

Radar Systems and Technology

Course No. 203

May 11-15, 1981



Continuing Engineering  
Education Program

SHORT COURSE NO. 203  
RADAR SYSTEMS AND TECHNOLOGY

May 11-15, 1981

George Washington University  
Washington, D.C. 20052

TIME	MONDAY	TUESDAY	WEDNESDAY	THURSDAY	FRIDAY
8:30 to 10:00	Introduction to Radar  SKOLNIK <i>NFL</i>	MTI Radar  SKOLNIK	Pulse Compression  HILL	Low Angle Tracking  BARTON	Synthetic Aperture Radar  SKOLNIK
	BREAK	BREAK	BREAK	BREAK	BREAK
10:15 to 11:45	Introduction to Radar (cont'd)  SKOLNIK	MTI Radar (cont'd)  SKOLNIK	Track-while-Scan ADT CFAR  HILL	Measurement Accuracy  BARTON	Remote Sensing Film of FPS-85  SKOLNIK
	LUNCH	LUNCH	LUNCH	LUNCH	LUNCH
1:00 to 2:30	Design of Air-Search Radar  SKOLNIK	Clutter Characteristics  SKOLNIK	Tracking Radar  BARTON	Phased Array Radar  HILL	ECCM, Over-the- Horizon Radar  SKOLNIK
	BREAK	BREAK	BREAK	BREAK	BREAK
2:45	Design of Air-Search Radar (cont'd)  SKOLNIK	Detection of Targets in Clutter  SKOLNIK	Tracking Radar (cont'd)  BARTON	Phased Array Radar (cont'd)  HILL	Millimeter Waves Current Problems  SKOLNIK

SESSION I

INTRODUCTION TO RADAR

Merrill I. Skolnik

MTI  
moving target indication  
(continuous wave)  
00-00-00

## RADAR

Radar is an electromagnetic device for the detection and location of reflecting objects such as aircraft, ships, satellites and the natural environment. It operates by transmitting a known waveform, usually a series of narrow pulses, and observing the nature of the echo signal reflected by the target back to the radar. In addition to determining the presence of targets within its coverage, the basic measurements made by a radar are range (distance), and angular location. The doppler frequency shift of the echo from a moving target is sometimes extracted as a measure of the relative velocity. The doppler shift is also important in CW (continuous wave), MTI (moving target indication) and PD (pulse doppler) radars for separating desired moving targets (such as aircraft) from large undesired fixed echoes (such as ground clutter). The doppler frequency shift is also sometimes employed to achieve the equivalent of good angular resolution. In addition to the usual measurements of range, angular location, and relative velocity, radar can obtain information about a target's size, shape, symmetry, surface roughness, and surface dielectric constant.

The origins of radar go back to the pioneering experiments of Heinrich Hertz in 1886 who demonstrated the similarity of radio waves and light. Hertz showed that radio waves could be reflected (scattered) from objects on which they impinge. This is the fundamental mechanism of radar. Based on these experiments, C. Hulsmeyer in Germany patented and demonstrated in 1904 a "Hertzian-wave" echo-location device for the detection of ships. Although the components used in his device were primitive by modern standards, the basic concept and philosophy were like that of a classical radar. Radar did not evolve from the early work of Hulsmeyer since there was no serious need for it until much later, when the development of military aircraft progressed in the 1930s to where it represented a significant new threat. The maturing of the aircraft as a military weapon then lead to the independent and almost simultaneous re-invention of radar in many countries as a means for the detection and tracking of aircraft. The demands of World War II accelerated the practical deployment of radar. Its development and improvement have been continuous ever since.

Radar has found many important applications. It is widely used for air traffic control, both for the detection of aircraft in flight and the control of aircraft moving on the airport grounds. Radar technology also forms the basis for aircraft navigation and landing aids, as well as for cooperative beacon systems (such as secondary radar, IFF, ATRBS, and DABS). On board aircraft, radar is used for weather avoidance, terrain avoidance, and navigation. It is widely found on ships of the world for piloting and collision avoidance. Large, ground-based radars are employed for the surveillance and tracking of satellites and ballistic missiles.

On board spacecraft, radar has been used for landing, rendezvous and docking. It has been proposed for the survey from space of agriculture and forestry resources, and the monitoring of sea and ice conditions. It is used for the ground-based observation of the weather and for the investigation of extraterrestrial phenomena such as the ionosphere, meteors, and aurora. The study of birds and insects has also benefited from the application of radar. Radar is used in law enforcement for the detection of intruders and for the speed measurement of vehicles. The military, whose support has made possible most of radar's major advances, extensively employ radar for surveillance, navigation, and the control and guidance of weapons.

The "typical" ground-based radar for the long-range detection of aircraft might operate at a wavelength of about 23 cm and radiate a peak power of about a megawatt (with an average power of several kilowatts) from an antenna about 10 meters in width rotating at 5 or 6 rpm. The early microwave radars used a magnetron oscillator as the transmitter. It is still widely used; but when high average-power or controlled-modulation waveforms are required, the transmitter is often a power amplifier like the klystron, traveling-wave tube, or crossed-field amplifier. The solid-state transmitter, usually based on the transistor, is also used for its potential in increasing reliability and maintainability. Low-noise receivers, such as the transistor or the parametric amplifier, have also found their way into modern radar practice. The impressive advances in solid-state digital circuitry made in recent years have resulted in significant new capabilities in radar signal processing and data processing. Sophisticated doppler processing techniques for MTI radar have been reduced to practice because of the availability of low cost, small-size digital processing technology. Another significant example of the benefits of advances in digital circuitry is in the automatic detection and tracking (ADT) of aircraft targets. A single operator observing the output of a standard PPI radar display might be able to track but a handful of aircraft. However, the small size and low cost of digital computers make it possible to automatically detect and accurately track several hundreds of aircraft simultaneously so as to present to the operator fully processed tracks rather than raw radar data. The parabolic reflector antenna has been and will continue to be the antenna most commonly employed with operational radar systems. However, the phased array antenna with agile beam steering controlled by electronic phase shifters has been of interest for radar applications because of the ease and rapidity with which its beam can be pointed anywhere within its coverage. The large cost and complexity of electronically steered phased array antennas have limited their application. Limited phased arrays whose beam is scanned over limited angular regions are more practical and have seen wide use as 3D air-surveillance radars, aircraft landing radars, and hostile-weapons location radars.

The range resolution of a radar can be of the order of a fraction of a meter, if desired; but the beamwidths that are practical with a microwave antenna limit the resolution in the angle coordinate (or cross-range dimension) to many orders of magnitude greater than this. It has been possible to synthesize the effect of a large antenna and thus overcome the cross-range limitation by employing the radar on a moving vehicle (such as an aircraft) and coherently storing the received echoes in an electronic or photographic memory for a time duration equivalent to the length of a large antenna. This technique for achieving cross-range resolution comparable to the resolution which can be obtained in the range dimension is called synthetic aperture radar (SAR). The output of such a radar is a map or image of the target scene. The use of a stationary radar to image a moving or rotating target by using resolution in the doppler domain is called inverse SAR. It has been employed, for example, to image the surface of the planet Venus under its cloud cover.

Radar is generally found within what is known as the microwave region of the electromagnetic spectrum. It is possible, however, to apply the radar principle at HF frequencies (from several megahertz to perhaps 30 megahertz) to obtain the advantage of long "over-the-horizon" ranges by refraction of the radar waves in the ionosphere. Aircraft can be detected by one-hop ionospheric propagation out to ranges of about 2000 nmi. Radar has also been considered for use at frequencies higher than the microwave region, at millimeter wavelengths. Laser radars are found in the IR and the optical region of the spectrum, where they offer the advantage of precision range and doppler frequency measurement.

## MAJOR DEVELOPMENTS IN RADAR BY DECADES

1930's - EARLY DEVELOPMENT OF THE BASIC CONCEPT OF RADAR

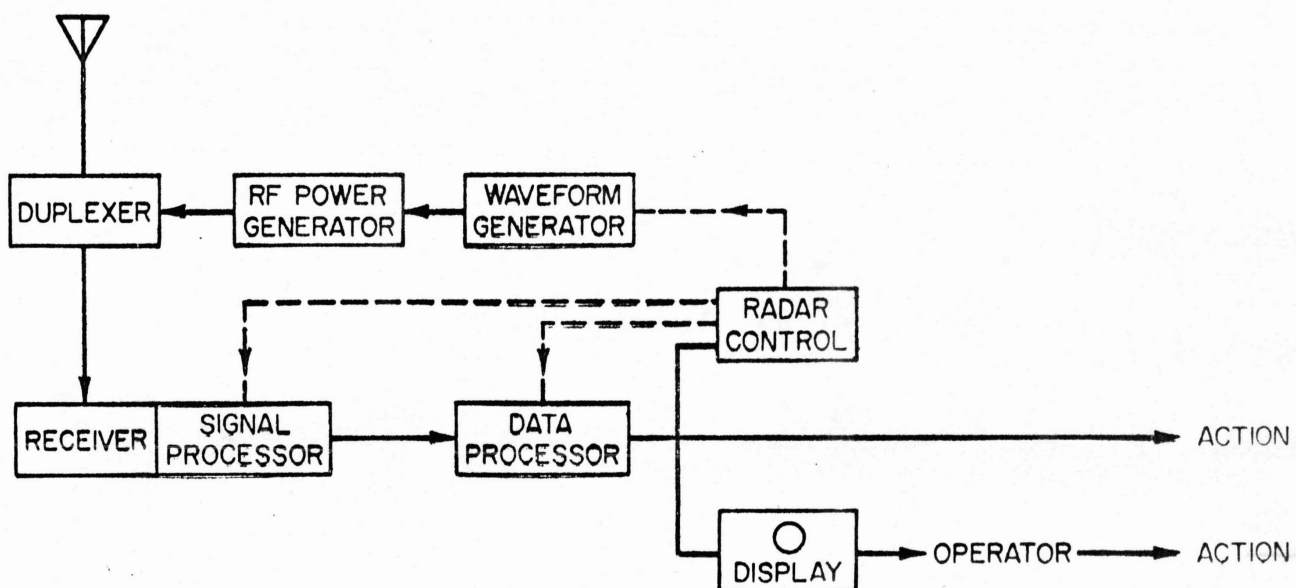
1940's - MICROWAVE RADAR

1950's - COHERENT RADAR, INCLUDING SYNTHETIC APERTURE AND MTI

1960's - DIGITAL PROCESSING, HF OTH RADAR

1970's - EXTRACTION OF INFORMATION, OTHER THAN LOCATION, FROM ECHO SIGNALS

# SIMPLE FUNCTIONAL BLOCK DIAGRAM





## Basic Radar Measurements

### LOCATION!

The following measurements can be made by radar:

Range - The accuracy of the range measurement is determined by the signal bandwidth. Accuracies of a few centimeters at a distance of several tens of miles are possible, with the basic limitation being the accuracy with which the velocity of propagation is known. *BT=1, WIDE BW WITH ACCURACY.*

Range rate - The doppler frequency shift provides a direct measure of the relative velocity. The longer the duration of the signal and the higher the frequency, the more accurate is the measurement. In radar the doppler frequency shift is often used to separate desired moving targets from undesired fixed targets (clutter). *MTI*  
The doppler frequency shift is also important for some types of radar imaging. *CAN ALSO GET ORTHOGONAL RATE, BUT DIFFICULT DERIVATIVE OF RATE*

Angle of Arrival - The angular location of the target is determined by use of a directive antenna. The larger the size of the antenna aperture (measured in wavelengths) the more accurate the measurement. *NO - 2D  
YES - 3D*

*10, BEST 0.1 mil 18 mil = 1 deg.*  
The above three measurements are what are normally made by a radar. They assume the target is a point scatterer, i.e., of infinitesimal size. When the target is distributed, of finite size, the following measurements apply:

Size - This is generally determined by use of a short pulse, or its equivalent (pulse compression). A measure of size can also be obtained by examining the variation of radar cross section with frequency.

Shape - The observation of the radar cross section from different aspect angles provides shape. Imaging of the target in range and angle also provides shape. *- mapping  
- synthetic aperture*

Change of shape - This is provided by the time variation of the radar cross section. A classical example is the modulation of the echo by aircraft propellers or jet engines.

Symmetry - The symmetry of a scattering object can be determined from observation of the target as a function of the polarization (direction of the electric field) of the radar signal. Symmetrical targets are insensitive to changes in polarization, asymmetrical targets are not. *CIRCULAR USED TO FULFILL MATH PLAN.*



In addition, the following two measurements can be made that describe something about the nature of the scattering material:

Surface roughness - The scale of surface "roughness" is measured in terms of the wavelength. When the surface variations are small compared to the wavelength, it is smooth. When it is large compared to the wavelength, it is rough. Measurements of backscatter as a function of wavelength can indicate the scale of surface roughness. (AMPLITUDE)

Dielectric constant - The reflection coefficient of a scattering surface depends on the dielectric constant. The measurement of the dielectric constant of a radar scatterer is difficult since it is necessary to know the surface roughness, shape, and the loss tangent. This is not a usual measurement in radar. However, the dielectric constant of the moon's surface was estimated many years ago from a series of radar measurements. The radar estimate was consistent with that measured with the moon rock samples brought back by Apollo. The measurement of dielectric constant is also of interest to NASA for estimating the soil moisture from a satellite-borne radar.

- SOIL MOISTURE
- FLOOD CONTROL
- WEATHER PREDICTION.

IEEE  
STANDARD RADAR-FREQUENCY LETTER BAND NOMENCLATURE

BAND DESIGNATION	NOMINAL FREQUENCY RANGE	SPECIFIC RADIOLOCATION (RADAR) BANDS BASED ON ITU ASSIGNMENTS FOR REGION 2
HF	3-30 MHz	138-144 MHz
VHF	30-300 MHz	216-225 MHz
"p" UHF	300-1000 MHz	420-450 MHz
L	1000-2000 MHz	890-942 MHz
S	2000-4000 MHz	1215-1400 MHz
C	4000-8000 MHz	2300-2500 MHz
X	8000-12 000 MHz	2700-3700 MHz
K <sub>u</sub>	12.0-18 GHz	5250-5925 MHz
K	18-27 GHz	8500-10 680 MHz
K <sub>a</sub>	27-40 GHz	13.4-14.0 GHz
mm	40-300 GHz	15.7-17.7 GHz
	94 GHz	24.05-24.25 GHz
		33.4-36.0 GHz

22 GHz WATER VAPOR ∴ SPLIT K-BAND

---

## APPLICATIONS OF RADAR

---

- **AIR TRAFFIC CONTROL** *60 miles* *200 miles*
  - AIRPORT SURVEILLANCE RADAR (ASR) – AIR ROUTE SURVEILLANCE RADAR (ARSR) – AIRPORT SURFACE DETECTION EQUIPMENT (ASDE) – LANDING RADAR (GCA OR PAR), *BEACON TRANSMITTER 1030-1090 MHz.*
- **AIRCRAFT NAVIGATION**
  - WEATHER AVOIDANCE – TERRAIN AVOIDANCE – TERRAIN FOLLOWING – RADAR ALTIMETER – DOPPLER NAVIGATOR – GROUND MAPPING
- **SHIP SAFETY**
  - PILOTING AND COLLISION AVOIDANCE – HARBOR SURVEILLANCE
- **SPACE**
  - RENDEZVOUS AND DOCKING – LANDING – SATELLITE SURVEILLANCE AND TRACKING – EARTH OBSERVATION

## TYPES

- PULSE
- HIGH RANGE RESOLUTION (PULSE COMPRESSION)
- CW (DEVELOPED  $\rightarrow$  NOISE + DOPPLER + LONG RANGE USES SEPARATE SITES)
- FMCW
- HTI (HE AMBIGUITY IN RANGE)
- PULSE DOPPLER
- SYNTHETIC APERTURE RADAR

---

## **APPLICATIONS OF RADAR (Cont'd)**

---

- **REMOTE SENSING**
  - WEATHER – RADAR ASTRONOMY – IONOSPHERIC SOUNDER – EARTH RESOURCES SURVEY – OCEAN CONDITIONS – INDUSTRIAL MEASUREMENTS – ORNITHOLOGY – ENTOMOLOGY
- **LAW ENFORCEMENT**
  - INTRUSION DETECTION – POLICE SPEED METER
- **INSTRUMENTATION**
  - RANGE INSTRUMENTATION – SURVEYING
- **MILITARY**
  - SURVEILLANCE – NAVIGATION – CONTROL AND GUIDANCE OF WEAPONS – RECONNAISSANCE – DAMAGE ASSESSMENT – FUZING – NON-COOPERATIVE TARGET RECOGNITION

### Examples of the Radar Range Equation

Type of Interference	Searchlighting or Tracking	Volume Search
Receiver Noise	$R_{\max}^* = \frac{P_{av} G_e A_r \sigma t_o}{(4\pi)^2 k T_a (E/N_o)}$	$R_{\max}^* = \frac{P_{av} A_r \sigma}{4\pi k T_a (E/N_o)} \cdot \frac{t_a}{\Omega}$
Volume Clutter (rain)	$R_{\max}^2 = \frac{\sigma G_e}{\eta 4\pi (c\tau/2) (S/C)_{\min}}$	$R_{\max}^2 = \frac{\sigma}{\eta f_p (c\tau/2) (S/C)_{\min}} \cdot \frac{t_a}{\Omega}$
Surface Clutter	$R_{\max} = \frac{\sigma}{\sigma^0 \Theta_b (c\tau/2) \sec \phi (S/C)_{\min}}$	<p>Correlated clutter: same as for 'searchlighting'</p> <p>Uncorrelated clutter:</p> $R_{\max} = \frac{\sigma f_p}{\sigma^0 (c\tau/2) \sec \phi (S/C)_{\min}} \cdot \frac{t_a}{\Omega_a}$
External Noise (jamming)	$R_{\max}^2 = \frac{P_{av} t_o G_e}{4\pi} \cdot \frac{\sigma}{E/N_o} \cdot \frac{1}{N_{oi} G_i}$	$R_{\max}^2 = P_{av} \frac{\sigma}{E/N_o} \cdot \frac{1}{N_{oi} G_i} \cdot \frac{t_a}{\Omega}$

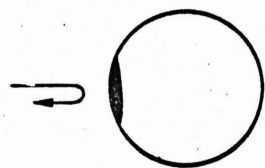
$R_{\max}$  = max radar range,  $P_{av}$  = average transmitter power,  $G_e$  = antenna gain,  $A_r$  = effective aperture,  $\sigma$  = target cross section,  $t_o$  = integration time,  $k$  = Boltzmann's const.,  $T_a$  = system noise temperature,  $E/N_o$  = signal-to-noise energy ratio req'd for detection,  $t_a$  = search time,  $\Omega$  = angular search volume,  $\eta$  = clutter (rain) cross section per unit volume,  $c$  = velocity of propagation,  $\tau$  = pulse width,  $(S/C)_{\min}$  = signal-to-clutter (power) ratio required for detection,  $f_p$  = pulse repetition frequency,  $\Theta_b$  = azimuth beamwidth,  $\phi$  = grazing angle,  $\Omega_a$  = azimuth coverage ( $2\pi$  rad),  $N_{oi}$  = noise power per Hz radiated by jammer,  $G_i$  = jammer antenna gain.

mjs

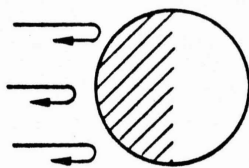
## Scattering from a Sphere

Scattering of electromagnetic energy results from discontinuities in the dielectric constant of the scattering object that are comparable to the radar wavelength. For example, the echo from a smooth, metallic sphere whose radius is large compared to the wavelength occurs from a small spot (the first Fresnel zone) on the tip (Fig. 1a). For scattering to occur from the entire sphere the surface would have to be rough, or diffuse (Fig. 1b), such as is a white billiard ball or the full moon when viewed at optical frequencies. When the radius of the sphere is comparable to the radar wavelength, there is a contribution to the backscatter due to a creeping wave that circles around behind the sphere as shown in Fig. 1c. This creeping wave causes constructive and destructive interference with the direct reflection so that the backscatter varies periodically as a function of  $a/\lambda$ . The classical description of the scattering from the sphere as a function of wavelength is sketched in Fig. 1d.

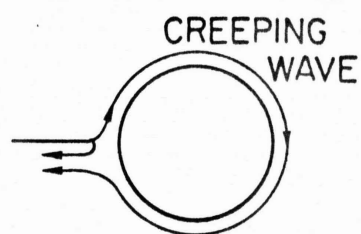
Some of the energy incident on a non-metallic (dielectric) sphere is reflected similar to that of a metallic sphere, but reduced by the reflection coefficient of the dielectric. Some energy penetrates the body of the sphere where it is partially reflected from the opposite side (Fig. 2a). This partially reflected component interferes with the direct backscatter from the front surface to produce a back-scatter cross section that depends on the size of the sphere, the dielectric constant, and the loss in propagating through the dielectric material. An example of the variation of the scattering from a dielectric sphere is shown in Fig. 2b.



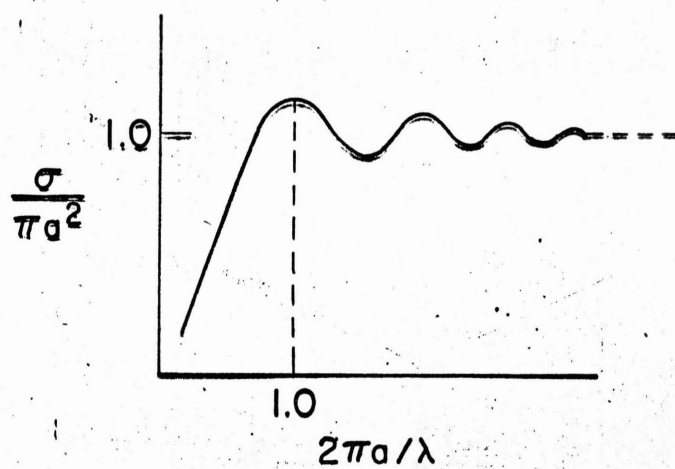
(a) SPECULAR SCATTER



(b) DIFFUSE SCATTER



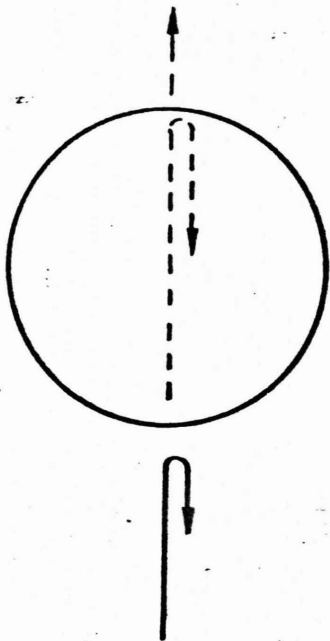
(c) RESONANT SCATTER



(d) RADAR CROSS SECTION

Fig. 1





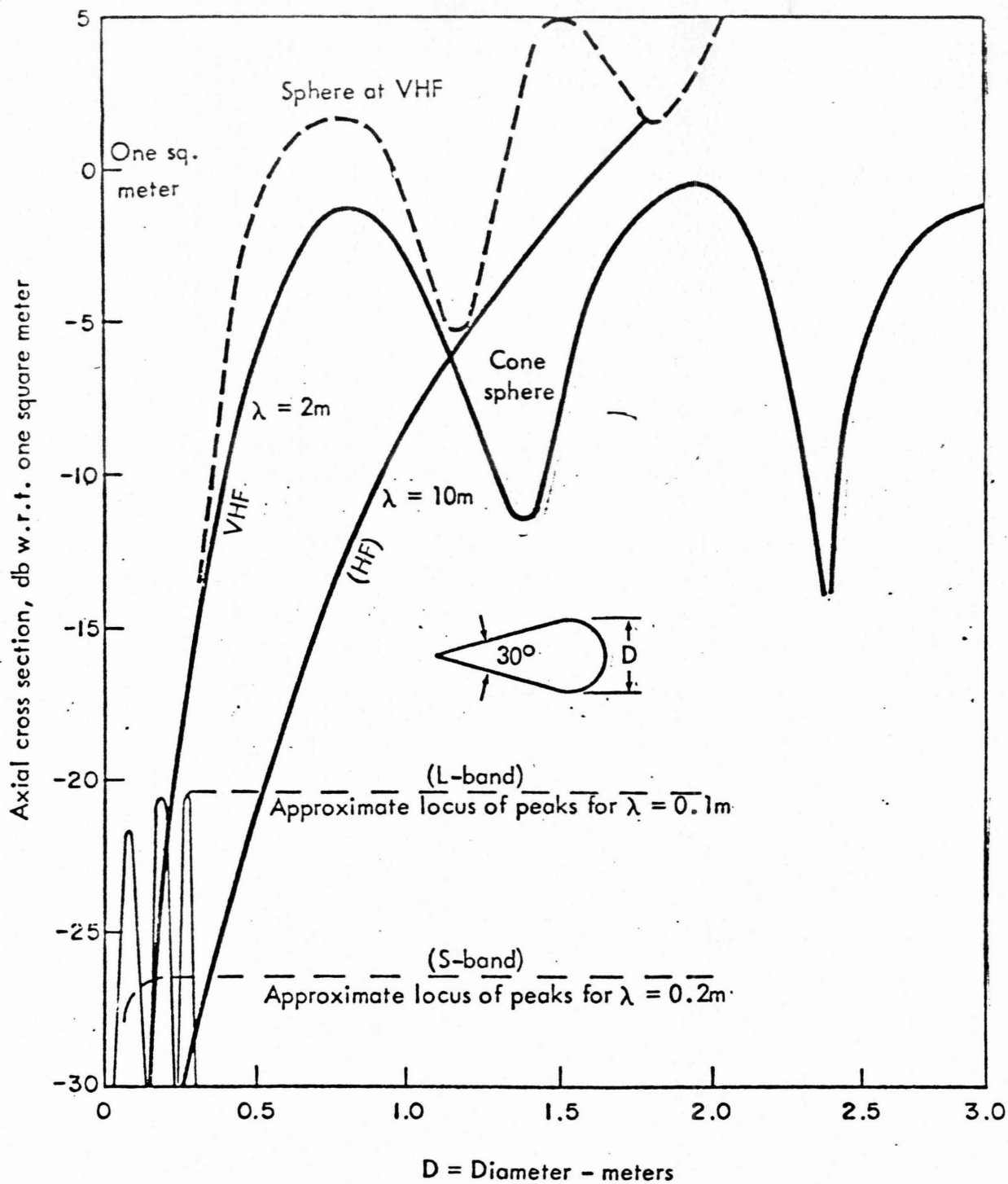
(a) RAYS IN DIELECTRIC SPHERE



Fig. 2

$2\pi a/\lambda$

(b) EXAMPLE OF RADAR CROSS SECTION



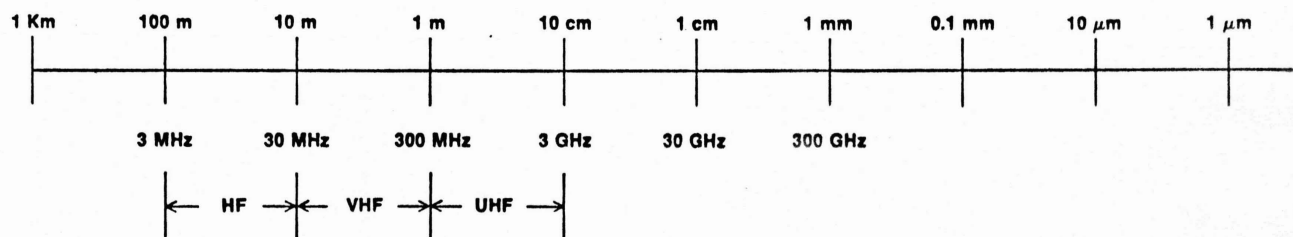
AXIAL RADAR CROSS SECTION OF A 30° CONE SPHERE FOR VARIOUS VALUES OF WAVELENGTH

## TYPES OF RADARS

- PULSE - CONVENTIONAL RADAR.
- HIGH-RANGE-RESOLUTION - RESOLUTION FROM A FEW CENTIMETERS TO SEVERAL METERS, USEFUL FOR SEEING DESIRED TARGETS IN CLUTTER. CAN USE PULSE COMPRESSION.
- CW (CONTINUOUS WAVE) - USES DOPPLER FREQUENCY SHIFT TO SEPARATE MOVING TARGETS FROM FIXED CLUTTER.

$$f_d = \frac{2v \cos \theta}{\lambda} \approx \frac{v_r(\text{kts})}{\lambda \text{ (m)}}$$

- FM-CW = FREQUENCY MODULATED CW, GENERALLY OF HIGH RANGE RESOLUTION BUT NO DOPPLER FREQUENCY SHIFT UTILIZED.
- MTI - MOVING TARGET INDICATION, A PULSE RADAR THAT EXTRACTS DOPPLER FREQUENCY SHIFT TO SEE MOVING TARGETS IN CLUTTER.
- PULSE DOPPLER - AN MTI WITH A SUFFICIENTLY HIGH PULSE REPETITION FREQUENCY TO AVOID AMBIGUITIES IN DOPPLER.
- SYNTHETIC APERTURE (SAR) - AN AIRBORNE IMAGING RADAR CAPABLE OF HIGH RESOLUTION IN BOTH RANGE AND ANGLE; CAN BE 3 M RESOLUTION.



Radar Frequencies									
HF	VHF	UHF	L	S	C	X	K <sub>a</sub>	K <sub>a</sub>	Millimeter

CO <sub>2</sub> laser	IR laser	Optical
--------------------------	-------------	---------

Surveillance } Information  
Combination

**Radar Frequencies**

# Radar Technology Applied to Air Traffic Control

WILLIAM W. SHRADER

**Abstract**—Use of primary radars for air traffic control (ATC) is discussed. The location and the parameters of various ATC radars are described. The clutter environment (land clutter, birds, automobiles, and weather) has had a major impact on the configuration of these radars. Signal-processing techniques and antenna techniques utilized to cope with the clutter are described. Future signal-processing techniques for the ATC radars are postulated.

## INTRODUCTION

PRIMARY radars are utilized by the Federal Aviation Administration (FAA) to provide control of air traffic, in addition to the beacon system (referred to as secondary radars). The primary radars are 60-mi airport surveillance radars, and 200-mi air route surveillance radars. Specifically, these radars are used to: 1) control nonbeacon equipped aircraft; 2) control aircraft with nonfunctioning beacons; 3) provide weather information to air traffic controllers; 4) provide coastal surveillance information to the military; and 5) provide weather information to the weather bureau in parts of the U.S.

There are approximately 124 ASR radars and 80 ARSR radars installed in the United States [1]. The locations, including future authorized locations, are shown in Fig. 1 and 2. These radars have been procured over the last 20 years. They have, however, been continually upgraded and currently are represented by 4 typical configurations, the ASR-6, ASR-7, ARSR-2, and FPS-66. In addition to the existing radars, the ASR-8 and ARSR-3 are currently being procured. Major characteristics of these radars are shown in Table I. Note that of the existing radars, only the ASR-7 has digital signal processing and solid-state circuitry.

The radar system coverage diagrams for the ASR-7 and the ARSR-2 are shown in Figs. 3 and 4. The coverage represents approximately 80 percent blip/scan ratio on a small jet aircraft.

## HISTORY

In February 1949, the Civil Aeronautics Administration (CAA) (predecessor to the FAA) granted authorization for commercial aircraft to use radar as a primary aid. This approval applied specifically to aircraft operating in the terminal area in inclement weather. The long-range (enroute) radar program began in 1953 with the commissioning, at Washington, D.C., of a microwave early warning (MEW) radar. The procurements of the existing modern enroute ATC radars

began in 1956 (the ARSR-1) and in 1957 (the ASR-4). Of significant interest is that, with the exception of antenna techniques, there has been no major improvement in the radar system concepts for air traffic control since 1956. For example, the ARSR-1 utilized a two-pole two-zero recursive moving target indicator (MTI) filter, which is conceptually identical to the MTI filter to be used in the ARSR-3 now being procured. Of course, solid-state and digital techniques will improve the reliability of the new systems, but the basic MTI performance capability will not change, for the reasons discussed in this paper. Of the approximately 200 ATC radars now in use, 90 percent of them utilize quartz delay lines for their MTI delay elements and vacuum-tube circuits throughout. Although the use of digital techniques does not inherently increase the MTI capability, the analog systems drift out of adjustment over a period of time. Thus, digital techniques result in improvement in the average performance obtained in the field.

## SIGNAL-PROCESSING PERFORMANCE

Emerson [2] and others predicted the performance of multiple delay feedback cancelers used in the ATC radars in a variety of clutter environments. The ATC radars fail to cancel clutter perfectly for two principal reasons: 1) the modulation of the clutter introduced by scanning of the radar antenna; 2) motion of the "fixed" clutter, primarily due to motion of the grass, trees, and leaves in the wind. In addition, weather clutter often fails to cancel because the average Doppler frequency induced by the wind falls outside the clutter rejection notch of the MTI filter. Barlow [3] and Grisetti *et al.* [4] predicted the performance of these radars in the various types of clutter. The clutter spectra had been measured, and by assuming linear signal processing, predictions were made of clutter residue at the system output.

When these multiple-delay MTI radar systems were built, they failed to perform as well as predicted. The MTI processing systems were much more severely limited by scanning modulation than had been expected. That is, with the antenna stationary, the clutter canceled well, but with the antenna rotating, the MTI improvement factor was as much as 20 dB worse than predicted. This fact was not discussed in the technical literature until 1967 [5] probably because no manufacturer would admit less MTI performance than was universally expected from such configurations.

Two other factors that may have obscured the actual performance being obtained from MTI radars are explained in the following.

VHF (30 to 300 MHz)

137-144 MHz

216-225 MHz

Economical surveillance radars

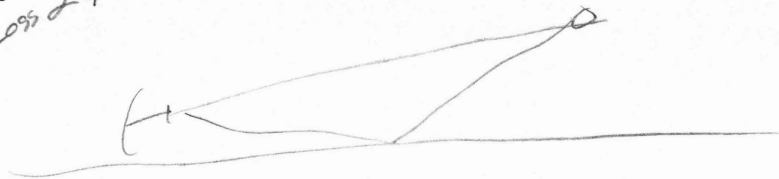
Easily achieved high power and large antennas

Extended range due to surface reflection

Weather-free

BECAUSE OF  
TOKYO-AMERICA

PATH  
LOSS  $\propto f^4$



LONG  
PATTERN

UHF (300 to 3000 MHz)

420-450 MHz

890-940 MHz

Economical surveillance radar with good  
MTI and free from weather.

Detection and tracking of extraterrestrial  
targets.

*satellites ICBMs  
by missile*

*"INSTRUMENTS OF WARFARE"  
GOOD BOOK ON EARLY ECM.  
ALSO "WIZARD WAR"*

L Band (1000 to 2000 MHz)

1215-1400 MHz

Popular for aircraft-surveillance radar

Extraterrestrial detection and precision track

SEVERAL REFLECTIONS SHOWN FROM TO EARTH/BACK GROUND  
REFLECTION.

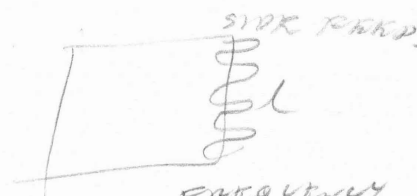


+45° EASY  
WITH CHASE

S Band (2000 to 4000 MHz)

2300-2550 MHz

2700-3700 MHz



FREQUENCY  
CHANGE PHASE  
SHIFT ALONG  
TO CHANGE  
HEIGHT,

Moderate-range aircraft surveillance

Height-finding

Combined surveillance and track-while-scan

Shipboard multifunction weapon control

Terminal defense ABM

Low environmental noise → LESS LIGHTNING + ATMOSPHERIC ABSORPTION,

Land-based weather observation

DUAL RELIABILITY SYSTEMS USED SIMULTANEOUSLY  
TO GET REDUNDANCY + FREQUENCY DIVERSITY,  
11-12-8 dB IMPROVEMENT,

C Band (4000 to 8000 MHz)

5255-5925 MHz

Precision, long-range tracking

Landbased multifunction weapon control

X Band (8 to 12.5 GHz)

8500 to 10,700 MHz

Tracking and missile guidance

Ship navigation

Airborne weather-avoidance X-Band VS, C-Band  
X-Band HRTF

Intrusion detection

Hostile-weapons location

Precision approach

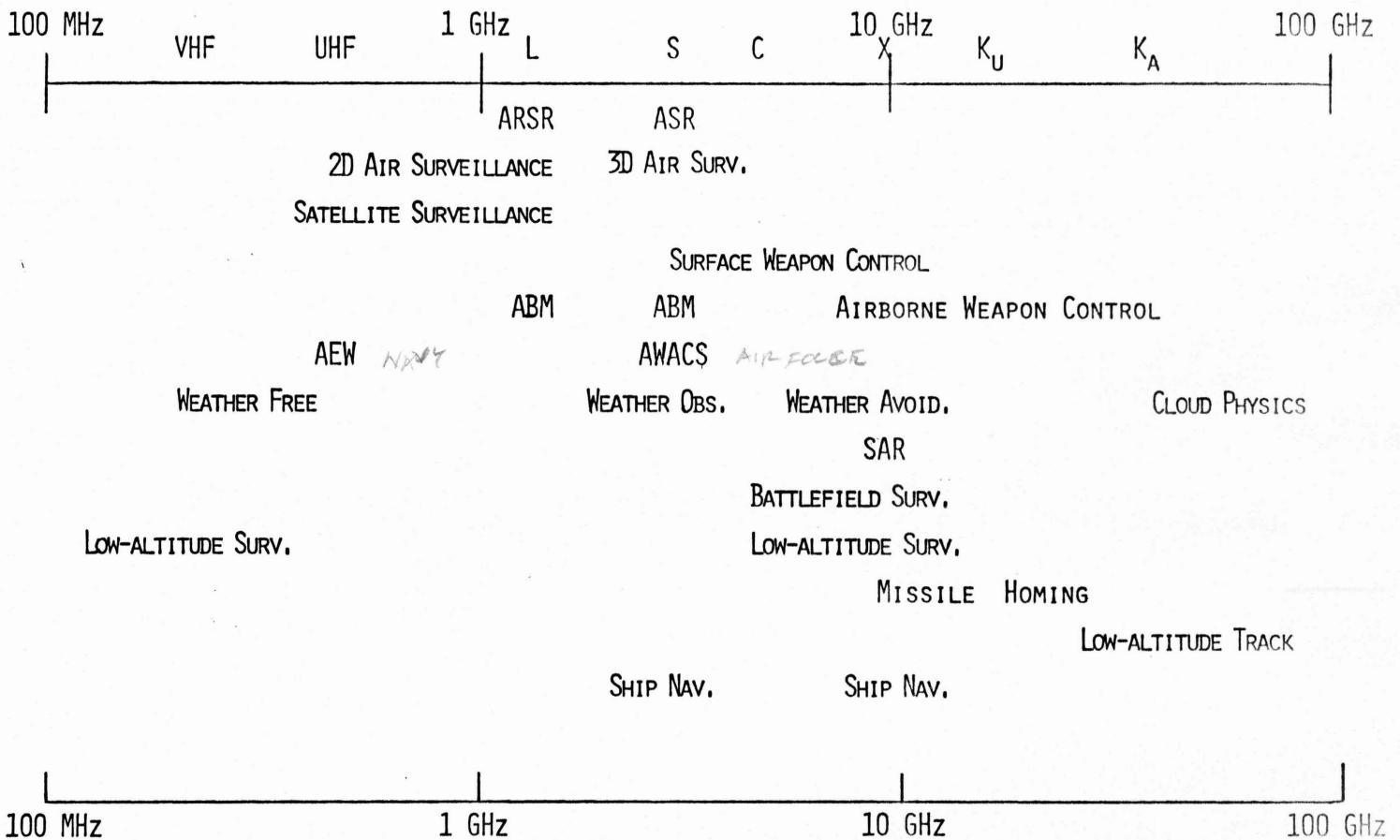
# K Bands (12.5 to 40 GHz)

13.4 to 14.4 GHz	}	K <sub>u</sub>
15.7 to 17.7 GHz		
23 to 24.25 GHz		K
26.5 to 40 GHz		K <sub>a</sub>

## Military airborne radar

THIS ANTENNA HAS NO DEPORTURE BLOCKING.

# CARRIER FREQUENCY



SPECTRAL BANDWIDTH REQUIREMENTS IN RADAR

1 MHz

10 MHz

100 MHz

1000 MHz

AIR SURVEILLANCE

SATELLITE SURVEILLANCE

WEAPON CONTROL

SHIP NAVIGATION

IMAGING (SYNTHETIC APERTURE)

BALLISTIC MISSILE DEFENSE

TARGET CLASSIFICATION

TARGET/CLUTTER ENHANCEMENT

ECCM →

Each frequency region has its own particular characteristics that make it better for certain applications than other frequencies. In the following, the usefulness of the various portions of the electromagnetic spectrum at which radars have been operated is examined and the major advantages and limitations of each frequency band are described. The divisions between the frequency regions defined here are not as sharp in practice as is the precise nature of the nomenclature. The following generalizations are only approximate representations of radar practice and should not be interpreted too rigidly.

**Lower than HF (below 3 MHz)** At the long wavelengths a significant portion of the radiated energy can be propagated by diffraction beyond the radar horizon. This is sometimes called the *ground wave*, or the *surface wave*. The lower the frequency, the less is the attenuation of the diffracted wave. The advantage of this mode of propagation is that the wave essentially follows the curvature of the earth. Because of the large antennas required for directive beams, the high ambient noise level, unwanted echoes (clutter) from ground objects, and the crowded electromagnetic spectrum, the frequencies below HF are not attractive for general radar application.

**HF (3 to 30 MHz)** The first operational radar system installed by the British just prior to World War II radiated in the HF band at a frequency between 22 and 28 MHz. These were the radars that provided detection of aircraft during the Battle of Britain. They operated at this frequency not because it was optimum for the application but because it was the highest frequency at which reliable high-power components were then available. The choice of this nonoptimum frequency reflected the often-quoted "Cult of the Imperfect" slogan of Sir Watson Watt, the British inventor of radar: "Give them the third best to go with; the second best comes too late; the best never comes." The ground-wave mode of propagation was employed, and ranges of 200 miles were obtained against aircraft. In addition to the ground wave, the sky wave at this frequency reflects off the ionosphere and can result in unwanted echoes. The reflection from the ionosphere is not always undesirable and can be a means for detecting targets at long ranges beyond the line of sight. The upper portion of the HF band has been used for radar astronomy, especially for obtaining echoes from the sun's ionized atmosphere. Ionospheric sounders that measure the height of the various layers of the ionosphere employ the radar principle. The same objections mentioned in the previous paragraph concerning radar at frequencies below HF apply almost equally well to the HF region.

**VHF (30 to 300 MHz)** The early radars developed in this country just prior to World War II operated in this frequency region. Some notable examples were the Navy CXAM, the Army SCR-270 surveillance radar, and the Army SCR-268 fire-control radar. They all used extensions of the then current technology in vacuum tubes and mechanically positioned array antennas. Because of the present crowded spectrum at VHF, modern radars are not found extensively in this region. However, it is an important region for the application of certain types of long-range radar with large antenna apertures and large radiated power such as might be used for satellite surveillance. VHF is probably the most economical region in which to build and operate large radars. Although the external noise is not as low as at higher frequencies, it is significantly lower than that in the HF region. The angular resolution of VHF air-surveillance radars is generally poor but the coverage is usually good and the equipment is relatively simple and reliable.

Radar technology is usually easier to achieve at the lower frequencies, and VHF is a compromise between the increasing noise level found at lower frequencies and the more difficult implementation of long-range radars found at the higher frequencies. Antennas for air-surveillance radars are more likely to be arrays of dipoles mechanically rotated than the parabolic reflectors commonly used at the higher frequencies. With horizontal polarization over a good ground plane, such as the sea, the interference

between the direct wave and the wave reflected from the surface can result in a substantial increase in the maximum range against aircraft. Another advantage of VHF is the good MTI performance that can be obtained against moving targets. Good MTI requires stable transmitters and receivers which are easier to achieve at the lower frequencies. Also, it is important that there be no blind speeds within the expected range of doppler velocities. The lower the frequency, the greater is the blind speed, everything else being equal. Radars at VHF are also free from weather echoes or attenuation. VHF is a good region in which to design a short-range "poor man's radar" and would undoubtedly be more widely used if the demands of other radio services did not take precedence for the available spectrum.

**UHF (300 to about 1,000 MHz)** Much of what has been said above concerning VHF radar applies to UHF as well. Narrower antenna beams are easier to achieve, and the external noise is less than at VHF. It is a good frequency band for reliable, long-range surveillance radar, with freedom from weather effects and with good MTI capability. Its application is limited by the wide spectrum allotted to UHF television.

**L Band (1,000 to 2,000 MHz)** This is a popular frequency band in the United States for aircraft-surveillance radar. It sacrifices some of the lower-frequency advantages of high power, large antenna apertures, and good MTI but provides improved angle resolution and low external noise.

**S Band (2,000 to 4,000 MHz)** Most of the radar applications below S band are for surveillance whereas most of those above are for information gathering such as precise target location and tracking. Good angular resolution can be obtained at S band with reasonable-size antennas, and the external-noise level is low. However, MTI at S band is usually noticeably worse than at UHF. Although weather effects are not as bothersome as at the higher frequencies, they can significantly degrade the radar performance in some applications. S band is of interest as a compromise radar frequency for medium-range aircraft detection and tracking when a single radar must be used for both functions.

**C Band (4,000 to 8,000 MHz)** This band lies between the S and X bands and can best be described as a compromise between the two. It has been successfully used for moderate-range surveillance applications where precision information is necessary, as in the case of ship-navigation radar. It is also the frequency at which one can find precision long-range instrumentation radars as might be used for the accurate tracking of missiles. Relatively long-range military-weapon control radars might also operate in this band.

**X Band (8 to 12.5 GHz)** This is a popular frequency band for military weapon control and for commercial applications. Civil marine radar, airborne weather-avoidance radar, and doppler navigation radars are found at X band. At X band the radar is generally of convenient size and is thus favored for applications where mobility and light weight are important. X band is advantageous for information gathering or short-range surveillance, but it is not very well suited for long-range surveillance. Sufficient bandwidth is available to make it more convenient to generate narrow pulses than at the lower frequencies. Narrow beamwidths are also easy to achieve at X band with small physical size apertures. A 1° beamwidth can be obtained with an antenna about 6 ft in width. An X-band radar may be small enough to hold in the hand, or it may be as large as the Haystack Hill radar used for radar astronomy with a 120-ft-diameter antenna and an average radiated power of about 500 kW CW.

**K<sub>u</sub>, K, and K<sub>a</sub> Bands (12.5 to 40 GHz)** The original K-band radars developed during World War II at the MIT Radiation Laboratory were centered at a wavelength of 1.25 cm (24 GHz). This proved to be a poor choice since it was soon found that it was too close to the resonance wavelength of water vapor (22.2 GHz), where the absorption is high. Later this band was subdivided into two bands on either side of the water-absorption frequency. The lower-frequency band, K<sub>u</sub>, covers 12.5 to 18 GHz; the upper band, K<sub>a</sub>, extends from 26.5 to 40 GHz. K<sub>a</sub> band is about the highest frequency at which one finds operational radar. Although radars have been built at higher frequencies, they have been mainly for experimental purposes or special applications. The K-band frequencies offer the advantage of good resolution in both angle and range with little mutual interference. High power is difficult to achieve,

and the antennas are small. There is increased atmospheric attenuation, external noise, and less sensitive receivers. These factors result in relatively short range. Limitations due to rain clutter and attenuation are increasingly serious at higher frequencies.

**Millimeter Wavelengths** This part of the frequency spectrum offers wide bandwidth and narrow antenna beams from relatively small apertures. It suffers the same limitations as the K bands, only more so. Even moderate power is difficult to achieve, and receiver internal noise is generally high. The external-noise level, the atmospheric absorption, and weather clutter increase rapidly with increasing frequency. The increase in attenuation is not monotonic, and there are "windows" where it is relatively less than at neighboring frequencies. Applications for millimeter-wave radar have been limited. It might be employed when the wide spectral range is needed to avoid interference from other electromagnetic services. The wide bandwidths and relatively narrow beamwidths might be of advantage when it is desirable to obtain information that might help to classify the type of target. The disadvantages, however, have tended to outweigh any advantages of operation at millimeter wavelengths.

**Laser Frequencies** Coherent power of reasonable magnitude and efficiency along with narrow directive beams can be obtained from lasers over the infrared, optical, and ultraviolet regions of the spectrum. The good angular resolution and range resolution possible with lasers make them useful for target information-gathering applications such as ranging or imaging. Lasers are less suited for surveillance because of the relatively small receiving aperture area and the difficulty of searching a large volume with a narrow beam. A serious limitation of the laser is its inability to operate effectively in rain, clouds, or fog.



# AFTERTHOUGHTS ON "INSTRUMENTS OF DARKNESS"

by Flight Lieutenant Alfred Price

As any author will testify, the time of publication of a book of this nature is in one respect a moment of sadness. It is then that one thinks of all the stories that one would have liked to have put in. But because they arrived too late, or were a bit too technical for the lay reader, or were "chopped" in the last-minute scramble to get the book to the exact size stipulated by the publishers, they had to stay out. Chas. W. Knight asked me to jot down a few such stories for the interest of members.

The most fascinating part of writing *Instruments of Darkness* was that of reconstructing the Intelligence battles, in which we tried to find

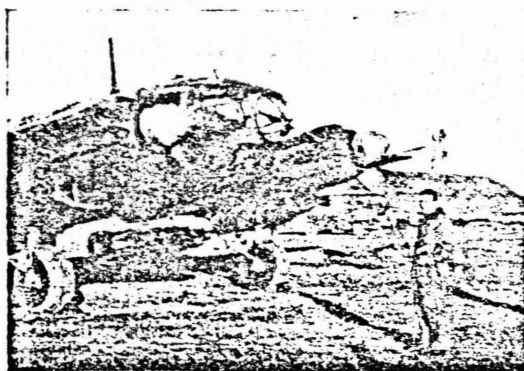
city between the two halves was measured electronically, and the idea was that a third conductor such as an aircraft in the vicinity would alter this capacity and thus set off the fuse. In practice it all fell down because of the very small change in capacity caused by the aircraft, due to the fact that the two halves of the shell were so close together. But the ironic part of the story is that while the German proximity fuse did not work, it sparked off research into this field in Britain. This resulted in the radar proximity fuse which worked so well that by the end of the V1 attack in 1944 an average of only 77 such shells was necessary to destroy one flying bomb.

The discovery of the German radio beams really did come as a shock to the British War Cabinet. The first of the special units using the beams to be discovered was *Kampfgruppe 100*; with some thirty Heinkel 111's it was based at Meucon airfield near Vannes in Brittany. This *Gruppe* operated as pathfinders, and had marked Coventry for the rest of the *Luftwaffe* during the heavy attack on the night of 14th November, 1940. Through its agents, the British Intelligence service had learnt that the German aircrewmembers were billeted in the town of Vannes. Prior to each operation they drove to Meucon in a couple of busses. The stakes were high: could



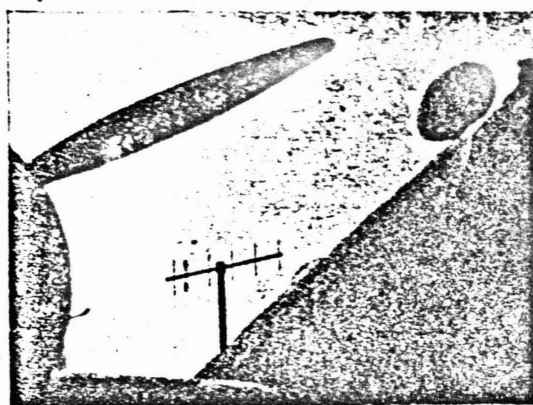
Did you ever get that feeling that you were being watched? A wartime infra-red photograph of the Chain Home station near Dover, taken by a German cameraman near Calais.

out about the German radar and they tried to find out about ours. It was all a bit like putting together a two-sided detective story, while at the same time being in the privileged position of knowing the technical facts that both sides were trying to gain. Far and away the most intriguing piece of espionage was the so-called "Oslo Report", which arrived in Britain via our embassy in Oslo in November 1939. Sent by a "well wishing German scientist", it contained a wad of papers giving information of the latest German technical devices, including radar. I discussed the report in some detail in my book, but one point I did not mention was that it did not stop at descriptions of secret devices—the packet actually contained one of them. The device in question was the prototype of a proximity fuse for an anti-aircraft shell, which worked on the capacitive principle. The shell was constructed in two parts, the front one of which was electrically insulated from the rear. The capa-



Major Victor von Lossberg, the commander of the German pathfinder unit III./K.G. 26, seen standing in front of his Heinkel 111 in 1941. The special post aerial for the Y-Gerat beam bombing system may be seen just behind the cockpit.

not the busses be ambushed by a specially parachuted in team of agents, and the highly-trained German crewmen killed? Eventually the idea reached the ears of the Chief of the Air Staff, Air Chief Marshal Sir Charles Portal, who was called upon to supply an aircraft for the enterprise. Portal was horrified. He said he would not be a party to any scheme where a "gang of assassins" murdered uniformed members of the enemy air force. Once started, where might such a course end? Eventually a compromise was reached: the ambushing team was to comprise uniformed soldiers. So it came about that on the night of the 15th March, 1941 seven heavily armed parachutists were dropped 8 miles outside Vannes, in open country. The soldiers



*Talking about aircraft with funny aerials, how about this? A highly directional Yagi, fitted to a "Ferret" Wellington during the war. Inside the fuselage . . .*

linked up with agents from the town, only to learn that the Germans had changed their habits: now the crewmen drove to Meucon in twos and threes in small cars, instead of being conveniently concentrated together in the busses. Since there was now no favourable opportunity for an ambush the operation was called off. The parachutists dispersed, and returned to Britain individually.

Amongst the most successful countermeasure to the German pathfinder tactics in the spring of 1941 was the "Starfish" fire decoy site. Responsible for these sites was Colonel J. Turner, onetime head of the R.A.F. works department and "Konky Bill" to his friends. During this time Major Victor von Lossberg commanded the second of the beam-flying path-

finder units, the Third Gruppe or Kampfgeschwader 26 at Poix, also equipped with Heinkel 111's. He says his own and Kampfgruppe 100 usually put up a total of 18 to 25 aircraft per raid, but such a small force often could not start a conflagration large enough to compete with the carefully prepared British decoys.

During one of the attacks on Liverpool in the spring of 1941 von Lossberg recalls that his Gruppe flew in as high as possible, at around 22,000 feet, in order to get the greatest possible range from their V.H.F. (42-48 megacycles) beam transmitters near Cherbourg. The Heinkels trailed long white condensation trails from each engine, together looking rather like railway lines in the moonlight. Suddenly von Lossberg saw one of the pairs of lines begin to twist and curve, then disappear altogether: British night fighters were active. The beam signals ended some seven minutes flying time short of the city, near Wrexham, and he continued on to the target using dead reckoning. Suddenly below him, in a position he knew to be well short of Liverpool, von Lossberg observed fires blazing up on the ground. In fact this was the decoy "Liverpool", built ten miles to the south of the city near Neston on the mouth of the Dee. The pathfinders went on to release their incendiaries accurately, but as they headed south afterwards they were helpless spectators as they watched bomber after bomber in the follow-up force release its load on the decoy. More than two thirds of the bombs intended for Liverpool were seduced away by the decoy.

Sir Robert Cockburn tells a nice little story of the "Mandrel" radar jamming device he designed. After it was first used in action, on the night of the 6th December, 1942, the British monitoring service reported that the band of frequencies it covered fell somewhat short of the intended 10 megacycles. On the following day Cockburn was driving from London to Malvern, wondering how he could devise a simple modification for the 150 "Mandrels" in service. In a flash it came to him, and within days the sets had been modified to jam out the necessary frequencies. His solution: a piece of tinfoil, bolted on to the chassis near the main tuning condenser; as the aircraft's motors turned they vibrated the foil which in turn varied the output frequency. To set up the jammer one merely ran the engines, then clipped off bits of tinfoil

until the desired frequency spread was obtained. Believe it or not, it worked!

In the same vein was Mr. R. Light's method of overcoming the previously successful jamming of British radar sets in Malta, in the summer of 1942. Light examined the jamming on an oscilloscope, and observed that it was heavily modulated at 100 cycles per second. More important than the frequency of the modulation was the fact that the depth of the modulation was 100 per cent., so the jamming strength varied between zero and a maximum one hundred times per second. The solution worked out by Light and Flight Lieutenant Jones, the commander of one of the radar stations, was almost ingenious in its simplicity. They used a radio receiver to pick up the jamming, which was then de-modulated. The output sine wave was fed to the radar's waveform generator, where it was arranged to trigger the set on when the jamming was at zero. In this way it was possible to "cancel out" the effect of the jamming. There was an interesting sequel. After the war Light met the man who had been his German counterpart during the incident. The latter burst out laughing when he heard what had been done to defeat his jamming. Yes, he had realised that a weakness existed which the British might exploit, but he had no choice: his smoothing condensers had broken down, and it was taking a long time to get new ones from Germany.

Both sides' radio monitoring services played a vitally important part in the radio war. It may come as a shock to some to learn that the Germans profited handsomely from the seemingly harmless practice of ground testing our bombers' T.1154 transmitters prior to each operation. It was not difficult to pick up these signals on the Continent, where they were carefully collated. The Germans were looking for a pattern: heavy test traffic in the morning and little or none in the afternoon—when the crews were at briefing—generally presaged a heavy attack. If no raid was planned the testing was spread evenly throughout the day. Colonel Hajo Herrmann,

who commanded the Berlin defence area during the crucial battles in the winter of 1943, has told me that at 5 o'clock each evening his chief signals officer would give him a fairly detailed estimate of the number of bombers the R.A.F.



... screwed to the top of the special operator's makeshift table, sat the tools of his trade: Hallicrafter receiver, signal generator and oscilloscope.

planned to use that night. Herrmann says he would order up to one quarter of his force to cockpit readiness on the strength of such information. Once the British Pathfinders were airborne their powerful H2S radiations were picked up in Germany, and the vanguard of the attacking force could be tracked relatively easily using these. As soon as the first H2S signals were received Herrmann would scramble his immediate readiness force. The distance from Berlin to Essen is roughly the same as that from Lincoln to Essen. So if the penetration was a shallow one, say to the Ruhr, Herrmann's crews would have been hard pushed to get there in time to engage without the information from the listening service.

The German signals people had a favourite catchphrase: *Aller Funkverkehr ist Landesverrat*—all radio traffic is treason. We in the fighting services should do well to remember it still.

SESSION II

DESIGN OF AIR SEARCH RADAR

Merrill I. Skolnik

Session II DESIGN OF AIR TRAFFIC CONTROL SURVEILLANCE RADAR

The purpose of this session is to outline how a radar system design is formulated. The example will be a long-range air surveillance radar as might be used for civilian air traffic control. The attached paper by W. W. Shrader will be used as a general reference on the subject. The topics to be discussed include:

1. Establishment of user and system requirements.
2. Use of the surveillance radar equation as a basis for design.
3. Determination of a typical set of radar parameters.
4. Considerations in the choice of components.
5. Limitations to sensitivity.
6. Other factors in radar design.
7. 3D and height finder radar
8. Airborne aircraft-surveillance radars.

The question of MTI design, clutter, and automatic detection and tracking will be discussed in other sessions.

ARSR AIR ROUTE SURVEILLANCE RADAR  
ASR AIRPORT SURVEILLANCE RADAR

200mi (L)  
60mi (S)

2D, 3D, height finder

G.C.I. ACQUISITION RADAR

DEW, <sup>AWACS</sup> AIRBORNE WARNING + CONTROL

CALIBRATION SPHERES  $\pm 6$ dB ACCURACY.



Fig. 1. ASR locations, March 1972.

AIRPORT SURVEILLANCE RADAR  
S-BAND, 60-MILE RANGE



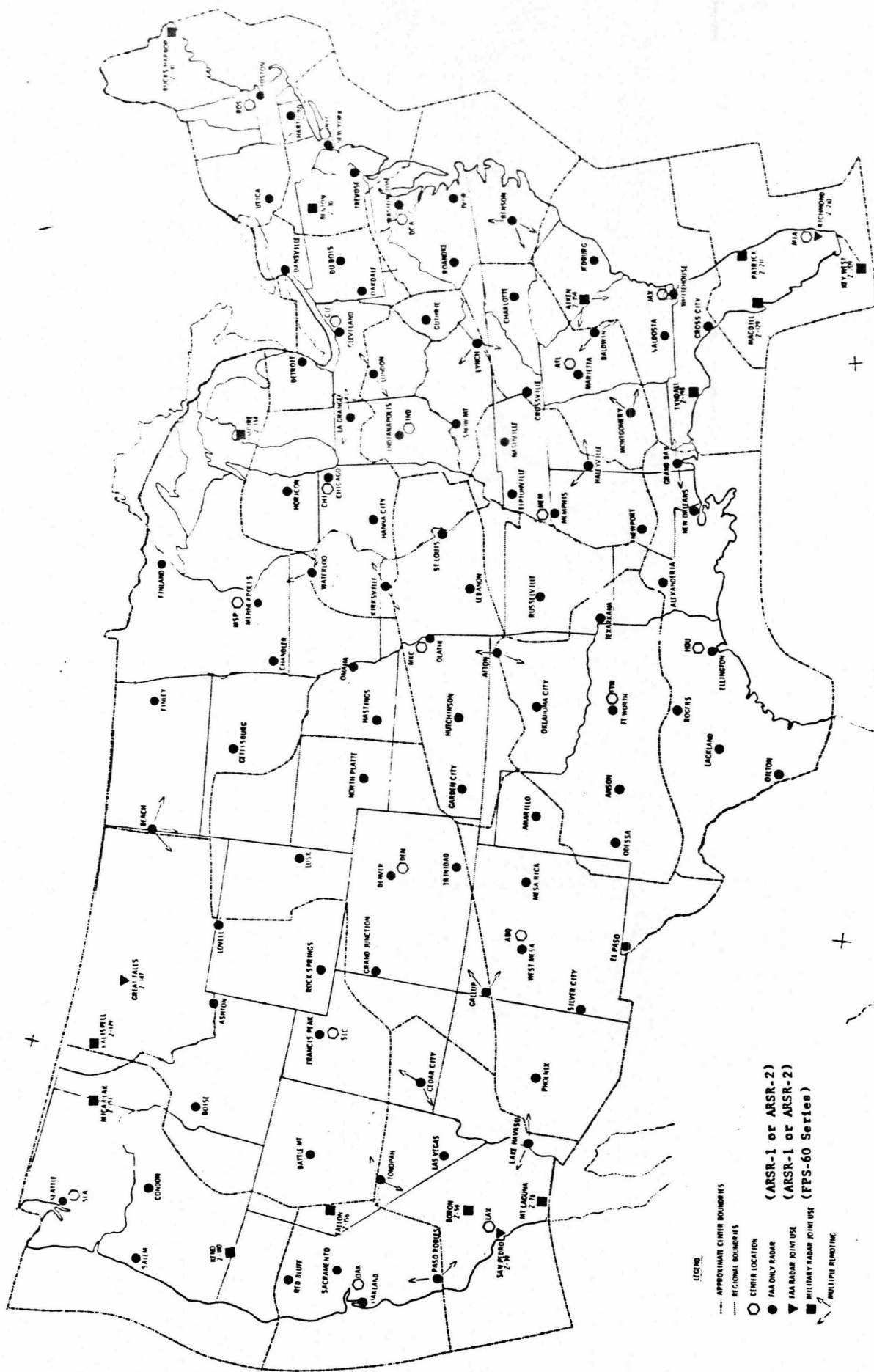


Fig. 2. ARSR locations, October 1970.

L-BAND  
200 MILE RANGE

TABLE I  
ATC RADAR CHARACTERISTICS

CHARACTERISTIC	ARSR-1/ARSR-2	FPS-66	ASR-6	ASR-7	ASR-8	ARSR-3
Antenna scan rate, rpm	5	5	15	13	12.5	5
Range, n.m.	200	200	60	60	60	200
Pulse Width, $\mu$ s	2	6	0.833	0.833	0.6	2
Azimuth Beamwidth, deg.	1.2	1.3	1.4	1.4	1.4	1.2
Elevation Coverage, deg.	0.2-45	0.2-45	0.2-30	0.2-30	0.2-30	0.2-46
Polarization (Selectable)	Hor/Circ	Hor/Vert/Circ	Vert/Circ	Vert/Circ	Vert/Cir	Hor/Vert/Circ
Prf, Hz (average)	360	360	700 to 1200	713, 950, 1050 1120, 1173, 1200	1030	360
Frequency, GHz	1.28-1.35	1.25-1.35	2.7-2.9	2.7-2.9	2.7-2.9	1.25-1.35
Diplex operation	no	yes	no	no	yes	yes
Subclutter Visibility, dB	27	25	25	25	28	30
MTI Improvement factor, dB	33	30	30	30	34	39
Blind Speeds, knots	1150	80	1250	2000	800	1200
Antenna Gain, dB	34	35	34	34	33.5 (lower beam) 32.5 (upper beam)	34.5 (lower beam) 33.5 (upper beam)
Peak Power, kW	4000	2000	400	425	1000	5000
Average Power, W	2900	4320	400	425	618	3600
Receiver Sensitivity, dBm	-116	-114	-109	-109	-110	-114
Noise Figure, dB	4	8	4	4.75	4	4
Circuitry	Tubes	Tubes	Tubes	Solid State	Solid State	Solid State
Signal Processing	Analog	Analog	Analog	Digital	Digital	Digital
	EXISTING RADARS			UNDER DEVELOPMENT		

Note: All of these radars have two complete transmitting-receiving channels and one antenna. Diplex operation is using both transmit-receive channels simultaneously for greater probability of detection. The ASR-8 uses frequency diplexing, while the FPS-66 and ARSR-3 are diplexed using orthogonal transmit polarizations.

1) The measurement of MTI improvement factor<sup>1</sup> or subclutter visibility is very difficult to make accurately with real clutter (and mistakes usually result in excessively good answers—thus if one gets a poor answer that may be accurate he tries again until he gets a good answer).

2) If an MTI system has been properly adjusted, it is impossible to determine from a PPI presentation how much subclutter visibility is being achieved. The PPI picture can be made to look very good while the MTI improvement factor is very poor.

The MTI systems are built with adjustable IF limiters preceding the canceling circuits as shown in Fig. 5. The limiter suppresses the strongest clutter sufficiently so the additional attenuation of clutter in the canceler results in the clutter residue being equal to the system noise level. If the limit level is set too low, there is a "black-hole" effect on the PPI. If set too high, the clutter residue obscures part of the PPI. When the limit level is set properly, the clutter residue blends with the noise on the PPI. The limiter also suppresses targets

that are superimposed on the strong clutter, but the amount of target suppression cannot be determined by looking at a PPI. The dynamic range of signals out of the limiter, however, is a direct indication of the MTI performance being achieved (assuming that the rest of the canceler processing is linear). The MTI improvement factor will be approximately equal to the dynamic range at the input to the canceler.

Unfortunately, the limiter causes the spectrum of strong clutter to spread so that the linear analysis of performance no longer applies [6]–[9]. Fig. 6 shows the clutter spectrum both before and after limiting, and also shows the response of a two-delay canceler. The limiting causes the clutter spectrum to spread into the passband of the canceler, which results in performance as shown in Fig. 7 for a two-delay canceler. ( $\sigma_v$  is the rms velocity spread of the clutter,  $\lambda$  the radar wavelength,  $f_r$  the pulse repetition frequency,  $\sigma_L$  the amount that the rms value of the clutter signal exceeds the receiver IF limit level, and hard limiting the asymptotic condition where  $\sigma_L$  becomes infinite.) The effect of this clutter spectral spreading is shown in Fig. 8, assuming that the clutter was hard limited before being processed in a two-delay canceler. ( $V_B$  is the first ambiguous blind velocity for a system without pulse interval staggering.) Fig. 9 shows a comparison of one

<sup>1</sup> MTI improvement factor is the average increase in signal-to-clutter ratio attributable to the moving-target-indicator system on targets distributed uniformly over the radial velocity spectrum; clutter attenuation normalized for uniformly distributed radial target velocities [18].



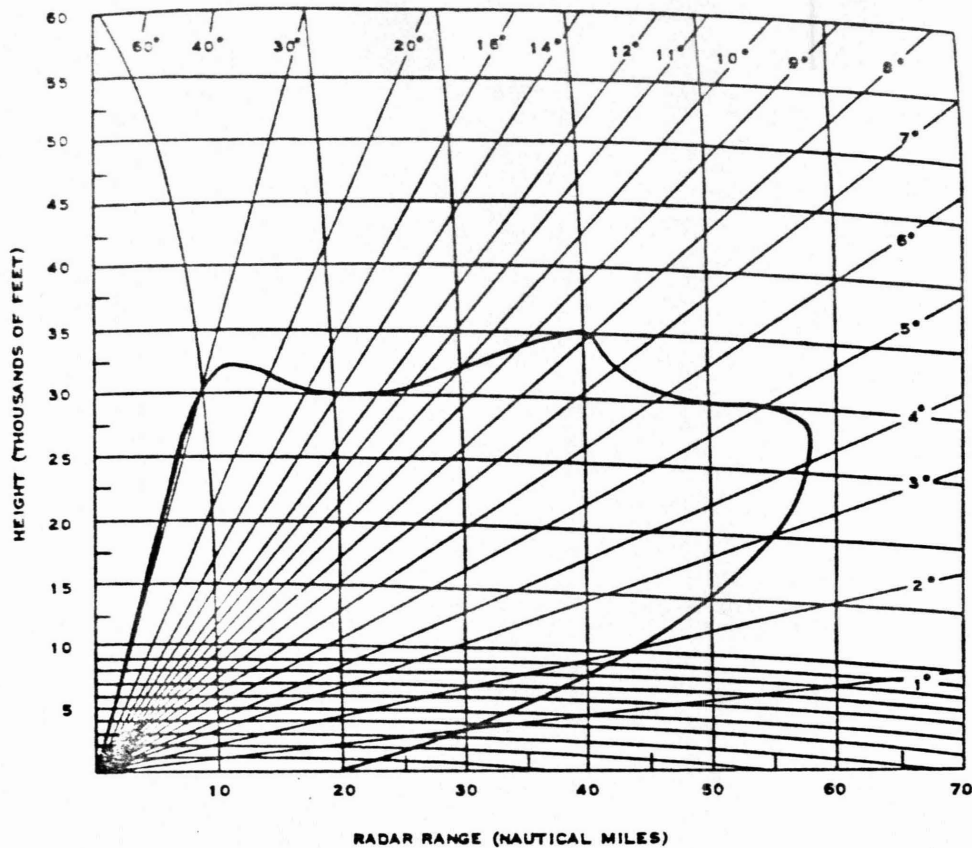


Fig. 3. ASR-7 radar system coverage.

delay, two-delay, and three-delay cancelers with limiting. The more complex three-delay canceler does not improve the situation much over the two-delay canceler. This is because the clutter spectral energy has been spread so far by the limiting, it will be in the passband for any canceler configuration. The majority of the clutter residue from the more complex cancelers comes from frequencies at the center of the MTI passband. The nature of the residue from limited clutter is very spiky compared to the target returns that exist for at least a beamwidth [6].

(The limiter is used in conjunction with MTI signal processors to provide constant false alarm rate (CFAR) performance in strong clutter. The limiter has been used for this purpose for more than 26 years (see [17, p. 649]), and no adequate substitute has been demonstrated. It might appear obvious that if limiting degrades the cancellation of clutter, then linear signal processing would be preferred. The key problem, however, is that linear signal processing must provide at least 60 dB of clutter attenuation to prevent a large number of false alarms from occurring in a real land clutter environment. Many linear signal-processing techniques have been implemented that did not provide 60 dB of clutter attenuation and thus the resulting false alarms made the system unusable. Following is a simple conceptual test to determine the usefulness of a proposed signal-processing technique: if the clutter residue from either point clutter 60 dB above noise, or distributed clutter 60 dB above noise, will be interpreted as a target, the system will be

demonstrated to be unusable in a real clutter environment.)

When the actual signal-processing performance being obtained from the ATC radars was recognized, attention was given to determining why they seemed to perform well in strong clutter environments, when other MTI radars with equivalent MTI improvement factors, but larger resolution cells, had been inadequate. Previous analyses of the adequacy of an MTI radar had been based on the assumption that the clutter was Rayleigh distributed. Thus, increasing the size of the resolution cell by a factor of two would only increase the clutter power by the same amount. An analysis of the distribution of clutter [10] showed that ground clutter was not Rayleigh distributed, but rather had a log-normal distribution (Fig. 10), resulting in a cumulative probability distribution of clutter reflectivity as shown in Fig. 11.

The mean clutter power exceeds the median clutter power by about 20 dB, and this gives the ATC radar, compared to a low-resolution radar, approximately a 20-dB advantage in being able to detect targets in a clutter environment. The ATC radar excludes the strong point clutter reflectors from most of the resolution cells and provides detection of the targets in the resolution cells where the clutter is weak, whereas a lower resolution radar will average the clutter over large areas. Fig. 12 shows a PPI display of all the ground clutter observed at one radar site. When the clutter was attenuated by 60 dB, the remaining strong points of the clutter are shown in Fig. 13. Although a significant number of points of

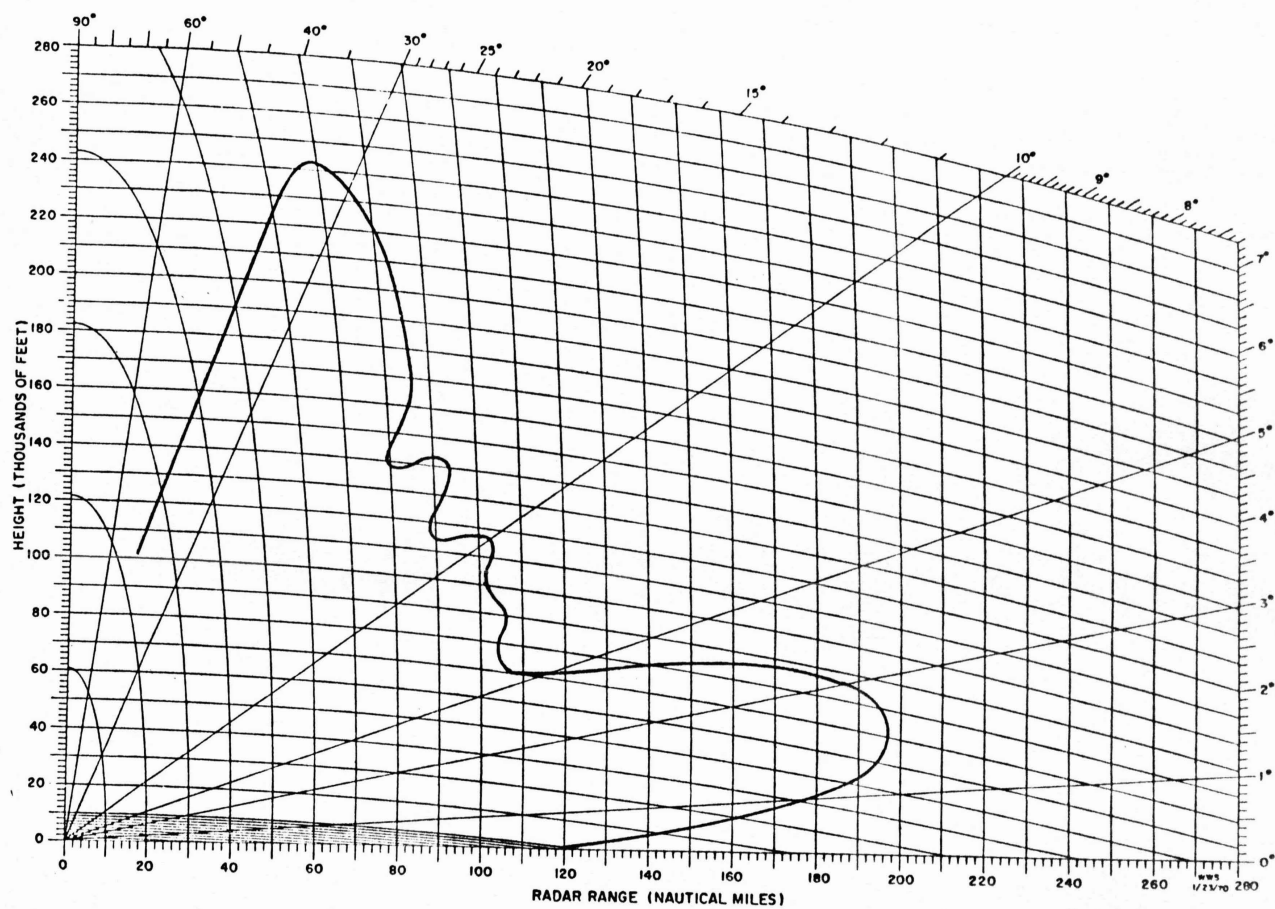


Fig. 4. ARSR-2 radar system coverage.

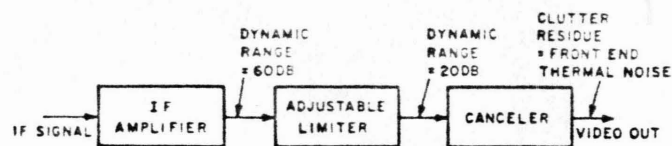


Fig. 5. Limiter consideration.

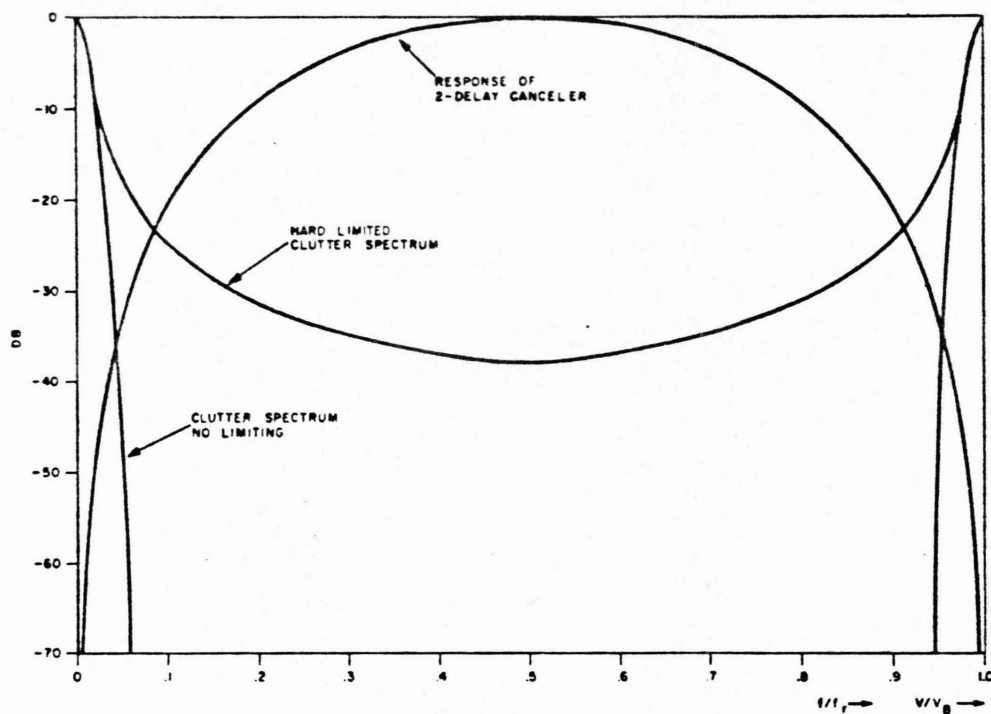


Fig. 6. Spectrum of limited clutter compared to two-delay canceler response.

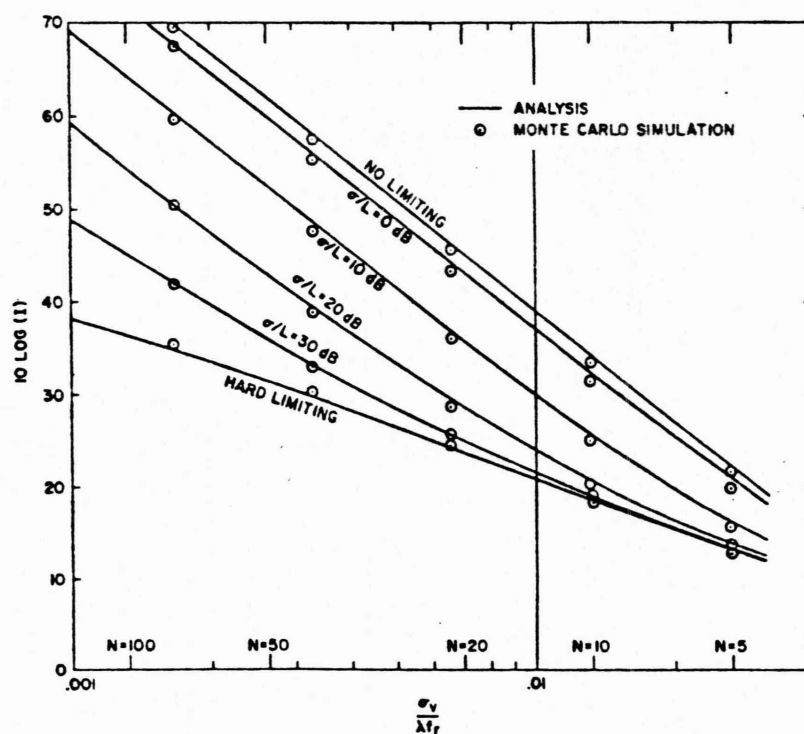


Fig. 7. Two-delay canceler performance with limited clutter [6].

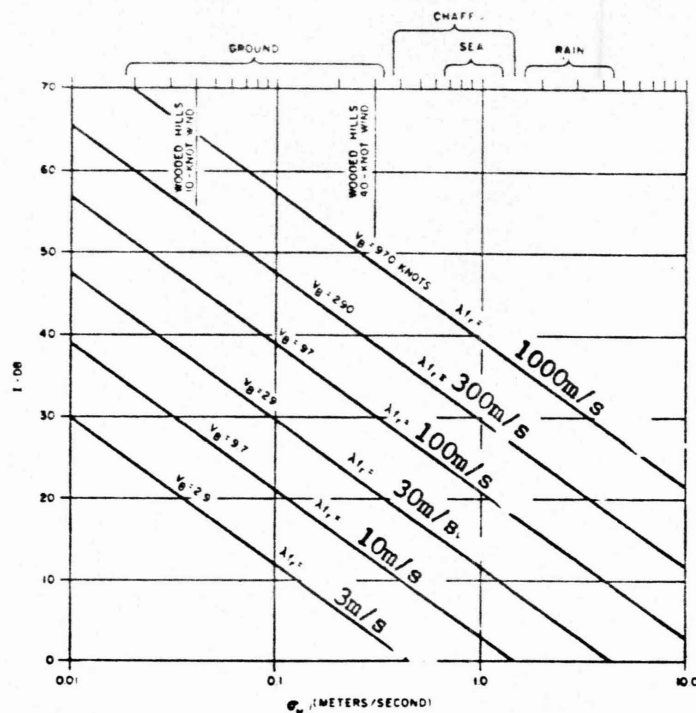


Fig. 8. Improvement factor limitation caused by clutter motion. Two-delay canceler. Hard-limited clutter.

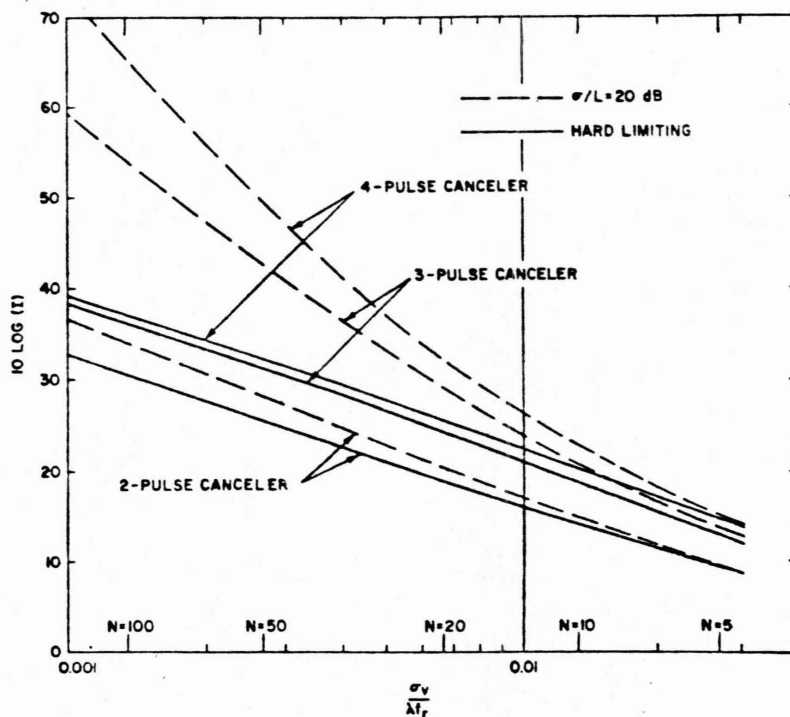


Fig. 9. Comparison of improvement factor limitation caused by clutter limiting for various cancelers [6].

strong clutter still exist, they occupy only a relatively few resolution cells. If an aircraft flying through this area were not detected on one scan of the antenna when it was in the resolution cell with one of the pieces of strong clutter, it would probably be detected on the next scan of the antenna.

#### PROBLEMS

Existing ATC radars suffer from several problems, the least of which is lack of sufficient subclutter visibility. The most severe problem is detection of unwanted moving targets such as the birds, automobiles, and insects. A second problem is

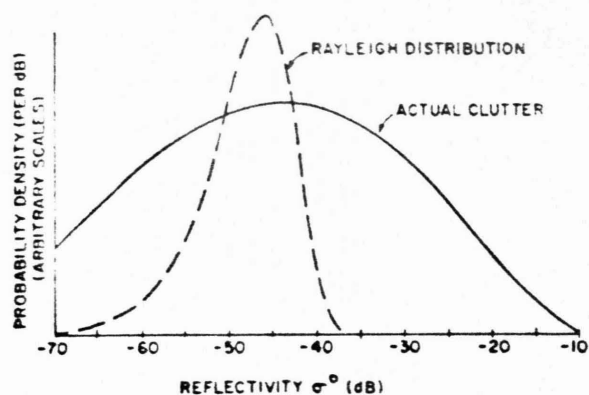


Fig. 10. Probability density of heavy ground clutter [10].

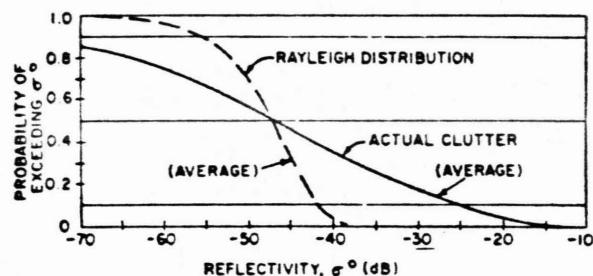


Fig. 11. Reflectivity distribution of heavy ground clutter [10].

fading of tangentially flying desired targets when using the MTI processor. A third problem is the occurrence of anomalous propagation (ducting) that is frequently observed. The anomalous propagation greatly aggravates the problem of tangential target fading because it requires that the MTI receiver be used at much longer ranges than would be otherwise required.

The reason these radars are so sensitive to unwanted moving targets can be seen from Fig. 14, the velocity response curve for the ARSR-2. The maximum response occurs at a velocity of about 40 knots. The feedback has very little effect on the response at this velocity. There is appreciable response to targets moving at 20 knots. Birds typically fly at speeds of 20 to 30 knots and when this is added to the wind speed, the birds will often be moving at 30 to 40 knots with respect to the radar. Because the velocity response curve is mainly determined by the frequency and the pulse repetition period of the radar, the only way the MTI processor could be made to reject the birds would be to either reduce the frequency of the radar or increase the pulse repetition frequency. The pulse repetition frequency is already as high as possible commensurate with the required unambiguous range. To significantly reduce the transmitter frequency would require a much larger antenna to maintain the same azimuth resolution and may result in undesired lobing in the vertical coverage pattern. Furthermore, if the rejection notch is widened to eliminate the birds, this results in the loss of many more tangentially flying desired targets.

Fig. 15 shows a pair of PPI photographs taken of birds in the midwestern United States. This is not an unusual display.

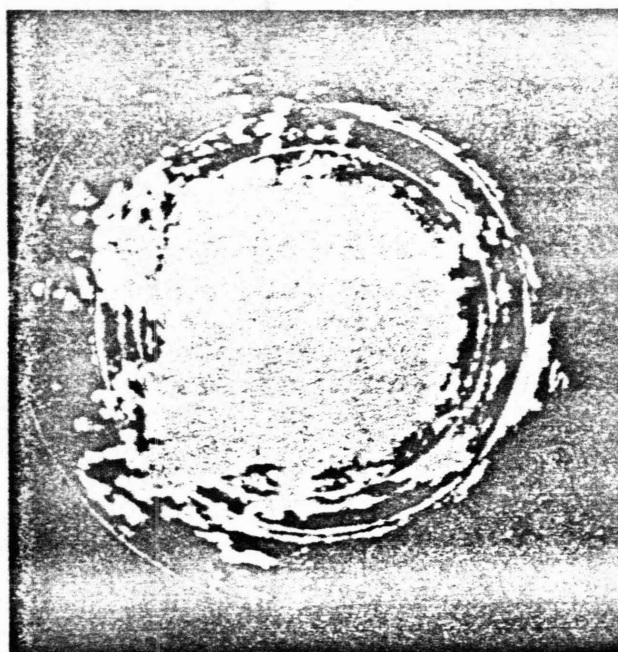


Fig. 12. All clutter return at a particular radar site. 0 dB.

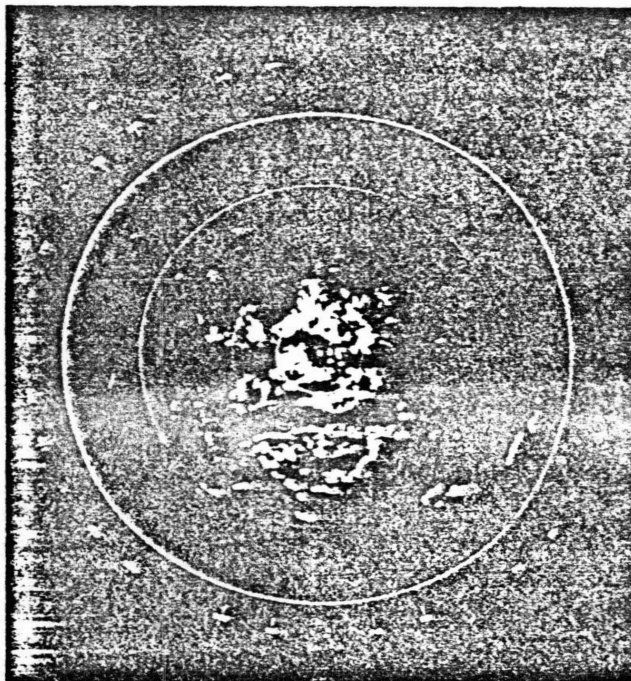


Fig. 13. Clutter return 60 dB above minimum discernible signal (MDS) at the radar site of Fig. 12.

The ARSR radar can detect a large bird in the peak of the antenna beam at a range of 50 mi. Fig. 15(b) shows the use of a moderate amount of sensitivity time control (STC) or swept gain. This eliminated most of the birds from the display. Fig. 16 was taken at the same location just after dusk. The clutter returns in this photograph are from insects. Again, the use of a moderate amount of STC has greatly reduced the intensity of the insect returns. It is not possible to eliminate



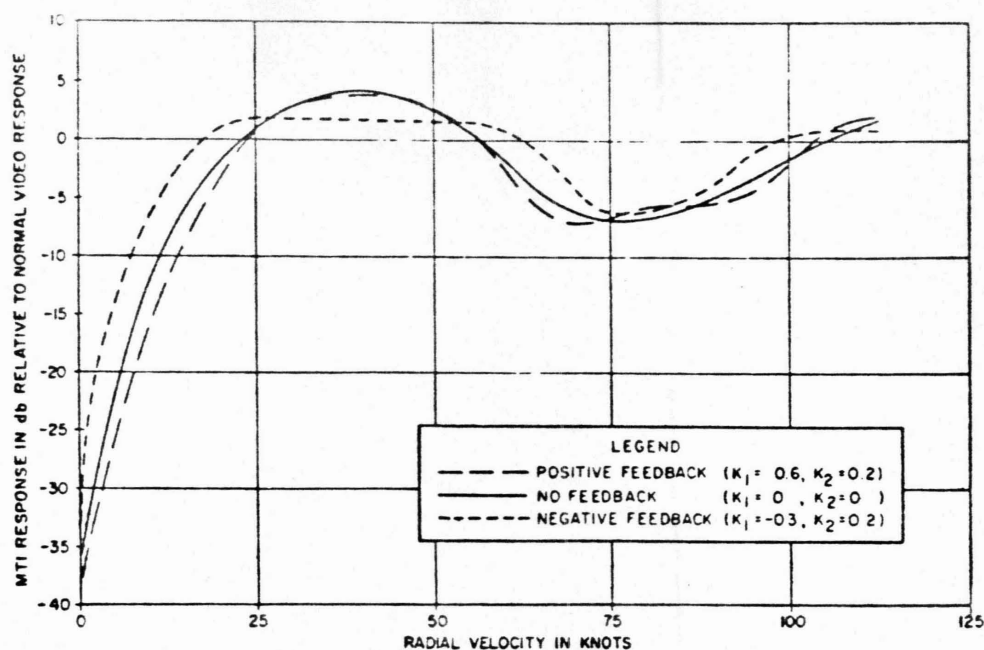


Fig. 14. Effects of feedback on ARSR-2 velocity response.

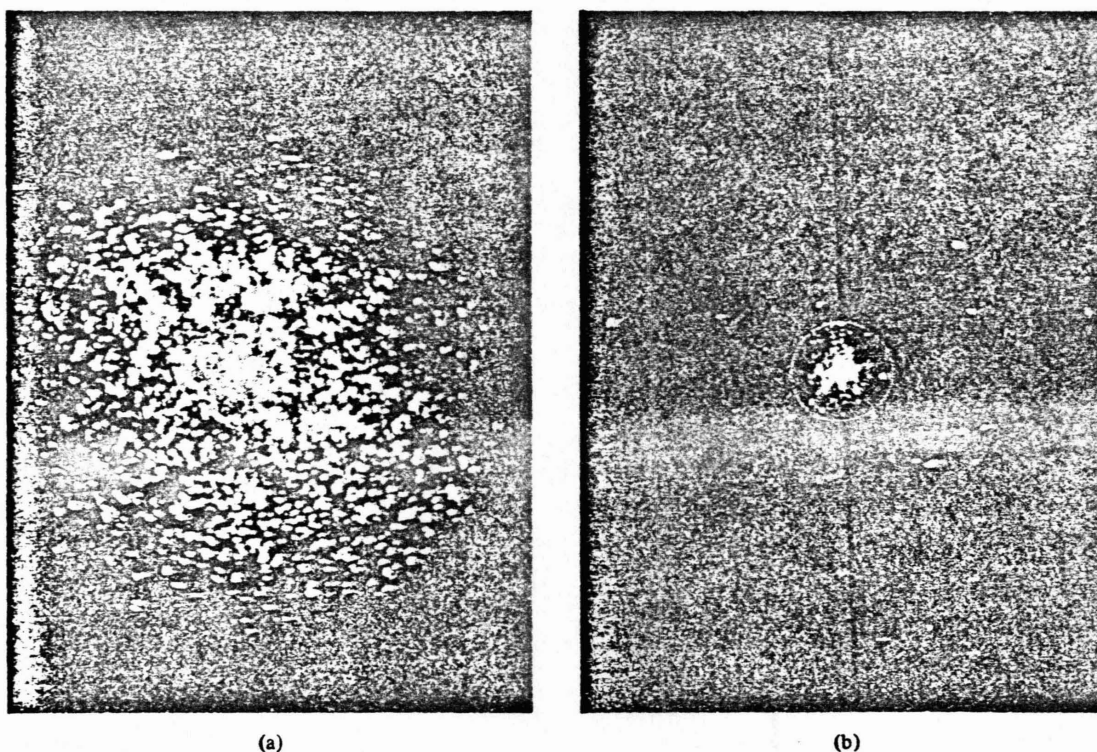


Fig. 15. STC can greatly reduce the number of birds displayed. Range—25 nmi. (a) Birds seen with MTI. (b) Birds seen with MTI and STC.

automobiles from the display by the use of STC, because they have radar cross sections equivalent to small aircraft.

#### ANTENNA TECHNIQUES

Since the incorporation of the two-delay feedback canceler in the 1950's, the only significant improvement in ATC radar

systems concepts has been through antenna techniques. The ASR and ARSR radars of the 1950's had antenna patterns with "cosecant-squared" coverage. (The gain of the antenna was a cosecant-squared function of elevation, which results in constant received echo power from a target flying at a constant altitude.) The cosecant-squared coverage is inadequate,

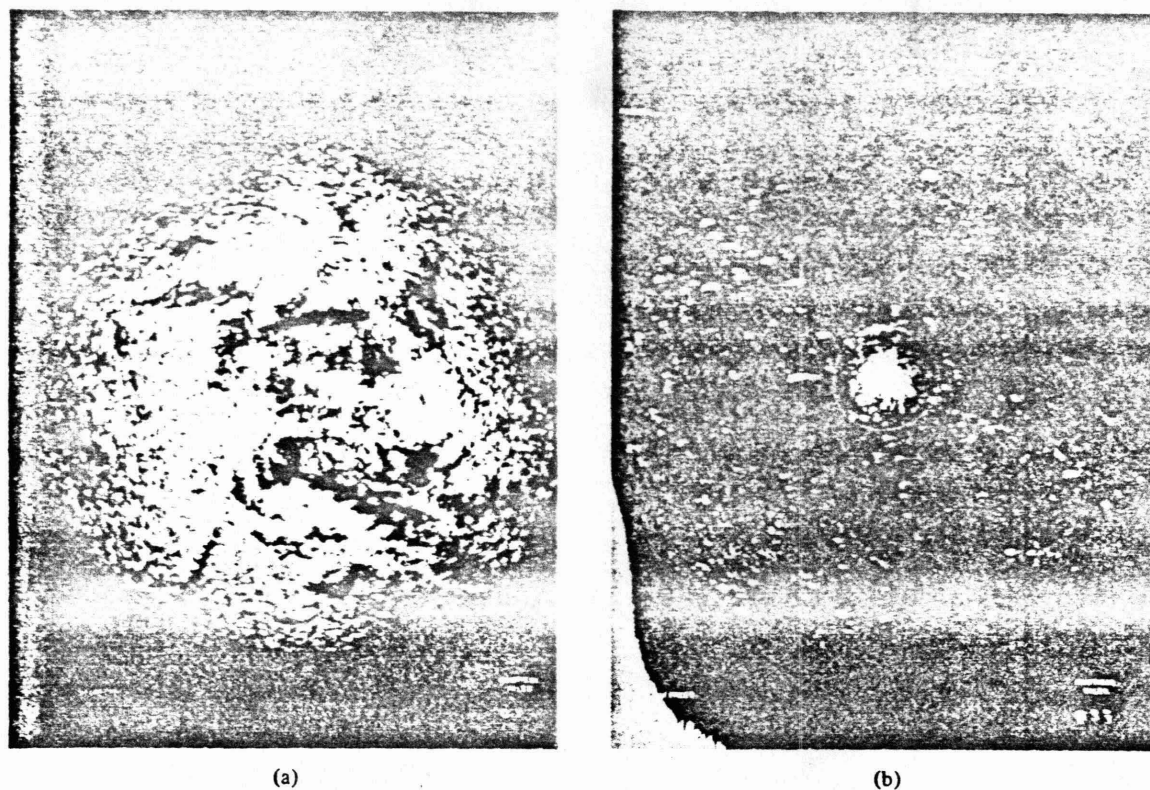


Fig. 16. Insects with and without STC. Range—25 mi. (a) Insects seen with MTI. (b) Insects seen with MTI and STC.

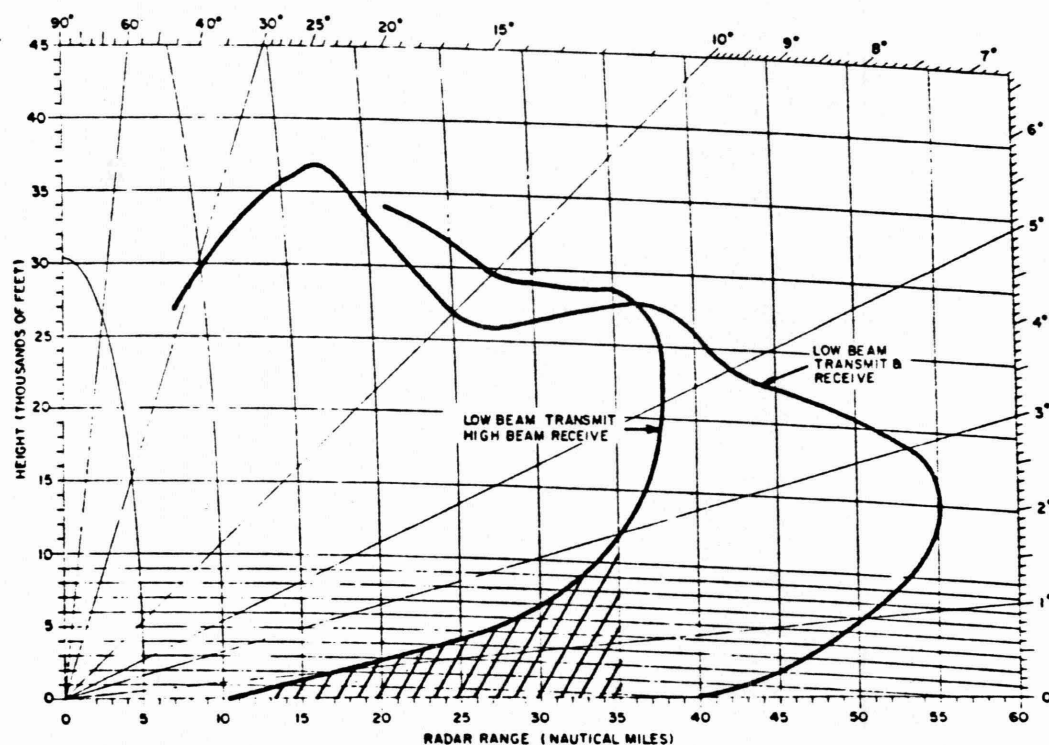


Fig. 17. Example of coverage obtained with two-beam antenna.

however, for the ATC radars, because the closer an aircraft comes to the radar, the stronger the clutter signals with which the aircraft signal must compete. Thus, the ARSR-2 antenna (see [11], [12]), first delivered in 1961, greatly increased the energy radiated at high elevation angles to increase the ratio

of target signal-to-clutter signal. This extra radiated energy shows clearly on the coverage diagram of Fig. 4. Although this ARSR-2 antenna greatly improved the situation, it still was not adequate for eliminating all the unwanted targets.

The most significant approach to solving the unwanted tar-

get problem has been based on spatial resolution. Most of the unwanted targets lie at very low elevation angles. Two-beam antenna techniques to take advantage of the spatial effects have been evolving for more than a decade. First, back-to-back antennas were used [13]. Then two beams were generated with separate feedhorns on a single reflector antenna. This is done by adding a second receive-only feedhorn beneath the high-power normal transmit-and-receive feedhorn. The coverage patterns are approximately as shown in Fig. 17. The near-in high-angle coverage is obtained by transmitting on the lower beam but receiving on the upper beam. At some pre-selected range the receiver is switched from the upper beam to the lower beam and normal coverage results beyond that range. Note the shaded area in Fig. 17 where coverage is not obtained when using the high beam. The choice of range where the receiver is switched from the high beam to the low beam is a compromise between losing low-angle targets and switching as far in range as possible. To quote from [14]: "The distance to which the high beam can be used is limited, because of the loss of low angle coverage on air craft. At Sydney this range is about 15 nautical miles."

Raytheon undertook an R&D program from the FAA to study the feasibility of combining the received energy from the two beams to provide intermediate beam positions [15]. The hardware resulting from this program has been evaluated on an ASR system and on an ARSR system at the FAA's NAFEC facility. Fig. 18 shows the physical layout of the ASR antenna with the two horns. The second receive-only horn is placed as close as possible to the original horn to make the two beams as close as possible. The beams are added in the RF-combining network shown in Fig. 19. The phase shifters of this combiner can be adjusted to give the antenna patterns (ARSR-2) shown in Fig. 20 [16].

The ASR-8 and the ARSR-3 will both have two-beam antennas. However, the beams will not be combined, because the feasibility of appropriate phase control between the two waveguide runs had not been established at the time of the ASR-8 and ARSR-3 procurements. Instead, the two beams of each antenna are specified closely enough so that combining is unnecessary.

It should be noted that all the ASR and ARSR antennas have relatively large vertical apertures, (e.g., 9 ft for the ASR, 23 ft for the ARSR-2). The large vertical aperture permits careful control of the radiation pattern in elevation. An additional feature of the larger aperture is that it enables a sharp cutoff on the lower edge of the beam. This results in very little energy radiated below the horizon, which greatly enhances the ability to provide accurate azimuth estimation on targets near the horizon.

#### ANOMALOUS PROPAGATION

Fig. 21 is a pair of PPI displays showing anomalous propagation (ducting). These were taken with an ARSR-2 radar mounted on a 50-ft tower in flat country near Atlantic City, N.J. One would expect the line of sight to be about 10 mi. It can be seen however, that the clutter actually goes out to 100 mi. This type of propagation is seen very often with mod-

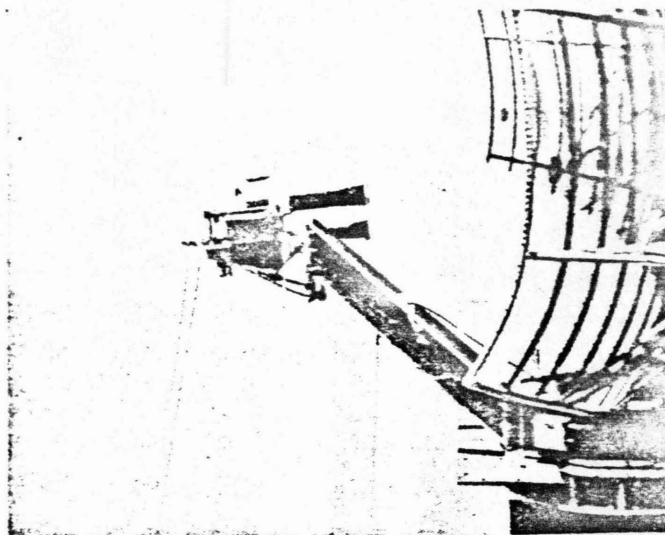


Fig. 18. Two-beam antenna.

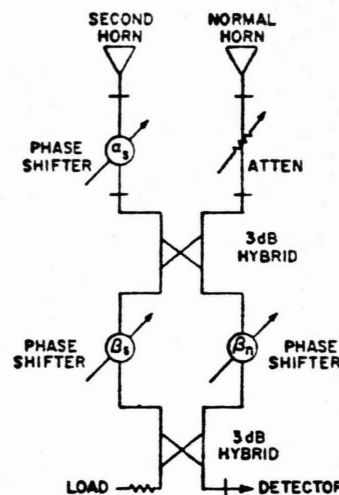


Fig. 19. Schematic of RF-combining network [16].

ern sensitive radars. The intracoastal waterway can be seen in this picture. The bridges across this waterway can be seen just inside the coastline. When anomalous propagation such as this occurs, it forces the MTI to be used to the full range of the clutter returns. This greatly aggravates the loss of targets that are rejected by the MTI clutter notch when they pass tangentially to the radar.

Various gating techniques have been considered to select the MTI only when clutter is present. The most common technique is the pulse-length discriminator. If a target longer than the pulse length of the radar is encountered, it is assumed that it is clutter and the MTI is selected. The principal shortcoming of this technique comes from the fact that many of the clutter targets are only of 1-pulse-length duration. Fig. 21 shows that although close-in clutter may be solid and continuous, much of the clutter at longer ranges is coming from point reflectors and thus would be displayed if the MTI is selected by a pulse-length discriminator.

The approach to be utilized in the ASR-8 and ARSR-3 for



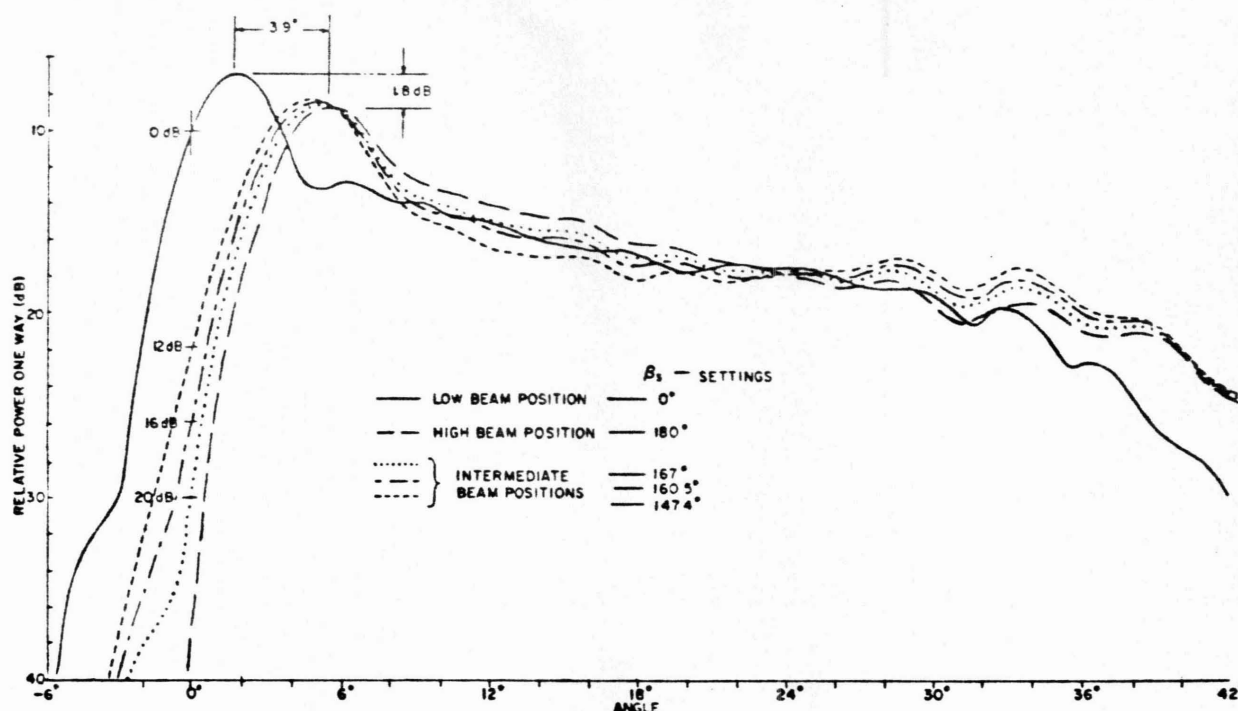
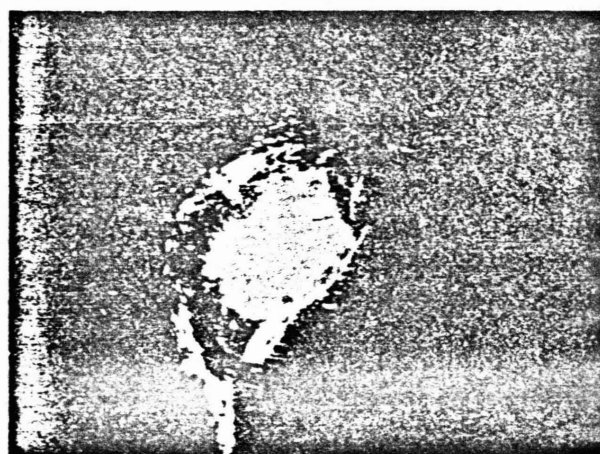


Fig. 20. Measured secondary patterns for combined operation [16].



(a)



(b)

Fig. 21. Anomalous propagation (ducting). (a) 100-nmi range. 20-nmi markers. (b) 50-nmi range. 5-nmi markers.

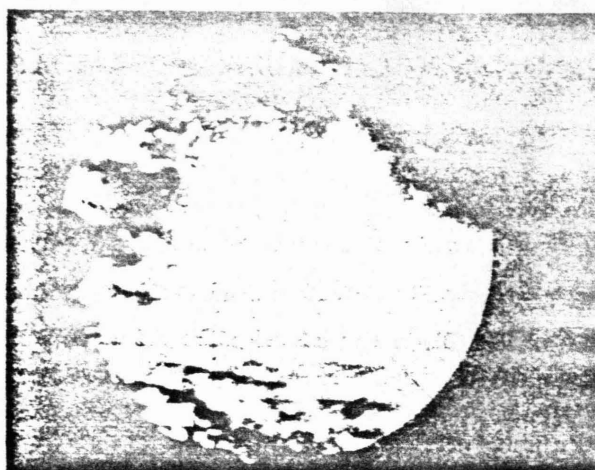
selecting the MTI is a device where the operator can preselect the various areas in which he wants the MTI. This technique is not as good as desired, because propagation conditions can change quite rapidly. When ducting occurs, the preset MTI selector will not be properly set.

It is probable that the most effective device to be developed for automatic MTI selection will be a storage device that remembers the clutter map of the entire area being scanned. Based on the history of the past several scans, the device will decide for each resolution cell whether the MTI or normal video should be selected.

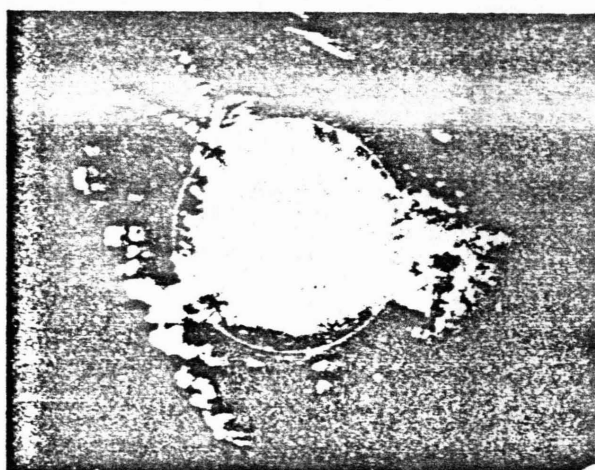
#### WEATHER

Fig. 22 shows the returns received from weather with an ARSR-2. The display range is 40 mi. Fig. 22(a) shows the weather returns with linear polarization. Fig. 22(b) shows the effect of circular polarization. This provides about a 20-dB reduction of the weather, but also reduces target signal strength about 4 dB. It can be seen that the weather reduction is not sufficient to permit tracking of targets through the entire area. The most promising solution to the weather problem is the use of a log-fast time constant (FTC) receiver. Because the amplitude fluctuation of the weather usually has a Rayleigh distribution, this type of receiver will reduce the weather to look like noise on the PPI. The use of a log-FTC receiver following an MTI receiver will also do an effective job of reducing the weather-to-noise level in the MTI video. The log-FTC technique is employed in the ASR-7, ASR-8, and ARSR-3.

After the weather is removed from the display of an air traffic control radar, the controller then has the problem of determining where the weather actually is. He does not want



(a)



(b)

Fig. 22. Weather returns as seen on an L-band ARSR radar. 40-nmi range. 10-nmi range rings. (a) Linear polarization. (b) Circular polarization.

to vector aircraft into areas of strong weather. To solve this problem, weather contours will be displayed. The contours will be derived from signals received through the orthogonal channel of the circular polarizer and passed through a separate rotary joint to a separate radar receiver. It is important that the noise figure of this weather channel be as good as possible, otherwise sensitivity will not be sufficient to provide a good outline of all the weather.

The advent of digital techniques will have a significant impact in two areas of ATC radars. The first is the relative simplicity (with the attendant reliability) of constructing MTI filters and feedback integrators. Higher feedback ratios can be used to obtain more carefully shaped velocity response curves. The second major advantage of digital techniques is the ease of implementing complicated pulse interval stagger ratios. Digital techniques have made it possible to construct MTI filters much more complex than the dual-delay feedback canceler, but because of the spectral spread of limited clutter, very little improvement in operational capability is accomplished. A digital MTI system, when compared with a similar properly adjusted analog MTI system, does not provide greater

inherent subclutter visibility. The analog MTI system, as mentioned earlier, eventually drifts out of adjustment. This does not happen with the digital system. Thus, in the long run, the digital system gives much better performance.

#### FUTURE SYSTEMS

The problems with the present ATC systems are fundamental. They are caused by the requirements for unambiguous range, operating frequency, data rate, and resolution in azimuth. Improved circuitry using today's concepts will not provide better performance. The particular problems that must be addressed in any future ATC radar concept are rejection of unwanted moving clutter signals (weather) superimposed on fixed clutter signals and rejection of slow-moving targets (birds and automobiles). Faster moving targets (aircraft), even though their radial velocity may be relatively small, must be displayed. An aircraft passing almost tangentially to the radar will have a radial velocity less than that of the bird flying straight towards the radar, but the aircraft must be retained, while the bird is rejected.

One type of system the author envisages for the future (after applying all the antenna techniques and STC techniques available) would consist basically of a fast Fourier transform processor combined with a large digital memory. Scan-to-scan comparisons will be made of each resolution element (range, azimuth, and velocity). To take full advantage of this type of processing the resolution cells must be considerably smaller than the gross radar parameters would suggest. On each scan, the radar will compare the range, azimuth, and velocity of each signal received with the comparable signals from several previous antenna scans. If a similar target existed in about the same place, then the target will be rejected. If the target has reasonable absolute velocity, such as an aircraft would, then it will move sufficiently between scans to be detected. Unwanted targets, such as weather superimposed on fixed clutter, will appear in the same range, azimuth, and velocity resolution cell on consecutive scans and therefore will be rejected. An aircraft simultaneously passing through the same range and azimuth cell as weather and fixed clutter would be retained as long as its radial velocity differs from both that of the weather and the fixed clutter. Several scans must be stored to ensure adequate rejection of unwanted targets with low blip/scan probability.

This type of processor has not been practical in the past because of the very large digital memory required to provide the necessary resolution. However, with digital memories becoming less and less expensive, this may well represent the signal processing to be utilized in ATC radars of the future.

#### ACKNOWLEDGMENT

Much of the introduction of this paper, as well as the locations of ASR and ARSR radars, was taken from [1].

#### REFERENCES

- [1] H. C. Moses, "Air traffic control radar systems definition report," Fed. Aviation Admin. Rep. FAA-EM-72-1, Mar. 1972.
- [2] R. C. Emerson, "Some pulsed Doppler MTI and AMTI tech

- niques." Rand Corp. Rep. R-274, DDC Doc. Ad 65881, Mar. 1, 1954 (not generally available).
- [3] E. J. Barlow, "Doppler radar," *Proc. IRE*, vol. 37, pp. 340-355, Apr. 1949.
  - [4] R. S. Grisetti, M. M. Santa, and G. M. Kirkpatrick, "Effect of internal fluctuations and scanning on clutter attenuation in MTI radar," *IRE Trans. Aeronaut. Navig. Electron.*, vol. ANE-2, pp. 37-41, Mar. 1955.
  - [5] W. W. Shrader, "MTI radar," Tech. Mono. TMO 67/003, Selenia S.p.A., Rome, Italy, July 1967.
  - [6] H. R. Ward and W. W. Shrader, "MTI performance degradation caused by limiting," 1968 *IEEE EASCON Rec.*, pp. 168-174; also *IEEE Trans. Aerosp. Electron. Syst.* (Abstracts), vol. AES-4, pp. 913-923, Nov. 1968.
  - [7] H. R. Ward, "The effect of bandpass limiting on noise with a Gaussian spectrum," *IEEE Proc.*, vol. 51, pp. 2089-2090, Nov. 1969.
  - [8] G. Grasso, "Improvement factor of a nonlinear MTI in point clutter," *IEEE Trans. Aerosp. Electron. Syst.*, vol. AES-4, pp. 640-644, Nov. 1968.
  - [9] G. Grasso and P. F. Guarguaglini, "Clutter residues of a coherent MTI radar receiver," *IEEE Trans. Aerosp. Electron. Syst.*, vol. AES-5, pp. 195-204, Mar. 1969.
  - [10] D. K. Barton and W. W. Shrader, "Interclutter visibility in MTI systems," in *EASCON '69 Tech. Conv. Rec.*, pp. 294-297, Oct. 1969.
  - [11] W. W. Shrader, "Antenna considerations for surveillance radar systems," in *Proc. 7th Annu. East Coast Conf. Aeronautical and Navigational Electronics*, Oct. 1960.
  - [12] —, "Results of antenna pattern considerations," in *Proc. 8th Annu. East Coast Conf. Aerospace and Navigational Electronics*, Oct. 1961.
  - [13] A. M. Patrick, "Primary radar in air traffic control," *Interavia*, vol. 16, pp. 851-853, June 1961.
  - [14] E. B. Mulholland and F. R. Soden, "Australia's ATC radar network," *Interavia*, vol. 22, pp. 511-513, Apr. 1967.
  - [15] Dep. Transp., Contr. DOT-FA69WA-2129.
  - [16] C. F. Winter, "Dual vertical beam properties of doubly-curved reflectors," presented at the 19th Annu. U.S.A.F. Antenna Research and Development Symp., Univ. Illinois, Robert Allerton Park, Monticello, Ill., Oct. 1969.
  - [17] A. G. Emslie and R. A. McConnell, "Moving target indication," in *Radar System Engineering* (Radiation Lab. Series), L. N. Ridenour, Ed. New York: McGraw-Hill, 1947, no. 1, ch. 16.
  - [18] *IEEE Standard Dictionary of Electrical and Electronic Terms*. New York: Wiley, 1972.



William W. Shrader (SM'68) was born in Foochow, China, on October 17, 1930. He received the B.S.E.E. degree from the University of Massachusetts, Amherst, in 1953, and the M.S.E.E. degree from Northeastern University, Boston, Mass., in 1961.

From 1953 to 1956 he worked in the Physical Research Unit at the Boeing Airplane Company, Seattle, Wash. Since 1956 he has been with the Raytheon Company, Wayland, Mass. He was a Project Engineer on a number of surveillance radar systems, including the ARSR-1 and ARSR-2. Currently, he is a Consulting Scientist on the staff of the Manager of the Radar Systems Laboratory. He is the author of "MTI radar" in M. Skolnik, Ed., *Radar Handbook* (New York: McGraw-Hill, 1970).

## Dissemination of System Time

G. ERIC ELLINGSON AND RICHARD J. KULPINSKI

**Abstract**—This paper considers the problem of estimating the offset in timing of like events at geographically separated locations as a basis for establishing common knowledge of time and, hence, system synchronism. Configurations discussed involve interrogation and reply between a user and a single donor, and one-way propagation between a user and the multiple sites of a reference system. The latter category includes navigation systems, which are shown to be appropriate means for disseminating time.

Further ramifications of time dissemination are discussed, including the characteristics of clocks suitable for airborne application. Variables and their relationship and solution are defined for stationary and moving users, and for users of atomic and crystal clocks. For the case in which frequency is offset between clocks, as is likely when crystal oscillators are used, methods are described that permit the estimate of offset in frequency as well as in time. Recursive minimum-variance methods are examined in some detail, and a parametric analysis of performance relative to random and systematic sources of error is given.

### I. INTRODUCTION

THIS paper describes alternative methods of estimating the discrepancy in timing of like events at geographically separated units as a means of establishing a common knowledge of time among participants in a system. The importance of common knowledge of time is increasingly being recognized; collision avoidance is an obvious example of the many ways in which it can be usefully applied. Apart from this and other ranging applications including position determination and area navigation, common knowledge of time creates the basis for dramatically improved coordination and discipline in large-scale systems. The synchronism it establishes can greatly improve efficiency in the use of time and frequency resources.

Conversely, the lack of synchronism and interunit coordination is an important factor impairing our ability to do the air traffic control job today. Present practice enables us to establish time rapport only between pairs of units; the growing need for real-time knowledge of interelement range

Manuscript received July 20, 1972; revised December 7, 1972. This work was supported by the Electronics System Division, Air Force Systems Command, under Contract XR/ESD F19628-71-C-0002.

The authors are with the Mitre Corporation, Bedford, Mass. 01730.



- [6] C. V. Robinson, "Electrical scanners," in *Radar Systems Engineering* (M.I.T. Rad. Lab. Ser., vol. 1). New York: McGraw-Hill, 1947, p. 291.
- [7] C. Porterfield, "Ground-controlled approach—Its development and early operational use," *IRE Trans. Aeronaut. Navig. Electron.*, vol. ANE-6, pp. 71-75, June 1959.
- [8] R. I. Colin, "Some sidelights of early GCA," *IEEE Trans. Aerosp. Navig. Electron.*, vol. ANE-10, pp. 87-89, June 1963.
- [9] A. C. Clarke, "You're on the glide path—I think," *IEEE Trans. Aerosp. Navig. Electron.*, vol. ANE-10, pp. 90-93, June 1963.
- [10] L. W. Alvarez and L. H. Johnson, "GCA, ground controlled approach," M.I.T. Rad. Lab. Rep. 438, Cambridge, Mass., Oct. 1943.
- [11] L. Melancon, "A limited scan antenna," in *EASCON 71 Conf. Rec.* (IEEE Publ. 71C34-AES, Oct. 1971), p. 190.
- [12] K. O. Bowright, "Return of special Logan radar urged," *Boston Globe* (Boston, Mass.), Dec. 24, 1973, p. 4.

## New Techniques Applied to Air-Traffic Control Radars

CHARLES E. MUEHE, LINCOLN CARTLEDGE, WILLIAM H. DRURY,  
EDWARD M. HOFSTETTER, MEMBER, IEEE, MELVIN LABITT, MEMBER,  
IEEE, PETER B. MCCORISON, AND VINCENT J. SFERRINO

**Abstract**—During the past two years a program has been carried out to show how new techniques can greatly improve the performance of radars used for air-traffic control. A survey of problems associated with presently used radars was undertaken. This survey indicates that primary radar in an automated air-traffic control system can be made significantly more effective by the use of new techniques. The radar's handling of extraneous reflections (clutter) is critical to its performance.

Three types of interfering clutter were found to predominate: ground clutter, weather clutter, and angels. Angels are generally accepted to be radar returns from flocks of birds. In addition, second-time-around clutter is often troublesome. For each type of clutter, all known remedies for improving the signal-to-clutter ratio were studied and radar systems were configured using appropriate sets of remedies.

Some specific solutions incorporated in the resulting radar systems are: a) the use of linear large dynamic range, near-optimum digital signal processors to filter signals from clutter, b) the use of electronically step-scanned antennas to improve the correlation of aircraft and clutter returns from pulse to pulse, c) the use of multiple PRF's instead of staggered PRF's together with coherent transmitters to keep second-time-around clutter returns well correlated while still overcoming blind speeds, d) the use of a fine grained ground clutter map to give superclutter visibility on tangential targets, and e) the use of lower operating frequencies to greatly reduce weather and angel returns.

Two demonstration radar systems have been implemented, an S-band radar using a mechanically rotating antenna and a UHF radar using an electronically step-scanned cylindrical antenna. Experimental results are described.

### I. INTRODUCTION

PERHAPS the most important application of radar in this country, especially to the frequent air traveler, is as a sensor in the nation's air-traffic control system. The system is served by 84 high-power long-range L-band enroute radars serving the Air Route Traffic Control Centers and ap-

proximately 125 medium-power S-band Airport Surveillance Radars (ASR) serving the terminal areas.

These radars, both terminal and enroute, while generally giving good service in a manual control environment, have certain deficiencies which make their use difficult in the fully automated systems being implemented by the Federal Aviation Administration (FAA). The principal difficulties are either an excessive number of false alarms which will overload the automation computers or else aircraft detection so spotty that the computer cannot make long continuous tracks of all aircraft.

Over the last two years, a concerted effort was made to gain a good understanding of the root causes of these deficiencies, to study all the ways the radars can be improved, and, finally, to design and demonstrate new signal processing techniques which should, together with certain antenna techniques, eliminate the problems.

We will first, briefly, describe the basic radar problems then discuss improvements to solve them. Finally, we describe signal processing techniques being built and tested.

### II. RADAR PROBLEMS

The poor performance previously mentioned is due to the competition of aircraft radar returns with the so-called "clutter" returns and the response of circuits used in the radar to overcome these clutter returns. It is convenient then to classify the problems according to the type of clutter return. These are fixed ground clutter, second-time-around effect, precipitation clutter, angels, and surface vehicles. We will describe these in terms of the ASR radars. The extension to the enroute radars is fairly obvious.

#### A. Fixed Ground Clutter

By far the largest undesired radar reflections come from fixed objects on the ground. Ground clutter generally extends out to about 20 nmi except in very hilly or mountainous areas where it may extend out to the maximum radar range (~60

Manuscript received September 4, 1973; revised January 16, 1974. This work was sponsored by the Federal Aviation Administration under Interagency Agreement DOT-FA72-WA1-242 and the Department of the Air Force.

The authors are with M.I.T. Lincoln Laboratory, Lexington, Mass. 02173.

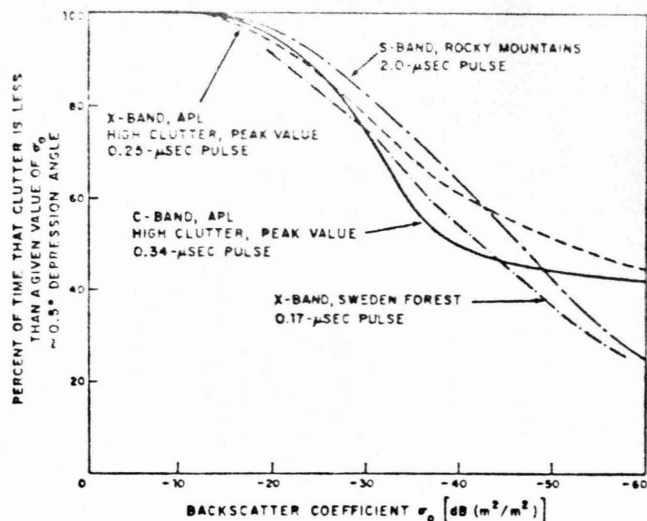


Fig. 1. Land clutter backscatter distribution from surface radars (from [1]).

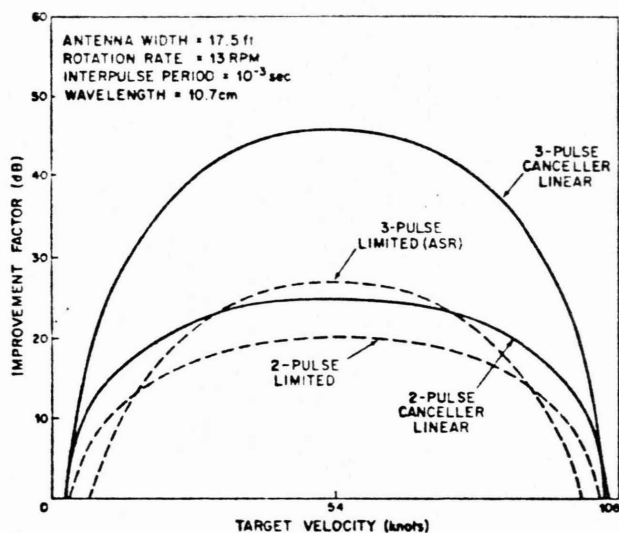


Fig. 2. Performance of S-band cancelers. The improvement factor is the ratio of signal-to-clutter out of the canceler to signal-to-clutter in. The latter ASR radars use three-pulse cancelers following a limiter shown above by the curve "3-Pulse Limited (ASR)."

nmi). Its natural or intrinsic spectrum is very narrow compared to the spectral spread caused by antenna scanning motion.

Ground clutter varies appreciably from spot to spot in the area of coverage. Typical distributions of the mean values  $\sigma_0$  are shown in Fig. 1. It tends to be highest from cities.

In the present ASR radars, ground clutter is reduced by three mechanisms: MTI, antenna tilt, and by mounting the antenna close to the ground to take advantage of the shielding effect of nearby objects. Fig. 2 shows the MTI filtering performance achievable using one and two delay line cancelers with and without limiting. Previous ASR radars have all employed limiting in the IF followed by a phase detector. The purpose of the limiting is to normalize the video output so that clutter residue from the MTI filter is reduced to the average noise level. This allows the video gain to be adjusted so the clutter will not show up on the controller's scope. Unfortunately, this limiting action spreads the clutter spectrum

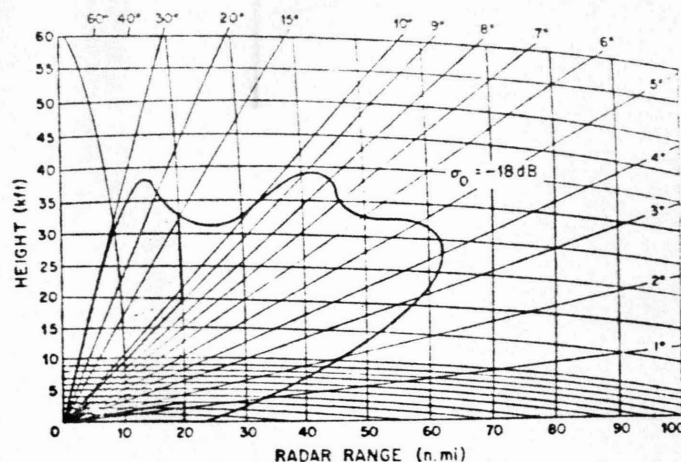


Fig. 3. Solid curve is coverage of ASR-7 radar against a  $2\text{-m}^2$  target in receiver noise [2]. Cross hatched region shows region of poor performance against ground clutter.

so that considerably poorer subclutter visibility (SCV) is achieved than if the normalization had been done by some other mechanism not involving nonlinearities.

If we consider the parameters of a typical terminal radar (ASR-7, see Section III-A 1) at 15 nmi, and  $\sigma_0$  from Fig. 1 that is exceeded only 5 percent of the time, we find that for a  $1\text{-m}^2$  target (typical small aircraft) the input signal-to-clutter ratio is  $-31$  dB. Since an output signal-to-clutter ratio of about 15 dB is needed for adequate target visibility, an improvement factor of 46 dB is required. We see from Fig. 2 that this is not achievable with the present configuration. It is, thus, common practice to achieve greater signal-to-clutter advantage by tilting the antenna upward (see Fig. 3) by  $2^\circ$  to  $5^\circ$  depending on the local clutter situation. If tilted, as shown in Fig. 3, there is a 17-dB advantage (maximum range divided by zero elevation range to the fourth power) in input signal to clutter for an aircraft flying in the peak of the antenna pattern. This advantage is degraded as the aircraft gets out of the peak of the antenna pattern so that, typically, detection gets spotty due to competition with ground clutter for small aircraft below about  $1.5^\circ$  or above about  $9^\circ$ . These angles change depending on the antenna tilt and ground clutter intensity. It is estimated that a 20-dB increase in improvement factor would be required for really adequate detection of small aircraft at all altitudes.

Another undesirable feature of the improvement curves in Fig. 2 is the very wide notch around zero and the first blind speed. The notch around the first blind speed is usually removed by using staggered PRF. The notch around zero means that targets will be lost for a considerable distance on the scope when the aircraft flies tangential to the radar. It will be observed that the three-pulse canceler with limiting is worse in this respect than the two-pulse canceler with limiting. Below, we shall describe how more advanced signal processing techniques and antenna techniques can both provide a large degree of improvement in SCV, and much better performance near zero velocity.

A further limitation in performance of existing ASR's is the presence at many sites of buildings or hills which limit the minimum elevation visible to the radar. Increasing the height of the antenna to overcome this limitation causes an undesirable increase in ground clutter level which could be overcome by improvement in SCV.

### B. Second-Time-Around Clutter

In the so-called "second-time-around" clutter effect, returns are being received due to illumination of clutter beyond the nonambiguous range by the next-to-last pulse transmitted. These returns are prevalent where conditions for anomalous propagation exist such that the radar waves are bent back downward with range and intercept the ground at great distances (greater than that corresponding to the interpulse period). This effect is also prevalent in regions where mountains exist beyond the nonambiguous range.

Present ASR's use magnetron transmitters that transmit pulses with random phase from pulse to pulse. Thus it is impossible to maintain the phase relation between the first- and second-time-around clutter returns and the two cannot be filtered out simultaneously.

Further, the present ASR's use pulse trains with staggered interpulse periods so as to avoid Doppler blind speeds. But this causes the second-time-around clutter return to be from a different range cell on succeeding returns so there is no hope of filtering it out. To effectively filter out second-time-around clutter, a fully coherent transmitter (one coherent from pulse to pulse) and a constant PRF must be used. The PRF need not be constant forever, but only over an interval sufficient to collect a group of pulses for processing. If the PRF is changed from group to group of pulses, the radar is said to use "multiple PRF."

### C. Precipitation Clutter

The backscatter from precipitation has been studied extensively. Fig. 4 shows the mean volume reflectivity from rain at 15 mm/h. This is considered a heavy rain found only 0.04 percent of the time at New Orleans [1]. This heavy rainfall is usually found only in relatively small-size cells in the center of storms. The radar should be designed to reject at least this level and as much higher a level as possible.

Also marked on Fig. 4 is the point where the volume reflectivity is such as to cause a 1-m<sup>2</sup> return at 30 mi in an ASR radar (rain return from a typical cell with precipitation extending from the surface to 10 000 ft). Rain at 15 mm/h is about 13 dB above this value. Remembering that these are average reflectivities and that ~15-dB signal-to-noise ratio is required for automatic detection, we need about 30-dB rain rejection for good performance.

The rain clutter spectrum is spread around some mean value determined by the wind velocity. The spectral spread observed by the radar is fixed by wind shear conditions [1]. The standard deviation of the rain velocity spectrum typically reaches values of 4 m/s at 30 nmi and increases with range.

Circular polarization is normally used to reduce rain clutter by about 15 dB while reducing the signal level to some extent. The use of MTI helps reduce rain clutter except when the antenna is looking toward or away from the wind direction. In these directions, the rain clutter spectrum is such that all of the rain clutter signals may pass through the MTI filters.

Log-FTC-antilog circuits [2], [3] reduce the receiver gain in proportion to the average level of rain clutter for about a mile in range surrounding the cell of interest. It, thus, normalizes the rain clutter level just as limiting is used to normalize ground clutter at the output of the MTI circuit. Its purpose is to suppress the rain clutter on the scope. At the same time, of course, it suppresses the signal. For adequate detection, the signal amplitude must be appreciably above the clutter residue from the MTI filters.

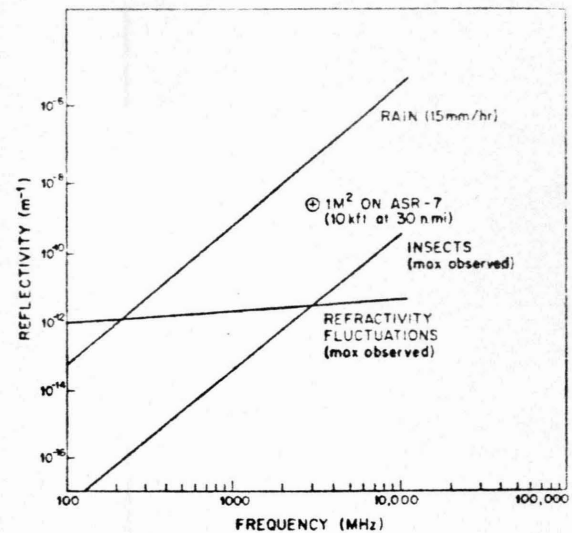


Fig. 4. Reflectivity of various moving clutter sources [1], [4].

### D. Angel Clutter

The so-called "angel clutter" refers to all returns which cannot be explained as being ground or precipitation clutter or targets. Much effort has been spent in studying angels. It is now believed that nearly all, if not all, angels are caused by bird flocks. Two other sources were considered possible.

Swarms of insects have been observed by meteorologists using powerful radars [4]. The swarms may cover large areas and, in general, drift with the winds. Well organized layers of turbulent refractivity in the atmosphere associated with changes in the refractive index have been observed. The maximum volume reflectivity associated with these types of returns is plotted in Fig. 4. It will be observed that both are much lower than a 1-m<sup>2</sup> target so should cause little difficulty when trying to detect aircraft.

Returns from single birds [5] at S band range in size between 10<sup>-4</sup> and 10<sup>-2</sup> m<sup>2</sup>. The return is principally from the body with very little from the wings. For large birds, the body is resonant near L band (1300 MHz) and is in the Rayleigh region at UHF. Typically, there may be anywhere from one to several hundred birds in a resolution cell. Although the mean return from a typical flock of birds may be low (~10<sup>-2</sup> m<sup>2</sup>), the tail of the distribution has been observed to return up to 10 m<sup>2</sup>. Although birds have been seen as high as 12 000-ft altitude, they usually fly less than 7000 ft. The usual appearance on the scope is as so called "dot angels." "Ring angels" are also caused by birds as a large group leave their nesting place at sunrise.

Of particular interest are the bird migrations in spring and fall. These have been described as "night effect," "falling leaves," "seasonal AP angel clutter," and have been reported by many terminals in the eastern part of the United States. The appearance on the scope when the radar is using MTI is that of two well-defined lobes. In Fig. 5, there is a strong migration in an easterly direction so MTI notches appear north to south. The lobes appear to be made up of a multitude of spots which move like falling leaves.

These migrations occur at night when there is a favorable wind. Migration will be very heavy on favorable nights so that most of the migration occurs on relatively few nights (5 to 15) each spring and fall. The number of birds associated with these migrations may be very large. One author esti-



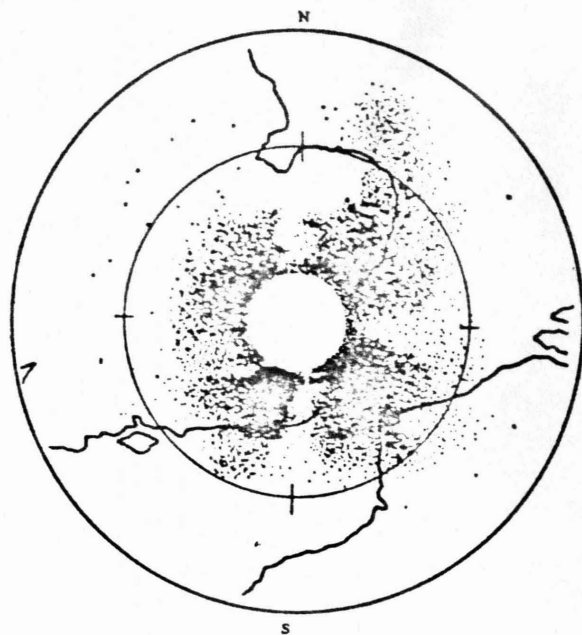


Fig. 5. Migrating birds as seen using MTI radar (from [5]).

mated that a few million birds crossed a 100-mi front during one of the busy nights of the autumn migration in the Cape Cod region [5].

Birds fly between 15 and 45 knots true air speed. Taking into account winds, radial velocities over the range  $\pm 80$  knots or so may be observed.

A fairly effective radar improvement used against bird clutter is a carefully tailored sensitivity time control (STC) [6]. The STC varies the radar gain with range and is adjusted so that the minimum detectable target is a specific value, say,  $1 \text{ m}^2$ . This calls for an  $R^{-4}$  attenuation law.

#### E. Surface Vehicles

The cross section of ground vehicles is in the same range as aircraft; namely, from  $1$  to  $100 \text{ m}^2$ . Radial velocities range over  $\pm 60$  knots.

Some reduction in ground vehicle returns is achieved by tilting the antenna upward. The only other solution found so far, as is practiced at the Atlanta airport, is to blank out areas on the scope known to contain visible roads carrying cars with radial velocities outside the notch at zero velocity. This has proven effective and causes only small holes in the coverage.

### III. RADAR IMPROVEMENTS

From the previous discussion, it is obvious that there is no single solution to the problem of providing high probability of detection with low false alarm rate in an automated system under all conditions. Rather, several changes must be made and the resulting system examined to see how well it corrects all the various problems.

We will now discuss a series of improvements which could be made to the radar and tell how each would help solve the above problems.

#### A. Signal Processing Techniques

1) *Optimum Signal Processing:* We first concentrate on fixed ground clutter since this presents the biggest clutter problem. To give complete flexibility in siting and tilting the antenna

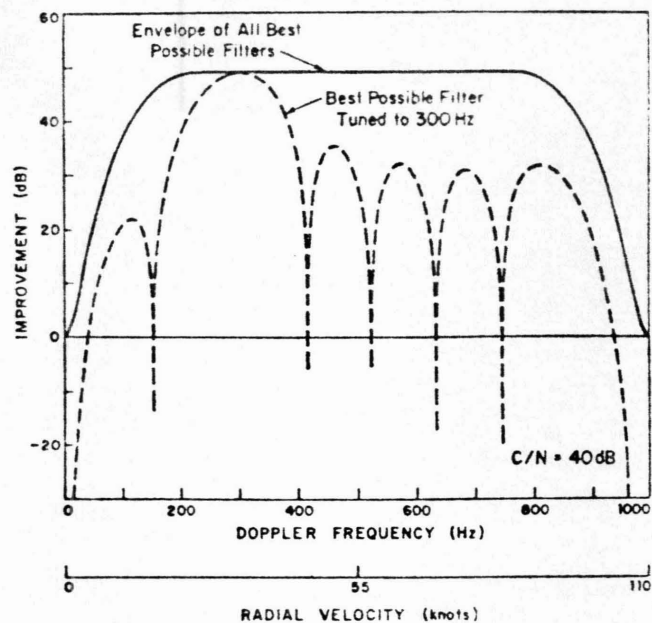


Fig. 6. Improvement of target-to-interference ratio, scanning antenna.

while still rejecting ground clutter, an approximate 20-dB improvement in performance should be provided in the signal processor. It is obvious that this requires processing linear clutter and target signals and that one must avoid all nonlinearities in the receiver. To narrow the blind speed region, one should also process more pulses.

In order to assess quantitatively what could be considered a "good" MTI processor for improving the performance of ASR radars against fixed ground clutter, calculations were made of the performance of the so-called "optimum processor." Given the initial conditions, the optimum processor has the highest target-to-interference (interference is defined as clutter plus front-end noise) ratio improvement of any processor. By knowing the performance of such a processor, one can judge how well a conventional easily implemented or any other processor (i.e., suboptimum) can approach the theoretical limit. The processor considered here can be defined as a device that takes  $M$  complex signal returns  $V_i$ , multiplies these returns by a complex filter weight  $\bar{W}_i$ , adds them, and then takes the square of the amplitude

$$R = \left| \sum_{i=1}^M \bar{W}_i V_i \right|^2.$$

$V_i$  is composed of target, noise, and clutter. The theory of optimization will not be shown here but follows that of DeLong and Hofstetter [7]. The clutter spectrum, which in this case is essentially all caused by the antenna scanning motion, is modeled by an antenna having a Gaussian beam shape as in Emerson [8].

Two general cases have been studied: the mechanically rotating antenna as in the ASR radars and the step-scan antenna. In both of these cases the transmitter pulses are assumed uniformly spaced. Fig. 6 shows the target-to-interference improvement in decibels that is possible (optimum) for the mechanically rotating antenna. The results in this section assume the use of a sufficiently stable coherent transmitter. Poorer, as yet undetermined, results will be obtained using a magnetron transmitter. The parameters are (similar in most

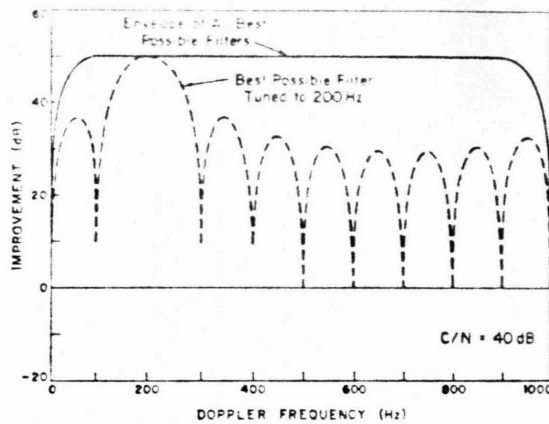


Fig. 7. Improvement of target-to-interference ratio, step-scan antenna.

respects to the ASR-7):

antenna width	5.25 m
antenna rotational speed	1.36 rad/s
wavelength	0.107 m
PRF	1000 pulses/s
number of pulses processed, look	10
clutter-to-noise ratio	40 dB.

The maximum clutter-to-noise ratio which can be handled will be set by the dynamic range of available analog-to-digital (A/D) converters. Mean clutter-to-noise ratios of 40 to 50 dB can be handled in available A/D converters with adequate sampling rates.

The upper curve in Fig. 6 is the improvement obtained when the optimum filter is tuned to the Doppler frequency of the target as the target Doppler is varied. The lower curve is the improvement when the optimum filter is tuned to a fixed Doppler (300 Hz) as the target Doppler is varied. The lower curve represents the frequency response of the particular optimum filter tuned to 300 Hz.

The following general characteristics of the optimum processor should be noted:

a) The upper curve (Fig. 6) levels out at about  $M \times C/N = 10^5$  where  $M$  is the number of pulses processed and  $C/N$  is the clutter-to-noise ratio, unless  $M$  is small. This points up the need for wide dynamic range A/D converters as explained above.

b) At the so-called "blind speeds" (0 and 1000 Hz), there is no improvement, but there is no deterioration either, thus a target whose cross section is sufficiently above clutter can be seen.

c) For filters that are not tuned on or close to blind speeds, there are very deep nulls at the blind speeds.

d) The width of the notch about the blind speeds increases with antenna rotational speed when all other parameters are held constant.

e) The filter cannot, in general, be approximated by a discrete Fourier transform (DFT) except in certain special cases.

f) Because the optimum weights  $W_i$  are a function of clutter-to-noise ratio, the optimum processor requires some *a priori* knowledge. However, this ratio can be determined in principle by the application of a proper algorithm in the receiver, together with ground clutter memory from scan to scan.

The step-scan case is shown in Fig. 7. Because the antenna

is not scanned and ground clutter can be considered to be time-stationary (constant voltage), the clutter spectrum is just an impulse at zero frequency. The intrinsic ground clutter spectrum (motion of trees) is ignored because it is too narrow to have any effect upon the results. It should be pointed out that the only input parameters needed for the step-scan case are the PRF, the number of pulses per look ( $M$ ), and the clutter-to-noise ratio. Thus these curves are directly applicable to other radar frequencies as well as S band. The parameters used in Fig. 7 are the same as in the scanning case.

The following properties of the step-scan curves (Fig. 7) should be noted:

g) The notches at the blind speeds are now very narrow. There would be much less chance of losing a target in clutter with near tangential velocity.

h) In most instances a DFT can replace the optimum filter and thus improve computation efficiency.

i) Although it cannot be seen on this figure, the improvement at the "blind speeds" is 0 dB as in the scanning case of Fig. 6.

By comparing these results with those of Fig. 2, we see the amount of clutter rejection achieved in the present radars as well as other conventional MTI systems is far less than the best that can be done, whether scanning or not.

2) *Near-Optimum Signal Processing:* In the scanning antenna case, the implementation of the optimum processor for every range-azimuth cell calls for  $M$  complex multiplications for each target velocity examined. Usually, if  $M$  pulses are being processed, a filter bank with  $M$  filters will give adequate coverage for all target velocities. Thus  $M^2$  complex multiplications must be performed for every range cell. For a typical ASR, 800 range cells per sweep must be sampled on 10 sweeps and processed every 10 ms. If optimum filters were used, 8 000 000 complex multiplications per second would be required or 32 million simple multiplications.

A simpler processor can be built. The optimum processor can be broken into two parts, a clutter filter followed by a target filter. The filter used to reduce clutter multiplies the signal vector by the antenna weighting and by the inverse of the interference covariance matrix. The target filter used to enhance the target is a DFT. The near-optimum processor could consist of a digital filter which approximates as closely as possible the frequency response of the clutter filter followed by a DFT for the target filter. This combination will give improvement factors within a few decibels of the optimum shown in Fig. 6 and require fewer multiplications per second than previously indicated. It will also provide Doppler information on the target.

Through direct comparison it has been found that a simple three-pulse canceler without feedback forms the clutter filter portion of a near-optimum processor for the scanning antenna.

For the step-scan case, Fig. 7, the clutter filter is nothing more than a dc removal filter and as such is very easy to implement.

3) *Ground Clutter Map:* The near-optimum ground clutter processor would not be complete without adequate thresholding. For a typical ASR, ground clutter will appear only in the zero Doppler filter and the filters immediately adjacent on each side. Ground clutter is very spotty in character. It varies greatly in size from one resolution cell to the next. Thus averaging nearby cells will not give a good estimate for thresholding purposes.



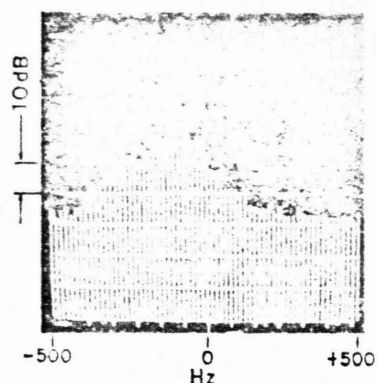


Fig. 8. Typical storm spectrum taken using an S-band radar. Receiver noise level is -57 dB.

A practical way to accurately set ground clutter thresholds is to use a digital ground clutter map which remembers the ground clutter in every range-azimuth resolution cell averaged over a sufficient time period (number of scans).

Such a clutter map provides superclutter visibility. Whenever an aircraft's cross section is larger than the clutter over which it is flying it will be seen even if it has zero radial velocity (tangential target). The operator makes no decision concerning the selection of MTI or normal video to be displayed on the scope. The best detection is provided automatically in each range-azimuth cell because detection in each velocity is optimized separately.

4) *Filter Bank for Precipitation Filtering:* It is fortunate that the optimum or near-optimum filtering against ground clutter utilizes a filter bank since this is a good approach to eliminating weather clutter. We need about 30-dB weather clutter rejection of which 15 dB is provided by circular polarization. Filtering of some sort is a viable solution to obtaining the remaining 15 dB. The filtering could be near-optimum as in the case of ground clutter except for the fact that the weather clutter spectrum (see Fig. 8) changes with time. This change could be measured and the filter adapted to the spectrum, but this would result in an intolerable amount of hardware.

A good alternative is to use the filter bank produced by the near-optimum ground clutter filter. It is only necessary to set the threshold on each filter adaptively. A so called "mean-level" threshold is employed. Since storms are rarely less than about 1 mi in extent, the moving clutter is averaged over a half mile on either side of the cell being examined for a target. Each velocity is averaged separately so that filters containing only noise and not weather clutter will not be penalized.

If further, a multiple PRF system is used so that high-speed aircraft typically will fall in different filters in the filter bank on successive PRF's, there is a very high likelihood that the target return will be competing with noise only on one of two PRF's. Only for aircraft whose true (not aliased) radial velocity coincides with that of the rain will there be a degradation in detection performance.

In summary, a modern radar for air-traffic control use employing a scanning antenna would have a fully coherent transmitter; a linear, large dynamic range receiver; a signal processor containing a near-optimum ground clutter filter bank; a fine grained ground clutter map to set ground clutter thresholds; mean-level thresholding on weather; and would employ multiple PRF's for elimination of blind speeds.

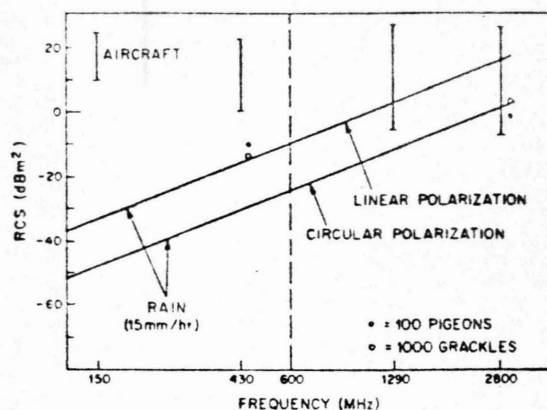


Fig. 9. Radar cross section of aircraft and moving clutter (rain and birds) as a function of frequency [1].

### B. Lower Frequency Radar

Another approach to the clutter problem is to choose radar parameters such that the target-to-clutter ratio at the input to the radar is much more favorable. For instance, the clutter cell size could be reduced by using very narrow beams or the range resolution reduced by using pulse compression. These are not very attractive solutions because they imply large antennas or very wide bandwidths in already overcrowded radar bands. A viable solution would be to go to lower frequencies.

Fig. 9 shows a summary of aircraft and moving clutter cross-section data as a function of frequency. For rain we have assumed a fan beam with a  $1.5^\circ$  azimuth beamwidth at 30-nmi range. It is quite clear that the aircraft return is maintained at the same size or larger as the frequency decreases, whereas the moving clutter, precipitation and birds, decreases in size. The clutter sizes shown are mean values so that an approximate 15-dB ratio between target and clutter is required for automatic detection. The dashed line at 600 MHz is the highest frequency where rain and birds are not considered a problem. Below 600 MHz, the radar need not even use circular polarization to combat rain.

### C. Antenna Improvements

1) *Dual Beam Antennas:* The present ASR antenna suffers because of two facts. First, it is tilted up several degrees (see Fig. 3) to reduce the ground clutter signals, thus degrading its low altitude performance at long ranges. Secondly, it has a cosecant-squared pattern with inadequate gain at the high elevation angles. Because of the latter fact, an aircraft at, say, 9 mi and 15 000 ft suffers a 20-dB disadvantage because of its position in the antenna pattern compared to some moving clutter at the peak of the beam (9 mi and 3000-ft altitude). A cosecant-squared pattern is a poor pattern to use when the elimination of birds and weather clutter is desired.

The ideal pattern is one that is uniform with elevation angle. Then an  $R^{-4}$  STC curve together with thresholding against noise will produce a constant cross-section discrimination against birds and weather. This ideal pattern would however have about 9 dB less peak gain than the present ASR antennas so it is out of the question. An antenna whose vertical pattern changes with range on receive is needed. It could maintain long-range low-altitude coverage and correct the high-elevation short-range problem as well. The ASR-8 radar

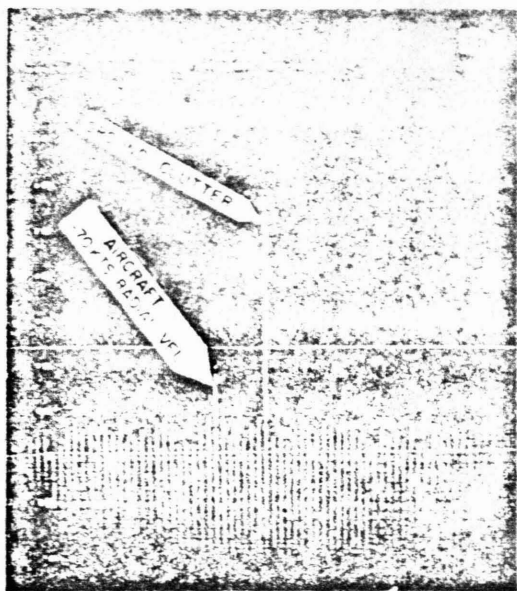


Fig. 10. Doppler spectrum of ground clutter and light single engine aircraft as observed by a UHF radar employing an electronically step-scanned antenna.

presently being developed will provide a dual beam on receive which will improve the long-range low-altitude coverage but will do little for the short-range high-angle coverage. Improvements of the SCV by 20 dB or more using improved processing techniques should remove enough restrictions on the antenna designer to solve the second problem.

2) *Step-Scanned Antennas*: An electronically step-scanned antenna is highly desirable for incorporation in an ASR because it reduces the spectral width of the ground clutter return to a narrow band. It is so narrow in fact that it is possible to completely separate the aircraft with slow velocities from the ground clutter. This is illustrated in Fig. 10 which is the spectral output of a 435-MHz radar using an electronically step-scanned cylindrical array antenna (Fig. 11). Notice that all of the ground clutter appears in one of the filter outputs and that the aircraft competes only with receiver noise. The SCV of the radar is limited only by the size of clutter the radar can handle and this, in turn, is limited only by the dynamic range of available A/D converters.

Although not entirely ruled out at *S* band, these cylindrical arrays are easier to build at lower frequencies and the large aperture they provide substantially reduces the required transmitter power, which in turn permits all the antenna switching to be accomplished with solid-state components. Cylindrical arrays have been used in a few radars at UHF and one is being designed for ATCRBS use at *L* band by Hazeltine.

Step-scanning a mechanically rotating antenna would produce a meaningful improvement although probably not as dramatic as that shown in Fig. 10.

#### IV. SOME RESULTS

Two demonstration radars utilizing the radar signal processing techniques described in Section III are being tested at Lincoln Laboratory, one at UHF and the other at *S* band.

##### A. UHF Radar with Step-Scan Antenna

This radar utilizes a fully coherent transmitter, an electronically step-scanned cylindrical array (see Fig. 11), and a

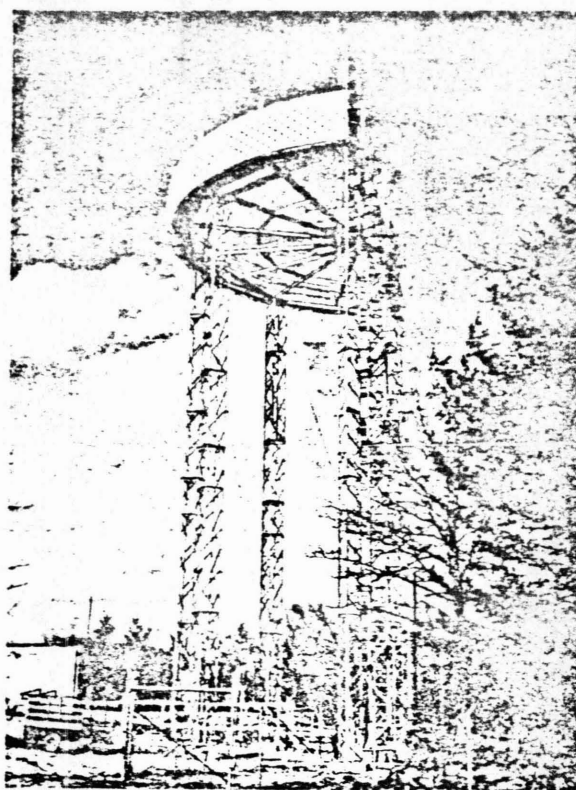


Fig. 11. Semicircular electronically step-scanned antenna used with UHF radar.

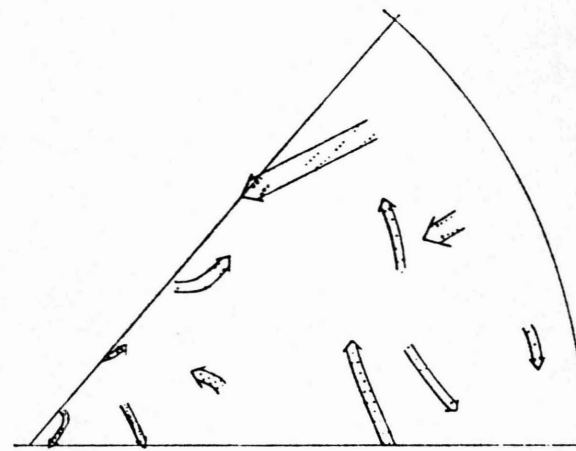


Fig. 12. Scan history display showing the detection of many aircraft. Arrows were added for emphasis.

wide dynamic-range linear signal processor. The antenna scans over a  $45^\circ$  sector and  $\frac{1}{4}$ -nmi range gates are processed out to 30 nmi every 3 s. A picture of typical synthetic video output for a period of 60 s is shown in Fig. 12. The processor was implemented using a minicomputer. It simply removes the dc from the quadrature video and noncoherently integrates two groups of 16 pulses on each azimuth. Detections on both groups of pulses are required before display. No ground clutter was seen confirming the results shown in Fig. 10. False alarms occurred in two regions and are believed due to automobile traffic. These could easily be removed by a tracking computer. Absolutely no rain was seen even on a rainy day. However, rain measuring equipment was not available to determine the rate of rainfall.

A few words should be said concerning the obvious breaks in the data. The antenna has a  $15^\circ$  elevation beamwidth centered at  $0^\circ$  elevation. It is, thus, very susceptible to ground lobing effects. The breaks in the tracks occur at about the right interval for ground lobing to be the cause. A properly designed antenna would have a sharp cutoff in its vertical pattern at zero elevation to reduce the strong antenna gain variations with elevation. Typically, we could see single-engine aircraft over the whole field of view and almost until they actually landed on a nearby runway.

#### B. S-Band Radar with Rotating Antenna

A greatly modified FPS-18 radar has been put into operation to test some of the signal processing concepts outlined in this paper. The stability of its klystron transmitter was improved so as not to be a limit in system performance. The antenna was servo driven, so that the ground clutter map would repeat itself every scan. A new, wide-bandwidth, linear receiver was provided. A processor employing the techniques described in Section III was simulated in real time on a general-purpose digital signal processor (the Lincoln Laboratory Fast Digital Processor, FDP) [9]. Signals were processed over  $35^\circ$  of arc by 8 mi in range. Ten complex video samples were processed as a batch using  $\frac{1}{4}$ -nmi range gates.

As of the present date, only a few results have been obtained using the S-band system. These results have been in consonance with the predictions of Section III.

#### V. CONCLUSIONS

The problems associated with air-traffic control surveillance radars to be used in a highly automated environment have been studied in detail. The general problem is one of aircraft returns competing with various kinds of clutter returns; ground clutter, weather clutter, birds, second-time-around clutter, and ground traffic. Radar solutions applicable

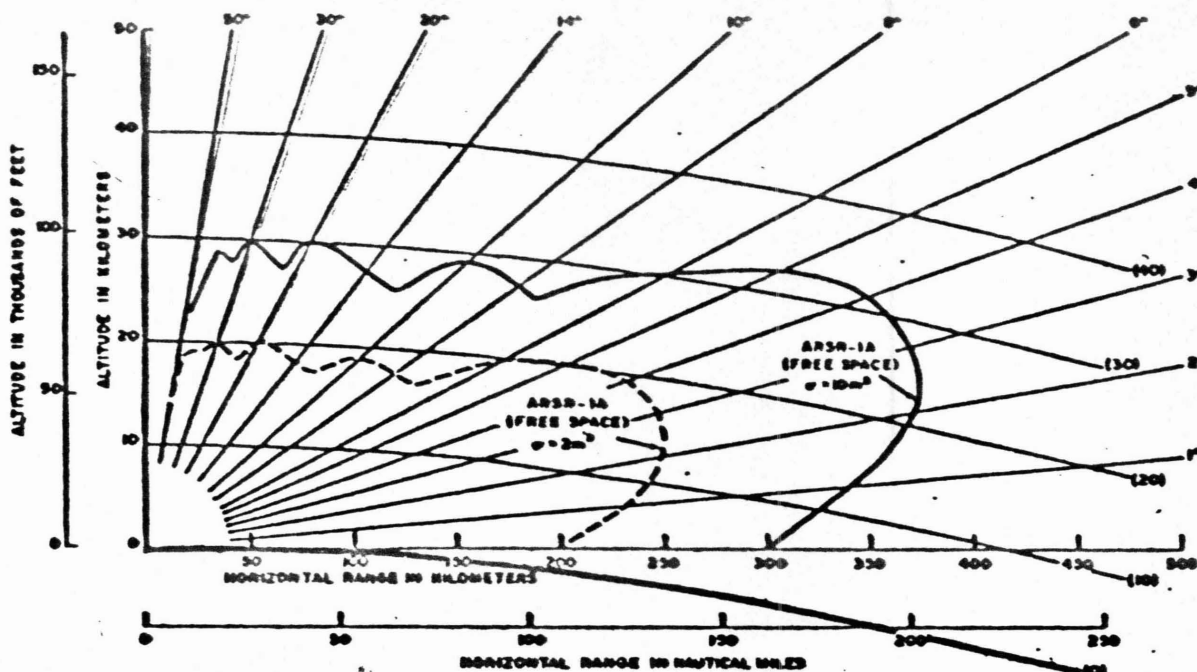
to the elimination of each type of clutter have been studied. Sets of these solutions were brought together to define radars which would be suitable to use in automated systems. Two such radars, a UHF radar employing an electronically step-scanned array and an S-band radar using a scanning antenna, have been built for demonstration purposes.

#### ACKNOWLEDGMENT

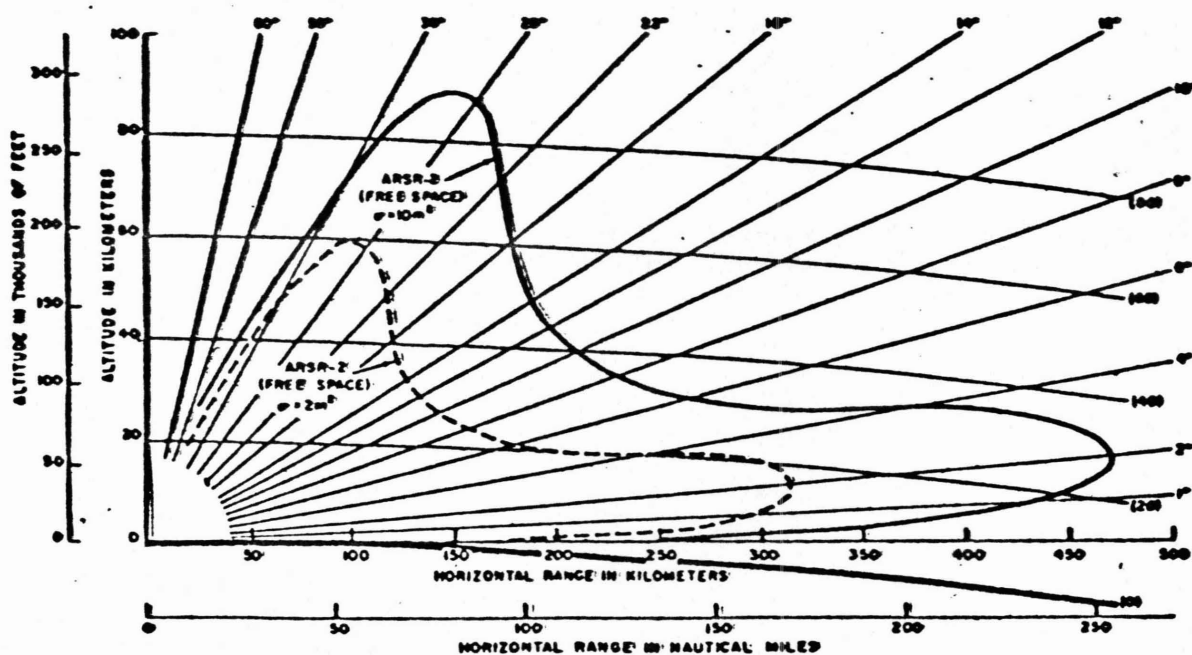
The work described above depended for its success on all the members of Group 43 at Lincoln Laboratory. R. G. LeBlanc, H. P. McCabe, and M. A. Nader are to be particularly commended for their contribution. T. M. Hendricks helped work out the suboptimum ground clutter processor. The authors also wish to thank H. G. Weiss and P. R. Drouilhet for their constructive direction and the Federal Aviation Administration for their sponsorship of this work and, in particular, K. Coonley and D. Hopson for their help and encouragement.

#### REFERENCES

- [1] F. E. Nathanson, *Radar Design Principles*. New York: McGraw-Hill, 1969.
- [2] "A brief description of the solid-state ASR-7 airport surveillance radar," Texas Instruments Inc. Rep., May 1970.
- [3] J. Croney, "Clutter on radar displays, reduction by use of logarithmic receivers," *Wireless Eng.*, pp. 83-96, Apr. 1956.
- [4] K. R. Hardy, "CPS-9 radar investigation of clear-air convection," in *13th Radar Meteorology Conf. Proc.*, pp. 236-240, Aug. 1968.
- [5] E. Eastwood, *Radar Ornithology*. London, England: Methuen & Co., Ltd., 1967.
- [6] R. E. Richardson, J. M. Stacey, H. M. Kohler, and F. R. Naka, "Elimination of a type of natural clutter in L-band radars," M.I.T. Lincoln Lab., Tech. Rep. 178, April 15, 1958, ASTIA Doc. AD 133851.
- [7] D. F. DeLong, Jr., and E. M. Hofstetter, "On the design of optimum radar waveforms for clutter rejection," *IEEE Trans. Informal. Theory*, vol. IT-13, pp. 454-463, July 1967.
- [8] R. C. Emerson, "Some pulse Doppler MTI and AMTI techniques," Rand Corp. Rep. 274, p. 104, Mar. 1, 1954.
- [9] B. Gold, I. L. Lebow, P. G. McHugh, and C. M. Radar, "The FDP, a fast programmable signal processor," *IEEE Trans. Comput.*, vol. C-20, pp. 33-38, Jan. 1971.

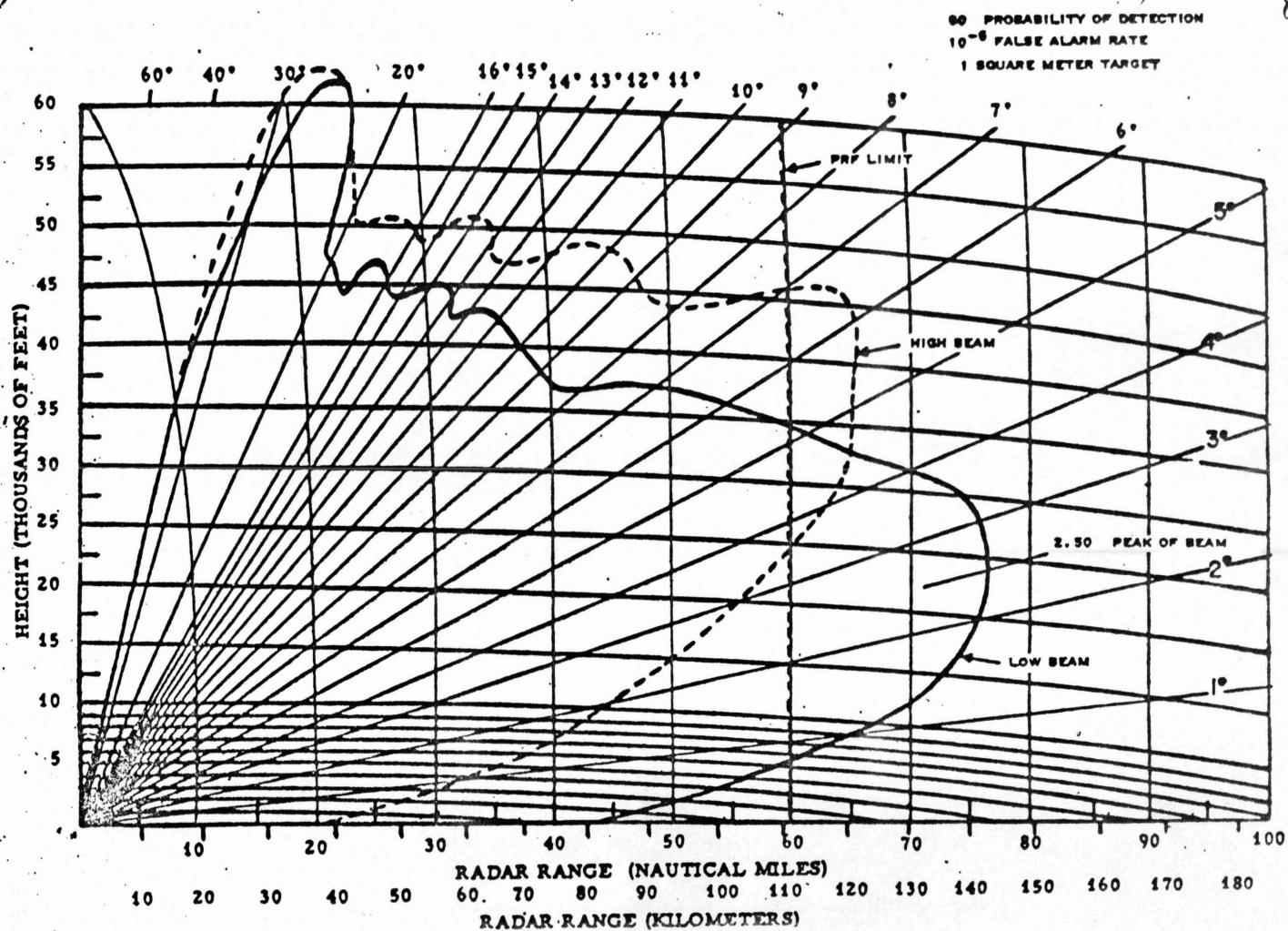


RANGE COVERAGE PATTERN FOR ARSR-1A



RANGE COVERAGE PATTERN FOR ARSR-2





(POWER)(APERTURE)PRODUCT IS ONLY IN CONSTANT FREQUENCY

Further questions relating to Sessions I and II

1. Compare the relative advantages of VHF (220 MHz) and S band (3000 MHz) for air surveillance radar application.

LESS WEATHER LOSS

RESOLUTION

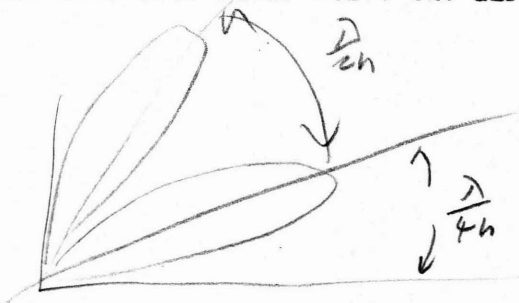
2. Under what circumstances might a 3D radar be favored over a 2D radar for air surveillance?

WHEN YOU NEED HEIGHT EG. YOU DON'T. RADAR IS POOR FOR HEIGHT.

3. Derive the surveillance radar equation given in class.

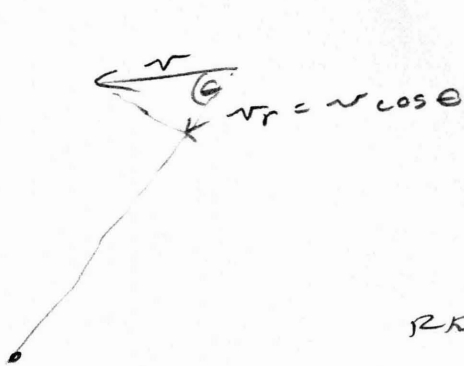
4. How well does radar solve the air-traffic control problem?

WELL, EXCEPT FOR HEIGHT + IDENTITY.



DRAGON WOULD WITH LOWEN

ASSR III IS VERY GOOD



TRANSMITS SINUSOID  
RECEIVE:  $\sin \omega(t-T)$

$$R = R_0 - v_r t$$

$$T = \frac{2R}{c}$$

$$T = \frac{2R_0}{c} - \frac{2v_r}{c} t$$

RECEIVE:  $\sin \left[ \omega t - \frac{2\omega R_0}{c} + \frac{2\omega v_r}{c} t \right]$

$$= \sin \left[ \omega \left( 1 + \frac{2v_r}{c} \right) t - \frac{2\omega R_0}{c} \right]$$

$\frac{2\pi f t + \frac{4\pi f v_r}{c} t}{c}$   
↑ CONSTANT PHASE SHIFT  $\phi_r$

DOPPLER FREQ,  $= f_d = \frac{2\pi f v_r}{c}$

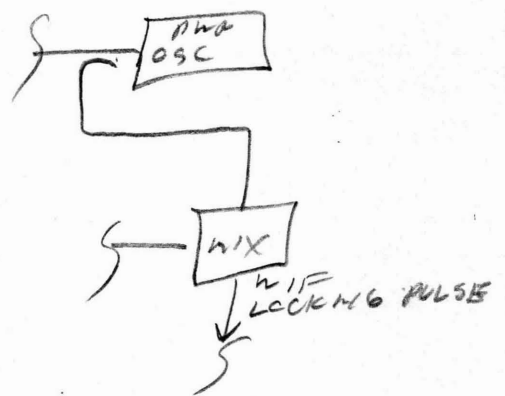
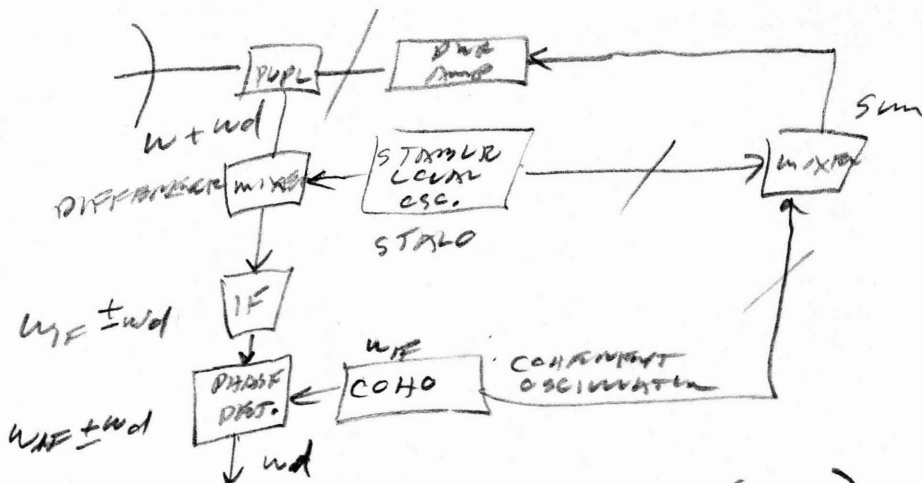
DOPPLER FREQ,  $= \frac{2v \cos \theta}{\lambda}$

### SESSION III

### MTI RADAR

MERRILL I. SKOLNIK

FEEDBACK PATHS



$$f_d = \frac{2v_r}{\lambda} \quad f_d (\text{Hz}) = \frac{v_r (\text{KNOTS})}{\lambda (\text{meters})} = \frac{300}{0.1} = 3 \text{ KHz} \quad \text{eg.}$$

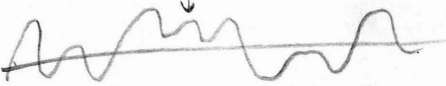
$$\sin(2\pi f_d t - \phi_r)$$

↑ CONSTANT

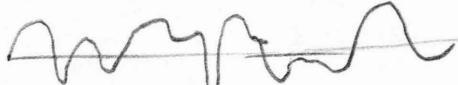
# FILTERING: HISTORY

WORKING TAXONOMY

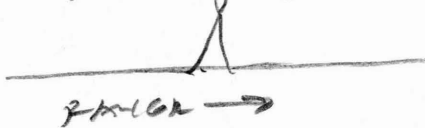
time ①



②

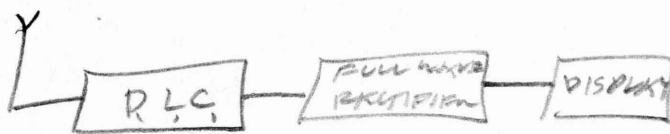


①-②



∴ USE DELTA LINE CHARACTER

nd



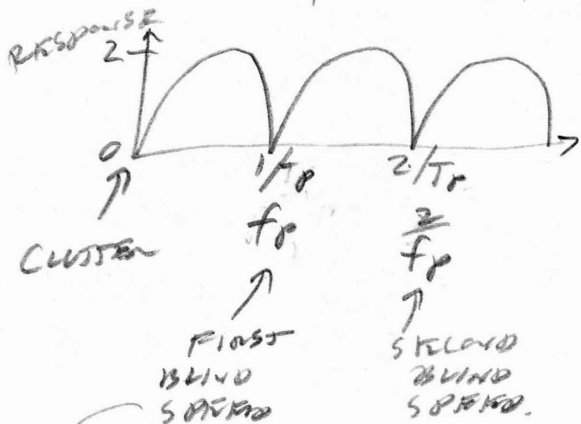
$$V_1 = K \sin(2\pi f_d t - \phi_0)$$

$$V_2 = K \sin(2\pi f_d (t - T_r) - \phi_0)$$

$$\sin A - \sin B = 2 \left( \sin \left( \frac{A-B}{2} \right) \right) \left( \cos \left( \frac{A+B}{2} \right) \right)$$

$$V_1 - V_2 = 2K \sin \pi f_d T_r \cos [2\pi f_d (t - T_r) - \phi_0]$$

$$RESPONSE = |2 \sin \pi f_d T_r|$$



$$\pi f_d T_r = 0, \pi, \dots, n\pi$$

$$f_d = 0, \frac{1}{T_r}, \dots, \frac{n}{T_r}$$

$$f_d = 0, f_p, n f_p$$

$$v_b = v_b \text{ WHEN } f_p = f_d = \frac{2v_r}{\lambda} \quad \therefore v_b = \frac{\lambda f_p}{2}$$

$$v_p (\text{KNOTS}) = \lambda (m) f_p (\text{Hz})$$

$$\text{LIST } \lambda = 100m \quad f_p = 400\text{Hz} \quad v_b = 0.1 \times 400 = 40 \text{ KNOTS}$$

3 KHz =  $f_d$  SAMPLED DATA SYSTEM @ 400 Hz  
∴ AMBIGUITIES.

$$\text{IF } f_p = 6\text{KHz}$$

$$\therefore v_b = 0.1 \times 6000 = 600 \text{ KNOTS}$$

$$6000 = \frac{80}{6} = 13.7 \text{ BUT ONLY RANGE.}$$

$$\text{LIST } v_b = 600 \text{ knots, } 400 = f_p$$

$$\therefore \lambda = 1.5m \quad (200 \text{ MHz})$$



Session MTI Radar

The doppler frequency shift of the echo signal can be used to determine the relative velocity of a target, but it is more often used as means to discriminate desired (moving) targets from unwanted (stationary) clutter, as in the Moving Target Indication (MTI) radar. The air search radar discussed in Session II usually is of the MTI type. MTI radar technology will be discussed by means of the following topics:

Block diagram of an MTI radar

Delay line canceller as a doppler filter

Blind speeds and their avoidance, including the staggered prf waveform

Multiple delay line cancellers for improved filtering

Limitations of MTI performance

Digital MTI and pulse doppler

MTI from a moving platform

The use of digital methods has made it possible to eliminate most of the problems associated with analog delay lines that have limited MTI performance in the past. There still exist fundamental problems in MTI design that limit the ability to achieve the theoretical performance, especially at the higher microwave frequencies. One of the toughest radar problems is that of providing MTI from a moving platform, such as an aircraft.

∴, RAISE  $f_p$ , ∴, RAISE AMBIGUITIES  
LOWER  $\lambda$ , ∴, PROBLEMS WITH LOW FREQ.

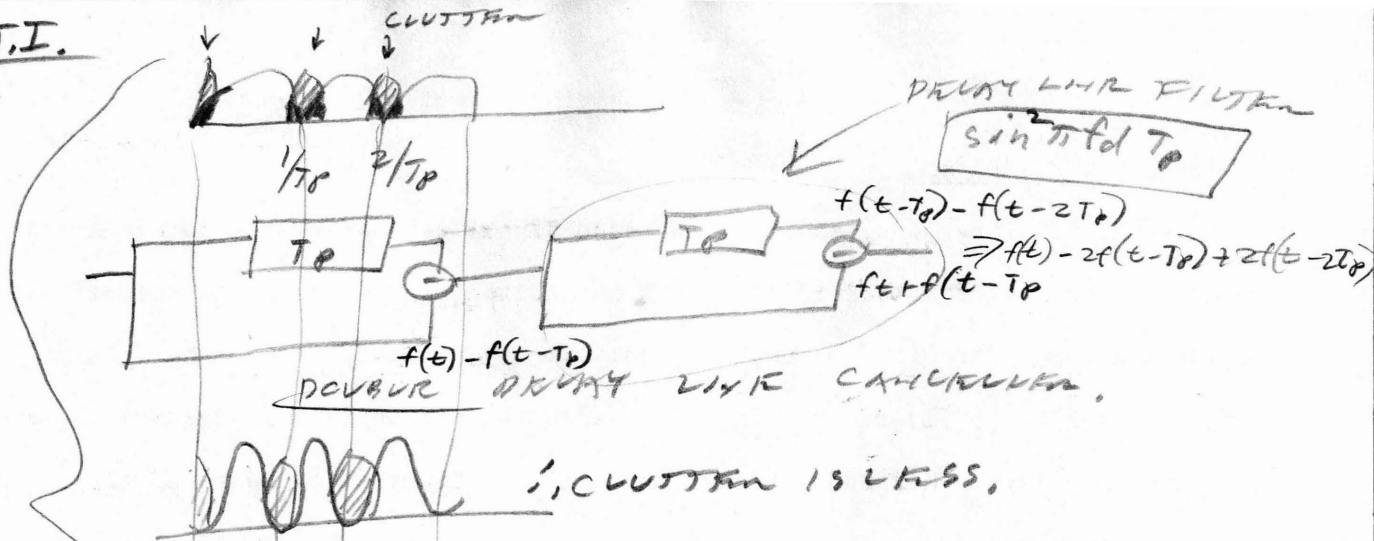
MTI RADAR — AMBIGUOUS DOPPLER BUT  
UNAMBIGUOUS RANGE

PULSE DOPPLER — UNAMBIGUOUS DOPPLER BUT  
AMBIGUOUS RANGE.

∴,  $f_p$  DETERMINES TYPE OF PLATFORM.

∴, VARY FILTER  $f_p$  OR  $\lambda$  TO  
REDUCE AMBIGUITIES. (EMERGENCY SOS.)

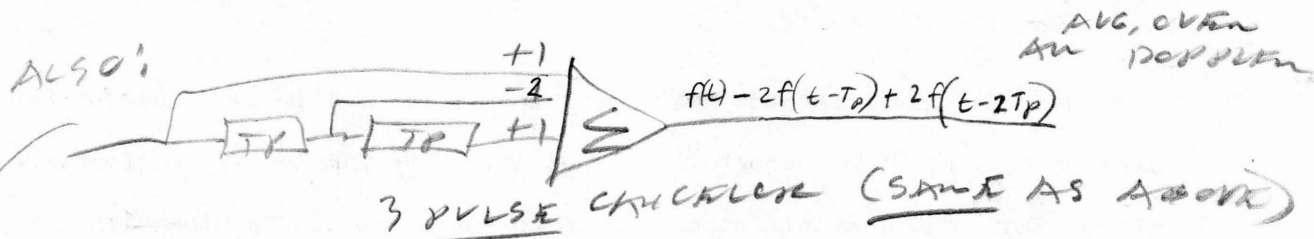
M.T.I.



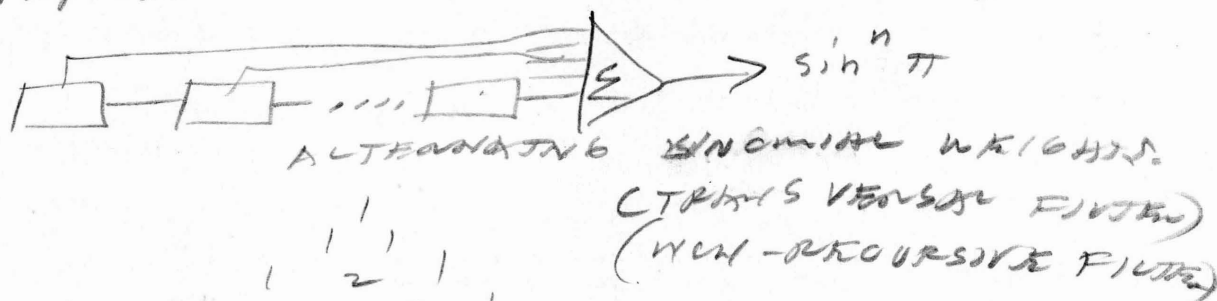
CAN ALSO GET  $\sin^3, \sin^4, \sin^5$ , etc.  
OPTIMUM UNDER ASSUMPTIONS MADE,  
MINIMIZES CLUTTER

$I =$  IMPROVEMENT FACTOR

$$I = \frac{\frac{\text{Signal}}{S_{\text{out}}/C_{\text{out}}}}{\frac{S_{\text{in}}}{C_{\text{in}}}} = \frac{S_{\text{out}}}{S_{\text{in}}} \times \frac{C_{\text{in}}}{C_{\text{out}}} = \frac{S_0}{S_1} \times \frac{\text{CLUTTER}}{\text{ATTEN}} \left( \text{AUG, OVER AN IDOPPER} \right)$$

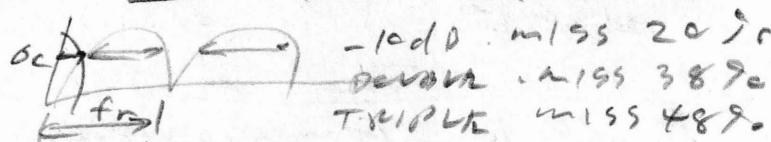


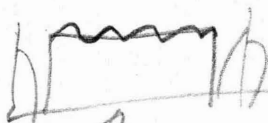
$n$ -pulse canceller ( $n-1$  DELAY LINKS)



			1			
			1	1		
		1	2	1		
	1	3	3	1		
1	4	6	4	1		
1	5	10	10	5	1	

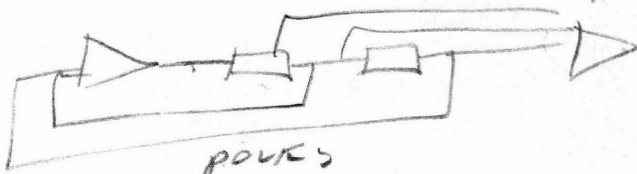
BUT STILL MISS TARGETS





↑ TRANSDUCER FILTERS (CARRY WEIGHTS)

CAN ALSO USE FEEDBACK LINKS AS WITH  
AS PERFORMING ZEROS



LATE 60'S.

BUT TRANSIENTS UPSET FILTER. (CAUSES RINGING)

MULTIPLE P.R.F. SYSTEMS INHIBITED BY FIXED  
ANALOG DELAY LINES.

ACOUSTIC - WATER + MERCURY WWII  
- SOLID QUARTZ WITH INTERNAL REFLECTIONS  
(MID 50'S)



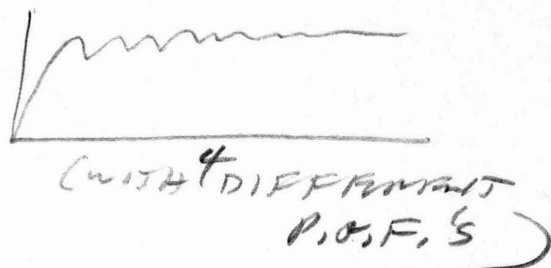
LC - FILTERS (ON LOW I. NOT USED MUCH.)

DIGITAL SYSTEMS MADE MULTIPLE SYSTEMS PRACTICAL

∴ STAGGERED

SESSION IV

CLUTTER



MERRILL I. SKOLNIK

T<sub>1</sub> 21.25

T<sub>2</sub> 22.30  $\frac{v_1}{v_0} = \frac{n_1 + n_2 + n_3}{N}$

T<sub>3</sub> 23.27

T<sub>4</sub> 24.31

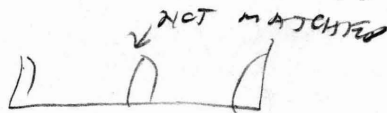
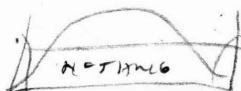
$\frac{v_1}{v_0} = 28.25$

eg.

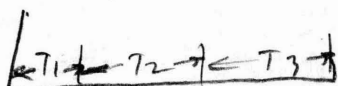
∴  $v_0 = 50 \text{ KNOTS (FAIR)}$

∴  $v_1 = 1400 \text{ KNOTS (4 FAIR)}$

M.T.I.

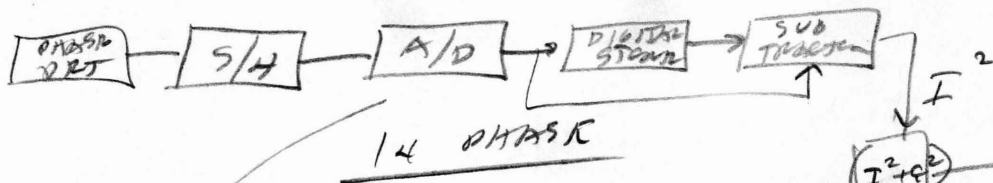


∴ COULD USE FILTER BANK  
OTHERWISE M.T.I. DEGRADES S/H.



REPEAT VARIOUS  
SIMPLE PRACTICES IN SAME  
ORDER.

# DIGITAL MTI DELAY LINK CANCELLER

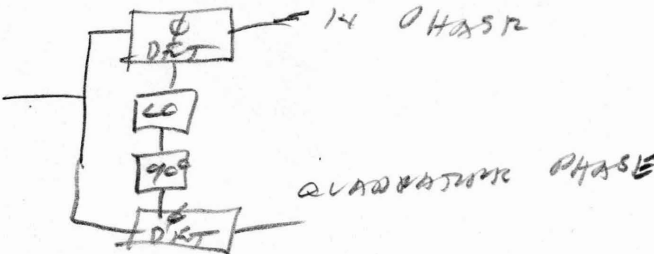
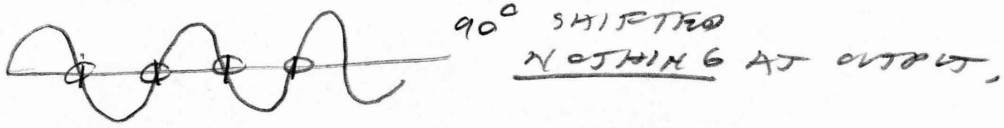
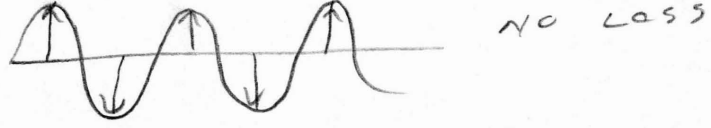
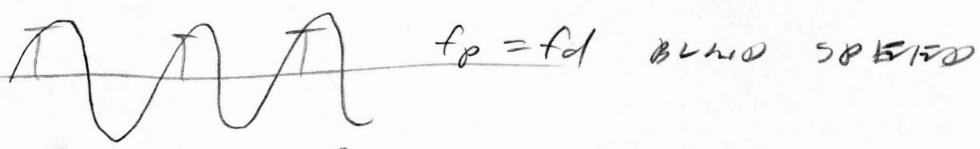


1/4 PHASE

QUADRATURE CHANNEL

(SOME)

BECAUSE OF BLIND PHASES

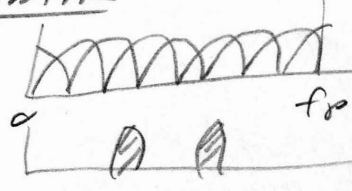


HOLDS FOR ANY OUTPUT.

NO. OF BITS DETERMINES EFFICIENCY.  
RESIDUE COULD MAKE STATIONARY TARGET  
LOOK LIKE MOVING TARGET  
EACH STRIP  $\rightarrow$  2 IN VOLTAGE  
 $\therefore$  6 dB PER BIT.

$\therefore$  50 dB IMPROVEMENT FACTOR  
 $\therefore$  NEED AT LEAST 9 BITS.  
BUT LIMITED BY SAMPLING RATE.

## FILTER BANK



1. MATCHES TARGET SPECTRUM  
BETTER (FAST FOURIER  
TRANSFORM)
2. ALSO CAN SEPARATE TWO TARGETS
3. ALSO KILL MATCHES FOLD OVER  
AMBIGUITIES WITH VARYING PRF

## CLUTTER AND RADAR

### INTRODUCTION

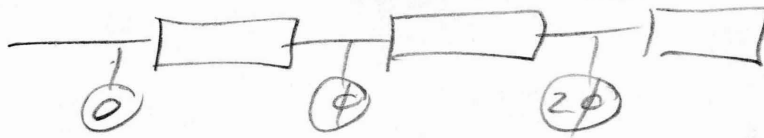
Radar echoes from the ground, sea, weather, atmospheric effects, birds and insects are called clutter since they usually interfere with the detection of desired targets such as aircraft or ships. Clutter is generally of a distributed nature although some types may be considered as point targets (water towers or other man-made objects, for example). When clutter is sufficiently intense it, rather than noise, can set the limits to receiver sensitivity and, hence, to the range of radar operation. When clutter is the factor limiting radar performance, the design of the radar for optimum detection is often different than when noise is the dominant effect.

Clutter echoes are not always undesirable targets to be eliminated.\* Radar has been widely used to study the nature of targets known as clutter. Two well-known applications have been weather radar and radar for measurement of the sea state. It has also been successfully used for the study of the flight of birds.

The study of clutter can be divided into two classes, which are 1) surface clutter from the land or the sea, and 2) volume clutter as from weather or the atmosphere. In this course both classes of clutter targets will be discussed. Clutter will be viewed both as a nuisance that interferes with the detection of desired targets and as a desired target itself. The study of surface clutter will concentrate on the sea since there exists far more information about radar scattering from it as compared with that from land.

over  
→

# DOPPLER FILTER BANK

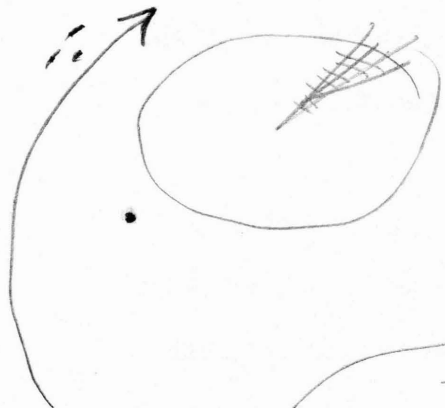
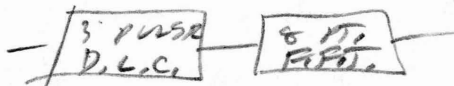


↑ SHIFT PHASIES WITH FAST  
FAST FOURIER TRANSFORMS TO  
FORM FILTER BANK.

FIG. 4-27 P. 127.

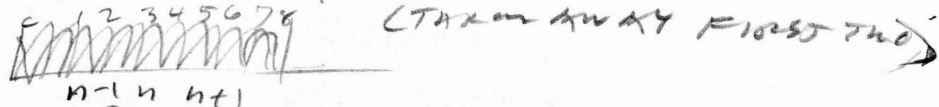
M.I.T. MOVING TARGET DETECTOR (MTD) (ASR-8)

3 PULSE D.L.C. FOLLOWED BY 8 PULSE FFT FILTER  
BANK. 47.5 nm RANGE QUANTIZED INTO 16 nm INTERVALS  
ANGLE QUANTIZED INTO  $\frac{3^\circ}{4}$  INTERVALS



∴ 365,000 RANGE ANGLE RESOLUTION.

10 PULSES - CPI, COHERENT PROCESSING  
INTERVAL.

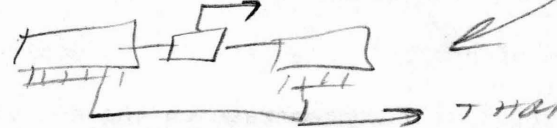


OVERLAP WITH  $\frac{\sin x}{x}$   
FILTERS.

∴ USE FREQUENCY DOMAIN WEIGHTING TO REMOVE SIDELOBES.  
∴ USE 3 PULSE D.L.C. TO REMOVE CLUTTER.

∴ 2,920,000 RANGE, ANGLE, DOPPLER  
RESOLUTION SIDE. EACH HAS ITS OWN  
ADAPTIVE THRESHOLD.

a) FILTERS 2-6 USE CLUTTER OF AR



b) FILTER 0 EXTRACT (FIG. 4-27 P. 127)

AND PUT IN CLUTTER MAP.

SLOWLY CHANGE IT ( $\frac{1}{8}$ ) WITH ( $\frac{1}{8}$ ) OF NEW INFO.

∴ SLOWLY CHANGE CLUTTER.

∴ ALLOWS CROSSING TARGETS TO BE  
SEEN (SINCE  $v_d = 0$ ).

c) FILTERS 1 AND 7 USE COMBINATION OF TWO.  
- P.R.F. IS CHANGED EVERY 10 PULSES.



### Definition of $\sigma^c$

The parameter used to describe the radar scattering from surface targets is the clutter cross section per unit area of illumination. This is designated  $\sigma^c$ . The geometry of the illuminated area is defined by Fig. 1.

### Radar Equation for Detection in Sea Clutter

When clutter dominates receiver noise, the radar range equation can be expressed as

$$R_{\max} = \frac{\sqrt{\sigma_t}}{(S/C)_{\min} \sigma^c \theta_b (c\tau/2) \sec \phi}$$

where  $R_{\max}$  = maximum range,  $\sigma_t$  = target cross section,  $(S/C)_{\min}$  = minimum signal-to-clutter ratio required for detection,  $\theta_b$  = azimuth beamwidth,  $c$  = velocity of propagation,  $\tau$  = pulse width, and  $\phi$  = grazing angles. This form of the radar equation applies for grazing angles that are not too large.

### Characteristics of $\sigma^c$

Fig. 2 illustrates the dependence of  $\sigma^c$  on grazing angle, frequency, and polarization. Other factors which affect  $\sigma^c$  are sea state, wind, rain, contaminants, pulse length, shadowing, and others we probably don't even know about.

### Theoretical Model of Sea Clutter

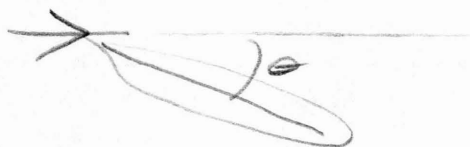
There have been several different models postulated to explain the nature of the radar echo from the sea including the sinusoidal surface,

9/12/3

- BW is improved BECAUSE CAN USE HIGHER BANDWIDTH.
- HELICOPTER HAS ROTOR BLADE SIGNATURE  $\therefore$  CAN SEE IT.
- POST PROCESSOR GROUPS HITS INTO EACH TARGET.
- MULTIPLE PERIOD PRF DOES NOT CANCEL 2ND TIME AROUND CLUTTER BECAUSE OF ALIASED PRF.  $\therefore$  USE CONSTANT PRF.

### MOVING RADAR (AIRBORNE)

problem: CLUTTER IS NO LONGER AT DC.



- $\therefore$  HAVE TO COMPENSATE FOR SHIFTING DOPPLER, AS BEAM ROTATES.
- $\therefore$  CHANGE COHERENT OSCILLATOR FREQUENCY WITH CHANGING DOPPLER FREQUENCY.

RADAR SAMPLES CLUTTER AND USES IT TO SHIFT OSCILLATOR.

CLUTTER-LOCKED AMTI  
 $\uparrow$   
 AIRBORNE

### "TACR"

"TIME ADVANCED CLUTTER COHERENT AIRBORNE RADAR" FEEDBACK SYSTEM.

problem:

$$f_d = \frac{2v \cos \theta}{\lambda}$$

$$\Delta f_d = \left( \frac{2v \sin \theta}{\lambda} \right) (\Delta \theta)$$

$$\Delta f_d = \frac{2v \sin \theta}{\lambda} (\theta)$$

$\therefore$  NEED VARIABLE B.W. FILTER AS WELL

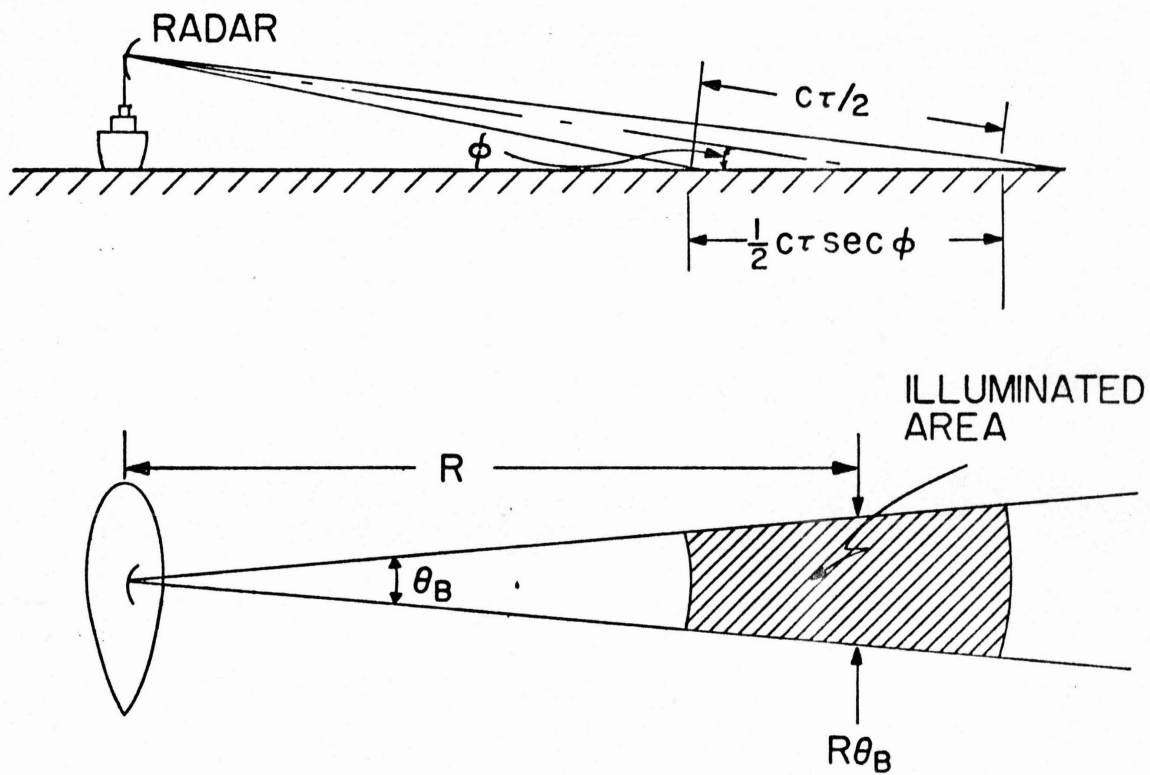
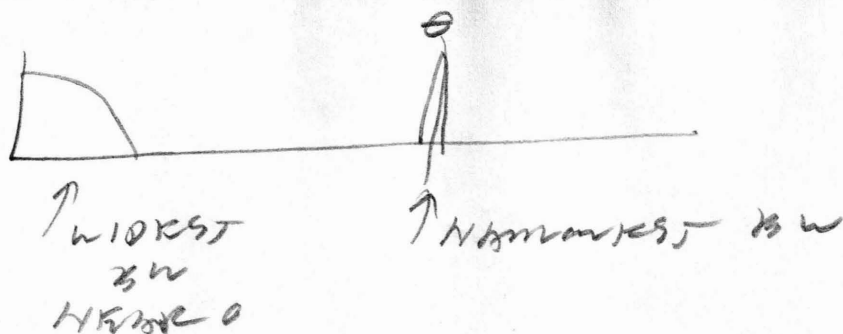


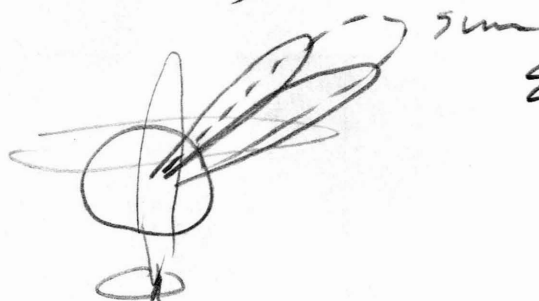
Fig. 1 - Area illuminated by radar at low grazing angles.  
(a) side view, (b) plan view. (Symbols defined in text.)



## DISPLACED PHASE CENTER ANTENNA

(2 IDENTICAL SYSTEMS)

(2 PULSES AT SAME STATIONARY POSITION)



$$\Sigma = j k \Delta$$

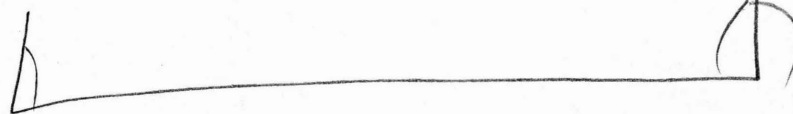
VARIES WITH ANGLE  
AND SPEED OF  
AIRBORNE,

problem

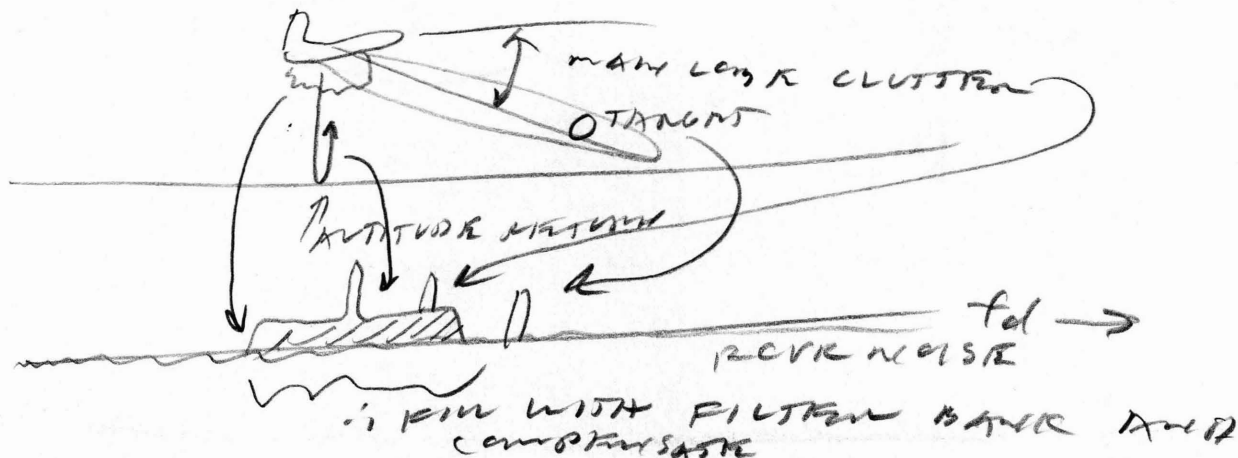
- BASING EVERYTHING ON TWO HITS ONLY.

## PULSE DOPPLER p. 146

STATIONARY



AIRBORNE



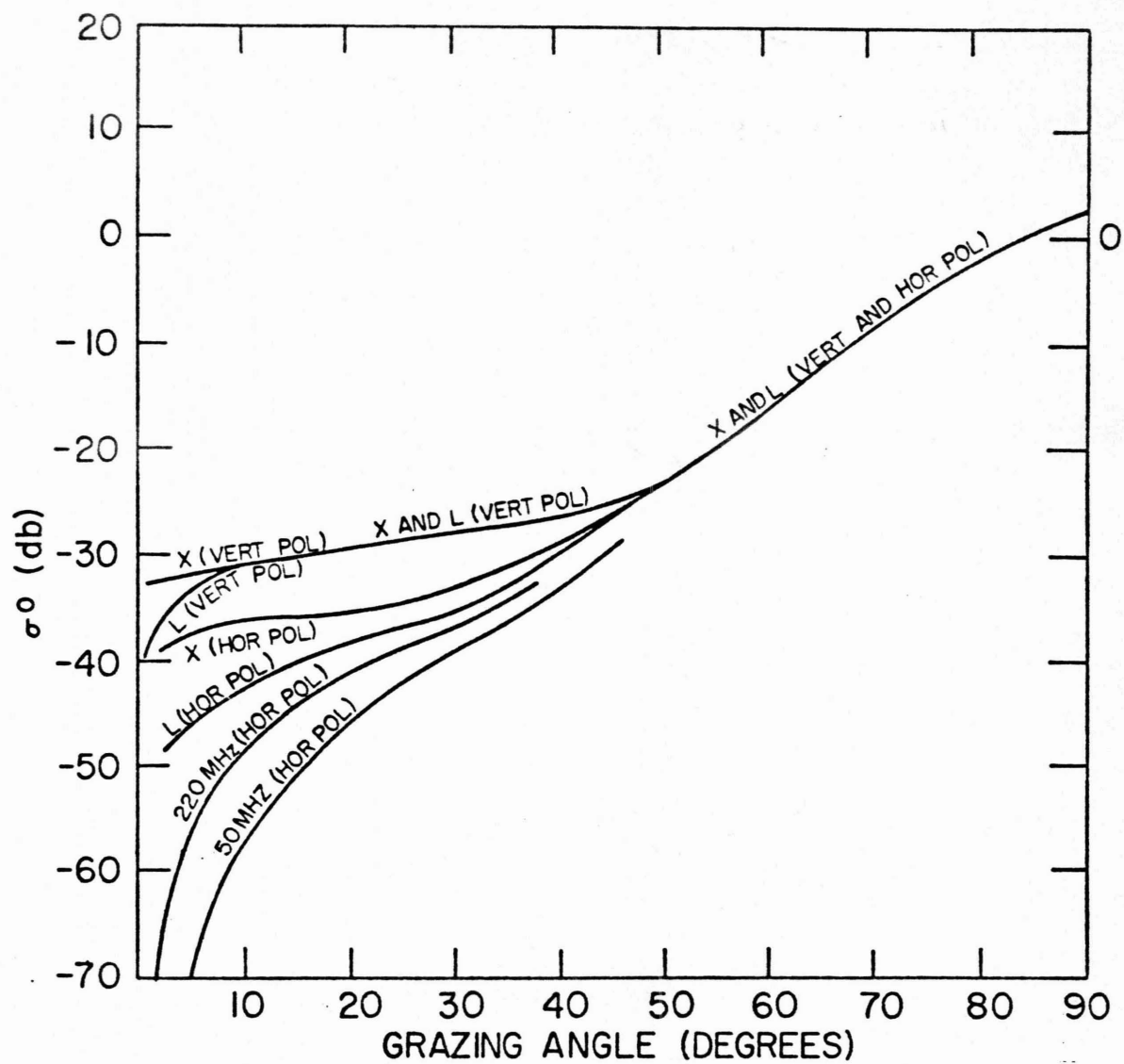


Fig. 2 - Composite of data showing the variation of  $\sigma^0$  with grazing angle, frequency and polarization for a "medium" sea.

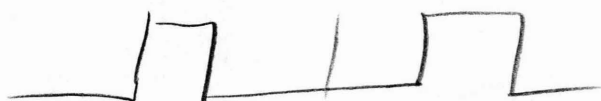
∴ PULSE-DOPPLER HAS MORE CLUTTER TO DEAL WITH.

PULSE-DOPPLER MUST HAVE VERY LOW SIDELOBES COMPARED TO MTI.

MTI - LOW P.R.F. (AVOIDS RANGE AND GUTS)

PULSE-DOPPLER - HIGH P.R.F. (AVOIDS DOPPLER AMBIGUITIES)

HIGH P.R.F. PULSE DOPPLER



$\frac{1}{3}$  DUTY CYCLE

KEEPS PROCESSING REASONABLE,

## CLUTTER

WANTED IN REMOTE SENSING.

SURFACE - LAND, AIR

VOLUME - RAIN, CLIFF

POINT - BIRDS, INSECTS

METEORS, AURORA, ETC.

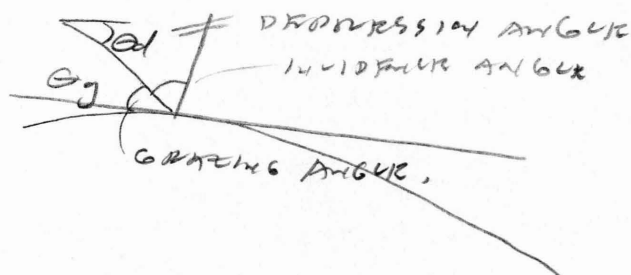
## SURFACE CLUTTER

- DOPPLER PULSWIDTH,  $\theta_{beam}$ , DOPPLER CLUTTER

$$\theta^\circ = \frac{\theta_c}{A} \quad \text{DEG UNIT AREA}$$

$\theta_{db} \Rightarrow A = \text{RADAR CROSS SECTION}$

$\theta_{beam} \Rightarrow \theta_{beam}$  ABOUT 1 SR. IN





droplets, and facets. The current theory is based on a composite surface model in which small ripples, or capillary waves, ride on top of the larger gravity waves, Fig. 3.

#### Techniques for Aiding the Detection of Targets in Sea Clutter

Methods for improving the detection of desired targets from undesired sea clutter include the following:

MTI (Moving Target Indication)--Does not help in detecting navigation aids such as fixed buoys.

Frequency--Lower frequencies produce less clutter (but it may be more difficult to direct radar energy on the surface at lower frequencies).

Polarization--Horizontal polarization produces less clutter.

Pulse width--Short pulse produces less clutter.

Beamwidth--Narrow beamwidth produces less clutter.

Antenna Scan Rate--A very rapidly rotating antenna decorrelates sea clutter and allows an improvement with pulse integration.

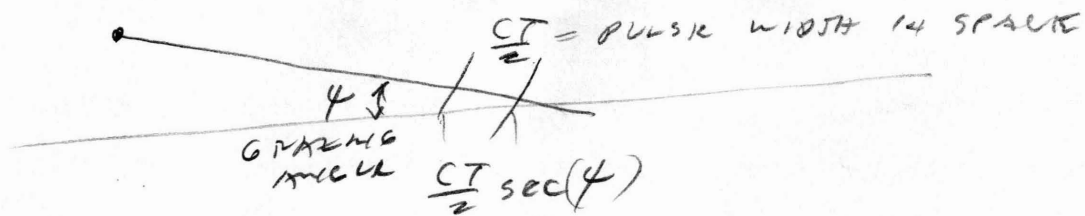
Target Time-Correlation--Observation of target over an interval of time allows discrimination from sea clutter because of target "persistence."

Matched Clutter Filter--Difficult to implement.

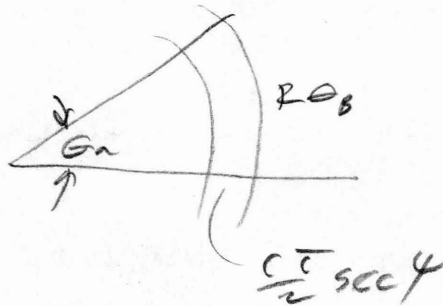
Frequency Agility--Clutter echo decorrelates with frequency but point target does not.

Clutter Range-Gating--When looking at normal incidence to the sea surface with high range resolution radar the clutter is at a greater range than a ship and so can be gated out.

Detector Design--The usual receiver detector design is based on the assumption that noise or clutter has a Rayleigh probability



ASSUME PFWIDTH IN ELEVATION IS BROAD.



$$A = R\theta_B \frac{CT}{2} \sec \psi$$

$$P_r = \frac{P_t G^2 \lambda^2 \sigma}{(4\pi)^3 R^4}$$

$$S = \frac{P_t G^2 \lambda^2 \sigma}{(4\pi)^3 R^4}$$

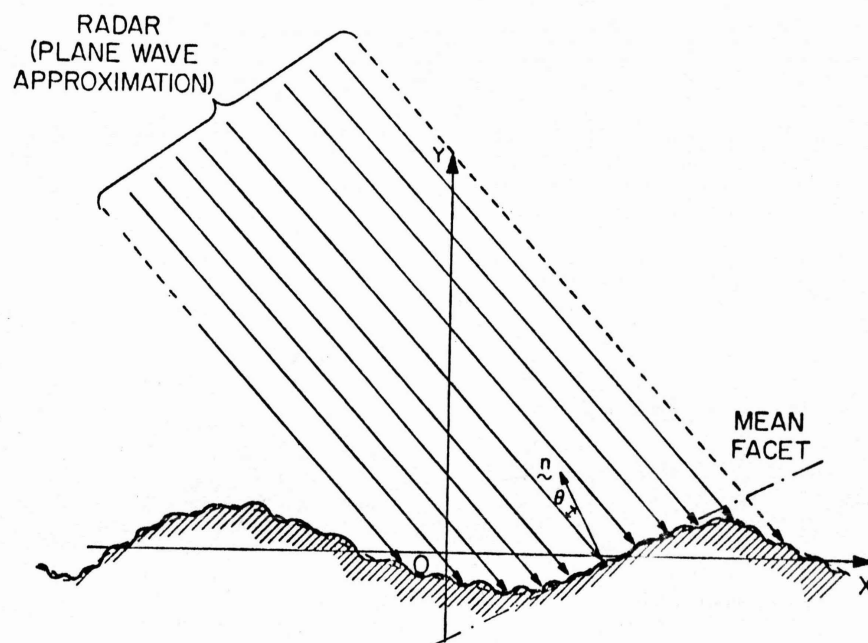
$$C = \frac{P_t G^2 \lambda^2 \sigma R\theta_B \frac{CT}{2} \sec \psi}{(4\pi)^3 R^4 R^3}$$

ASSUME  $C \gg \text{NOISE}$

$$\frac{S}{C} = \frac{\sigma_t}{\sigma^0 R\theta_B \frac{CT}{2} \sec \psi}$$

$$\rightarrow P_{MAX} = \frac{\sigma_t}{\sigma^0 \theta_B \frac{CT}{2} \sec \psi \left( \frac{S}{C} \right)_{min}}$$

MAXIMUM RADIATION FOR POINT SOURCE IN SURFACE CLUTTER,



### COMPOSITE ROUGH SURFACE

FIGURE 3. COMPOSITE SURFACE MODEL

- DOUBLE THE POWER, NO CHANGE
- HALF THE POWER, NO CHANGE.
- DOUBLE THE PULSE WIDTH, HALF THE RANGE  
(OPPOSITE OF NORMAL CASE)

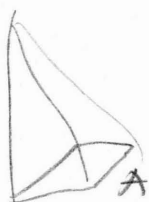
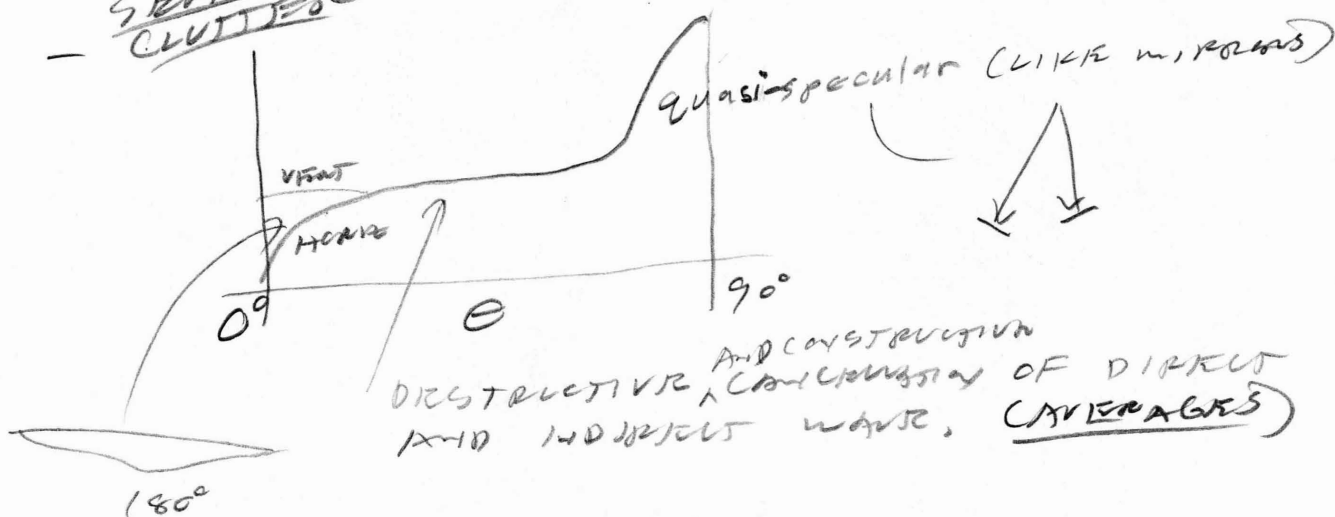
$\therefore$  WANT NARROW BEAM WIDTH  
+ NARROW PULSE WIDTH

- <sup>CHANGE</sup> n PULSES, NOTHING HAPPENS
- IF DECORRELATE CLUSTERS (CHG. POSITION, ETC.)  
WOULD HELP WITH n PULSES.
- ALTIMETER



WANT  
 $R^2 \sigma \rho_B$

- SEA CLUTTER (EASIER TO ANALYZE THAN LAND CLUTTER)



$$\sigma = \frac{4\pi A^2}{\lambda^2}$$

$$\text{LET } \lambda = 9.1$$

$$\therefore \sigma = 10^3 A$$

RADAR CROSS SECTION  $\gg$  PHYSICAL

distribution. Sea clutter is not always described by such a distribution so that other detection criteria are indicated.

STC (Sensitivity Time Control)

Log FTC--Logarithmic receiver characteristic followed by a high pass filter.

IAGC (Instantaneous Automatic Gain Control)

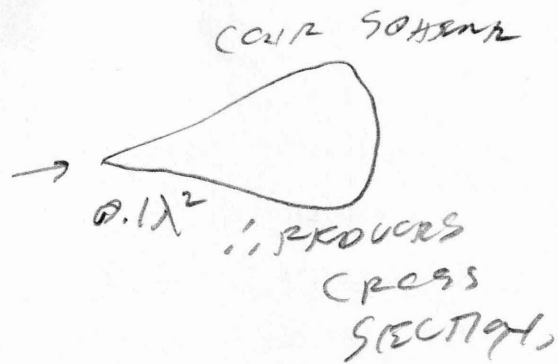
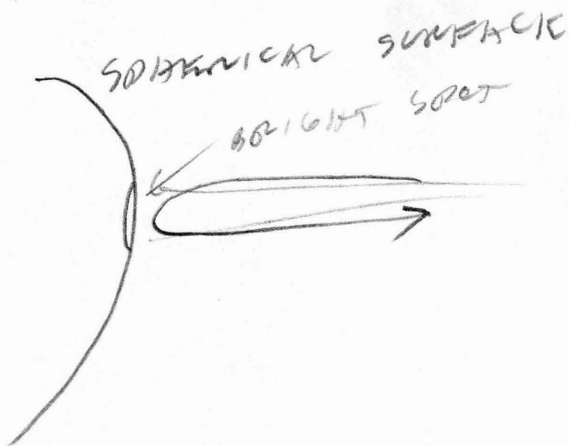
Pulse Width Discrimination--Clips pulses due to extended targets.

Automatic Video Thresholding--A form of constant false alarm rate (CFAR) receiver for clutter.

The basic desire in designing a radar to see targets in clutter is to increase the ratio of target-signal-to-clutter power. A method that reduces clutter in of itself is not necessarily desirable if target signal is reduced as well. (A trivial example is the raising of the antenna beam over the water. The sea echo is reduced, but so is the echo from any other surface target. A clutter fence would have the same effect.) Some of the above techniques do improve the target-to-clutter ratio, and some do not. Those that do not are generally used to prevent the receiver or the display from saturating. In the presence of large distributed clutter echoes, the receiver might be saturated and not allow the detection of desired point-targets even though they were much greater than the clutter. Methods for automatically "turning down the gain" or maintaining the false alarm rate constant are used to maintain the performance of the radar even though they offer no "subclutter visibility" or improvement in target-to-clutter ratio.

#### Remote Sensing of Sea Conditions by Radar

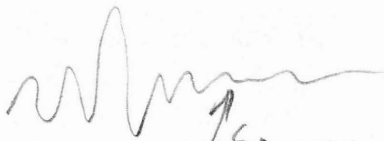
Several methods have been proposed or have been used to measure by use or radar techniques the condition of the sea. Some of these methods attempt



SPHERICAL	$A = 1m^2$	$\lambda = 0.1m$
FLAT PLATE	$\frac{4\pi A^2}{\lambda^2}$	$\frac{6}{1m^2}$
CONE SECTION	$0.1\lambda^2$	$10^3m^2$
		$10^{-3}m^2$

$\left. \begin{matrix} 10^3m^2 \\ 10^{-3}m^2 \end{matrix} \right\} 10^6 \text{ DIFFERENCE}$

## SEA CLUTTER



↑ SHOR WAVE CAPILLARY WAVES



COMPOSITE ROUGH SURFACE,

DEBRIS

USE SHORT PULSES + NARROW BEAMWIDTHS.

BUT STILL DOES NOT EXPLAIN LOSSES,

1. RUSSIANS BELIEVE SPRAY.

OR 2. WHITE FOAM

3. DISCONTINUITY BEFORE BREAKING WAVE,



to determine the sea state, or average wave height, but some can provide much more information. These methods may be classified as follows:

- a) Scatterometer--which measures the curve of  $\sigma^0$  vs angle and infers by such a measurement the state of the sea, Fig. 4.
- b) Precision altimetry--By observing the sea at normal incidence with a very short pulse the surface roughness, and therefore the sea state, can be deduced from the smearing of the echo pulse.
- c) HF doppler radar--The doppler spectrum of an HF radar echo from the sea yields information on the magnitude and direction of the wind at sea. This is described in the attached reprint from ONR Reviews.
- d) Imaging radar--Mapping of the wave patterns with high resolution sidelooking radar can allow the determination of the sea spectrum.

Other techniques that might be considered include polarization ratios, critical angle determination, absolute measurement of  $\sigma^0$  at normal incidence, and variation of  $\sigma^0$  with frequency to determine the crossover from diffuse to specular reflection.

#### Land Clutter

The radar echo from land clutter is more difficult to deal with than sea clutter, both in theory and in practice. The echo from land is much larger than from the sea by an order of magnitude or more. In addition, it is more difficult to quantify and classify the nature of land echo. The echo from land depends upon the type of terrain and its composition. Desert, forests, vegetation, bare soil, cultivated fields, cities, roads, lakes, and mountains all have different scattering characteristics. Furthermore, the echo will depend upon the stage of growth of any vegetation and the moisture content. A snow cover can also change the scattering. By contrast, sea

- LAND CLUTTER CROSS SECTION GREATER THAN THAT FOR WASTELAND AT LOW GROUND ANGLES. (OPPOSITE AT VERTICAL)
- LAND MORE LOSS BECAUSE OF ABSORPTION.

CLUTTER IS DEPENDENT ON ANTENNA GAIN.

GROUND ECHO IS HARD TO ANTICIPATE!!

## WEATHER CLUTTER

- VOLUMETRIC

RADAR METEOROLOGY

SER. 13.5 pp. 498-592

[SER DERIVATION]

ELLIPTICAL  $\therefore \frac{\pi}{4}$  FACTOR

GAUSSIAN BEAM  $\therefore \div 2 \ln 2$

~~$$G = \frac{4\pi}{\theta_H \theta_V}$$~~

$$G = \frac{\pi^2}{\theta_H \theta_V} \text{ more ACCURATE}$$

$R D^6 \therefore$  LARGE PRODUCTS ONLY AFFECT REFLECTIVITY.

$$\sum_i D^6 = a r^6 = 200 r^{1.6} \text{ TYPICAL.}$$

$$\overline{P_r} = \frac{2.486 \pi r^{1.6}}{R^2 \lambda^2} \times 10^{-8}$$

(mm/hr)

$$\eta = 17 f^4 r^{1.6} \times 10^{-12}$$

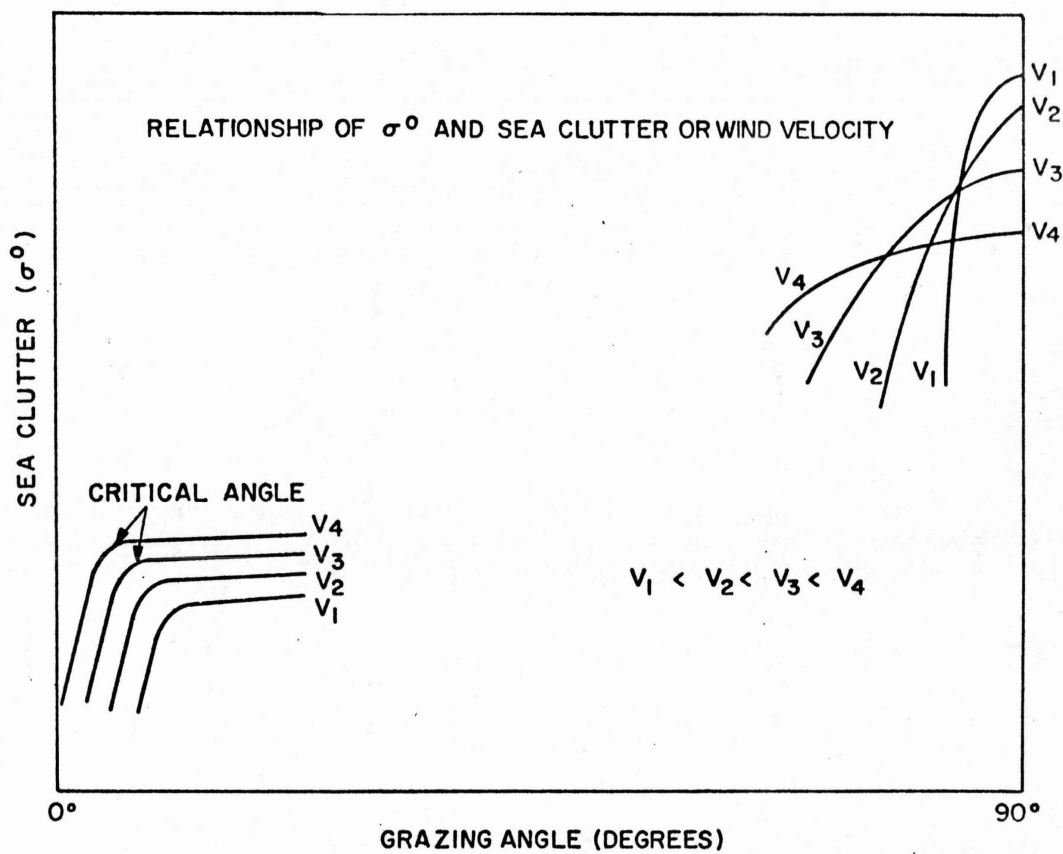
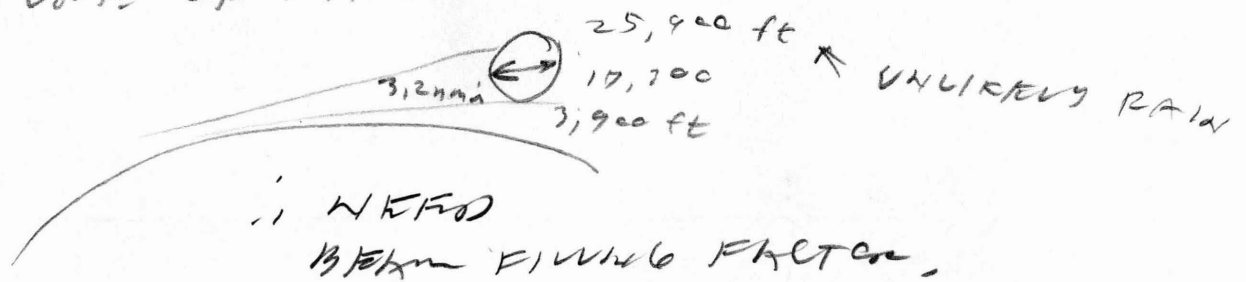


Fig. 4 Relationship of  $\sigma^0$  and wind speed, or sea clutter.

- BUT RAIN IS NOT UNIFORM, ESPECIALLY WITH ALTITUDE.

- CURVATURE OF EARTH



- CLEAR AIR (ANGELS)

1. POINT (BIRDS OR INSECTS)
2. DISTRIBUTED (CLEAR AIR TURBULENCE)

$$R^4 = \frac{\sigma}{\sigma_0}$$

$$R_{MAX} = \frac{\sigma_0}{\sigma_0 \theta_B \frac{1}{2} \sec^2 \phi (S/C)_{min}}$$

∴ cross section more important with clutter.

### TECHNIQUES TO SEEK TARGETS IN CLUTTER

1. MOVING TARGET INDICATOR
2. DOPPLER (CW)
3. PULSE DOPPLER
4. POLARIZATION (USE CIRCULAR) ( $W^x, S^{\text{ca}}$ )
5. BEAM WIDTH  $\theta_B$ , PULSE WIDTH  $\tau$  (ALL)
6. FREQUENCY ( $W^x, S^{\text{ca}}$ )

echo is much more uniform. The radar echo from the sea in the North Atlantic is not that much different from the sea in the South Pacific under the same wind and fetch conditions. Although our knowledge of radar sea echo is far from complete, it is in better shape than our knowledge of land echo. Fig. 5 illustrates the diverse nature of radar echo from various land surfaces.

#### Weather Clutter

Weather clutter, just as was the case for sea clutter, is of interest for the information it can provide about weather<sup>h</sup> phenomena as well as be an impediment to the detection of desired targets. Many of the techniques for improving the detection of targets in sea clutter apply to weather clutter. One of the most effective is the reduction of frequency. Since the clutter echo is proportional to the fourth power of the frequency, significant benefit is obtained in operating at lower frequency. For example, the radar reflectivity of rain at 1250 MHz (L band) is 35 db less than that at 9375 MHz (X band). Thus the lower the frequency, the less concern about weather effects.

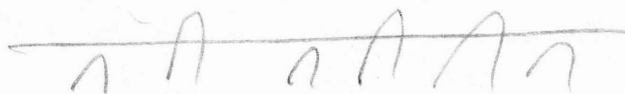
When radars must operate at the higher microwave frequencies where rain echo is large, the adverse effects of rain can be mitigated by use of circular polarization and by high resolution in range and angle. The use of circular polarization takes advantage of the fact that raindrops are symmetrical (spherical) while most targets of interest, like aircraft, are not.

Radar is of interest as a sensor of weather effects and it has been widely used for this purpose. It is in everyday use to aid meteorologists in monitoring rain and storm conditions; and it has been employed for measurement of precipitation, the study of the physics of clouds, tornadoes,

DOES NOT IMPROVE  
S/C

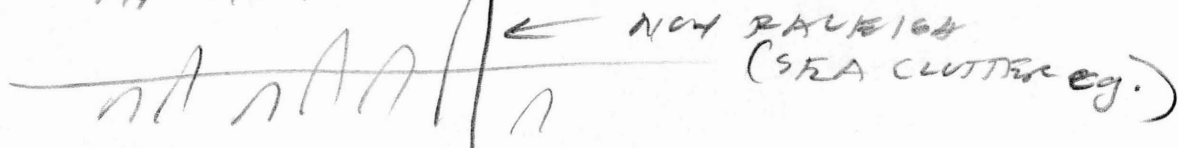
7. IN OUT OF A  
CLUTTER

IN HITS CLUTTER  
IN HITS TARGET



IN OUT OF A DETECTION.

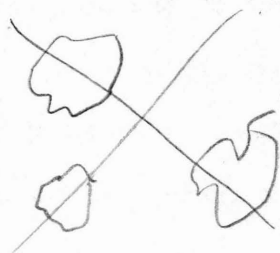
BETTER THAN CONVENTIONAL  
IN NON-STATISTICAL



NON RAYLEIGH  
(SEA CLUTTER eg.)

8. LOGARITHMIC DETECTION ALSO HELPS  
WITH SEA CLUTTER

9. INTERCLUTTER VISIBILITY  
LAND CLUTTER



PATCHY  
INTERCLUTTER VISIBILITY  
CAN SEE  
 $\therefore$  IN PROVES CLUTTER.

10. ANTENNA SCAN RATE (SEA)

20 rpm 60 hits  
600 rpm 2 hits

SEA CLUTTER UNCORRELATED WITH  
FASTEN SCAN RATE.

$\therefore$  INTEGRATION IMPROVEMENT.

HORIZONTAL POLARIZATION NOISE  
WITH SEA CLUTTER.

11. FREQUENCY AGILITY (W, L)

$df = \frac{1}{\text{PULSE WIDTH}}$   $\therefore$  RELATIVE PHASES  
1 MHz 1 ms CANCEL,

SCOPK LOOKS SMOOTHER WITH CLUTTER IN  
SEA CLUTTER, NOT LAND (ALREADY  
DECORRELATED)



hurricanes, and clear air turbulence.

The basis for the use of radar as a measuring tool for precipitation is the radar equation:

$$P_r = \frac{P_t G^2 \lambda^2 \sigma}{(4\pi)^3 R^4}$$

where  $P_r$  = received power,  $P_t$  = peak power of transmitter,  $G$  = antenna gain,  $\lambda$  = radar wavelength,  $\sigma$  = target cross section, and  $R$  = range. Since rain and other hydrometeors are volumetric targets, the target cross section  $\sigma$  will depend on the volume of clutter illuminated. It is therefore convenient to express the scattering properties of rain on a per-unit-volume basis. Thus we write

$$\sigma = \frac{\pi}{4} (R\theta_B) (R\phi_B) (c\tau/\lambda) \sum_i \bar{\sigma}_i$$

where  $\theta_B$  and  $\phi_B$  are the half-power beamwidths of the radar antenna in the azimuth and elevation planes,  $(c\tau/2)$  is the width of the resolution cell in range when the pulse width is  $\tau$ ,  $c$  is the velocity of propagation,  $\bar{\sigma}_i$  is the radar cross section of the individual precipitation particles, and the summation is taken over a unit volume. With this definition, and using the relationship  $G = 4\pi A_e/\lambda^2$  between the antenna gain  $G$  and the effective area  $A_e$  to eliminate one of the  $G$ 's in the radar equation, and noting that  $G = 4\pi/\theta_B\phi_B$  to eliminate the other, we get

$$\bar{P}_r = \frac{P_t A_e h}{32 R^2} \sum_i \bar{\sigma}_i$$

In this equation the bar over the received signal power signifies the average value. We have also substituted  $h = c\tau$ , a practice common among radar

- FENCE DOES NOT HELP WITH LOW ANGULAR TARGETS.

12. - CLUTTER FENCE (TILTED)

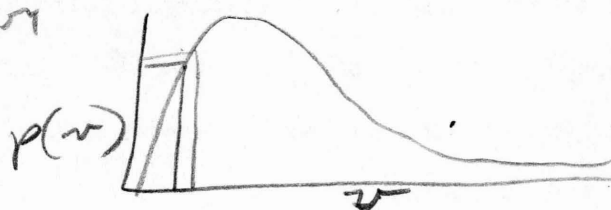
13. S.T.C. SENSITIVITY TIME CONTROL.  
(DOES NOT IMPROVE S/C)

10. LOG F.T.C.,

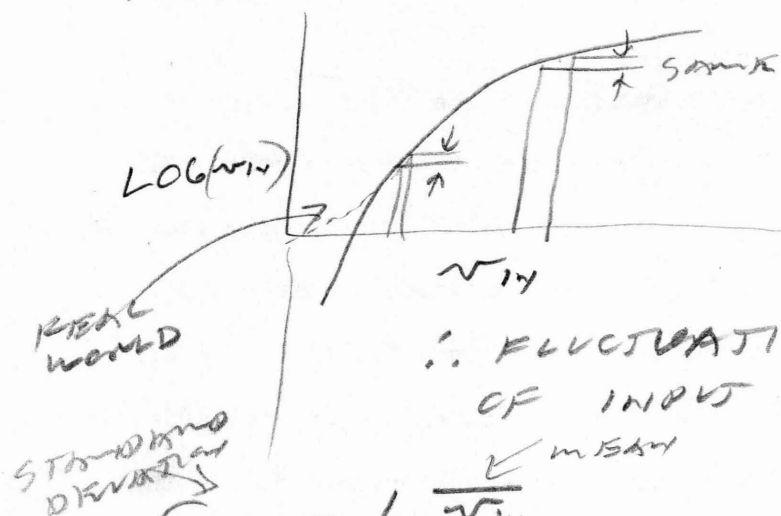
RAYLEIGH CLUTTER pp 506-507

PROBABILITY

$$p(v) = \frac{2v}{\sigma^2} e^{-\frac{v^2}{\sigma^2}}$$



AMPLITUDE OF FLUCTUATION ABOUT MEAN IS PROPORTIONAL TO MEAN.



∴ FLUCTUATION IS INDEPENDENT OF INPUT LEVEL.

$$\sigma_{v_{in}} = b \sqrt{v_{in}}$$

$$v_{out} = a \log v_{in}$$

$$\text{slope } \frac{\Delta v_{out}}{\Delta v_{in}} = \frac{a}{v_{in}}$$

$$\text{@ } \sqrt{v_{in}}, \text{ SLOPE } \frac{\Delta v_{out}}{\Delta v_{in}} = \frac{a}{\sqrt{v_{in}}}$$

$$\sigma_{v_{out}} = \sigma_{v_{in}} \times \text{SLOPE}$$

$$= \sigma_{v_{in}} \times \frac{1}{\sqrt{v_{in}}} = ab$$

= CONSTANT

meteorologists (but not widely used by other radar engineers).

Since precipitation particles are almost always much smaller than the radar wavelength, the cross section can be expressed by the Rayleigh formula

$$\sigma_c = \pi^5 D^6 |K|^2 / \lambda^4$$

Substituting into the previous radar equation, we get,

$$\bar{P}_r = \frac{\pi^5 P_t A_e h}{32 R^2 \lambda^4} |K|^2 \sum_c D^6$$

The factor  $|K|^2$  depends on the dielectric constant of the scatterers. For ice at all temperatures and microwave frequencies  $|K|^2 = 0.197$ . The value for water varies with temperature and frequency. (It can be found in a number of sources.) As an example  $|K|^2 = 0.93$ , for water at  $10^\circ\text{C}$  and a wavelength of 10 cm. The difference in the value of  $|K|^2$  for ice and water is one reason that radar operation is degraded less in snow than in rain.

Radar meteorologists define

$$Z = \sum_c D^6$$

There is a relationship between  $Z$  and the rainfall rate  $r$ , of the following form:

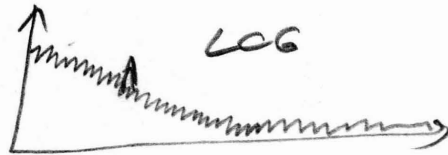
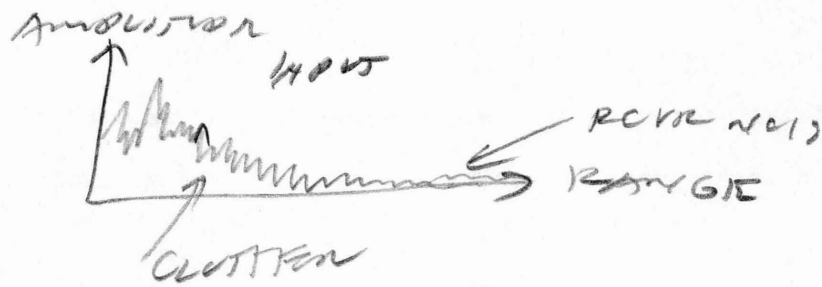
$$Z = ar^b$$

where  $a$ ,  $b$  are empirically determined constants. There is much variability in the values of these constants, but a commonly used relation is

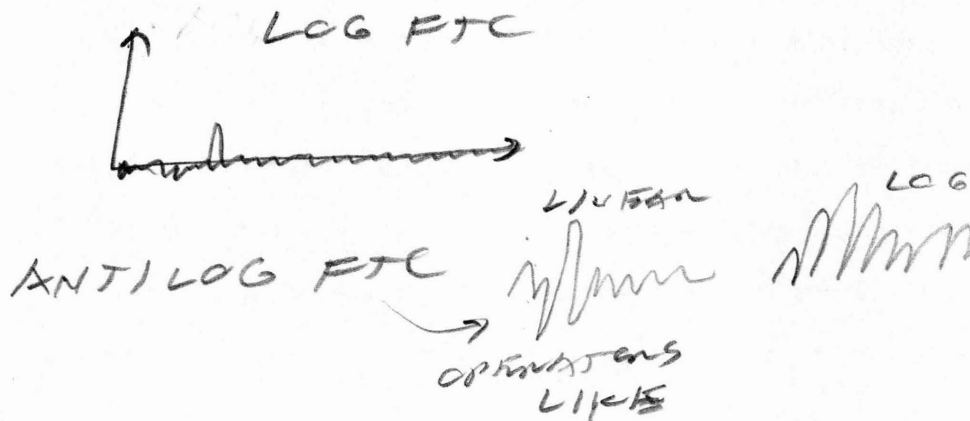
$$Z = 200 r^{1.6}$$

where  $Z$  is in  $\text{mm}^6/\text{m}^3$  and  $r$  is in  $\text{mm/hr}$ . The radar equation for rain is then

1. FLUCTUATION IS INDEPENDENT OF LEVEL



$\log FTC \Rightarrow \log \text{FAST TIME CONSTANT}$



$$\bar{r} = \frac{\pi^5 F_t A_e h}{32 R^2 \lambda^4} \quad 0.93 \times 2 \times 10^{-16} r^{1.6}$$

For snow the corresponding relationship between Z and r is

$$Z = 2000r^2$$

where r now refers to the precipitation rate based on the equivalent water content of melted snow.

#### Detection of Targets in Weather

Many of the techniques mentioned previously for aiding the detection of targets in sea clutter apply as well to weather clutter. A short pulse and narrow beamwidth will reduce the amount of clutter with which the target must compete. A log-FTC receiver, AVT or IAGC can provide some relief, but do not provide subclutter visibility. The usual MTI is not as effective as one might like. Circular polarization provides an improvement in target-to-clutter ratio, but the biggest reduction occurs by employing lower frequencies.

#### Applications of Weather Radar

The use of radar as a means to study and measure the effects of weather represents an important application. The uses of radar in this regard include:

- Routine observation of storms and precipitation
- Hurricane tracking
- Quantitative measurement of precipitation
- Airborne weather avoidance
- Meteorological research

Angels

Radar echoes obtained from regions of the atmosphere where no "apparent" reflecting sources exist have been called ghosts or angels. Such echoes can, for the most part, be explained as one of the following: birds, insects, weather fronts, layered clear air turbulence, convective bubbles, second-time-around echoes, or lightning. The use of radar for the detection of clear air turbulence has been of recent interest. Although radar can detect CAT, it is probably uneconomical to do so on the basis of what is currently known. It should also be mentioned that birds can provide extensive clutter in an air surveillance radar and can limit the capability of a radar to detect targets just as can land or rain clutter. The elimination of clutter due to birds is not always an easy task, but STC can be of help.



Table 1\*  
**BEAUFORT SCALE**  
**WITH CORRESPONDING SEA STATE CODES**

Beaufort number	Wind speed				Seaman's term	World Meteorological Organization (1964)	Estimating wind speed		Hydrographic Office		World Meteorological Organization	
	knots	mph	meters per second	km per hour			Effects observed at sea	Effects observed on land	Term and height of waves, in feet	Code	Term and height of waves, in feet	Code
0	under 1	under 1	0.0-0.2	under 1	Calm	Calm	Sea like mirror.	Calm; smoke rises vertically.	Calm, 0	0	Calm, glassy, 0	0
1	1-3	1-3	0.3-1.5	1-5	Light air	Light air	Ripples with appearance of scales; no foam crests.	Smoke drift indicates wind direction; vanes do not move.	Smooth, less than 1	1	Calm, rippled, 0-14	1
2	4-6	4-7	1.6-3.3	6-11	Light breeze	Light breeze	Small wavelets; crests of glassy appearance, not breaking.	Wind felt on face; leaves rustle, vanes begin to move.	Slight, 1-3	2	Calm, rippled, 15-135	2
3	7-10	8-12	3.4-5.4	12-19	Gentle breeze	Gentle breeze	Large wavelets; crests begin to break; scattered whitecaps.	Leaves, small twigs in constant motion; light flags extended.	Moderate, 3-6	3	Slight, 2-4	3
4	11-16	13-18	5.5-7.9	20-28	Moderate breeze	Moderate breeze	Small waves, becoming longer; numerous whitecaps.	Dust, leaves, and loose paper raised up; small branches move.				
5	17-21	19-24	8.0-10.7	29-38	Fresh breeze	Fresh breeze	Moderate waves, taking longer form; many whitecaps; some spray.	Small trees in leaf begin to sway.				
6	22-27	25-31	10.8-13.8	39-49	Strong breeze	Strong breeze	Larger waves forming; whitecaps everywhere; more spray.	Larger branches of trees in motion; whistling heard in wires.				
7	28-33	32-38	13.9-17.1	50-61	Moderate gale	Near gale	Sea heaps up; white foam from breaking waves begins to be blown in streaks.	Whole trees in motion; resistance felt in walking against wind.				
8	34-40	39-46	17.2-20.7	62-74	Fresh gale	Gale	Moderately high waves of greater length; edges of crests begin to break into spindrift; foam is blown in well-marked streaks.	Twigs and small branches broken off trees; progress generally impeded.				
9	41-47	47-54	20.8-24.4	75-88	Strong gale	Strong gale	High waves; sea begins to roll; dense streaks of foam; spray may reduce visibility.	Slight structural damage occurs; slate blown from roofs.				
10	48-55	55-63	24.5-28.4	89-102	Whole gale	Storm	Very high waves with overhanging crests; sea takes white appearance as foam is blown in very dense streaks; rolling is heavy and visibility reduced.	Seldom experienced on land; trees broken or uprooted; considerable structural damage occurs.				
11	56-63	64-72	28.5-32.6	103-117	Storm	Violent storm	Exceptionally high waves; sea covered with white foam patches; visibility still more reduced.					
12	64-71	73-82	32.7-36.9	118-133								
13	72-80	83-92	37.0-41.4	134-149								
14	81-89	93-103	41.5-46.1	150-166								
15	90-99	104-114	46.2-50.9	167-183								
16	100-109	115-125	51.0-56.0	184-201								
17	109-115	126-136	56.1-61.2	202-220	Hurricane	Hurricane	Air filled with foam; sea completely white with driving spray; visibility greatly reduced.	Very rarely experienced on land; usually accompanied by widespread damage.				
									Confused	9	Phenomenal, over 45	9

Note: Since January 1, 1955, weather map symbols have been based upon wind speed in knots, at five-knot intervals, rather than upon Beaufort number.

\*From Bowditch, "American Practical Navigator," U.S. Navy Hydrographic Office H.O. Pub. No. 9, 1968. Appendix R.

## Rain Model

There does not exist any generally agreed upon model for a rain storm. The radar scattering characteristics of uniform rain of any particular rainfall rate are well known, but actual storms are not uniform. They contain cells of more intense rain than the surroundings and the mean intensity of rainfall decreases with increasing altitude. Also, intense storms generally occur at lower altitudes and have a smaller extent than less severe storms. The problem is further complicated by the different scattering properties of rain and of the ice particles found at the higher altitudes in storm clouds.

The model for rain that will be assumed here is based on that given by Edgar et al,<sup>1</sup> as modified. For the design of surveillance radars they assume the precipitation rate of rain to be uniform throughout the affected volume and that the volume affected by rain varies with the precipitation rate as follows:

PRECIPITATION RATE	DIAMETER	CEILING	DURATION
2mm/hour	300km	4km	13 hours
4	45	4	5.0
8	35	8	1.8
16	20	8	0.6
32	8	8	0.2
64	1	8	0.06

(The "duration" is the maximum duration to be expected at any one place with a frequency of once per year. Its value

---

1. A.K. Edgar, E.J. Dodsworth and M.P. Warden, "The Design of a Modern Surveillance Radar," International Conference on Radar - Present and Future, 23-25 Oct. 1973, IEE Conference Publication No 105, pp 8-13.

will vary with location.) The radar reflectivity of rain when linear polarization is used is given by

$$\eta = 7.0 \times 10^{-48} \times f^4 \times r^{1.6} \quad \text{m}^2/\text{m}^3 \quad (1)$$

where  $f$  is the radar frequency in Hz and  $r$  is the precipitation rate in mm/hour. The apparent reflectivity when using circular polarization will be less by about 15db.

The velocity spectrum of rain moving with the wind is also given by Edgar et al. This is important for the design of MTI and pulse doppler radars. They take the shape of the spectrum to be gaussian, centered on the wind velocity, with a standard deviation of

$$\sigma_v = [1 + (7.3 \times 10^{-3} \times k \times R \times \Phi_b)^2]^{1/2} \quad \text{m/sec} \quad (2)$$

where  $k$  is the wind-shear across the vertical beamwidth in m/sec/m,  $R$  is the range in meters, and  $\Phi_b$  is the vertical two-way half-power beamwidth in degrees. Nathanson<sup>2</sup> suggests that for radar calculations the value of  $k = 5.7 \times 10^{-3}$  m/sec/m be used for radars pointing in the direction consistent with that of the primary high-altitude winds.

The rain area as given above from the paper by Edgar et al differs from that given by Nathanson (Ref 2 p 197), which is

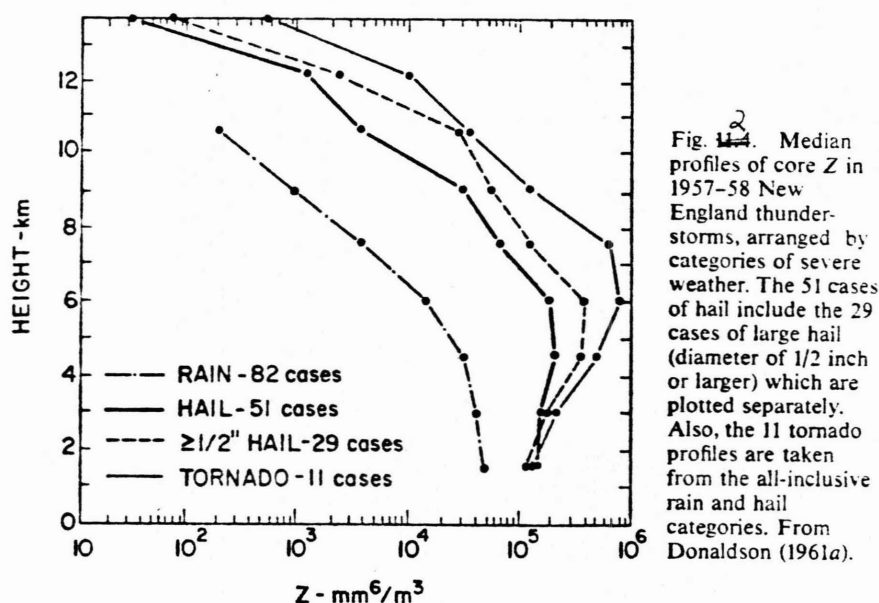
---

2. F.E. Nathanson, Radar Design Principles, McGraw-Hill Book Co., 1969, pp 206-209.

$$\text{diameter (n mi)} = 25.9 - 14.7 \log r \quad (3)$$

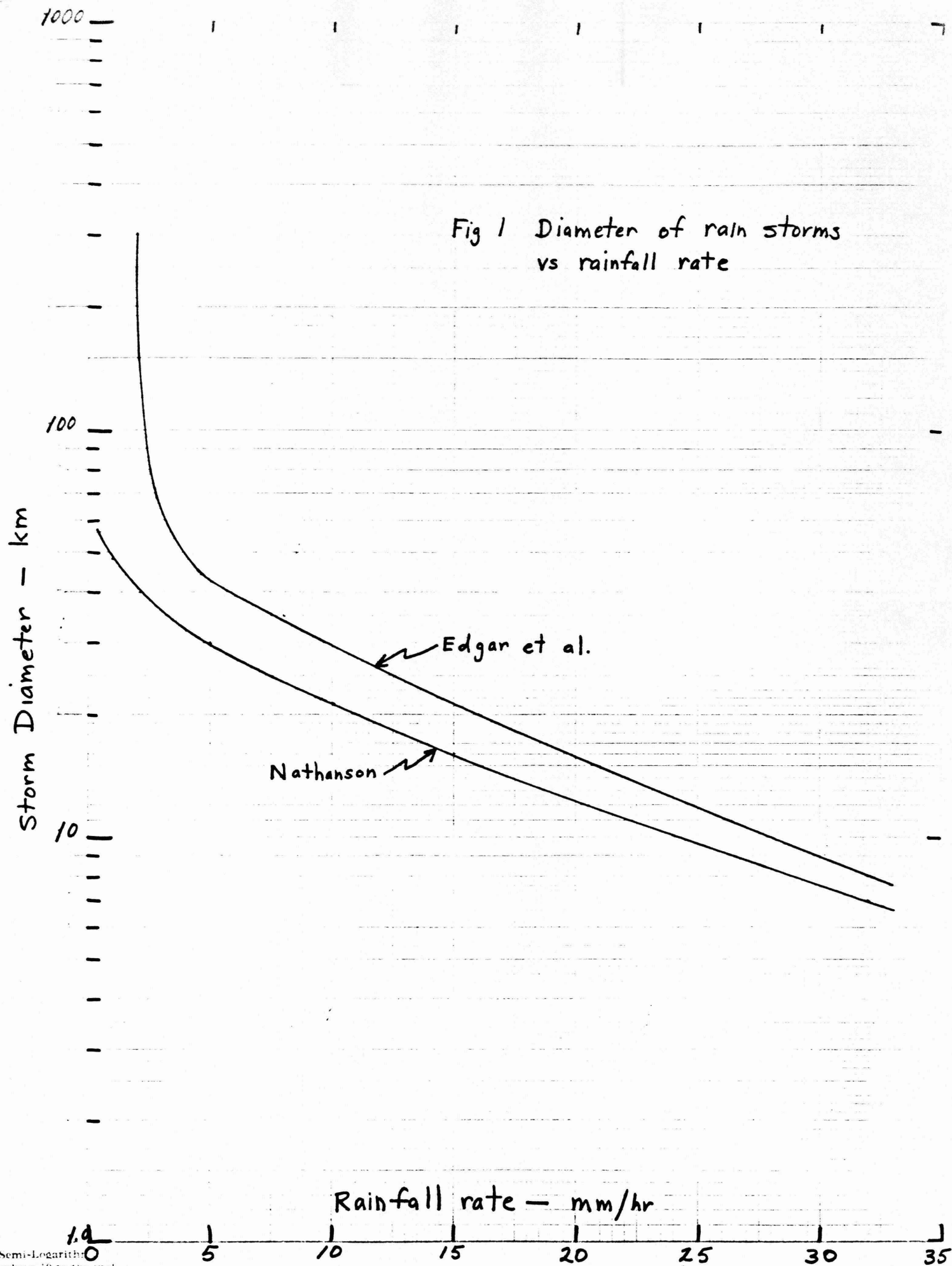
This is shown plotted in Fig. 1 along with the data of Ref 1. Nathanson's storm sizes are less than those of Edgar et al and deviates considerably at low rates of rainfall.

Figure 2, taken from Battan<sup>3</sup> plots the median profiles of  $Z$  in  $\text{mm}^6/\text{m}^3$  ( $Z=200r^{1.6}$ ) for New England thunderstorms. The heights here are different than in table I but are consistent for medium rain. Note



that an  $r$  of 4 mm/hr corresponds to a  $Z$  of  $1.7 \times 10^3$ , and  $r = 32$  mm/hr corresponds to  $Z = 5 \times 10^4$ .

3. L.J. Battan, Radar Observation of the Atmosphere, University of Chicago Press, Chicago, 1973, p 207.



Further questions relating to Sessions III and IV

1. What problems occur if the MTI radar is on a satellite?
2. Does a step-scan radar with MTI suffer a "scanning fluctuation"?
3. Does the digital MTI do something the "ideal" analog MTI does not?
4. Are there any other methods for improving the target-to-clutter ratio, in addition to high resolution, when the target and clutter are both stationary?
5. Would you expect  $\sigma^0$  for land clutter to decrease, increase, or remain constant as a function of grazing angle, at very low grazing angle?



## PULSE COMPRESSION

A PART OF "SIGNAL PROCESSING"  
WHY P.C.?

SHORT PULSE AND RESOLUTION  
ENERGY AND SENSITIVITY  
LOTS OF BOTH

BASIC THEORY

SPECTRUM OF A PULSE

EXAMPLES OF P.C.

FM - LUMPED CONSTANT  
- DISPENSIVE

PHASE CODING; BARKER CODES

DEFINITION: MATCHED FILTER

RANGE SIDELOBES - WEIGHTING

DOPPLER EFFECTS

DEFINITION: T.B.

P.C. RATIO

PROCESSING "GAIN"

AMBIGUITY.

OUTLINE

## I. SIGNAL PROCESSING

- USER INTERFACE (IN GENERAL)

A. - PRE-DETECTION

B. - POST DETECTION

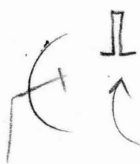
A. PRE-DETECTION

1. AMPLITUDE + PHASE

∴ COHERENT (PULSE COMPRESSION, E.G.)  
(USUALLY FIRST IF.)

2. AMPLITUDE ONLY

∴ NON-COHERENT



X-X



SHORT PULSE

CAN DISTINGUISH CLOSER TARGETS

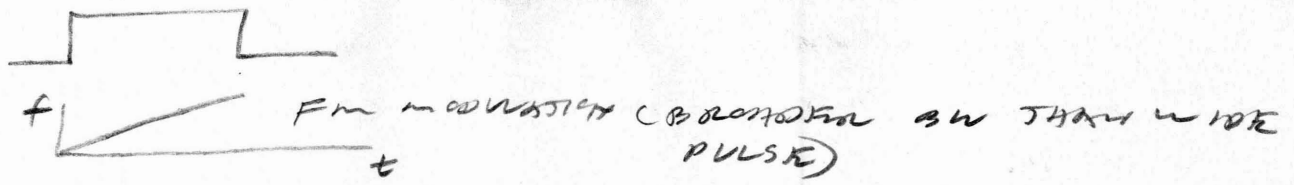
∴ BETTER RANGE RESOLUTION, BUT WEAK.

PRF POWER HAS BREAKDOWN LIMITATIONS

∴ HAD TO LIMIT RANGE RESOLUTION.

BUT BANDWIDTH HIGH PRF,

CONSTITUENTS CAUSE RESOLUTION.



SUPERPOSITION  $\Rightarrow$   $\Delta$  PCM

## SESSION V

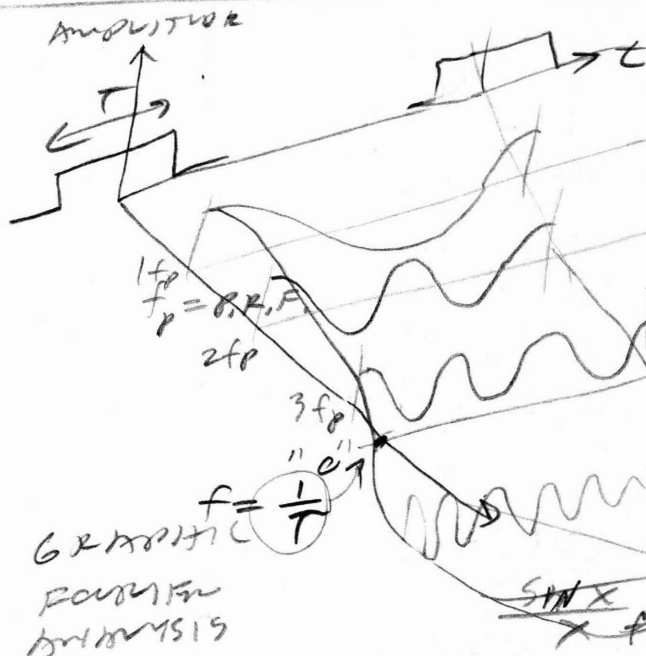
### PULSE COMPRESSION

#### TRACKING WITH SURVEILLANCE RADAR

#### -- AUTOMATIC DETECTION AND TRACKING

ROBERT T. HILL

#### SPECTRUM OF PULSE



FIRST  $\approx$  APPROXIMATELY  
SNR MAX = BW LIMITED  
PULSE WIDTH

CONTRIBUTION

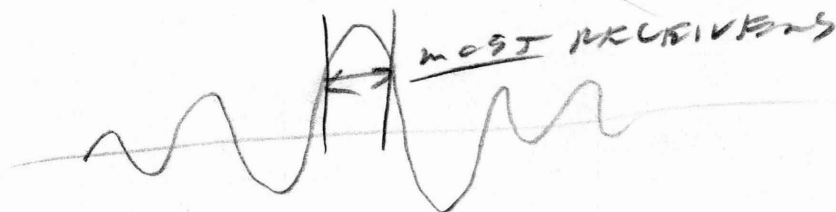
IS ANALYSIS FREQUENCY SPECTRUM, IN CO. F. C. V. E. F. M.  
REMOVED THE FUNCTION APPROX. OF PULSE SPECTRUM.  
RECTANGULAR PULSE  $\Rightarrow$   $\frac{\sin x}{x}$  PULSE SPECTRUM

IF  $T$  IS VERY SMALL,  $\infty$  PEAKS OF  $\infty$  COMBINATION.  $\therefore$  CONTINUOUS CHAIN OF IMPULSES.

IF  $T$  IS  $\infty$  SMALL,  $\infty$  FLAT SPECTRUM. (CONTINUUM)

NARROW PULSES HAVE BROAD SPECTRA  
WIDE PULSES HAVE NARROW SPECTRA  
CW PULSER HAVE 1 CARRIER

SEMI-RE PULSER ( $\pm$  PULSER WIDTH =  $\pm$  PERIOD)



$\therefore$  PERIODS  $\frac{1}{T} \approx \omega$

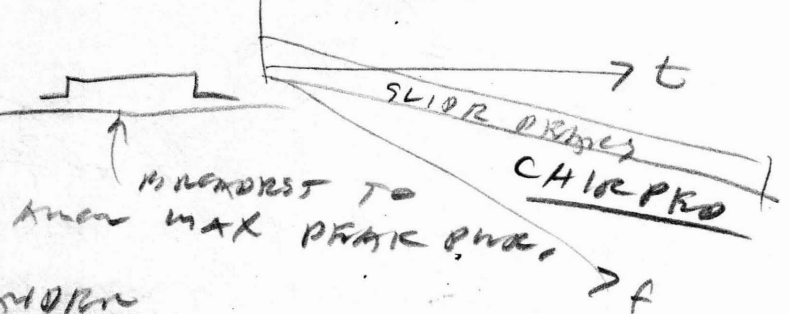
SOME PULSES USE  $(\frac{1,2}{T})$

EXAMPLE OF PULSER COMPRESSION:

NARROW  
PULSER



T  $\neq$  T AMPLITUDE



PULSER EXPANSION

(PULSER COMPRESSION IS OPPOSITE)

TYPICAL PULSE RX PATTERN RATIOS  $\Rightarrow 128:1$

CAN BUILD OVER RX PATTERN / PULSE COMPRESSOR  
IN ONE UNIT, DO AT 30 MHz IF, eg.  
MIX WITH 3000 S BAND SIGNAL.

$$\begin{array}{lcl} 30 + 3000 \text{ XMT } & = & 3030 \\ 3060 - 30 \text{ RCV } & = & 3030 \end{array} \left. \vphantom{\begin{array}{l} 30 + 3000 \\ 3060 - 30 \end{array}} \right\} \begin{array}{l} \text{USE SAME} \\ 30 \text{ MHz RX PATTERN /} \\ \text{COMPRESSOR.} \end{array}$$

Session V

A. PULSE COMPRESSION

B. TRACKING WITH SURVEILLANCE RADAR

- AUTOMATIC DETECTION AND TRACKING

A session on two subjects, a part of the course

RADAR SYSTEMS AND TECHNOLOGY

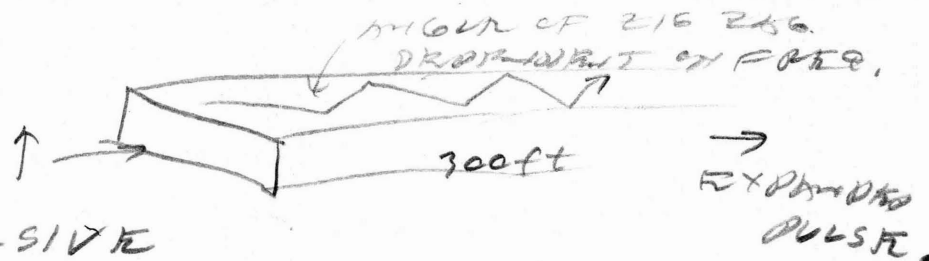
-203-

George Washington University, Washington D.C.

R. T. Hill

November 1978

WAVEGUIDE

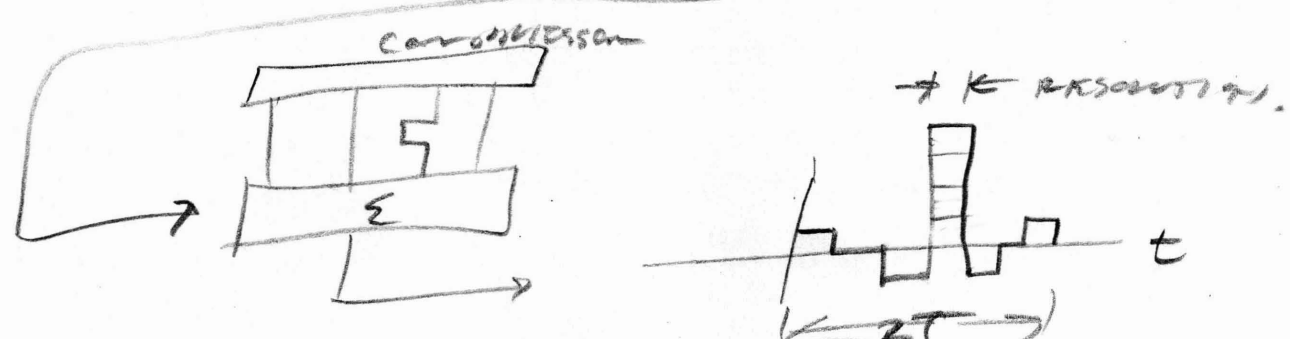
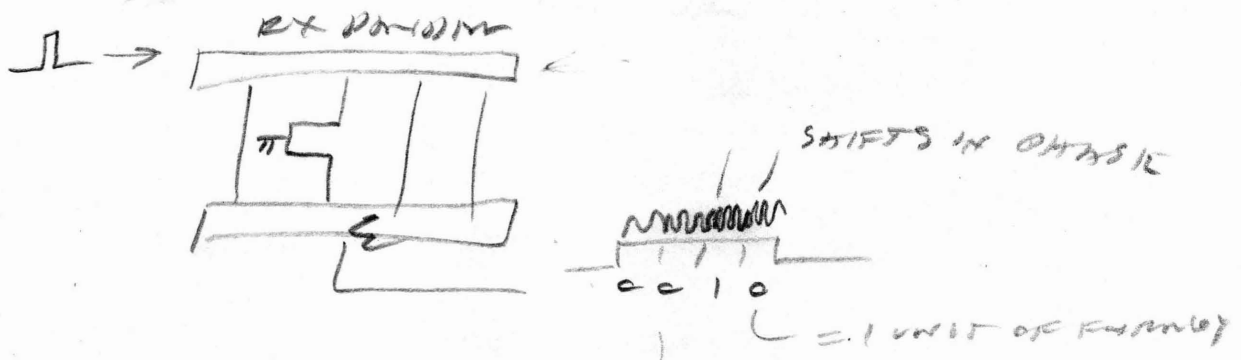
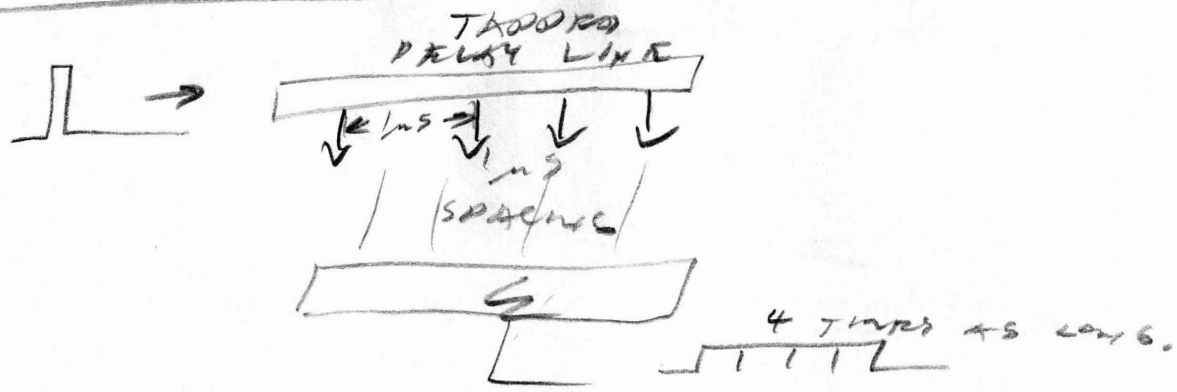


DISPENSIVE

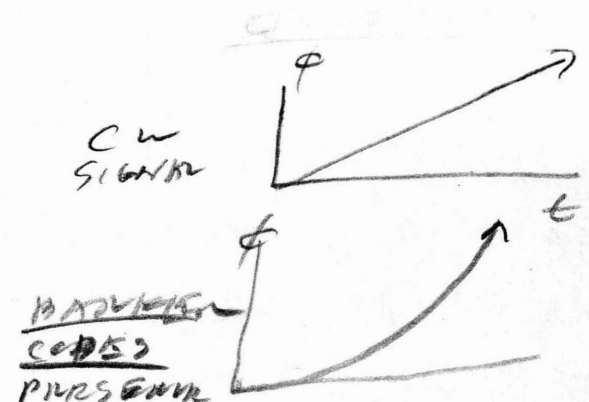
ACOUSTIC TRANSDUCERS WITH SAME  
WAY IN DIELECTRIC MEDIUM STRIP.

MIXED DISPENSIVE STRIPS NEXT  
RX PATTERN / COMPRESSOR  
FOR LINEAR F.M.

# PHASE CODING



SEVERAL COPIES THAT GIVE NO MORE THAN 40% SIDELOBES = MARKER CODES (13 MAX.)



INCREASING RATE OF CHANGE OF PHASE, VS. TIME.

## Session Overview

This session treats two important subjects in radar system technology - the first, an essential element of the greater subject "signal processing" and the second, a process that brings real utility to modern radars in a way not possible only a decade or so ago.

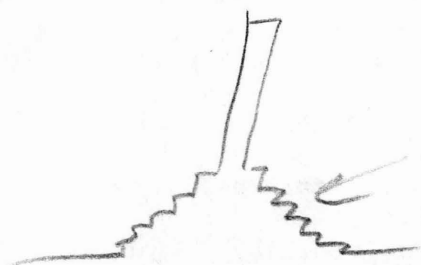
"Signal processing" is a term usually describing the treatment of the received signal in a radar prior to (and can include) the detection of the envelope of the radio signal in the receiver. Certainly the taking of signals from the antenna, the amplifying and mixing of them with radio signals used as a reference (as from a "local oscillator" to establish a convenient "intermediate frequency"), the treatment of successive returns (as in a Moving Target Indicator or in a signal "integrator" of some sort) all constitute a part of signal processing. When this processing involves attention to not only the amplitude of the signal at hand but also its phase we speak of it as "coherent"; when only the amplitude of the signal is important (as in some "video processing" following envelope detection), we speak of it as "noncoherent" signal processing. "Pulse compression" deals with the response of a radar to its particular signal (with attention to both amplitude and phase) and is, therefore, in the realm of "coherent signal processing". It is assumed in these notes that the other aspects of coherent signal processing are at least casually familiar to the student, or that he will have other access to them.

It is important for a modern surveillance radar to "finish the job"



- ACTUALLY HAVE BEEN BUILDING MATCHED FILTERS (MAXIMUM PEAK RESPONSE NOT REPRODUCTION) (CONJUGATE GIVES MAXIMUM PEAK OUTPUT)

- OTHER CONDS:



BUTTER SIDELOBES  
BUT RECEIVED  
HIGHLIGHTED

∴ LOSS OF SENSITIVITY.

CAN KEEP RINGING DOWN.

- MOVING TARGETS

IF MOVE 1 PULSER DISTANCE  
RETURN PULSER. ( $\frac{1}{2}\lambda$  WILL  
CANCEL)

PROBLEM WITH LONG PULSES (SLOWER  
TARGETS) ∴ STAGGER CODE  
PROGRESSION

of estimating the presence of reflecting bodies thought to be of interest to a user. The automatic detection and track features just now finding their way into radar systems generally treat the output of the envelope detector, well after pulse compression and the rest of coherent signal processing, to estimate reliably the presence and locations of targets that are of interest to the user, and to sustain these estimates (to form tracks) for the continued benefit of the user. Terms used to describe the process range from "noncoherent signal processing", "video processing", "threshold processing", "plot extraction" or "automatic target detection" where the presence and measured location of a target are concerned, to "data processing" or even "information processing" where the subsequent stages of track formation are concerned. We will be content with "Automatic Detection and Tracking" to embrace the whole process.

#### V. A. Pulse Compression

In this lecture, we will suggest why pulse compression is important in radar design, develop with some simple diagrams the basic theory, and illustrate, again with simple diagrams, the two basic types of pulse compression, namely frequency modulation ("linear f.m.-ing" or "chirping") and phase coding.

Why pulse compression? - While the earliest "radars" may not have used pulses, nonetheless it was quickly reasoned that a short pulse transmitted and a listening period to follow (one long enough to permit time for reflected returns from the greatest of reasonable target ranges) permitted an easy measurement of the range of reflecting bodies. Certainly such operation permitted one-antenna transmit and receive systems (duplexed radars) without fear of turning

the whole system into an oscillator! Very convenient.

It was also apparent that a very short pulse permitted the measurement of range to each of two separate but closely spaced targets, whereas a longer pulse would cause the separate reflections to overlap, denying the "resolution" of the two targets in the received signal. So, it could be argued, short pulses made a better radar.

Of course, it was also apparent that if one wanted to see small targets a long way away, one needed lots of electromagnetic energy in his pulse - one needed a strong signal.

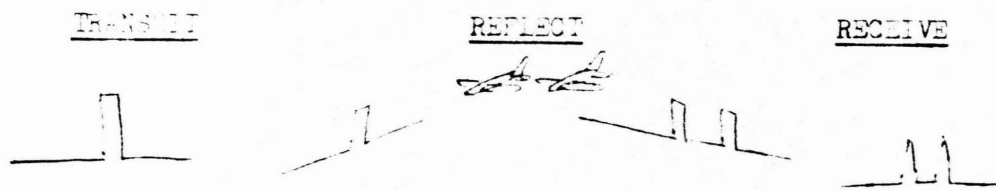
Fine - short pulse, lots of energy - go to high peak powers in the transmitted pulse.

However, as performance needs increased, the obvious limitations on peak power (waveguide and tube breakdown, arcing, for example) put a bound on this dimension. So the question was, how to get more energy per pulse without sacrificing the range resolution of a short pulse.

Then, more elegant examination of how receivers respond to signals showed that the resolution in range came not uniquely from the fact that the pulse was short in time, but rather from the fact that it had a broad spectrum of frequencies in its modulation. It's those high frequency constituents (or far out "sidebands") that shape the narrow pulse that would allow a receiver to distinguish the range-difference between two closely spaced returns. (To appreciate this more fully, a basic understanding of modulation theory is required - the next few paragraphs supply this.)

So, both a strong signal and good range resolution can be had simultaneously by using long pulses that keep the bandwidth of a much

narrower pulse and a receiver that will respond to that particular signal (that will "compress" the long but wide band pulse). Figure 1 restates this fundamental idea.

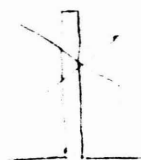


i.e. a very short pulse..

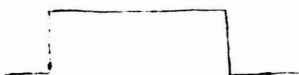
..allows reflections from  
two closely spaced targets...

..to be seen by  
the receiver..

BUT there's not much energy there, it gives a weak signal  
relative to receiver noise.



A stronger (higher peak power) pulse would do  
- but transmitter equipment may limit this  
dimension.



This is another strong signal (more energy)  
but the signal will "overlap" from the two  
targets

but, if there's a deliberate  
modulation on the pulse  
(as in this example)...

..then the reflections..

..may still be  
separated by a  
proper "pulse  
compression" receiver.

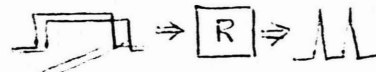
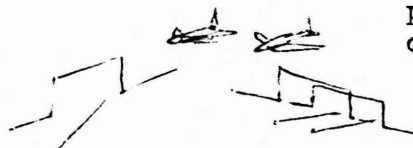
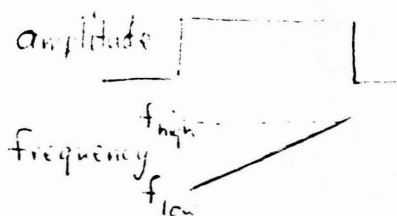


FIGURE 1 Pulse Compression Overview

The basic theory - spectrum of a pulse - It is not necessary to develop completely the relationships between a pulse and its spectrum, but a few relationships are essential. The diagram of Figure 2 reminds us of how a modulation envelope (which we will later apply to a carrier) is in fact "composed" of frequency constituents (which will be the "sidebands" on each side of the carrier when we so modulate the carrier).

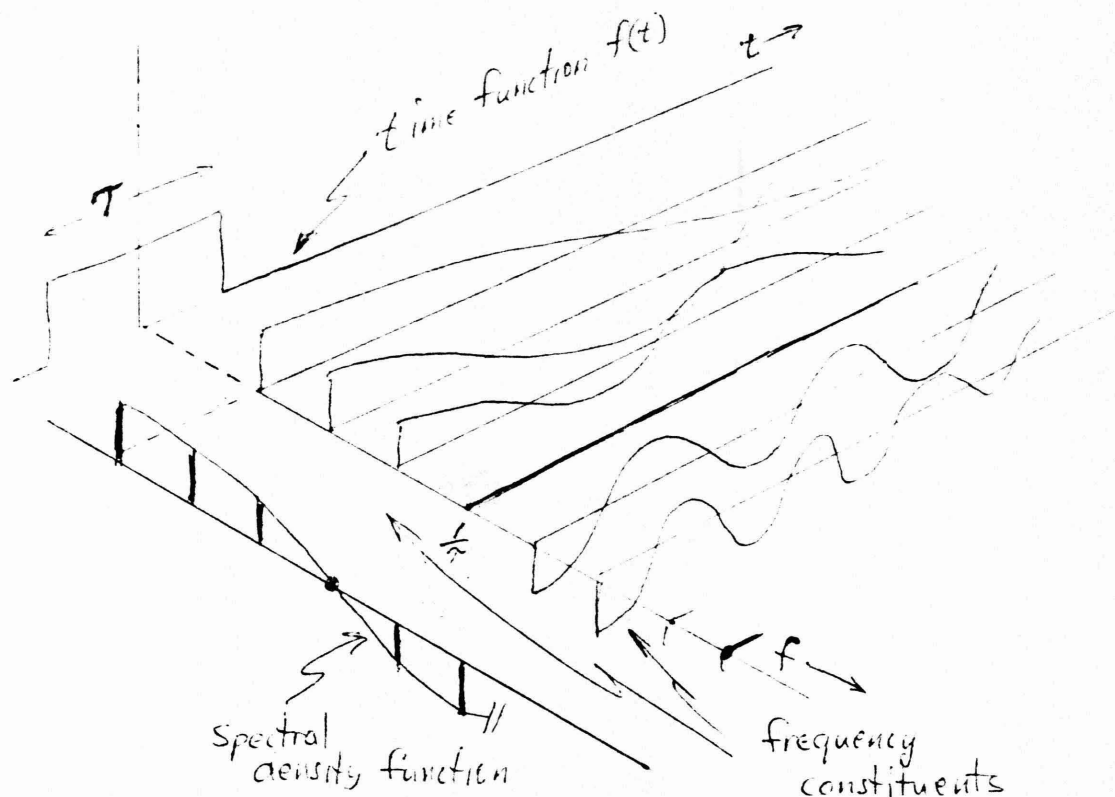


FIGURE 2 Spectrum of pulses

The student is reminded of a few fundamentals:

a) If the waveform  $f(t)$  is in fact a train of pulses, this "shaping" of the pulse we see in the figure must recur periodically to form the train - therefore that first sine wave we see must be of the pulse repetition frequency itself and each of the other constituents must be integral multiples of it, i.e. we have a line spectrum with the prf being the line spacing.

b) If the waveform  $f(t)$  consists of one pulse only on an infinite axis (unlike radar) we note the recurrence cannot be permitted, therefore all frequencies "in between" the lines of case a) above must be present, giving us the shaping here at  $t_0$  but never again - the spectrum of a single pulse is a continuum of frequency constituents.

c) If the pulse involved is particularly narrow in time, there must be higher-frequency constituents before the first spectral "zero crossing" shown to make it narrow. If it were particularly broad in time, the opposite is true - the spectrum is narrower. In fact, the zero crossing will be at a modulation frequency exactly the reciprocal of the pulse width.

The student should consider the nature of the spectrum of an infinitesimally narrow pulse, an impulse. And he should consider the other extreme: a single line of frequency being a continuous wave in time.

It may help the student to visualize in the framework of Figure 2 the frequency constituency of a train of pulses in which the pulse width equals one half the repetition frequency, so the spectral zero crossings



are at 2 prf, 4 prf, 6 prf, etc. and we have only odd frequency constituents, just as we should realize from

the elementary graphing above.

In our radar work, the student should remember that these spectra represent the modulation put on the r.f. carrier - so they are the sidebands on either side of that carrier in the complete spectral representation of the signal.

IMPORTANT - WIDE PULSES HAVE NARROW SPECTRA, NARROW PULSES HAVE WIDE SPECTRA.



The basic theory - pulse compression - Consider a device as

follows: a number of filters (very narrow band) feed differing delay lines, the outputs of which go to a summing device (below). If I were

to feed a narrow pulse

(containing these  $n$  frequency constituents) to this network,

I would have a signal

out that is the recombination of

these "progressively delayed"

frequencies, and it would appear to have a longer time envelope. The

figure to the right shows

this composition with the

"original" narrow pulse

dotted in. Such a network

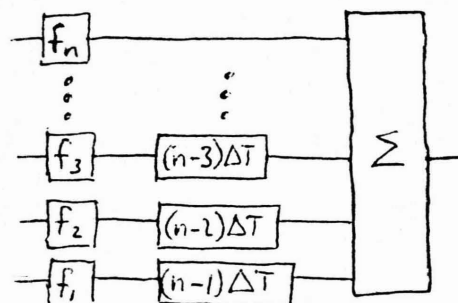
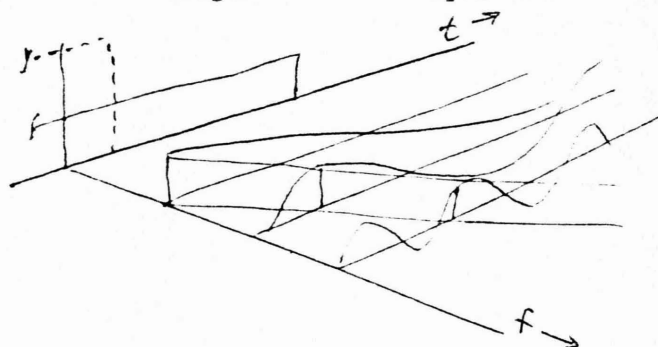
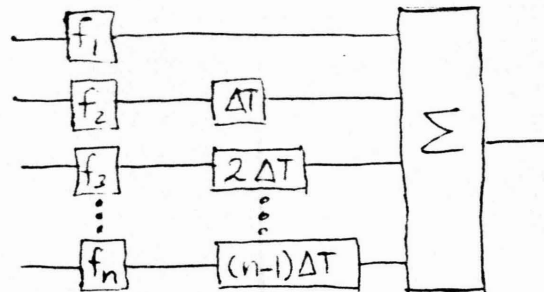
would be a pulse "stretcher".

But the longer pulse would

still have all the frequencies of the narrower original. It is now a frequency modulated pulse, NOT just the longer envelope on the carrier which would have a much narrower spectrum. This stretched pulse has the same energy content as the original but the peak power is proportionately less and can now be amplified without as great a fear of overdriving a peak power limited device.

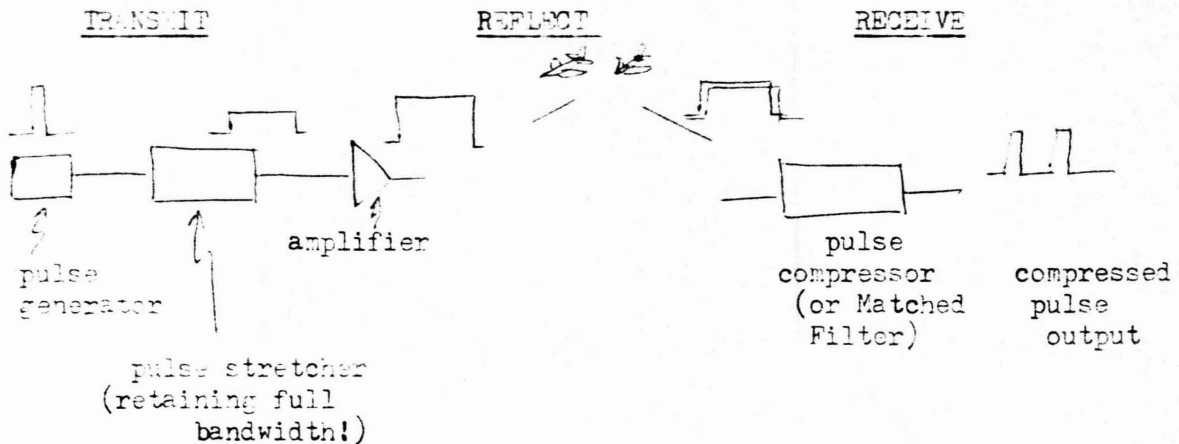
Now, if on receive we had a second filter bank which REVERSED the frequency-delay relationship (shown at right), we see that the stretched pulse would be reconstituted, the frequencies would

be re-aligned to form again the narrow pulse. This network would be



a pulse compressor for that particular stretched pulse - it is (albeit only "notionally" derived here) a "matched filter".

So a pulse compression radar in very general terms might look like this:



Types of pulse compression - the lumped-constant network shown before is in fact typical of early (1950's) pulse compression devices - crystal lattice filters and time delay lines. Then it was recognized that many microwave devices perform in a similar way, that is they are "frequency dispersive". A length of waveguide is frequency dispersive because the total path length traveled by energy at any one frequency is a function of that frequency and the guide's dimensions - and since the pathlengths differ, the pulse is "spread out" somewhat when received at the far end. But a few hundred feet of waveguide doesn't make a very good circuit element so other frequency-dispersive devices have been developed - employing acoustic dispersion in metal strips (with piezoelectric transducers at each end) is typical.

Incidentally, in radar it is often convenient to use the very same

network to generate the stretched pulse and to compress it on receive. This is possible by a trick in the mixing. The basic expansion might be done at an intermediate frequency, then this i.f. is added to a transmit "local oscillator" signal and the sum taken as the radiated frequency:

$$f_{if} + f_{Lo} = f_{radiated}$$

e.g.  $30 \text{ MHz} + 3000 \text{ MHz} = 3030 \text{ MHz}$

Then on receive, this received frequency ( $f_{radiated}$ ) could be mixed with an LO above it by the intermediate amount and the difference taken as the i.f.:

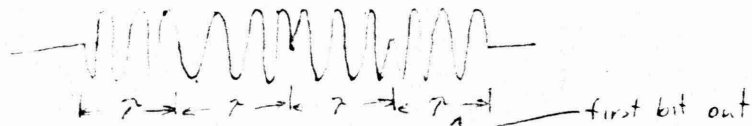
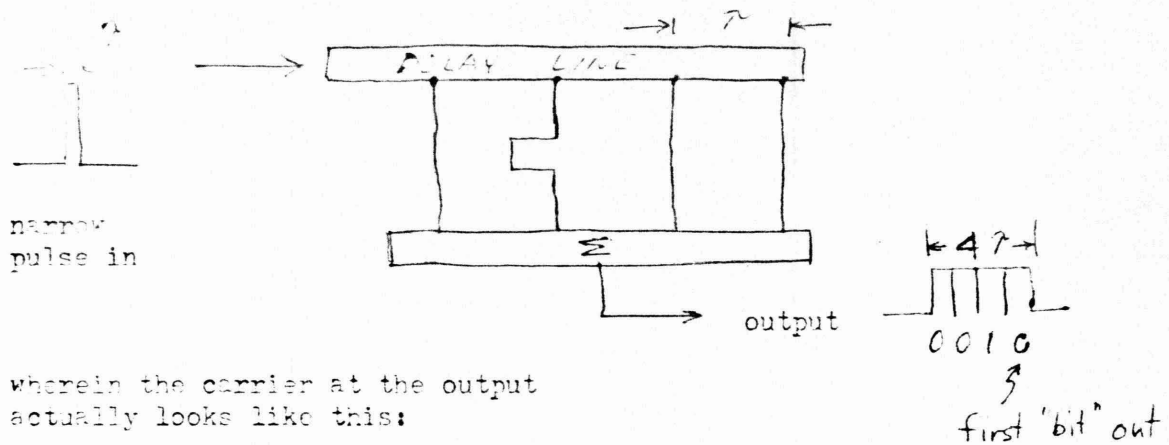
$$f_{Lo} - f_{radiated} = f_{if}$$

e.g.  $3060 \text{ MHz} - 3030 \text{ MHz} = 30 \text{ MHz}$

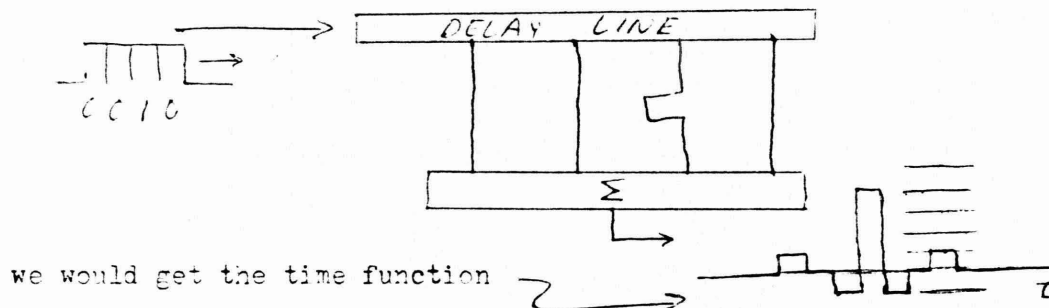
By doing this, the high sidebands of the modulation become the low sidebands on receive and vice versa... and the same frequency dispersive device (assumed here to be working at the i.f.) that expanded the pulse on transmit now will compress the pulse on receive.

Because frequency dispersion results in a monotonic (usually linear as well) frequency-time function within the pulse, it is called "f.m."-ing or use of "linear f.m." or "chirp" processing, etc.

Another type of pulse compression involves the use of phase modulation (actually with a phase progression not unlike that resulting from linear frequency dispersion - so these techniques really aren't so terribly "different" in theory). We can illustrate the generation of an expanded pulse and its subsequent compression by considering a tapped delay line, a number of  $180^\circ$  phase shifters (lengths of line will do) and a summer (top of next page):



Then if this signal were amplified, transmitted, reflected and received by an exactly compensating network:



Networks like these can be made with "surface acoustic wave (SAW)" devices.

More vivid in this second kind of pulse compression was the concept of "time-" or "range-sidelobes", characteristic of all pulse compression receivers. It is possible by weighting the individual frequencies in the f.m. technique and by weighting the taps of the delay line to alter the shape of the whole output waveform somewhat. When this is done (to keep very low range sidelobes, say), the main pulse in the response will never be quite as strong or narrow as when no weighting is used. But it may well be an advantage to take a slight "mismatch" or weighting penalty to achieve very low range sidelobes.

The particular set of binary phase sequences that have no time sidelobes greater than value one are called the Barker codes - the 4-bit code was an illustration. The student might enjoy drawing and testing the network for the 13-bit Barker: 0000011001010.

Ratios of expanded to compressed pulse lengths (the "pulse compression ratio") vary considerably - in some special purpose radars this figure is in the tens or hundreds of thousands. For many more "ordinary" radars, however, a few tens or a hundred or so to one should be considered useful and typical. Designers speak of the "time-bandwidth product" involved. Recall a pulse not stretched in the frequency dispersive manner (or in the analogous tapped delay line manner) will have a spectrum containment (most of the energy) within a passband of about the reciprocal of the pulse width - a time-bandwidth product of unity. The modulation techniques result in a waveform, then, with greater than unity T-B product. With no weighting for sidelobe shaping, the pulse compression ratio and the T-B product can be regarded as equal - the pulse transmitted in a 100:1 pulse compression system has a T-B product of 100.

The student may want to read more of matched filter theory, of resolution and ambiguity characteristics in such processes and of the process of convolution and superposition principles in the theory of linear networks.

Pulse compression permits high power radar operation to be achieved without high peak power risks while retaining the high resolution of broadband signals.

end

# AUTOMATIC DETECTION AND TRACKING

RADAR HAS MAJOR INFLUENCE ABOUT ENVIRONMENT IN MODERN RADAR.

## 1. OPEN LOOP "SEARCHING" RADAR ("SCANNING" RADAR)

- NOT VERY ADAPTIVE
- CAN STILL GIVE INFLUENCE OF LOCATION OF OBJECTS OF INTEREST TO USER.
- CAN CONTRAST SCAN TO SCAN AND ESTIMATE MOTION EQUATION.

"TRACK WHILE SCAN"

## 2. CLOSED LOOP "TRACKING" RADAR

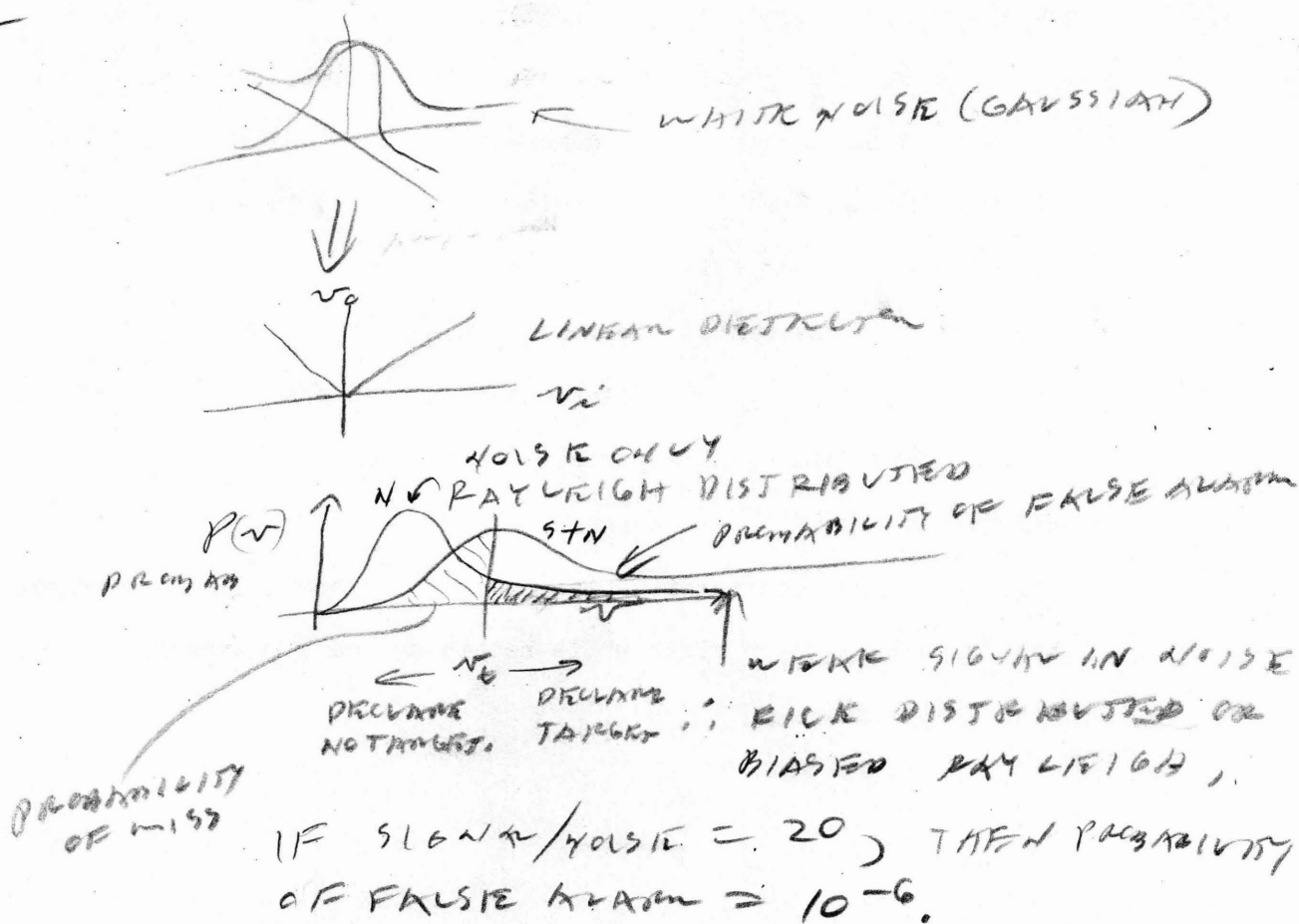
eg. PHASED ARRAY RADAR.

- FOCUS ON ONE OBJECT

- SIDELOBES AND CLUTTER CAN FALSE AUTOMATIC DETECTORS.

- THRESHOLD DETECTION (AFTER ENVELOPE DETECTION)

- ASSUME SINGLE PULSE BASIS.



V. B. Tracking with Surveillance Radar

- Automatic Detection and Tracking

- - Dr. Skolnik's notes on this subject follow and provide quite a thorough list of references. Mr. Hill's lecture follows the sequence of these notes. The lecture brings added emphasis to the "serial" importance of clutter and undesired signal suppression in the radar signal procession itself, of the reliable and accurate "extraction" of target detections and of the establishment and maintenance of tracks formed from those detections from one or more such radars with attention to any dissimilarities among them.

R.T.H.



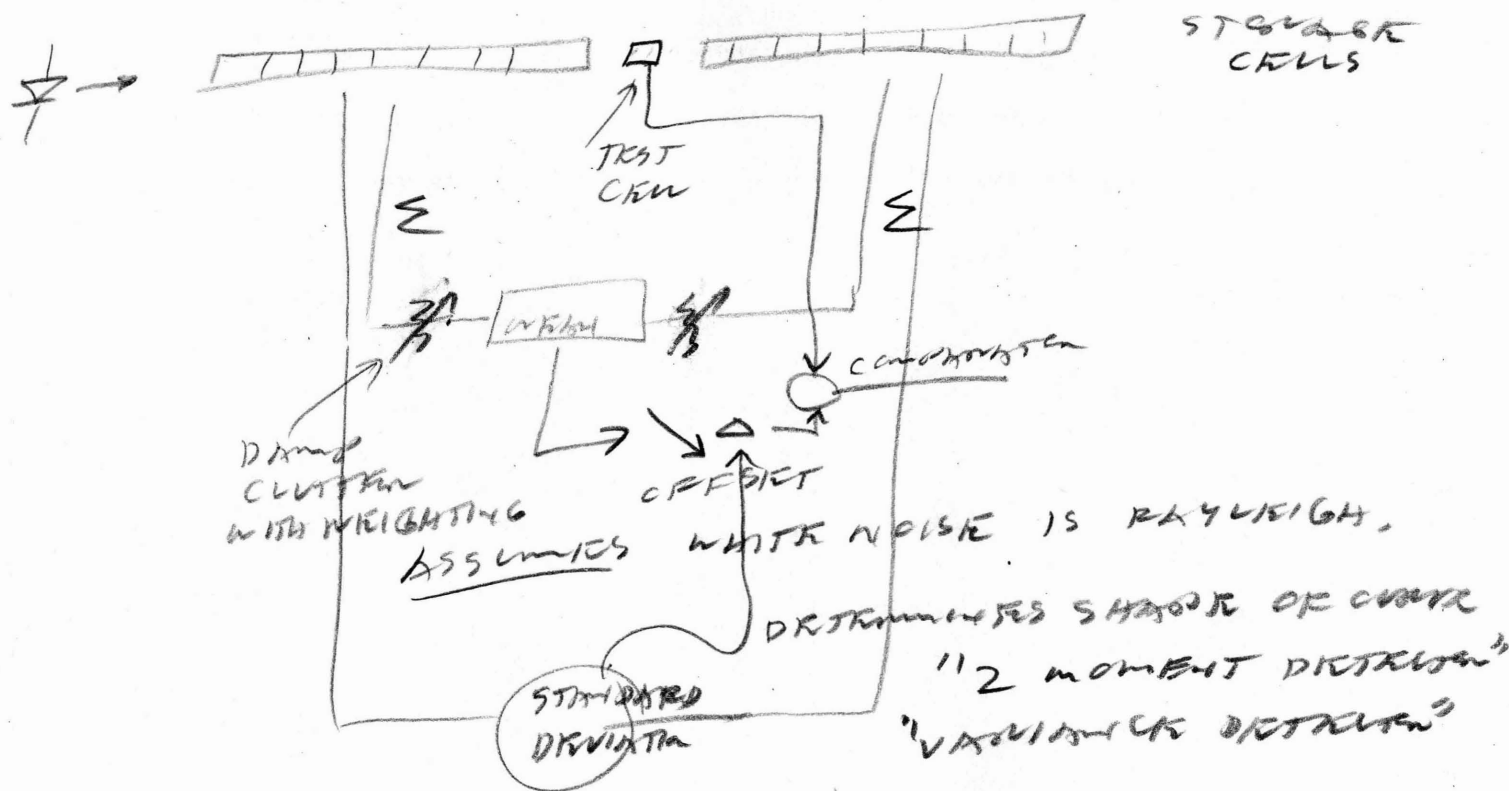
PROBABILITY DENSITY FUNCTION IS A PLOTTING OF  $KOEA = 1$ .

$W =$  CRITERIA OF DETECTION

PROBABILITY OF DETECTION  $P_{DET} = 1 - P_{MISS}$ .

ALL ABOVE IS BASED ON SINGLE PULSE BASIS. INTEGRATION CAN IMPROVE SITUATION.

WEIGHT LEVEL DETECTOR MLD



$\therefore$  CONSTANT FALSE ALARM RATE.

CAN ALSO AVERAGE SUCCESSIVE STORAGE CELLS.

$\therefore$  TAKE "m out of n" TESTS.

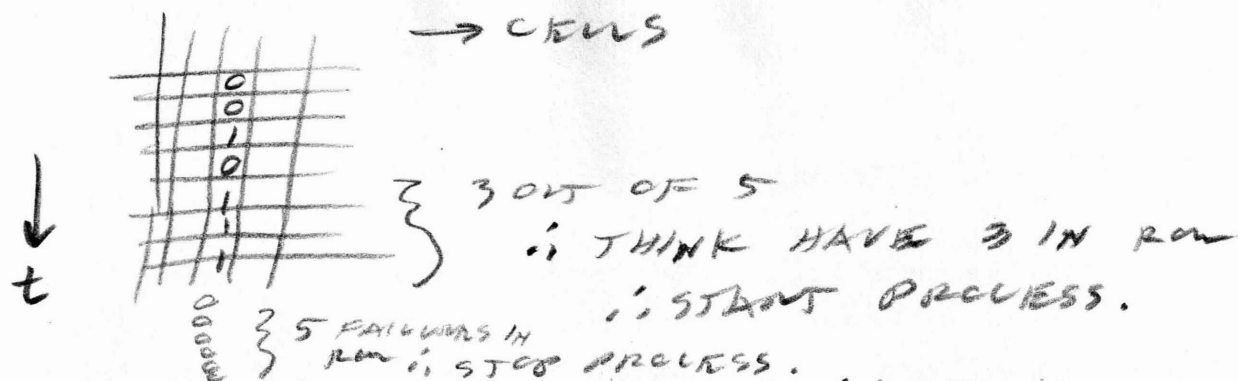
HUMAN  $\Rightarrow$  2 IN A ROW FOLLOWED BY 1 OUT OF 2.  
RESPONSE TO SUCCESSIVE SIGNALS.

## Tracking with Surveillance Radar

The track of a target can be determined with a surveillance radar from the positions of the target as measured from scan to scan. The quality of such a track will depend on the time between observations, the location accuracy of each observation, and the number of extraneous targets that might be present in the vicinity of the tracked target. A surveillance radar that develops tracks on targets it has detected is sometimes called a track-while-scan (TWS) radar.

One method of obtaining tracks with a surveillance radar is to have an operator manually mark with a grease pencil on the face of the cathode-ray tube the position of the target on each scan. The simplicity of such a procedure is offset by the poor accuracy of the track. The accuracy of track can be improved by using a computer to determine the trajectory from inputs supplied by an operator. A human operator, however, cannot update target tracks at a rate greater than about once per two seconds. Thus, a single operator cannot handle more than about six target tracks when the radar has a twelve-second scan rate (5 rpm antenna rotation rate). Furthermore, an operator's effectiveness in detecting new targets decreases rapidly after about a half hour of operation. The radar operator's traffic handling limitation and the effects of fatigue can be overcome by automating the target detection and tracking process with data processing called automatic detection and tracking (ADT). The availability of digital data processing technology has made ADT economically feasible. An ADT system performs the functions of target detection, track initiation, track association, track update, track smoothing (filtering) and track termination.

The automatic detector part of the ADT quantizes the range into intervals equal to the range resolution. At each range interval the detector integrates  $n$  pulses, where  $n$  is the number of pulses expected to be returned from a target as the antenna scans past. The integrated pulses are compared with a threshold to indicate the presence or absence of a target. An example is the commonly used moving window detector which examines continuously the last  $n$  samples within each quantized range interval



JAMMING WILL HAVE SAME EFFECT AS CLUTTER. I WILL STILL DETECT TARGET.

I. CENTROIDING

ALSO NEAREST NEIGHBOR COMPARISONS.

0100110001  
100100110001  
I, MOVING?

TRACT FORMATION

CENTROIDED TARGET POSITION IS DEFINED AS "CONTACT", "PLOT", (AFTER DECLARATION)  
"hit", "strike" (per pulse)

and announces the presence of a target if  $m$  out of  $n$  of these samples cross a pre-set threshold. By locating the center of the  $n$  pulses, an estimate of the target's angular direction can be obtained. This is called beam splitting.

If there is but one target present within the radar's coverage, detections on two scans are all that is needed to establish a target track and to estimate its velocity. However, there are usually other targets as well as clutter echoes present, so that three or more detections are needed to reliably establish a track without the generation of false or spurious tracks. Although a computer can be programmed to recognize and reject false tracks, too many false tracks can overload the computer and result in poor information. It is for this same reason of avoiding computer overload that the radar used with ADT should be designed to exclude unwanted signals as from clutter and interference. A good ADT system therefore requires a radar with a good MTI and a good CFAR (constant false alarm rate) receiver. A clutter map, generated by the radar, is sometimes used to reduce the load on the tracking computer by blanking clutter areas and removing detections associated with large point clutter sources not rejected by the MTI. Slowly moving echoes that are not of interest can also be removed by the clutter map. The availability of some distinctive target characteristic, such as its altitude, might also prove of help in relieving the computer when performing track association. Thus, the quality of the ADT will depend significantly on the ability of the radar to reject unwanted signals.

When a new detection is received, an attempt is made to associate it with existing tracks. This is aided by establishing for each track a small search region, or gate, within which a new detection is predicted based on the estimate of the target speed and direction. It is desired to make the gate as small as possible so as to avoid having more than one echo fall within it when the traffic density is high or when two tracks are close to one another. However, a large gate area is required if the tracker is to follow target turns or maneuvers. More than one size gate might therefore be used to overcome this dilemma. The size of the small gate would be

determined by the accuracy of the track. When a target does not appear in the small gate, a larger gate would be used whose search area is determined by the maximum acceleration expected of the target during turns.

On the basis of the past detections the track-while-scan radar must make a smoothed estimate of a target's present position and velocity, as well as a predicted position and velocity. One method for computing this information is the so-called  $\alpha$ - $\beta$  tracker (also called the g-h tracker), which computes the present smoothed target position  $\bar{x}_n$  and velocity  $\bar{\dot{x}}_n$  by the following equations

$$\text{smoothed position: } \bar{x}_n = x_{pn} + \alpha(x_n - x_{pn})$$

$$\text{smoothed velocity: } \bar{\dot{x}}_n = \bar{\dot{x}}_{n-1} + \frac{\beta}{T_s} (x_n - x_{pn})$$

where  $x_{pn}$  = predicted position of the target at the nth scan,  $x_n$  = measured position at the nth scan,  $\alpha$  = position smoothing parameter,  $\beta$  = velocity smoothing parameter, and  $T_s$  = time between observations. The predicted position at the  $n + 1$ st scan is  $\bar{x}_n + \bar{\dot{x}}_n T_s$ . (When acceleration is important a third equation can be added, with  $\gamma$  = acceleration smoothing parameter, to describe an  $\alpha$ - $\beta$ - $\gamma$  tracker.) For  $\alpha = \beta = 0$ , the tracker uses no current information, only the smoothed data of prior observations. If  $\alpha = \beta = 1$ , no smoothing is included at all. The classical  $\alpha$ - $\beta$  filter is designed to minimize the mean square error in the smoothed (filtered) position and velocity, assuming small velocity changes between observations, or data samples. One criterion for selecting the parameters of the  $\alpha$ - $\beta$  tracker is to choose  $\beta = \alpha^2/(2-\alpha)$ . The particular choice of  $\alpha$  within the range of zero to one depends upon the system application, in particular the tracking bandwidth. Using as a criterion the best linear track fitted to the radar data in a least squares sense gives the values of  $\alpha$  and  $\beta$  as

$$\alpha = \frac{2(2n-1)}{n(n+1)} \quad \beta = \frac{6}{n(n+1)}$$

where  $n$  is the number of the scan or target observation ( $n > 2$ ).

The standard  $\alpha$ - $\beta$  tracker does not handle the maneuvering target. However, an adaptive  $\alpha$ - $\beta$  tracker is one which varies the two smoothing parameters

to achieve a variable bandwidth so as to follow maneuvers. The value of  $\alpha$  can be set by observing the measurement error  $x_n - x_{pn}$ . At the start of tracking the bandwidth is made wide and then it is narrowed down if the target moves in a straight-line trajectory. As the target maneuvers or turns, the bandwidth is widened to keep the tracking error small.

The Kalman filter is similar to the classical  $\alpha$ - $\beta$  tracker except that it inherently provides for the dynamical or maneuvering target. In the Kalman filter a model for the measurement error has to be assumed, as well as a model of the target trajectory and the disturbance or uncertainty of the trajectory. Such disturbances in the trajectory might be due to neglect of higher order derivatives in the model of the dynamics, random motions due to atmospheric turbulence, and deliberate target maneuvers. The Kalman filter can, in principle, utilize a wide variety of models for measurement noise and trajectory disturbance; however, it is often assumed that these are described by white, Gaussian noise with zero mean. A maneuvering target does not always fit such an ideal model, since it is quite likely to produce correlated observations. The proper inclusion of realistic dynamical models increases the complexity of the calculations. Also, it is difficult to describe a priori the precise nature of the trajectory disturbances. Some form of adaption to maneuvers is required. The Kalman filter is sophisticated and accurate, but is more costly to implement than the several other methods commonly used for the smoothing and prediction of tracking data. Its chief advantage over the classical  $\alpha$ - $\beta$  tracker is its inherent ability to take account of maneuver statistics. If, however, the Kalman filter were restricted to modeling the target trajectory as a straight line and if the measurement noise and the trajectory disturbance noise were modeled as white, gaussian noise with zero mean the Kalman filter equations reduce to the  $\alpha$ - $\beta$  filter equations with the parameters  $\alpha$  and  $\beta$  computed sequentially by the Kalman filter procedure. As the dynamic system model is made more complex, the Kalman filter becomes increasingly more difficult to implement.

The classical  $\alpha$ - $\beta$  tracking filter is relatively easy to implement. To handle the maneuvering target, some means may be included to detect maneuvers and change the values of  $\alpha$  and  $\beta$  accordingly. In some radar

systems, the data rate might also be increased during target maneuvers. As the means for choosing  $\alpha$  and  $\beta$  become more sophisticated, the optimal  $\alpha$ - $\beta$  tracker becomes equivalent to a Kalman filter even for a target trajectory model with error. In this sense, the optimal  $\alpha$ - $\beta$  tracking filter is one in which the values of  $\alpha$  and  $\beta$  require knowledge of the statistics of the measurement errors and the prediction errors, and in which  $\alpha$  and  $\beta$  are determined in a recursive manner in that they depend on previous estimates of the mean square error in the smoothed position and velocity.

(The above discussion has been in terms of a sampled-data system tracking targets detected by a surveillance radar. The concept of the  $\alpha$ - $\beta$  tracker or the Kalman filter also can be applied to a continuous, single-target tracking radar when the error signal is processed digitally rather than analog. Indeed, the equations describing the  $\alpha$ - $\beta$  tracker are equivalent to the Type II servo system widely used to model the continuous tracker.)

If, for some reason, the track-while-scan radar does not receive target information on a particular scan, the smoothing and prediction operation can be continued by properly accounting for the missed data. However, when data to update a track is missing for a sufficient number of consecutive scans, the track is terminated. Although the criterion for terminating a track depends on the application, one example suggests that when three target reports are used to establish a track, five consecutive misses is a suitable criterion for termination.

One of the corollary advantages of ADT is that it effects a bandwidth reduction in the output of a radar so as to allow the radar data to be transmitted to another location via narrow-band phone lines rather than wide-band microwave links. This makes it more convenient to operate the radar at a remote site, and permits the outputs from many radars to be communicated economically to a central control point.

When more than one radar, covering approximately the same volume in space, are located within the vicinity of each other, it is sometimes desirable to combine their outputs to form a single track file rather than form separate tracks. Such an automatic detection and integrated tracking system (ADIT) has the advantage of a greater data rate than any single



radar operating independently. The development of a single track file by use of the total available data from all radars reduces the likelihood of a loss of target detections as might be caused by antenna lobing, fading, interference and clutter since integrated processing permits the favorable weighting of the better data and lesser weighting of the poorer data.

### References

Plowman, J.C.: Automatic Radar Data Extraction by Storage Tube and Delay Line Techniques, J. Brit. IRE, vol. 27, pp. 317-328, October, 1963.

Caspers, J.W.: Automatic Detection Theory, Chapter 15 of "Radar Handbook," Edited by M. I. Skolnik, McGraw-Hill Book Co., New York, 1970.

Oakley, B.W.: Tracking in an Air Traffic Control Environment, Chapter 30 of "Radar Techniques for Detection, Tracking, and Navigation," Edited by W. T. Blackband, Gordon and Breach, N.Y., 1966.

Benedict, T.R. and G. W. Bordner: Synthesis of an Optimal Set of Radar Track-While-Scan Smoothing Equations, IRE Trans., vol. AC-7, pp. 27-32, July, 1962.

Simpson, H.R.: Performance Measures and Optimization Condition for a Third-Order Sampled-Data Tracker, IEEE Trans., vol. AC-8, pp. 182-183, April, 1963.

Quigley, A.L.C.: Tracking and Associated Problems, International Conference on Radar - Present and Future, 23-25 Oct 1973, London, pp. 352-359, IEE Conference Publication No. 105.

Hampton, R.L.T. and J. R. Cooke: Unsupervised Tracking of Maneuvering Vehicles, IEEE Trans., vol. AES-9, pp. 197-207, March, 1973.

Thorp, J.S.: Optimal Tracking of Maneuvering Targets, IEEE Trans., vol. AES-9, pp. 512-519, July, 1973.

Singer, R.A. and K.W. Behnke: Real-Time Tracking Filter Evaluations and Selection for Tactical Applications, IEEE Trans., vol. AES-7, pp. 100-110, January, 1976.

Kalman, R.E.: A New Approach to Linear Filtering and Prediction Problems, Trans. ASME, J. Basic Engrg., vol. 82, pp. 34-45, March, 1960.

Schooler, C.C.: Optimal  $\alpha$ - $\beta$  Filters for Systems with Modeling Inaccuracies, IEEE Trans., vol. AES-11, pp. 1300-1306, November, 1975.

Kanyuck, A.J.: Transient Response of Tracking Filters with Randomly Interrupted Data, IEEE Trans., vol. AES-6, pp. 313-323, May, 1970.

Morgan, D.R.: A Target Trajectory Noise Model for Kalman Trackers, IEEE Trans., vol. AES-12, pp. 405-408, May, 1976.

Leth-Espensen, L.: Evaluation of Track-While-Scan Computer Logics, Chapter 29 **of** "Radar Techniques for Detection, Tracking, and Navigation," Edited by W. T. Blackband, Gordon and Breach, New York, 1966.

Cantrell, B.H., G. V. Trunk, J. D. Wilson, and J. J. Alter: Automatic Detection and Integrated Tracking, IEEE 1975 International Radar Conference, pp. 391-39-, Arlington, VA, April 21-23, 1975.

## [54] AUTOMATED RADAR DATA PROCESSING SYSTEM

[75] Inventors: Alexander Kossiakoff, Brookville; James R. Austin, Gaithersburg, both of Md.

[73] Assignee: The United States of America as represented by the Secretary of the Navy, Washington, D.C.

[22] Filed: Mar. 31, 1975

[21] Appl. No.: 563,908

[52] U.S. Cl. .... 343/5 VQ

[51] Int. Cl.<sup>2</sup> .... G01S 9/02

[58] Field of Search .... 343/5 DP, 5 VQ

## [56] References Cited

## UNITED STATES PATENTS

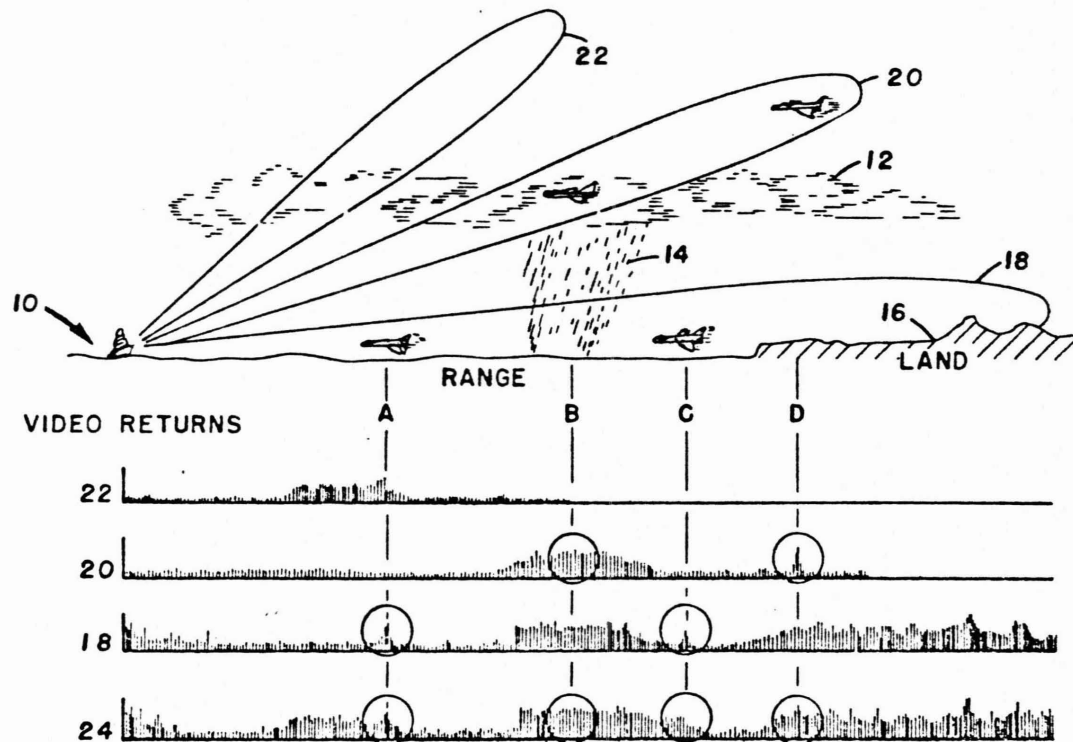
3,213,448	10/1965	Foley	343/5 DP X
3,353,177	11/1967	Wilmot	343/5 DP
3,359,442	12/1967	Groginsky	343/5 DP
3,460,137	8/1969	Ralston	343/5 DP
3,680,095	7/1972	Evans	343/5 DP X
3,836,964	9/1974	Evans	343/5 DP X
3,870,992	3/1975	Hanna, Jr.	343/5 DP
3,919,707	11/1975	Evans	343/5 DP

Primary Examiner—Malcolm F. Hubler

## [57] ABSTRACT

An automated radar data processing system comprised of signal processing circuitry and programmed general purpose digital computer apparatus performs detection, classification and tracking of all targets within the field of view of the radar. The signal processing circuitry includes an adaptive video processor which receives the raw radar video signals and which derives a threshold from the noise, clutter, or electronic countermeasures signals in the immediate vicinity of the target and passes only those incoming signals which satisfy the detection criteria in terms of signal to noise ratio and extent. The signal processing circuitry is interactive with target track data derived and stored in the computer apparatus, so that the specific signal processing applied to any target by the adaptive video processor is optimized in accordance with the track status of that target. The proposed system also better enables a human operator to take a system management position wherein he can set up or establish data processing conditions so as, for example, to optimize target detection in highly variable or critical environments.

20 Claims, 24 Drawing Figures



Further questions relating to Session V

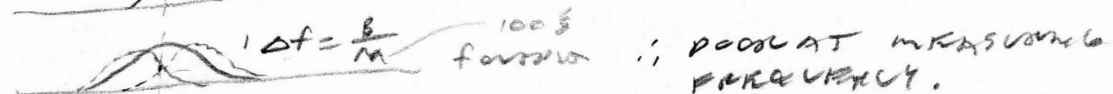
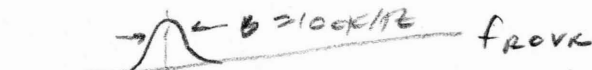
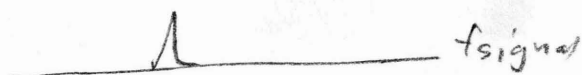
1. What problem might occur in trying to design a single pulse compression waveform to see small targets at both short and long range?
2. How would you have to find the best coded-pulse waveform for pulse-compression ratios greater than 13?
3. How can pulse compression aid the low-angle tracking problem? The glint problem?
4. Does pulse compression have a role in radar altimeters?
5. Can ADT be made to work without CFAR?

SESSION VI

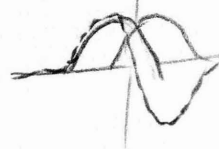
TRACKING RADAR

DAVID BARTON

# RADIO MEASUREMENTS



INTERPOLATION WOULD IMPROVE ACCURACY.  
"SEQUENTIAL MEASUREMENT" IN RADAR TECHNOLOGY.



TWO TUNED CIRCUITS

DISCRIMINATION WITH AFC

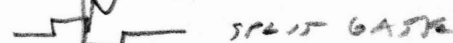
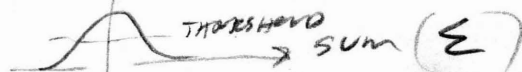
"SIMULTANEOUS COMPARISON" IN RADAR TECHNOLOGY.

ANGULAR MEASUREMENT IN RADAR IS STILL A LOT OF "SEQUENTIAL" MEASUREMENT.

## ANGULAR MEASUREMENT



$\theta_3$  = HALF POWER BEAM WIDTH  
 $t_0$  = time on target



↑ EXACT ANGLE POSITION, DEPENDENT ON SLOPE

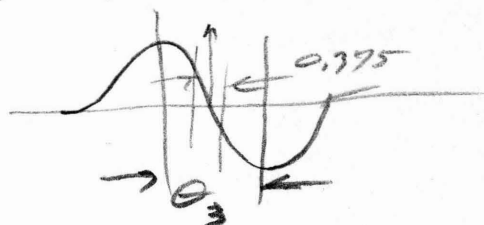
SLOPE DEPENDS ON SIGNAL STRENGTH.

∴  $\frac{\Delta}{\Sigma}$  SLOPE IS INDEPENDENT OF TARGET AMPLITUDE.

$$K = d\left(\frac{\Delta}{\Sigma}\right) / d\theta / \theta_3$$

SLOPE IS CONSTANT FOR AW SYSTEM?

USUALLY  $K = 1.5$



## Radar Tracking

by David K. Barton  
Raytheon Company  
Bedford, Massachusetts 01730

M21-62

617-274-17100 X 3509

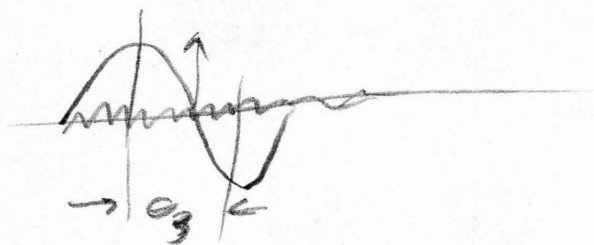
X 2588

- A. Fundamentals
  - 1. Detection, Resolution, and Interpolation
  - 2. Basic Measurement Processes
  - 3. Fundamental Considerations of Accuracy
- E. Angle Tracking Techniques
  - 1. Sequential Lobing
  - 2. Conical Scanning
  - 3. Linear Scanning
  - 4. Monopulse
- C. Tracking Radar Antennas
  - 1. Lobing and Scanning Antennas
  - 2. Monopulse Feeds
  - 3. Phased Array Trackers
  - 4. Pedestals and Mechanical Design
- D. Tracker Signal Processing
  - 1. Angle Tracking Receivers and Processors
  - 2. Range Trackers
  - 3. Doppler Trackers
  - 4. Examples of Trackers Using Doppler

References



# INTERFERENCE



$$\sigma_{\theta_3} \text{ (STANDARD DEVIATION NORMALIZED TO HALF PWR BEAM WIDTH)} = \frac{E_n}{K E_s}$$

$$\sigma_{\theta_3} = \frac{1}{K E_s/E_n} = \frac{1}{K \sqrt{2 S/N}} \quad \text{POWER RATIO}$$

$$\sigma_{\theta_3} = \frac{1}{K \sqrt{2 S/I}} \quad \text{14 TEMPERATURE RATIO,}$$

$$\therefore \sigma_{\theta} = \frac{\theta_3}{K \sqrt{2 S/I}} \quad K=1.5$$

0.01° ACCURACY WITH 1° BEAM WIDTH

$$\sqrt{2 S/I} = 67$$

$$S/I = 2200 = +33.5 \text{ dB}$$

FOR ONE PULSE MEASUREMENT,  
BETTER WITH AVERAGING.

AS LONG AS  $S > I$ , THEN  $\text{AVG} = N \text{ PULSES}$ .  
improvement

## RADAR TRACKING

### A. FUNDAMENTALS

1. Detection, Resolution and Interpolation. Any radar detection of a target provides some information on target coordinates, although the data may be very coarse. The PPI display of a conventional 2D search radar gives range and azimuth data in the form of an intensified blip whose width in azimuth is approximately the beamwidth of the antenna and whose range extent is the transmitter pulsewidth, perhaps compressed by signal processing or stretched by limited display bandwidth or excessive spot size. The simplest type of automatic radar measurement consists of reporting the azimuth or range resolution cell in which the target is detected, or the cell containing the largest signal if two or more contiguous cells give alarms. In this case, the measurement is simply the identity of a particular resolution cell in space (and possibly in Doppler frequency) which is known to contain, or at least to adjoin, the target position.

More refined estimates of target location are made by interpolation within a cell or between two cells. The human operator places a cursor scale at the apparent center of the PPI blip to obtain interpolation to a fraction of the beamwidth. An automatic target extractor may integrate signal pulses in contiguous, fixed gates, and make an estimate based on the relative amplitudes; or it may perform a continuous integration and produce an output when the output begins to decline from its peak value. These are all interpolation processes which can be applied to search, track-while-scan, or tracking radar. The distinctions among these terms can be seen from their definitions [ 1 ]:

Search radar. A radar used primarily for the detection of targets in a particular volume of interest.

Track-while-scan. A target tracking process in which the radar antenna and receiver are not part of the tracking loop, but provide periodic video data from the search scan, as inputs to computer channels which follow individual targets.

Tracking radar. A radar (or mode of a radar) in which the target is tracked by a closed-loop servo which controls the antenna (for angle-tracking) or receiver gates or filters (for range or Doppler tracking).

Thus, the tracking radar is distinguished by the fact that its antenna or receiver is "tuned" to the point in radar space in which the target signal is expected to appear, so that interpolation may be performed more efficiently and accurately. Modern tracking radars may be time-shared between targets, or may interlace tracking and search modes with a single antenna, so it is not total dedication to a single target which serves to identify the tracker. In subsequent sections, while emphasis will be placed on tracking radar techniques, the operation and measurement performance of track-while-scan and search radars will be covered for purposes of comparison.

2. Basic Measurement Processes. The measurement of target angle, by interpolation within the main lobe of the antenna pattern, is representative of all radar measurement processes. Typically, a narrow "pencil" beam (Fig. 1a) is pointed toward the target, and when the signal is detected steps are taken to center the antenna axis at the target azimuth and elevation angles. Ideally, the beam would be aligned with the antenna axis (for maximum gain and lowest sidelobes), and would be pointed to obtain the maximum signal. All mainlobe patterns have essentially the same shape near the axis (where a quadratic approximation matches both the  $\sin x/x$  and Gaussian patterns), and the slope of the pattern falls slowly through zero at the axis. Accurate alignment of the beam axis with the target requires the formation of a first derivative of the pattern in the angular coordinate to be measured (Figs. 1b, 1c). The beam is then adjusted until this derivative response is exactly zero, indicating perfect alignment with the target. Since the derivative is an odd function, and essentially linear for a fraction of a beamwidth each side of the axis, an output other than zero can be interpreted directly as a pointing error and used to control the antenna servo.

In measuring echo time delay (to obtain target range), the received and processed pulse envelope is analogous to the antenna pattern in angular

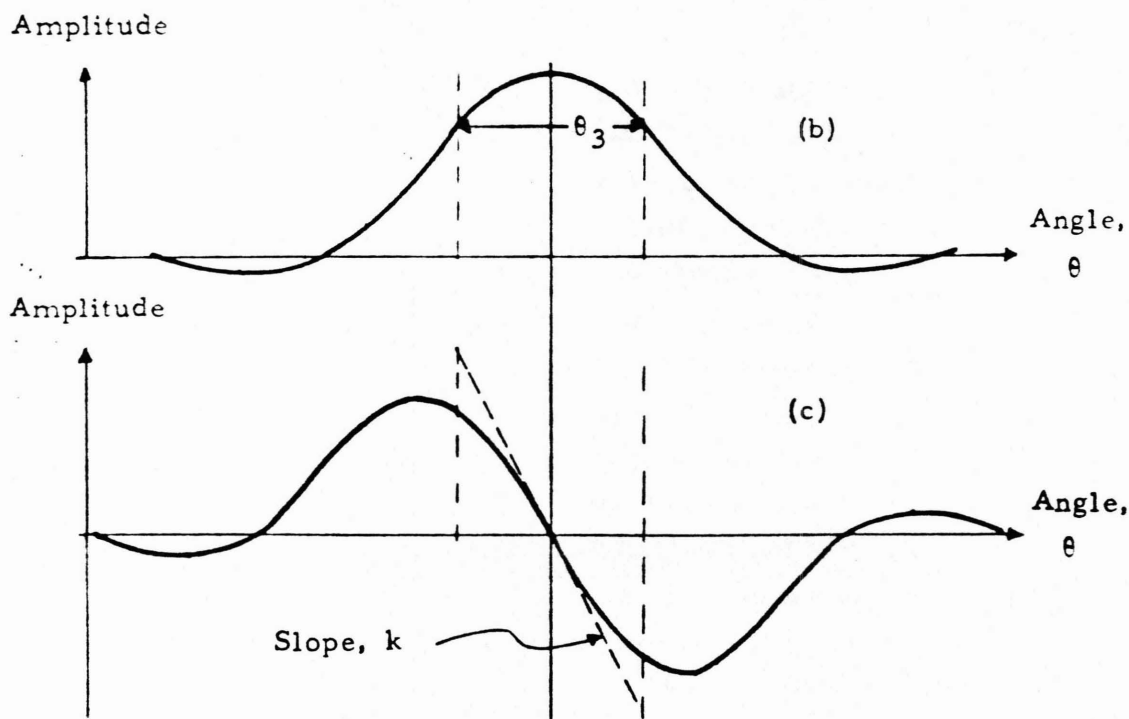
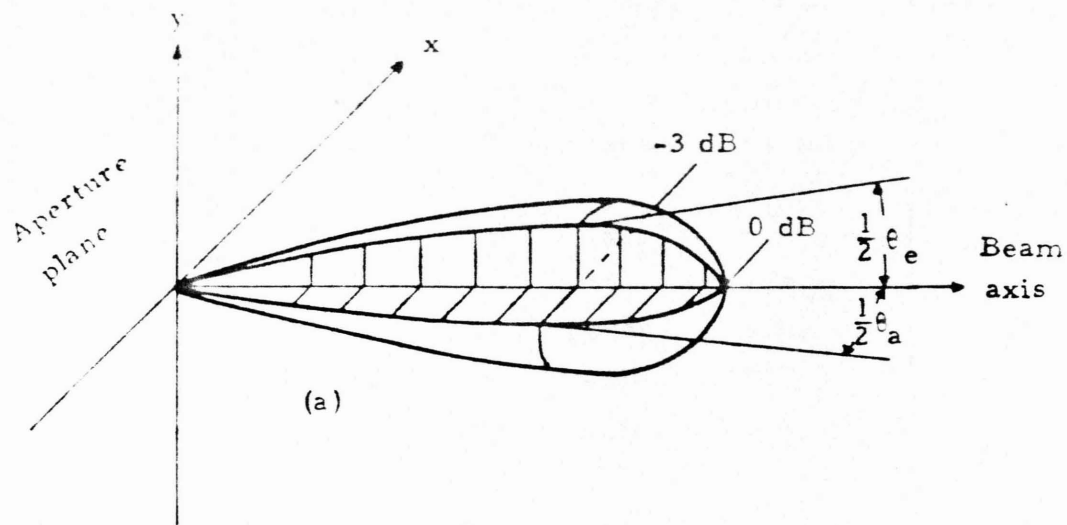


Figure 1. Tracking radar antenna patterns: (a) Pencil beam main lobe. (b) Amplitude vs. angle in plane through the beam axis. (c) Derivative of amplitude pattern, showing linear slope with null at axis.

measurement. The delay to the peak of this envelope is measured, relative to the peak of the transmitter signal, which is similarly processed to remove bias. While a rectangular pulsed transmission, viewed by a wideband (mismatched) receiver, may preserve its flat top without a recognizable peak, the output of a more nearly matched system will have a curved peak similar to the antenna lobe. In pulse compression systems, the analogy to antenna patterns is exact, including multiple "time sidelobes" beside the mainlobe. Doppler frequency measurements use the shift in signal spectrum, relative to the transmission. In this case, too, the response of the filter to the signal, as its frequency is varied, forms a curved lobe analogous to the antenna pattern. The derivative response can be formed directly by a frequency discriminator.

In each radar coordinate (angle, delay, or frequency), the radar designer has a choice of forming the derivative response either by sequential or simultaneous comparison of two adjacent channels (Fig. 2), which can represent beams, gates, or filters. Sequential comparison is often used in angle, where the expense of additional feeds and receivers may be a major consideration. The degree to which the difference between two displaced beams can approximate the derivative of the on-axis beam is indicated by Fig. 3, which was calculated for beam patterns formed by a cosine-illuminated aperture. The difference between two beams offset  $\pm 0.3$  beamwidths from the axis (crossing at their -1 dB points, one-way) follows the ideal derivative very closely. The same consideration applies to generation of a frequency discriminator curve from two detuned filters, or of a time discriminator function from outputs of two adjacent range gates. In these cases, however, the cost of a second simultaneous channel is small, and sequential comparison is seldom used. Figure 4 shows typical measurement systems for any coordinate.

3. Fundamental Considerations of Accuracy. It is apparent that the accuracy of a radar measurement depends upon the width of the response lobe within which interpolation is made. For the usual lobe shapes, this

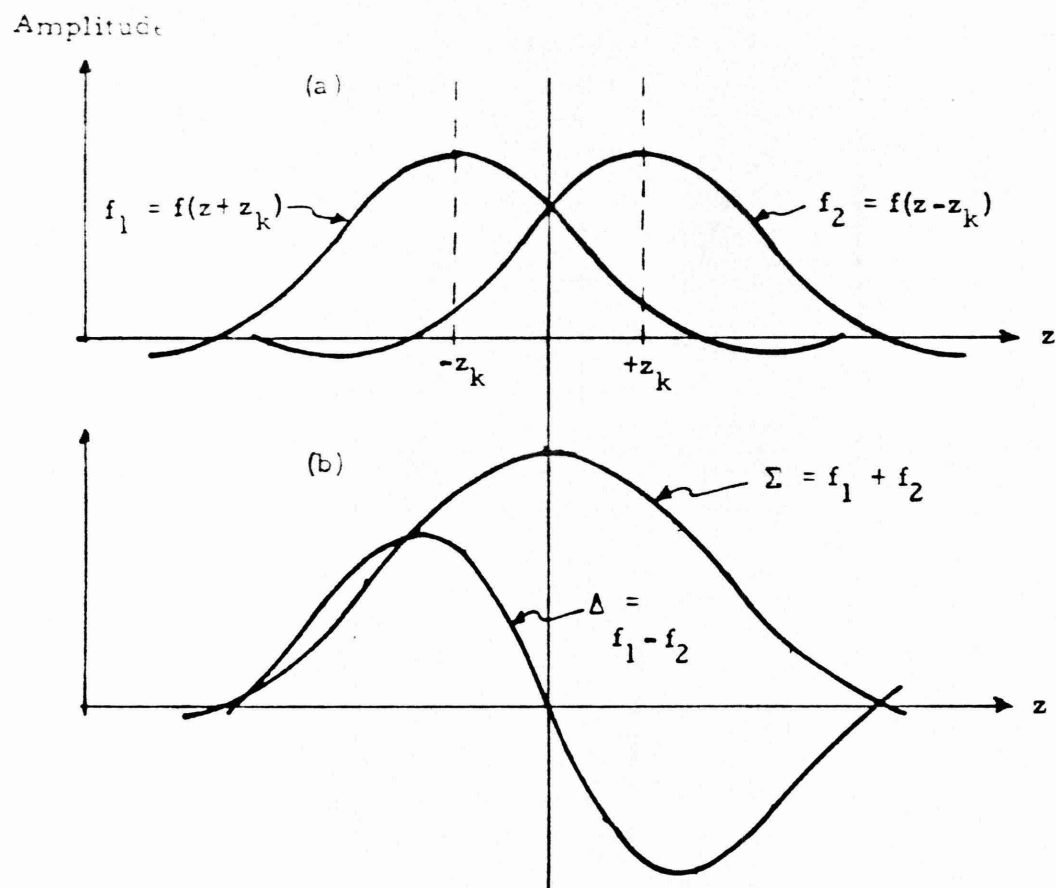


Figure 2. Approximation of derivative response formed by two offset channels: (a) Responses of two adjacent signal channels. (b) Sum and difference channels formed from two adjacent channels.

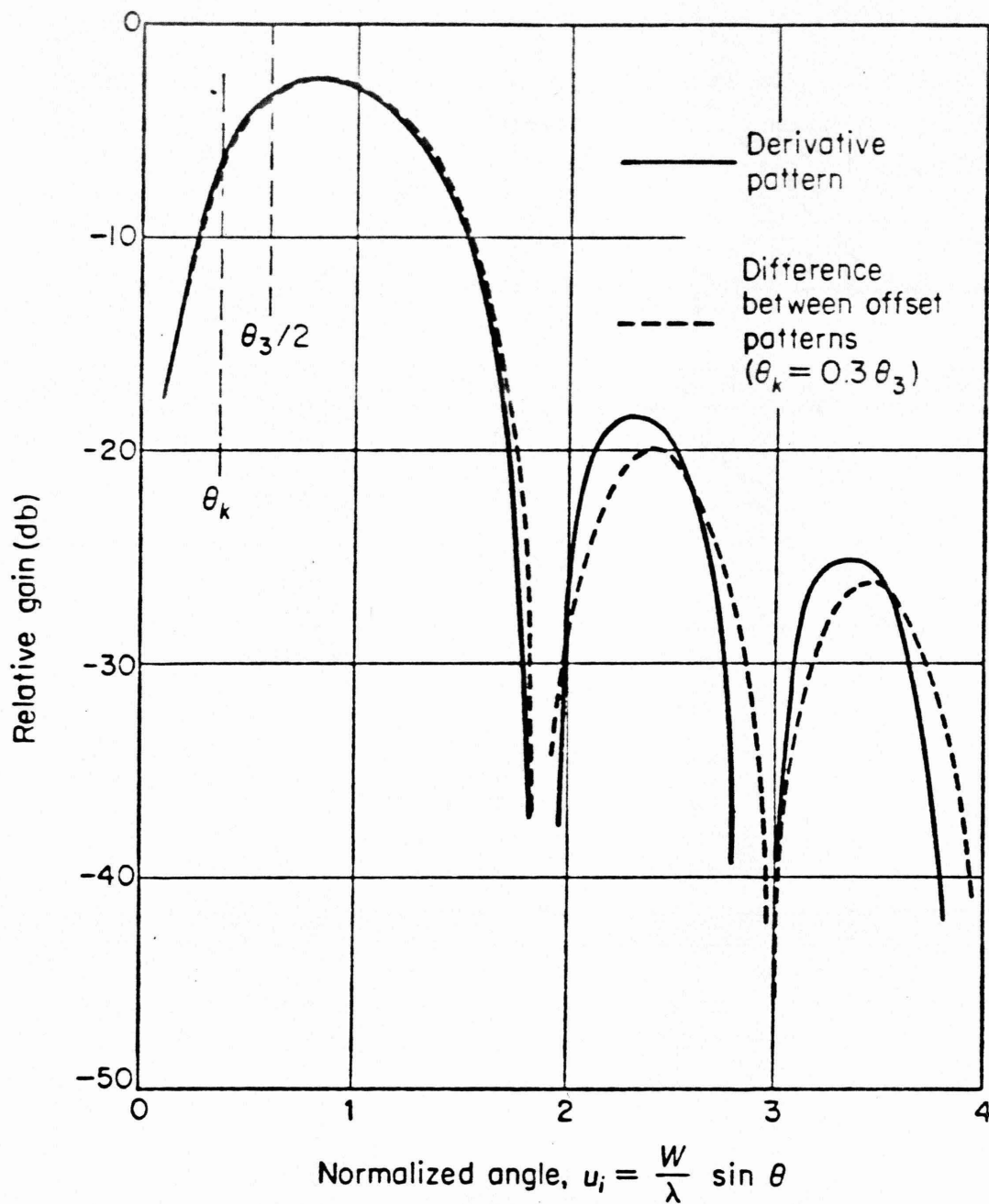


Figure 3. Comparison of difference-pattern response of conical scan and monopulse trackers [ 2 ].

*∴ SAME*



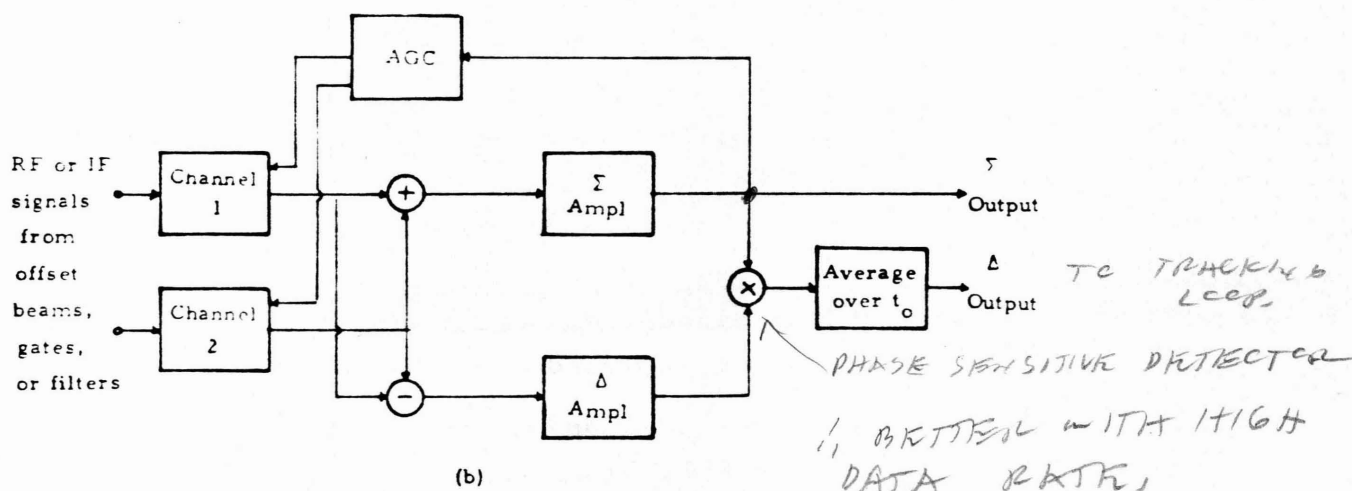
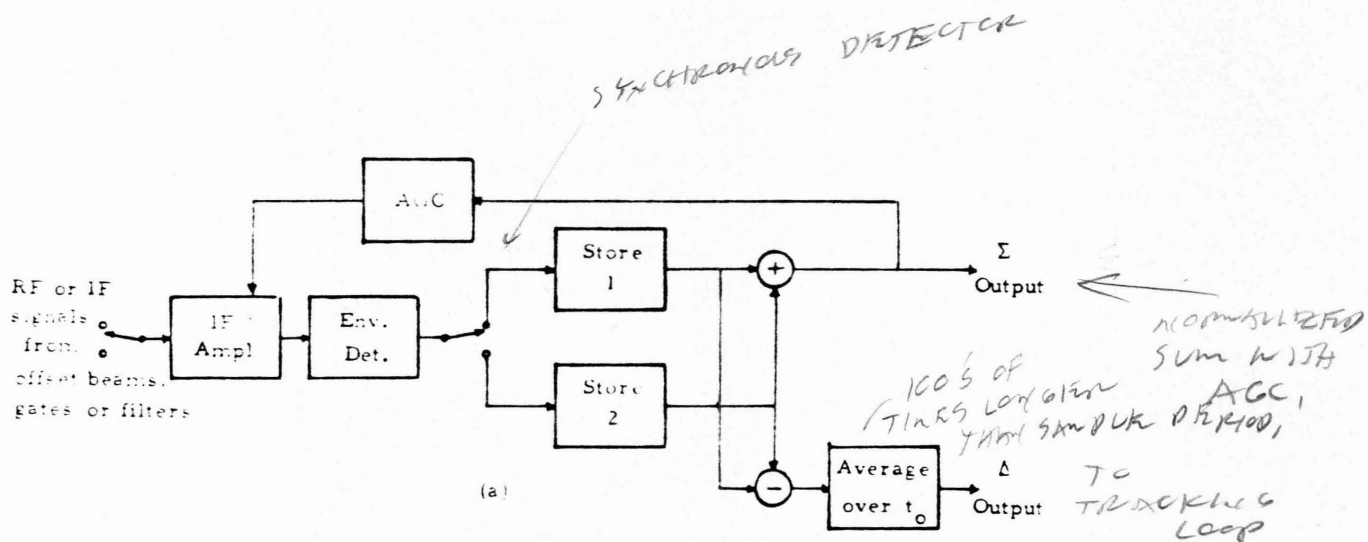


Figure 4. Typical measurement systems using AGC normalization and sequential or simultaneous formation of  $\Sigma$  and  $\Delta$  response: (a) Sequential-channel system. (b) Simultaneous-channel system. (CHANCE PULSES)

width is uniquely related to the slope of the derivative response, which represents the "sharpness" (second derivative) near the center of the original lobe. In Fig. 5, it can be seen that the noise error in output of the measurement discriminator is proportional to the electrical noise voltage divided by the slope of the derivative response. If the gains of the  $\Delta$  and  $\Sigma$  channels are adjusted for equal noise outputs, and the S/N ratio in the  $\Sigma$  channel is large enough to avoid small-signal suppression effects in the error detector, the standard deviation of the measurement can be expressed in terms of the half-power width of the resolution cell:

$$c_z = \frac{z_3}{k_z \sqrt{2(S/N) n}}$$

where the factor of two results from suppression of the quadrature component of noise in the detector, and  $n$  is the number of independent noise samples integrated in the output filter time constant  $t_0$ .

The normalized slope  $k_z$  is a dimensionless quantity near unity for most practical measurement systems. In order to reduce error, for a given S/N and integration time, the width of the resolution cell  $z_3$  must be reduced. This implies a narrow field of view in angle; narrow pulses, gates, spectra and filters in range and Doppler; or instrumentation of many contiguous beams, gates, and filters to cover a broader interval. This trade-off between sensitivity, field of view, and complexity is one of the basic reasons for use of specialized tracking radars to cover specific targets rather than broad search volumes.

The width and shape of the resolution cell or "response function" in a given coordinate are determined by the weighting applied to signals received over an interval in the "transform coordinate." For example, Fig. 6 shows the transform relationships between the antenna illumination in the x-coordinate across the aperture and the antenna pattern in angle. Uniform weighting of signals transmitted or received over the aperture leads to the narrowest beam, but gives high sidelobes. Tapered illumination or weighting gives a broader beam with lower sidelobes. The two-way

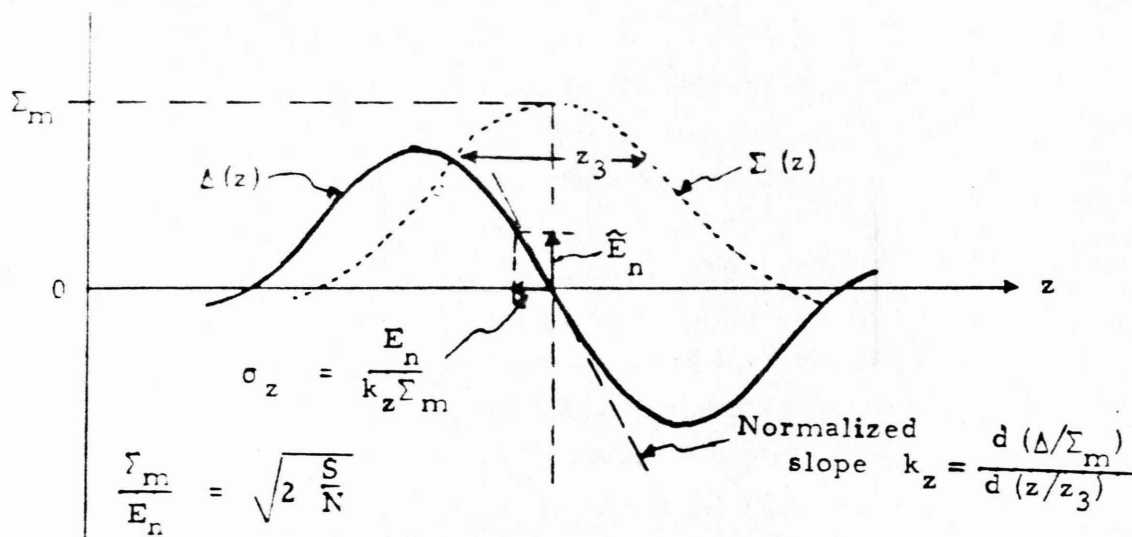


Figure 5. Conversion of small in-phase noise voltage to measurement error.

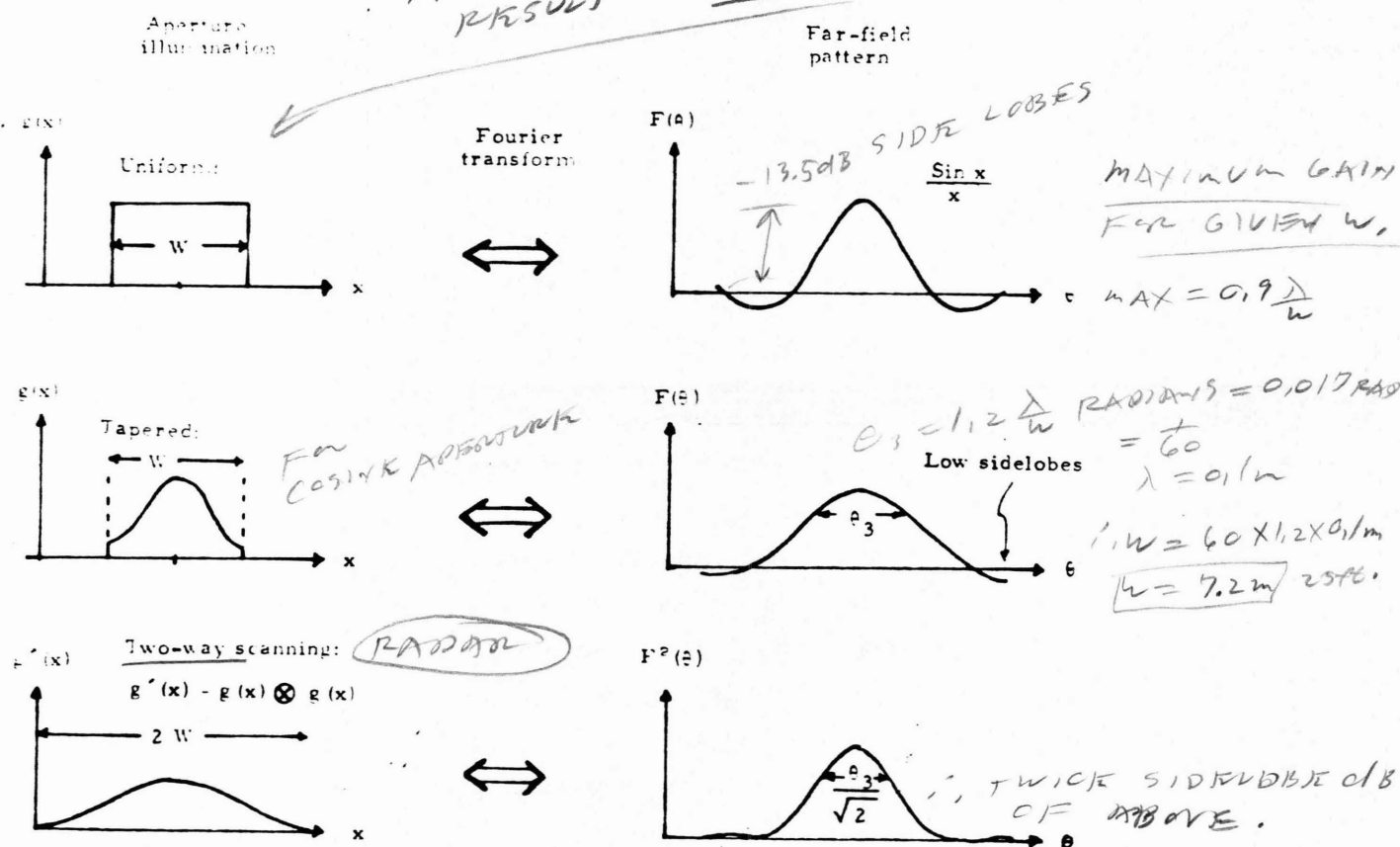


Figure 6. Antenna transform relationships.

scanning pattern is the square of the one-way pattern, and has an equivalent illumination given by the convolution of the actual illumination function with itself (which would require twice the aperture width if produced with a nonscanning antenna). In delay-Doppler coordinates, the Fourier transform relates the frequency spectrum to the time response of the radar. For example, a chirp transmission with uniform spectrum over a bandwidth  $B$  produces a  $(\sin t)/t$  time response with a 3-dB compressed pulse width  $t_3 = 0.886/B$ . Weighting or taper applied to the received spectrum can reduce sidelobes at the expense of a wider output pulse. Doppler filtering of a train of uniform pulses transmitted over a time  $T$  can produce a resolution bandwidth  $B_3 = 0.886/T$  with high sidelobes, or wider bandwidths with lower sidelobes. Because the shapes of all these response functions are similar, within the 3-dB points, the measurement potential in a given coordinate can be related to the illumination or weighting function in the transform coordinate:

Angle error $\sigma_\theta$ depends on $\lambda/w$	}	or more precisely to the rms widths of the weighting in these transform coordinates.
Delay error $\sigma_t$ depends on $1/B$		
Doppler error $\sigma_f$ depends on $1/T$		

Quantitative relationships will be described in a later section.

## B. ANGLE TRACKING TECHNIQUES

1. Sequential Lobing. The earliest tracking radars used sequential lobing (Fig. 7) for angle error detection. The system was derived from the old A-N radio beacons, in which two overlapping beams were keyed alternately to produce a continuous tone at the crossover axis. In early radar, successive groups of pulses were transmitted in the A and B beams, and the "Type K" display showed the two sets of returns with slightly different delays on an amplitude-vs-time sweep. The tracking servo consisted of an operator who turned the antenna handwheel until the two signals were balanced in amplitude. Referring to Fig. 4a,

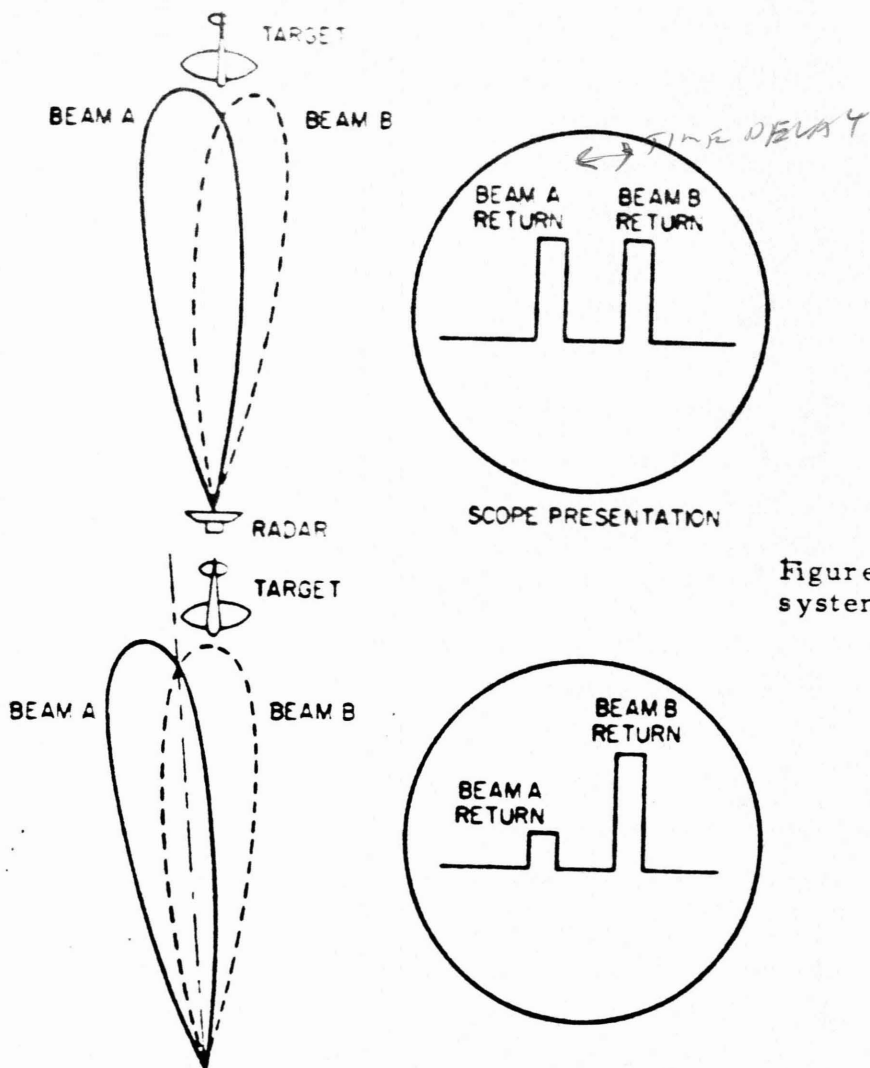


Figure 7. Sequential lobing system [ 3, p. 21-6].

*RADAR  
HANDBOOK BY  
W. H. P. H. H.*

*EARLY WWII (1938)  
SCR 268.*

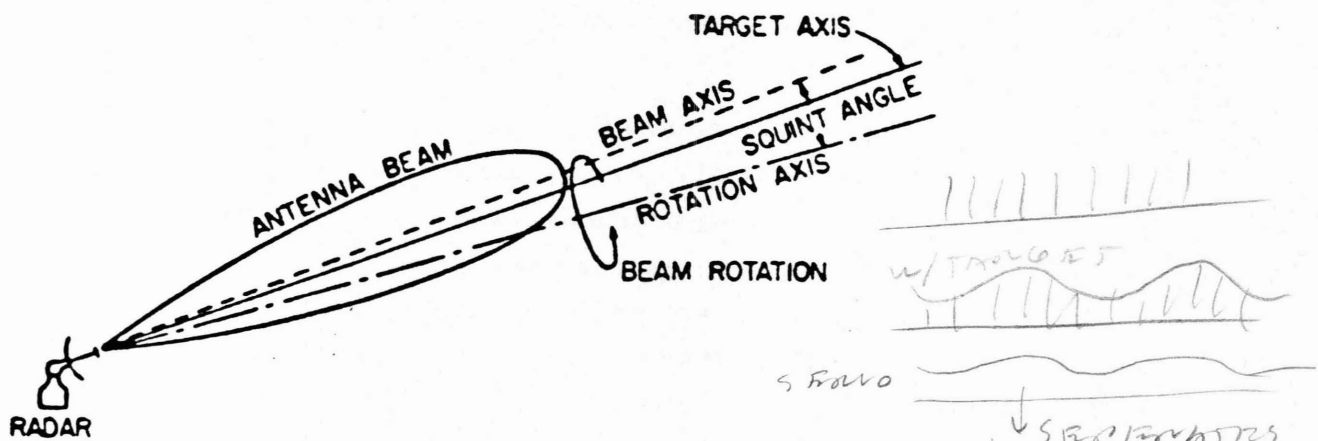


Figure 8. Conical-scan tracking [ 3, p. 21-6]. 1943

*RECEIVING  
+ AEMUTH  
RESOLVED  
FOR  
TRACKING.*

the two input channels are alternating beams formed by the antenna, connected to receiver with manual gain control or slow AGC (to average over both beams). The summing and differencing operations are performed visually, the display-operator combination providing adequate storage of the sequential data and integration over periods in the order of seconds. For tracking in both angular coordinates, the pulses are divided into four groups, so that elevation and traverse sensing is time multiplexed, with separate displays and operators.

2. Conical Scanning. When microwave radar was developed during World War II, narrow pencil beams became available and the technique of conical scanning was introduced (Fig. 8). The beam is offset from the tracking axis by the squint angle  $\theta_k$ , and is rotated rapidly around that axis, producing sinusoidal modulation of the received signal envelope. This modulation is recovered after the second (envelope) detector (Fig. 9), and demodulated by a reference voltage synchronized to the scan, producing elevation and traverse error signals which control the pedestal servos. As with lobe-switching sequential scan, the received energy is shared between the two coordinates. Conical scan antennas may use either rotating or nutating feeds (the latter maintaining constant polarization), or the scan may be generated by electronic combination of clustered feedhorns. If the scan modulation is generated electronically in the receiving channel, the system is known as "silent lobing" or COSRO (conical-scan-on-receive-only). Since many pulses (at least four) must be received in each scan cycle, and many scan cycles averaged in the servo, the system bandwidth is limited to a very small fraction of the repetition rate.

3. Linear Scanning. Since the closing phases of World War II, the precision approach radars of ground-controlled approach and landing systems have used the scanning procedure illustrated in Fig. 10. Two separate beams are generated, one scanning in azimuth and one in elevation, and usually time sharing a single transmitter and receiver. Each beam is narrow in the scanned coordinate and broad enough in the other coordinate to cover a good part of the scanning field of the other

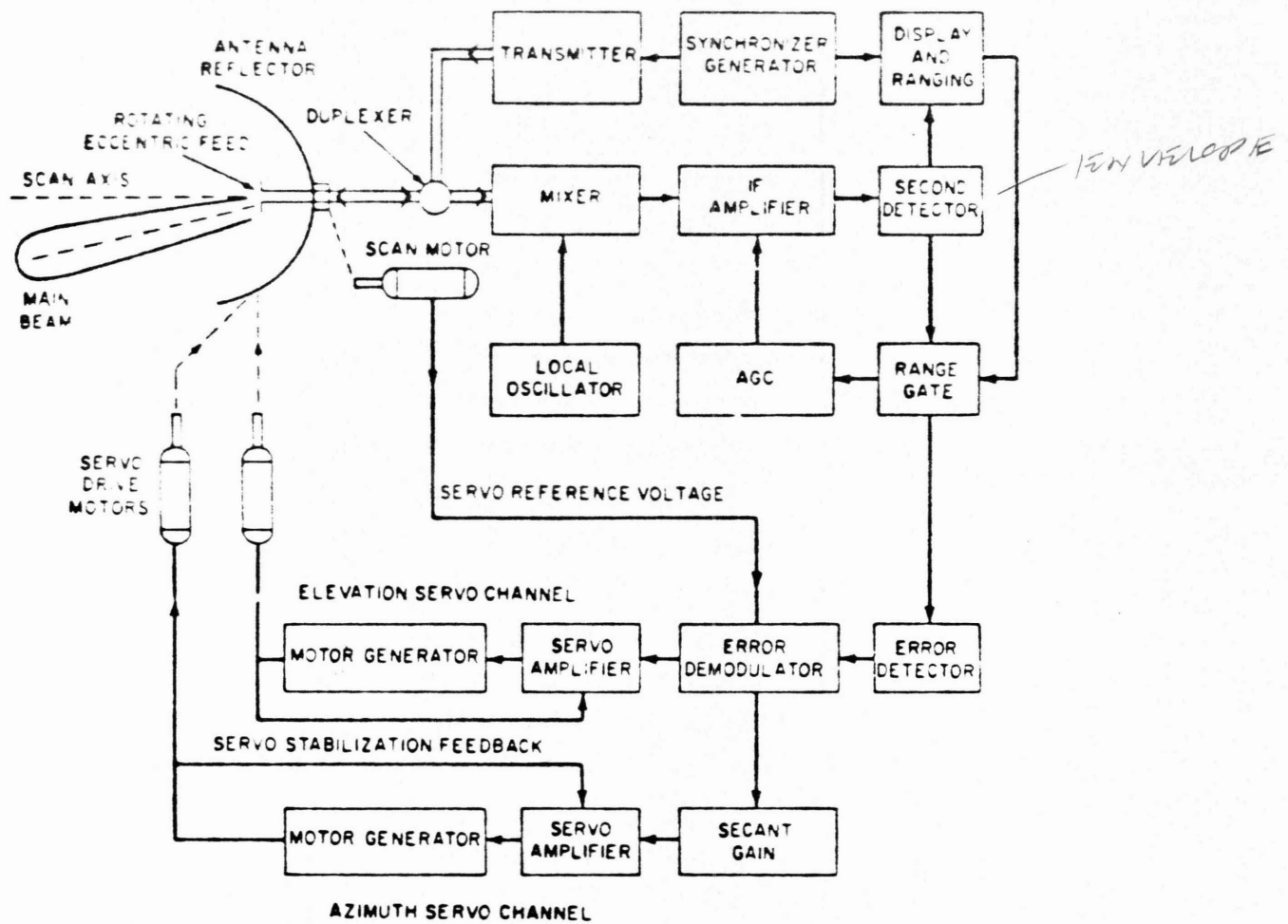


Figure 9. Block diagram of a conical-scan radar [ 3, p.21-7 ].

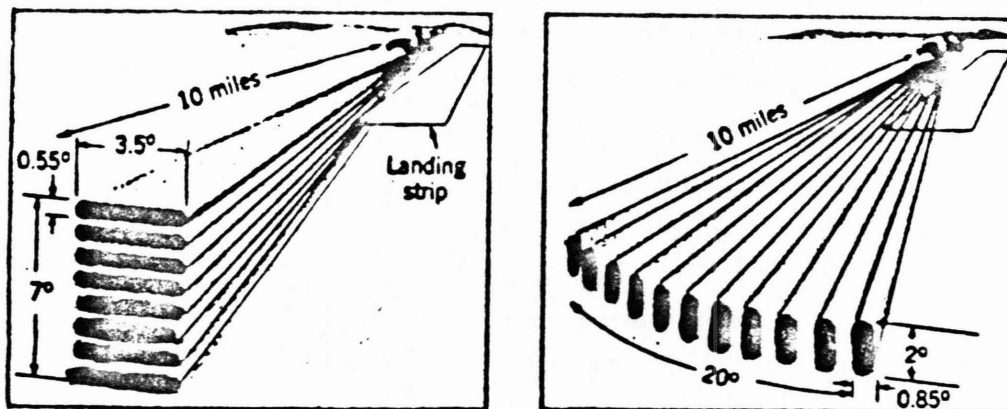


Figure 10. Two-coordinate, linear-scanning system for precision approach radar [ 10 ]. AS ACCURATE AS BEST MONOPULSE SYSTEM.

↑  
ALSO RUSSIAN SA2 AND SA3 SYSTEMS CAN TRACK SIMULTANEOUS TARGETS.



beam. In each coordinate, an intensity-modulated CRT produces a narrow blip on a range-angle display calibrated with range marks and the established approach path. The operator interpolates visually the center of each blip and advises the pilot of his deviation from the intended approach. This is a case of track-while-scan within a limited scan sector, and the loop is closed through verbal commands to the pilot. A similar scan procedure is used with automatic tracking gates (angle gates) in some foreign equipment for missile command guidance, and in one coordinate the procedure is commonly applied for track-while-scan in 2D search radars and nodding height finders.

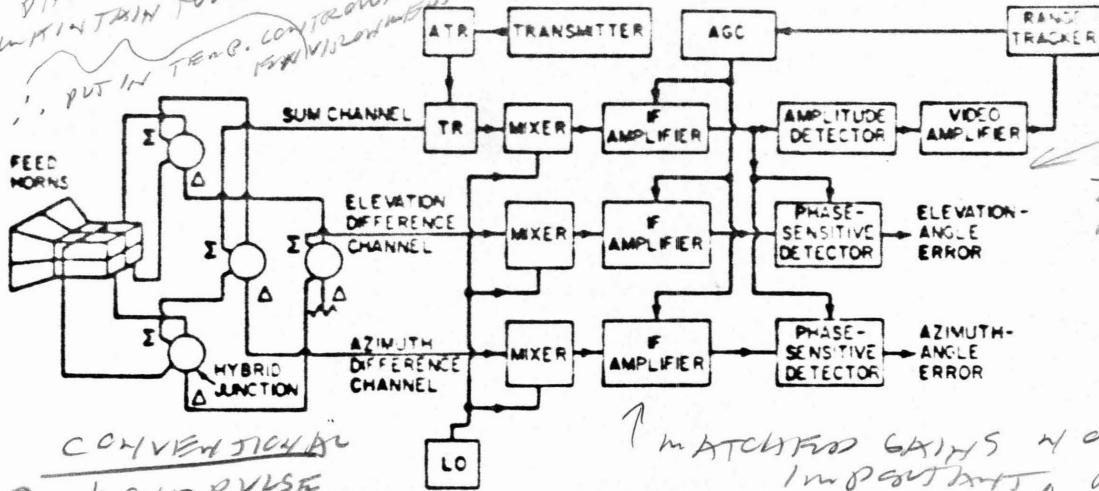
4. Monopulse. The monopulse tracker makes the best use of signal energy by forming simultaneously the on-axis  $\Sigma$  beam and its derivative patterns in traverse and elevation (Fig. 11). The on-axis target produces maximum signals in the  $\Sigma$  channel and nulls in both  $\Delta$  channels. A small deflection of the axis from the target in either coordinate produces a proportional signal in the corresponding  $\Delta$  channel, with a phase of 0 or 180 deg indicating the direction of the error. The signal energy diverted to the  $\Delta$  channel is only that which is lost from the  $\Sigma$  channel due to misdirection of the  $\Sigma$  beam, and both  $\Delta$  channels receive the benefit of each received pulse, providing complete data on target position in a single pulse interval. At the same time the target is illuminated with the full on-axis gain of the  $\Sigma$  pattern, to which the transmitter is connected. In addition to its greater efficiency in use of energy, the monopulse system is insensitive to natural target amplitude fluctuations (scintillation) and to AM jamming from the target.

The type of monopulse tracker most often used is the sum-and-difference amplitude-comparison system shown in Fig. 11, which may be considered to form each  $\Delta$  pattern by subtracting squinted receiving beams (Fig. 2). In fact, since the horn phase centers are less than a wavelength apart and may involve multiple-mode excitations, there may be no individually generated beams, but only the composite  $\Sigma$  and  $\Delta$  patterns. In stacked-beam height finders and some array radars, the individual beams are generated in the antenna, received and processed

"STATIC SPLIT" (BRITISH MONOPULSE)  
(NOTHING MOVES.)

NOTED AMPLITUDE + PHASE  
STABILITY AND SIMILARITY.

DIFFICULT TO  
MAINTAIN TOLERANCES.  
PUT IN TEMP. COMPENSATION



CONVENTIONAL  
MONOPULSE

↑ MATCHED GAINS NOT  
IMPORTANT, BUT STILL  
NEED PHASE TRACKING.

Figure 11. Block diagram of a conventional monopulse tracking radar [3, p. 21-13].

TODAY  $\frac{1}{200}$  OF BEAMWIDTH  
→ ACCURACY AND  
PRECISION & PROBABILITY  
BIAS PROVED.

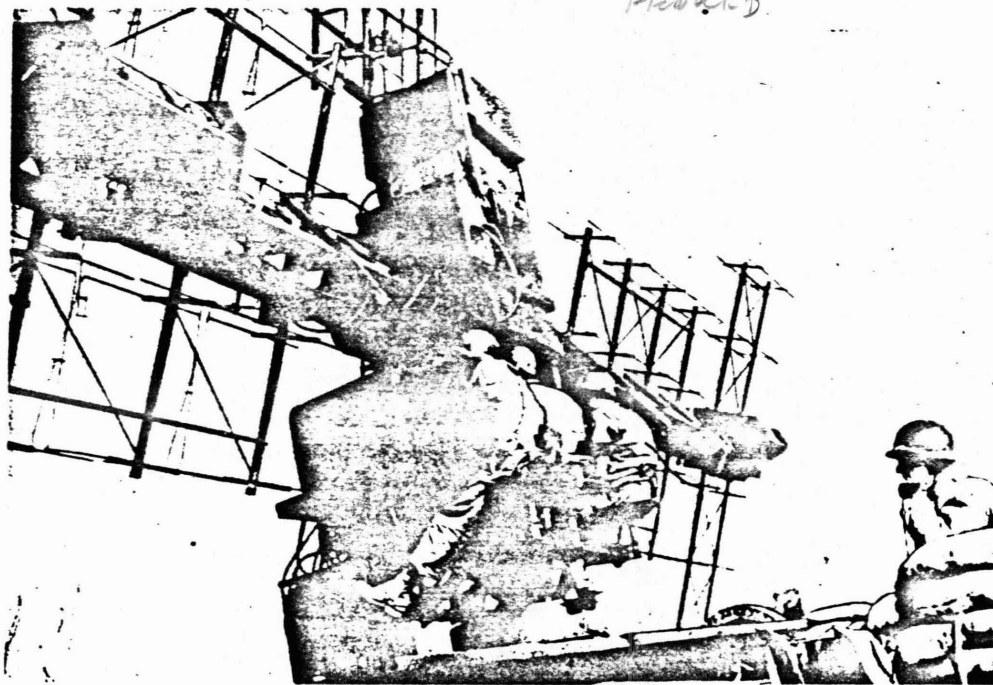


Figure 12. The SCR-268 sequential-lobing radar.

BRITISH MONOPULSE

REQUIRED WATCHED GAINS



separately, and combined in  $\Sigma$  and  $\Delta$  networks at IF or video, to give a true "amplitude comparison monopulse" system. The other major type of monopulse system uses "phase comparison" between signals received by separate (generally contiguous) antennas. Combination phase-amplitude systems have also been built. It is important to note that the distinction between amplitude and phase monopulse is in the phase-center spacing between antenna feed points, and that subsequent networks at RF or IF can transform the angle information of either system into amplitude- or phase-coded form.

### C. TRACKING RADAR ANTENNAS

1. Lobing and Scanning Antennas. The earliest U.S. tracker to use sequential lobing was the SCR-268, a VHF dipole array system which used human servos for pointing (Fig. 12). By alternately switching small phase shift sections in the feed network, the beam could be offset up and down or right and left, generating the target angular measurement function. The system had a very respectable power-aperture product and range, but at 200 MHz its beamwidths were so great ( $\approx 20$  deg) that it was used only to designate optical fire control systems, rather than as the source of gun orders. In 1943, the SCR-584 (Fig. 13) became available for antiaircraft fire control [ 4 ]. The first of the microwave, pencil-beam trackers, this radar used an offset dipole, spinning at 30 Hz to scan the 4-deg beam in a cone around the tracking axis. Automatic angle tracking to about 2 mr accuracy was provided on typical aircraft targets, the primary source of error being target scintillation components at the 30 Hz scan rate.

Apart from the conventional 2D search radars and nodding height finders, which measured azimuth or elevation over a wide field of scanning, the prime use of linear scanning techniques has been in GCA systems. The "Eagle scanner," Fig. 14, was originally developed for an aircraft radar, but its major application has been in the X-band precision approach radars AN/MPN-1 and derivative types (still in use today). This antenna uses two linear phased array feeds to illuminate cylindrical reflectors for azimuth and elevation scanning. The feeds are of the waveguide type,

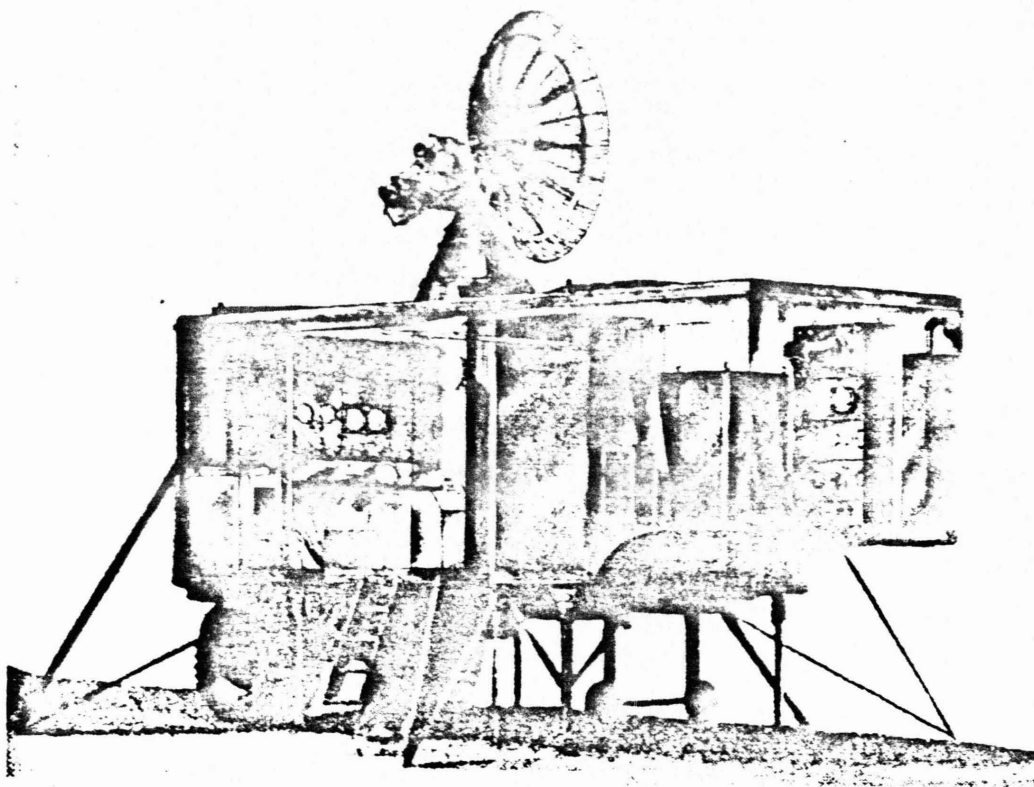
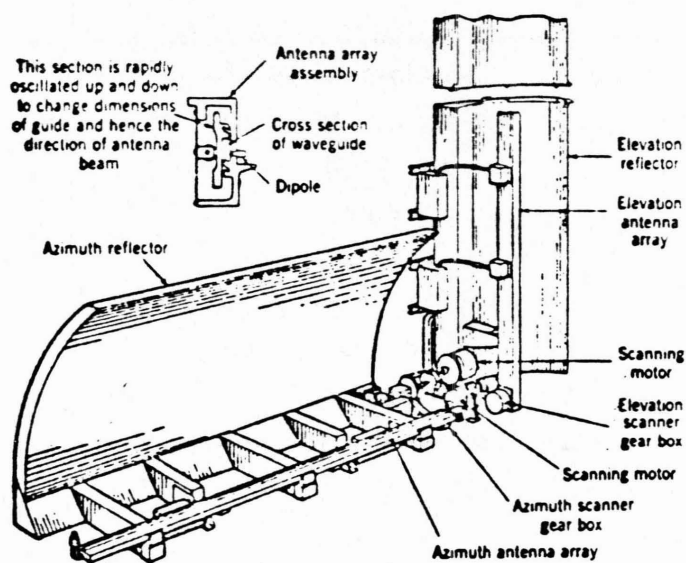


Figure 13. The SCR-584 conical-scanning radar.



(WAVEGUIDE (UNIFORM PHASE SLOTS),  
MODULATED WIDTH OF WAVEGUIDE CAN TO SHIFT  
Figure 14. Eagle scanner for GCA azimuth scan [10]. PHASE,  
(SOME ARE STILL IN USE)

with dipoles coupled into the guide with probes. The width of the guide is varied mechanically to change the phase velocity in the guide and hence the incremental phase shift between radiating elements. Beam-width in the scanning plane is 0.6 to 0.8 deg, with a 2-sec total scan time for both coordinates. Scanners of this type have operated for years with only moderate maintenance problems.

2. Monopulse Feeds. The early monopulse antenna was designed from the viewpoint of a cluster of four feed horns, producing four beams squinted in space. Two 90-deg phase shifters and four microwave hybrids (Fig. 15) were used to form the  $\Sigma$  and  $\Delta$  outputs. The optimization problem involved choosing the horn dimensions to obtain the best compromise among  $\Sigma$  efficiency,  $\Delta$  slopes, and sidelobe levels in all three patterns. It was shown by Hannan [ 5] that this simple feed could not approach very closely the optimum functions for  $\Sigma$  and  $\Delta$  illuminations over the lens or reflector aperture, as derived by Kirkpatrick [ 6].

Considering only gain and slope optimization, for a given aperture, Kirkpatrick repeated the classic derivation showing that the ideal  $\Sigma$  illumination was uniform over the aperture, and then proceeded to show that the ideal  $\Delta$  illumination (for maximum slope) was a linear-odd function. These illuminations, however, give high sidelobes (Fig. 16), which fall off very slowly with angle. Furthermore, they cannot be generated in horn-fed systems without excessive spillover loss (and accompanying lobes near 90 deg). When sidelobes and horn limitations are considered, both illumination functions become tapered (Fig. 17), but the horn size which gives an efficient  $\Sigma$  taper has large  $\Delta$  spillover and sidelobes, while the larger horn for good  $\Delta$  illumination gives an inefficient  $\Sigma$  illumination. A useful view of the problem is given by Dunn and Howard [ 7] in terms of the fields in the focal plane of the lens (or reflector), shown in Fig. 18. The focussed spot representing the target moves as the target deviates from the antenna axis, producing unequal fields in the four horns. If the horn cluster is matched to the size of the focussed spot, to obtain optimum  $\Sigma$ -channel gain, the individual horn dimensions are too small to accept the full energy from an off-center spot, as needed for high  $\Delta$ -channel gain and slope.

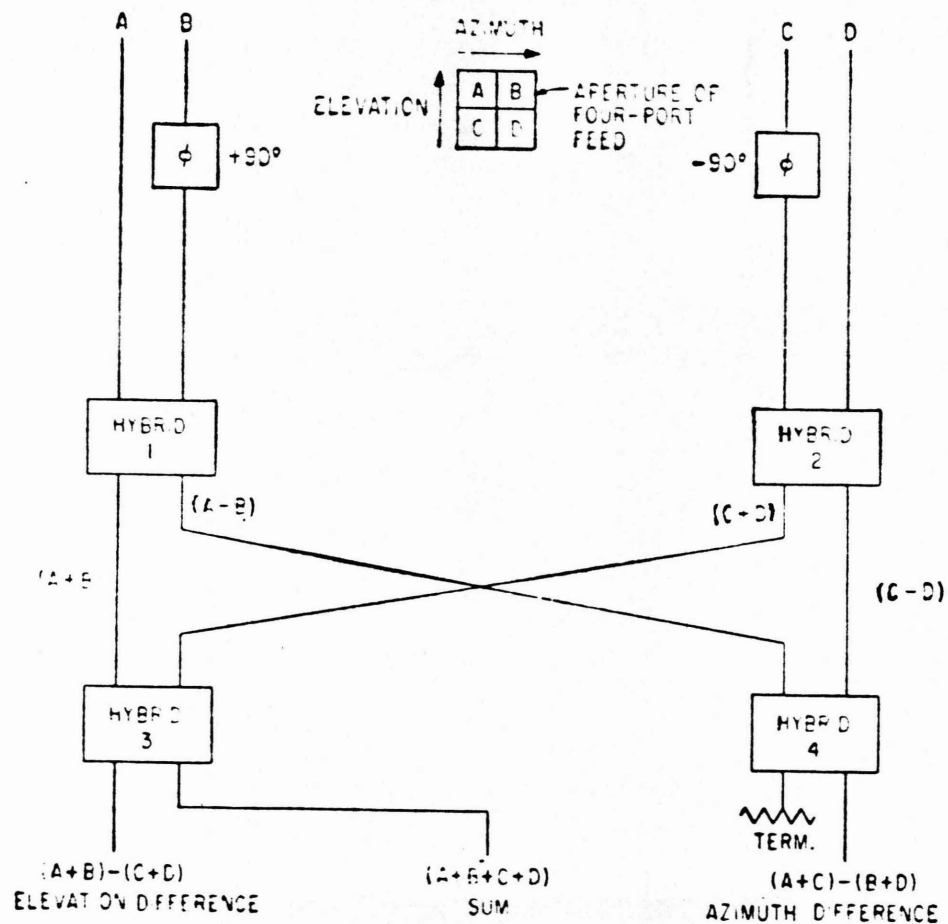


Figure 15. Microwave comparator circuit forming sum and difference channels from four-horn monopulse feed [ 7 ] .



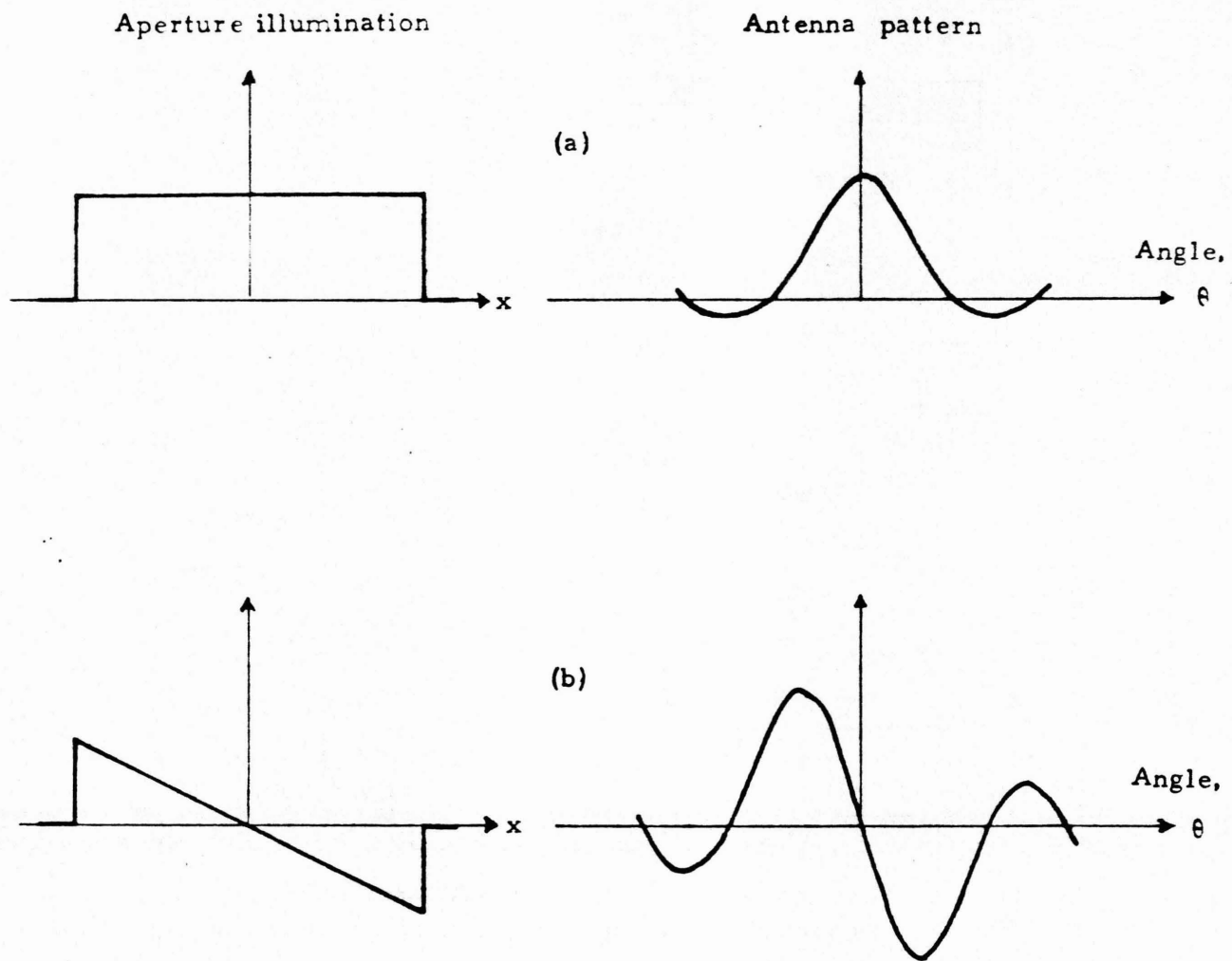


Figure 16. Illuminations and patterns for maximum  $\Sigma$  gain and  $\Delta$  slope with a given aperture: (a)  $\Sigma$  channel; (b)  $\Delta$  channel.



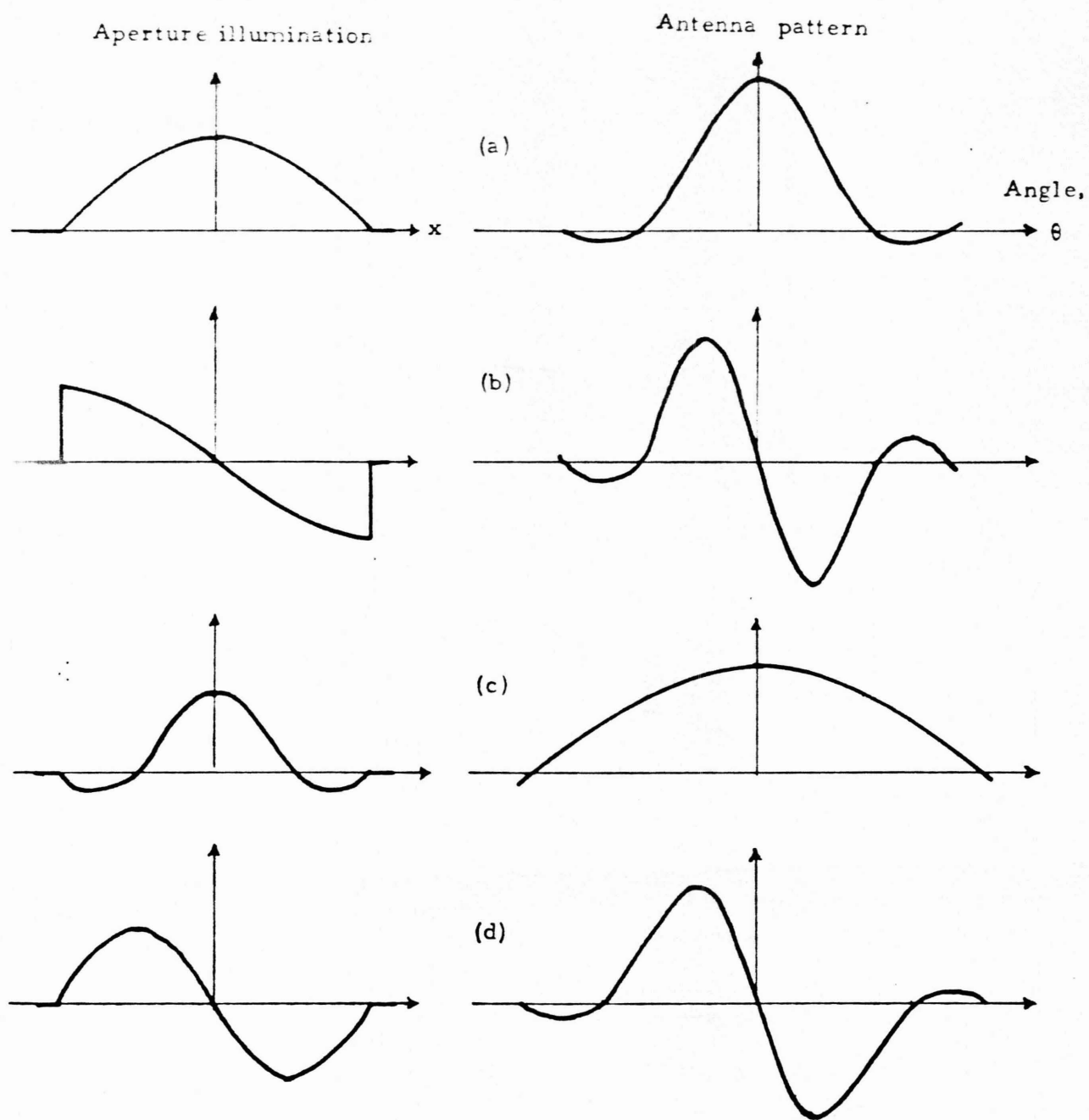
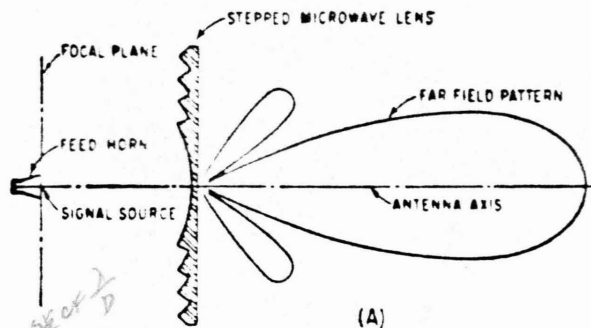
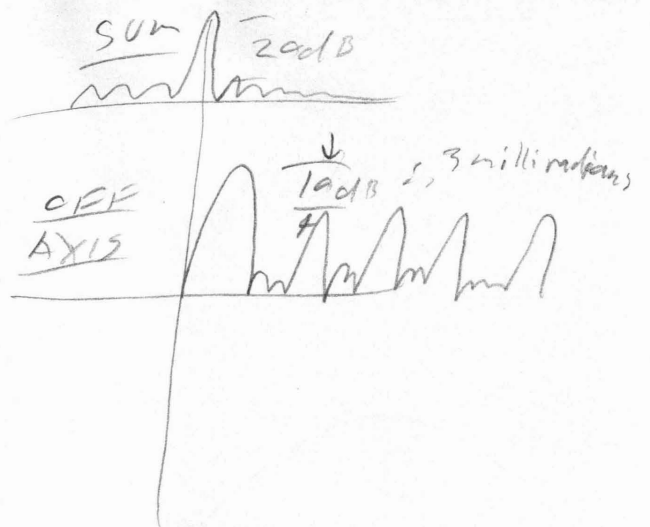
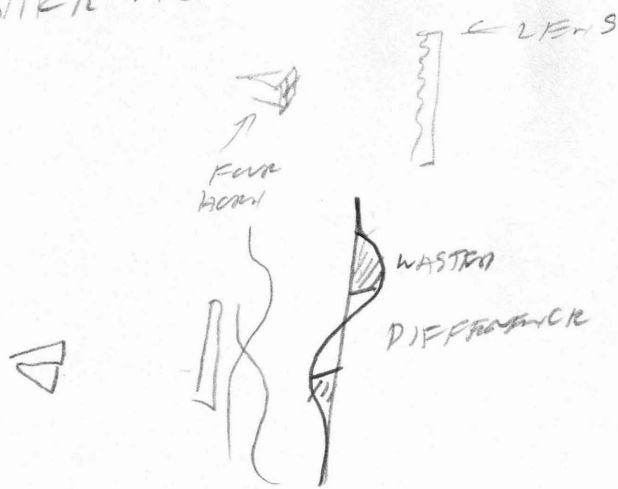
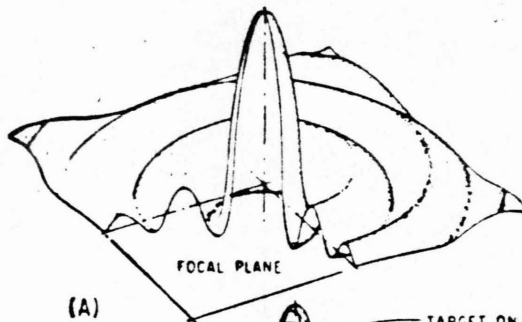


Figure 17. Patterns for tapered illuminations using four-horn clusters: (a, b) small horn cluster; (c, d) large horn cluster.

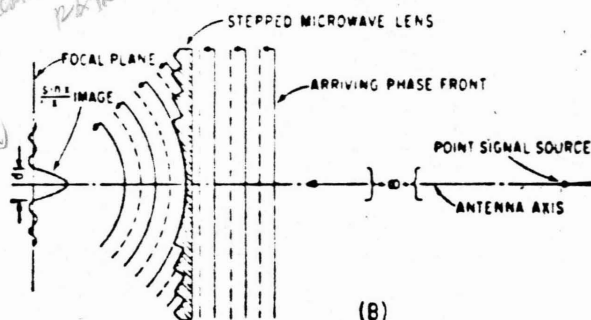
NICK-AJAX



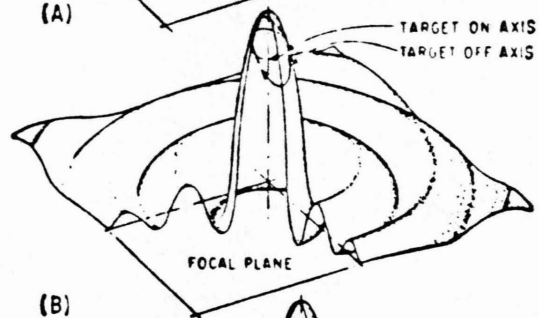
(A)



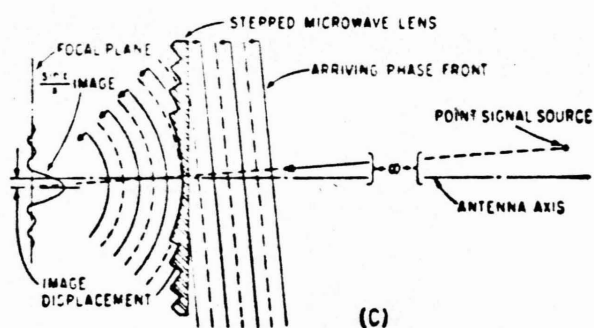
(A)



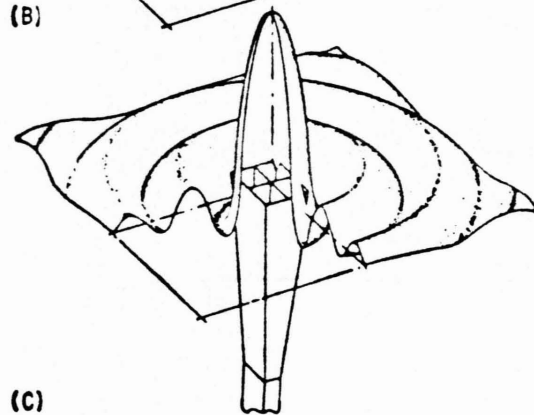
(B)



(B)



(C)



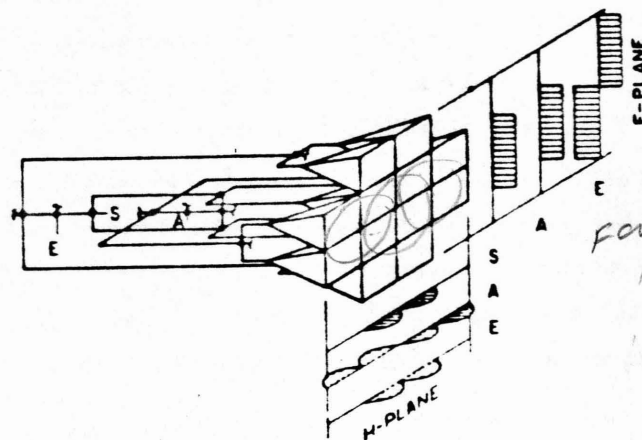
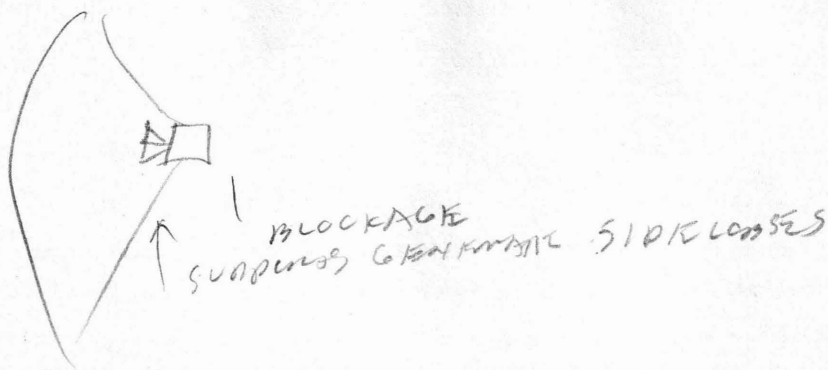
(C)

Figure 18. Two- and three-dimensional views of received energy in focal plane: (A) single, on-axis feed; (B) offset feed with conical scanning; (C) four-horn cluster [7].

The solution to this optimization problem, developed during the late 1950's, is to use a larger array of horns (Fig. 19), with multimode excitation or additional hybrids. The  $\Sigma$ -channel excitation appears in the central region of the  $4 \times 4$  array, matching the on-axis focal spot. Each  $\Delta$  channel excites the outer regions of the feed array (with opposite polarities) to maintain high  $\Delta$  gain and slope. These "four-level" feeds are larger and more complex, and can best be used with lens antennas or Cassegrainian reflectors, which minimize blockage problems. Early monopulse trackers included the Nike Ajax (Fig. 20) and the AN/FPS-16 Instrumentation Radar (Fig. 21), both of which used four-horn feeds. The 25-m diameter AN/FPS-49 dish (Fig. 22), operating at 425 MHz, was fed by a 5-horn configuration, with only the central  $\Sigma$  horn designed to handle the 300-kw average transmitter power. A four-layer, multimode feed was used in Nike Hercules (Fig. 23), achieving major improvements in gain and sidelobe levels as compared to Nike Ajax.

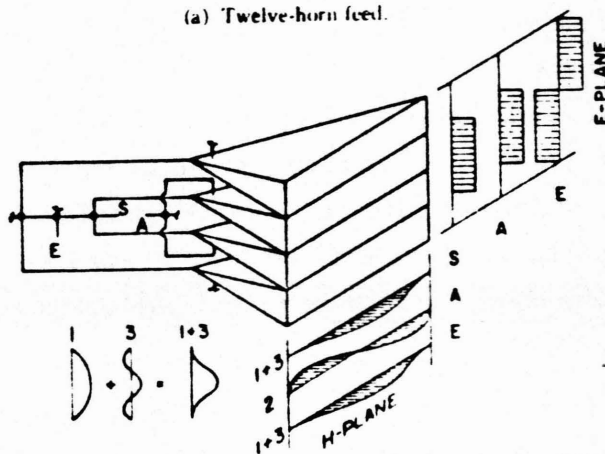
3. Phased Array Trackers. The corporate-fed phased array presents special problems in monopulse beam forming. In principle, the optimum illumination functions for all three patterns can be formed using a set of three hybrids for each set of four symmetrically located elements. The  $\Sigma$ ,  $\Delta_e$  and  $\Delta_a$  outputs of the hybrids are combined in three separate corporate feed networks, giving completely independent control of the three illumination functions, at the expense of extreme complexity. At the opposite extreme, the aperture can be divided into quadrants and these four outputs combined in three hybrids, giving a choice of poor  $\Delta$  sidelobes or poor  $\Sigma$  sidelobes (Fig. 24a).

Three general approaches have been used to overcome this compromise between complexity and poor performance. The subdivision of the array into more modules or subarrays (Fig. 24b) reduces the sidelobes with modest increase in numbers of hybrids. The AEGIS antenna [ 13 ] is an example of this approach (Fig. 25). The "Lopez feed" uses a dual ladder network (Fig. 26) to synthesize smooth, tapered illumination functions in both  $\Sigma$  and  $\Delta$  channels. In a two-coordinate array, such networks must be used for each row, and two additional networks then combine the rows



FOUR HORNS — FOR EACH output,  
NEW LAYS?

(a) Twelve-horn feed.



(b) Four-horn triple-mode feed.

Figure 19. Multilayer monopulse feeds [ 5 ] .

WHETHER LAYS.

(SIMILAR TO NEW LAYS SYSTEM)

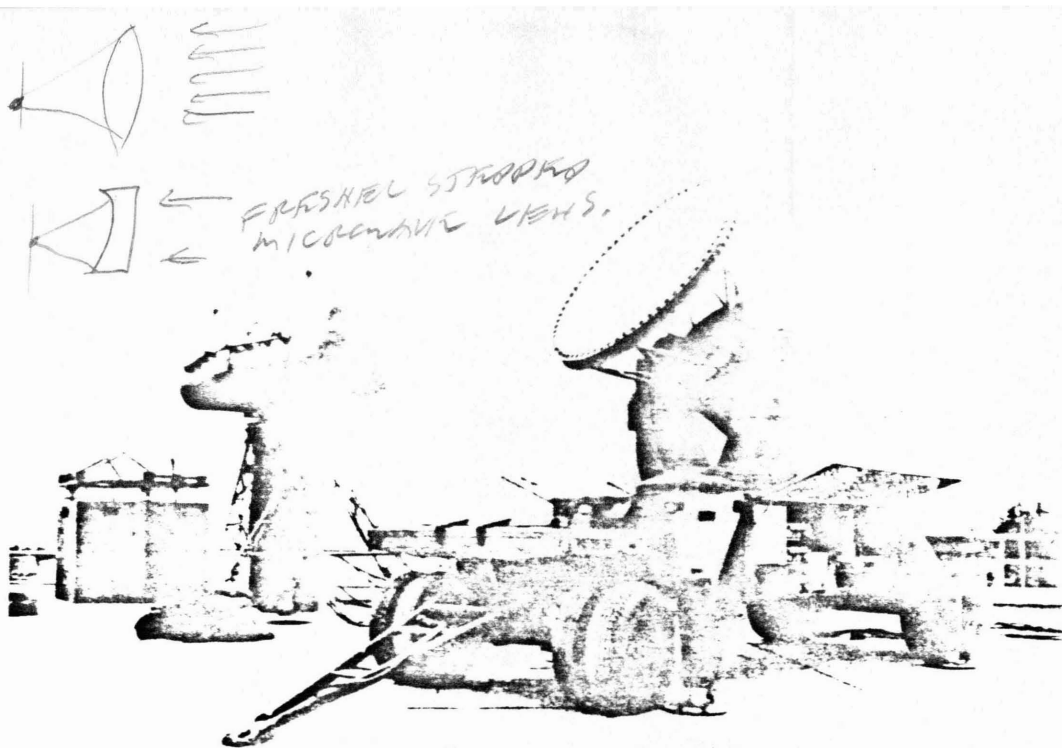


Figure 20. Nike AJAX tracker, using a 1.8-m diameter lens with 4-horn feed at 9 GHz. In the background is a search radar used for acquisition.

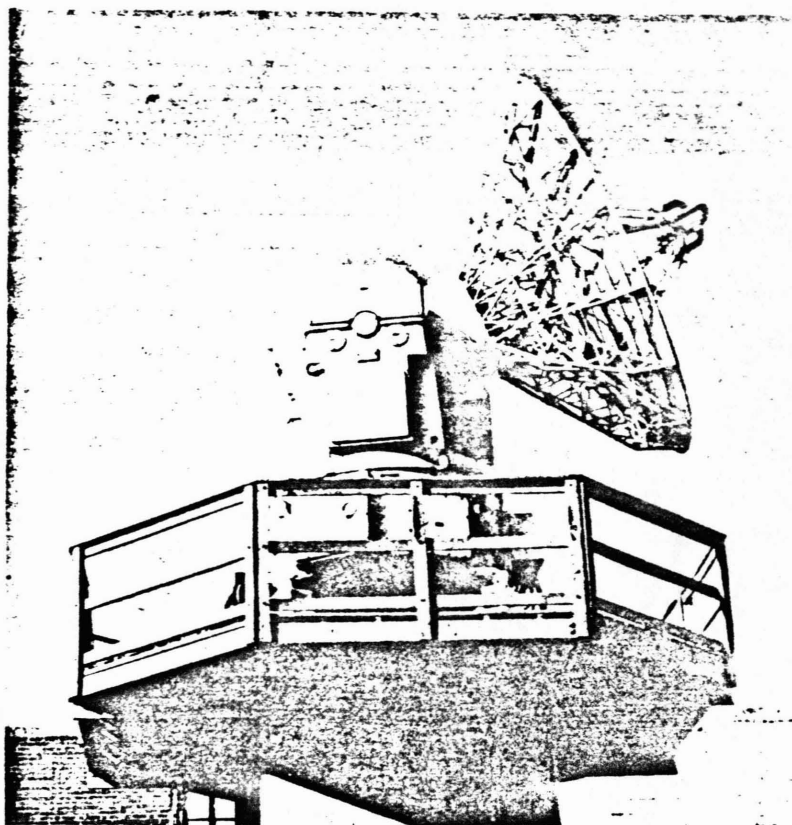


Figure 21. AN/FPS-16 instrumentation radar, using a 3.6-m reflector and 4-horn feed at 5.6 GHz, with multimode excitation in the azimuth plane.

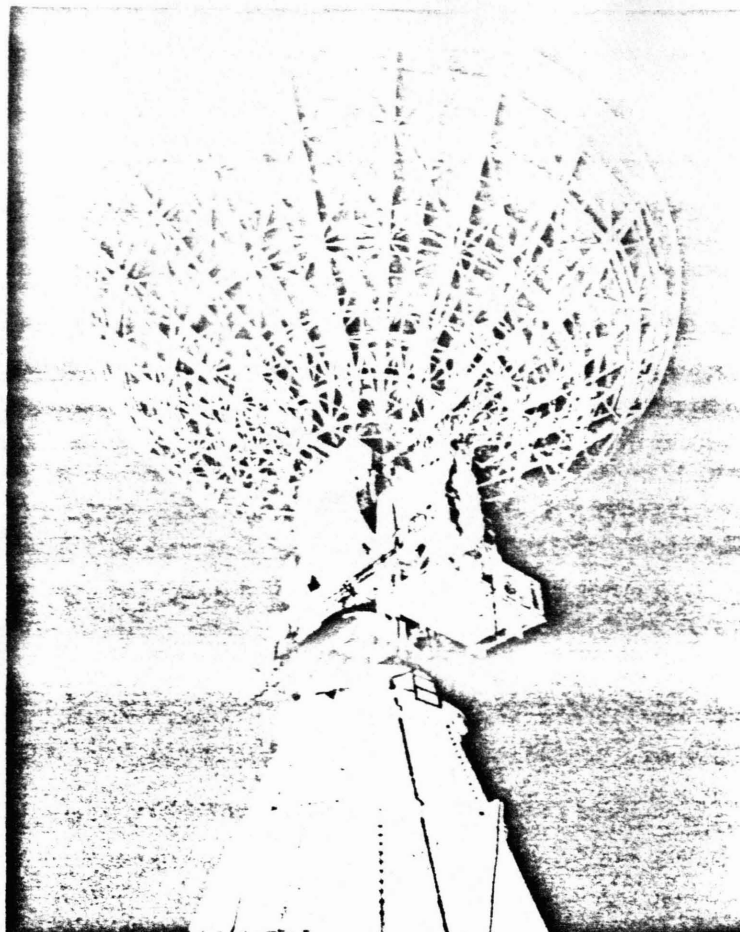
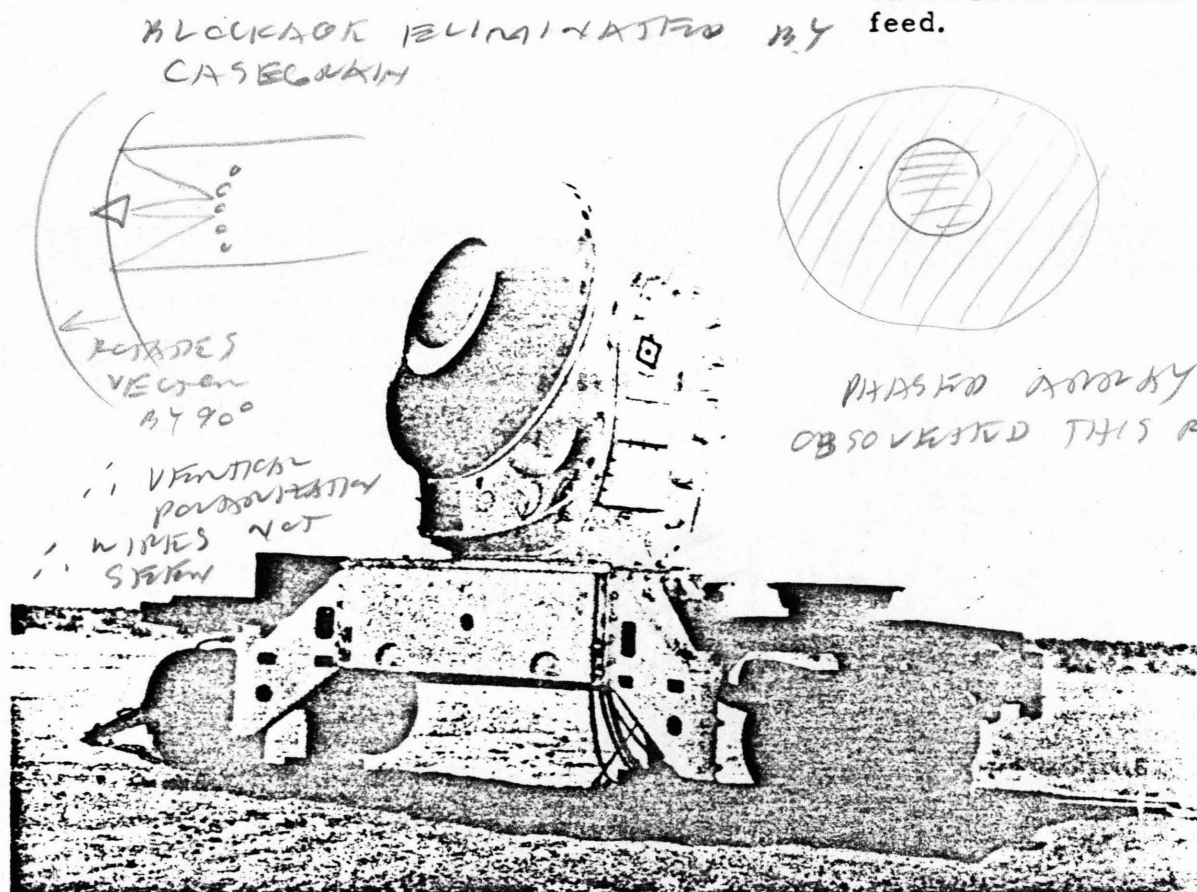
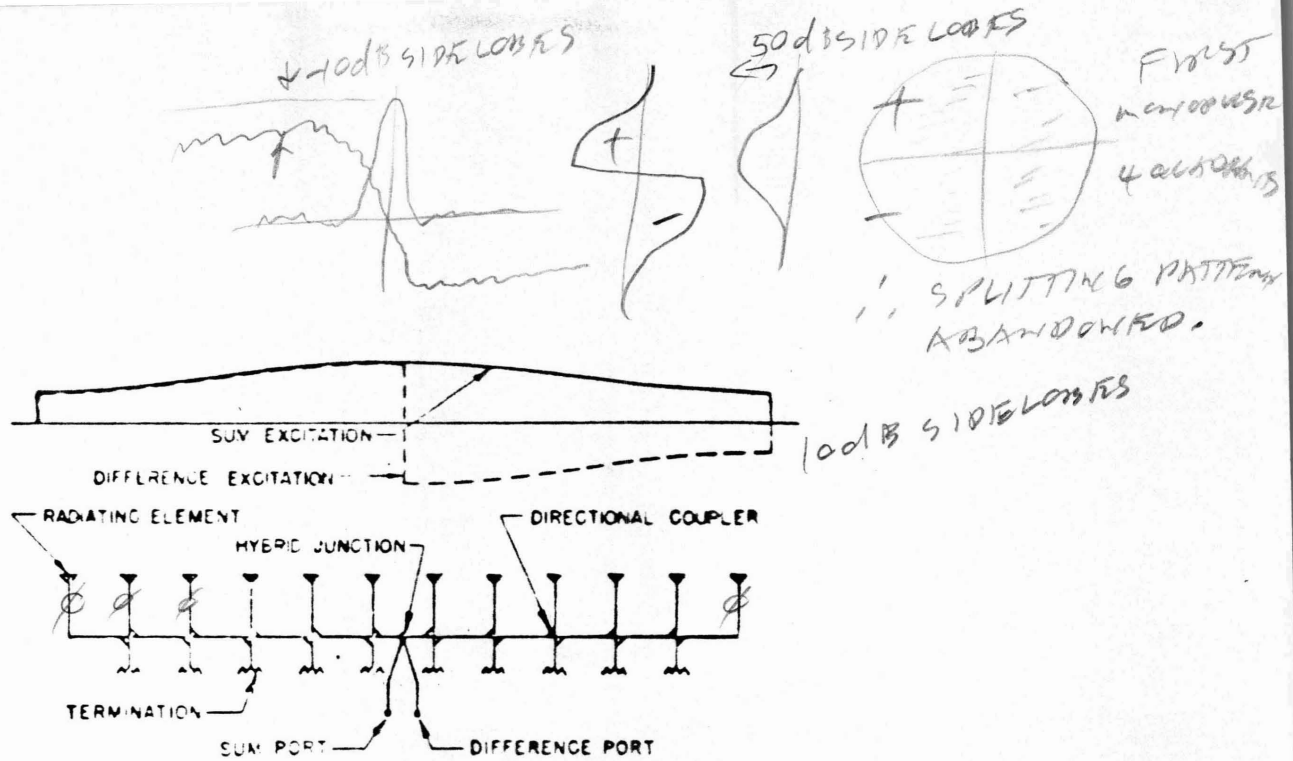


Figure 22. AN/FPS-49 BMEWS search-track radar, with a 25-m reflector and 5-horn monopulse feed, at 425 MHz.

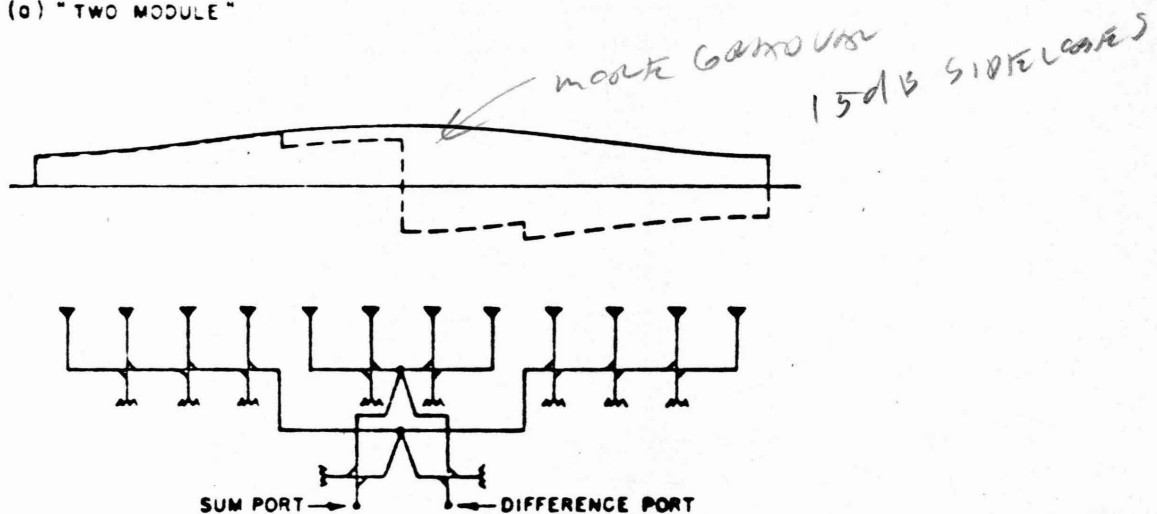
Figure 23. Nike Hercules tracking antenna, a Cassegrainian system with 2.4-m main reflector and 4-level multimode feed.







(a) "TWO MODULE"



(b) "FOUR MODULE"

Figure 24. Monopulse series-feed networks for linear arrays [12].

WHETHER 4/10 S.

$$\text{For } 10 \text{ } w = 72\lambda$$

$$10 \times 10 \text{ } w \times h = 72 \times 72\lambda^2$$

$$\therefore D = 72\lambda \text{ SQUARE APERTURE,}$$

$$\begin{matrix} \frac{\Delta}{2} \\ \frac{\Delta}{2} \end{matrix} \leftarrow \frac{\pi}{2} \pi \pi \pi \pi \pi \pi$$

$$\therefore N_D = 14.4 \text{ ELEMENTS (ACTUALLY 100 ELEMENTS)}$$

$$\therefore T = 10^4 \text{ TOTAL ELEMENTS.}$$



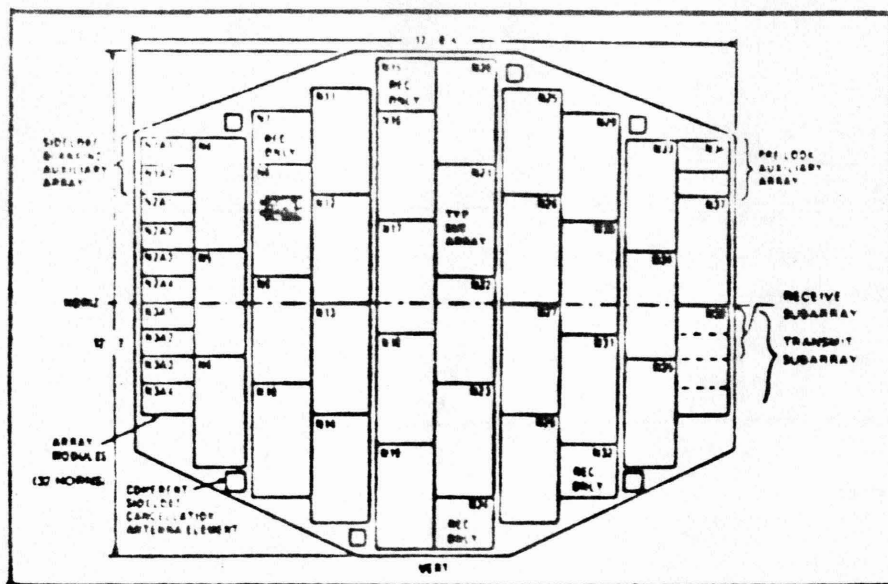


Figure 25. Arrangements of sub-arrays in AEGIS antenna [13].

ONLY 40 FEEDS  
WITH SEGMENTED FEEDS.  
STILL VERY EXPENSIVE.

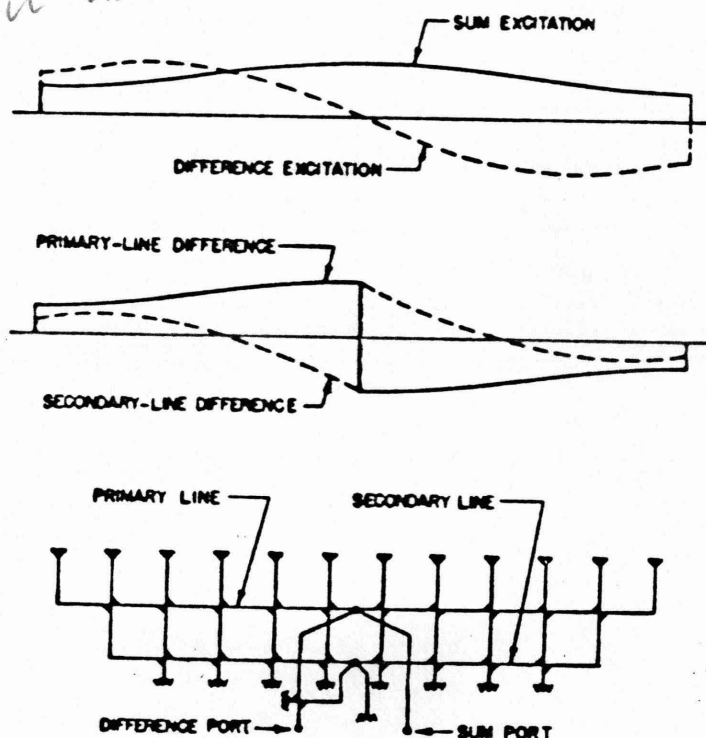


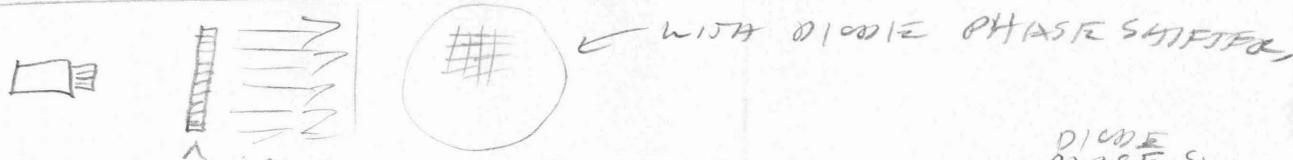
Figure 26. The Lopez feed: a dual-ladder network for separate optimization of  $\Sigma$  and  $\Delta$  excitation of a linear array.

WHENEVER HAS (HARD WHENEVER [LONG ISLAND] (GREAT NECK AREA))

28

- EXPENSIVE
- EXTREME TOLERANCES
- COMPLICATED.

∴ USE SUBARRAY APPROACH



to form a single  $\Sigma$  and two  $\Delta$  channels. The third array approach uses an optically-fed lens or reflector (Fig. 27), separating the beam steering function of the aperture elements from the monopulse feed design and permitting conventional multi-layer monopulse feeds to be used. This is the approach used in the SAM-D radar (Fig. 28), where an efficient, four-layer, multimode receiving feed horn is centered between two simple transmitting horns. The array elements are adjusted between transmitting and receiving to focus on the proper feed.

One further example of a monopulse tracking antenna is the limited-scan array-fed reflector of the AN/TPN-19 PAR (Fig. 29). A small (800-element) array, analogous to the subreflector of a Cassegrainian antenna, is illuminated by a multimode monopulse feed horn assembly. Control of the array element phase shifters changes the illumination over the main reflector to scan the monopulse beam cluster over a limited field of view ( $15 \times 20$  deg). The  $0.75 \times 1.4$  deg beam would normally require some 10,000 phasing elements in a planar array, with appropriate feed networks for three-channel monopulse operation. This radar, deployed as in Fig. 30, represents the only production phased-array radar system in the U.S. (if frequency scan 3D radars are excluded).

4. Pedestals and Mechanical Design. Except for fixed array designs with electronic steering, the tracking radar is dependent on rapid, smooth and accurate antenna pointing by its pedestal, and extraction of angular data from shaft angle encoders. The art of pedestal and antenna mechanical design has progressed steadily from the SCR-584 through Nike AJAX and Hercules, AN/FPS-16, and larger systems such as AN/FPS-49 and Rampart (Fig. 31). A prime requisite of all these systems is a very rigid structure with high mechanical resonance frequencies. This makes it possible to close the servo loops with high enough gain to overcome slowly varying wind loads and wide enough bandwidth to minimize tracking lags. Other considerations include low friction and stiction, accurate and stable alignment of axes, freedom from thermal expansion errors, and provisions for accurate boresighting and calibration. In most cases, radomes are not used and the antenna is exposed to wind and

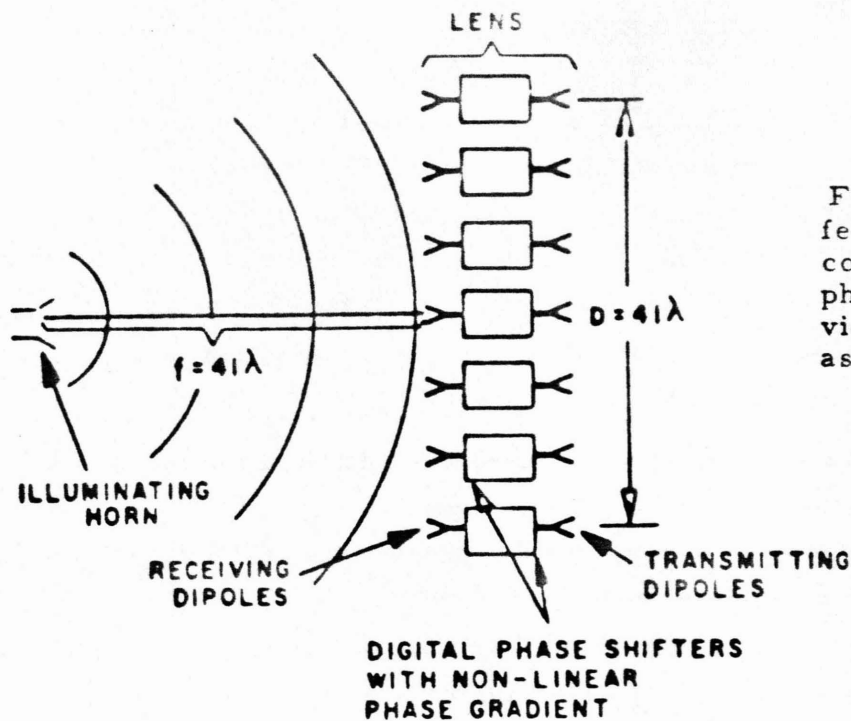


Figure 27. Optically-fed lens array, using computer control of phase shifters to provide collimation as well as beam steering [ 14 ].

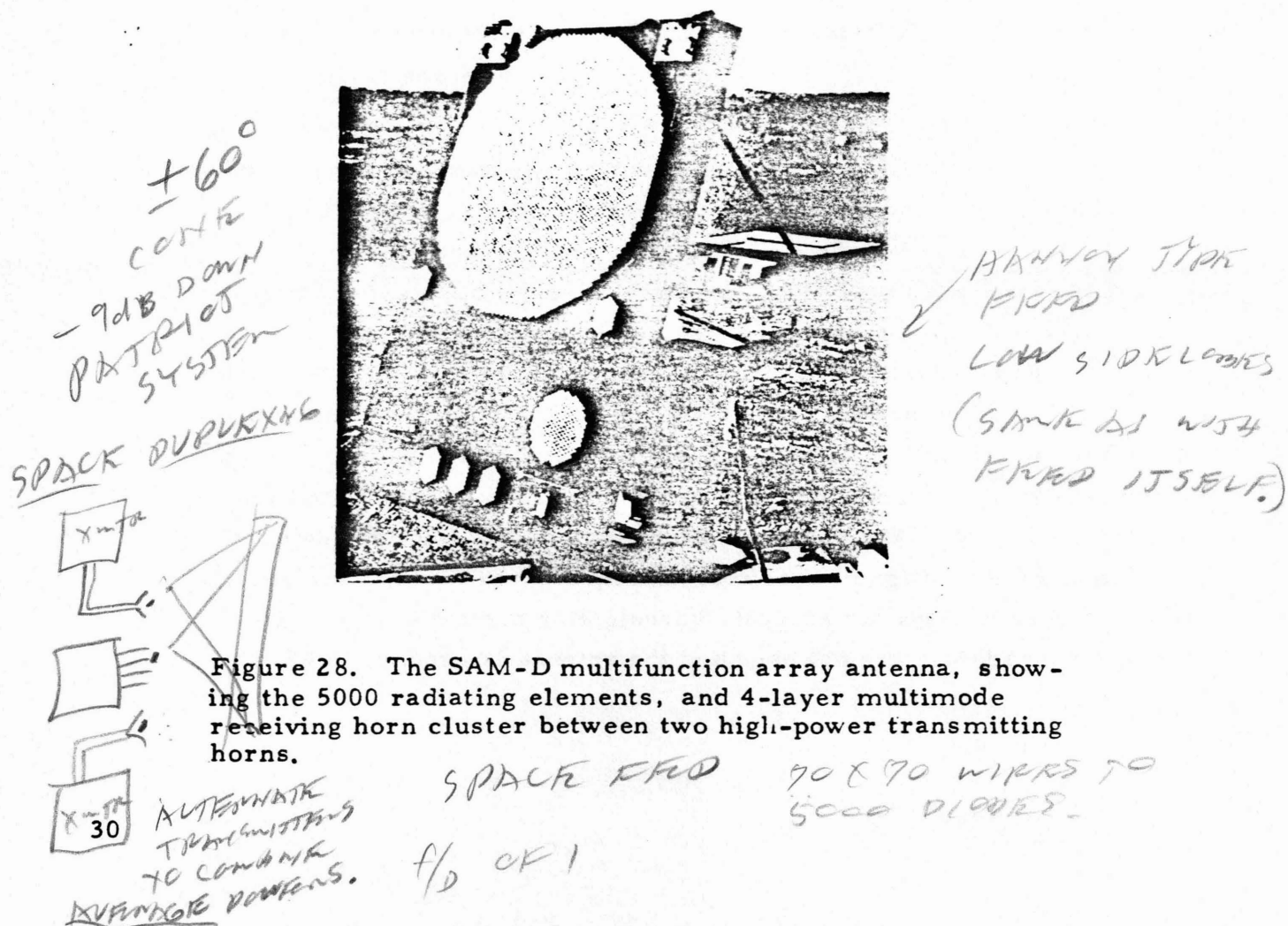


Figure 28. The SAM-D multifunction array antenna, showing the 5000 radiating elements, and 4-layer multimode receiving horn cluster between two high-power transmitting horns.

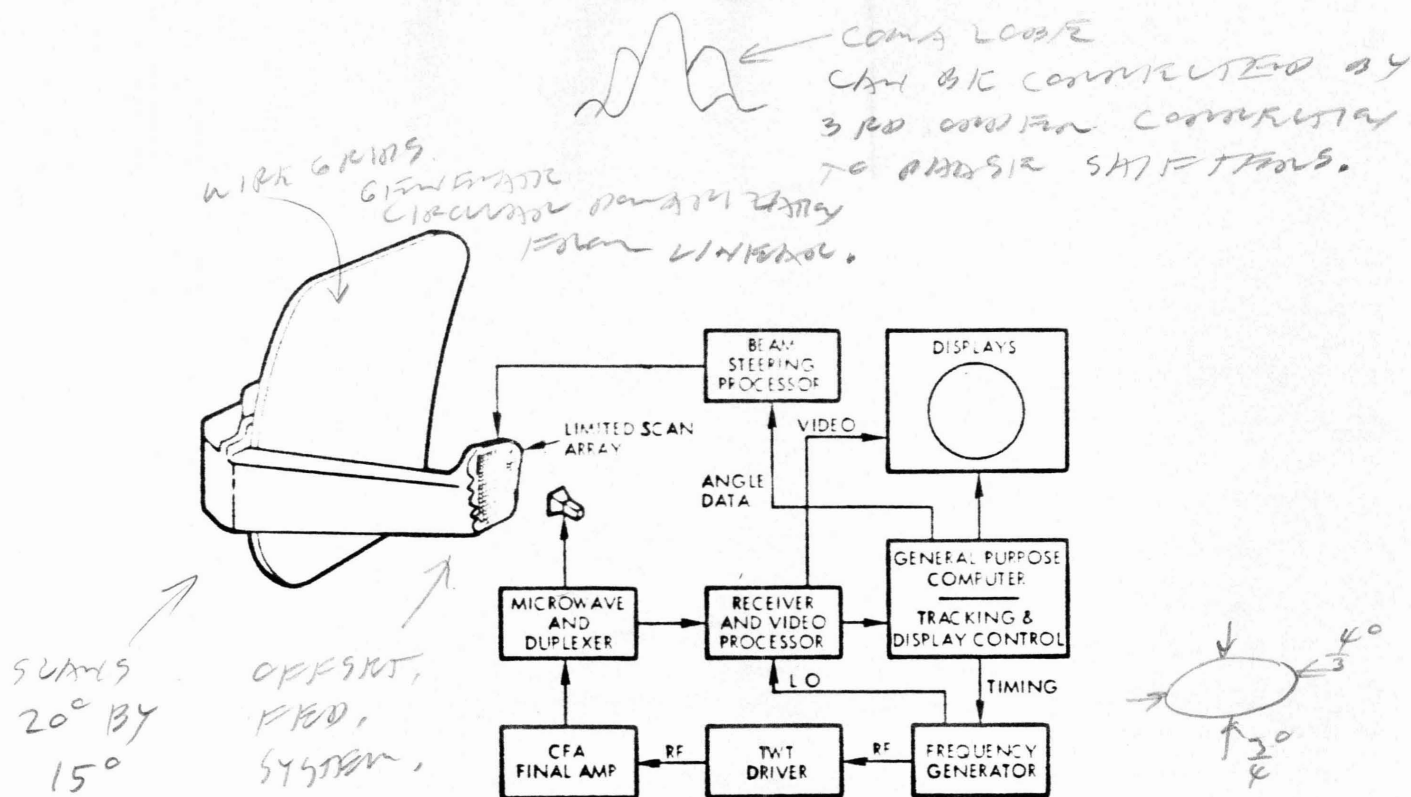


Figure 29. Block diagram of AN/TPN-19 precision approach radar, a monopulse scan-track radar with limited electronic scan [ 10 ].

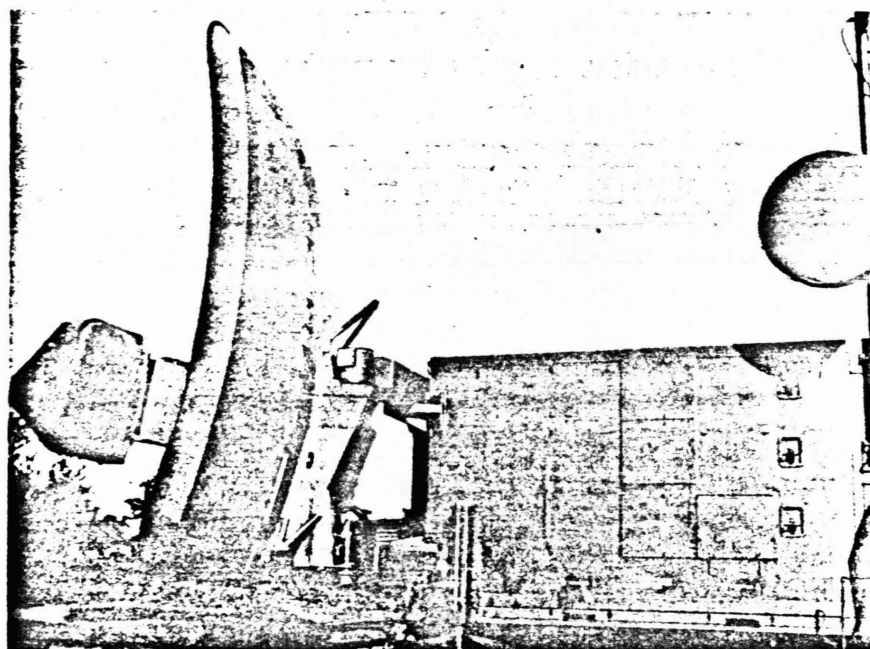


Figure 30. AN/TPN-19 precision approach radar, showing 800-element array which illuminates the 2.8 x 3.6-m reflector to scan a monopulse beam cluster [ 10 ].

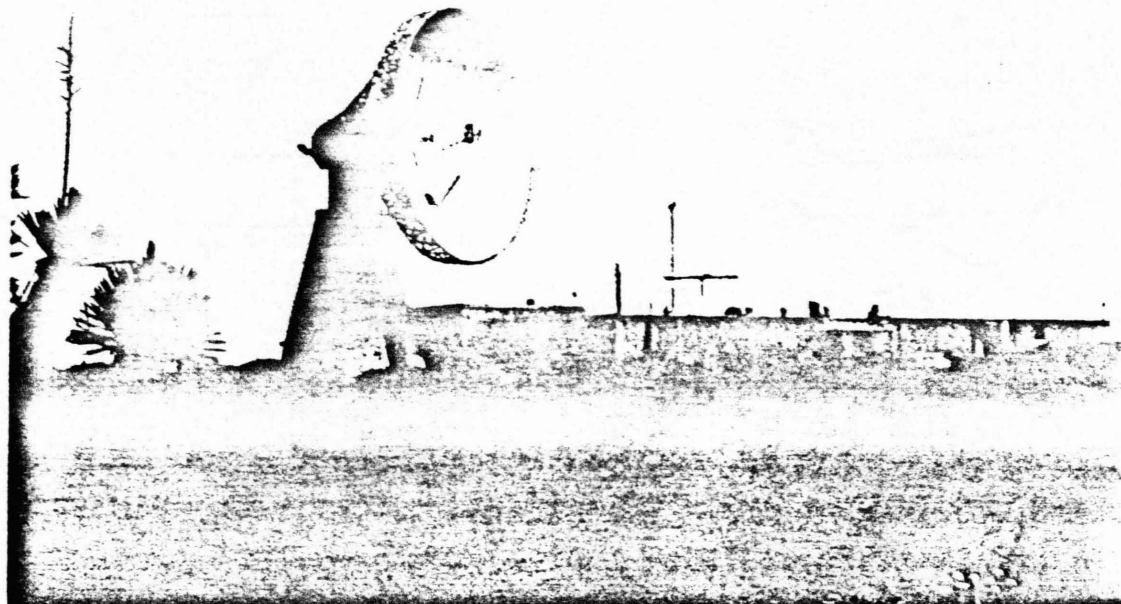


Figure 31. Rampart radar at White Sands Missile Range. This monopulse tracker uses an 18-m reflector in a Cassegrainian system, with 4-horn monopulse feed.

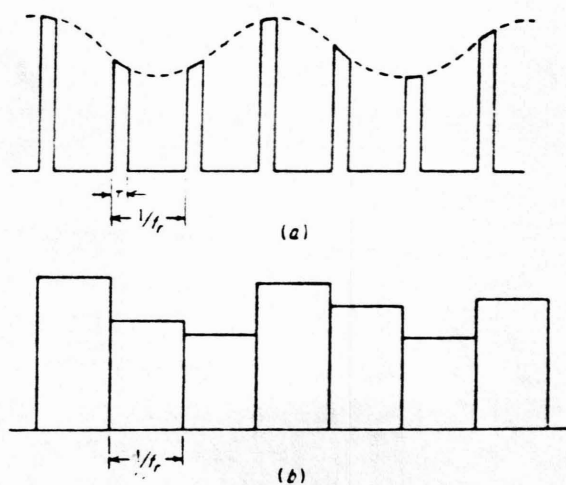


Figure 32. Processing of conical-scan pulse train to recover scan modulation component. (a) Pulse train with conical-scan modulation; (b) Same pulse train after passing through boxcar generator [ 11 ] .

weather. The presence of a radome introduces a variety of possible errors, caused by nonuniformity in the dome material, by water or ice films, by reflections which increase sidelobe levels, or by inability to use optical alignment techniques. Modern radome materials and use of radioastronomical sources for boresighting may alleviate most of these problems in the future, but data to verify this are lacking.

#### D. TRACKER SIGNAL PROCESSING

1. Angle Tracking Receivers and Processors. Tracking radar signal processors must perform several functions:

- Amplification of the target signals to levels adequate for envelope detection;

- Thresholding for target acquisition;

- Furnishing IF or video signals for operation of the range (and Doppler) tracking loops;

- Amplification of the two signals required in each angular coordinate to form the error signal;

- Normalization of the error signal with respect to target amplitude;

- Formation and filtering of the error signal to provide inputs to the antenna servo.

Depending on the type of tracker, these operations may be carried out in one or several RF, IF and video channels, and the requirements on these channels will vary with the system. The block diagram of Fig. 4a describes adequately the processing for a sequential lobing radar, where the input switch is generally an RF device, and the output switch, storage, filtering and adders may take the form of an incremental delay device, producing offset images on a K-scope (as in Fig. 7). The requirement for normalization can be met visually if IF and video gains are adjusted to avoid saturation, on the one hand, and fading of the signal to too small a scope deflection on the other. This processing may also be performed automatically. The gain must remain constant over the lobing cycle and



yet change rapidly enough to remove the larger variations in target cross section. Separate paired video channels are required for elevation and traverse (or azimuth).

Conical scan processing uses a similar sequence of elements, as indicated in Fig. 9. The input "switch" is a continuous mechanical rotation of the feed. The output switch is an error demodulator using the reference voltage from the scan drive shaft. An AGC holds the gain constant over the scan cycle, but adjusts for slower target fluctuations. The error detector accepts the modulated video pulse train from the range gate and performs a "boxcar" or sample-and-hold operation to reduce unwanted high-frequency components while preserving the audio envelope at the scan frequency (Fig. 32). When multiplied by the audio scan reference voltages (two quadrature components, corresponding to elevation and traverse channels) and filtered, the outputs are DC voltages proportional to off-axis position components of the target.

Monopulse receivers require parallel RF and IF channels as shown in Figs. 4b and 11. To reduce requirements for phase and amplitude balance between channels, most practical systems form the  $\Sigma$  and  $\Delta$  channels in passive RF networks, as shown in Fig. 11. The  $\Sigma$  channel then controls AGC for normalization of the error signals, and provides a phase reference for the error detectors. A fast AGC may be used to eliminate target fluctuation, since each pulse is error-detected independently and error filtering follows the detectors. In this type of  $\Sigma$  and  $\Delta$  monopulse, the position of the tracking null is determined almost entirely by the balance of the RF network. The individual IF amplifiers have relatively lax tolerances on phase matching, and unmatched gains affect only the loop gain of the tracking servo. Other systems of normalization and error detection may be used in special circumstances. The limiter, or " $\Sigma + j\Delta$ " circuit of Fig. 33 involves recombination of amplified  $\Sigma$  and  $\Delta$  signals in an IF hybrid, followed by hard limiting in two matched amplifiers. The subsequent addition gives normalized signals  $2\Sigma$  and  $2j\Delta$ , which are processed through the amplifier or 90-deg phase shift, output adders, linear detectors, and an output subtractor to obtain a bipolar video signal proportional to angular error. The advantage of this circuit



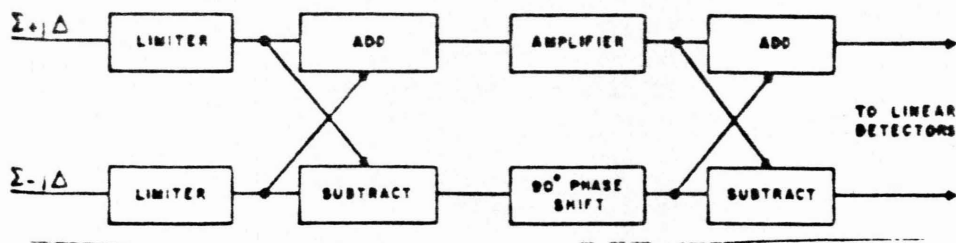


Figure 33. Normalization of monopulse signals in limiter circuits [ 6 ].

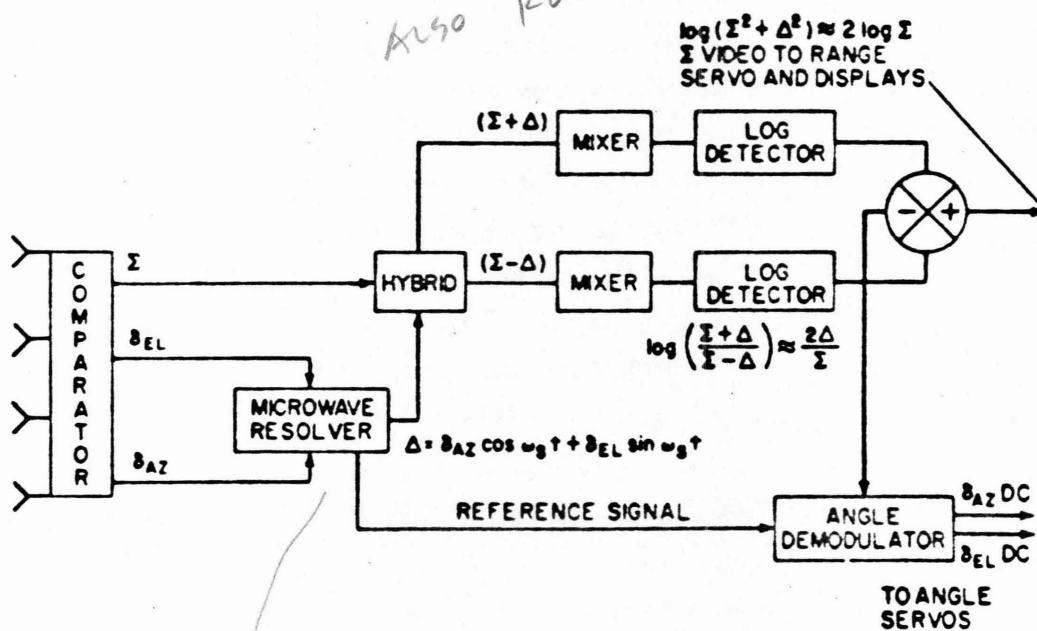
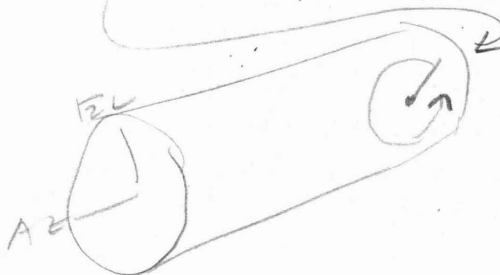


Figure 34. Block diagram of a two-channel monopulse radar system, after R. S. Noblit [ 3, p. 21-30 ].

CHUBB RECEIVER  
(ORIGINAL WITH  
SPERRY.



is that it can process many targets, of differing amplitudes, in a single beam position, without using multiple AGC loops. An alternative process providing instantaneous normalization uses matched log amplifiers with  $\Sigma + \Delta$  and  $\Sigma - \Delta$  channels.

It is also possible to process two-coordinate monopulse signals in a two-channel receiver. This can be done in the mixed phase-amplitude comparison system devised by Hausz [ 8 ], in which phase difference carries one angular error and amplitude difference carries the other, or in a time-multiplexed fashion (Fig. 34). The time sharing of angle sensing involves a 3-dB sacrifice in angular sensitivity, since half the energy in each  $\Delta$  channel is unused, but it retains the advantages of instantaneous normalization and freedom from scintillation error. The log detector system shown can be replaced by limiter normalization, with a 90-deg phase shift introduced at RF. In the system shown, which uses a rotating resolver, omission of one receiver channel would produce a COSRO system, assuming transmission through a duplexer in the  $\Sigma$  channel. If the transmitter is duplexed into the  $\Sigma + \Delta$  channel, the result is a conically scanned system with an auxiliary receiving channel, scanning 180-deg out of phase with the main channel. This is equivalent to using a pair of rotating feeds squinted in opposite directions, the "scan with compensation" system described in Soviet literature [ 9 ].

2. Range Trackers. The generalized two-channel measurement system shown in Fig. 4b is representative of the "split gate" type of range tracker. The inputs  $f_1$  and  $f_2$  are now derived from a common IF or video amplifier (e. g. the  $\Sigma$  channel of a monopulse receiver) by time gating, typically using a pair of contiguous, rectangular gates extending somewhat beyond the width of the received pulse (Fig. 35). The resemblance to monopulse angle sensing functions is apparent. If implemented at IF, the phase of the  $\Delta$  signal is reversed at the center of the split gate. When multiplied in the error detector by the  $\Sigma$  signal, and passed through a low-pass filter, the output is a DC voltage proportional to displacement of the target from the center line. The split gate in this form is used whenever the S/N ratio for a single pulse may be low, since averaging of the DC output over many pulses can yield a smoothed estimate of error.

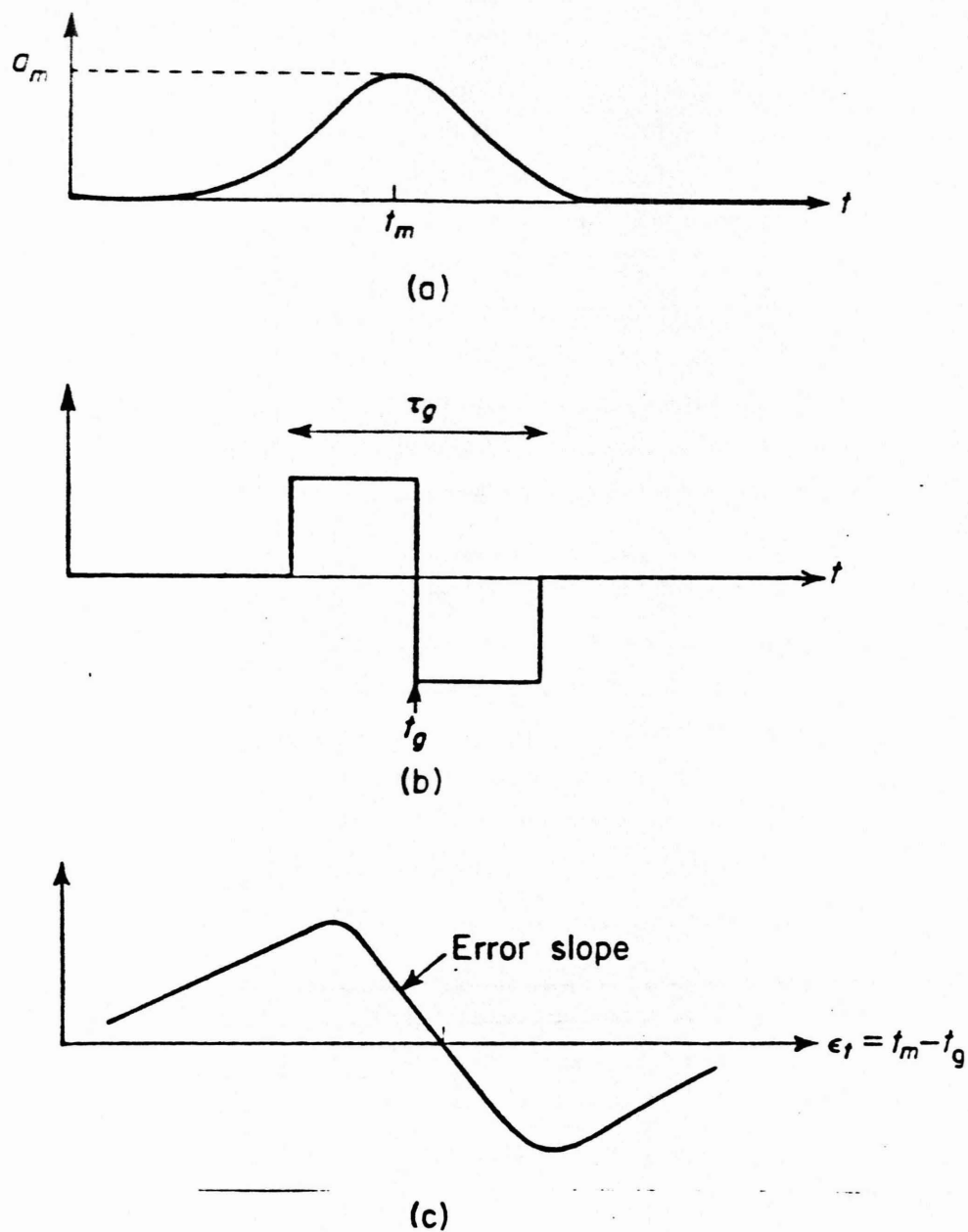


Figure 35. Waveforms and response of split-gate range tracker: (a) signal envelope; (b) gate function; (c) output error voltage vs. displacement of signal from gate center [ 2 ].

When single-pulse estimates are to be made at high S/N ratio, the range tracker can form each estimate by passing the IF or video waveform through a differentiator (Fig. 36). The undifferentiated  $\Sigma$  signal is compared to a threshold, and when it exceeds this threshold the occurrence of a negative-going zero crossing in the differentiated ( $\Delta$ ) channel is identified as the time of peak signal. Obviously, there will be zero crossings from noise, occurring at an average rate equal to the channel bandwidth, but if S/N is high enough these can be suppressed by setting a high  $\Sigma$  threshold, without missing true signals. Averages over many pulses may still be formed at the output, to reduce the error further. The split-gate (correlator) and differentiator (filter) processors are mathematically equivalent for strong signals, and differ only when nonlinear effects are taken into account.

A variant of the split gate tracker is the leading-edge tracker (Fig. 37). Here, the nominally rectangular pulse is amplified in a wide-band receiver, envelope detected, and differentiated before being applied to a narrow split gate (matched to the pulse rise time). The unwanted trailing-edge response is deleted by clipping of negative video or is ignored after designation of the gate to the location of the leading edge. The leading edge is selected to avoid the effects of trailing chaff or slightly delayed interference such as multipath reflections or repeater jamming.

3. Doppler Trackers. In pulsed radar, Doppler tracking is often applied to hold a filter on the fine line of the spectrum found by a coherent train of pulses (Fig. 38). The envelope of the transmitted spectrum is typically some megahertz in width, and within it the coherent pulse train energy is concentrated in lines a few hertz wide, spaced at the repetition rate of a few hundreds of hertz. The reflected signal is shifted by

$$f_d = \frac{2 v_t}{\lambda} ,$$

typically a few kilohertz. After wideband IF amplification and range gating, the signal may be heterodyned into a narrow bandpass or lowpass filter (using in-phase and quadrature processing in the latter case), at which

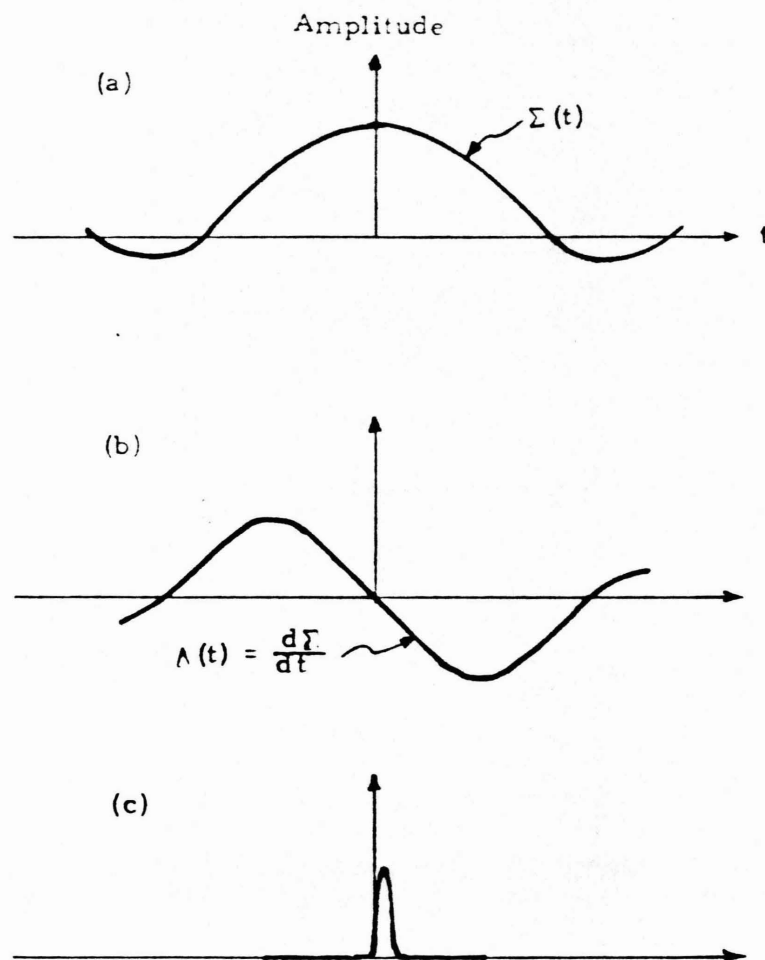


Figure 36. Differentiator range tracker waveforms;  
 (a) signal envelope; (b) differentiated signal;  
 (c) zero-crossing marker indicating location of signal  
 peak.

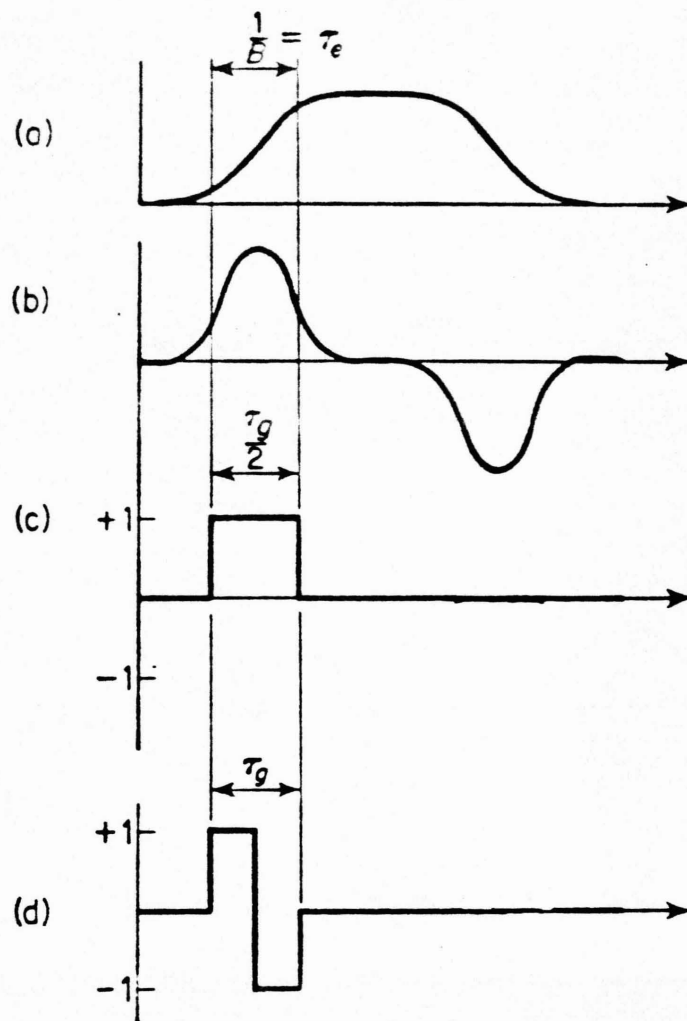


Figure 37. Leading-edge range tracker waveforms; (a) signal envelope of bandlimited rectangular pulse; (b) differentiated signal; (c) gate for angle tracking; (d) split gate for range tracking.

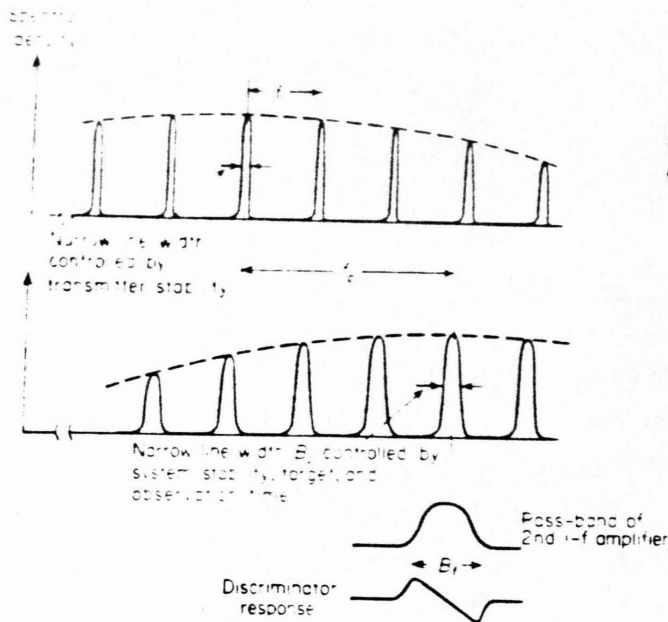


Figure 38. Line spectra in coherent Doppler track [ 2 ].

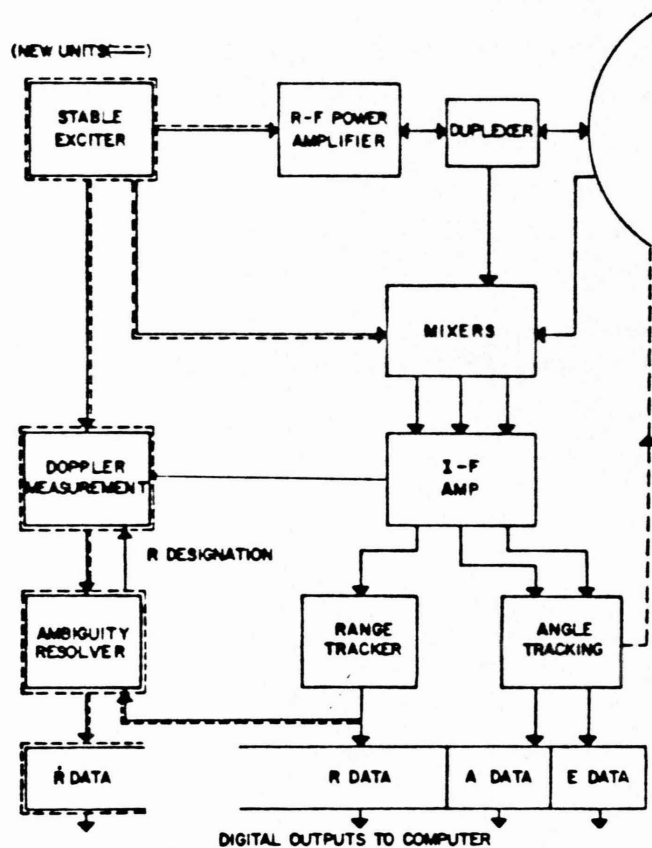


Figure 39. Block diagram of coherent velocity measurement modification to conventional mono-pulse tracker.



point a conventional frequency discriminator will produce the desired  $\Delta$ -channel response. Narrowband AGC in the second IF  $\Sigma$  channel provides the desired normalization process. The Doppler tracking loop is closed by applying the filtered discriminator output as a DC control voltage to the variable oscillator used to heterodyne the wideband IF signal into the second IF.

4. Examples of Trackers Using Doppler. The Doppler tracking potential of a coherent pulsed radar may be used in two ways. In Fig. 39, the three position loops operate in normal fashion, using wideband IF amplifiers as in the noncoherent radar. A range-gated  $\Sigma$  output at IF is applied to the Doppler measurement unit, which consists of a narrowband second IF, controlled offset oscillator, and an ambiguity resolver which uses differentiated range data to select the center line of the target spectrum. The Doppler  $\dot{R}$  data is far more precise than the differentiated range data previously available.

The other advantages of Doppler tracking are the improved S/N and S/C ratios resulting from narrowband processing of all signals (range and angle channels as well as the Doppler channel itself). In Fig. 40, the narrowband second-IF filters are inserted in all three receiver channels, processing angle  $\Delta$  channels as well as the  $\Sigma$  channel used in ranging and Doppler tracking. The acquisition process is more complex, since all four loops must acquire before tracking begins. However, once a target is in track it can be retained even if the S/N and S/C ratios in the wideband IF fall below unity. Radars of this type, especially those using digital signal processing and prf control to avoid blind ranges and blind velocities, have been applied to instrumentation and weapon control.

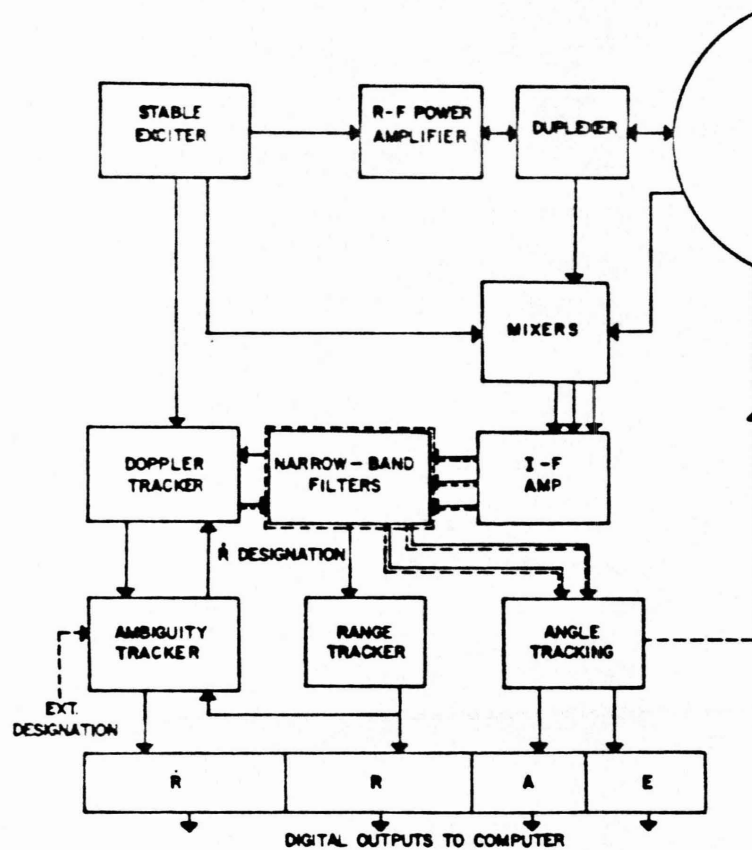


Figure 40. Block diagram of coherent velocity tracker using narrowband filters in all channels.

## References. Radar Tracking

- [ 1 ] IEEE Standard Definitions: Radar and Navigation Aid Terms, No. 172 (Rev. 1976, to be issued).
- [ 2 ] D. K. Barton and H. R. Ward, Handbook of Radar Measurement, Prentice-Hall, 1969.
- [ 3 ] M. I. Skolnik, Radar Handbook, McGraw-Hill, 1970.
- [ 4 ] I. A. Getting, "The SCR-584 Radar and Mark 56 Naval Gun Fire Control System," IEEE Trans. AES-11, No. 5, Sept. 1975, pp. 921-36.
- [ 5 ] P. W. Hannan, "Optimum Feeds for all Three Modes of a Monopulse Antenna," IRE Trans. AP-9, No. 5, Sept. 1961, pp. 444-61, (reprinted in Monopulse Radar, Vol. 1 of Radars, Artech House 1974.)
- [ 6 ] G. M. Kirkpatrick, Final Report on Angular Accuracy Improvement, " August 1952 (reprinted in Monopulse Radar, as above).
- [ 7 ] J. H. Dunn and D. D. Howard, "Precision Tracking with Monopulse Radar," Electronics, Apr. 22, 1960 (reprinted in Monopulse Radar, as above).
- [ 8 ] W. Hausz and R. A. Zachary, "Phase-Amplitude Monopulse System," IRE Trans. MIL-6, No. 2, April 1962, pp. 140-46 (reprinted in Monopulse Radar, as above).
- [ 9 ] P. A. Bakut, et al., Questions of the Statistical Theory of Radar, Vol. II, Soviet Radio, Moscow (1964); translation: AD645775.
- [ 10 ] H. R. Ward, C. A. Fowler and H. I. Lipson, "GCA Radars: Their History and State of Development," Proc. IEEE 62, No. 5, June 1974, pp. 705-16.
- [ 11 ] M. I. Skolnik, Introduction to Radar Systems, McGraw-Hill, 1961.

References. Radar Tracking

- [ 12] A. R. Lopez, "Monopulse Networks for Series Feeding an Array Antenna," IEEE Trans. AP-16, No. 4, July 1968, pp. 436-40 (reprinted in Monopulse Radar, Vol. 1 of Radars, Artech House, 1974).
- [ 13] R. M. Scudder and W. H. Sheppard, "AN/SPY-1 Phased-Array Antenna," Microwave J., Oct. 1974, pp. 51-55.
- [ 14] P. J. Kahrilas, "Design of Electronic Scanning Radar Systems," Proc. IEEE 56, No. 11, Nov. 1968, pp. 1763-71.

SESSION VII

LOW ALTITUDE TRACKING

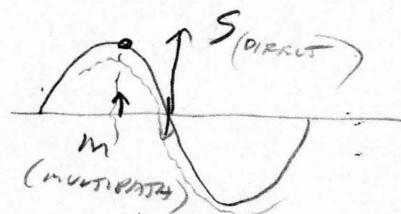
RADAR ACCURACY

DAVID BARTON

# LOW ALTITUDE TRACKING WITH SMOOTH SURFACE

$$\sigma_{\theta} = \frac{\sigma_3}{K \sqrt{2} S/I_D}$$

SPECULAR  
MODEL



SPECULAR  
REFLECTING  
COEFFICIENT

(GROUND REFLECTIVITY)

SEE p. 2

LKT  $h_t = 100m$   $h_r = 10m$   $R = 10km$

$$\theta_t = \frac{90}{10,000} \text{ RAD} \rightarrow 9 \text{ milliradians}$$

$$\psi = \frac{110}{10,000} \text{ RAD} \rightarrow 11 \text{ milliradians (GRAZING ANGLE)}$$

$$\frac{2h_t}{R} = 20 \text{ milliradians}$$

TARGET WILL HAVE DOPPLER SHIFT,  $\therefore$  USE M.T.I.  
TECHNIQUES TO ELIMINATE CLUTTER,  
BUT BOTH TARGETS WILL HAVE SAME DOPPLER.

$\delta$  = RANGE DUE TO 3RD ORDER TARGETS

$$\delta = \frac{2h_r h_t}{R} = \frac{2 \times 10 \times 100}{10,000} = 0.2 \text{ meters}$$

$$c = 3 \times 10^8 \text{ m/s}$$

$$300 \text{ m/ns}$$

0.3 m/ns  $\therefore$  BW  $> 7 \text{ GHz}$  TO RESOLVE  
TARGETS WITH 0.2 meters.

$\therefore$  RANGE RESOLUTION IS NOT  
PRACTICAL FOR MOST RADARS.

TYPICAL DOPPLER SHIFTS  $\leq 1 \text{ Hz}$ .  
 $\therefore$  IMPRACTICAL ALSO.

Low-Altitude Tracking  
and Radar Accuracy

by David K. Barton  
Raytheon Company  
Bedford, Massachusetts 01730

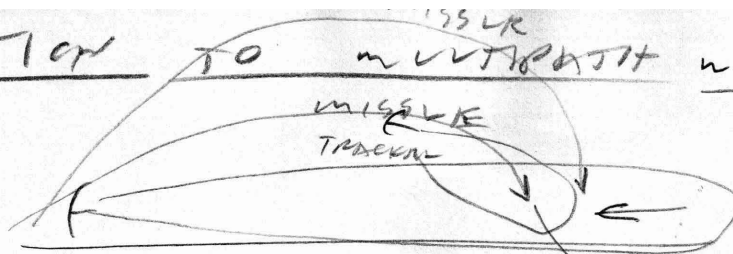
- A. Surface Reflection Phenomena
  - 1. Specular Reflection
  - 2. Diffuse Reflection (forward scatter)
  - 3. Backscatter (clutter)
- B. Multipath Errors in Tracking
  - 1. Reflections in Antenna Sidelobes
  - 2. Reflections in Main Lobe
  - 3. Range and Azimuth Errors
- C. Anti-Multipath Techniques
  - 1. High-Resolution Radar
  - 2. Off-Axis Tracking
  - 3. Multiple-Target Estimators
  - 4. Complex Angle Monopulse
  - 5. Other Techniques
- D. Accuracy of Radar Measurements
  - 1. Thermal Noise
  - 2. Clutter and Interference
  - 3. Target Noise
  - 4. Lag Errors
  - 5. Instrumentation Errors
  - 6. Atmospheric Propagation
- E. Example of System Error Analysis
  - 1. Classification of Errors
  - 2. Combination of Errors
- F. Typical Low-Altitude Tracking Problem

References

January 1978



# SOLUTION TO MULTIPATH WITH FLAT SURFACE



∴ DON'T USE RADAR ELEVATION INFORMATION.  
 BACKSCATTER ANGLE TO REDUCE REFLECTION.  
 ∴ DIRECT SIGNAL SIGNIFICANTLY STRENGTHENED.

## ROUGH SURFACE

$\sigma_h$  {  $\sigma_\alpha$  RMS DRV. SLOPE IN RADIANS  
 $\beta_0$



SMOOTH SEA  $\sigma_h = 0.15$

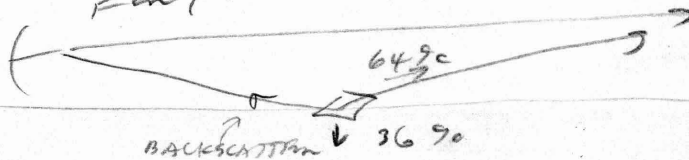
$\sigma_\alpha = 0.02$  TO  $0.03$  RADIANS

ROUGH TARGET

$$\rho = \rho_0 \rho_s$$

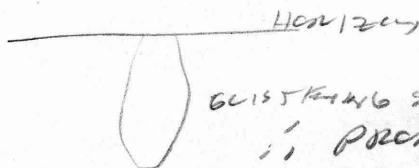
SPERULAN GRAB-6 ANGLE

FOR  $\rho_0 = 0.8$



$\rho_0$  = FOKSNIER COEFFICIENT (ABSORPTION COEFFICIENT)

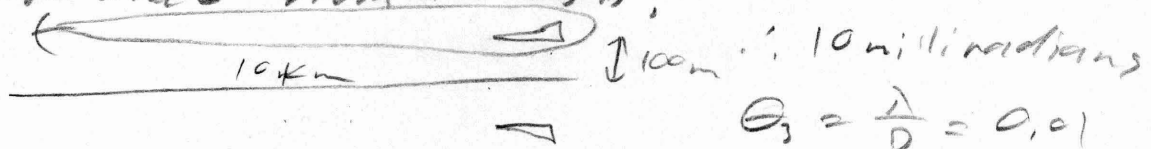
∴ STRENGTH (∝ ABSORPTION AT SPREAD ANGLE)



∴ PROBABLY USING INTERFEROMETRY TO PLACE MUCH TARGET

SYNTHETIC APERTURE RADAR HELPS BY

NARROWING BEAM WIDTH



$$\theta_s = \frac{\lambda}{D} = 0.01$$

∴ 3 m ANT @ X-BAND.

1.9 m ANT @ Ka BAND. → BRITISH RADAR.

m, L.S. / 6 CA SYSTEM

$$\therefore \theta = \frac{300}{15,000} = 20 \text{ radians} \approx 1^\circ$$

$$5 \text{ m radians} \approx 0.25^\circ$$

# LOW-ALTITUDE TRACKING AND RADAR ACCURACY

5000 ft  
10,000 ft  
50 ft  
300 ft @ 13° elevation  
3000 ft  
15,000 ft  
CIVIL CASR IS 51 m / 1 km

## A. SURFACE REFLECTION PHENOMENA

The radar tracker is designed to point its directional beam at the selected target, and to discriminate against interfering signals to the greatest possible extent with a combination of angle, range, and Doppler resolution. In a real environment, however, signals reflected from the target (or emitted by a transponder) arrive at the antenna from several surface-reflected paths as well as directly (Fig. 1). When the target elevation angle  $\theta_t$  is low (from a few beamwidths to about 1.5 beamwidths), these reflections enter the principal sidelobes of the  $\Delta$  pattern, and below that angle they begin to enter the main  $\Delta$  lobe. The geometry of the paths will be described, along with other factors which affect the spatial distributions and magnitudes of the different reflected components.

1. Specular Reflection. The reflected ray from a flat surface may be treated as arriving at the antenna from an image target below the surface, or in terms of an image antenna viewing the real target (Fig. 2). Equations for the several angles and for the difference in lengths between the direct and the reflected paths are shown in Table I. Also shown are the relationships for the spherical earth, where Fig. 3 defines the symbols. Although it is possible to obtain  $\delta$  and  $\psi$  directly by solving a cubic equation, use of the graphs (Figs. 4 and 5) for correction factors J and K is usually the more convenient procedure for the spherical-earth case. The relative amplitude of the reflected ray is given by the Fresnel reflection coefficient  $\rho_o$ , plotted in Fig. 6. Hence, for a smooth earth, the total signal voltage at the antenna output is

$$E = A_t f(\theta_t) + A_r \rho_o D f(-\theta_r) e^{-j\alpha} \quad (1)$$

where  $A_t$  and  $A_r$  represent the free-space field strengths of the target signal at the antenna and image antenna,  $f(\theta_t)$  and  $f(\theta_r)$  are the voltage

→ AZIMUTH ERROR IS LOW WITH REFLECTION DISPERSION. Ka BAND 3-4 km RANGE IN RAIN.

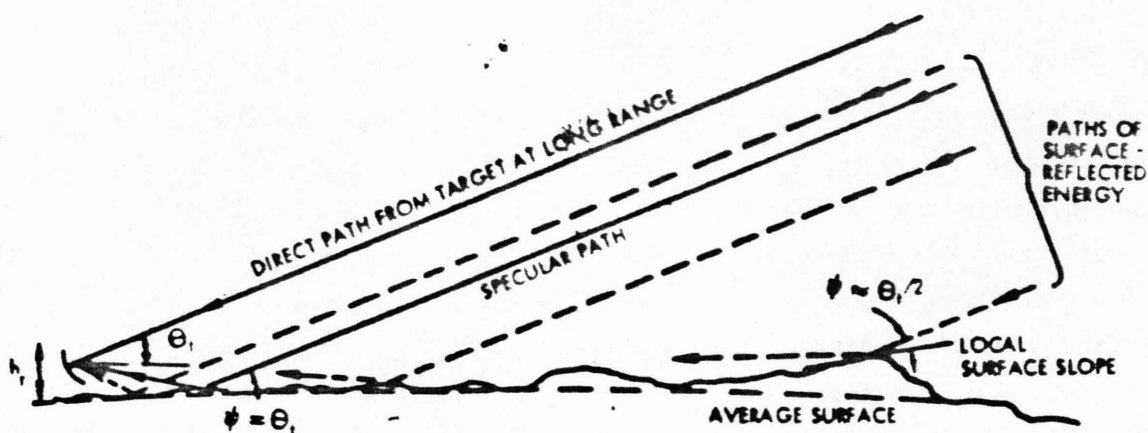


Figure 1. Specular and diffuse paths for a typical rough surface, showing variation of local grazing angle  $\psi$  from  $\psi \approx \theta_t/2$  for large features near the horizon [1].

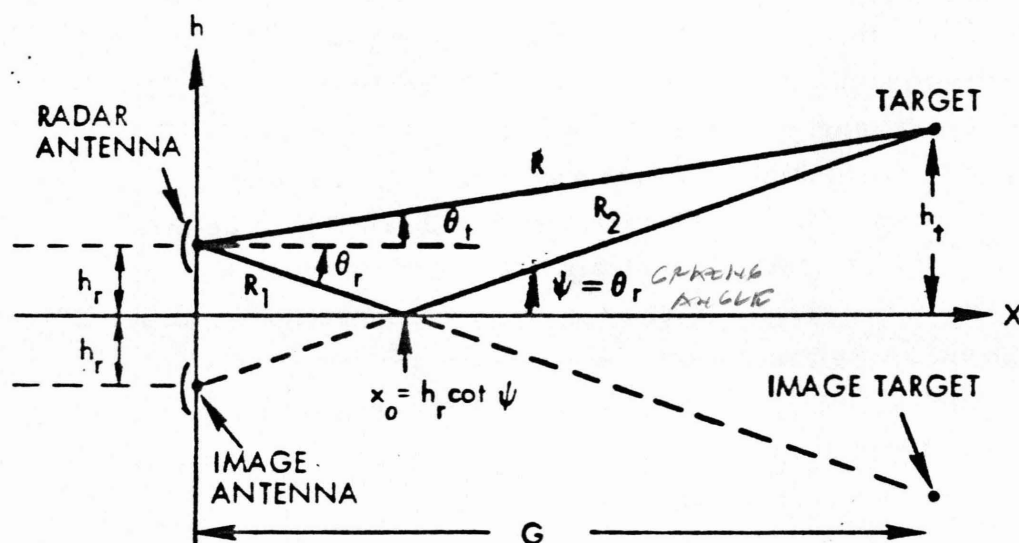
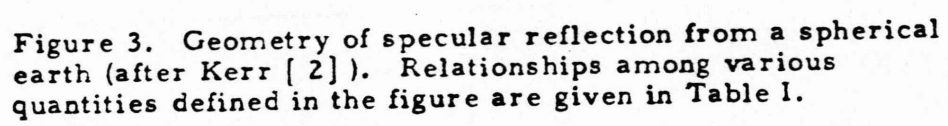


Figure 2. Geometry of specular image.

Assume  $\sin \theta_t = \frac{h_t}{h_r}$  ; small angle assumption  
 $\therefore \theta_t = \frac{h_t}{h_r}$  radians

	Flat Earth	Curved Earth, $h_r \ll h_t$	Curved Earth, general case
Target elevation, $\theta_t$	$\frac{h_t - h_r}{R}$	$\frac{h_t - h_r}{R} - \frac{R}{2ka}$	$\frac{h_t - h_r}{R} - \frac{G_t^2 - G_r^2}{2kaR} - \frac{G_r}{ka}$
Pathlength difference $\delta$	$\frac{2h_r h_t}{R}$	$\frac{2h_r h_t}{R} J(S,T)$	J and K are correction factors, plotted in [2] or [3] as a function of normalized range S and height ratio T.
Grazing angle, $\psi$	$\frac{h_r + h_t}{R}$	$\frac{h_r + h_t}{R} K(S,T)$	
Normalized range, S	---	$\frac{R}{R_{h1} + R_{h2}}$	
Height ratio, T	---	$\sqrt{h_r / h_t}$	$\sqrt{\frac{h_r}{h_t}}$ or $\sqrt{\frac{h_t}{h_r}}$
Horizon range, $R_{hi}$	---	$\sqrt{2ka h_i} = 4130 \sqrt{h_i}$ ( $h_i$ in m)	
Image angle, $\theta_r$	$\psi$	$\psi + \frac{G_r}{ka}$	
Range to reflection point, $G_r$	$\frac{R h_r}{h_r + h_t}$	$\frac{h_r}{\psi} \left( 1 - \frac{h_r}{4ka \psi^2} \right)$	$ka \psi \left[ \sqrt{1 + \frac{2h_r}{ka \psi^2}} - 1 \right]$

Table 1. Radar-target geometrical relationships for low-angle target ( $\psi \approx \tan \psi$ ,  $R \approx G$ ). For standard atmosphere, the effective earth radius  $ka = 8.5 \times 10^6$  m.



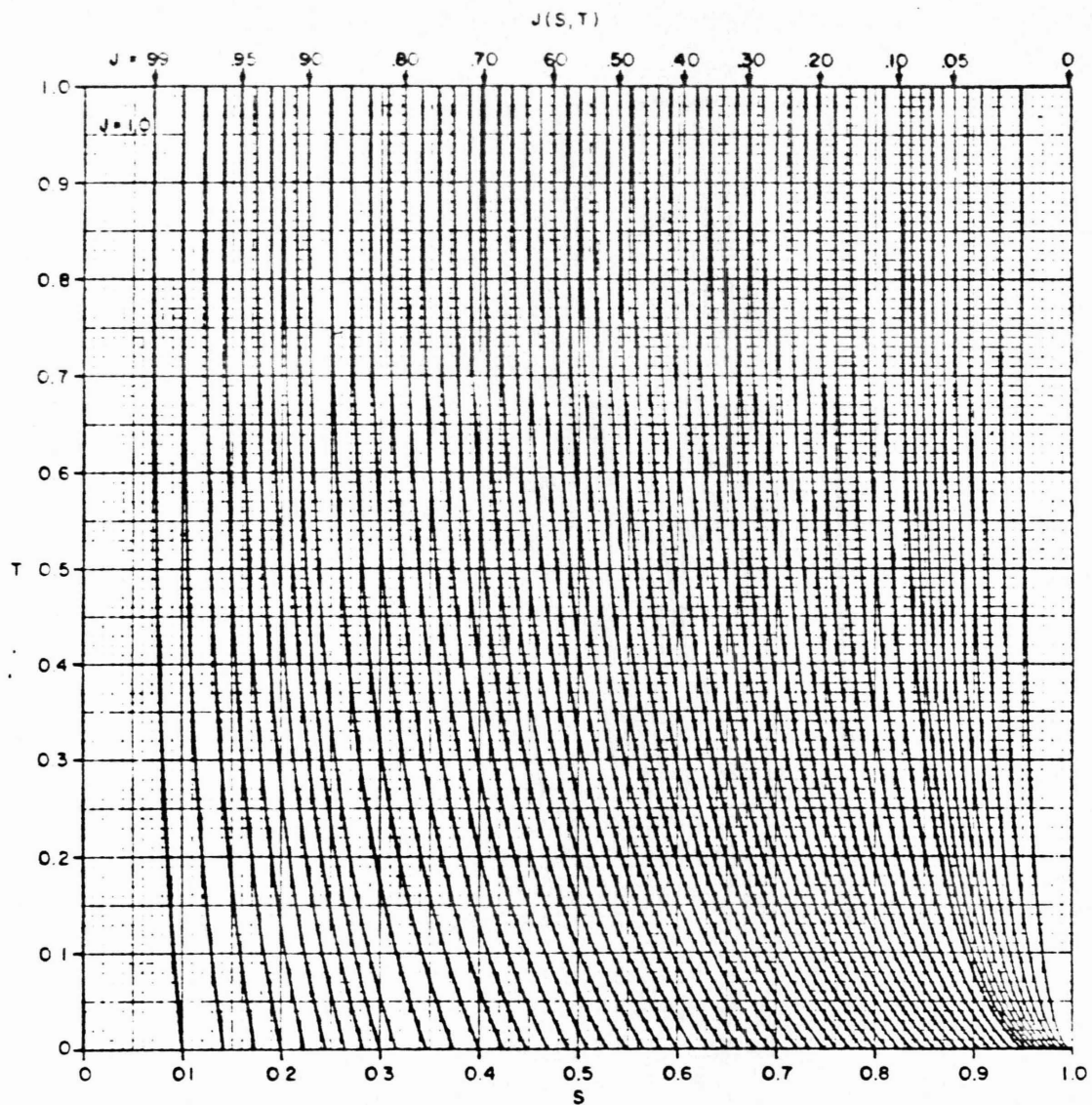


Figure 4. Correction factor  $J(S, T)$  used for calculation of pathlength over curved earth (from Blake [3]).



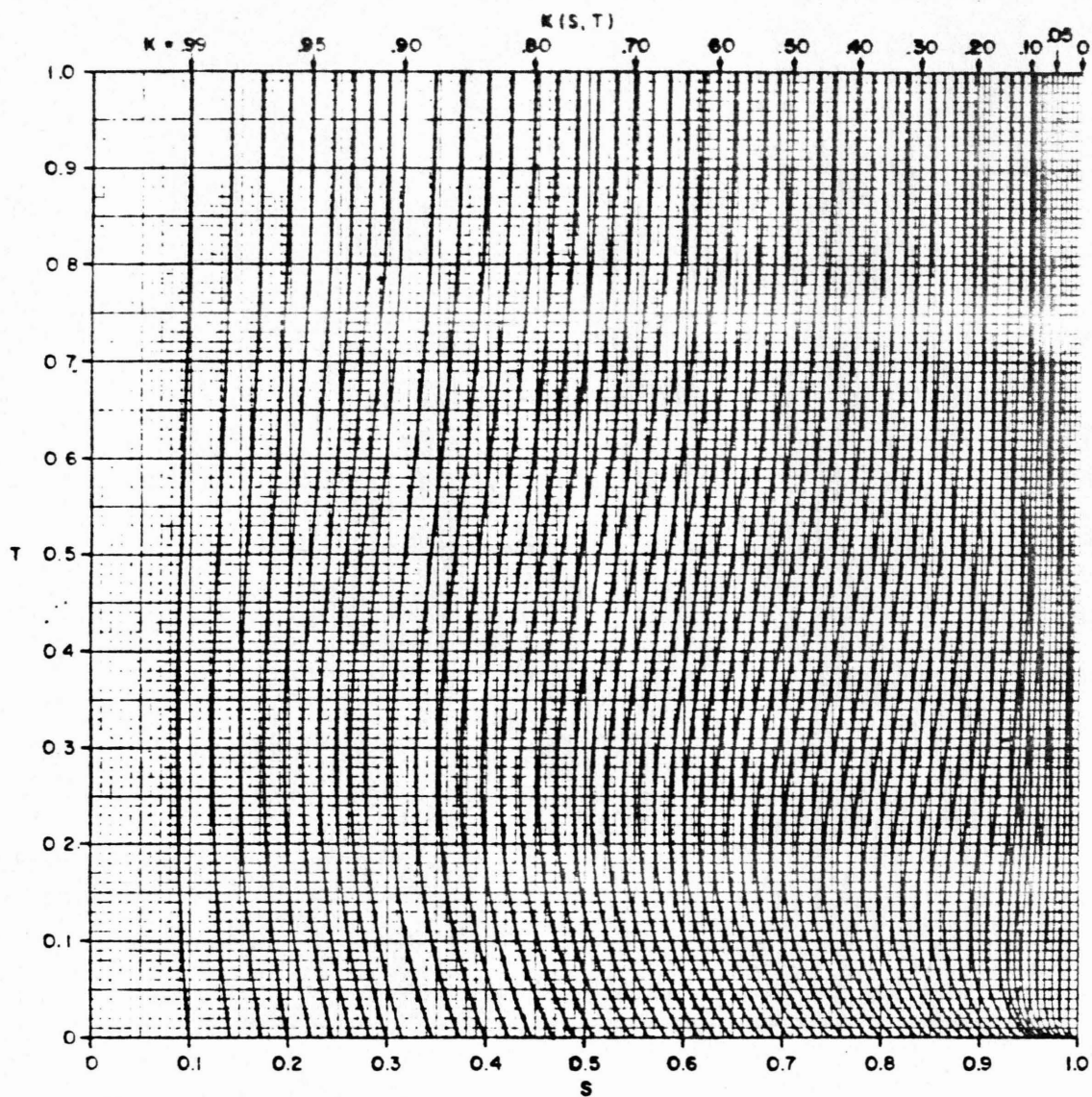
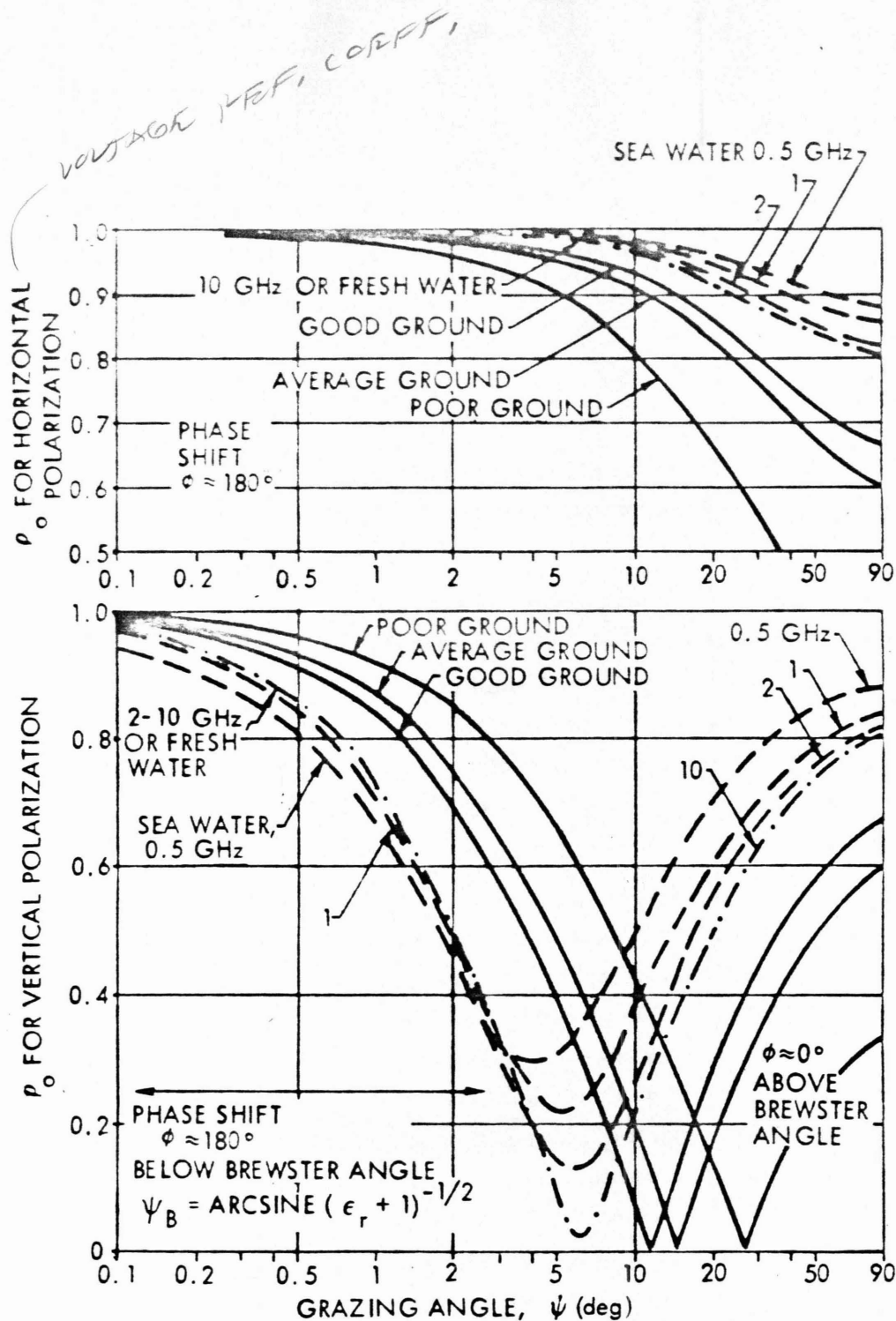


Figure 5. Correction factor  $K(S, T)$  used for calculation of grazing angle at the surface of a curved earth (from Blake [3]).





$\phi = 0^\circ$  FOR  
ONLY PERFECT  
CONDUCTION

Figure 6. Fresnel reflection coefficients  $\rho_0$  for horizontal and vertical polarizations, at different frequencies and for water and land surfaces [1]. Note that the phase shift at reflection is 180 deg for both components, below the Brewster angle, so that the sense of a circularly polarized wave is not reversed upon reflection at the low angles of interest in radar multipath problems.

*CUTTER*

9810 FORWARD  
SCATTER FROM  
SHARP CUTTER.

gains of the antenna along the direct and reflected paths, respectively,  $D$  is the divergence factor [ 2, 3] and  $\alpha$  is the total phase shift of the reflected signal:

$$\alpha = \frac{2\pi\delta_0}{\lambda} + \phi \quad (2)$$

where  $\phi$  is the phase angle of the Fresnel reflection coefficient. In most surface-based radar cases, it is adequate to set  $D = 1$  for paths not dominated by diffraction effects.

Reflections from a rough surface differ in three ways from the smooth-surface case: the amplitude of the specular component is reduced, diffuse components are introduced, and radar energy from the transmission may be backscattered from surface elements beneath the target. The amplitude of the specular reflection is now given by the product  $\rho_o \rho_s$ , where the specular scattering coefficient  $\rho_s$  is described by Fig. 7. If the surface is covered by vegetation, another factor  $\rho_v$  is included to account for absorption.

2. Diffuse Reflection (forward scatter). The region on the surface from which tilted facets may reflect energy to the antenna is known as the "glistening surface" [ 4], and is generally an ellipse surrounding the point of specular reflection. Viewed in azimuth-elevation coordinates, the sources of reflection vary with surface conditions as shown in Fig. 8. The distribution of diffuse energy in elevation angle, for the low-elevation target, is typically as shown in Fig. 9, with a large fraction of the energy appearing from just below the horizon, beneath the target. Although these "horizon" components have greater relative pathlengths than the specular component, substantial energy originates from regions with very small excess delay and Doppler shift and yet within or near the "horizon spot" (see Figs. 10 and 11).

Integration of the power in three different parts of the glistening surface yields three components of the diffuse reflection coefficient  $\rho_d$ , plotted in Figs. 12 and 13. Note that the rss sum of these components

$\rho = \rho_{op}$      $\sigma = 0.15m$      $\lambda = 0.3$      $\left. \begin{matrix} \rho_0 = 0.8 \\ \rho_{av} = 0.64 \end{matrix} \right\} 1.6 \lambda = 5$   
 $\therefore \rho_s = 0.8$  FROM CHART,  $\rho_0 = 0.8$      $\therefore$  OPTICS HAS  
 $\therefore \rho_{av} = 0.64$     ADVANTAGE

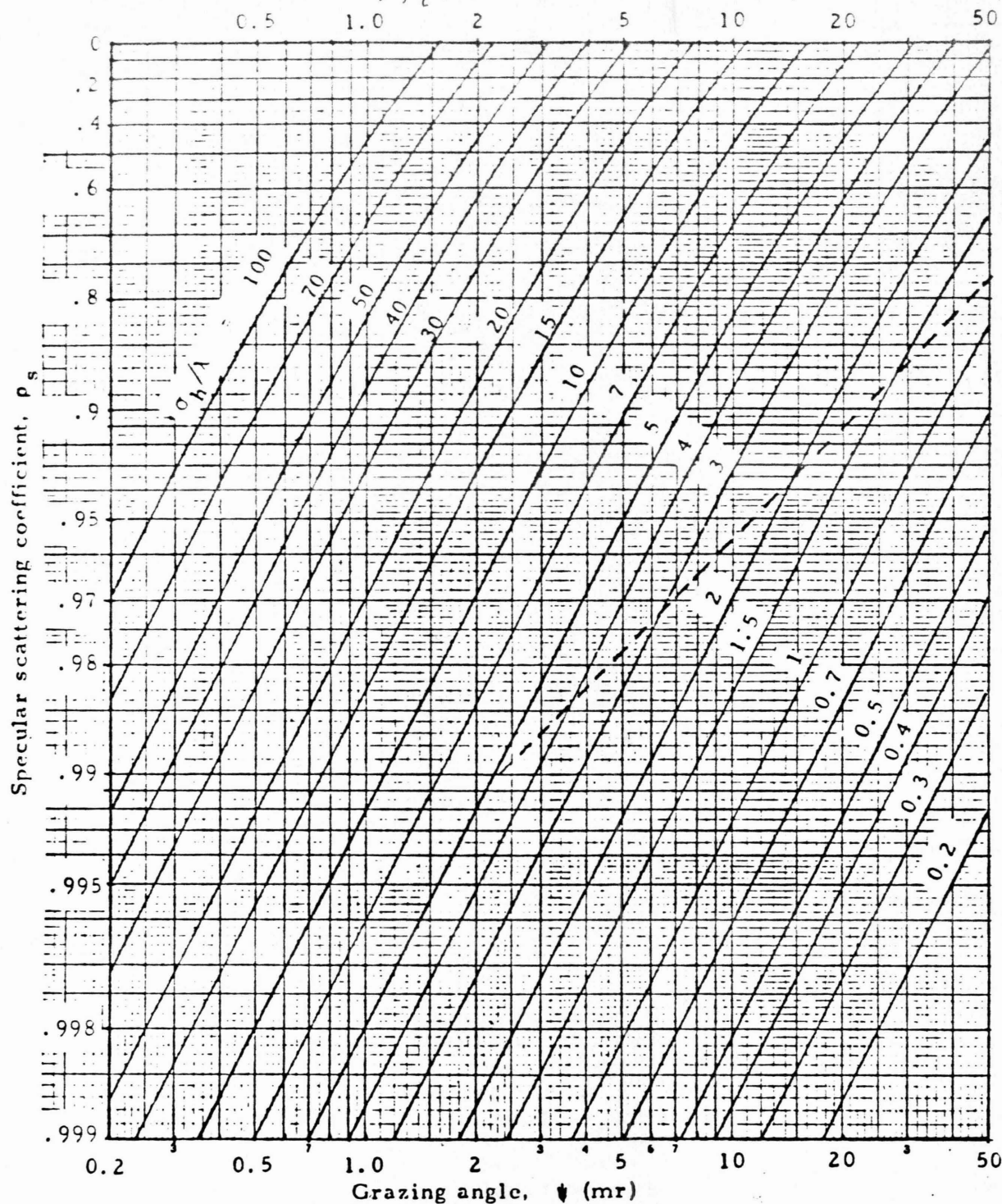


Figure 7. The rms specular scattering coefficient  $\rho_s$  for a Gaussian surface with height deviation  $\sigma_h$ . This is a plot of the expression

$$\rho_s^2 = \exp \left[ - \left( \frac{4\pi \sigma_h \sin \psi}{\lambda} \right)^2 \right]$$

The dashed curve represents  $\rho_0$  for average ground and vertical polarization, expanding that curve from Fig. 6.

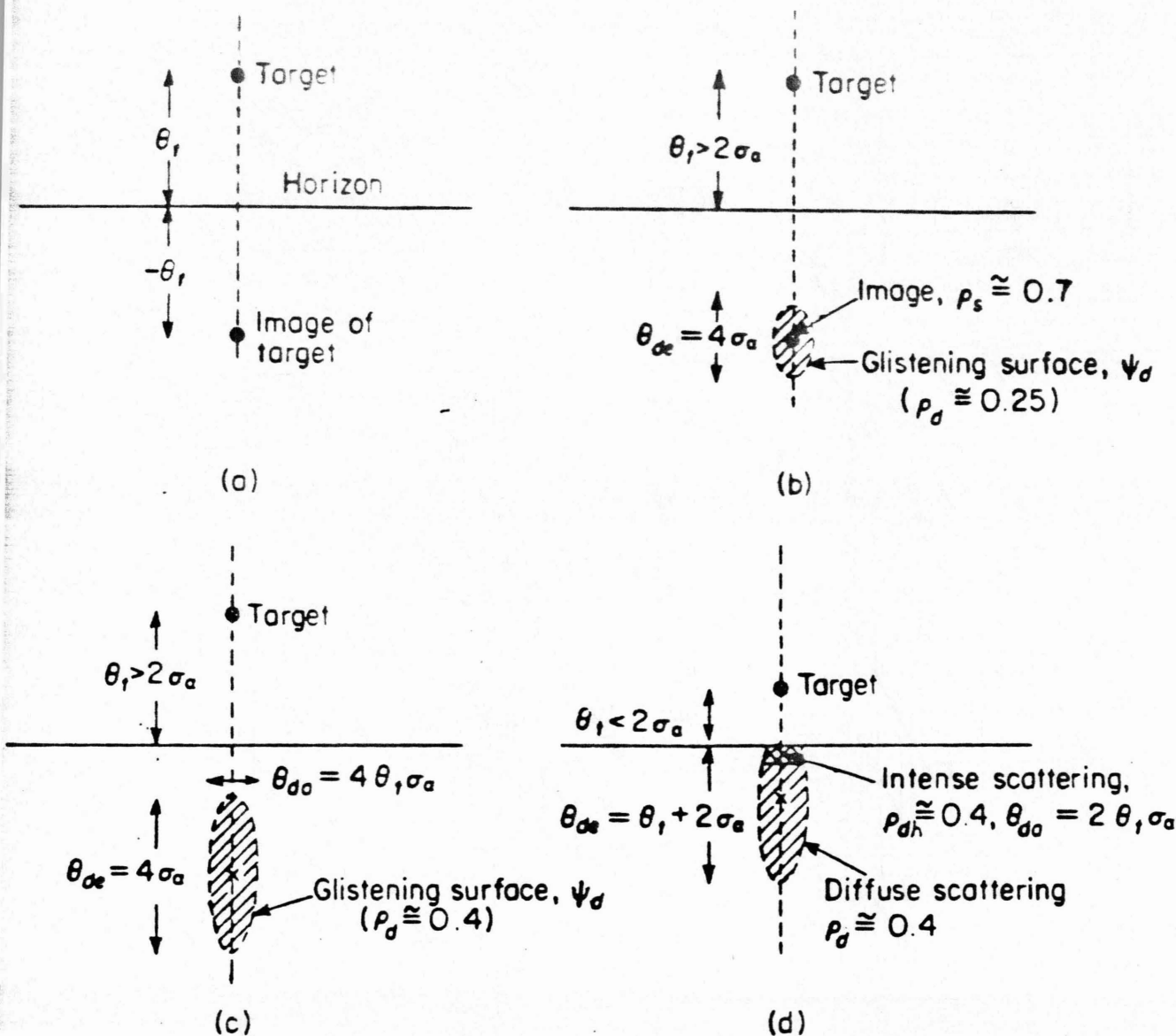


Figure 8. Angular spread of multipath reflections for a long-range target and low-sited radar [ 5 ] : (a) specular reflection; (b) slight roughness, characterized by rms slope  $\sigma_a \ll \theta_t$  and rms height deviation  $\sigma_h \approx 0.06 \lambda / \sin \theta_t$ ; (c) rough surface,  $\sigma_h > 0.16 \lambda / \sin \theta_t$  and  $2\sigma_a < \theta_t$ ; (d) rough surface with  $2\sigma_a > \theta_t$ , producing intense horizon spot. The major and minor axes of the elliptical glistening surface are  $\theta_{de}$  and  $\theta_{da}$ , while  $\rho_s$  and  $\rho_d$  are the specular and diffuse scattering factors. The elliptical glistening surfaces shown here represent the -4 dB contours of a Gaussian function, rather than sharp limits on reflection areas.

REFLECTION DIFFUSION MEASUREMENTS PRESENTED  
AT 1979 IEASCON BY RAYTHEON

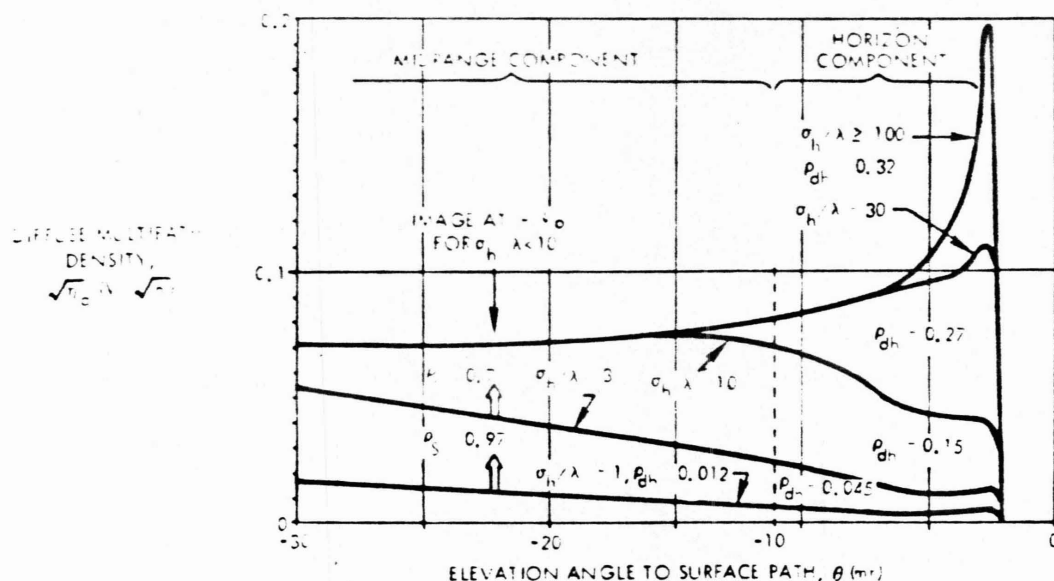


Figure 9a. Typical voltage density of diffuse components in elevation angle, computed according to [ 6a ] with correction for low-grazing-angle geometry, using the following parameters:

$$\begin{aligned} h_r &= 10 \text{ m} & a_t &= 18 \text{ mr} \\ h_t &= 100 \text{ m} & \psi_o &= 22 \text{ mr} \\ R &= 5 \text{ km} & \sigma_a &= 0.05 \text{ rad} \end{aligned}$$

The horizon component  $\rho_{dh}^2$  is defined as the area under the curve of power density  $\eta_d^2$  from the horizon to  $-\psi_o/2$ , and the midrange component  $\rho_{dm}^2$  from  $-\psi_o/2$  to  $-2\psi_o$ . Below that angle, the foreground component  $\rho_{df}^2$  extends to the lower end of the glistening surface at an elevation  $-2\sigma_a - \theta_t = -0.118 \text{ rad}$ . Directive antennas normally eliminate most of the foreground component, and often the midrange component as well, but the effect of the horizon component remains until the target rises above about 1.5 beamwidths.

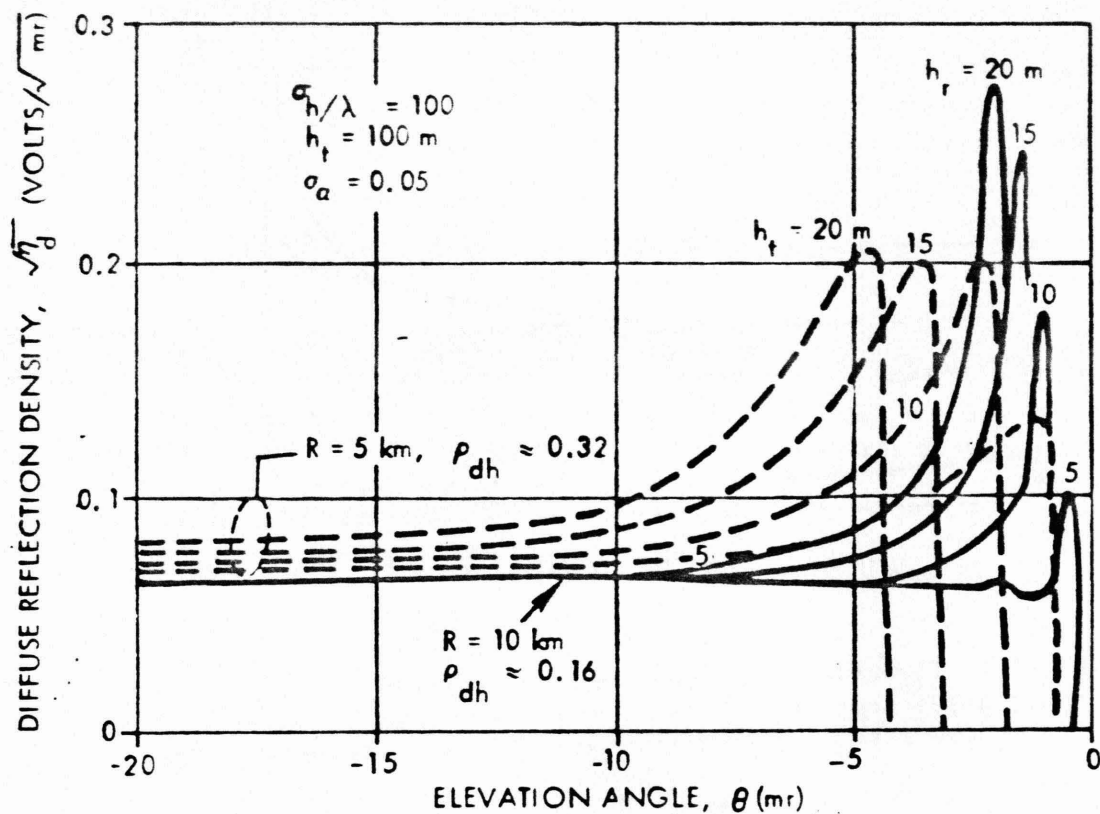
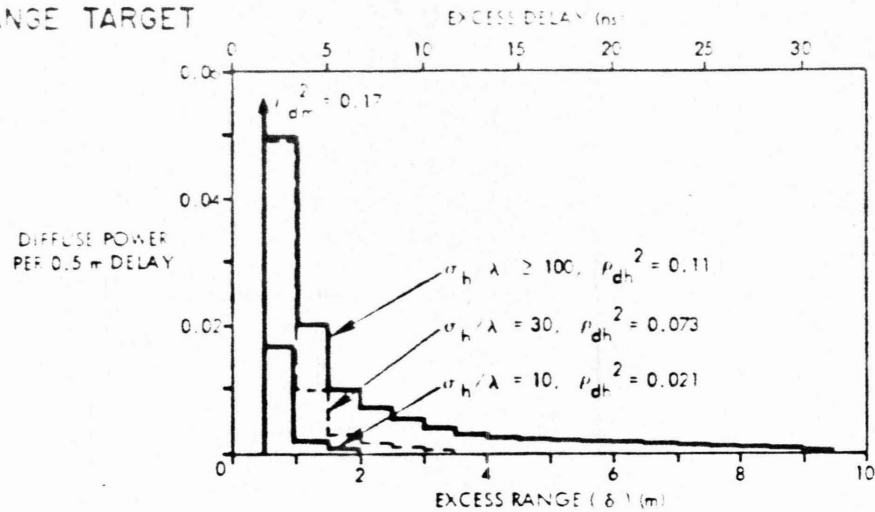


Figure 9b. Reflection densities for a rough surface viewed from different antenna heights with targets at 5 km and at 10 km. Note that the intense horizon spot predicted by [ 4 ] and [ 6 ] tends to disappear as antenna height is reduced and target range is increased, because of the low-grazing-angle correction introduced in [ 6a ] .



d) SHORT RANGE TARGET



b) LONG RANGE TARGET

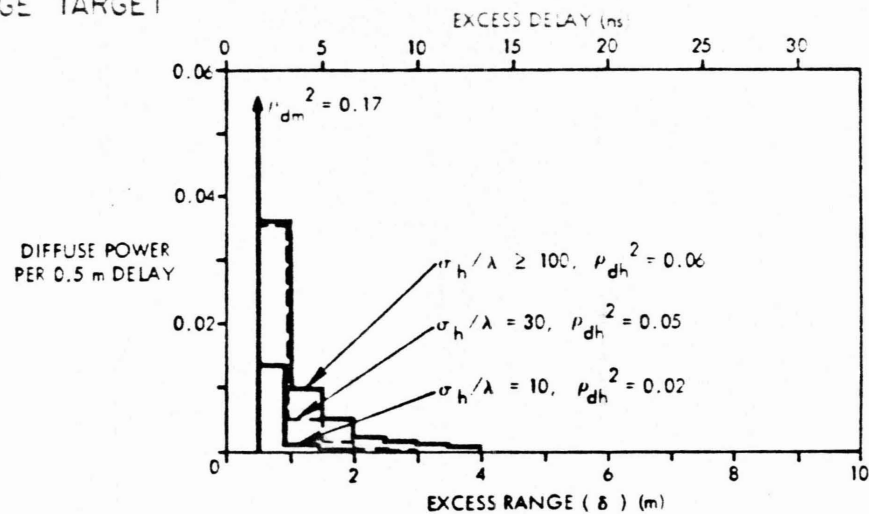


Figure 10. Typical power density of diffuse components in range (delay) relative to direct ray. Components with appreciable delay ( $> 1$  m), for the short-range target over rough terrain, originate in regions of the glistening surface nearer the target, and are greatly reduced for moderate roughness or longer target range. The midrange component  $\rho_{dm}^2$  has essentially the same delay (0.4 m) as the specular component. The foreground component is not included here, as it will normally be eliminated by a directive antenna. Range gating on narrow pulses, or averaging over a frequency-agile pulse train, can reduce the components whose delay exceeds the reciprocal of signal bandwidth, but since most of the power is received with less than 3 ns delay there will be few systems having sufficient bandwidth to affect the error of low-sited radars. In (a), the target is at 5 km range with conditions as tabulated in Fig. 9a, while in (b) the target is at the same elevation angle at long range.



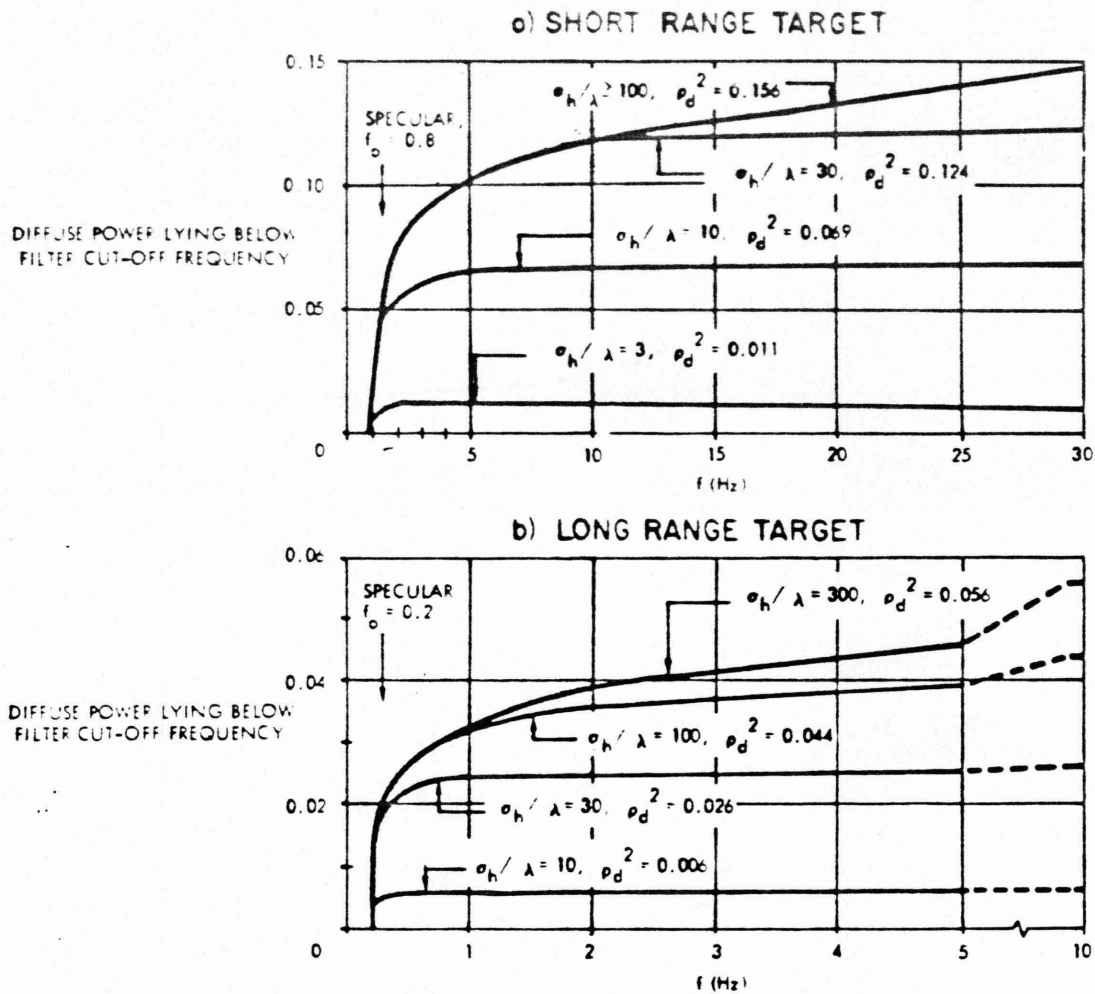


Figure 11. Diffuse reflected power vs. filter passband, considering  $\rho_d^2$  to include all components originating beyond the point of specular reflection. In (a), the target is at 5 km range with conditions as in Fig. 9a and a velocity  $v = 10,000 \lambda$  per sec, placing significant power above typical tracker bandwidths. In (b) the target is at the same altitude and velocity but at 10 km range, reducing the frequency spread of the multipath so that essentially all the power lies within a typical tracker bandwidth of 2 Hz.

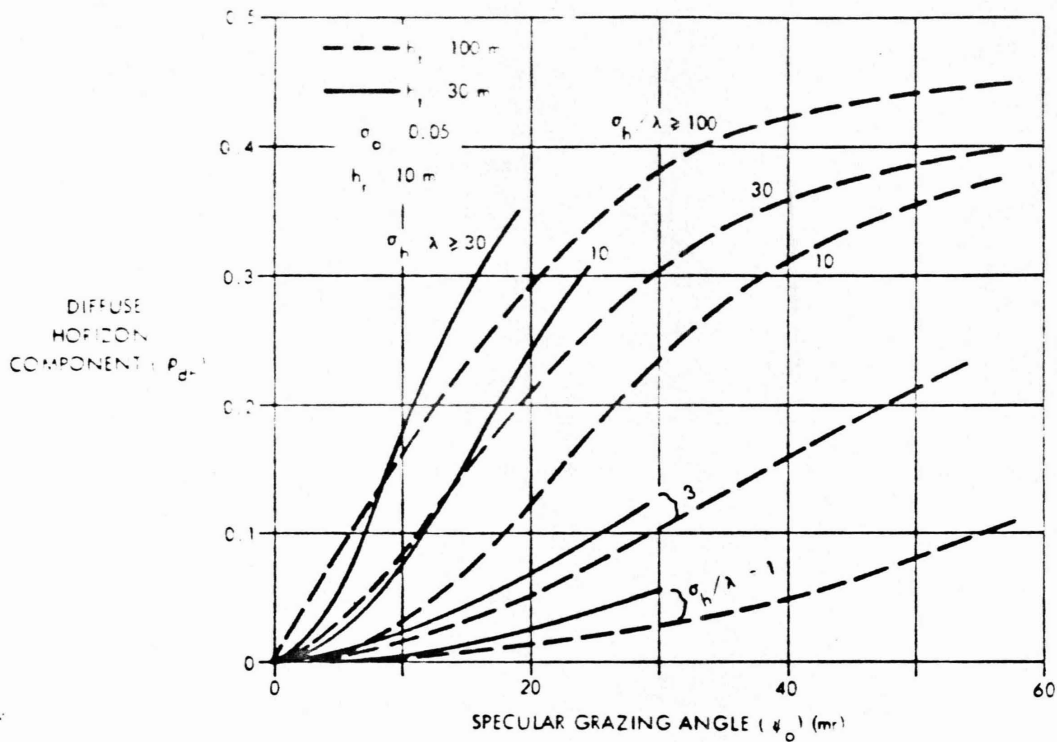


Figure 12a. Magnitude of the horizon diffuse component as a function of grazing angle, for two target altitudes and different degrees of surface roughness. For a given grazing angle, the horizon component is reduced as target altitude increases, because the target illuminates the surface more strongly at longer ranges from the radar, where  $\psi_1$  is small and the low-grazing-angle correction reduces the contribution to  $\rho_{dh}$ .

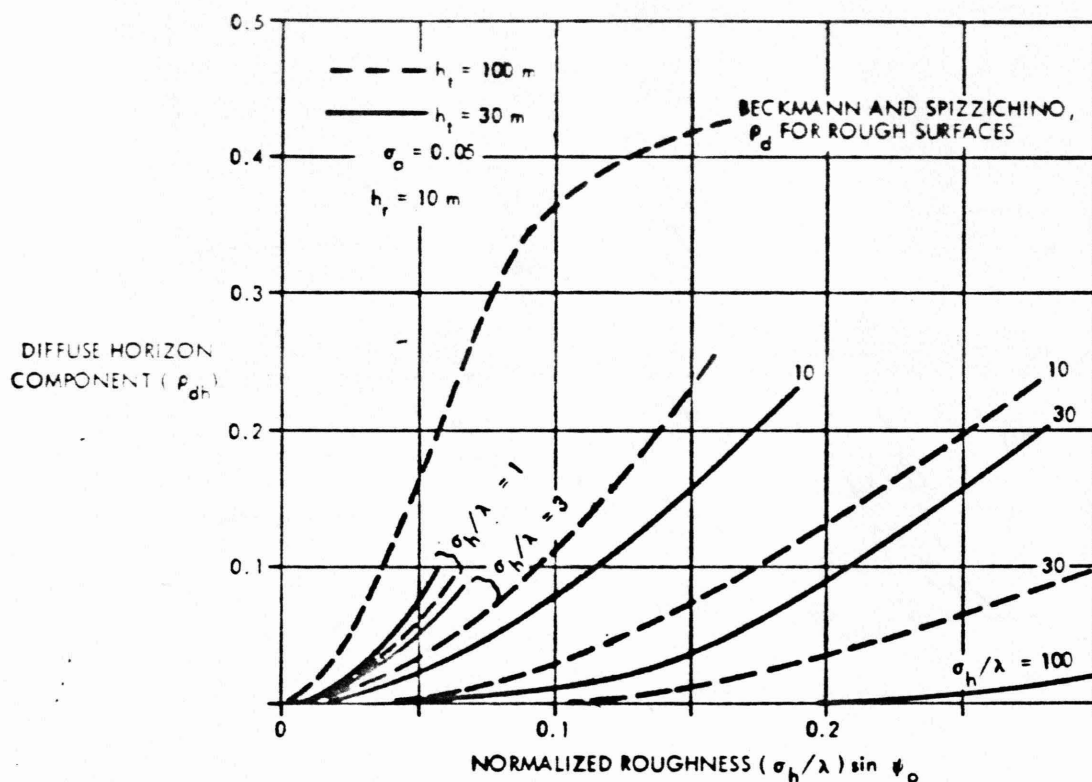


Figure 12b. Data from Figure 12a is replotted here as a function of the normalized roughness, for comparison with uncorrected values from [ 4 ]. For medium and rough surfaces,  $\sigma_h/\lambda > 10$ , the plotted curves cover situations with very low grazing angles where the horizon component is greatly reduced.

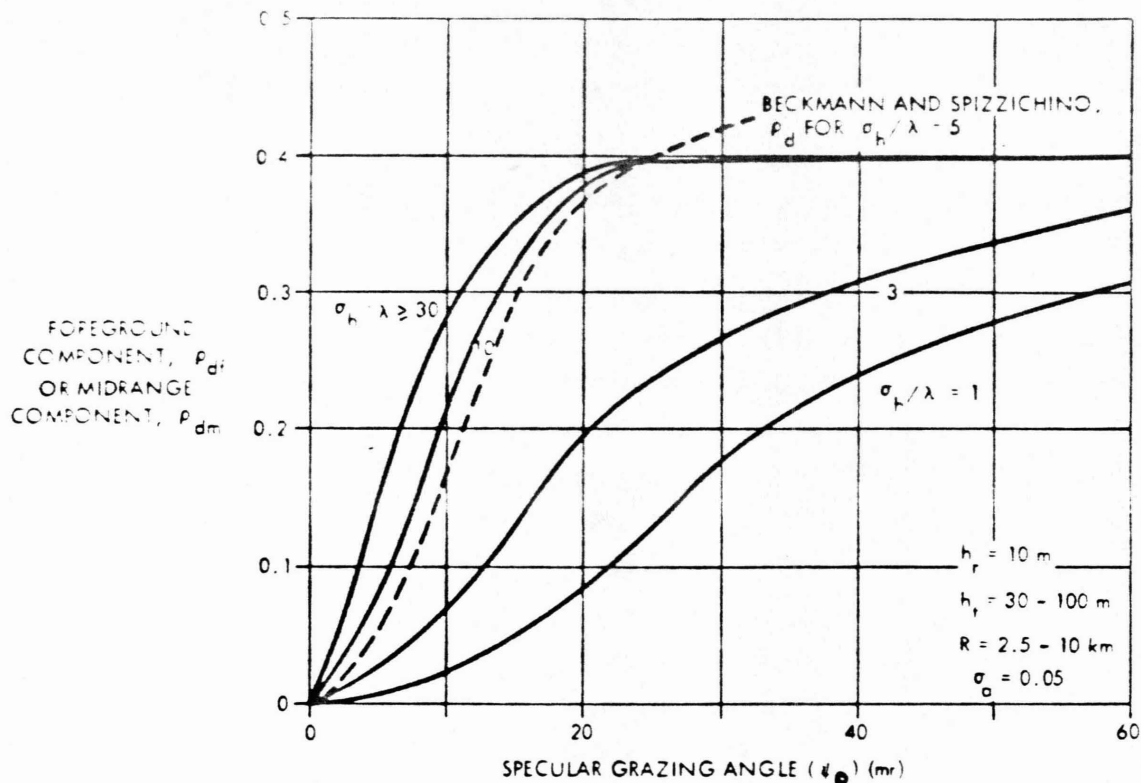


Figure 13. Magnitudes of the foreground component,  $p_{df}$ , and the midrange component,  $p_{dm}$ , of diffuse reflection. Note that these components, for  $\sigma_h/\lambda \gg 10$ , are dependent essentially on grazing angle and not on normalized roughness. In most experiments, and most radar applications,  $p_{df}$  is excluded by the directive antenna. For rough surfaces,  $p_{df}^2 = p_{dm}^2 \approx p_{dh}^2 \approx 0.16$ , so that total diffuse power is about half that of the direct signal, for the typical geometries considered here. At very low target angles ( $\psi_0 < 5$  mrad) where all diffuse components are small, the dominant multipath terms are from specular reflection (over smooth surfaces) or from diffraction, a subject not adequately discussed in the literature of low-angle tracking. However, see [15] for a method of calculating the magnitude of the diffracted field from a knife edge below the direct path to the target.

is considerably larger than most previously reported values [ 4], because antenna resolution has not been considered. In many practical cases, the foreground component is rejected entirely, and often the horizon component is the most significant. The effect of diffuse reflections on tracking accuracy will be described below.

3. Backscatter (clutter). The specular and diffuse reflections are reflected or emitted from the target before being scattered from the surface, and hence they have approximately the same delay and Doppler shift as the direct target signal. Surface clutter is generated by direct illumination from the radar, a small fraction of which is backscattered to the radar receiver. Only the clutter within the same spatial resolution cell as the target will contribute to tracking error, although in some cases this cell must be extended to include sidelobe response as well as the main lobe. Two-way antenna patterns are used in evaluating clutter power, as contrasted with the use of receiving-only patterns for multipath components. Equations for calculating S/C ratios with and without MTI or Doppler processing have been given in a separate lecture, and the effects of clutter or clutter residue on tracking accuracy will be summarized below.

## B. MULTIPATH ERRORS IN TRACKING

The multipath component of tracking error for a given situation depends upon the reflected power and the antenna response at the angles from which it is received, relative to the slope of the target error characteristic. It is convenient to evaluate tracking error using monopulse sum and difference patterns for a typical pair of illumination functions, and it can be shown that conical scan and other sequential lobing systems will have similar errors if their beams resemble the monopulse sum beam. Figures 14-20 are based on cosine illumination of a rectangular aperture (with a difference pattern which is the derivative of the sum pattern), and are typical of a large class of antennas, both rectangular and elliptical, whose sum and difference sidelobe ratios are near 23 and 18 dB respectively, and whose difference peaks are about 3 dB below maximum sum gain. Equations in Table II are generalized for any pattern or illumination.

General expression for interference error, normalized to 3-dB elevation beamwidth

$$\frac{\sigma_{\theta}}{\theta_e} = \frac{1}{k_m \sqrt{2(S/I_{\Delta})n_e}} \quad (3)$$

Specular multipath in sidelobes, where  $\overline{G}_{se}$  is averaged over region near image,  $\approx 2\theta_t$  below target tracking axis

$$\frac{\sigma_E}{\theta_e} = \frac{\rho_o \rho_s \rho_v}{k_m \sqrt{2\overline{G}_{se} n_e}} \quad (4)$$

Diffuse multipath in sidelobes, where  $\overline{G}_{se}$  is averaged just below horizon,  $\approx \theta_t$  below target tracking axis

$$\frac{\sigma_E}{\theta_e} = \frac{\rho_o \rho_{dh} \rho_v}{k_m \sqrt{2\overline{G}_{se} n_e}} \quad (5)$$

Multipath component in main  $\Delta$  lobe, at angle  $\theta < 1.5\theta_e$  from tracking axis ( $\rho = \rho_o \rho_d \rho_v$  or  $\rho_o \rho_s \rho_v < 0.5$ )

$$\frac{\sigma_E}{\theta_e} = \frac{\rho \Delta(\theta)/\Sigma(0)}{k_m \sqrt{2 n_e}} \quad (6)$$

Diffacted component in main  $\Delta$  lobe, at angle  $\theta < 1.5\theta_e$  from tracking axis.  $A(\theta)$  is the voltage of the diffacted component, and  $A(0)$  that of the direct target component [14].

$$\frac{\sigma_E}{\theta_e} = \frac{A(\theta) \Delta(\theta)}{\sqrt{2} k_m A(0) \Sigma(0)} \quad (6a)$$

Diffuse multipath error in azimuth measurement over narrow glistening surface ( $\theta_{da} < \theta_a$ )

$$\frac{\sigma_A}{\theta_{da}} = \frac{\rho_o \rho_d \rho_v}{2\sqrt{2\overline{G}_{sr}}} \quad (7)$$

Specular multipath error in range measurement where  $\overline{G}_{sr}$  is averaged over region near image

$$\sigma_r = \frac{\rho_o \rho_s \rho_v h_r \theta_t}{\sqrt{2\overline{G}_{sr}}} \quad (8)$$

Table II. Multipath error equations for specular and diffuse components and for diffraction.

1. Reflections in Antenna Sidelobes. When the radar is tracking a target at elevation  $\theta_t$ , the specular image arrives at depression angle  $\theta_r \approx \theta_t$  (for  $h_r \ll h_t$ , see Table I). If this target-image separation  $\approx 2\theta_t$  is sufficient to place the image in the sidelobe region of the  $\Delta$  pattern, as in Fig. 14, the specular component will introduce a small, approximately sinusoidal error voltage whose power, relative to the sum signal, is

$$I_{\Delta}/S = \frac{(\rho_o \rho_s \rho_v)^2}{\bar{G}_{se}} \quad (9)$$

The resulting error expression is given in Table II, as derived from the general expression for interference error. Since the phase angle  $\alpha$  of the specular component changes with target elevation, there will be a slow oscillation of this error, with a frequency

$$f = \frac{1}{2\pi} \frac{d\alpha}{dt} \approx \frac{2h_r}{\lambda} \frac{d}{dt} \left( \frac{h_t}{R} \right) = \frac{2h_r}{\lambda} \dot{\theta}_t \quad (10)$$

In most cases, this frequency is low enough so that no smoothing effect is provided by the servo ( $n_e \approx 1$ ).

Diffuse error has a similar effect, except that it is more random and may be reduced by smoothing (see Fig. 11 for typical frequency spectra). However, the depression angles from which the diffuse components arise cover the entire interval from the horizon to  $\approx 2\sigma_\alpha$ , so evaluation of  $I_{\Delta}/S$  is more difficult. It is often sufficient to evaluate only the horizon component, since this lies closest to the main lobe of the  $\Delta$  channel.

2. Reflections in Main Lobe. Targets below about 1.5 beamwidths will produce diffuse components in the main  $\Delta$  lobe, and below 0.75 beamwidths the specular component enters this lobe. An expanded plot of typical  $\Sigma$  and  $\Delta$  patterns is shown in Fig. 15. Reflections from this region can cause either of two types of error, depending on their magnitudes relative to the direct ray.



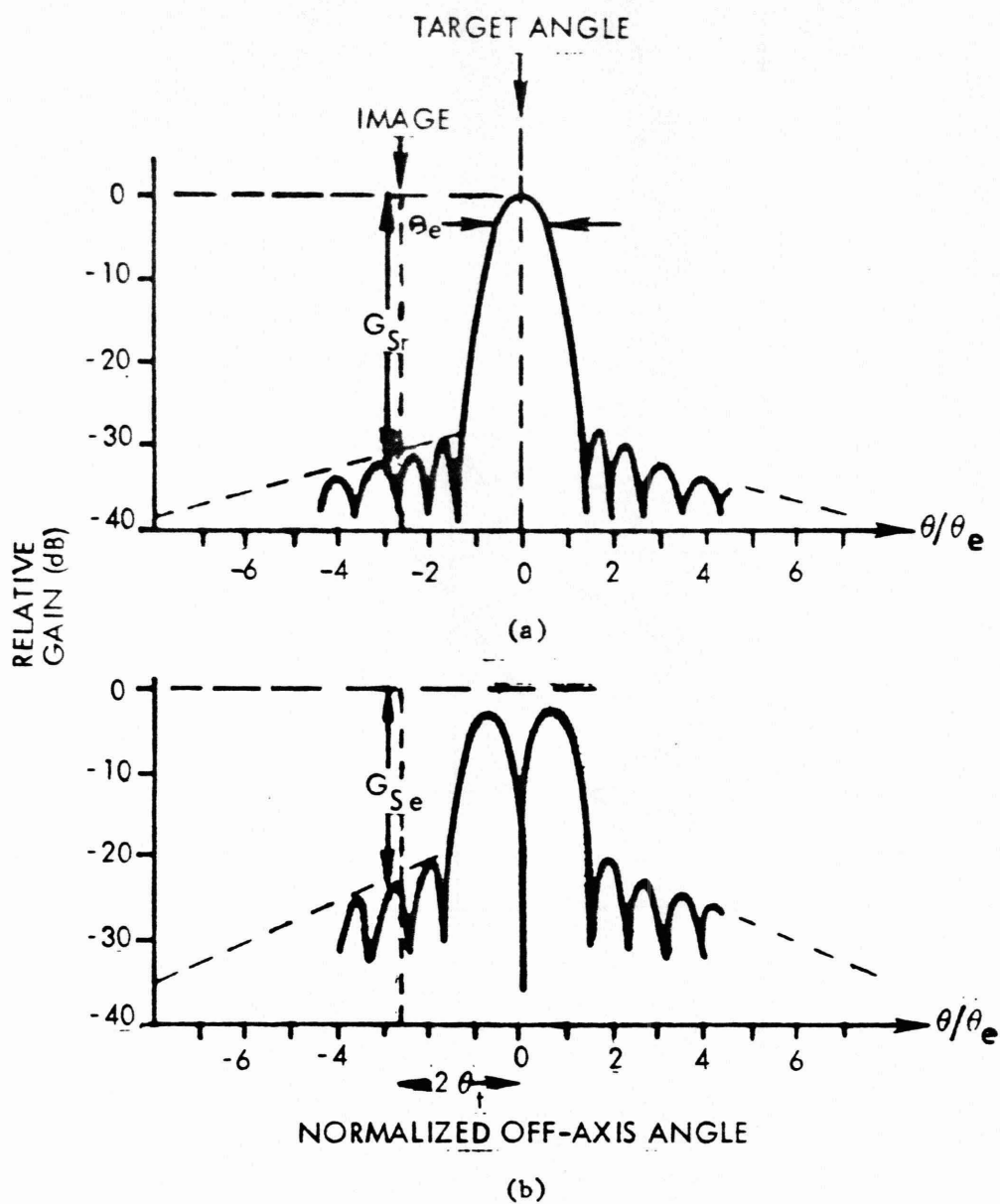


Figure 14. Typical monopulse patterns, showing definitions of sum and difference sidelobe ratios  $G_{sr}$  and  $G_{se}$  (evaluated at the angle from which reflections<sup>sr</sup> arrive).<sup>se</sup>

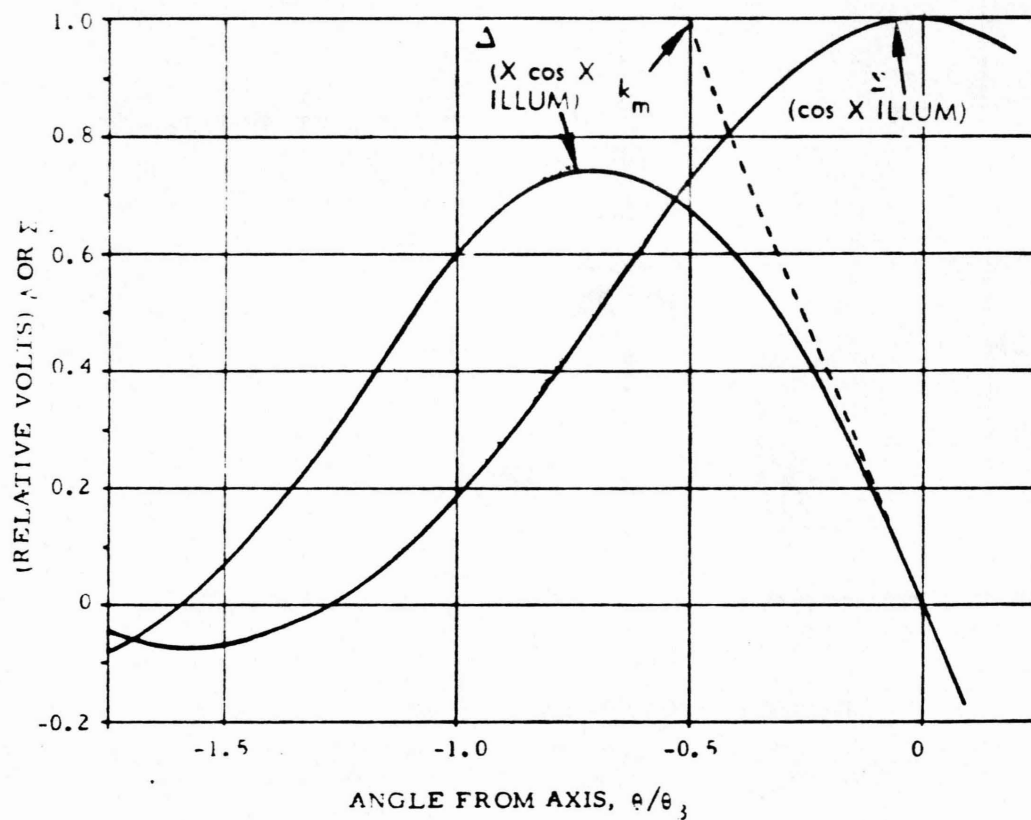


Figure 15. Expanded plot of mainlobe region for sum and difference patterns. The dashed line is at the on-axis tracking slope  $k_m = 1.96$ , where the slope is defined in normalized units [ 5 ] :

$$k_m \equiv \left. \frac{\partial(\Delta/\Sigma)}{\partial(\theta/\theta_3)} \right|_{\theta=0}$$

For small reflections ( $\rho < 0.5$ ), the tracking angle deviates symmetrically about the target angle, as with sidelobe reflections, and the target remains within the region of linear difference slope. The specular multipath-to-signal ratio is

$$I_{\Delta}/S = \left[ \frac{\rho_o \rho_s \rho_v \Delta(\theta)}{\Sigma(0)} \right]^2 \quad (11)$$

and the resulting error is given by Eq. 6 in Table II. Here,  $\Delta(\theta)$  is the difference-channel voltage gain averaged over the angles from which the reflections arrive, and it is assumed that the resulting error (Fig. 16) is small enough that the direct signal is received with the full gain  $\Sigma(0)$  of the sum channel.

The same expression applies to diffuse components, with  $\rho_d$  replacing  $\rho_s$  and with appropriate adjustment of the reflection angle. For example, in Fig. 16, if the horizon diffuse component  $\rho_{dh}$  is substituted for  $\rho_s$ , the source of reflections will be half way from the target to the image, and the target elevation angles in the abscissa will run from zero to  $2.4 \theta_e$ . Hence, significant mainlobe diffuse errors will commence at target elevation  $\theta_t \approx 1.5 \theta_e$  rather than at  $\theta_t \approx 0.75 \theta_e$ . Two typical curves for horizon diffuse error  $\sigma_{\theta h}$  are shown in Fig. 17, taking into account the variation of  $\rho_{dh}$  with target elevation for rough and medium surfaces. At the lower elevations, where the horizon component approaches the  $\Delta$ -pattern null, diffuse scattering at greater depression angles becomes important. The error from these regions, near the specular point (mid-range) and below it (foreground), are shown in Fig. 18. The density of these reflections is inversely proportional to the surface slope, and the reflected power (integrated over the  $\Delta$  mainlobe) is proportional to the beamwidth, giving a family of curves which depend on  $\theta_e/\sigma_\alpha$  as shown.

A different type of error appears when strong specular reflections ( $\rho > 0.7$ ) are received, as may happen for surfaces where the normalized roughness  $(\sigma_h/\lambda) \sin \psi < 0.065$ . When such a reflection enters the main  $\Delta$  lobe some  $1.5 \theta_3$  below the target (see Fig. 15), and is in phase with

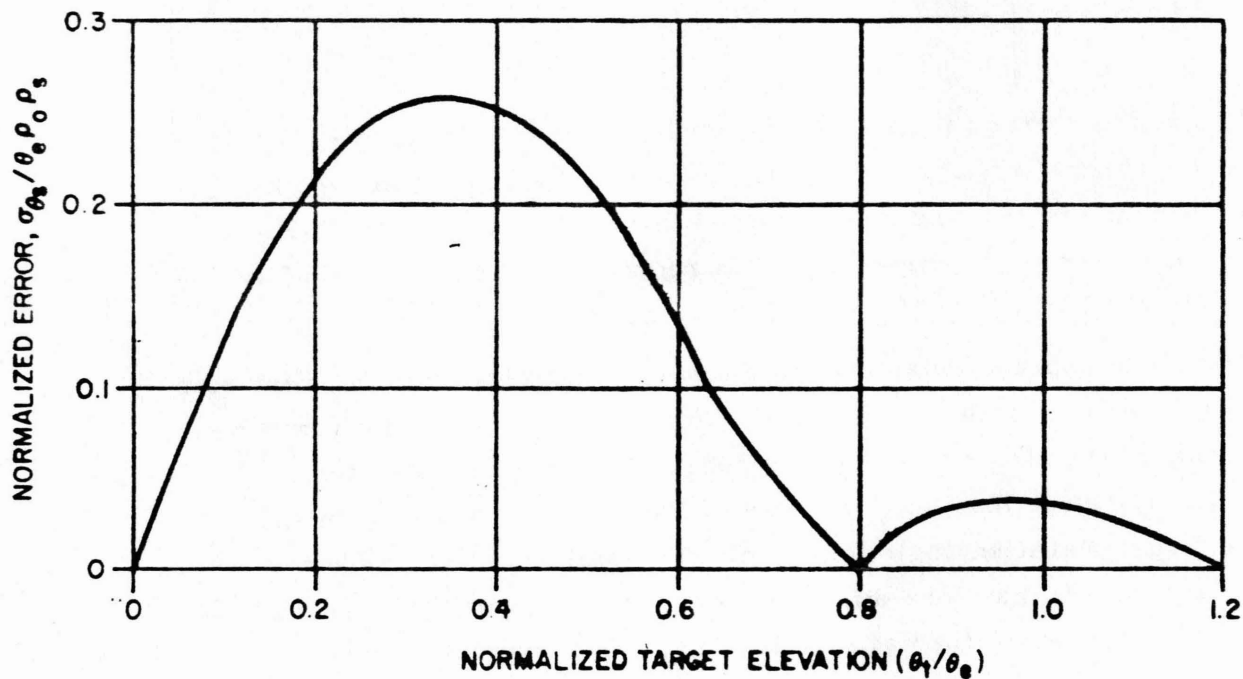


Figure 16. Normalized specular error component  $\sigma_{\theta_s}$  for  $\rho_0 \rho_s < 0.5$ , in which case the target remains within the linear region of the  $\Delta$  pattern and deep signal nulls are not encountered.

NO SKIDING OCCURS CLOSE IN WITHIN  
ANTENNA CAN NOT LOCK ONTO TARGET,

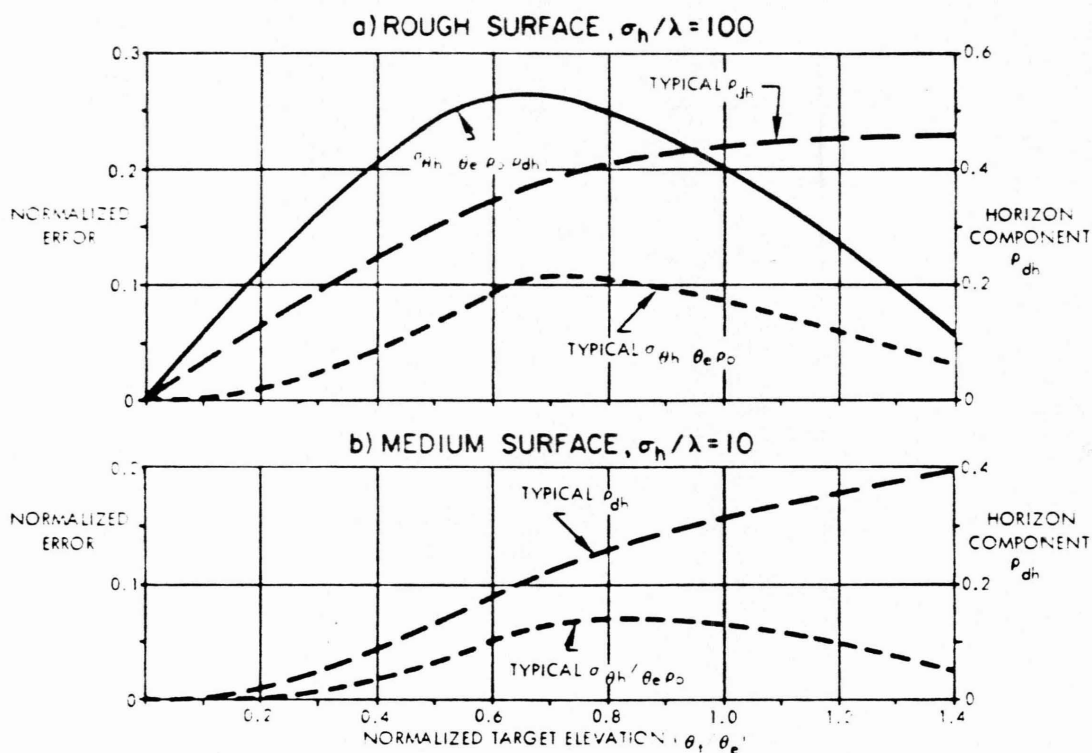


Figure 17. Normalized horizon component of diffuse multipath error (defined as originating between the horizon and  $-\psi_0/2$  in elevation angle). The dashed lines give typical values for the 100-m target of Fig. 9a at different ranges, as observed with a 40-mr radar beamwidth. For  $\sigma_h/\lambda > 10$ , the horizon component is concentrated near the horizon (about halfway between the target and the image), so the normalized curve of Fig. 16 can be used with 2:1 expansion in the elevation scale and with  $\rho_{dh}$  replacing  $\rho_s$ .

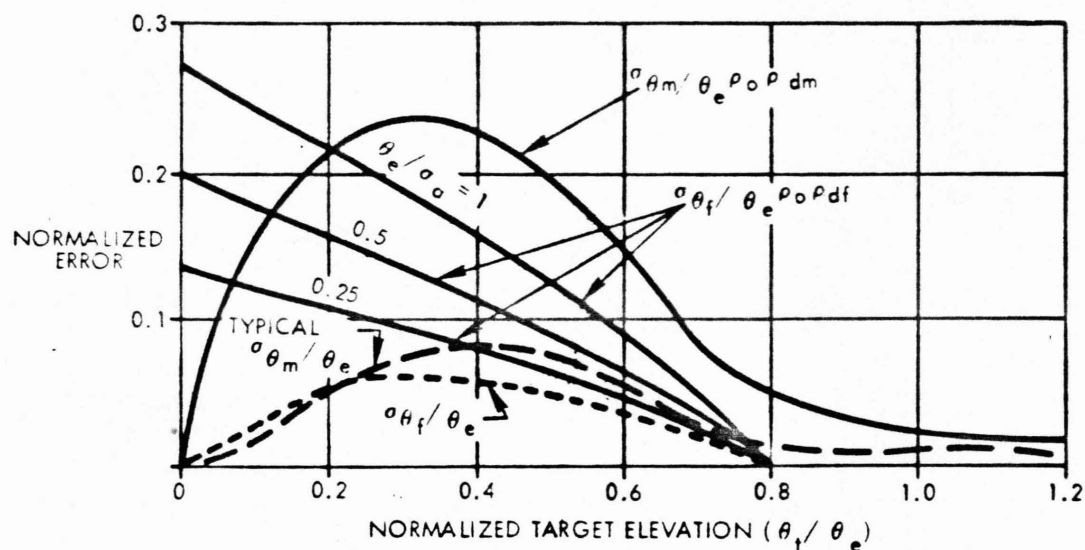


Figure 18. Normalized foreground and midrange components of diffuse multipath error, for different ratios of radar beamwidth to surface slope. These components are important for rough surfaces, where specular reflection is absent at the low angles for which  $\sigma_{\theta_m}$  and  $\sigma_{\theta_f}$  exceed  $\sigma_{\theta_h}$ . The typical curve shown by the dashed line is for medium and rough surfaces described in Fig. 13, observed with a 40-mr beamwidth.

the target signal, the tracking angle tends toward the horizon, forcing the target far up onto the upper  $\Delta$  lobe and the image farther up the lower lobe. When the image is out of phase, the servo forces the lower peak of the  $\Delta$  lobe to the horizon, placing the target and image symmetrically on the two shoulders of this lobe. In the in-phase case, the indicated elevation is near zero, independent of true target elevation, while in the opposing case it is near 0.7 beamwidths, independent of target elevation. This phenomenon, known as "nosediving," is shown in idealized form in Fig. 19. In actuality, the track may be lost due to  $\Sigma$ -channel fading as the relative phase approaches 180 deg, or the antenna may be deflected downward rather than upward, either as a result of random noise or apparent increase in reflected power from diffuse components. Even if range and azimuth tracking is preserved, the elevation data are useless. Smoothing of the elevation data can delay the onset of nosediving, as shown approximately in Fig. 20, provided the smoothing time exceeds the period of the multipath error. This figure also shows the diffuse components and the normalized specular component for cases where  $\rho_o \rho_s < 0.5$ .

3. Range and Azimuth Errors. Both specular and diffuse reflection components can also introduce errors in range data, and diffuse components cause a small azimuth error as well. The spatial distributions of Figs. 8 and 10 give an idea of the spread in these two coordinates. The composite direct-plus-reflected signal may be viewed as an extended target giving glint errors in range and azimuth, as listed in Table II.

### C. ANTI-MULTIPATH TECHNIQUES

Many radar tracking operations are carried out within the region  $\theta_t < 1.5 \theta_e$ , where the  $\Delta$  mainlobe reaches the horizon and the second  $\Delta$  sidelobe reaches the image. Often, tracking is desired even for  $\theta_t < 0.5 \theta_e$ , where strong specular reflection in the mainlobe will normally cause erratic tracking or total loss of track. A number of techniques have been devised to reduce multipath error, but most of these are based on the purely specular reflection model, and are of limited value over irregular surfaces. For example, low-sidelobe antenna design can suppress the response to the specular image for  $\theta_t > 0.8 \theta_e$ , but at the expense of a broader mainlobe and increased diffuse error.



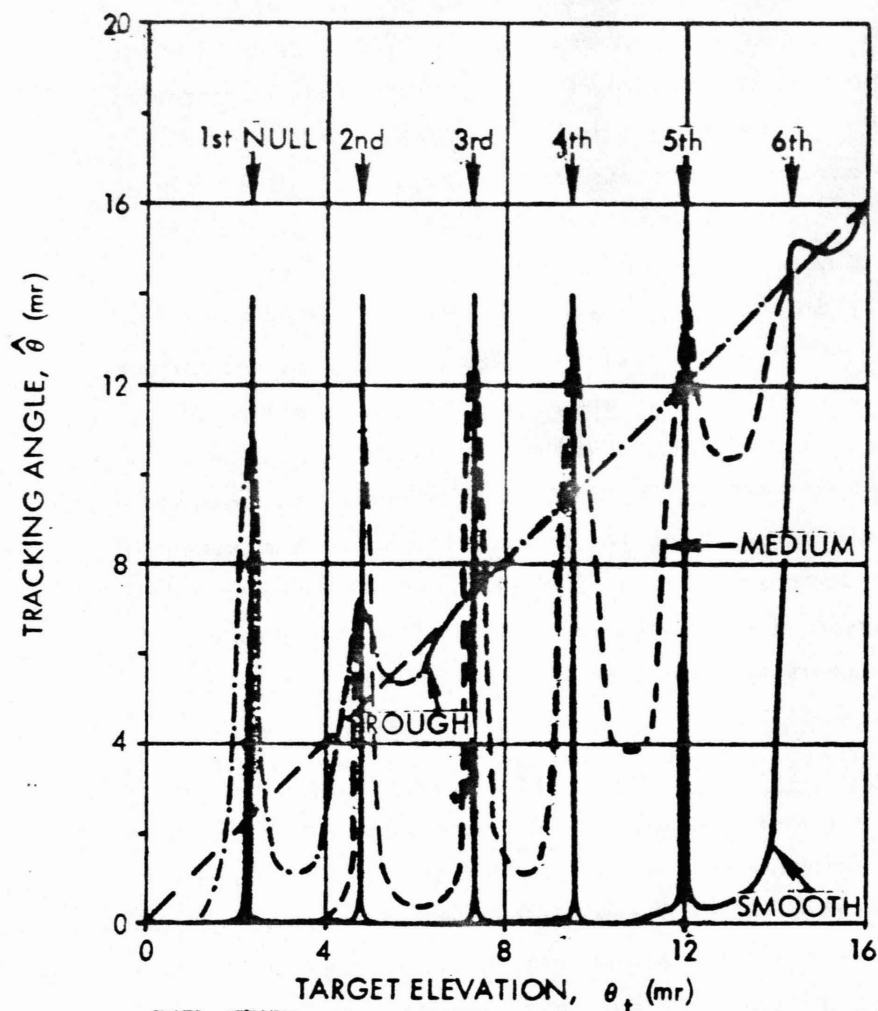


Figure 19. Tracking angle vs. target angle with a specular image of varying amplitude according to Fig. 7. The smooth, medium and rough surfaces correspond to  $\sigma_p/\lambda$  of 1, 5 and 20 respectively. The radar beamwidth  $\theta_b = 20$  mr, and the antenna height  $h_a = 200 \lambda$ , giving signal nulls at elevation intervals  $\lambda/2 h_a = 0.0025$  rad. The phenomenon known as "nosediving," in which the radar tracks the centroid between target and image, with abrupt jumps to a fixed angle above the target, occurs for  $\theta_t < 0.7 \theta_e$  when  $\rho > 0.75$ . In practice, the antenna may jump to an angle below the image, causing loss of track. Effects of diffuse reflection are not shown.

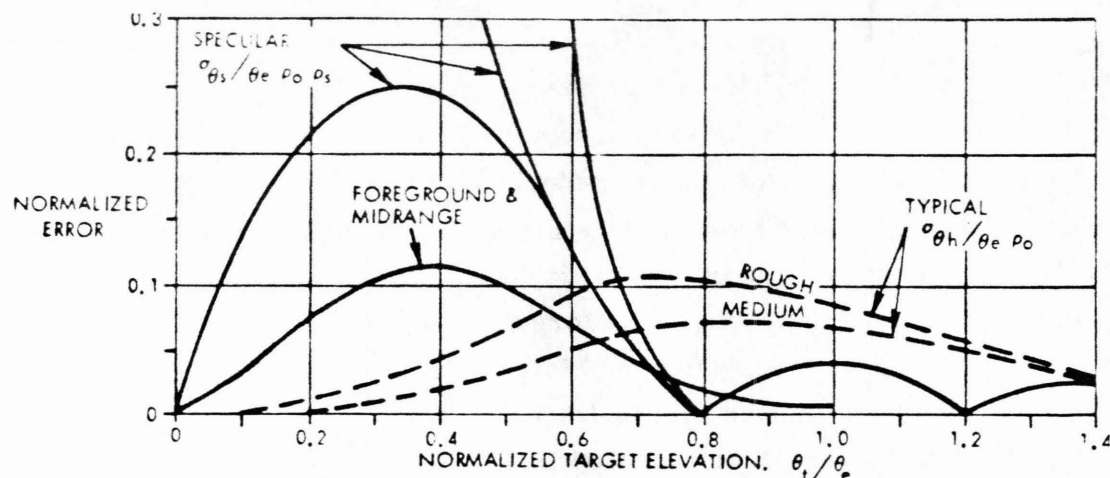


Figure 20. Combined multipath error envelopes for a typical tracker, showing relative magnitudes of specular component and diffuse components from horizon and nearer regions. The diffuse curves are drawn for  $\theta_e = 40$  mr,  $h_e = 10$  m,  $h_t = 100$  m and  $\sigma_a = 0.05$ , but for other cases the magnitudes of separate components are found using Figs. 9-18 and combined in rss fashion:

$$\sigma_{\theta}^2 = \sigma_{\theta_s}^2 + \sigma_{\theta_h}^2 + \sigma_{\theta_m}^2 + \sigma_{\theta_f}^2$$

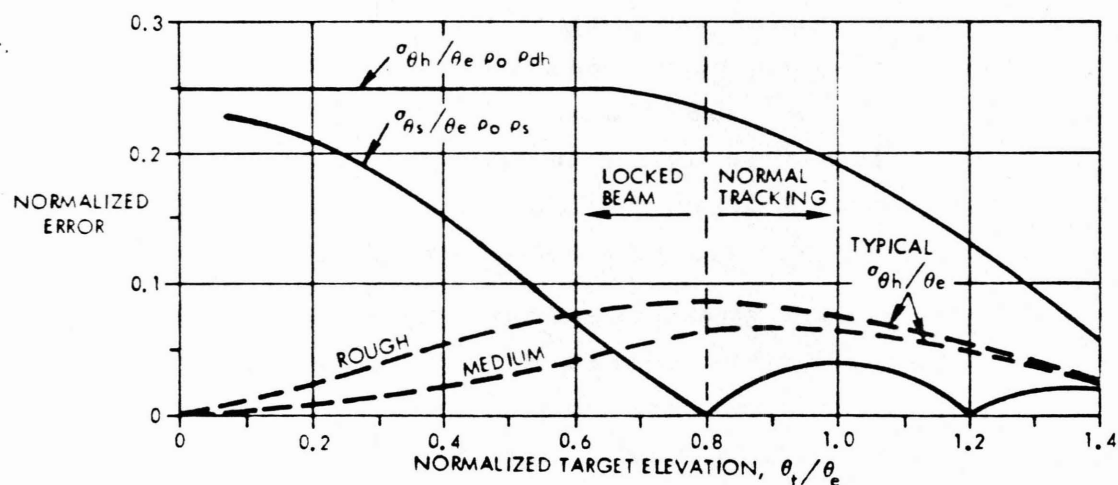


Figure 21. Normalized multipath error components for off-axis monopulse tracker, in which the beam is locked at  $\theta_b = 0.8\theta_e$  for targets below that angle. Typical horizon components are for the same case used in Fig. 20.

1. High-Resolution Radar. The use of narrow beams is the most basic technique for avoidance of multipath error, and this explains the preference for high frequencies in tracking radar. Narrowing the elevation beam is beneficial in two ways: first, the multipath errors for a given S/I ratio are directly proportional to beamwidth  $\theta_e$  (see Table II); secondly, the S/I ratio for a given target elevation is generally improved with decreasing  $\lambda/D$  ratio (where D is antenna diameter), and beamwidth is usually reduced by this means (rather than by decreasing the taper). Since tactical systems are limited in antenna size, the trend has been toward higher frequencies:  $K_u$ -band (16 GHz),  $K_a$ -band (35 GHz), or even higher, for short-range systems. Some of the limiting factors are discussed by Thompson and Kittredge [ 7 ], who conclude that the higher bands are usable, in a typical case, to about 10-km range in rain up to 4 mm/h.

Resolution in range or Doppler is of limited value for most (low-sited) radars. The spread of diffuse multipath is typically only a few nanoseconds in range delay (Fig. 10), and one to a few hertz in Doppler (Fig. 11). The spread of the specular components is even smaller, often only one or two wavelengths of the RF and a fraction of a hertz, respectively. Airborne or high-sited surface radars can sometimes use range or Doppler resolution to advantage. The expressions in Table III summarize the conditions under which these steps are useful.

Frequency agility or diversity gives some of the benefits of range resolution, although the error components are averaged over the tunable band rather than being excluded from the receiver output. The limitations as to applicability are similar to those of range resolution, but the tunable bandwidth  $\Delta f$  may be greater than the instantaneous bandwidth of practical waveforms.

2. Off-Axis Tracking. A simple procedure suggested in 1952 by Kirkpatrick [ 8 ] consists of locking the antenna at an elevation  $\theta_b \approx 0.8\theta_e$  for targets descending below that elevation, and following the targets in an open-loop error estimation mode. The expected errors for different surface conditions are shown in Fig. 21.

Techniques	Sidelobe region, $\theta_t > 1.5 \theta_e$ , $\sigma_E < 0.03 \theta_e$	Mainlobe region, $0.3 \theta_e < \theta_t < 1.5 \theta_e$ $0.03 \theta_e < \sigma_E < 0.3 \theta_e$	Horizon region, $\theta_t < 0.3 \theta_e$ peak error $\rightarrow \theta_e$
Narrow beamwidth	Error = $C \theta_e / \sqrt{G_{se}}$	Error and region proportional to $\theta_e$	Region of large error proportional to $\theta_e$
Range resolution with signal bandwidth B	Effective for $\frac{h_r h_t}{R} > \frac{c}{2B}$	Effective only if $h_r \theta_e > \frac{c}{2B}$	Ineffective
Data smoothing or Doppler resolution	Effective for $\frac{2 h_r \theta_t}{\lambda} > \frac{1}{t_0}$	Effective for $\frac{2 h_r \theta_t}{\lambda} > \frac{1}{t_0}$	Ineffective
Frequency agility or diversity	Effective for $\frac{h_r h_t}{R} > \frac{c}{2 \Delta f}$	Effective only if $h_r \theta_e > \frac{c}{2 \Delta f}$	Permits track on centroid at horizon, but no height data
Off-axis mono-pulse tracking	Ineffective	Provide stable track with $\sigma_E \rightarrow 0.2 \theta_e$ as $\theta_t \rightarrow 0.3 \theta_e$	Provides stable track with increasing error until loss of signal
Double-null tracker	Degenerates to normal monopulse	Effective, giving $0.02 < \sigma_E / \theta_e < 0.1$	Provides stable track with minimum error
Symmetrical $\Delta/\Sigma$ pattern	Inapplicable	Effective for smooth and medium surfaces	Relatively large diffuse error and deep fades limit applicability
Asymmetrical monopulse	Inapplicable	Effective, giving $0.05 < \sigma_E / \theta_e < 0.2$	Provides stable track with increasing error until loss of signal
Complex angles	Ineffective	Effective for specular reflection at low sites	Possible data over calibrated surface until loss of signal
Multiple-target estimation	Ineffective	Effective for smooth and medium surfaces	Impractical except as implemented with asymmetrical beams
Radar fences	Effective	Effective when main-lobe clears fence	Detrimental: extends horizon to top of fence
Circular polarization	Ineffective unless $\theta_t \gg$ Brewster angle; not applicable for narrow beams		
Use of a priori altitude	Inapplicable	Poor tracking is better than a priori data	Permits continued range and azimuth track until loss of signal

Table III. Effectiveness of anti-multipath techniques in three regions of elevation tracking [ 6 ].

3. Multiple-Target Estimators. Some years ago it was recognized that the conventional monopulse tracker, while near optimum for measuring a single target, was far from the ideal (maximum likelihood) estimator for one of two or more closely spaced targets. Several schemes were devised and tested for simultaneous measurement of two unresolved targets, or of a target over a reflecting surface. The basic papers on this approach appear in [ 1 ], with White [ 9 ] giving the clearest discussion of the results. Having synthesized the maximum-likelihood tracker for low-angle targets over a smooth surface, he showed that the resulting  $\Delta$  patterns, while placing a second null at the image, had large response lobes at the horizon and at angles below the image. Following an intuitive preference for reduced response in these regions, White arrived at the "tempered double-null tracker," which maintained the second null at the image point but with generally reduced response at and below the horizon. The estimated errors for this technique, using the diffuse reflection models described above, are shown in Fig. 22. For a smooth surface, there would be no error except that resulting from thermal noise, clutter, or circuit deficiencies.

A second approach to the target-image problem, described by Dax [ 10 ], used a broadened  $\Sigma$  pattern to produce a  $\Delta/\Sigma$  ratio having symmetry with respect to the peak of the lower  $\Delta$  lobe. The antenna was locked to place the axis of symmetry at the midpoint between target and image (as calculated from range data), making the output estimate independent of phase and amplitude of the specular reflection. White [ 9 ] proposed a similar scheme for phased-array trackers which could not afford the time to control adaptively the double-null pattern. A pair of asymmetrical patterns was generated whose ratio  $F_B/F_A$  was symmetrical relative to the target-image midpoint (as with the Dax system). By "squinting" the two patterns so that each was asymmetrical, the response below the horizon could be minimized. Even with squint, this approach leads to a large response from the horizon component of diffuse reflection, giving errors as shown in Fig. 23. Again, for a smooth surface, this approach yields zero error for strong enough signals.

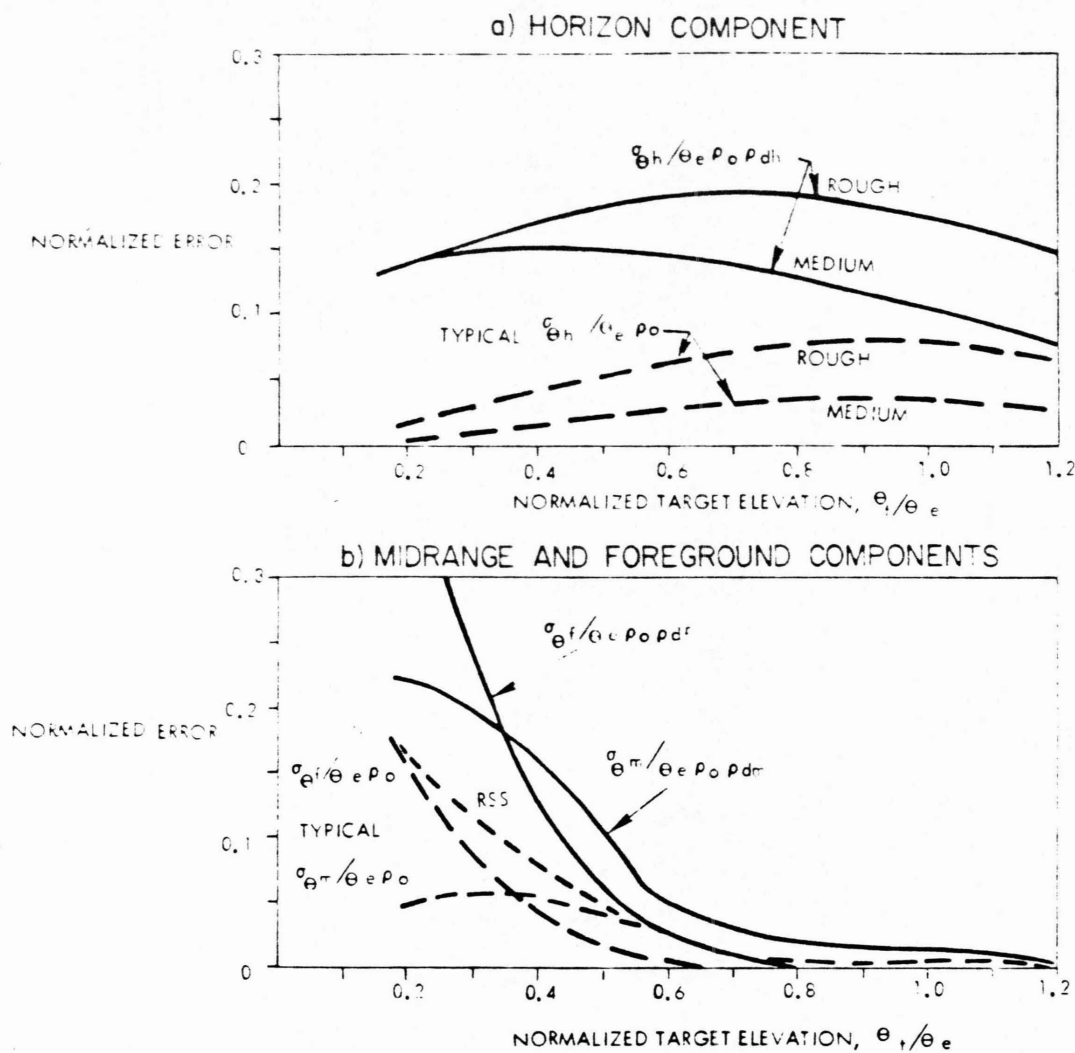


Figure 22. Normalized diffuse multipath error for tempered double-null tracker [9]. The presence of specular reflection at low target elevation angles tends to increase the sensitivity to noise and to diffuse components arriving at angles different from the image angle. Note, however, that the horizon components of error are lower than for tracking or off-axis monopulse, especially for medium surfaces which lack the enhanced horizon spot. Below  $\theta_t = -0.3\theta_e$ , the foreground components rise quite steeply equaling or exceeding those of conventional monopulse systems. To obtain direct comparison with the conventional monopulse systems using the same aperture size, the beamwidth  $\theta_e$  is taken as  $1.2\lambda/D$  ( $\approx 40$  mr for the typical curves), and White's standard beamwidth is assumed to be  $\lambda/D$ . The actual modified sum beamwidth is somewhat broader than  $\theta_e$ .



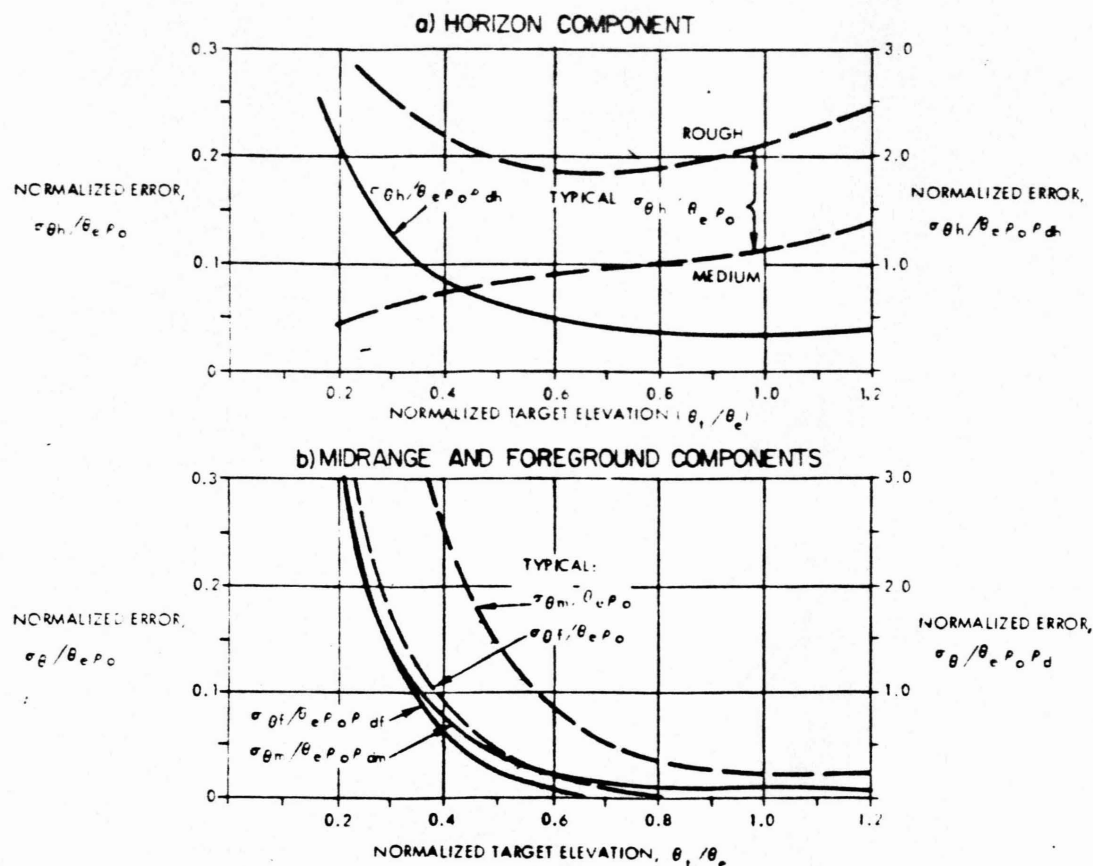


Figure 23. Normalized diffuse multipath error for fixed asymmetrical-beam monopulse estimator [9]. The effect of specular reflection is to increase the sensitivity to noise and diffuse components for  $\theta_t < 0.6 \theta_e$ . The relatively large response to horizon components of diffuse multipath results from the high gain at zero elevation of the broadened pattern of one of the two beams used in this system. Typical values are shown for the case used in previous figures, with  $\theta_e = 1.2 \lambda / D = 40$  mr.



Each of the linear multiple-target estimation techniques can be described by its antenna pattern functions or by the equivalent aperture weighting functions (the two functions being related by the Fourier transform). Aperture weighting or sampling is the more complicated description, in that it involves many more elements than the number of beams used to synthesize the corresponding patterns in space.

4. Complex Angle Monopulse. It has been shown by Sherman [ 11] that the quadrature component of the monopulse error signal contains information which is rejected in the normal monopulse error detector, and which can provide data on a second, unresolved target. Subsequent work applied this to the low-angle tracking problem, showing that a series of observations could be interpreted to yield true target elevation to high precision. Experiments show that the actual complex  $\Delta/\Sigma$  ratio does not follow the regular spiral path with increasing target elevation over the ground, but instead has both systematic and random variations in phase and amplitude (presumably as a result of diffuse components). Attempts have been made to match measured data, over one or more loops of the spiral, to a calibration curve prepared for the target azimuth angle, with considerable success for a test target at fixed range. However, diffuse reflection theory predicts that such calibrations will be valid only within very narrow intervals in target azimuth and range. The greatest prospect for success of the complex angle technique is in lower frequency radars, sited low and looking over the sea, such that diffuse components are minimized.

5. Other Techniques. Three further techniques for multipath reduction should be mentioned. Radar fences have been used at fixed sites, and natural obstacles are often available for use by mobile radars, to reduce clutter and multipath. Fences are of particular value in reducing multipath in the antenna sidelobes, for targets above  $\approx 2\theta_e$ . The top of the fence causes diffraction and produces an equivalent source above the angle from which multipath would have arrived. Hence, for lower target elevations where this diffraction component may enter the main  $\Delta$  lobe, the error may actually be increased. Siting of the radar just above the height of a distant line of trees can minimize error on low-elevation targets.

Use of circular polarization is sometimes proposed to reject reflected components from a flat surface. This would be effective over an infinite metallic ground plane, but unfortunately, the earth's surface does not cause a reversal of the sense of circular polarization at angles below the Brewster angle (Fig. 6), and this approach is useless.

The final technique involves reliance on non-radar sources of altitude data: a priori trajectory information, optical data, or barometric altimeter data. Each of these has its own sources of error, which are beyond the scope of this course.

#### D. ACCURACY OF RADAR MEASUREMENTS

Several sources of measurement error have been discussed above. This section will review the basic error components and the factors which affect them, leading to an example of tracking radar error analysis.

1. Thermal Noise. The basic expression for noise error in interpolation within a resolution cell of width  $z_3$  has been given:

$$\sigma_z = \frac{z_3}{k_z \sqrt{2(S/N) n}} \quad (12)$$

Table IV gives the expressions for thermal noise errors in angle estimation, in terms of the on-axis energy ratio

$$\mathcal{R} = 2(S/N) n L_m \quad (13)$$

and the error slope constants which apply to each case. Numerical values of monopulse slope  $k_m$  are shown in Fig. 24, as a function of  $\Sigma$ -channel sidelobe ratio. Table V shows corresponding values for horn-fed apertures. Conical-scan error slope for two-way scanning systems is shown in Fig. 25 as a function of squint angle. One-way (COSRO) systems have somewhat lower values  $k_s/\sqrt{L_k} \leq 1.2$ , with correspondingly larger errors. The equations shown in Table IV do not include the effects of small-signal suppression (detector loss) or of inefficient signal processing (e.g.  $L_m > 1$ ), which can be accounted for by inclusion of loss factors to reduce  $\mathcal{R}_m$ . Detailed discussion of these losses will be found in [ 5 ].

Ideal, rectangular aperture

$$\sigma_{\theta} = \frac{\sqrt{3} \lambda}{\pi w \sqrt{R_0}} \quad (14)$$

Ideal, circular aperture

$$\sigma_{\theta} = \frac{2 \lambda}{\pi D \sqrt{R_0}} \quad (15)$$

Monopulse null track ( $k_m \approx 1.5$ )

$$\frac{\sigma_{\theta}}{\theta_3} = \frac{1}{k_m \sqrt{R_m}} \quad (16) \quad \frac{0.7}{\sqrt{R_m}}$$

Linear scan ( $k_p / \sqrt{L_p} \approx 1.4$ )

$$\frac{\sigma_{\theta}}{\theta_3} = \frac{\sqrt{L_p}}{k_p \sqrt{R_m}} = \frac{0.7}{\sqrt{R_m}} \quad (17)$$

Conical scan ( $k_s / \sqrt{L_k} \approx 1.4$ )

$$\frac{\sigma_{\theta}}{\theta_3} = \frac{\sqrt{2 L_k}}{k_s \sqrt{R_m}} \quad (18) = \frac{1}{\sqrt{R_m}}$$

Additional error component for estimation at angle  $\theta$  off axis

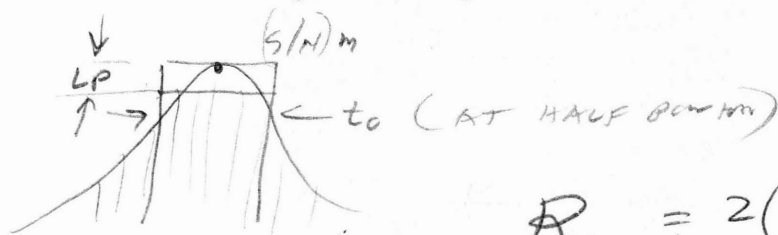
$$\frac{\sigma_{\theta}}{e} = \frac{1}{\sqrt{R}} \quad (19)$$

Note:  $R_0$  calculated for uniform illumination,

$R_m$  calculated on axis for actual illumination,

$R$  calculated at target angle  $\theta$ .

Table IV. Thermal noise errors in angle tracking and measurement



$$R_m = 2 \left( \frac{S}{N} \right)_m t_0 t_n$$

$$\text{SEARCH} \quad \frac{\sigma_{\theta}}{\theta_3} \approx \frac{0.7}{\sqrt{R_m}} = \frac{1}{k_m \sqrt{R_m}}$$

$$\sigma_{\theta} \approx 0.1 \theta_3 \text{ TOTAL}$$

NOT MATCH PRESENT IN TABLE

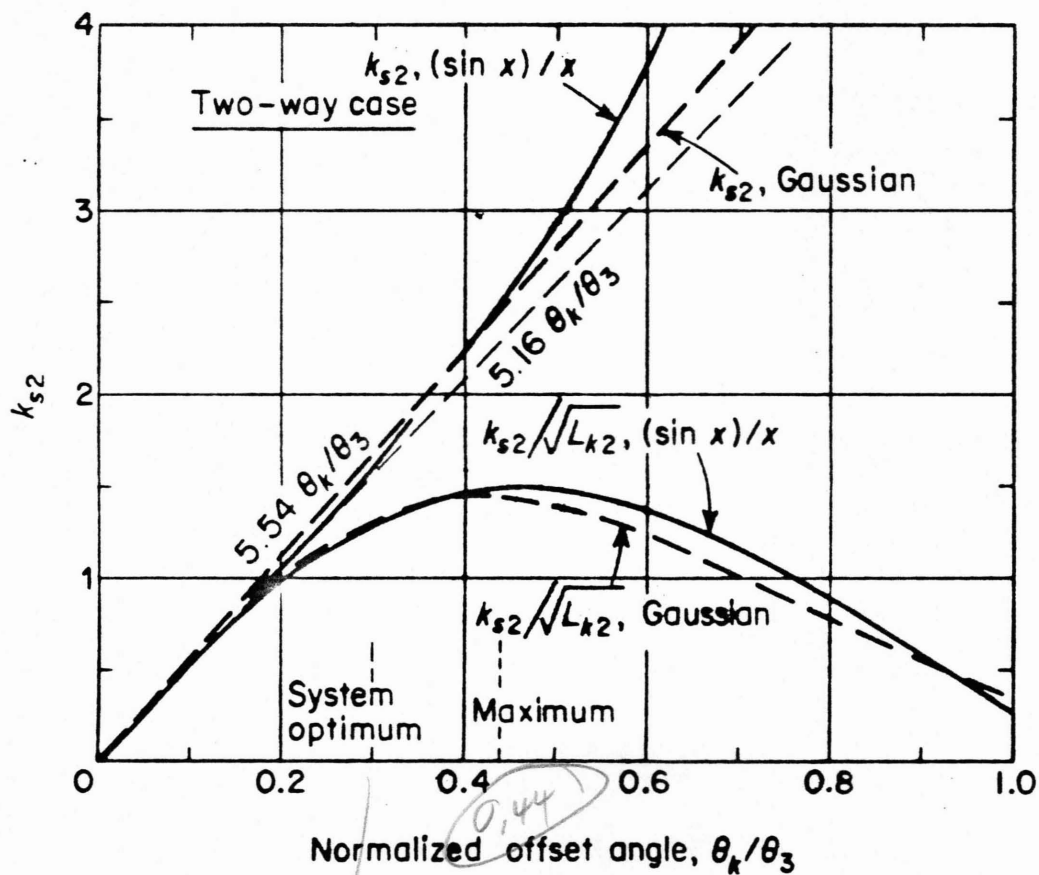
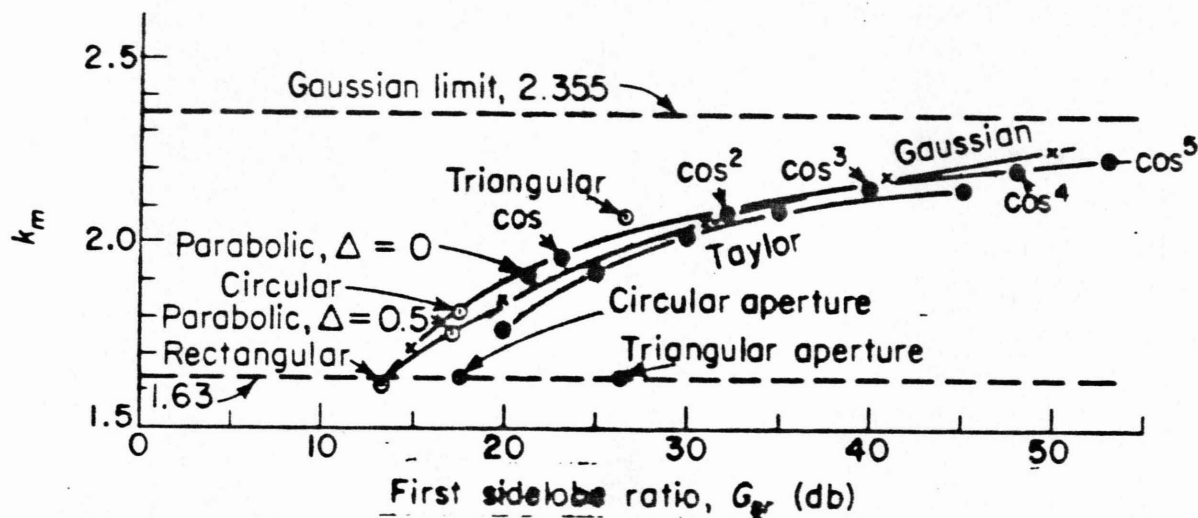


Figure 25. Conical-scan error slopes vs. offset angle [ 5 ].

BECAUSE STRONGER SIGNAL.

! PRACTICAL FORMS BETTER  
WORK.

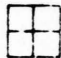
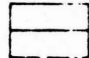
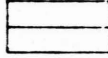
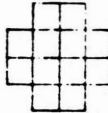
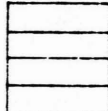
Type of horn	$\eta_a$	$k_m$	$k_m$	$G_{sr}$ (db)	$G_{se}$ (db)	Feed shape
Simple four-horn	0.58	1.2	1.2	19	10	
Two-horn dual mode	0.75	1.6	1.2	19	10	
Two-horn triple-mode	0.75	1.6	1.2	19	10	
Twelve-horn	0.56	1.7	1.6	19	19	
Four-horn triple-mode	0.75	1.6	1.6	19	19	

Table V. Performance of horn-fed antennas:  $\eta_a$  is  $\Sigma$ -channel efficiency,  $G_{sr}$  is  $\Sigma$ -channel sidelobe ratio,  $G_{se}$  is  $\Delta$ -channel sidelobe ratio.

Errors in range delay or Doppler measurement are found from equations in Table VI, and from Figs. 26 and 27. The normalized ranging slope  $K\tau_{3a}$  is analogous to  $k_m$  in monopulse angle measurement, as is the normalized Doppler slope  $K_f B_{3a}$ . Except for ranging slope on the rectangular pulse, all these normalized slopes have optimum values near unity. In Doppler measurement, the spectral width  $B_{3a}$  will be the width of the spectral envelope (Fig. 28) for noncoherent (single-pulse) processing, and width of the fine spectral line for pulsed Doppler processing.

2. Clutter and Interference. The general expression for error caused by small interfering signals is

$$\sigma_x = \frac{x_3}{k_x \sqrt{2(S/I_\Delta)n_e}} \quad (26)$$

where  $(S/I_\Delta)$  is the ratio of  $\Sigma$ -channel signal to  $\Delta$ -channel interference, and  $n_e$  is the number of independent interference samples averaged in one measurement. Equations for  $S/I_\Delta$  in clutter may be obtained from those discussed in earlier lectures by multiplying  $\Sigma$ -channel  $S/C$  ratios by the receiving gain ratio  $(\Delta/\Sigma)^2$  in the channel under consideration (elevation, azimuth, range or Doppler). This is especially significant in elevation tracking over a clutter surface. If Doppler processing is used, the  $S/I_\Delta$  ratio may be increased by the MTI or Doppler improvement factor.

3. Target Noise. Most radar targets consist of several scattering or reflecting elements, distributed in angle and range with respect to a "center of gravity" which is to be measured. Two types of target noise can be identified [ 12 ] : glint, which is associated with the phase relationships of the reflected signal; and scintillation, in which amplitude fluctuations of the reflected signal are converted by radar processing into apparent shifts in target position. Glint is present in all four measurement coordinates, and can be approximated by normally distributed errors with standard deviations shown in Table VII. Typical measured distributions are shown in Fig. 29.

SKOTCHDOPOLE  
LAG FORMULA

$$\epsilon_v = \frac{v_t}{kv} \rightarrow 0$$

$$\epsilon_a = \frac{a_t}{ka} \quad \text{LRT } ka = 2.5 \quad ka = 2.5 B_n^2 = 90 \left(\frac{1}{t_a}\right)^2$$

LRT  $R = 6000m$

LRT rms  $R_{min} = 1m$  ;  $\epsilon_a \leq 6m$  ;  $ka \geq 10 = 2.5 B_n^2$  ;  $B_n^2 = 4$   
Ideal (filter matched to signal with rms bandwidth  $B_a$ )

$$\sigma_t = \frac{1}{B_a \sqrt{R}} \quad (20) \quad B_n = 2Hz$$

CAN  
ADAPT  
TO  
RMSE  
AND  
S/N

Mismatched filter for signal pulse-width  $\tau_{3a}$  (where  $k\tau_{3a} \leq 1.2$ )

$$\frac{\sigma_{th}}{\tau_{3a}} = \frac{1}{k\tau_{3a}\sqrt{R}} = \frac{1}{\sqrt{R}n} \quad (21) \quad \text{AFTER INTEGRATION SAME.}$$

Pulse compression with output pulsewidth  $\tau_{3x}$

$$\frac{\sigma_t}{\tau_{3a}} = \frac{1}{k\tau_{3x}\sqrt{R}} = \frac{\sqrt{L_m}}{k_m\sqrt{R}} \quad (22)$$

Rectangular pulse with adaptive filter (see Fig. 27)

$$\frac{\sigma_t}{\tau} = \frac{\sqrt{2}}{R} \text{ or } \frac{1}{\sqrt{2B}\tau R} \quad (23)$$

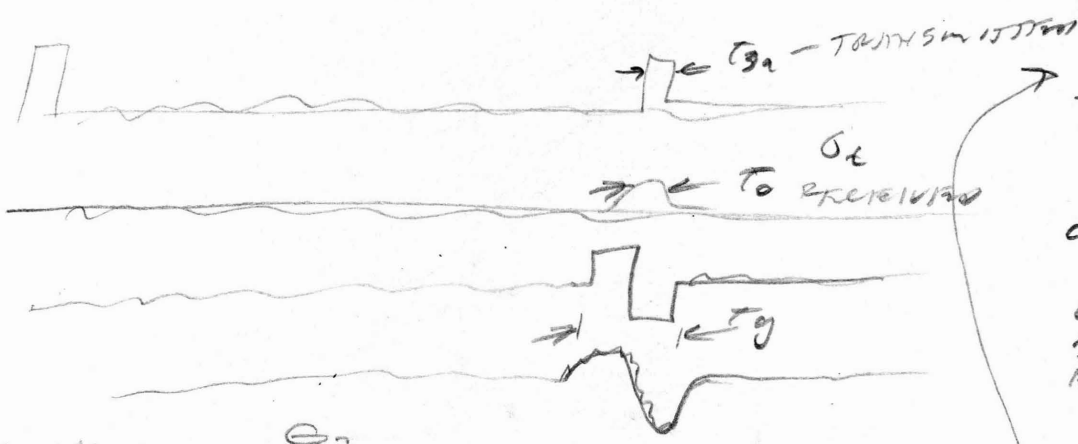
Ideal Doppler estimate for rms signal duration  $\tau_a$

$$\sigma_f = \frac{1}{\tau_a \sqrt{R}} \quad (24)$$

Mismatched filter for signal bandwidth  $B_{3a}$  (where  $k_f B_{3a} \leq 1.2$ )

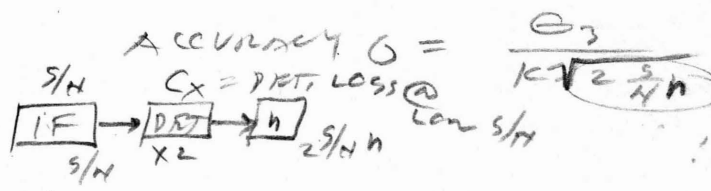
$$\frac{\sigma_f}{B_{3a}} = \frac{1}{k_f \tau_{3a} \sqrt{R}} \quad (25)$$

Table VI. Thermal noise errors in range and angle tracking



S/N	n
100	1
10	10
1	100 X 2
0.1	10,000

LIMITED BY LAG FORM IN TRACKING LOOP. ALSO LOOP GAIN  $\rightarrow 0$  ; GOES UNSTABLE



S/N below 1,  $C_x$  LOSS IS INTRODUCED.

Now  $2 C_x S/N h$

$$\sigma_e = \frac{\sigma_3 \sqrt{C_x}}{K \sqrt{2 S/N h}} \quad C_x = \frac{S/N + 1}{S/N} \quad \therefore \sigma_e = \frac{\sigma_3 \sqrt{(S/N) + 1}}{K S/N \sqrt{2 h}}$$

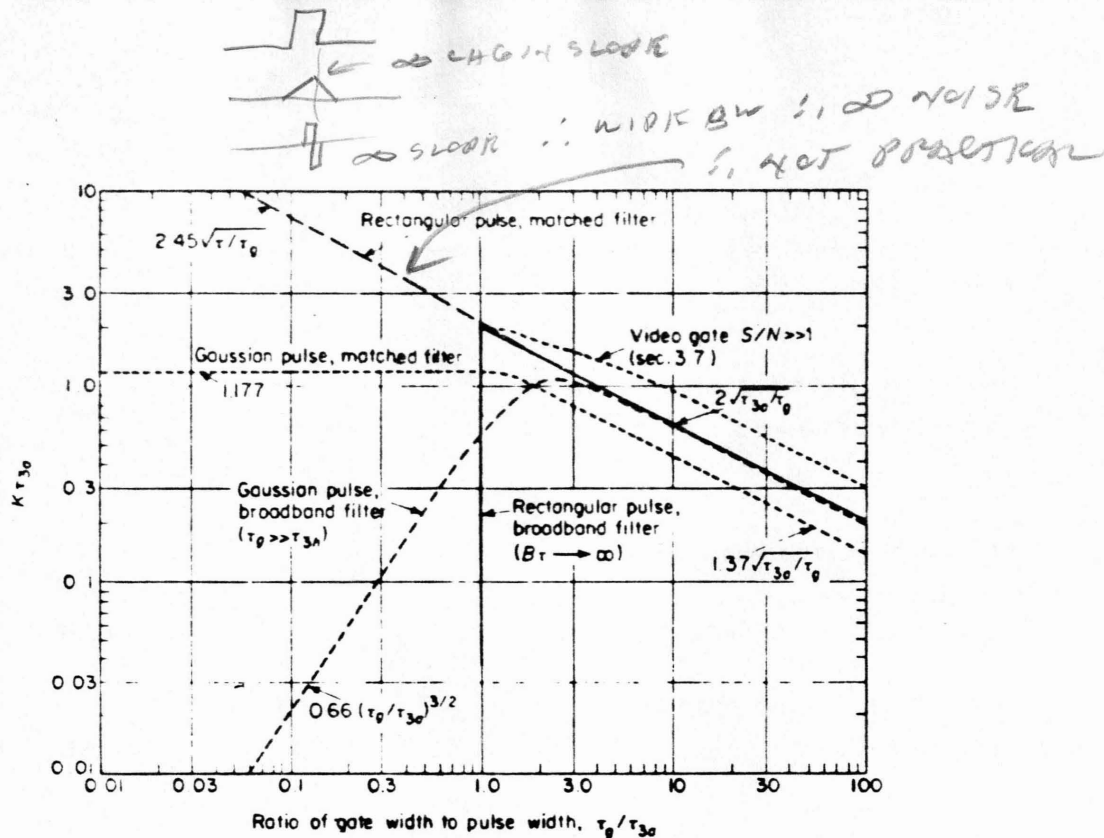
ENERGY RATIO = 100

$$\therefore S/N = 50, n = 1$$

$$S/N = 1, n = 50$$

BUT  $S/N = 0.1, n = 500$





$\therefore$  WIDE  $\tau_0 \approx 2\tau_{30}$  FOR BEST RESULTS

Figure 26. Normalized slope for split-gate discriminator [ 5 ].

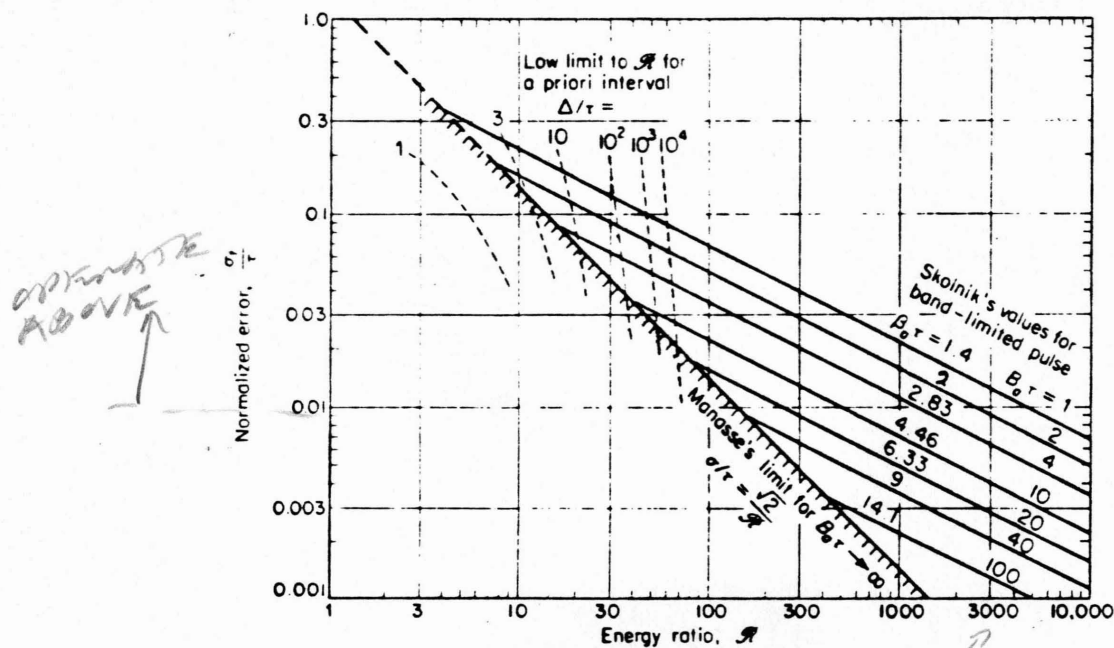


Figure 27. Measurement accuracy vs. energy ratio for rectangular pulse [ 5 ].

BUT INCREASING NOISE OBSCURES.

GLINT:

$$\sigma_H = 0.35 L_x / R$$

CROSS RANGE RXTHT OF TARGET

← RANGE

$$\sigma_r = 0.35 L_r$$

← RANGE LENGTH

$$\sigma_f = 0.35 (2 L_x \omega_a / \lambda) \text{ Hz}$$

## SCINTILLATION IN SEQUENTIAL MEASUREMENT SYSTEMS (INCLUDING FREQUENCY SCANNING)

Table VII. Target noise components, including Doppler error for target rotation rate  $\omega_a$ .

Class of error	Bias components	Noise components
Radar-dependent tracking errors	Boresight axis setting and drift Torque caused by wind and gravity Servo unbalance and drift	Thermal noise Multipath Torque caused by wind gusts Servo noise Deflection of antenna caused by acceleration
Radar-dependent translation errors	Pedestal leveling Azimuth alignment Orthogonality of axes Pedestal flexure caused by gravity force Pedestal flexure caused by solar heating	Bearing wobble Data gear nonlinearity and backlash Data takeoff nonlinearity and granularity Pedestal deflection caused by acceleration
Target-dependent tracking errors	Dynamic lag	Glint Dynamic lag variation Scintillation or beacon modulation
Propagation errors	Average refraction of troposphere Average refraction of ionosphere	Irregularities in refraction of troposphere Irregularities in refraction of ionosphere
Apparent or instrumentation errors	Stability of telescope or reference instrument Stability of film base or emulsion Optical parallax	Vibration or jitter in reference instrument Film transport jitter Reading error Granularity error Variation in parallax

Table VIII. Inventory of angle error components for tracking radar [13].

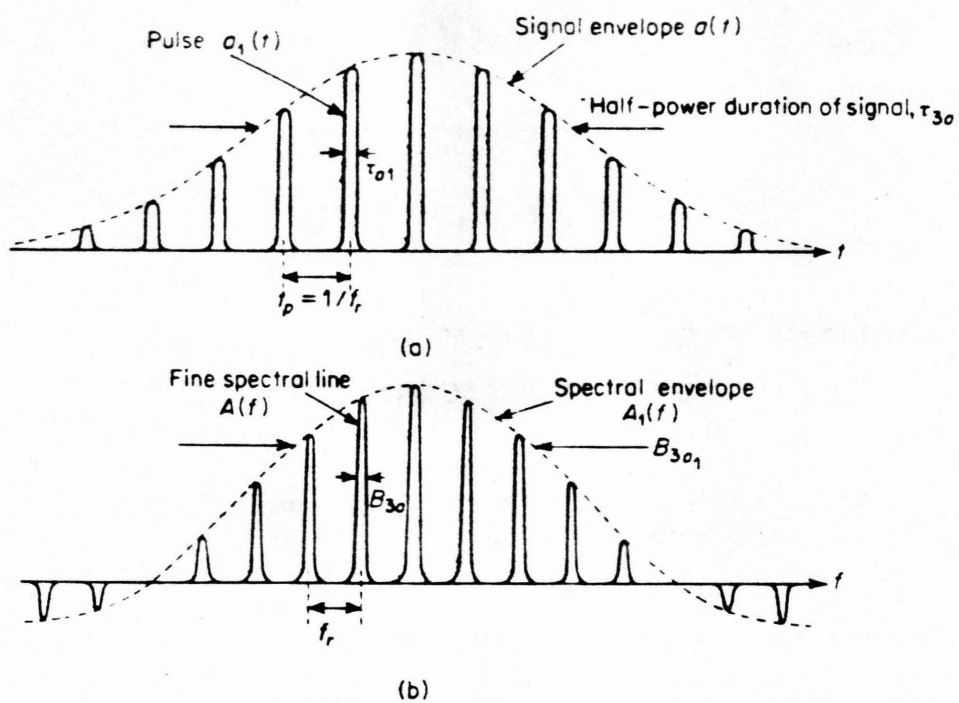


Figure 28. Pulse train waveform and spectrum:  
 (a) waveform, modulated by antenna pattern;  
 (b) spectral envelope and fine line structure [ 5 ] .

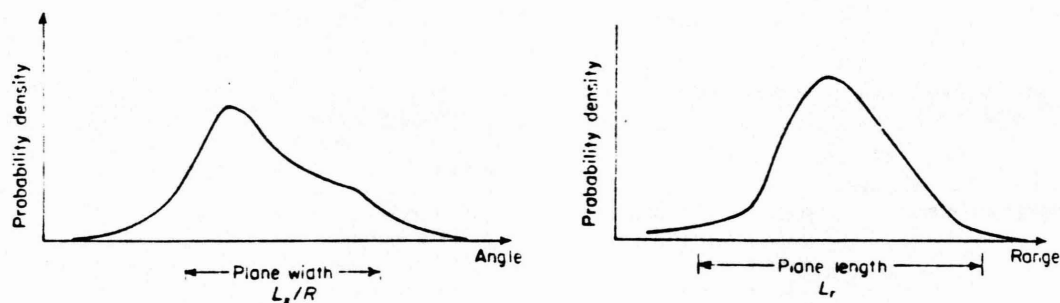


Figure 29. Typical aircraft glint distributions in angle and range.

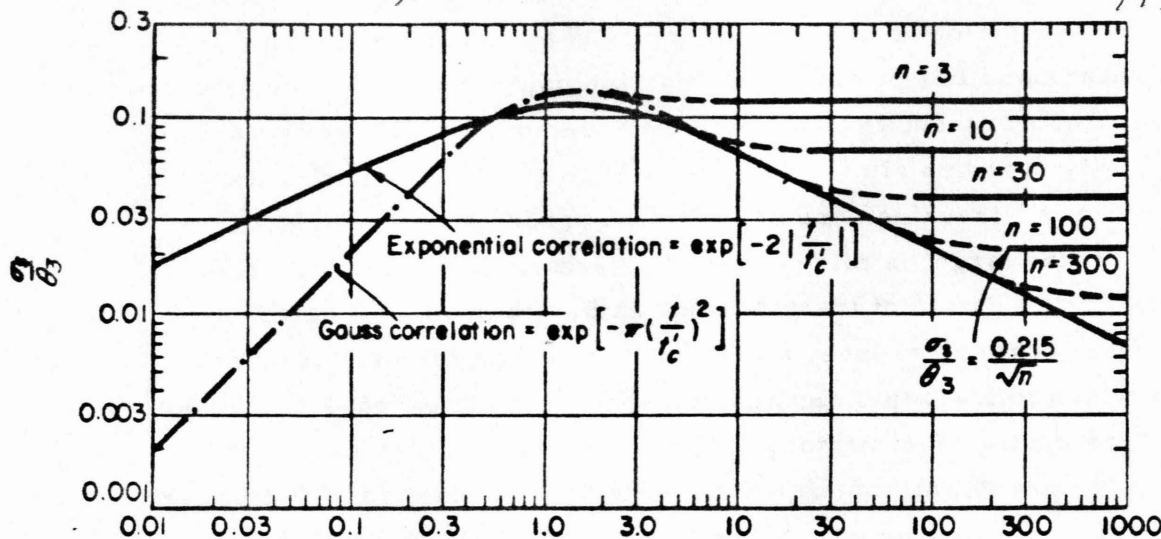
Scintillation error is normally associated with sequential lobing or conical scanning for angular measurement, where target fluctuation components at the lobing rate are interpreted as target deviations. Search radars and linear-scan systems, including frequency scanners, are also affected as shown in Fig. 30. Range and Doppler trackers are normally based on simultaneous processing of two channels, as is monopulse angle tracking, and scintillation errors should be small. However, if the target is offset from the  $\Delta$ -channel null, scintillation can cause a modulation of tracking-loop gain, resulting in a noise error. This error is reduced by fast AGC or other normalization procedures which follow rapid signal fluctuations, at the expense of greater glint errors during brief periods of  $\Sigma$ -channel signal fades (Fig. 31). In principle, perfect normalization on a Rayleigh signal leads to infinite variance of the measurement, but in practice the limited dynamic range and bandwidth of processing leads to truncation of the error distribution.

**4. Lag Errors.** All tracking systems exhibit some lag errors on maneuvering targets, as a result of their smoothing properties. As the noise of individual measurements increases, a longer smoothing time must be used to avoid excessive tracking error (increasing  $n$  in Eq. 9, for instance, and decreasing the tracking loop bandwidth  $B_n$ ). The ability of the tracker to follow target maneuvers is reduced by smoothing, and a common problem in tracker design is to balance the noise and lag errors for the cases of greatest interest. One way of describing servo response is to specify "error constants"  $K_v, K_a, \dots$  for velocity, acceleration, and higher derivatives. The lag error is then expressed as the sum of terms corresponding to each derivative of target motion in the tracked coordinate:

$$\epsilon = \frac{v_t}{K_v} + \frac{a_t}{K_a} + \dots$$

The velocity error coefficient  $K_v$  can be made infinite, after a long settling time to achieve steady-state conditions, but the acceleration error coefficient is closely tied to servo bandwidth:

$$K_a \approx 2.5 B_n^2$$



$$(n_e - 1) = \frac{\theta_3}{\omega t_c} = \frac{n p}{t_c} = \text{Number of independent amplitude-difference samples}$$

Figure 30. Scintillation error in a linear-scanning radar [ 5 ].

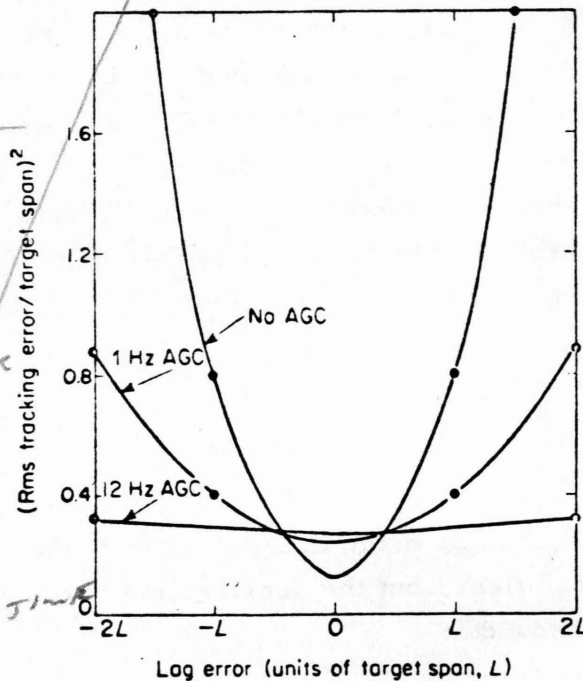
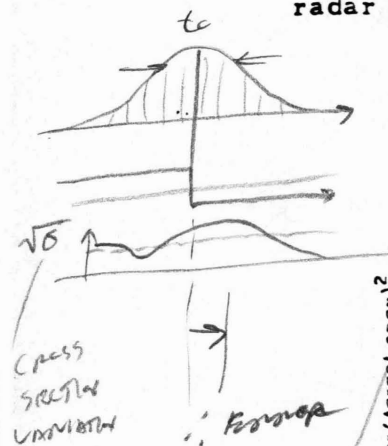


Figure 31. Radar tracking noise for different AGC and widths [ 12 ].

$$\lambda = 0.03 \sim$$

$$V_b = 200 \text{ m/s}$$

$$R = 10 \text{ km}$$

$$L_x = 10 \text{ m}$$

$$0.02 \text{ RAD/SEC}$$

$$t_c = \frac{(0.03)^{1.5}}{2 \cdot (0.02) \cdot (10)} = 0.075 \text{ SEC}$$

TYPICAL SKEWNESS  
 $2^\circ \quad 360^\circ/10$   
 $10 \times \frac{2^\circ}{360} = 0.022 = t_c$   
 $\therefore \frac{0.55}{1095}$   
 $\therefore$  STILL 10% FASTER  
 $\therefore$  SPEED UP SKEW RATE.

Thus, for a given S/N ratio, it is possible to find an optimum bandwidth which minimizes the RSS sum of thermal noise and lag error [ 13, pp. 307-308, 372] .

5. Instrumentation Errors. There are many potential sources of error in practical radar equipment, including polarization sensitivity of the antenna [ 12] , unbalances, drifts and circuit noise in the RF and receiving systems, quantizing noise in A/D converters, and mechanical errors in the antenna-pedestal system. No general analysis of these errors can be given, but each radar must be analyzed individually to arrive at realistic values of instrumental error in each coordinate.

6. Atmospheric Propagation. Most radars operate through the troposphere, which slows and bends the RF rays. For a standard atmosphere and a radar at sea level, Figs. 32 and 33 show the average elevation and range errors. These may be scaled to the actual refractivity at the radar site, if this is measured or calculated as differing from  $N_0 = 313$  units. Paths through nonstandard tropospheric profiles may be calculated by ray tracing to obtain corrections to within one or two per cent of the original bias error, but generally the five to ten per cent accuracy available from the scaling to surface refractivity is adequate.

Random fluctuations in the troposphere cause smaller errors in all radar coordinates, with azimuth error (and elevation error, for tracking antennas) as shown approximately in Fig. 34. Interferometers or arrays extending along the ground and tracking by phase measurement will have greater elevation errors [ 5] .

Especially at the lower radar frequencies, the ionosphere can introduce significant errors. Typical values are shown in Fig. 35, but the seasonal, daily, and random variations are large and only rough estimates are possible. Corrections can be made using measured profiles of electron density, or by comparing the measured data on two or three separated frequencies.

MARINE CORPS

TPN-22 (15 MHz ELEVATION FREQUENCY SEARCH)

HELPS WITH INTEGRATION.

$$\frac{\Delta f}{f_c} = \frac{\text{TIME TO SEARCH}}{\text{CHIRP BANDWIDTH}} = \frac{10 \text{ MHz}}{15 \text{ MHz}} \therefore 0.67 \therefore \text{STILL 10\% BANDWIDTH}$$

$$f_c = \frac{c}{2Lp} = \frac{300 \text{ m/msec}}{2(10)} = 15 \text{ MHz}$$

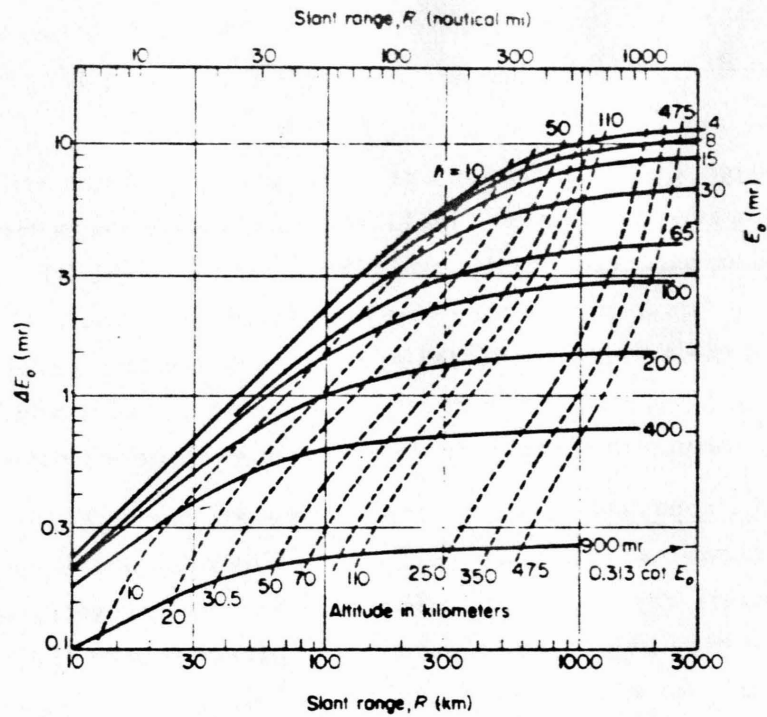


Figure 32. Elevation bias error in standard (exponential) atmosphere [ 13 ].

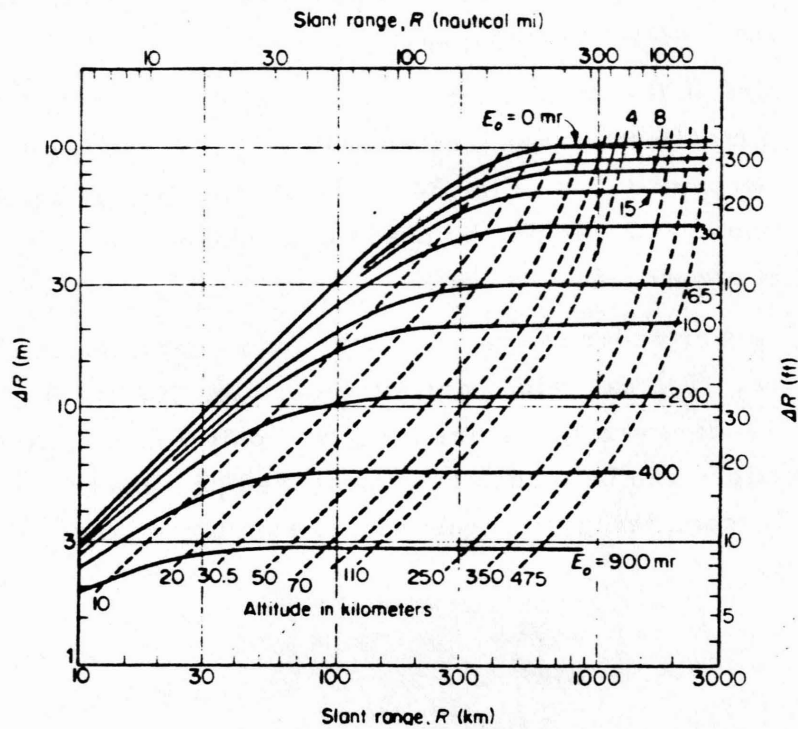


Figure 33. Range bias error in standard (exponential) atmosphere [ 13 ].



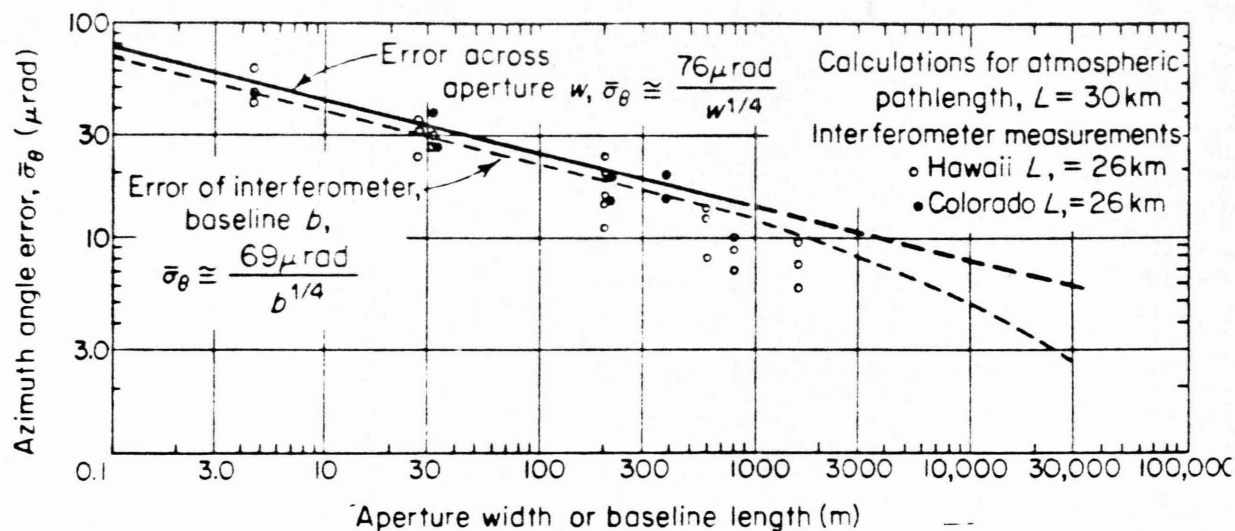


Figure 34. Tropospheric fluctuation error vs. aperture width or baseline length in average atmosphere [ 5 ] .

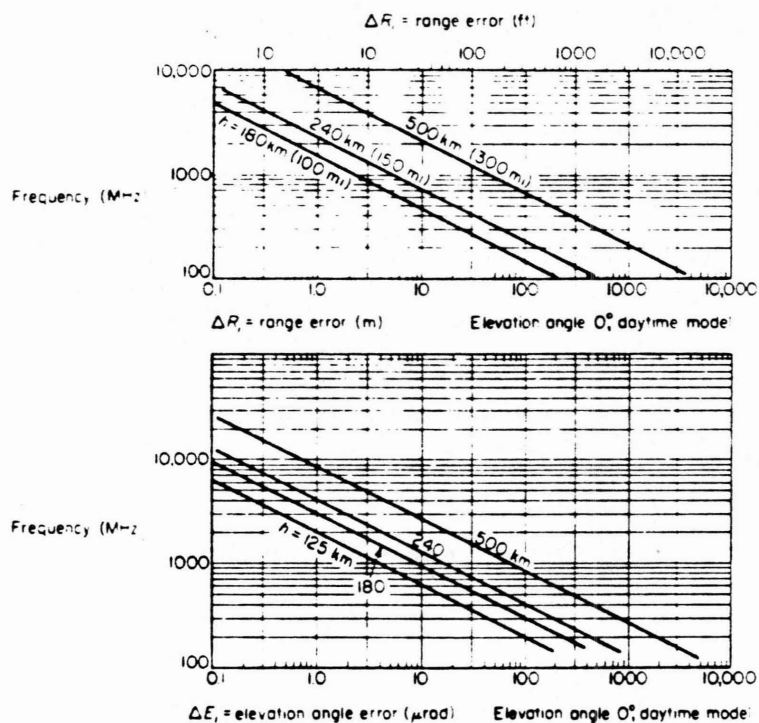


Figure 35. Typical ionospheric errors in range and elevation, vs. radar frequency [ 13 ] .

## E. EXAMPLE OF SYSTEM ERROR ANALYSIS

1. Classification of Errors. Radar errors may be classified by their sources, by spectral characteristics, and by their amplitude distributions. In a conventional tracker, for example, the sources can be divided between radar imperfections which cause the tracking axis to deviate from the target, those which cause the angles of this axis to be incorrectly translated into the chosen coordinate system, target-dependent deviations of the tracking axis from the center of gravity, propagation errors, and apparent errors which are in fact attributable to reference instrumentation (see Table VIII). Each of these may further be divided into bias and noise components, or more finely into true bias (zero frequency), apparent bias (very low frequency, but changing from one test to the next), low frequency (relative to servo bandwidth), cyclic, and white noise (see Fig. 36). Individual components within these classifications may be normally distributed, uniformly distributed over some interval, or sinusoidal.

2. Combination of Errors. Because the many sources tend to produce independently varying errors, a summation of variances (RSS addition) is usually valid. For a given target type, range, elevation angle, and environment, the several components are RSS added in each coordinate, and their variation with range is then used to prepare a plot similar to Fig. 37. Families of such curves for different elevation angles and target types may be prepared. A description of errors in the original AN/FPS-16 is given in the reprinted IRE paper, Appendix A. More detailed analyses will be found in [ 5 ] and [ 13 ], indicating the different levels of complexity with which radar errors can be analyzed and described.

- THERMAL NOISE  $n = f r t_0$
- MULTIPATH
- LAG
- GUNT
- SCINTILLATION
- CLUTTER  $n_c \leq f r t_0 = \left(1 + \frac{t_0}{t_c}\right)$
- PROPAGATION
- MECHANICAL

50

Summing Formulas  $G = \sqrt{G_1^2 + G_2^2 + G_3^2}$   
ROOT MEAN SQUARE  
ASSUMES UNCORRELATED  
BIAS FORMS → ADD LINEARLY OR CALIBRATE OUT

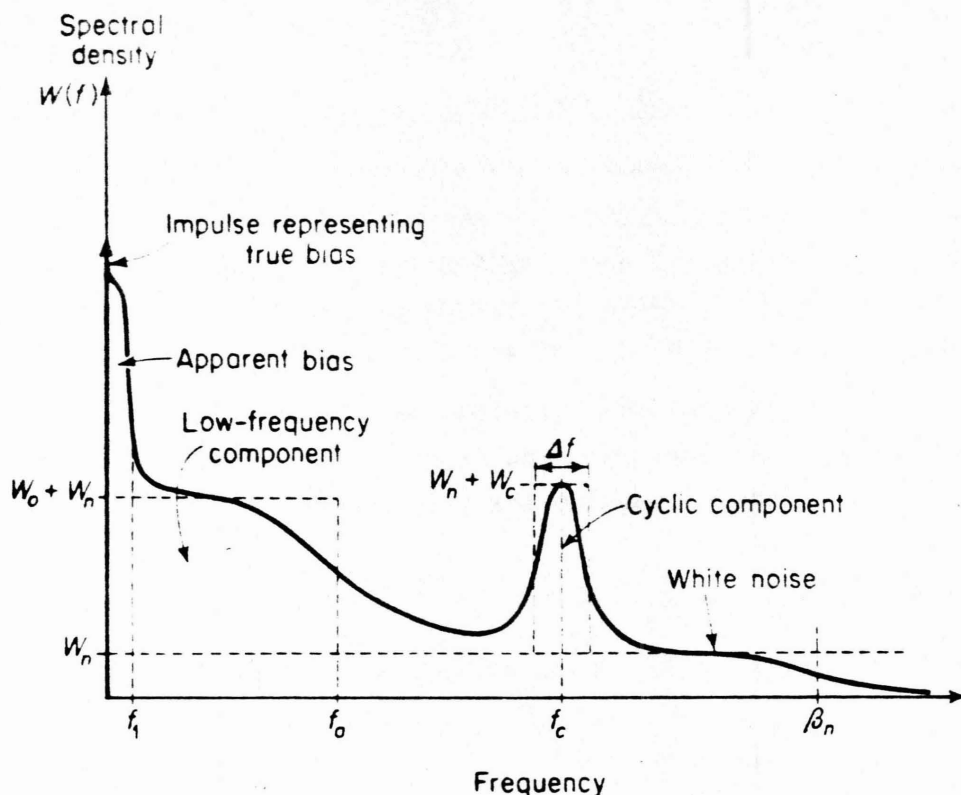


Figure 36. Typical angle-tracking error spectrum [ 13 ] .

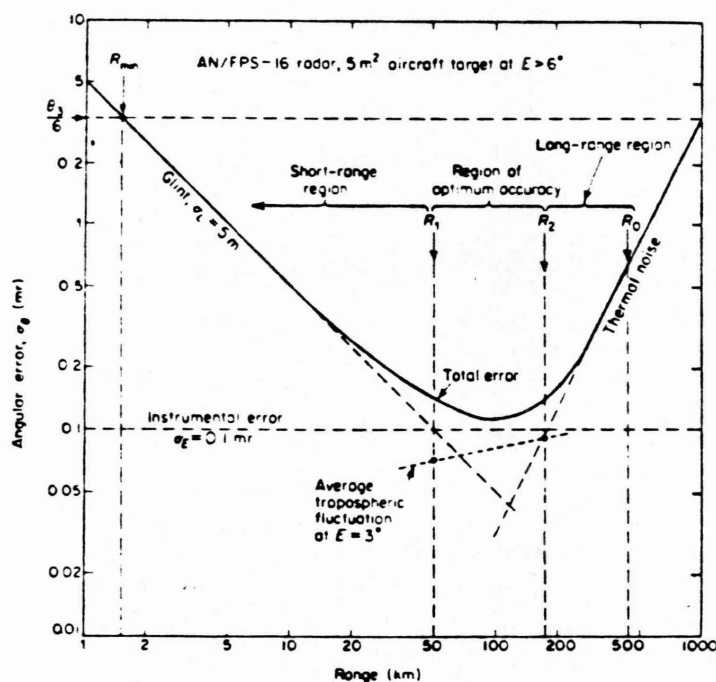


Figure 37. Monopulse tracking error vs. range [ 5 ] .

→ PRACTICAL PRECISION  $\sigma_r = 1 \text{ m}$   
 BUT INSTRUMENTATION  $\sigma_\theta = 0.1 \text{ mr}$  AT LEAST 67% OF TIME,  
 EXTENSIVE CALIBRATION AND UPKEEP.  $\sigma_\theta \text{ TACTICAL} \approx 0.5 - 1 \text{ mr}$   
 TO JUST ILLUMINATED.  $\sigma_\theta \text{ MISSILE HOMING} \approx 4 - 5 \text{ mr}$

SHIPPING AND AIRCRAFT WORK DIFFICULT

## F. TYPICAL LOW-ALTITUDE TRACKING PROBLEM

The following problem illustrates the effects of relatively smooth and rough sea conditions on a shipboard tracking radar with and without special anti-multipath features. For the ranges given, the flat-earth assumption is adequate for use in error estimation, as can be seen by reference to Figs. 4 and 5 with  $S = 0.09$  and  $T = 0.32$ .

Calculations are made for one target location at an elevation angle of approximately one-half beamwidth, and error components are described by frequency to indicate whether they are subject to reduction by filtering.

### 1. Radar-Target Geometry

Shipboard radar:  $\lambda = 0.03$  m (X-band)  
 $D = 1$  m ( $\theta_e = \theta_a = 35$  mr or 2 deg)  
 $h_r = 10$  m  
Aircraft target:  $R = 5$  km  
 $h_t = 100$  m  
 $v_t = 300$  m/s inbound  
Sea state: State 2 (slight sea,  $\sigma_h = 0.15$  m,  $\sigma_a = 0.05$ ,  
relatively smooth surface at X-band); or  
State 4-5 (rough sea,  $\sigma_h = 0.5$  m,  $\sigma_a = 0.05$ ,  
relatively rough surface at X-band)

Calculated angles (assume flat earth):

$$\text{Target elevation, } \theta_t = \frac{h_t - h_r}{R} = 0.018 \text{ or } 18 \text{ mr}$$

$$\text{Grazing angle, } \psi_o = \frac{h_t + h_r}{R} = 0.022 \text{ or } 22 \text{ mr}$$

$$\text{Reflection lobe width, } \lambda / 2h_r = 0.0015 \text{ or } 1.5 \text{ mr}$$

Other geometrical factors:

$$\text{Range to specular reflection point, } x_o = \frac{h_r}{\tan \psi_s} = 455 \text{ m}$$

$$\text{Delay of specular reflection, } \delta_o = \frac{2h_r h_t}{R} = 0.4 \text{ m}$$

$$\text{Normalized elevation angle, } \theta_t / \theta_r = 0.52$$

$$\text{Effective elevation rate, } \frac{\dot{\theta}_t + \dot{\psi}_o}{2} = \frac{h_t v_t}{R^2} = 0.0012 \text{ rad/s}$$

## 2. Reflection Coefficients

Fresnel reflection coefficient,  $\rho_o = 0.7$  (Fig. 6)

(for specular, midrange and foreground components)

Fresnel coefficient at  $\psi_o/2$ ,  $\rho_o = 0.83$

(for horizon component)

Specular scattering factor,  $\rho_s = 0.37$  (SS 2,  $\sigma_h/\lambda = 5$ )  
(Fig. 7)  $= 0$  (SS 4,  $\sigma_h/\lambda = 16$ )

Horizon diffuse component,  $\rho_{dh} = 0.11$  (SS 2)  
(Fig. 12a)  $\rho_{dh} = 0.19$  (SS 4)

Midrange component,  $\rho_{dm} = 0.29$  (SS 2)  
(Fig. 13)  $\rho_{dm} = 0.39$  (SS 4)

Foreground component,  $\rho_{df} = 0.29$  (SS 2)  
(Fig. 13)  $\rho_{df} = 0.39$  (SS 4)

The angular relationships of these components to the monopulse antenna patterns are shown in Fig. 38.

## 3. Computation of Error

Specular error:

$$\frac{\sigma_{As}}{\theta_e \rho_o \rho_s} = 0.2 \text{ (Fig. 16)}$$

For SS 2:  $\sigma_{As} = 0.2 \times 35 \times 0.7 \times 0.37 = 1.8 \text{ mr}$

For SS 4:  $\sigma_{As} = 0$

Horizon component:

$$\frac{\sigma_{Ah}}{\theta_e \rho_o \rho_{dh}} = 0.25 \text{ (Fig. 17a)}$$

For SS 2:  $\sigma_{Ah} = 0.25 \times 35 \times 0.83 \times 0.11 = 0.8 \text{ mr}$

For SS 4:  $\sigma_{Ah} = 0.25 \times 35 \times 0.83 \times 0.19 = 1.4 \text{ mr}$

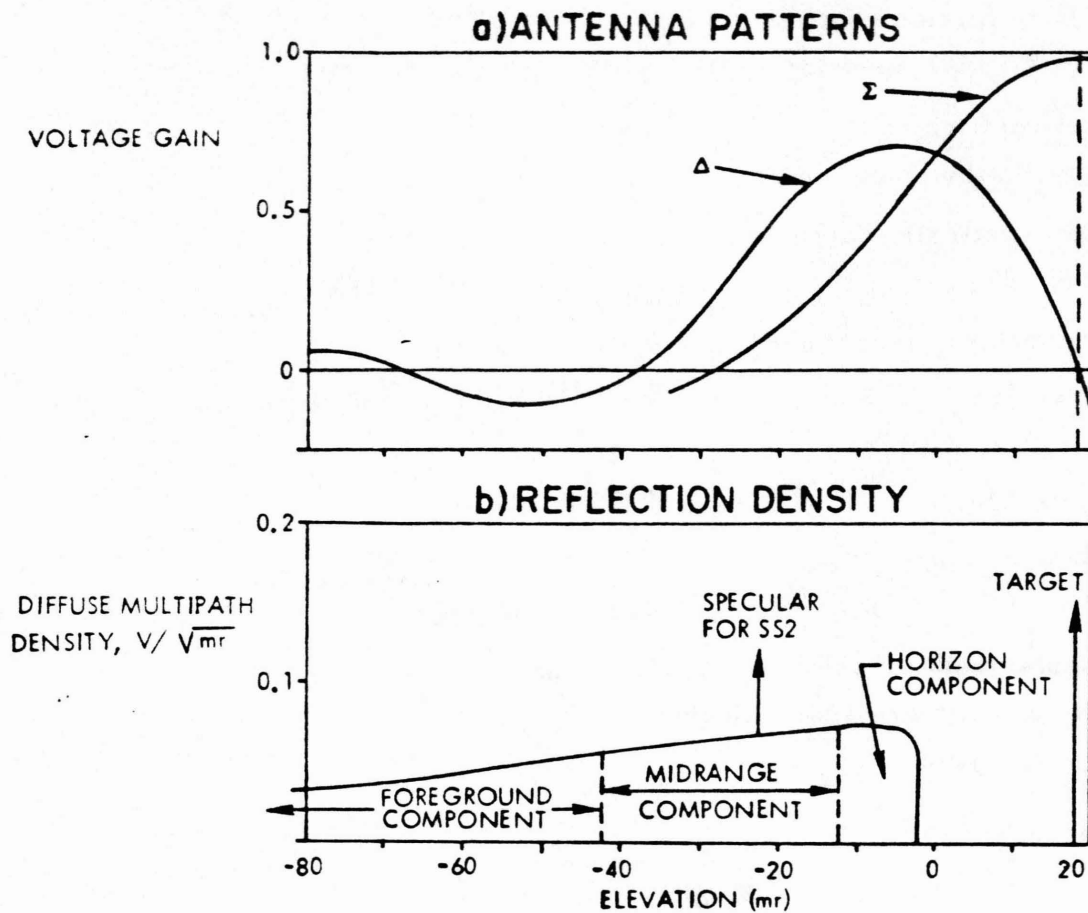


Figure 38. Relationship of antenna patterns to multipath reflection density for typical problem.

Midrange component:

$$\frac{\sigma_{\theta m}}{\theta_e \rho_o \rho_{dm}} = 0.185 \text{ (Fig. 18)}$$

For SS 2:

$$\sigma_{\theta m} = 0.185 \times .29 \times 35 \times 0.7 = 1.31 \text{ mr}$$

For SS 4:

$$\sigma_{\theta m} = 0.185 \times 0.39 \times 35 \times 0.7 = 1.77 \text{ mr}$$

Foreground component:

$$\frac{\sigma_{\theta f}}{\theta_e \rho_o \rho_{df}} = 0.1 \text{ (Fig. 18)}$$

For SS 2:

$$\sigma_{\theta f} = 0.1 \times 0.29 \times 35 \times 0.7 = 0.71 \text{ mr}$$

For SS 4:

$$\sigma_{\theta f} = 0.1 \times 0.39 \times 35 \times 0.7 = 0.96 \text{ mr}$$

Total multipath error:

$$\sigma_{\theta} = \sqrt{\sigma_{\theta s}^2 + \sigma_{\theta h}^2 + \sigma_{\theta m}^2 + \sigma_{\theta f}^2}$$

For SS 2:

$$\sigma_{\theta} = 2.47 \text{ mr or } 0.071 \theta_e$$

For SS 4:

$$\sigma_{\theta} = 2.45 \text{ mr or } 0.070 \theta_e$$

#### 4. Frequency Characteristics of Error

Specular component:

$$f = \left( \frac{\dot{\theta}_t + \dot{\psi}_o}{2} \right) \frac{2h_r}{\lambda}$$

$$= 0.0012 \frac{20}{0.03} = 0.8 \text{ Hz}$$

Horizon component:

$$f = \frac{v}{\lambda} (\cos \theta_t - \cos \psi_2)$$

(900 < x < 4000)

$$\psi_2 = \tan^{-1} \frac{h_t}{5000-x}$$

For x = 900,

$$f = \frac{300}{0.03} (\cos .018 - \cos 0.024)$$

$$= 10,000 (.99984 - .9997)$$

For x = 4000,

$$f = 1.35 \text{ Hz } \left\{ \begin{array}{l} \text{Largely beyond} \\ \text{servo passband} \end{array} \right.$$

$$f = 48 \text{ Hz}$$



Midrange component:

$$(240 < x < 900)$$

For  $x = 240$ ,  $f = 0.6$  Hz } Within servo  
 For  $x = 900$ ,  $f = 1.35$  Hz } passband

Foreground component:

$$(40 < x < 240)$$

For  $x = 40$ ,  $f = 0.4$  Hz } Within servo  
 For  $x = 240$ ,  $f = 0.6$  Hz } passband

Total error at output of 1.5-Hz filter:

For SS2:  $\sigma_{\theta} \approx 2.3$  mr or  $0.069 \theta_e$

For SS4:  $\sigma_{\theta} \approx 2.0$  mr or  $0.057 \theta_e$

## 5. Applicability of Anti-Multipath Techniques

### (a) Off-axis monopulse:

Specular component:

$$\frac{\sigma_{\theta s}}{\theta_e \rho_o \rho_s} \approx 0.1 \text{ (Fig. 21)}$$

For SS2:  $\sigma_{\theta s} = 0.1 \times 35 \times 0.7 \times 0.37 = 0.91$

For SS4:  $\sigma_{\theta s} = 0$

Horizon component:

$$\frac{\sigma_{\theta h}}{\theta_e \rho_o \rho_{dh}} \approx 0.25 \text{ (Fig. 21)}$$

For SS2:  $\sigma_{\theta h} = 0.25 \times 35 \times 0.83 \times 0.11 = 0.80$  mr

For SS4:  $\sigma_{\theta h} = 0.25 \times 35 \times 0.83 \times 0.19 = 1.38$  mr

Midrange component:

$$\frac{\sigma_{\theta h}}{\theta_e \rho_o \rho_{dm}} = 0.1 \text{ (Fig. 21)}$$

(use curve for  $\sigma_{\theta s}$   
 with  $\rho_{dm}$  replacing  $\rho_s$ )

For SS2:  $\sigma_{\theta m} = 0.1 \times 35 \times 0.83 \times 0.29 = 0.84$  mr

For SS4:  $\sigma_{\theta m} = 0.1 \times 35 \times 0.83 \times 0.39 = 1.13$  mr

Foreground component: negligible

Total multipath error:

For SS 2:  $\sigma_{\theta} = 1.47 \text{ mr or } 0.042 \theta_e$

For SS 4:  $\sigma_{\theta} = 1.78 \text{ mr or } 0.051 \theta_e$

(or about 0.6 to 0.7 times the previous error)

Total multipath error at output of 1.5-Hz filter:

For SS 2:	$\sigma_{\theta} \approx 1.23 \text{ mr or } 0.035 \theta_e$	} Results are 1.9 to 1.5 better than tracking monopulse
For SS 4:	$\sigma_{\theta} \approx 1.38 \text{ mr or } 0.039 \theta_e$	

(b) Double-null tracker:

Specular component: negligible

Horizon component:  
(medium surface)  $\frac{\sigma_{\theta h}}{\theta_e \rho_o \rho_{dh}} \approx 0.15 \text{ (Fig. 22a)}$

For SS 2:  $\sigma_{\theta h} = 0.15 \times 35 \times 0.83 \times 0.11 = 0.48 \text{ mr}$

For SS 4:  $\sigma_{\theta h} = 0.15 \times 35 \times 0.83 \times 0.19 = 0.83 \text{ mr}$

Midrange component:  $\frac{\sigma_{\theta m}}{\theta_e \rho_o \rho_{dm}} \approx 0.09 \text{ (Fig. 22b)}$

For SS 2:  $\sigma_{\theta h} = 0.09 \times 35 \times 0.7 \times 0.29 = 0.64 \text{ mr}$

For SS 4:  $\sigma_{\theta h} = 0.09 \times 35 \times 0.7 \times 0.39 = 0.86 \text{ mr}$

Foreground component:  $\frac{\sigma_{\theta f}}{\theta_e \rho_o \rho_{df}} \approx 0.055 \text{ (Fig. 22b)}$

For SS 2:  $\sigma_{\theta f} = 0.055 \times 35 \times 0.7 \times 0.29 = 0.39 \text{ mr}$

For SS 4:  $\sigma_{\theta f} = 0.055 \times 35 \times 0.7 \times 0.39 = 0.53 \text{ mr}$

Total multipath error:

For SS 2:  $\sigma_{\theta} = 0.89 \text{ mr} = 0.03 \theta_e$

For SS 4:  $\sigma_{\theta} = 1.31 \text{ mr} = 0.04 \theta_e$

Error at output of 1.5-Hz filter:

For SS 2:  $\sigma_{\theta} \approx 0.75 \text{ mr} = 0.02 \theta_e$

For SS 4:  $\sigma_{\theta} \approx 1.01 \text{ mr} = 0.03 \theta_e$

(results are factor of 1.7 to 1.3 better than off-axis monopulse)

(c) Asymmetrical-beam Estimator:

Specular component: negligible

Horizon component:  $\frac{\sigma_{\theta h}}{\theta_e \rho_o \rho_{dh}} \approx 0.6 \text{ (Fig. 23a)}$

For SS 2:  $\sigma_{\theta h} = 0.6 \times 35 \times 0.83 \times 0.11 = 1.92 \text{ mr}$

For SS 4:  $\sigma_{\theta h} = 0.6 \times 35 \times 0.83 \times 0.19 = 3.31 \text{ mr}$

Midrange component:  $\frac{\sigma_{\theta m}}{\theta_e \rho_o \rho_{dm}} \approx 0.35 \text{ (Fig. 23b)}$

For SS 2:  $\sigma_{\theta h} = 0.35 \times 35 \times 0.7 \times 0.29 = 2.5 \text{ m}$

For SS 4:  $\sigma_{\theta h} = 0.35 \times 35 \times 0.7 \times 0.39 = 3.3 \text{ mr}$

Foreground component:  $\frac{\sigma_{\theta f}}{\theta_e \rho_o \rho_{df}} \approx 0.2 \text{ (Fig. 23b)}$

For SS 2:  $\sigma_{\theta h} = 0.2 \times 35 \times 0.7 \times 0.29 = 1.4 \text{ mr}$

For SS 4:  $\sigma_{\theta h} = 0.2 \times 35 \times 0.7 \times 0.39 = 1.9 \text{ mr}$

Total multipath error:

For SS 2:  $\sigma_{\theta} = 3.4 \text{ mr or } 0.1 \theta_e$

For SS 4:  $\sigma_{\theta} = 5.0 \text{ mr or } 0.14 \theta_e$

Error at output of 1.5-Hz filter:

For SS 2:  $\sigma_{\theta} = 2.9 \text{ mr or } 0.08 \theta_e$

For SS 4:  $\sigma_{\theta} = 3.8 \text{ mr or } 0.11 \theta_e$

(Results are worse than conventional monopulse tracker by factor of 1.3 to 1.9)

(d) Narrower beam at  $K_u$ -band:

$$\theta_e = 1.2 \lambda / D = 1.2 \times .018 = 0.022 \text{ rad or } 22 \text{ mr}$$

$$\text{Normalized velocity } v_t / \lambda = 16700$$

$$\sigma_h / \lambda = 8 \text{ (SS 2) or } 28 \text{ (SS 4)}$$

$$\text{Normalized elevation: } \theta_t / \theta_e = 0.82$$

$$\rho_s = 0 \text{ for either sea state}$$

$$\rho_{dh} = 0.13 \text{ (SS 2) or } 0.33 \text{ (SS 4)}$$

$$\rho_{dm} = \rho_{df} = 0.39 \text{ for either sea state}$$

$$\text{Specular error: } \sigma_{\theta s} = 0$$

$$\text{Horizon component: } \frac{\sigma_{\theta h}}{\theta_e \rho_o \rho_{dh}} = 0.24$$

$$\text{For SS 2: } \sigma_{\theta h} = 0.24 \times 22 \times 0.83 \times 0.13 = 0.57 \text{ mr}$$

$$\text{For SS 4: } \sigma_{\theta h} = 0.24 \times 22 \times 0.83 \times 0.33 = 1.45 \text{ mr}$$

(Error frequencies extend from 2.25 to 80 Hz)

$$\text{Midrange component: } \frac{\sigma_{\theta m}}{\theta_e \rho_o \rho_{dm}} = 0.06 \text{ (Fig. 18)}$$

$$\text{For either sea state: } \sigma_{\theta m} = 0.06 \times 22 \times 0.7 \times 0.39 = 0.36 \text{ mr}$$

$$\text{Foreground component: } \frac{\sigma_{\theta f}}{\theta_e \rho_o \rho_{dm}} \approx 0 \text{ (Fig. 18)}$$

Total multipath error:

$$\begin{array}{ll} \text{For SS 2: } & \sigma_{\theta} = 0.67 \text{ mr} \\ \text{For SS 4: } & \sigma_{\theta} = 1.49 \text{ mr} \end{array} \left. \begin{array}{l} \\ \\ \end{array} \right\} \begin{array}{l} \text{essentially all} \\ \text{horizon component} \end{array}$$

Total error is 0.2 to 0.6 times that at X-band, and is largely beyond the servo passband for  $v_t = 300 \text{ m/s}$ .

## 6. Errors from Sea Clutter

Area of resolution cell:  $A_c = \frac{R \theta_a}{1.33} \frac{\tau_c}{2}$   
 (assume  $\tau = 0.5 \mu\text{sec}$ )  

$$= \frac{5000 \times 0.035}{1.33} \times 75 \approx 10^4 \text{ m}^2$$

Antenna  $\Delta$  gain at surface: 0.7 relative volts

Clutter reflectivity: for grazing angle  $\approx 2 \text{ mr} = 0.1 \text{ deg}$ ,

For SS2:  $\sigma^0 \approx -50 \text{ dB}$

For SS4:  $\sigma^0 \approx -40 \text{ dB}$

Clutter cross section:

For SS2:  $\sigma_c \approx 0.1 \text{ m}^2$

For SS4:  $\sigma_c \approx 1 \text{ m}^2$

Signal-to-clutter ratio: for  $\sigma_t = 2 \text{ m}^2$

For SS2:  $(S/C)_\Delta = 40 \text{ or } +16 \text{ dB}$  } Without

For SS4:  $(S/C)_\Delta = 4 \text{ or } +6 \text{ dB}$  } MTI

Clutter error:  $\sigma_\theta = \frac{\theta_e}{k_m \sqrt{2(S/C)_\Delta n_e}}$  (for  $S/C \gg 1$ )

For SS2:  $\sigma_\theta = \frac{2.0}{\sqrt{n_e}}$  } Without

For SS4:  $\sigma_\theta = \frac{6.3}{\sqrt{n_e}}$  } MTI

For SS2, with  $S/C \gg 1$ , the error varies from 2 mr (when the aircraft passes through an ambiguous velocity for which  $n_e \approx 1$ ) to a negligible level at other velocities. For SS4, however, the condition  $S/C \gg 1$  is not met and a cross-product term [14] appears which is correlated over the time required for the target to move through a resolution cell:

$$t_c = \frac{\pi c}{2} \times \frac{1}{v_t} = \frac{75}{300} = 0.25 \text{ sec}$$

$$n_e = \frac{1}{t_c \theta_n} = \frac{1}{0.25 \times 2} = 2$$

$$\sigma_\theta = \frac{\theta_3}{k_m (S/C) \sqrt{2 n_e}} = \frac{35}{1.96 \times 4 \times \sqrt{4}} = 2.2 \text{ mr}$$

Hence MTI is needed for good tracking within one beamwidth over a rough sea.

#### 7. Azimuth Error

$$\frac{\sigma_A}{\theta_{da}} = \frac{\rho_o \rho_v \rho_d}{2 \sqrt{2 G_{sr}}} \quad (\text{Table II})$$

$$\theta_{da} = 2 \sigma_\alpha (\theta_t + \theta_r) = 0.1 (18 + 8) = 2.6 \text{ mr for } \rho_{dh}$$

$$\overline{G}_{sr} = 1/\Sigma^2 = 1/.45^2 = 4.9 \text{ for } \theta_t + \theta_r = 26 \text{ mr} = 0.74 \theta_e$$

For SS 2:	$\sigma_A = \frac{2.6 \times 0.83 \times 0.11}{2 \sqrt{2 \times 4.9}} = 0.038 \text{ mr}$	} Both negligible relative to other errors
For SS 4:	$\sigma_A = 0.065 \text{ mr}$	

References, Low-Altitude Tracking and Radar Accuracy

- [ 1 ] D. K. Barton, Radars, Vol. 4: Radar Resolution and Multipath Effects, Artech House, 1975.
- [ 2 ] D. E. Kerr, ed., Propagation of Short Radio Waves, Vol. 13 of MIT Radiation Laboratory Series, McGraw-Hill, 1951.
- [ 3 ] L. V. Blake, "Prediction of Radar Range," Chap. 2 in Radar Handbook (M. I. Skolnik, ed.), McGraw-Hill, 1970 (graphs used in Blake's original-NRL reports are also reproduced in Radars, Vol. 2: The Radar Equation, Artech House, 1974).
- [ 4 ] P. Beckmann and A. Spizzichino, The Scattering of EM Waves from Rough Surfaces, Pergamon Press, 1963.
- [ 5 ] D. K. Barton and H. R. Ward, Handbook of Radar Measurement, Prentice-Hall, 1969.
- [ 6 ] D. K. Barton, "Low-Angle Radar Tracking," Proc. IEEE 62, No. 6, June 1974, pp. 687-704 (reprinted in [ 1 ]).
- [ 6a ] D. K. Barton, "Radar Multipath Theory and Experimental Data," IEE Radar-77, London, England, Oct. 25-28, 1977, pp. 308-312.
- [ 7 ] F. H. Thompson and F. A. Kittredge, "A Study of the Feasibility of Using 35 GHz and/or 94 GHz as a Means of Improving Low Angle Tracking Capability," NRL Rpt. 2249, May 1971 (reprinted in [ 1 ]).
- [ 8 ] G. M. Kirkpatrick, "Final Engineering Report on Angular Accuracy Improvement," General Electric Co., 1 August 1952 (reprinted in Radars, Vol. 1: Monopulse Radar, Artech House, 1974).
- [ 9 ] W. D. White, "Low-Angle Radar Tracking in the Presence of Multipath," IEEE Trans. AES-10, No. 6, Nov. 1974, pp. 835-52 (reprinted in [ 1 ]).
- [ 10 ] P. R. Dax, "Accurate Tracking of Low Elevation Targets over the Sea with Monopulse Radar," IEE Conf. Publ. No. 105, Radar-Present and Future, London, Oct. 1973 (reprinted in [ 1 ]).



References. Low-Altitude Tracking and Radar Accuracy

- [ 11] S. M. Sherman, "The Use of Complex Indicated Angles in Monopulse Radar to Locate Unresolved Targets," Proc. NEC 22, 1966, pp. 243-48 (reprinted in Radars, Vol. 1: Monopulse Radar, Artech House, 1974.)
- [ 12] J. H. Dunn and D. D. Howard, "Target Noise," Chap. 28 in Radar Handbook (M. I. Skolnik, ed.), McGraw-Hill, 1970.
- [ 13] D. K. Barton, Radar System Analysis, Prentice-Hall, 1964.
- [ 14] D. K. Barton, The Radar Equation, Vol. 2 in Radars, Artech House, 1974 (see p. 229).
- [ 15] R. C. Kirby, "Radio Wave Propagation," Secs. 18-63 through 18-111 of Electronics Engineers' Handbook (D. G. Fink, ed.), McGraw-Hill, 1975. See Sec. 18-80 for knife-edge diffraction.

SESSION VIII

PHASED ARRAYS

ROBERT T. HILL

## PHASED ARRAYS

A lecture on how phased arrays work  
and how they are built.

R. T. Hill

A part of a course in  
Radar Systems and Technology  
Continuing Engineering Education Program  
The George Washington University

Revised 4-76  
Orig. 5-75

## I. How Phased Arrays Work

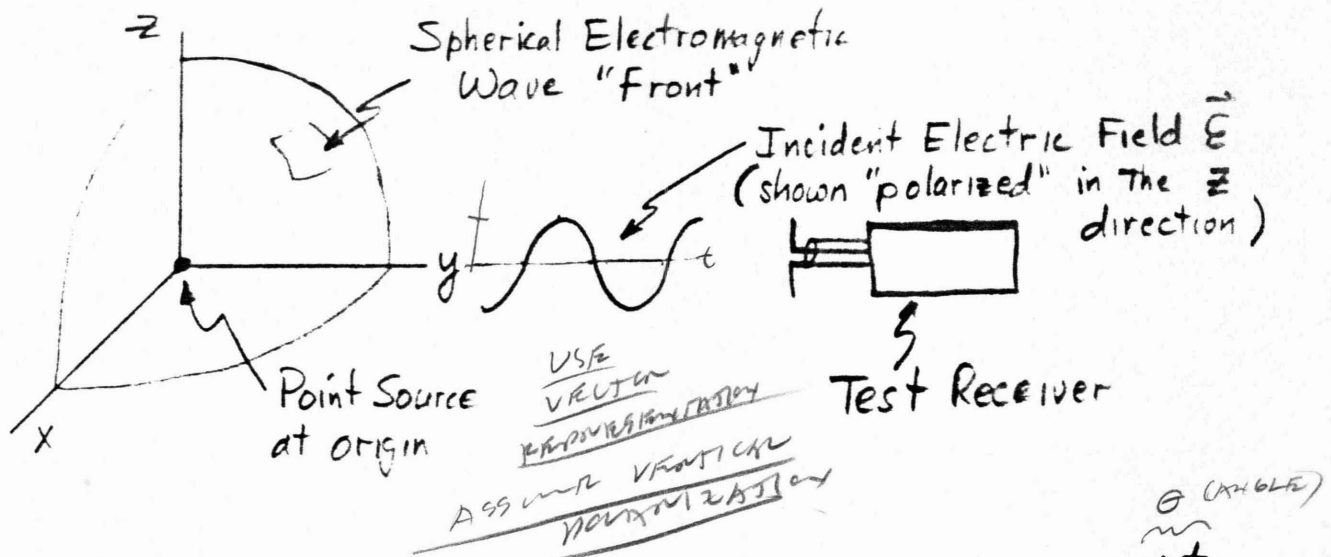
### Introduction

The several paragraphs to follow will take the student, even one who recalls very little of electromagnetic theory, antenna theory or even vector representations of fields, along a course of "synthesizing" a microwave phased array from the most elementary building blocks. The material is accurate, to be sure, but not particularly deep and rigorous. Certain properties of fields are assumed rather than developed, for example - but one who has ever pondered a pebble dropped into a pond (or better two pebbles side-by-side) will have no difficulty understanding phased arrays (or any microwave antenna for that matter) and how patterns are formed and steering is accomplished. We begin with a single radiating element, then a pair, then several that together constitute an "array", and in each case examine what their radiations look like together at points a long way away (the "far field").

### An Element

Consider a source of microwave electromagnetic radiation that is just a point, and assume it radiates in all directions (spherically). Assume that if one had a receiving device sensitive to the electric field (one constituent of the radiating electromagnetic field) and aligned it with that field (say the electric field is vertically "polarized" in the region of the receiver) one would sense a field intensity,  $\vec{E}$  (in, say, volts per meter), that goes through sinusoidal cycles of intensity at the carrier frequency  $f_c = \frac{\omega_c}{2\pi}$  (i. e.,  $\omega_c$  is  $f_c$  in radian measure) and the magnitude of  $\vec{E}$  would decrease in direct linear proportion with the receiver distance from our point source element (power spatial density,

being proportional to the square of  $\vec{E}$ , decreases as the square of the distance). This is illustrated below:

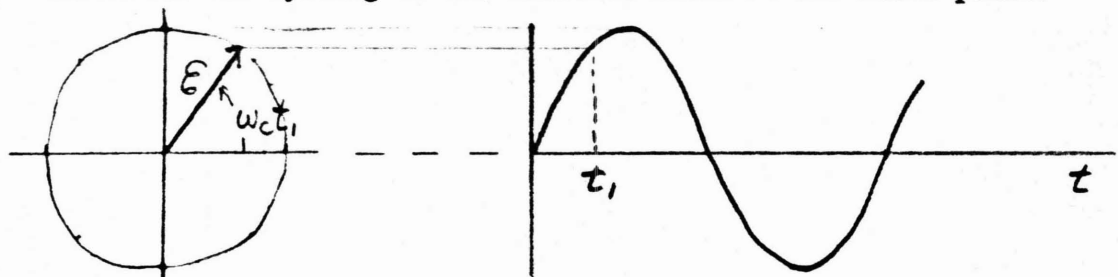


So, at some fixed distance the electric field is  $\vec{E} = E_{\max} e^{j\omega_c t}$  which is a vector  $E_{\max}$  "volts" long rotating in phase at  $\omega_c$  angular rate. For simplicity  $E_{\max}$  will be written  $E$ . The form is that of a simple vector  $\vec{A} = A e^{j\phi}$ :



which in our case has a time varying phase angle:  $\phi = \omega_c t = 2\pi f_c t$ .

$\vec{E}$  describes the cycling of the electric field at our field point:



Vector "generates" the graph to the right

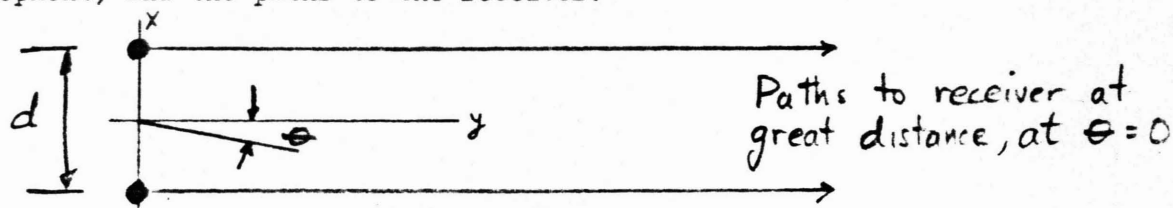
Graph of field intensity as a function of time at our field point

We have established that a radiating element produces a sinusoidally varying electric field that can be sensed from a remote point, the field point. It is further asserted that, with a proper orientation of our

receiving probe, the sensed electric field is invariant with angular location, the magnitude varying only with radial distance.

### Two Elements

Consider that two elements, each radiating like the first, are disposed along the x-axis separated by distance  $d$  straddling the origin. Consider further that our receiver is at such a great distance that the straight-line paths from each radiator to the receiver are essentially parallel. Consider finally that our receiver is located on the y-axis. This figure shows the x-y plane (sufficient locus for most of the following development) and the paths to the receiver:



At the receiver located on the normal to the element line (this normal or "broadside" field point angle is  $\theta = 0$ ) the incident electric field is the sum of the two vectors:

$$\begin{aligned}\vec{E} &= \sum_{n=1}^2 \vec{E}_n = E_1 e^{j(\omega_c t + \Phi_1)} + E_2 e^{j(\omega_c t + \Phi_2)} \\ &= [E_1 e^{j\Phi_1} + E_2 e^{j\Phi_2}] e^{j\omega_c t}\end{aligned}$$

where  $\Phi$  is the excitation phase of the element.

For the two elements being excited with equal amplitudes and in phase ( $E_1 = E_2$ ,  $\Phi_1 = \Phi_2 = 0$ ), this resultant has its maximum value since the two constituent vectors arrive at the receiver in phase, having traversed equal path lengths. The very simple vector diagram shows the sum to be  $2E$ .

$$\begin{array}{c} E \uparrow \\ E \uparrow \end{array} \quad 2E = E_{total} \propto E_1$$

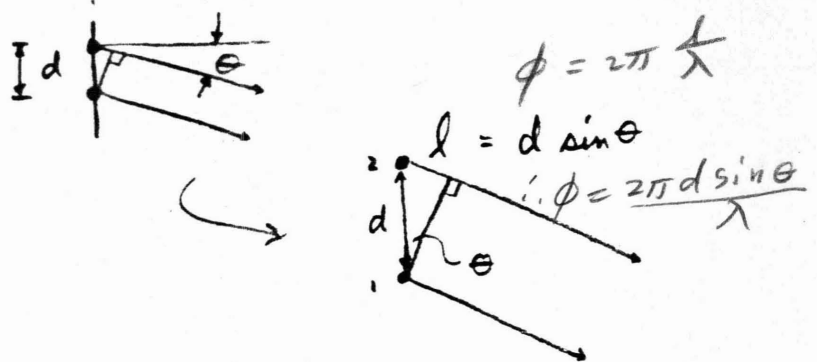
(From this point on, the carrier frequency operator  $e^{j\omega_c t}$  will not be written; the entire vector diagram will show relative arrival phases of

$$\phi = \text{PATH LENGTH DIFFERENCE PHASE DIFFERENCE}$$

constituent vectors and will be understood to be rotating at the carrier frequency to generate the time varying total field.)

Consider moving the receiver to other positions  $\theta \neq 0$  in the horizontal plane:

Now, of course, the path lengths from each element to the field point are NOT the same; they differ by the line



segment  $l$  in the figure, given by  $l = d \sin \theta$  so that the phase lag of the field from element "2" as seen at the distant receiver is, in radians:  $\phi_2 = 2\pi \frac{l}{\lambda}$   $\lambda$  is the carrier wavelength

(The convention will be  $\phi$  for excitation phase at the elements, and  $\phi$  for path-length induced phase seen in the far field.) This phase as a function of field point angle is  $\phi_2 = 2\pi \frac{d \sin \theta}{\lambda}$  and the vector sum of the two elements' contributions is seen in diagram:

It is evident that there exists some field point angle  $\theta$  for which  $\phi = \pi$  radians ( $180^\circ$ ) and the resultant goes to zero. This describes the first

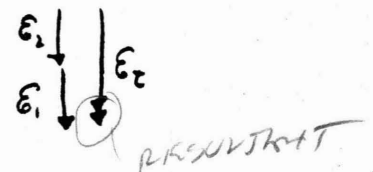
interference null off broadside; we can solve for the angle  $\theta$  for which that condition prevails:  $\phi = 2\pi \frac{d \sin \theta}{\lambda} \stackrel{\text{set}}{=} \pi$

$$\text{or } \theta = \sin^{-1} \left( \frac{\lambda}{2d} \right) \quad \text{and } E_t = 0$$

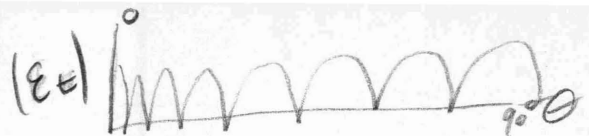
As the value of  $\theta$  increases further, the vectors continue their mutual rotation due to increasing path-length difference until they again align,

i.e., at  $\phi = 2\pi \frac{d \sin \theta}{\lambda} \stackrel{\text{set}}{=} 2\pi$

$$\text{or } \theta = \sin^{-1} \frac{\lambda}{d}$$

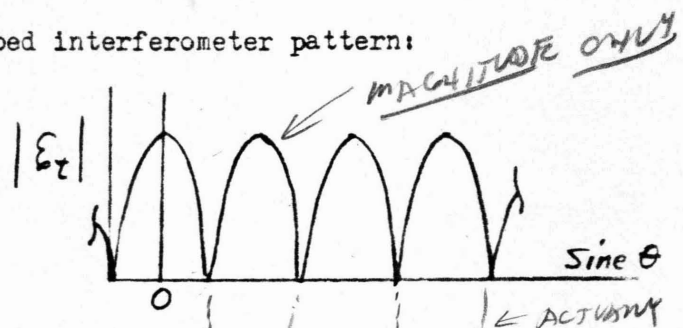






If we graph the resulting vector field magnitude as a function of the viewing angle, we have the familiar multilobed interferometer pattern:

Notice that only if we plot this as a function of sine  $\theta$  are the lobes uniformly spaced.

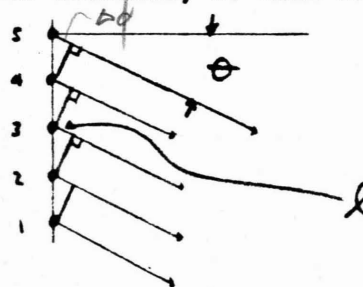


In " $\theta$ -space" they are more closely spaced in the broadside region than at the wider angles. Notice, too, that the spacing of the two elements measured in wavelengths,  $\frac{d}{\lambda}$ , determines the compactness of this lobed structure. Observe that if  $d$  is many wavelengths,  $\phi$  is "amplified" relative to  $\theta$  and many lobes appear in, say, the forward  $180^\circ$  of space; if  $d$  is only a few wavelengths, then the lobes are much thicker and only a few exist.

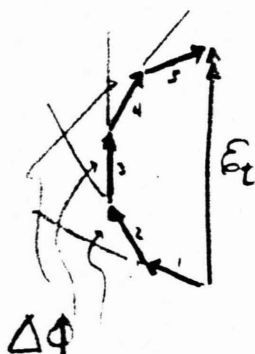
#### A Line of Elements

Having established that two radiators form an interference pattern, that it is multilobed in structure and that the lobe width and spacing are inverse functions of the spacing of the elements, we will add elements in the line of the two to make an array.

Consider  $N$  elements disposed as shown to the right with the paths shown to a distant receiver



at an angle of  $\theta$ . The vector diagram that results at that receiver is shown below with the element-to-element phase increment due to path



$$\text{where } \Delta\phi = 2\pi \frac{d}{\lambda} \sin \theta$$

as before

length differences  $\Delta\phi$

shown very clearly.

This, of course, is drawn for equal intensity at each element (a "uniform illumination function" at the

array), and assumes the elements were excited in phase so that the resultant is maximum (all the vectors adding in phase) when there is no path-length difference, a condition occurring at  $\theta = 0$ .

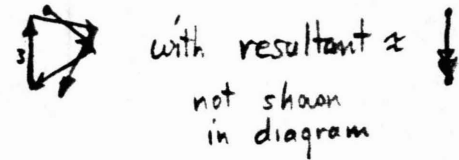
Now, consider other values of receiver position, of  $\theta$ . Certainly there is a value of angle  $\theta$  where the vector diagram closes on itself and produces a pattern null:



Continuing, there must be a

next "maximum" encountered,

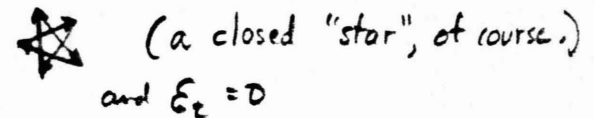
shown approximately in this diagram:



and that is in fact the peak of the first

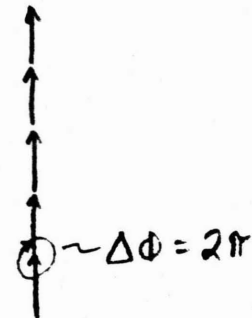
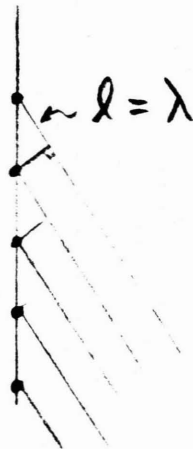
"sidelobe". And, at a still larger value

of  $\theta$ , another null occurs:



We note in this five-element

vector diagram that if the element spacing  $\frac{d}{\lambda}$  were such that, for reasonable viewing angle  $\theta$ ,  $\Delta\phi$  reaches  $2\pi$ , the vector sum would again maximize, as shown here:



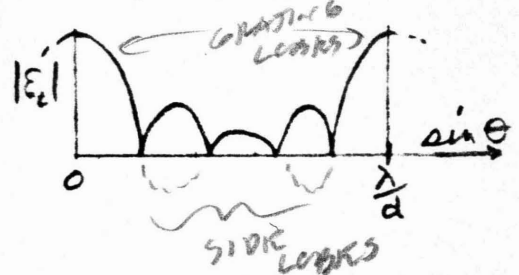
This full strength major lobe is called a "grating lobe" insofar as it occurs only with a grating or discrete array of sources. It occurs at an angle

$$\theta|_{d=\lambda} = \sin^{-1} \frac{\lambda}{d}$$

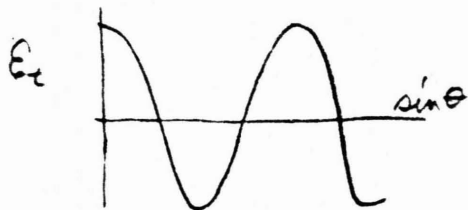
or in general at the several angles

$$\theta = \sin^{-1} \frac{m\lambda}{d} \quad \text{for integer } m$$

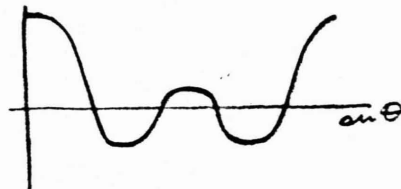
Just as in the case of the interferometer discussed in the last section, we can plot this succession of values of the resultants of these vector summations as a function of the viewing, or field point, angle and we see that the pattern is of this shape, recurrent with these grating lobes, and has a shape of the form  $\frac{\sin Nx}{\sin x}$  where N is the number of elements.



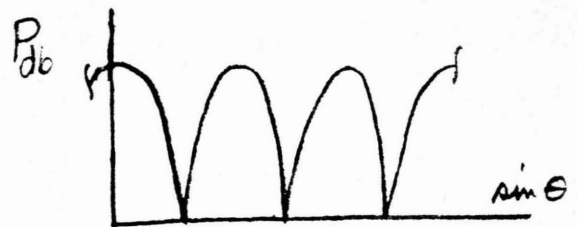
Incidentally, these patterns, insofar as we have been graphing the resulting total ELECTRIC FIELD at the field point, have POLARITY that should be recognized - that is, if the "test receiver" were actually at precisely the same distance from the center of rotation and moved very carefully IN ANGLE ONLY, then the polarization of the lobes one to another would be as we see on the left below, with  $180^\circ$  phase differences on alternate lobes. In most systems work, this is of little consequence, and we are much more interested in the angular distribution of power, proportional to the square of the electric field; hence POWER PATTERNS are correctly shown as on the right below. Furthermore, it is a great convenience to plot such patterns in logarithmic ordinate values, decibels.



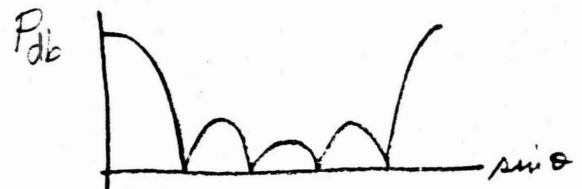
Interferometer Field Pattern



Line Array Field Pattern

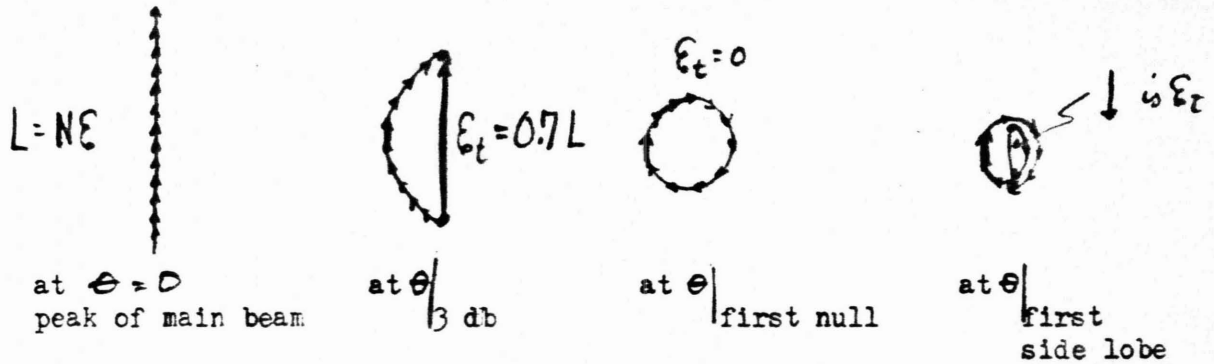


Interferometer Power Pattern



Line Array Power Pattern

It is an interesting exercise to consider a line array composed of many elements very closely spaced (still uniformly illuminated) in which case the vector summation diagrams would be like a piece of string of fixed length being wrapped in circles:



(In each case the phase reference is the center of this array, whose contribution is represented by the vertical elemental vector in each diagram above.) Elementary geometry says that the first sidelobe peak is roughly when the string wraps "once and a half around", or

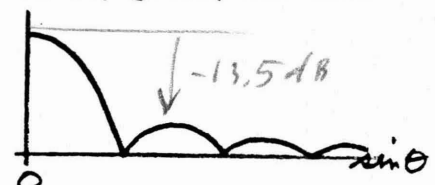
$$\frac{C}{\pi} = D \quad \text{or} \quad \frac{\frac{2}{3}L}{\pi} = \epsilon_t$$

$$\text{or} \quad \epsilon_t = .212 L$$

and squaring the coefficient,  $(.212)^2 = 0.045$ , and converting to decibels gives

$$\begin{aligned} \frac{P(\theta_{\text{sl}})}{P_{\text{max}}} &= 10 \log(0.045) \\ &= 10 \log(45) - 30 \\ &= 16.5 - 30 \\ &= -13.5 \text{ db} \end{aligned}$$

demonstrating with a piece of string rather than a Fourier Transform that indeed the first sidelobe peak of a uniformly illuminated aperture is "about 13.5 db down" as the common rule of thumb says. A graph of the resultant magnitude  $\epsilon_t$  as a function of  $\theta$  (graphed as power in db) gives, for this closely spaced filled array, a pattern function



of the familiar "sine x over x" shape, more properly:

$$\frac{\sin\left(\pi \frac{S}{\lambda} \sin \theta\right)}{\pi \frac{S}{\lambda} \sin \theta}$$

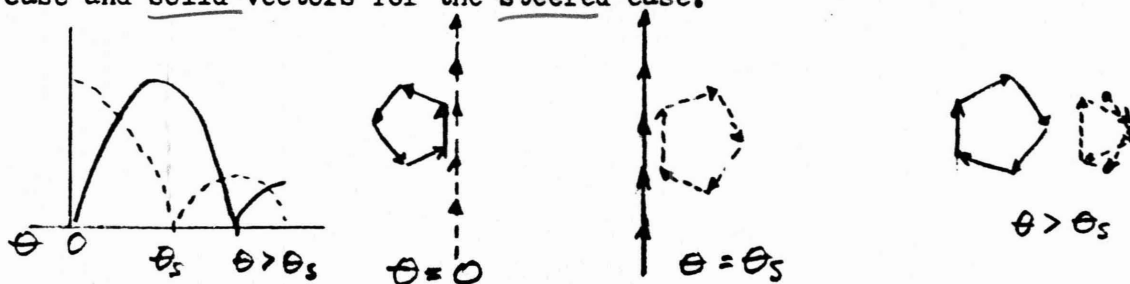
where  $S$  is the aperture width.

We note the nulls are trigonometrically positioned in angle  $\theta$  and that the null spacing (and hence width of the main beam) is inversely proportional to the aperture width. We also note that this array of elements so finely spaced than the aperture can nearly be considered a continuum is a special case of the discrete array of the previous discussion, and in fact, as we would expect, the discrete array pattern becomes the other as we pack more elements in:

$$\lim_{N \rightarrow \infty} \frac{\sin Nx}{\sin x} = \frac{\sin x}{x}$$

DIFFERENTIATING NUM. + DIVIDEN.  
AND TAKING LIMIT

We have discussed so far elements that have been excited with no phase difference among them, that is, elements that have been excited "in phase". If, however, it were desired that the maximum of the pattern not occur at  $\theta = 0$  but rather at some "steering angle"  $\theta_s$ , the elements can be excited with a phase increment between adjacent ones  $\Delta\Phi$  that exactly compensates for the path length difference between elements when viewed from  $\theta_s$ . That is, the phase lag of one element relative to another due to path length is precisely the advance in phase with which that element should be excited, in order that the vectors once again "line up in phase" in the direction desired,  $\theta_s$ . Again, for a  $N=5$  element array, the figure illustrates this steering, using dashed vectors for the "unsteered" ( $\Delta\Phi=0$ ) case and solid vectors for the steered case.



could also physically move elements (small as moving Antennas)

The illustration is for the steering angle  $\theta_s$  to be approximately at the first null of the normal or "unsteered" pattern. One might consider this as a "first" beam position to the right, for example, although obviously finer increments of  $\Delta\Phi$  permit much finer repositioning of the maximum (main beam). The vector addition equation is

$$\vec{E}_t = \sum_m \vec{E}_m e^{j m \Delta\Phi} e^{-j n 2\pi \frac{d}{\lambda} \sin \theta}$$

and, as evident, the condition for a vector maximum at  $\theta_s$  is

$$\Delta\Phi = -2\pi \frac{d}{\lambda} \sin \theta_s$$

or the excitation phase to be applied to the  $m^{\text{th}}$  element (numbered  $-\frac{N-1}{2}$  to  $+\frac{N-1}{2}$ )

is  $m \Delta\Phi = 2\pi \frac{nd}{\lambda} \sin \theta_s$  for odd  $N$

where both phase and position in the aperture are with respect to the center element in this indexing or to the center of the array (should there not be a center element) in general.

Incidentally, the form of the  $\vec{E}_t$  equation is clearly that of a Fourier Transform of a complex function. The complex function is  $\vec{E}_m e^{j m \Delta\Phi}$ , the "illumination function" at the aperture, and the Fourier operator  $e^{-j 2\pi f t}$  is in this case  $e^{-j 2\pi \frac{d}{\lambda} (\sin \theta) m}$  where  $m$  is the integration variable  $t$ , and  $(\sin \theta)$  the transform variable:

$$U(f) = \int_{-\infty}^{\infty} u(t) e^{-j 2\pi f t} dt$$

$$\vec{E}_t = \sum_m \vec{E}_m e^{-j 2\pi \frac{d}{\lambda} (\sin \theta) m}$$

We note that  $\frac{d}{\lambda}$  is a frequency (spatial "frequency") scale factor, i.e. the transform (pattern) is compressed or expanded in frequency (spatial angle) in proportion to aperture dimension (spacing of elements for a given number of them). The path length-induced phase differences from a straight line of radiators result in the pattern being a Fourier (linear trigonometric) Transform of the illumination function across the array.

STEERED PATTERN IS ASYMMETRIC WITH ANGLE.

Then the object of a phased array is to control the excitation phase of the elements in a fixed set of elements ( the fixed array) in order to position at will and inertialessly the position of the pattern maximum (the "main beam").

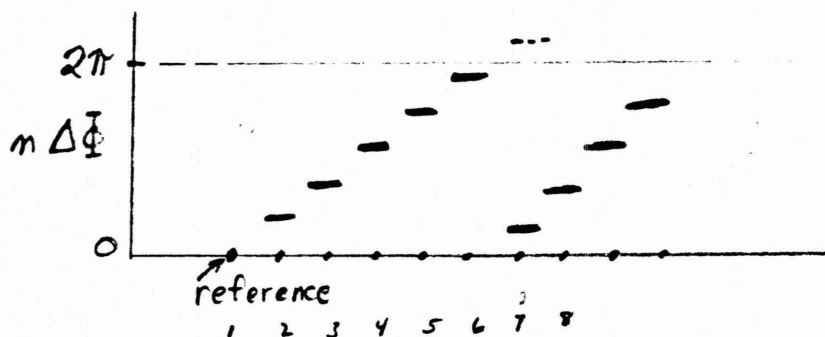
There exist many ways to do this (lenses, frequency sensitive serpentine, phase shifters) as revealed in the survey section to follow, but it serves the purpose here to continue as though a sort of phase shifter were being used at each element.

Observe that in a long array, the accumulation  $m\Delta\phi$  can become greater than  $360^\circ$  for even modest steering angles, yet phase shifters are commonly built to provide only  $360^\circ$  of phase shift. The adequacy of this can be illustrated in this vector

diagram for " $\theta_s$  = several beamwidths off normal" (distorted a bit for



clarity). We wish to compensate, by phase control in the excitation of the elements, for the path length induced phase differences of the diagram. Yet it seems foolish to compensate for, say, the seventh vector relative to the presumed reference (number one) by changing its phase  $2\pi$  plus the small angle shown - rather its contribution could be brought into alignment with the reference by the small angle adjustment alone. A graph of radiated phase across the aperture, then, would reveal this "zoning" in the phase front:

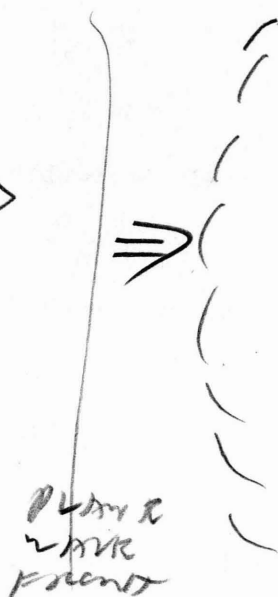




SIMPLE



FURNEL REFLECTION



PLANE  
WAVE  
FRONT



PRISMATIC

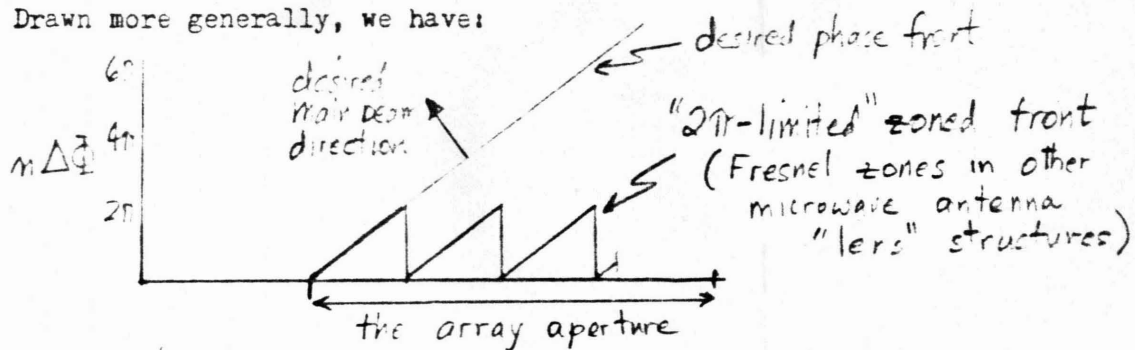
SPATIAL  
FILTER  
OF LEADING  
EDGE

BUT PROBLEM WITH LEADING EDGE OF  
PULSE FORMATION.

∴ BAND LIMITED ANTENNA

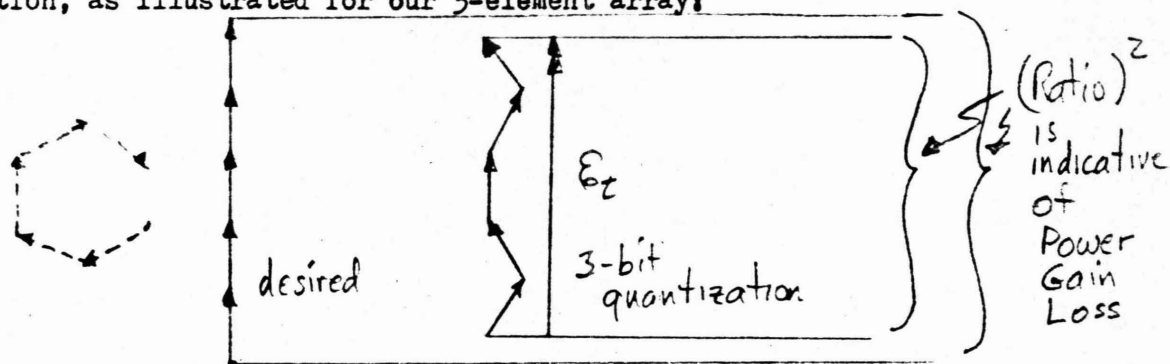
REAL TIME DELAY DEVICES WOULD  
NOT LIMIT BANDWIDTH, BUT  
USUALLY DO IN PRACTICAL SYSTEMS.

Drawn more generally, we have:



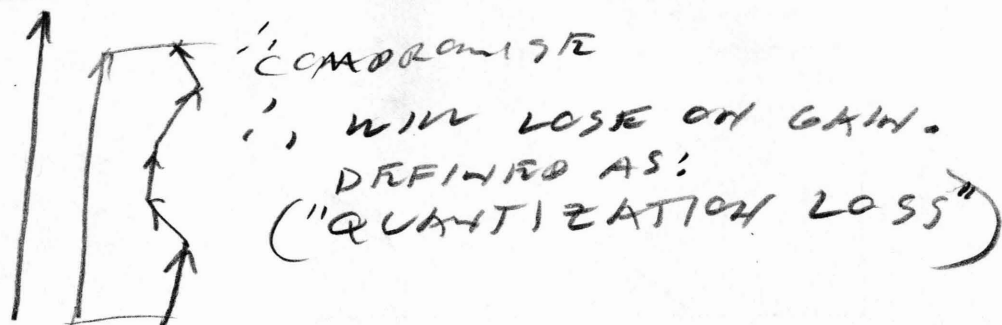
This economy results, however, in pulse edge transients (or in spectral filtering, if you like) because the entire front is not formed until after several cycles of the rf pulse (or because the missing  $n2\pi$  phase delay is precisely that value only for the center frequency and not exact for each modulation sideband of the pulsed transmission).

Another familiar matter is "quantization" in element phase control, a component economy matter again. If phase shifters provide, say, only eight choices of phase between 0 and  $2\pi$  (are "3 bit" phase shifters) the desired vector alignment at any chosen  $\theta_s$  is not achieved precisely. This does not mean that the beam cannot be positioned in extremely small steps in  $\theta$ . It simply says that for some  $\theta_s$  in  $\theta$ , the alignment will be an approximation, as illustrated for our 5-element array:



Seen is that the inability to compensate at  $\theta_s$  exactly for path length induced phase differences (shown alone in the dashed diagram on the left above) has resulted in a loss in the total field  $E_T$ , a loss in antenna gain that is referred to as "quantization loss". In large phased arrays quantization of 3, 4 or 5 bits is not uncommon, with gain losses (averaged

DIGITALLY CONTROLLED PHASE SHIFTERS  
ARE NOT CONTINUOUS.



BUT IF ARRAY IS LARGE  
GRANULATION CAN BECOME  
INSIGNIFICANT (eg. CHANGE ONLY  
ONE ELEMENT, WILL SLIGHTLY  
SHIFT BEAM)

### ELEMENT PATTERNS

✱  $\therefore$  MULTIPLY ENTIRE PATTERN  
OUTSIDE OF SIMULATION BY  
ELEMENT PATTERN.

✱ NON-LINEAR  
PHASE FRONTS WILL BE THE  
SAME FOR ALL ANGLES.

$\therefore$  CAN STILL LEAVE ELEMENT  
PATTERN OUT OF SUMMATION OF ARRAY.

- CAN USE PATTERNS OF ELEMENTS  
TO CANCEL GRATING LOBES

- ALSO WORRY ABOUT MUTUAL COUPLING.  
(EARLY ARRAYS USE EGG-CARTON & APPLIES,  
ETC.)

over the scan volume) of half a db and less.

We have been treating so far the radiating elements as though they themselves have no pattern but rather as though they radiate in all directions equally, are "idealized point sources". Actual radiators have themselves a pattern (the "element pattern")  $P_e(\theta_r)$  which scales the amplitudes of the vectors as a function of field point angle,  $\theta_r$ , relative to their own individual orientations. In a line array, all elements are oriented identically and this scaling treats all contributions the same, and can therefore be represented in the summing equation simply as:

$$\vec{E}_{total}(\theta_s, \theta) = P_e(\theta) \sum_n \epsilon_n e^{j2\pi \frac{d}{\lambda} n (\sin \theta_s)} e^{-j2\pi \frac{d}{\lambda} n (\sin \theta)}$$

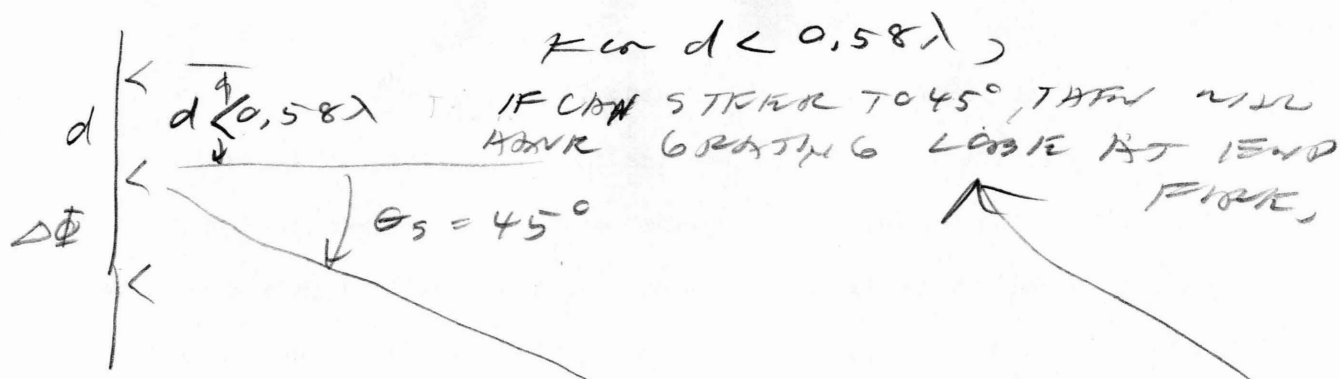
since  $\theta_r = \theta$   
in a line array  
of oriented elements

$$\therefore \vec{E}_{total}(\theta_s, \theta) = P_e(\theta) \cdot \vec{E}_a(\theta_s, \theta)$$

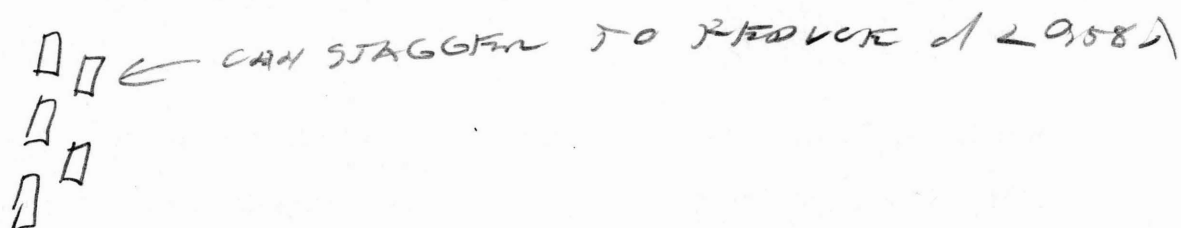
In other array geometries, the element pattern factor can be a function of the element index  $n$  and not so simply superpositioned. Also note that the total resulting pattern, subject to steering, is, in the ordinary line array case, the product of the element pattern which remains fixed in space regardless of the steering applied and the array pattern which, of course, is steered. From this point on, we will use the subscripts "e" for element and "a" for array - our previous vector summations for the idealized "point" radiators were actually array patterns.

As described before, the array pattern is cyclic, it has grating lobes. In rough terms this entire pattern moves with the steering of the main beam. It may well be that as the main beam is steered to the right, say, a grating lobe which had been at left "endfire" (and well attenuated by the element pattern, perhaps that of an open ended waveguide with a null in that direction) now steers into less attenuated regions:

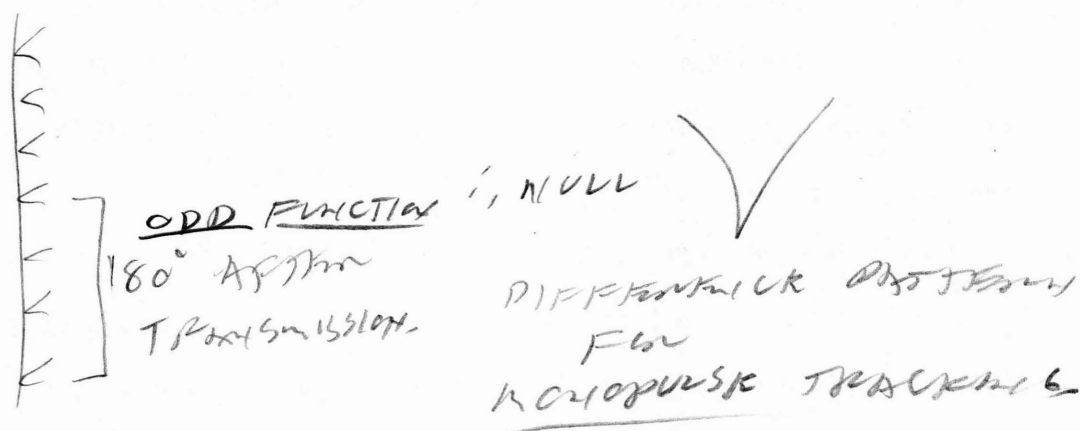




- DESIRE GRATING LOBE TO BE PAST  $90^\circ$  (NOT IN REAL SPACE)
- ASSUME THAT TOTAL PHASE IS LESS  $360^\circ$ .



CAN ALSO USE BANDWIDTH LIMITATION TO REDUCE NUMBER OF ELEMENTS.



CAN CALIBRATE WHEN ACQUIRE  
 $\therefore$  CAN USE AS BOTH SEARCH AND TRACK.

BUT NEED TWO DIFFERENT SETS OF PHASE SHIFTS FOR SUM AND DIFFERENCE,

and the grating lobe now becomes a detriment. Consequently, if the steering volume covers large angles and "drags in" a grating lobe in this manner, it will be necessary to space the elements so that the lobe is farther away in angle. A rough rule might be that for  $\theta_s = 45^\circ$ , the grating lobe should be no nearer than  $\theta = -90^\circ$ , just coming in to "real space". That is,

$$\begin{aligned}\Delta\Phi &= 2\pi \frac{d}{\lambda} \sin \frac{\pi}{4} & (\theta_s = 45^\circ = \frac{\pi}{4}) \\ &= 4.44 \frac{d}{\lambda}\end{aligned}$$

yet  $2\pi \frac{d}{\lambda} + \Delta\Phi$  should be less than  $2\pi$  to prevent a grating lobe in the endfire direction, giving

$$\max \frac{d}{\lambda} = 1 - \frac{\Delta\Phi}{2\pi} = 1 - .71 \frac{d}{\lambda} \text{ or } \underline{\underline{\max \frac{d}{\lambda} = 0.58}}$$

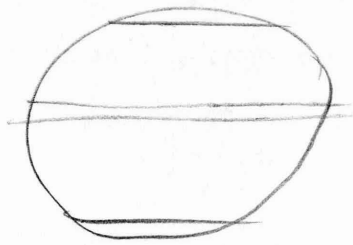
or, in other words, in a regularly spaced line array the elements should be spaced very little more than half a wavelength apart to prevent a grating lobe from appearing in real space for a reasonable steering angle.

It is also important to realize that any periodic component of the excitation function across the array (be it due to the discrete sources themselves or a regular phasing error across the array) forms a "grating" and transforms into some proportional pattern feature. Therefore, quantization round-off or similar matters (e.g. subarray construction) are often made aperiodic deliberately. Main lobe gain is not recovered in such randomization, but increased peak sidelobes can be avoided.

To this point, it has been assumed that all elements in an array are excited with equal intensity. We have seen that a "uniform illumination function" produces a "sine Nx over sine x" pattern. However, in some cases a modified pattern may be desired - one of considerably lower sidelobes. While no illumination function affords as much main beam gain for total power radiated as does the uniform function, it will generally be preferable to give up a little gain and widen the main beam a bit to achieve low sidelobes. Of course, with non-uniform weighting across the elements, their vector diagrams at each field point angle  $\theta$  in the far field can

## RULE OF THUMB

FOR CIRCULAR ARRAY, UNIFORMLY  
FILLED, GIVES 18dB SIDE LOBES



BECAUSE OF INHOMOGENEOUS  
WEIGHTING.

CAN ALSO DISTRIBUTE ELEMENTS  
ACROSS ARRAY WITH BUILT-IN  
WEIGHTING.

BUT UNIFORM WEIGHTING IS ONLY  
WRITTEN TO GIVE MAXIMUM  
GAIN.

OTHER WEIGHTING FUNCTIONS  
WILL DECREASE GAIN.

CAN ALSO SPACE TAPER ARRAYS  
BUT WILL LOSE GAIN AND  
RESOLUTION.

MAGIC TRICKS ANYBODY HAVE SUM  
AND DIFFERENCE PATTERNS.



no longer be represented by regular polygons or circle-approximations. To evaluate a weighted field summation, we must write it out:

$$\begin{aligned}\vec{E}_e(\theta_s, \theta) &= P_e(\theta) \sum_m \vec{E}_m(\theta_s) e^{-j2\pi \frac{d}{\lambda} (\sin \theta) m} \\ &= P_e(\theta) \sum_m E_m e^{jm\Delta\Phi} e^{-j2\pi \frac{d}{\lambda} (\sin \theta) m}\end{aligned}$$

or more properly

$$= P_e(\theta) \sum E_m e^{-j2\pi \frac{d}{\lambda} (\sin \theta - \sin \theta_s) m}$$

which becomes for large N

$$= P_e(\theta) \int_{-\infty}^{\infty} E(s) e^{-j2\pi \frac{d}{\lambda} (\sin \theta - \sin \theta_s) s} ds$$

where the variable "s" is space in the line of the array.

We see, then, that the pattern is the Fourier Transform of the complete complex illumination function.

Many transform pairs are familiar and tabularized in books in antenna theory, sampling theory or filter theory. As discussed in an excellent reference (The Theory of Array Antennas, J.L. Allen, Technical Report No. 323, 25 July 1963, MIT Lincoln Laboratory), various geometries of cosine, cosine squared (on pedestals of various heights), Dolph and Taylor weightings provide the designer choices of sidelobe levels, mainbeam broadening and efficiencies (main beam gain relative to that of uniform illumination).

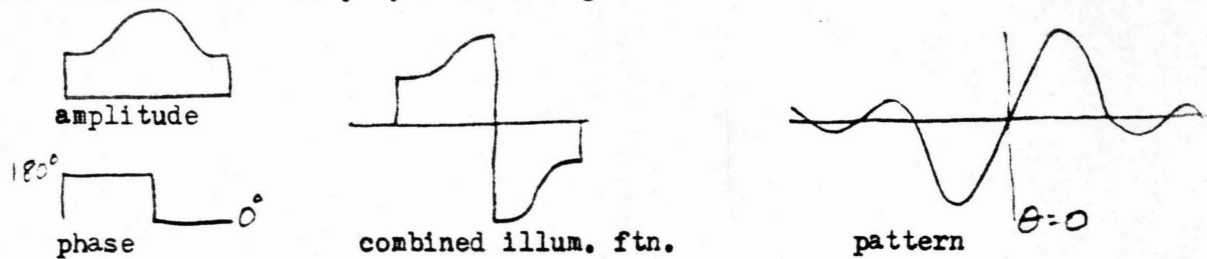
Generally speaking, a phased array permits (requires) a means of channeling power from the transmitter to the antenna in a determined controllable manner, permitting illumination functions with fairly high edge excitation, with even "peaked" edges and inflection points in the function. To illustrate, a "cosine-squared on a pedestal" function is shown, an illumination quite hard to achieve with a feedhorn and reflector.



Phased arrays also permit optimization in other ways. Duplexing can

# PLANTAR ARTERIES

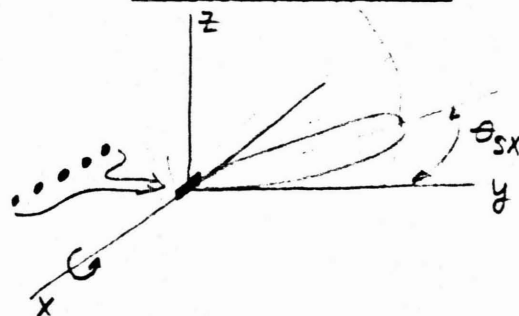
often be in the array structure so that uniform illumination can be used on transmit for maximum gain (power on target), yet a very low sidelobe pattern can be used on receive. Furthermore, a "difference" pattern can often be extracted from the array by introducing an odd-function across the array:



The resulting pattern is useful in precise angle measurement, as in angle monopulse operation. Generally, however, the simple  $180^\circ$  phase on half the array does not produce a good "difference" pattern for an illumination amplitude function that gives a good "sum" pattern otherwise. Some amplitude change is desirable, and feed systems have been developed (tandem feeds, for example, or multiple separately-weighted horn clusters) to separately weight the elements in combining the signals from them (forming the beams) on receive.

### Planar Arrays

In order to understand the operation of a planar array, it is necessary to examine a linear array in an enlarged space. The figure illustrates the domain of the pattern examined up to now, and since no assumption had been made about orientation dependence of the "point" radiators, we may correctly reason that a figure of revolution results for the array pattern. The polar plot in the xy-plane is the array pattern as we have previously presented it.

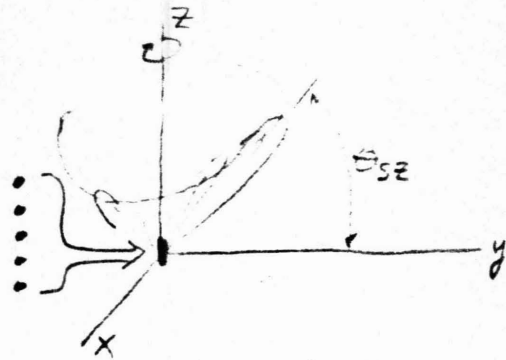


Steering (control of  $\Delta \Phi_x$ )

results in a changing of the angle of this main beam cone. Consider now

an array oriented on the z-axis:

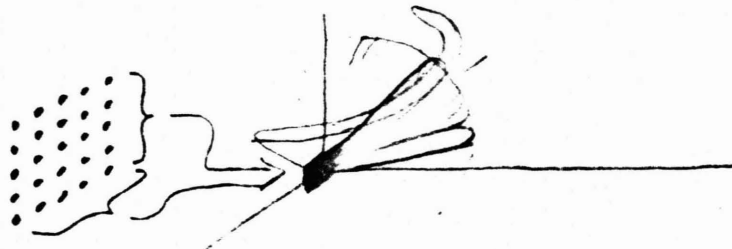
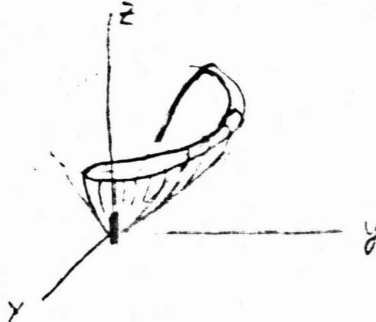
Just as before, a cone at some steering angle  $\theta_{sz}$  is formed by an appropriate control. Had these radiators had a directivity in the y direction (been  $\frac{\lambda}{4}$  from an xz ground plane, say), the cone would



appear reinforced in the "forward" direction, as pictured to the left.

Now, consider that such a z-axis line array is to be the element in an x-axis line array of such elements,

producing a steerable element pattern (the cones with the z-axis) that can be superimposed (as in the earlier equation accounting for an element pattern) on the x-axis-oriented cones of the array pattern:



Again, the locus of main beam positions with various  $\Delta\Phi_x$  for a fixed  $\Delta\Phi_z$  is shown to the right,

and the locus of main

beam positions with various

$\Delta\Phi_z$  for a fixed  $\Delta\Phi_x$

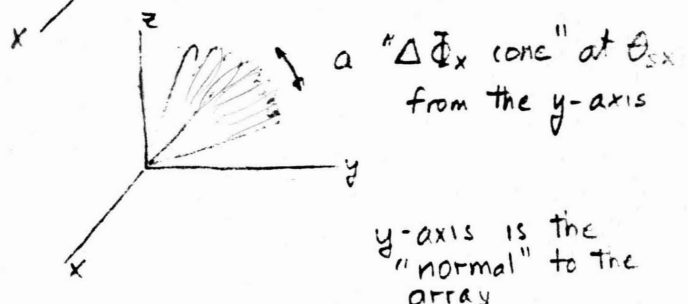
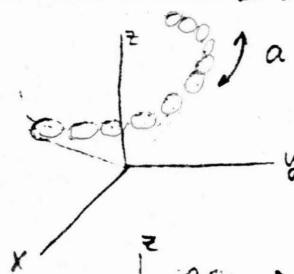
is shown in the lower

figure. These two orthogonal

phase gradients  $\Delta\Phi_z$ ,  $\Delta\Phi_x$

are the steering controls

that "beam steering computers" determine and feed to individual phase shifters



CONFORMAL USUALLY ASSUMES  
ARRAY HAD TO CONFORM TO SPECIAL  
SURFACE,

CYLINDRICAL ARRAYS ARE SYMMETRIC  
AND DO NOT DISTORT ABOUT SYMMETRY.

- ~~ARRAY~~ STEERING BY INDIVIDUAL ELEMENTS,

- STEERING BY PHASES,

in response to a commanded ( $\theta_{sx}, \theta_{sy}$ ) steering angle. The entire "array" pattern (as we've called the first figure of revolution here) is, of course, scaled by this entire "element" pattern (the orthogonal figure of revolution). This means that the main regions of sidelobes are along these "crossed cones".

#### Non-Planar Arrays

The previous development brought us to a planar array steered by linear phase gradients. Other geometries have been explored; our scope here is sufficient only to make a few remarks and definitions.

All arrays are "conformal"; that is, they conform to some geometric surface. The term is particularly significant, however, when the surface is shaped by some other demand entirely (aerodynamics, for example). Sometimes a section of a right circular cylinder will suffice as a part of a fuselage, the streamlined structure of a ship or a missile body, and often one refers to cylindrical array work as work in "conformal arrays". In a circular array (as one "row" of a cylindrical array), one must account for the element pattern orientation (radial to the circle, so that  $P_e(\theta)$  is indeed a function of the summing index  $n$  in the vector addition at a field point) and, of course, no single value of element-to-element phase increment will now permit the "path length difference" induced phase differences to be compensated. Often, a "template" of particular phase and amplitude values, appropriate for perhaps  $90^\circ$  of the circle to form a good pattern with the main beam along the central radial, is caused by the feed system (a switched lens system, perhaps) to be moved about the circle, forming the same pattern exactly at each of these "scan positions". In fact, in the line (planar) array one incurs a trigonometric beam distortion (beam broadening off-normal and a less-significant pattern lopsidedness squeezing the pattern structure away from array normal) is not seen at all, of course, in the scanning (moving the excitation template) of a circular array (cylindrical array in

the scan plane of the circles).

Other geometries (cones, truncated cones, spheres) have been explored. The student may ponder these without further benefit of these notes, save that he remembers that invariably the pattern is formed by viewing the excited array from a great distance and adding vectorially at each viewing angle the contributions made (with attention to path length phase differences and element pattern gain functions at the angle) by each element, then repeating that summing at other viewing angles to trace out the whole pattern. As a matter of further fact, this process of summing the contributions of each element with attention to amplitude and phase as seen at the viewing point applies at any field point no matter what distance from the domain of the elements - but up close to the array (in its "near field") the element-to-element path-length-induced phase differences in the summations are not so nicely (linearly) behaved as when viewed at such a distance that the paths may be considered parallel (consider the two figures at the bottom of page 5).

## II. How Phased Arrays Are Built

### Introduction

The second half of this discourse turns to array techniques. It is expeditious to use previously prepared material, specifically a feed system survey done a few years ago. While techniques may have changed in their state, the illustrative nature remains valid, particularly the categorization given. It alone is repeated here for ready reference.

### Categorization

The chart shows several ways of "getting from the transmitter to the individual elements of an array" with the proper phasing and illumination to form in the far field the desired beam and pattern. In the context of the



previous section, "beam steering" should be taken to mean the establishment of proper element excitation phasing ( $m\Delta\phi_x, m\Delta\phi_y$  in planar arrays) to form a field maximum (main beam) in the desired direction  $\theta_s$ .

The survey paper further develops these topics, as do many of the other papers in the book from which it is taken and to which the student is referred, Oliner and Knittel (editors), Phased Array Antennas, Artech House, Inc., Dedham, Mass.

#### Phased Array Categorization

##### A. Beam Steering within the power distribution system

###### A.1 Frequency Steering

###### A.1.1 Single dimension

###### A.1.2 Frequency-by-frequency

###### A.2 Multiple Beams

###### A.2.1 Lenses

###### A.2.2 Matrices

##### B. Beam Steering by devices at the elements

###### B.1 Space Feeding

###### B.1.1 Reflect

###### B.1.2 Feed through

###### B.2 Constrained Feeding

# Phased Array Feed Systems, a Survey

ROBERT T. HILL

Naval Ship Engineering Center  
Hyattsville, Maryland

## Abstract

The "feed system" in phased arrays is surprisingly hard to isolate from the rest of the system. It is rare that the feed is exclusively a power distribution or collection device. Although this function is primary, feed development has in this last decade embraced the functions of formation and steering of single and multiple beams, as well. Then, with the wider availability of phase shifters for individual elements, feed design has more recently emphasized the distributive role alone. Therefore, a categorization along the line of the inclusion and exclusion of beam steering is presented. Accomplishments of the 1960's are reviewed, and finally a discussion of relative merit, problems and design choices is presented. The survey is, for a variety of reasons, restricted primarily to radars of a civilian or military air-surveillance sort in the microwave region.

## Introduction and Scope of Survey

The "feed system" in phased arrays is surprisingly hard to isolate from the rest of the radar, much more so than in more conventional radars typically involving tower or mast mounted antennas of a feed horn and reflector type. These classically involve a clear separation of transmitter and receiver from the antenna system, quite foreign to many of today's phased array systems. The replacement of the mechanically rotating antenna structure with inertialess beam steering techniques promoted a blending of transmitter and receiver components into the antenna structure, with the promise of increased efficiency by the proximity to the antenna of both the transmitter and receiver r.f. amplifiers. The elimination of the "rotating joint" in a feed line brought a dispersive or modular potential to the amplifier and array relationship, as in systems involving sub-array amplification, which further counters a clear distinction of just what is, in fact, solely the "feed system". As we shall see in several of the systems discussed, this blending is not without exception; for particular applications, phased arrays may still be mounted on movable structure, and a clearer "feed system" is evident.

The opinions or assertions contained herein are those of the writer and are not to be construed as official or reflecting the views of the Navy Department.

It is, of course, impossible to survey absolutely all phased arrays developed to date. There should be no question, then, that this paper, largely because of the author's own background, responsibilities and, hence, contacts in the field, is concerned primarily with radars of a military or civilian nature wherein aircraft or to a lesser degree orbiting or re-entering bodies are the targets and which operate in or near the microwave region. Large arrays of other types, as in radio astronomy, and those operating well outside the microwave region simply could not be surveyed.

There is sufficient interest in the multiple purpose potential of the phased arrays surveyed, such as the detection of targets and the more accurate estimation of their position, to warrant attention to difference pattern characteristics as well as sum. Monopulse extraction is, therefore, discussed.

Finally, this paper is being prepared for presentation with a number of others in which particular feed systems are discussed. I will attempt to avoid these particular ones, and dwell instead on others. I hope to present a "second level" of information in some of these, data not previously reported, and the comments of the experimenters themselves regarding development difficulties, iteration and the like that led finally to the "published" data.

We proceed now with discussion of, first, a categorization of array feed types, and, second, review of the accomplishments of the last decade, and some of the recent proposed systems. Then we will review some of the arguments involved in design choices.

## Categorization

Categorization is valuable because it establishes a language. Phased array radars are most often described as being of a particular feed type before any further description is attempted. This survey

confirmed, however, that the last two decades have produced virtually tailor-made phased arrays with a resulting variety that nearly defies categorizing. A level or two of classification is possible, but further subclassification is very difficult indeed. I have chosen to describe first phased arrays in which the feed system itself dominates in the steering of the beam and second those in which the feed may play a part in forming the beam but does not beam steer. The wide-spread acceptance of discrete phase shifters for use at each element of an array took the field from the former to the latter type. I find it convenient to discuss the second type, those feeds which do not beam steer, in two further categories, space feeds and constrained feeds. Figure 1 illustrates this categorization with a few systems familiar to many named as examples.

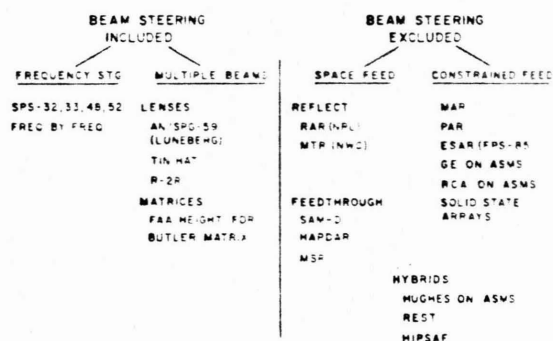


Fig. 1 Array Feed Systems (Table).

The categorization could, of course, be inverted—that is, a first level might have been Space Feed and Constrained Feed, and Frequency Steering Feeds could have been embraced under Constrained Feed. But the major distinction of, essentially, with and without element phase shifters better addresses the evolution of phased array development. It should be noted that in John Allen's 1962 survey of array radars (1), categorization follows slightly different lines, although the individual types can be found both in that work and here. The intent here is to classify feed systems alone, not total radars as was being done in that work.

#### Accomplishments of the 1960's

Using this categorization as an outline, we shall review some of the feeds developed in the last decade, trusting that, while it is not a complete survey, each major feed type is represented typically.

#### Beam Steering Included

**Frequency Steering** Generally familiar to radar engineers is the role of the "serpentine" waveguide feed of many phased arrays. These feeds are generally of a series tapped-line type, illustrated most simply in Figure 2(a). From the drawing we

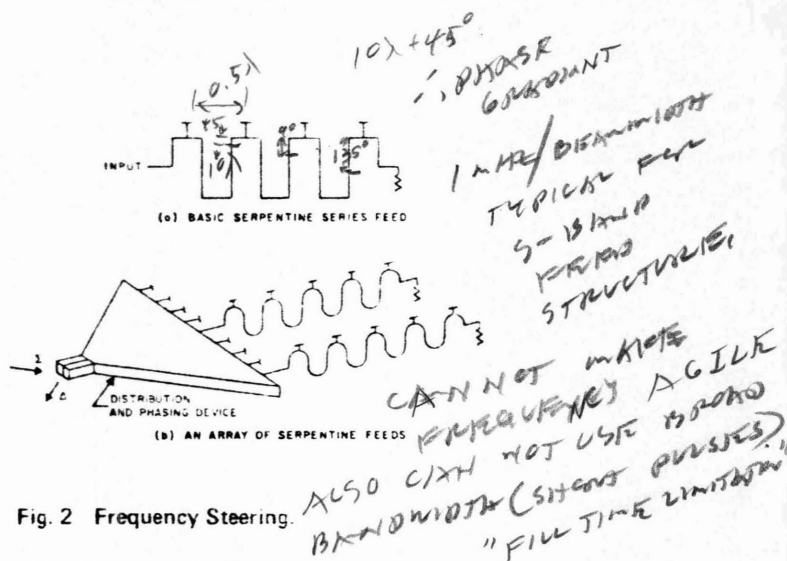
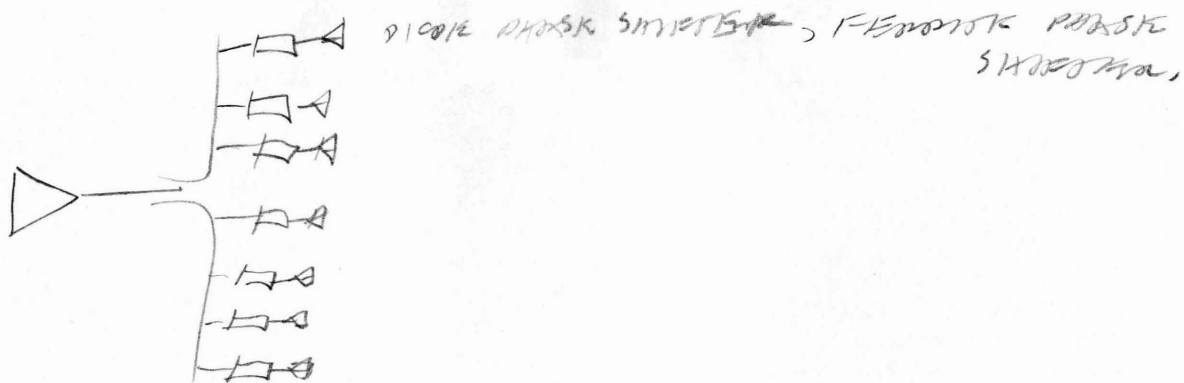
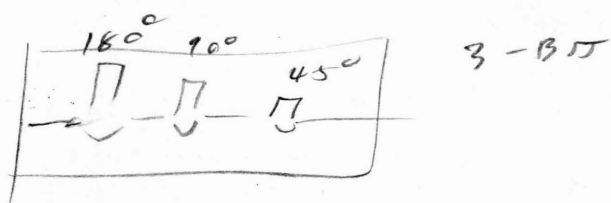


Fig. 2 Frequency Steering.

see that the taps (the radiating elements) bear a phase difference, one to the next, that depends on the number of guide wavelengths, measured in the feed, between them. This is, of course, determined by the frequency of the signal. As in any phased array, the phase difference between the elements determines the beam direction. The ratio of the path length in the feed line between the elements to the distance in space between the elements determines the spatial sensitivity of the frequency steering. This factor has been identified in the literature as the "wrap-up" factor (2), the bigger the wrap-up factor the greater the angle scanned for a given change in frequency. Several radars of significance use this feed principle. Figure 2(b) schematically illustrates the approach for the AN/SPS-33, the Hughes Aircraft built S-band 3-D radar for search and track, which has been operational on board the aircraft carrier Enterprise and the cruiser Long Beach for a number of years. In that system analog ferrite phase shifters are used between a parallel plate distribution device and the serpentine waveguides for steering in the direction orthogonal to the frequency steering. The illustration shows a hybrid feed at the input, providing a difference pattern port for the phase steering direction. Angle monopulse is in one plane only; sequential observations of a target at slightly different frequencies provide angular interpolation in the frequency steering direction. The serpentine feeds were made of quite light weight reduced height waveguide, "snaked" in the H-plane, that is using all H-plane bends. Broad-wall multihole waveguide couplers constituted the



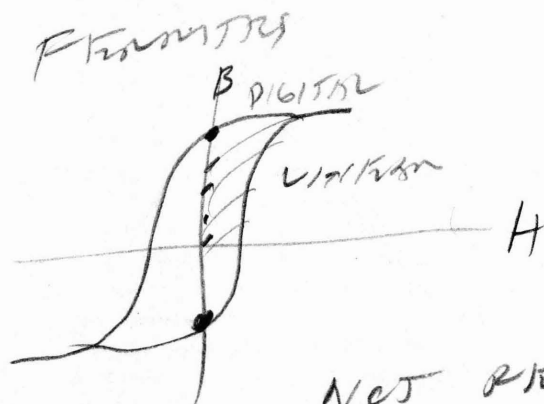
## DIODE PHASE SHIFTER



QUADRATURE HYBRID SHIFTER

DIODES  $\approx 1.1 \text{ dB LOSS}$

FERRITES  $\approx 0.7 \text{ dB LOSS}$



NOT RECIPROCAL

$\therefore$  MUST SHIFT NETWORKS  
TRANSMIT + RECEIVE,

"taps" for the elements. Making the couplers alternately forward and backward couplers allowed the open end of the auxiliary arms themselves to be the radiators, forming a planar array of open end waveguide elements, backed up immediately by the serpentines. The structure is extremely strong; the unfortunate explosions aboard the Enterprise last year sent debris into the arrays, requiring serpentine replacement, of course, but causing no interruption of the radar functions at the time. The steering sensitivity of the feed in the near normal region is approximately 3 MHz per degree, and the lines have approximately 3 dB loss.

Figure 3 shows the AN/SPS-48 radar antenna, in

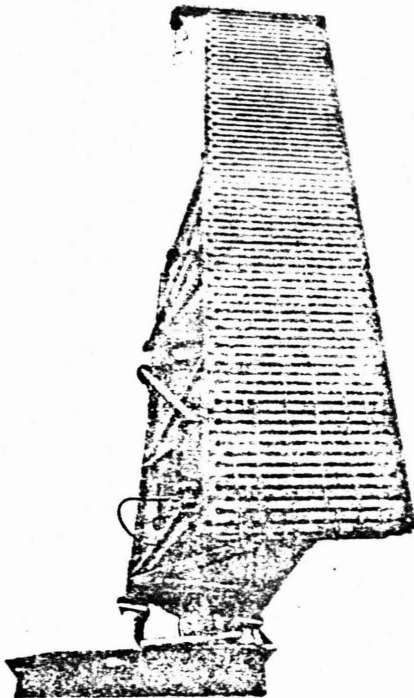


Fig. 3 AN/SPS-48 Array Feed.

which a single serpentine is used to feed horizontal straight waveguides with slot radiators. The antenna rotates in azimuth, frequency steering is used only in elevation. This Navy radar (and the Marine Corps counterpart AN/TPS-32) is built by ITT-Gilfillan. Operating in the S-band, it uses a serpentine with all E-plane bends and has a steering sensitivity comparable to the AN/SPS-33 and loss in the 1 to 2 dB region. The taps to feed the horizontal straight waveguides are simply slot couplers in the narrow wall of the serpentine, feeding at a right angle the butted horizontal waveguides. An iris structure in the serpentine opposite the slot contributes to proper match. With this feed arrange-

ment, by the way, comes a peculiarity, the "squinting" of the beam in azimuth as it is frequency steered in elevation. This results from the end feeding of the horizontal straight waveguides. The straight waveguides have, of course, a greatly reduced wrap-up factor and very little steering sensitivity; nonetheless, the azimuth shift of the beam is about one twentieth of the elevation steering (a rough average over the elevation scan region).

Another E-plane serpentine guide was designed and produced for an experimental phased array for the Navy several years ago by the Aero Geo Astro Corporation. It also used multihole broadwall couplers after every bend, but used only forward couplers and used coaxial cables to connect the coupler to the radiating element. This serpentine was designed by Dr. Judd Blass, of Terry Microwave at the time, under subcontract.

An array feed worth mentioning here, but not shown in the categorization of Figure 1, is in the class of a "low inertia" steering feed. ITT-Gilfillan, with Marine Corps sponsorship, has developed a phased array which is frequency scanned (by serpentine columns) in elevation and phase scanned in azimuth by a "Delta a" scanner and is illustrated in Figure 4. Essentially a tapped waveguide run in which the "a" dimension can be mechanically varied,

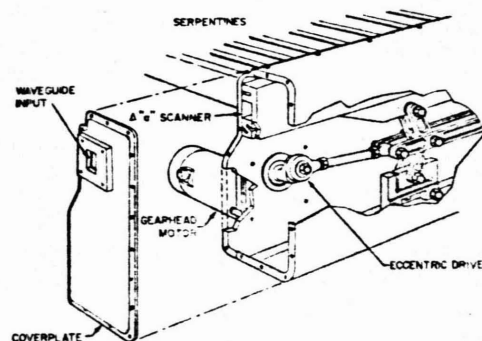


Fig. 4 A Low Inertia Scanning Feed.

the device is certainly appropriate in cases involving a regular and uninterrupted scanning program. The cyclic modulation of the "a" dimension modulates the guide wavelength, of course, changing the phase gradient in azimuth (tap to tap) and resulting in a cyclic and very rapid azimuth scan. The figure shows the linkage assembly to perform the scan. The serpentines for this system are constructed as machined halves of entire serpentines (E-plane) and

fitted together as shown in Figure 5.

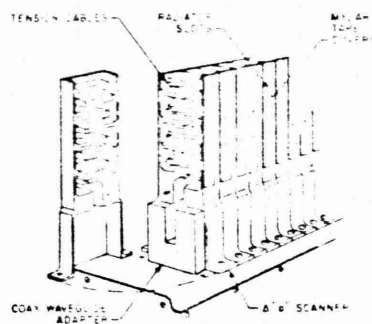


Fig. 5 A Construction of X-band Serpentine.

Frequency steering has been considered for scanning in both dimensions: Figure 6(a) shows such a scheme. If the helix has a wrap-up factor far in excess of that of the serpentine, a monotonic change of

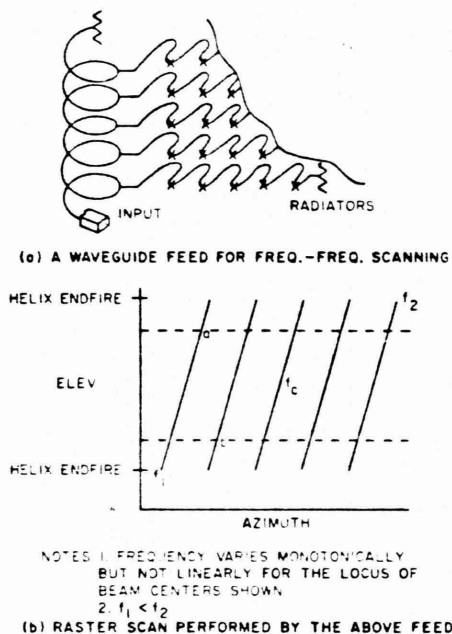


Fig. 6 Frequency by Frequency Steering.

frequency results in the raster scan pattern shown in Figure 6(b). The scheme depends upon the helix "cycling through" conditions of one elevation extreme, through normal, through the other extreme, through end-fire in that direction (and the opposite end-fire),

back to the first elevation limit and so on as the frequency is monotonically changed - this cycling has to occur while the serpentine goes through only a part of one such cycle in the azimuth steering. In use, the frequencies associated with undesired and poorly performing scan directions would not be transmitted (the scan region outside the dotted lines in Figure 6(b), for example). In this case the wrap-up factors must bear such a ratio that the movement of the beam center in azimuth from point "a" to point "b" is less than an azimuth beamwidth to assure continuous solid angle coverage. Waveguide structure was developed along this line several years ago by the Autonetics Division of North American Rockwell, Anaheim, California; the scheme is similar to that pursued by Dr. Croncy at the Admiralty Surface Weapons Establishment in England, as well.

**Multiple Beam Feeds.** Both two and three dimensional lenses or "analog computer" devices have been developed for beam switching - these certainly belong to the category of multiple beam feeds which perform beam steering. The Navy's aborted AN/SPG-59 radar development used a spherical Luneberg lens to transform a point feed into an appropriately phased set of signals which, when radiated from a spherical array, results in an equi-phase planar front. A two dimensional representation of such a lens is shown in Figure 7, from the basic examination given in Skolnik (3). The lens action demands a change of dielectric constant with radius from a relative value of unity at the circumference to a value of 2 at the center. In the AN/SPG-59 lens, more than 40 concentric shells were used

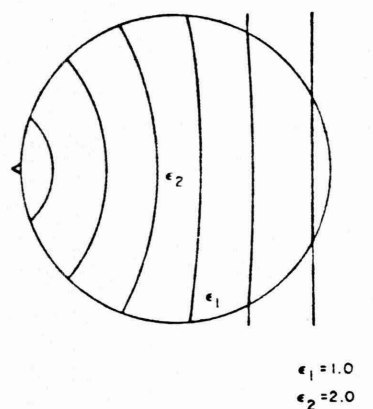


Fig. 7 Two Dimensional Representation of a Luneberg Lens.



in the transmit lens, the dielectric constant of each being controlled by the material density. The receive lenses were made by assembling small cubes, with inserted metal threads controlling the dielectric constant.

An array feed scheme using such a lens is shown in Figure 8. The switches permit each feed point on

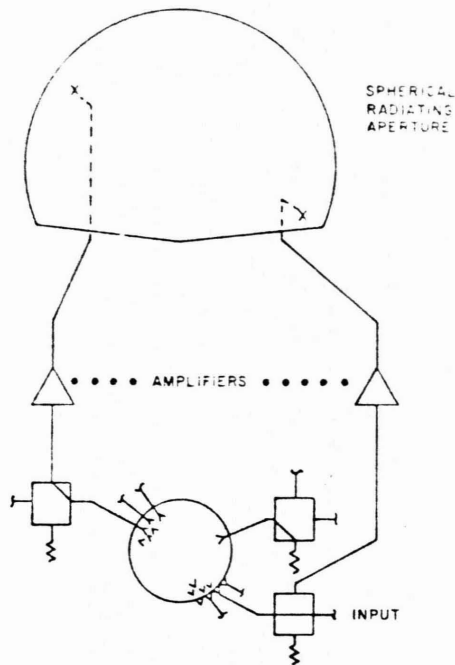


Fig. 8 Feed System Using Luneberg Lens.

the lens to be used as both as excitation point and a collector point. The general possibilities for such a feed include cabling to amplifiers in the one per element manner shown, or connection to include coherent mixing as well so that final amplification and radiation might be at a frequency other than the "phase computation" frequency of the lens. More switching could be included to take advantage of the fact that for any one beam position, less than half of the amplifiers shown in Figure 8 would be used; for example, the amplifier shown at the "input" element in Figure 8 certainly could be used for the diametrically opposite element. All of the amplifiers could by switching at both the lens and the aperture, be shared between diametrically opposite elements - and the same control that causes excitation of a particular input could switch amplifiers so that the hemisphere opposite the feed point is provided with amplification. Most radar applications would define regions on the lens for which excitation as beam inputs is never

required and/or for which there is no diametrically opposite element. These considerations complicate the illustrative "half of the amplifiers" and "hemispheric" schemes described here.

A lens similar in function to the two dimensional Luneberg lens is the so called "tin hat" or helmet device (4), a dome shaped parallel plate structure wherein the dome provides a path-length variation to the collector rim ports when one rim port is excited. This path-length variation has the same front forming effect as the dielectric gradient in the Luneberg lens. Figure 9 is a photo of a C-band

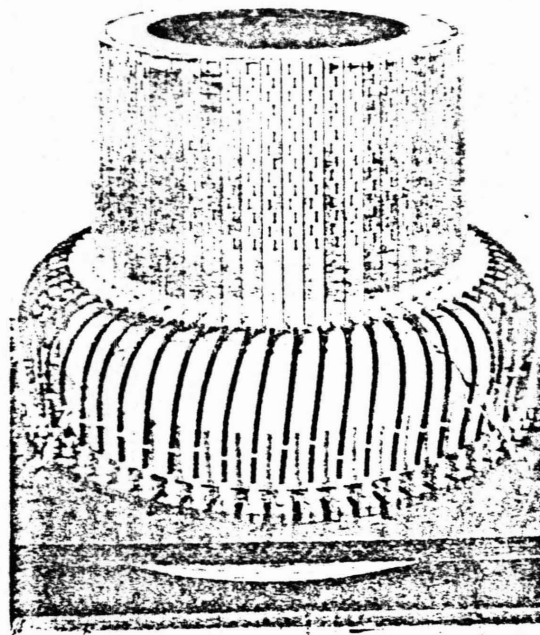


Fig. 9 A Tin Hat Feed.

cylindrical array in which each waveguide column is fed by an output port of the tin hat device at the base of the cylinder. This array was developed by the Hughes Aircraft Company several years ago.

Another feed of this type, that is of the switched beam lens type, is the R-2R lens. Convenient for the feeding of cylindrical or circular arrangements of elements, the lens makes use of the fact that if the elements on a circle of  $2R$  radius are fed through equal line lengths from collector ports on a circle of  $R$  radius excited from one port on its circumference, a linear wavefront is formed, providing the ports on



the R circle are spaced at twice the central angle of those on the 2R circle. The scheme is shown in Figure 10. It is widely known, the use of it as one of the circular array alternatives at the Naval Electronics Laboratory Center is one of the more recently reported cases (5), and involves a much more elaborate switching scheme to achieve both multi-port excitation for desired weighting and also 360 degree coverage.

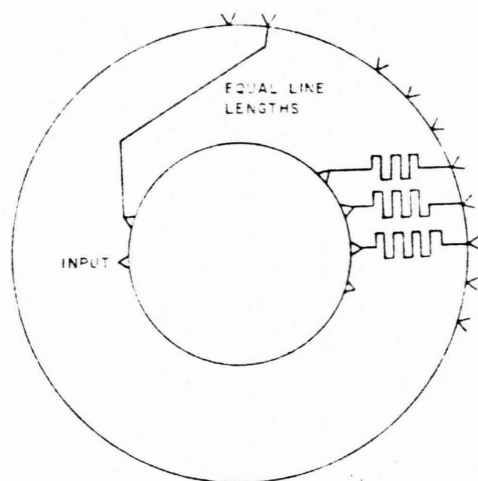


Fig. 10 The R-2R Scheme.

A multiple beam forming and steering feed device that has been used is the matrix of hybrid networks, or the Butler matrix. Such networks were reported nearly ten years ago; the Allen survey (1) and Skolnik (3) both cite several references (6, 7). Figure 11 shows a simple four beam device, composed of variations of the

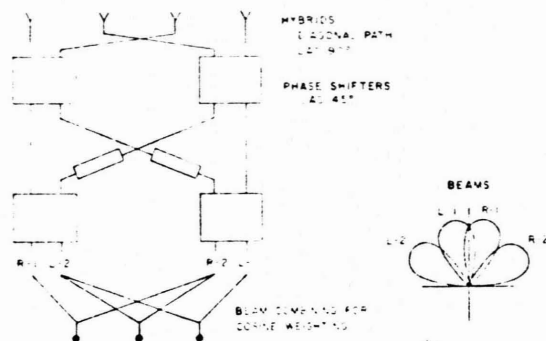


Fig. 11 Four Beam Matrix.

fundamental building block of a quadrature hybrid and a

fixed phase shift. The Navy sponsored significant development of such networks at the Naval Research Laboratory (8); an L-band system forming on receive eight beams in azimuth and three in elevation was constructed using eight element matrices in a stripline construction, stacked and crossed to form the pencil beams. Diode controlled switches in a similar construction were used for beam selection. A common practice (as in the NRL program) is to combine the ports of adjacent beams. A cosine aperture weighting then results, rather than uniform, with the often more desirable pattern characteristics. With this arrangement, monopulse processing of the squinted beam type is possible; that is, a magic tee would produce a signal proportional to the amplitude difference of the two inputs. The development of such monopulse switches in three-level stripline was a part of the NRL program. Also included was the specification and acquisition of a 64-element matrix, considered an essential part of any ultimately useful system. Built by Advanced Development Laboratories, Inc., Nashua, N. H., this low power L-band device (1200 to 1320 MHz) was measured by ADL and rechecked, including pattern measurement from a 64-element line array, by NRL. These measurements indicated a phase gradient error of less than 0.2 degrees (with element standard deviation of 6 or 7 degrees for some beam positions), insertion loss around 2 dB typically, beam port isolation greater than 40 dB and VSWR generally less than 1.5 to 1. The beam phase centering requirement for monopulse was treated with compensating fixed phase shift; for at least one beam pair null depth was still limited to approximately 18 dB.

The NRL developments required great patience and iteration in the network construction. The performance was quite sensitive to the tightness of screws holding the stripline plates together, etc. The construction itself was quite heavy, particularly so until crossovers in single layer stripline were developed. A number of concerns have successfully designed and produced crossovers that contribute to this type of feed and, of course, to many other stripline assemblies.

The Butler matrix has been used as a part of more complex array feeds as well, as beam forming networks combining the outputs of subarrays, for example.

A feed system that Hughes Aircraft has developed is the parallel plate radial feed, shown in Figure 12 as it might be used to feed a line array. It is included here in the multiple beam category insofar as higher order TE modes in the circular waveguide in the center correspond to greater phase gradients

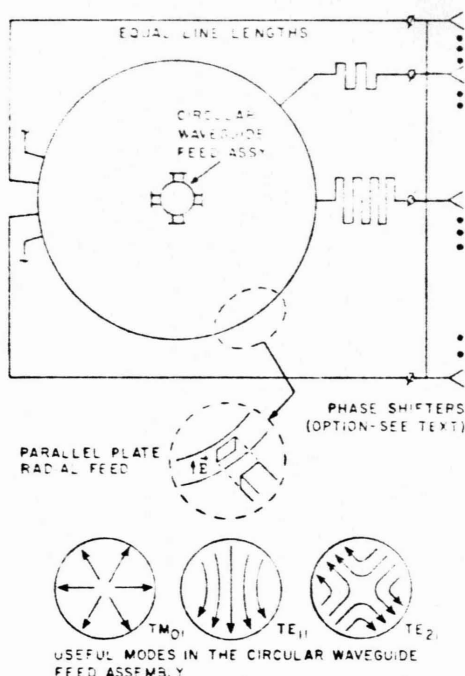


Fig. 12 Parallel Plate Radial Feed.

from port to port at the periphery. Hughes in the early sixties built an S-band radial feed and an appropriate waveguide feed in the center for establishing seven beams, the equivalent of an 8-port Butler matrix. It can be seen that the  $TM_{01}$  mode in the circular guide results in a uniform and in-phase excitation at the periphery. The  $TE_{11}$  mode results in a complete cosine cycle of amplitude weighting around the periphery. Proper phasing and weighting of the two modes, then, result in an aperture illumination of cosine squared on a pedestal, equi-phased. With this excitation, phase shifters as shown could be used for beam steering. On the other hand, the  $TE_{11}$  mode and higher order  $TE_{n,1}$  modes can be excited in the circular guide feed (with 90-degree phased and oriented pairs, for instance, to create rotating fields in the circular guide and spiral TEM fronts in the parallel plate region, where the pitch of the spiral and, hence, steering angle of the beam, is determined by the particular order of the TE mode) to form multiple beams with no phase shifters.

Hughes engineers report good performance with a simple rectangular waveguide transformation at the periphery as shown in the insert of Figure 12. A version of the feed that could be used to form monopulse squinted beams at the feed structure but with which the external

phase shifters would steer the beams has been proposed by Hughes as an improvement in the AN/SPS-33 and is under procurement by the Navy.

Similar parallel plate feed devices of the radial type used for distribution rather than for forming multiple beams have been reported to me by both Sylvania and Raytheon. Raytheon reports an X-band air dielectric device with 4-port contradirectional couplers (small stripline inserts) placed along radii with no wasting at the periphery and claims about 0.5 dB insertion loss. The 324 couplers are arranged in concentric hexagons in this particular experimental device.

The subject of feeds which form multiple beams cannot be left without mentioning the waveguide beam forming matrix (forming 111 receive beams), three of which are used in the AHSR-1 Height Finder of the Federal Aviation Agency and developed by the Maxson Corporation. Each antenna element of a vertical line array is connected to a waveguide line extending behind it. Another waveguide, a "beam forming" guide, taps to these element waveguides with crossed guide couplers. The beam forming guide in which the taps are equi-distant from the elements forms a beam normal to the array. Other beam forming guides tap at a variety of "slants" across the element waveguides, forming beams at various elevation angles. Skolnik (3) summarizes this radar, as well, with a diagram, photo and radar characteristics. A frequent first reaction is to contemplate why the beam forming waveguide using the last tap on each element waveguide is not "cheated" by all the directional couplers that precede it, implying that so little energy is left. A coherent analysis of the entire matrix, of course, discloses that the energy arriving in a plane front at a particular angle reinforces in the beam forming guide "parallel" to the arriving front, with only sidelobe response in the other beam forming waveguides.

#### Beam Steering Excluded

Relatively "safe" is the classification of feeds for arrays of phase shifting elements into "space" feeds and "constrained" feeds. I suggest "space" is a term slightly preferable to "optical" insofar as fields such as fiber or channeled optics attack the synonymy. Also, I prefer "constrained" as the general class of feeds that route in a manifold structure signal from transmitter or receiver to the array. "Corporate" I think of as a feeding of elements "in a body", i.e. in phase, as an equal line length type of constrained feeding. Corporate feeds are (usually) constrained feeds, but all constrained feeds

are not corporate. Finally, and inevitably, there are hybrids of these that I shall describe.

**Space Feeds** The paper by Kahrilas (9) in the 1968 special issue of the Proceedings of the IEEE on Electronic Scanning reviews the well-known HAPDAR radar, developed at Sperry, Great Neck, for ARPA and operating at White Sands for the last several years. This well designed space feed array involves the feeding of a circular aperture from the rear, a "feed-through" approach, and, as illustrated in Figure 13, uses 2:1 and 1:1 feedthrough devices in stripline to con-

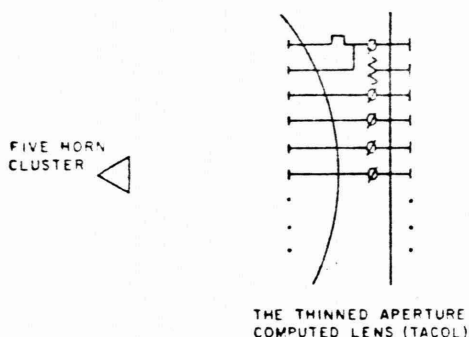


Fig. 13 A Representation of HAPDAR.

tribute to the desired illumination function across the array and yet preserve collection efficiency. This structure, Kahrilas reports, is called the TACOL for Thinned Aperture Computed Lens; the referenced article provides design and measured data and a number of photographs of the components. A five-horn cluster is used to provide independent sum and difference illumination of the collector surface, and is positioned behind the lens at a distance equal to the lens diameter, i.e.  $F/D=1$ . The horn cluster-TACOL combination provides about as much design freedom as has been seen in a space feed system.

The SAM-D radar also uses a feedthrough space fed array, mounted on a tracked vehicle. In this Raytheon development, the array is illuminated by either one of two transmit feedhorns (each connected to a separate transmitter for redundancy) or by the receive horn cluster, depending upon which feed the array is commanded to focus on. In this case we see, then, two interesting features: first, a space duplexing feature involving the refocusing of the array between trans-

mit and receive functions, and, second, a control of which of the two transmitter chains will be employed. The horns are positioned such that the  $F/D$  is unity, accommodating the stowage of the array by folding it onto the top of the vehicle. The receive horn cluster is a vertical stack of four multimode horns (10); that is, the elevation patterns are shaped by the four horns combined in the one plane, the azimuth patterns use the multimode sum and difference pattern extraction of each horn in that plane. Raytheon reports they are at this writing approximately 75% completed with the Army Missile Command specified tests on the array, installed in the MSR test facility at Bedford, Mass., since last December. Figure 14 shows an antenna

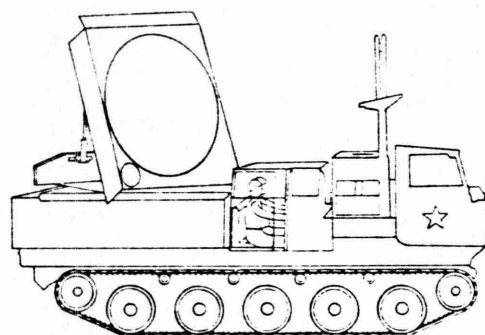


Fig. 14 SAM-D Antenna Mock-Up.

mock-up. Another radar to use the space duplexing feature of feedthrough space feeding is the S-band Missile Site Radar (MSR) (11), another Raytheon development and part of the Ballistic Missile Defense program.

The use of horn clusters to illuminate feedthrough space fed arrays was examined at some length at Westinghouse under the investigation of planar array alternatives late in the Navy's AN/SPG-59 program. Clusters of a dozen or more horns were examined with rather elaborate coupler and divider assemblies behind the horns to achieve the desired sum and difference illumination functions. Among the alternatives proposed by Westinghouse was a plane-mirror folding of the cone of the feedthrough area behind the array, so that four planar arrays could be fed, individually, in a rather entwined vertical structure, more compatible with the ship architecture at the time. This is a variant I've not seen elsewhere. The work on these feeds was done by Mr. H. Querido, to the best of my knowledge; reports are not known to me.

The other type of space feeding obviously involves illumination of the aperture from the front rather than from the back, so-called "reflect" feeding. While the feedthrough approach offers greater freedom in designing the feedhorn assembly (without blocking the aperture), the reflect array permits the area immediately behind the array to be used for phase shifter control and drive assemblies, structural members, heat removal apparatus and the like. The major disadvantage is that the suspended horn not only has an aperture limitation, but positioning and bracing structure must also be minimized, making it susceptible to inadvertent defocusing in the field.

As in the feedthrough approach, we can look to Raytheon for experience with the reflect approach as well. In the middle sixties, an independent research and development program there involved various array sizes leading to a 1300 element reflect array, circularly polarized. This work led to the X-band reflect array radar, developed by Raytheon and now operating at the Naval Weapons Center, China Lake, California. Figure 15(a) shows the array, Figure 15(b) its horn cluster

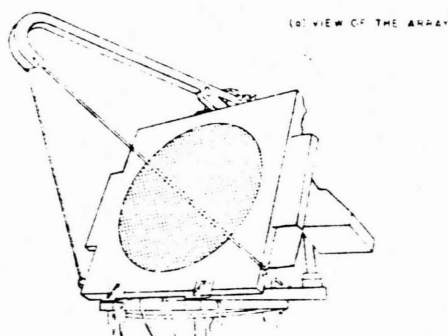


Fig. 15 a Multitrack Radar (MTR)

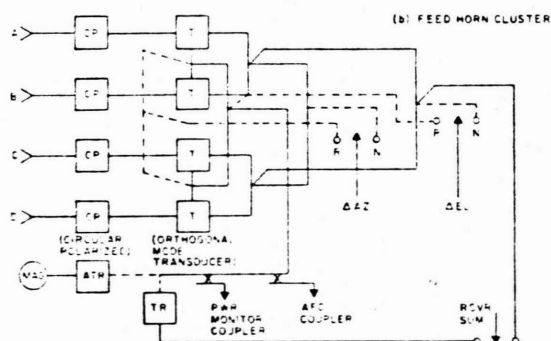


Fig. 15 b Multitrack Radar (MTR)

ter and monopulse assembly. NWC personnel (A. J. Paulsen and others) report that one of the difficulties encountered in the early operation was the alignment of the feed. The system was carefully aligned in June 1969. By September about 6 dB had been lost in monopulse null depth (an average with scan). Some failed phase shifters, a fairly localized set, were replaced and a dB or two was recovered. Moving the feed was not attempted at that time, due to the structural difficulty - it is suggested that a better arrangement of adjustable members would have been possible in design.

A later development at Raytheon is in their RARF radar, a reflect array at  $K_u$ -band featuring a polarization agile feed cluster of four horns. Each horn has a pair of orthogonal exciters, but rather than route eight waveguides to this assembly, the horns are summed and the two difference patterns formed for each of the two sets of exciters, so that six waveguides feed this assembly. The weighting and phasing of these two sets of three inputs determine the polarization degree of circularity and sense. The antenna is shown in Figure 16.

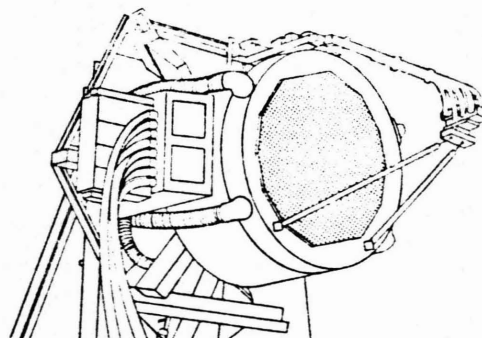


Fig. 16 Raytheon RARF Array.

A curious part of Raytheon's work in reflect arrays is that the use there of row and column phase control (wherein spherical correction is approximated by the product of two "crossed cylinder" factors) is somewhat incompatible with offset feeds. With the exception of some early FAD work, the centered feeds have been used. My recent discussions with Raytheon personnel indicate that if a different control scheme had been used, they might have exploited the offset feed to a greater extent.

At the Naval Research Laboratory, an S-band reflect array radar (RAR) has been operated for a number of years following its development by the Blass Antenna Electronics Company. It has employed a centered feed horn assembly which was a vertical stack of two multimode horns; that is, a



horn pair was used to form the elevation difference pattern, the multimode difference pattern extraction was used in azimuth. More recently, a single multimode aperture has been used to form difference patterns in both planes.

**Constrained Feeds.** The Bendix-built AN/FPS-85 radar (12) at Eglin Field, Florida, is an example of one kind of constrained or channeled feed system, one in which properly phased signals are generated at HF to be fed to each element after up-conversion and amplification. I've considered the beam steering mechanism as not being a part of the feed, although a feed-like structure (a clever tapped coaxial cable structure not unlike a set of serpentine lines in principle) was used in the ESAR predecessor at Bendix, and was proposed in the Navy's SEADAR studies there in the early 1960's, to generate at HF the required row and column phasing. SEADAR was a thorough study, carried well into component and materials selection phases with detailed full-scale mock-ups of several alternatives in the conversion, distribution and amplification region (the "feed") behind the array face. Many useful specifications came from this ambitious program, but finally the sheer size and weight of the potential system precluded its further development for shipboard use. This, like the ESAR and AN/FPS-85, used clusters of simultaneous beams to search for, acquire and track targets. The MAR radar, a predecessor of the PAR (11) under development by General Electric as a part of the Safeguard Program, and the PAR itself similarly use constrained feeds with amplification on either a per-element basis or a subarray basis, and form clusters of beams from which monopulse information is extracted. Some of these systems result in remarkable entanglements of semi-rigid coaxial cable behind the array face, to a degree that cannot be appreciated from the inevitably simplified notional drawings. I have found personal examination of the MAR, the AN/SPG-59, the ESAR and other cabled feeds most sobering indeed and have expressed concern that this "behind the face" area can be too easily slighted in early design. In more recent work under Provencher at the Naval Electronics Laboratory Center in San Diego, feed system hardware has received an impressive amount of early attention. Figure 17 shows this feed area for a part of a multi-band array, with both coaxial cable and stripline power dividers evident. Careful examination reveals the L-band 1:2 divider at the center foreground, the 1:4 S-band divider at the right feeding further dividers in stripline and the two levels of C-band division (at right and in the center stacks) both in stripline. Constrained feeding with coaxial cables forms a part of many other feed systems, such as connecting lenses to arrays, etc. Problems encountered in Navy work have included the flow of center conductor support material; in the AN/SPG-59 program, a spiral type teflon support was found unsatisfactory even after a holding-finger design at each connector was

tried. Finally, a five-ribbed spline support was developed and found satisfactory.

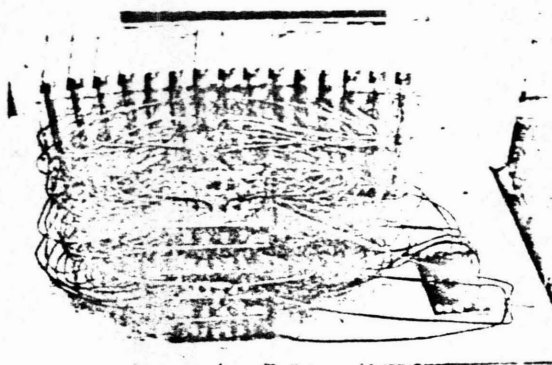


Fig. 17 NELC Three Band Feed.

Another type of constrained feed, and one of the more attractive for many applications, is the waveguide series feed. The center-fed series feed with cross-guide couplers at each element was carried into a rather advanced state of development by the General Electric Company, Syracuse, N. Y., under funding by all three services. This feed is illustrated schematically in Figure 18. The G. E.

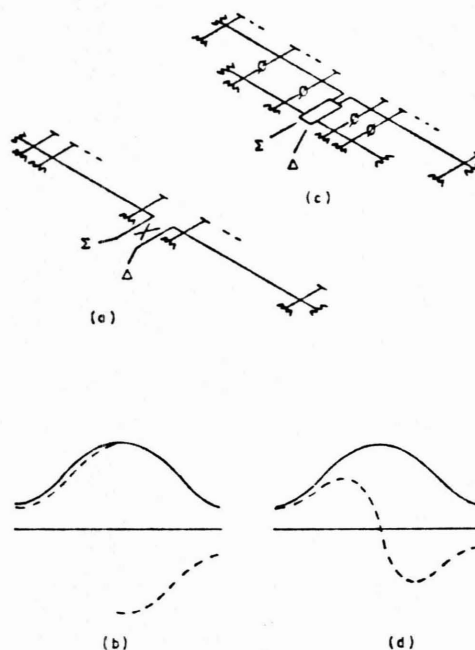


Fig. 18 Waveguide Series Feeds.

work included 1) design procedure, wherein coupler values could be upper bounded for acceptable broad band properties and all coupler values determined for desired illumination functions, 2) construction techniques, resulting in very light weight and inexpensive construction, 3) system trades, wherein illumination functions were investigated in an attempt to meet in one design both sum (as in search) and difference (as in track) pattern requirements, and 4) transient analysis, wherein "response function", "instantaneous bandwidth" or "signal distortion" properties of such a feed were investigated.

The Navy showed considerable interest in the earlier variation, Figure 18(a), in the ASMS program, as did the Army in the AADS-70 and SAM-D programs. To the Navy it represented a very controllable (in design) distribution device which could be used in feeding the rows, say, of a planar array, with a single vertical feed to connect the rows. The form factor, resulting in a more slab-like array structure than space feeding would allow, was attractive. The middle 1960's brought advancement in experimentation that was impressive. In considering it for a multi-function radar application, the Navy was uncertain as to the specific illumination function that would be optimum. While the center feeding with the hybrid allows a delightfully simple extraction of both sum and an interferometer type of difference pattern (in addition to the self duplexing feature through phase shifter control between transmit and receive), it is demanded that one illumination function be built into the device, and treated in halves in difference, as shown in Figure 18(b). This, it was recognized, was a "single degree of freedom" (one illumination function) in the design of a multiple purpose device. G.E. and others (15) dealt briefly with this dilemma, and, just as compromising looked the bleakest, a modified version offering two degrees of freedom in illumination function determination was made available. This author's exposure to it was in association with SAM-D and ASMS joint proceedings in 1967 and, in that effort at least, it was referred to as a "Lopez" feed, crediting A. Lopez of the Wheeler Laboratories with its development. Figure 18(c) shows the basic scheme, and Figure 18(d) the design freedom afforded. G.E. proceeded with this refinement of their previous work and refer to the feed as a "tandem" feed. It should be noted that in forming the sum and difference patterns at the combining network in the center, one need not associate either row of couplers uniquely with the sum or the difference pattern, although such combining is a special case, of course. In general, the two couplers per element and the combining or hybrid network assembly in the center allow individual illumination functions to be achieved for sum and difference pattern formation. The truncation of the back row is indicative of the fact that, in designing desirable sum and difference patterns, the illumination functions need not differ in the edge region,

but the central region is vital. A further design choice, the fixed phase shift between coupler rows, is handled in the G.E. work by a positioning or "slant" of one row relative to the other. A program of transient analysis was sponsored by the Navy at G.E. (contract N00024-65-C-1093) in which it was desired to synthesize the impulse response function (itself a function of steering angle) of a "tandem feed" through c.w. sampling. A computer simulation of the feed was made, involving c.w. excitation and a recording of amplitude and phase in the far field for various beam steering angles. This was spot checked with c. w. operation of an experimental array with good agreement. From these data, a convolution with any input waveform is possible to determine the distortion in the signal as might be received at any far field point.

Recent discussions with the Hughes Aircraft Company, Fullerton, disclose their development of a tandem feed in light weight reduced height waveguide and their development of design procedures. An S-band 24 element (12 per half) feed has been built in which no truncation is used in the back row. The particular design involves the sum pattern being uniquely determined by the front row. The design was iterated to balance coupler limitations with efficiency (waster load loss at the end of the feed) for a particular desired pair of illumination functions. In this design, the maximum coupler value is between 6 and 7 dB, and an efficiency of about 83 percent is achieved (power radiated to power input) for patterns of about 28 dB maximum sidelobes, sum and difference. The design process developed at Hughes by DuFort and Jones and soon to be reported in the literature, shows this achievement to be very nearly the upper bound on efficiency for the particular constraints.

Row feeding with such a waveguide structure can, of course, be regarded as "subarray" feeding, but certainly more familiar in the subarray concept is feeding in rectangular and nearly square subarrays, then forming an array by a "brick wall" assembly of these modules. The development of appropriate power dividers has been advanced at RCA, Moorestown, N.J., and at the Applied Physics Laboratory of the Johns Hopkins University. RCA has proposed such an array feed for the Multi-Function Array Radar (MFAR) of the AEGIS weapon system (formerly the ASMS) and are proceeding with that development. Both the RCA approach and the APL work supporting the Navy program are corporate feeds in a stripline type assembly, and are of the "reactive" type, that is at each junction there is no load device, as there is in a "matched" corporate assembly. The 1968 paper by Stark et al (14) describes a subarray feed assembly of the "matched"

type, an assembly of waveguide hybrid devices providing 1:24 division. The article points out the salient advantage of the matched type as reducing the effects of reflections which might otherwise cause spurious sidelobes. Recent discussions with Raytheon have disclosed in-house work on an X-band corporate feed in which a resistive film is used with a "tuning fork" power divider in a way that 4-port hybrid performance is achieved, providing a matched corporate feed in stripline.

Figure 19 shows a view of the 1:16 reactive feed (a) and the subarray module (b) with which it is used. The entire module has been power tested with both radiate and short circuit conditions at the elements in the region 25 to 40 kw peak. Incidentally, APL has

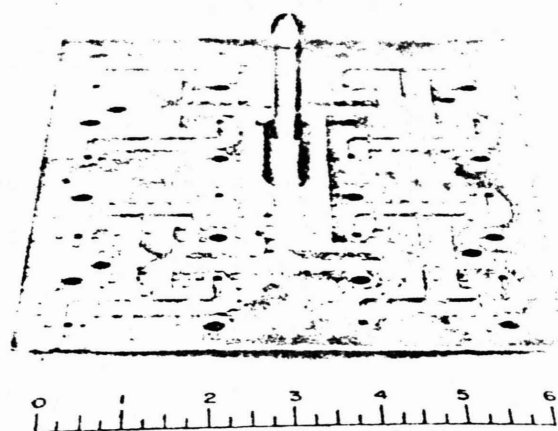


Fig. 19a A Corporate Feed

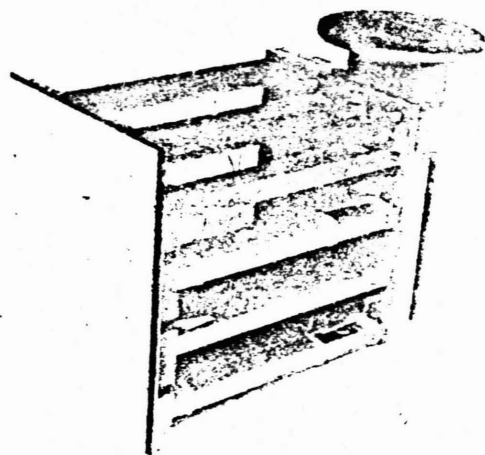


Fig. 19b A Corporate Feed

developed a power testing technique in which a radioactive source is used in proximity to stimulate free charges and resultant arcing. Proper control and statistical interpretation can shorten the time required for power testing markedly. A recent article by Robinson of RCA (15) illustrates their network.

Much of the community is involved in the race to "solid state arrays". Proposals generally involve a form of constrained feeding of these amplifiers (or locked oscillators), although not without exception. Meads, Harper and Hsiao at NRL have covered some aspects of feeding (multiple band conversion schemes, etc.) in recent memoranda. Other work involves very compact printed or stripline structure at each element, such as the experimental system at Ryan in San Diego, seen by myself about a year ago.

**Hybrid Systems.** The Hughes proposal in the recent AEGIS Contract Definition (under the General Dynamics, Pomona, team) is an example of a hybrid system and is illustrated in Figure 20. It

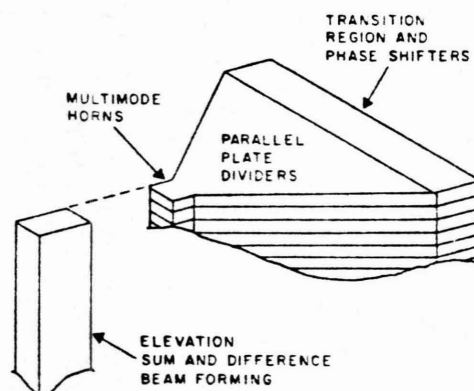


Fig. 20 A Hybrid Feed - Hughes on ASMS.

involves a stack of parallel plate TEM power dividers each feeding a row of elements in a one-dimensional space feed manner. Each of these dividers is fed by a multimode horn, using weighting of the  $TE_{10}$ ,  $TE_{20}$ ,  $TE_{30}$ , and  $TE_{40}$  modes for independent sum and difference pattern determination. (Later work, Hughes reports, has indicated that the  $TE_{40}$  contribution is probably not required.) The transition from the parallel plate device to the waveguide housed phase shifters has been studied at Hughes by DuFort and reported in the 1968 paper (16).



A hybrid feed for an array intended to scan only slight angles has been developed by RCA and is the subject of the paper by W. Patton in these proceedings, as well as an earlier report (17). The approach, under an Air Force program called REST, involves illuminating from a point feed a spherical collector surface, then cabling these signals through phase shifters to groups of radiating elements on the array. A notional sketch, Figure 21, illustrates this hybrid scheme.

Subarray feeding has previously been described, both with rows and also the more conventional rectangular subset of elements forming the subarrays. It was quickly established that the rectangular sub-

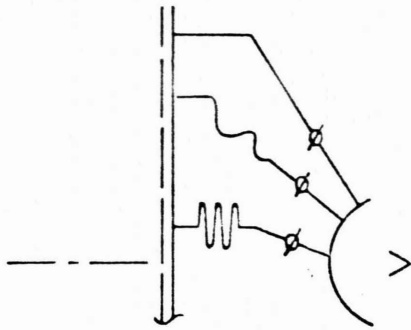


Fig. 21 A Hybrid Feed - RCA REST.

arrays should be stacked with some staggering (as in a brick wall) to reduce illumination quantization effects. This started an evolution of subarray feeding as follows, that leads to our final system surveyed. APL, and probably others, has studied subarrays, using the stripline type feed, that are not rectangular but rather "windmill" shaped so that adjacent subarrays are interlocked, reducing the spatial granularity in the complex illumination function. Next in the evolution, I have discussed with various concerns the interlacing of cabled subarrays, wherein a "subarray" may have a central density of elements but a few elements in extreme positions, further smearing aperture quantization effects by this interlacing. In each of these steps, in this evolution, elements are uniquely identified with a subarray (and, hence, with one amplifier or time delay device, etc.). The next evolutionary step is that of the HIPSAP system at Hughes a hybrid system wherein each element receives a contribution from each constituent "subarray" illumination function. These functions are space fed to the array and are shown as the beams in Figure 22, having been formed by an 8 by 8 crossed Butler matrix assembly. These devices are fed by a

1:32 stripline corporate feed. The Butler assembly has a spherical aperture for focusing at the collector surface of the feedthrough array,  $F/D$  of 0.5 is used, with a resulting high illumination efficiency - about 0.2 dB loss in the space feeding is claimed. Figure 23 shows the assembly, the crossed Butler is in waveguide (0.4 dB loss each way is claimed), the feedthrough array (not shown) uses open waveguide elements on both surfaces; the time delay mechanism is by cable lengths in the present breadboard. The entire feed promises very broadband operation, the Butler assembly providing a feed that exactly compensates for the migrating focus, with signal spectral (sideband) constituents, of the feedthrough array. Certainly a feed system offering the proverbial "something for everybody", and a fitting close to the survey.

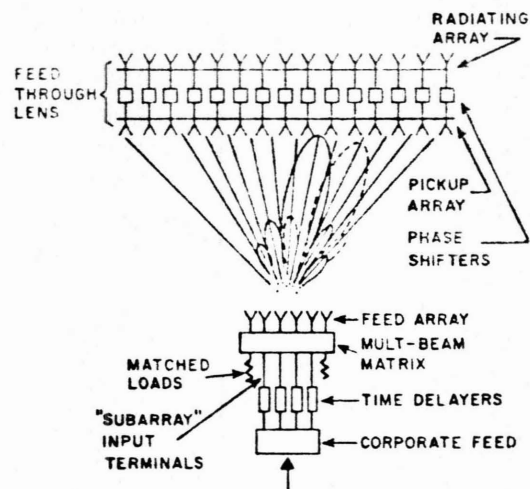


Fig. 22 HIPSAP Diagram.

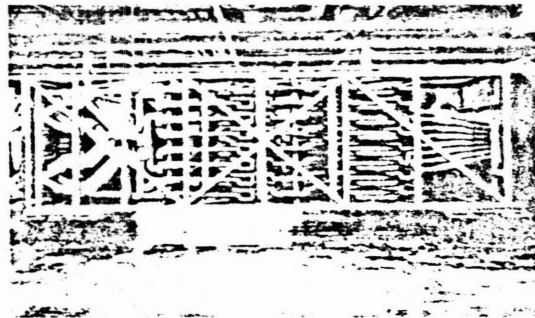


Fig. 23 HIPSAP Construction.

### Design Considerations

This author's participation in a number of the recent evaluations of proposed systems has revealed this fact that subtle design differences of fractions of a dB in loss (as in spillover versus insertion loss) and the like are certainly involved in setting the course of exploratory development, but in engineering development the more mundane matters of form factor, accessibility and cost quickly dominate. I don't find this inappropriate at all; it's simply ironic to devote one's attention to signal distortion in line feeds one minute and hail the rigidity the waveguide runs afford the array the next. A case from the SAM-D/ASMS joint design explorations in 1967 illustrates. One contribution involved a feedthrough array at C-band for the SAM-D user; but to meet the Navy requirement for S-band operation and the Navy's greater need for over-pressure, the peripheral mounting of the larger array simply would not suffice, and a waveguide constrained feed structure was offered instead. Other form factor matters are important, particularly those that bear on maintainability. The choice of feed structure must be jointly considered with phase shifter drive and control circuitry location, drive cabling, air flow for heat removal and the like.

I have previously mentioned "matched" and "reactive" feed types in the context of the constrained power dividers, and implied a concern with the energy reflected within the feed or at the elements. Reflections can cause VSWR sidelobes, secondary beams or a general pattern degradation if not absorbed in many types of systems, not only in the corporate feeds. In reflect space feeding, the effect of the image of the feed horn, in the plane surface of the array face has been observed by pattern measurements. It has come to my attention that in the HAPDAR a slight ripple on the signal due to reflective paths within the chamber behind this feed-through space fed array can be observed, although no pattern effects are evident. I recall attention in the design of serpentine feeds with reactive taps to slightly staggering the tap points, accepting slight loss in gain and other effects, to avoid the broadside resonance phenomenon in which reflective contributions from each tap add in phase at the input for regularly spaced taps, giving high VSWR and sudden gain loss.

The space feed versus constrained feed argument concerning loss deserves comment. The reflect approach does limit horn cluster design and taper, so that perhaps it remains least efficient with a 2 or 3 dB loss (spillover and face reflections); whereas the feed-through approach provides considerably more opportunity to shape the illumination for edge efficiency, 1.0 dB is possible. Most constrained feeds must run close to 1.0 dB in loss. The radial parallel plate devices per-

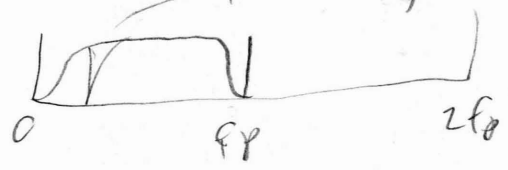
haps offer the greatest efficiency, with total insertion loss (taps included) of as little as half a dB, excluding admittedly any necessary cabling to the aperture.

Of course, the feed is one part of a signal filter and hence its contribution to distortion, its transfer or transient characteristics, are of interest. These topics are explored in early M.I.T. reports (18) and more recently by Adams (19) and Kinsey who, with Horvah, is contributing applicable material in these proceedings. Attention was given to feed and component transient characteristics by Ross (20) at Sperry, as well. For most applications of my association, signal bandwidths required do not rival the bandwidths of candidate array feeds for most reasonable criteria for band limits. However, just as need for more range resolution took us away from frequency steering feeds, demand for even greater information content (bandwidth in a single sample will continue to drive us toward time delay or frequency insensitive array geometries and feed systems.

### References

1. Allen, J.L.: Array Radars - A Survey of Their Potential and Their Limitations, The Microwave Journal, May 1962.
2. Allen, J.L.: The Theory of Array Antennas, Lincoln Laboratory Technical Report No. 323, July 25, 1963.
3. Skolnik, M.I.: Introduction to Radar Systems, McGraw-Hill, New York, 1962.
4. Johnson, R.C.: The Geodesic Luneberg Lens, The Microwave Journal, August 1962.
5. Boyns, J.E.: Circular-Array Radar Antenna, NELC Report 1535, February 2, 1968.
6. Butler, J. and Lowe, R.: Beam Forming Matrix Simplifies Design of Electronically Scanned Antennas, Electronic Design, Vol. 9, April 12, 1961.
7. Shelton, J.P. and Kelleher, K.S.: Multiple Beams from Linear Arrays, IRE Transactions, Vol. AP-9, March 1961.
8. Harper, W.H.: A Matrix-Steered Radar Concept Final Report, NRL Report 6863, April 4, 1969.

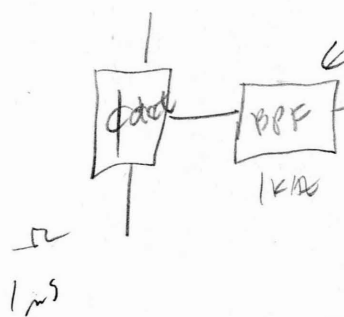
POORPER FILTER M.T.I,  
NOTCH HAS BEEN USED  
TO REJECT SIDES



$2f_p$  ALIAS  $3f_p$   
 $3f_p$  ALIAS  $4f_p$

$\therefore$  1ms PULSE LIKE IMPULSE  
 $\therefore$  STARTCH PULSE OUT

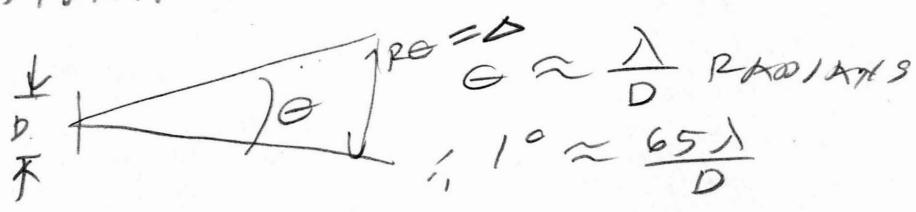
$\therefore$  WILL NOT WORK



BPF BW  $\approx \frac{1}{f_p}$

STATISTICAL APERTURE RADAR  
SICOLNIK (pp 517 - 529)

ANGLE RESOLUTION & RANGE RESOLUTION  
IN TYPICAL RADAR.



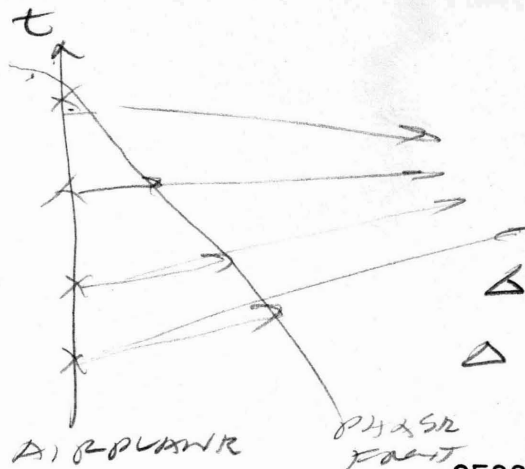
LET  $D = 3m$   $\lambda = 3cm$   $\therefore @ 100KHz$

$$RE \approx \frac{(105m)(3 \times 10^{-2} m/\lambda)}{3} = 10^3 m = \Delta$$

$\therefore$  NEEDED LARGE ANTENNA, BUT  
LIMITED BY MECHANICAL PROBLEMS.

$$\frac{D}{\epsilon} < 10^4 \quad \epsilon < 0.1 \lambda$$

TOLERANCE  $\rightarrow \epsilon$   $\frac{D}{0.1 \lambda} < 10^4 \quad \frac{D}{\lambda} < 10^3 \quad \therefore \frac{1}{20}$  MAXIMUM  
RESOLUTION  
WITH ONE ANTENNA



SEQUENTIAL BY GENIUS  
ADDITION - COHERENT  
SYSTEM

$$\Delta = R \theta_s$$

$$\Delta = R \frac{\lambda}{2L_s}$$

BECAUSE OF 2 WAY PATHS

SESSION IX

SYNTHETIC APERTURE RADAR

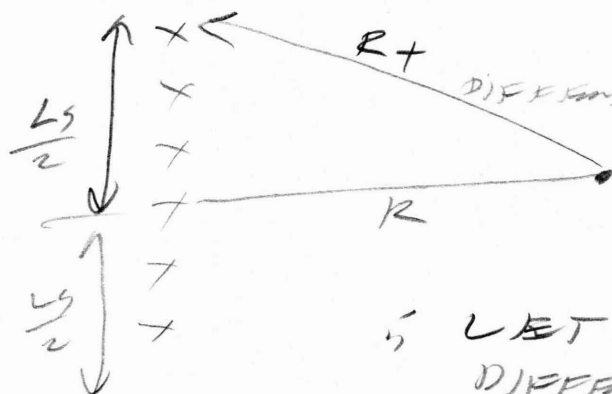
(SA, R,)

REMOTE SENSING WITH RADAR

MOVIE OF FPS-85 RADAR

MERRILL I. SKOLNIK

LIMITATIONS



NO LONGER PLANE  
WAVE

LET  $R + \frac{\lambda}{8}$  BE MAXIMUM  
DIFFERENCE.

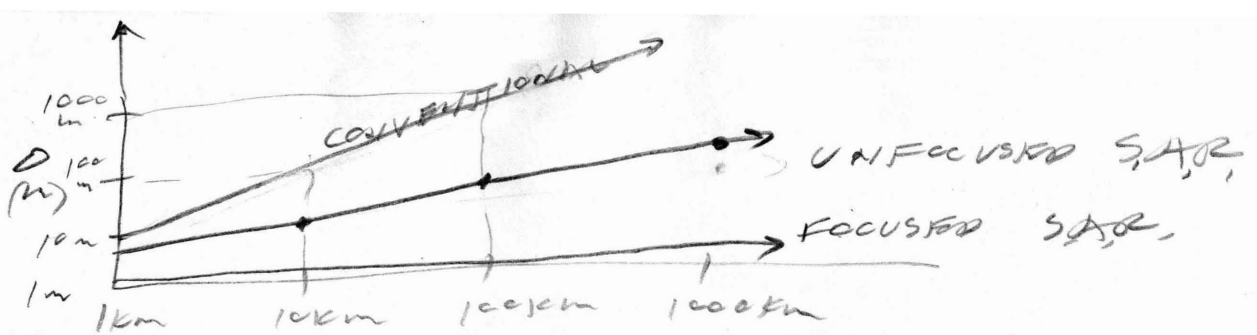
SETS LIMIT TO ANTENNA SIZE

$$R^2 + \frac{L_s^2}{2} = \left(R + \frac{\lambda}{8}\right)^2$$

$$R^2 + \frac{L_s^2}{2} = R^2 + \frac{R\lambda}{4} + \frac{\lambda^2}{64}$$

$$\therefore L_s = \sqrt{R\lambda}$$

$$\therefore \Delta_{\text{MAX}} = \frac{R\lambda}{2\sqrt{R\lambda}} = \frac{1}{2}\sqrt{R\lambda}$$

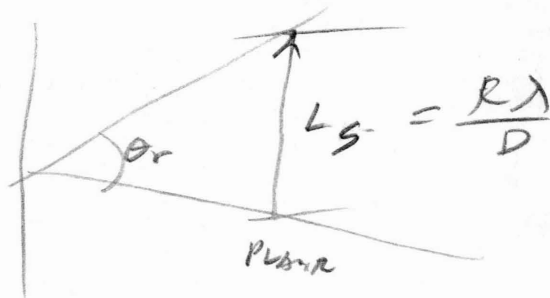


$$R\theta = \frac{R\lambda}{D} \quad @ 100km, \Delta = 1m$$

BUT also also correct for  
PHASE  $\therefore$  "FOCUS" ANTENNA.

$$\therefore \Delta = R\theta_s = R \frac{\lambda}{2L_s}$$

$\therefore$  ONLY LIMITATION IS BEING APPLICABLE  
TO SKK OBJECT OVER DISTANCE.



$$\Delta = \frac{R\lambda}{2 \cdot \frac{R\lambda}{D}} = \frac{D}{2}$$

$\therefore$  FOCUSED ANTENNA HAS RESOLUTION  
INDEPENDENT OF RANGE.

BUT AT EACH RANGE HAVE TO  
ADD DIFFERENT NUMBER OF  
PULSES AND ADJUST PHASES.

$$\text{PATTERN} \Rightarrow \frac{\sin x}{x} \text{ SAR}, \text{ PRRV ANTI} \Rightarrow \frac{\sin^2}{x^2}$$

SIDELOBES ARE PATTERNS.

Digital vs Optical Relative Merits

DIGITAL	OPTICAL
<b>Size</b> Prototypes currently large, but potentially "flyable" using LSI techniques	Current versions also large, and "flyable" systems unlikely due to mechanical stability requirements
<b>Speed</b> <u>Real-time rates possible</u>	Real-time rates possible with appropriate I/O transducers.
<b>Flexibility</b> Potential multimode capabilities via programmable approaches	Flexibility only within generic type (e.g., broadside imaging).
<b>Experience</b> Few "operational" processors, but heavier research experience in recent years	Most processing to date done optically
<b>Calibration</b> Natural processor calibration	Analog processor difficult to calibrate
<b>Dynamic Range</b> Wordlength, and therefore dollar, limited. Output image is also display limited	Output limited by display media unless direct viewing is used
<b>Signal and Image Storage</b> Current computer-compatible tapes and even high-density tapes very bulky. Large processor memories required	Film very efficient 2-D data storage and serves as processor memory as well
<b>Motion Compensation</b> Multipoint techniques available	Multipoint techniques difficult for processor-based corrections
<b>Focusing</b> Manual focusing impractical	Manual focus fast and simple
<b>Autofocus</b> Great flexibility and possible use of phase information	Techniques must be simple, are relatively fixed, and must be based on intensity measurements only
<b>Sidelobe Control</b> Straight-forward signal-data weighting techniques	Aperture weighting feasible, but difficult to implement without phase or SNR perturbations

REQUIRE STATE AUTHORITY

From D.A. Ausherman: Digital versus Optical Techniques in Synthetic Aperture Radar (SAR) Data Processing, Optical Engineering, vol. 19, No. 2, pp. 157 - 167, March/April 1980.

REQUIRE STABLE SYSTEM WITH TIME.

2 MODELS — ANTENNA  
— DOPPLER PROCESSOR  
(CARL WILBY)  
(INVENTOR)

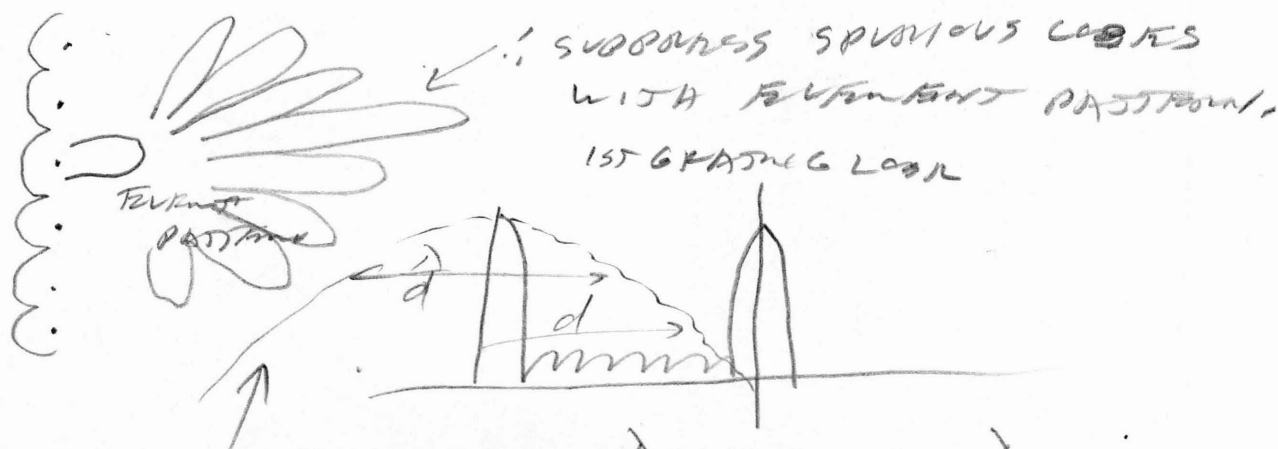
DOPPLER AMBIGUITIES  
TO BLIND SPOTS CAN ALSO OCCUR  
BECAUSE OF SAMPLING RATE.

$\downarrow$   
 $d_e < \lambda$  TO AVOID GRATING LOBS  
 $\uparrow$

$\downarrow$   
 $d_e < \frac{\lambda}{2}$  TO AVOID GRATING LOBS IN SAR.  
 $\uparrow$

$$d_e = v \cdot T_p = v / f_p < \frac{\lambda}{2} \quad \text{TOO SEVERE A RESTRICTION}$$

ARRAY PATTERN VS. ELEMENT PATTERN.



$$\frac{\lambda}{2d_e} = \theta_g = \frac{\lambda}{D}$$

$d_e = \frac{P}{2}$  i. 2 PULSES OFFSET  
MOVE ANTENNA

$$d_e = \frac{v}{f_p} = \frac{D}{2} \quad \left( f_p \geq \frac{2v}{D} \text{ TO AVOID GRATING LOBS} \right)$$

ACTUALLY  $f_p \geq \frac{4v}{D}$  BECAUSE OF OPTICAL PROCESSING.



## APPLICATIONS OF SAR

- MEASUREMENT OF SEA STATE AND WAVE SPECTRUM OF THE SEA (SEASAT)
- GEOLOGICAL AND MINERAL EXPLORATION (SIR-A)
- AGRICULTURAL MEASUREMENTS (SIR-B)
- OTHER REMOTE SENSING (MAPPING OF WATERSHEDS, FLOODS, ICE, OIL SPILL, PRECIPITATION, URBAN LAND USE, AND OTHERS)
- MILITARY

$$f_p \leq \frac{c}{2R_n}$$

$R_n = \text{UNAMBIGUOUS RANGE}$

$$\frac{D}{2} = \delta az$$

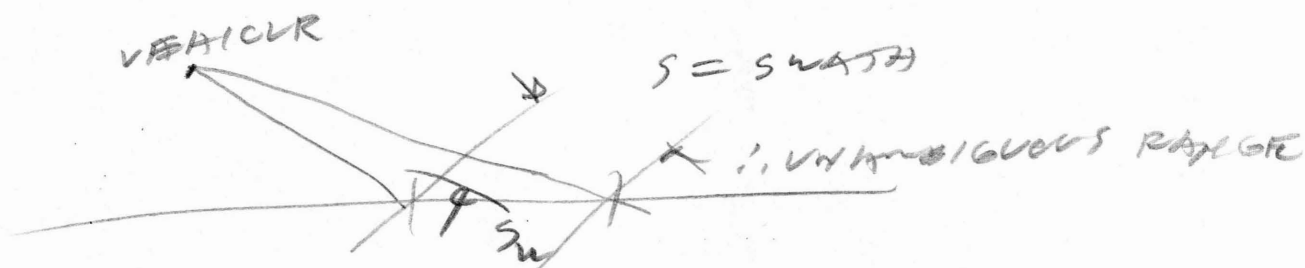
$$\therefore f_p \geq \frac{2v}{\delta az}$$

$$\therefore \frac{2v}{\delta az} \leq f_p \leq \frac{c}{2R_n}$$

$$\frac{2v}{\delta az} = \frac{c}{2R_n}$$

$$\therefore \boxed{\frac{R_n}{\delta az} = \frac{c}{4v}}$$

$\therefore$  MUST COMPROMISE BETWEEN RESOLUTION AND UNAMBIGUOUS RANGE.



$\therefore$  USE DIRECTIVE ANTENNA TO ILLUMINATE SWATH WIDTH TO ELIMINATE AMBIGUITIES.

$$R_n = S_n \cos \gamma$$

$$\frac{S_n}{\delta az} = \frac{c}{4v \cos \gamma}$$

PRODUCES IMAGE, AS WITH HOLOGRAM.

## ATTRIBUTES OF SAR OF INTEREST FOR REMOTE SENSING

- GOOD RESOLUTION IN CROSS RANGE, OR ALONG TRACK, DIMENSION.
- RESOLUTION CELL SIZE INDEPENDENT OF RANGE.
- ABILITY TO PRODUCE IMAGES FROM SATELLITE RANGES.
- ALL WEATHER.
- MAP-LIKE PRESENTATION.
- CAN BE UTILIZED WITH MULTIPLE FREQUENCIES, DUAL POLARIZATION, AND SPATIAL DIVERSITY.
- POTENTIAL ABILITY TO EXTRACT INFORMATION REGARDING ROUGHNESS, SYMMETRY, AND DIELECTRIC PROPERTIES.
- REAL-TIME PROCESSING AND DISPLAY.
- UNIQUE INFORMATION DUE TO USE OF MICROWAVE WAVELENGTHS.
- WELL DEVELOPED TECHNOLOGY. OPERATION POSSIBLE FROM VHF TO MILLIMETER WAVELENGTHS.

$$\frac{P_n}{\sigma_{az}} = \frac{C}{4\pi}$$

SEASAT  $\approx$  5 meters resolution  
over 100 km.

LANDSAT - optical imaging.

- 80 meter resolution

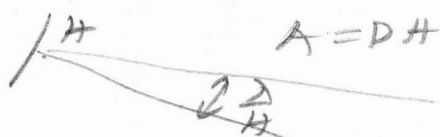
- problems with management  
of huge amounts of data.

Radar Equation (P. 521 Eq. 14-14.)

$$f_{ptc} \tau_c = \frac{L_s}{v}$$

$$\sigma = \sigma^0 \sigma_{az} \sigma_r \sec^4$$

AND GRT Eq. 14.15



EXPAND EQUATION WITH ABOVE  
RESTRICTIONS.

$$S/N = \frac{2 P_{av} \rho_a^2 \sigma^0 E_c(n) \sigma_{az} \sigma_r}{\pi f k T_0 F_n R S_w \sin^2 \theta}$$

$\therefore$  NEED HIGH AVERAGE POWER  
ALSO NEED TO COMPROMISE  $\sigma_{az}$  AND  $\sigma_r$   
ALSO POWER TRADES OFF WITH  
RANGE AND SWATH.

PROCESSING

$$= \sum_n S_n \underbrace{e^{j\phi_r(n)}}_{\text{FOCUSING}} \underbrace{w_n}_{\text{CORRELATION}}$$

FOR ILLUMINATING TAPER.

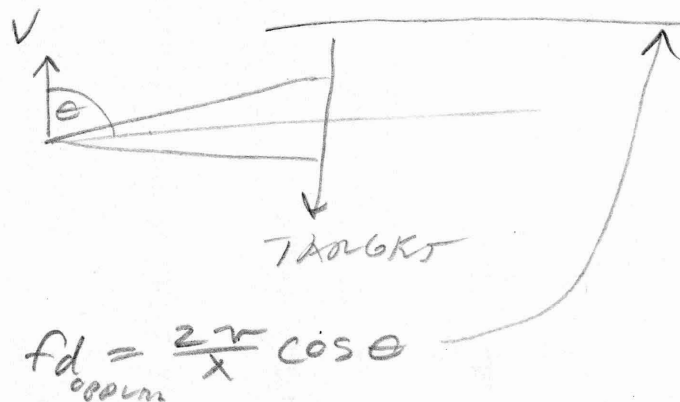
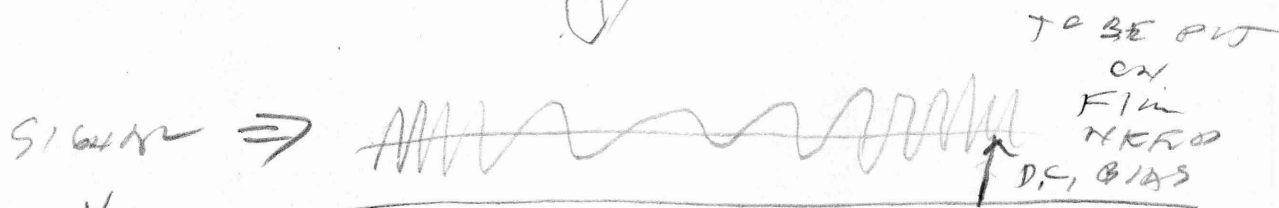
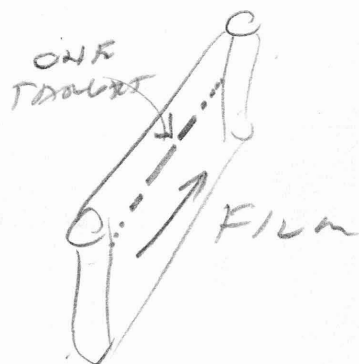
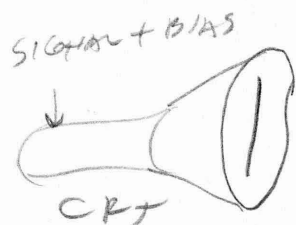
FIRST OPERATIONAL SYSTEM IN 1960s

## SIGNIFICANT DIFFERENCES BETWEEN SAR AND OPTICAL IMAGING

- $10^5$  DIFFERENCE IN WAVELENGTH
  - SAR AND OPTICS RESPOND TO DIFFERENT TARGET EFFECTS
- CONTROLLED, COHERENT ILLUMINATION (SAR) VS AMBIENT, INCOHERENT ILLUMINATION (OPTICS)
  - SAR DESIGNER CAN SPECIFY INCIDENT ANGLE
- SAR RESOLUTION CAN BE INDEPENDENT OF RANGE, AND CAN ACHIEVE GOOD RESOLUTION AT LONG RANGE
- SAR OPERATES ANY TIME OF DAY OR NIGHT, AND IN ADVERSE WEATHER

- FIRST SYSTEMS USED ELECTRONIC PROCESSING.
- OPTICAL PROCESSOR AIDS FOCUSING. - MOST SYSTEMS
- DIGITAL PROCESSING NOW

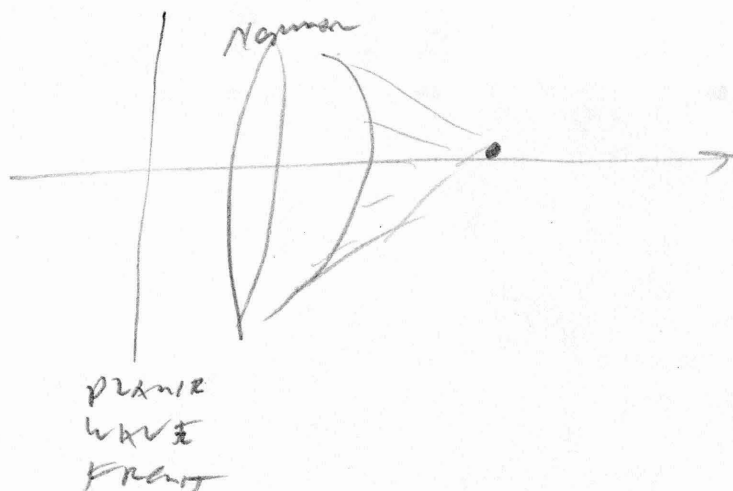
## OPTICAL PROCESSING FIG. 14.5



$$fd = \frac{2r}{\lambda} \cos \theta$$

PHASE VARIES AS SQUARE OF VELOCITY.

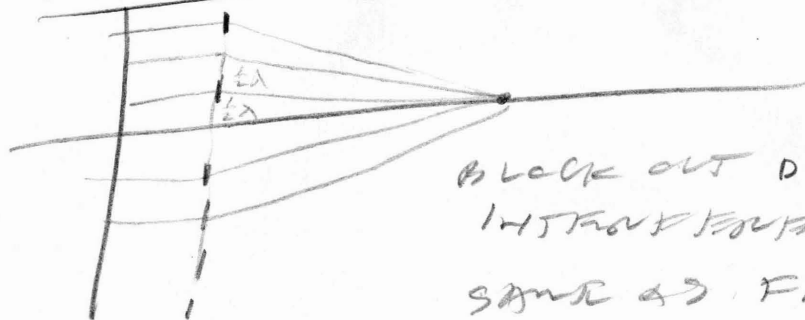
FRESNEL LENS (ACTS AS LENS)



<u>EARTH</u>	<u>OCEAN</u>	<u>ATMOSPHERE</u>	<u>TECHNOLOGY &amp; DATA PROCESSING</u>
o AGRICULTURE/RANGE/FORESTRY, INCL. SOIL MOISTURE	o SURFACE WINDS	o SEVERE STORMS	o IMAGING
o LAND USE/MAPPING, INCL. URBAN	o WAVE HEIGHT DIRECT (SPECTRUM)	o WEATHER MODIFICATION	o SOUNDING
o MINERAL RESOURCES, INCL. CIVIL ENGINEERING	o STORM SURGES, PILE UPS	o CLEAN AIR TURBULENCE (AIR NAVIGA- TION)	o DATA PROCESSING
o WATER RESOURCES, INCL. FLOODS, CONTINENTAL ICE AND GLACIERS	o TIDES, COASTAL WARNINGS	o INITIAL STAGE PARAMETER FOR WEATHER FORE- CASTING	
o LAND & FRESH WATER ENVIRONMENT & POLLUTION, INCL. WETLANDS	o CURRENTS/CIRCULATION (SEA-SURFACE TOPOGRAPHY)	PRECIPITATION	
o LAND/ATMOSPHERE INTERFACE (PRECIPITATION/DROUGHT)	o MARINE GEOID	WATER VAPOR	
o EARTHQUAKE PREDICTION CRUSTAL MOTION	o SEA-LAND INTERFACE	CLOUD PHYSICS PARAMETER	
o SOLID TIDES-GRAVITY FIELD, MAGNETIC FIELD	o SEA ICE	SOIL MOISTURE	
o POLAR MOTION, EARTH ROTATION	o SHIPPING/NAVIGATION	PARTICULATES (AEROSOL)	
	o COASTAL APPLICATIONS	o AIR-SEA INTER- ACTIONS	
	o FISHERIES	o AIR POLLUTION	
	o OCEAN/COASTAL POLLUTION		



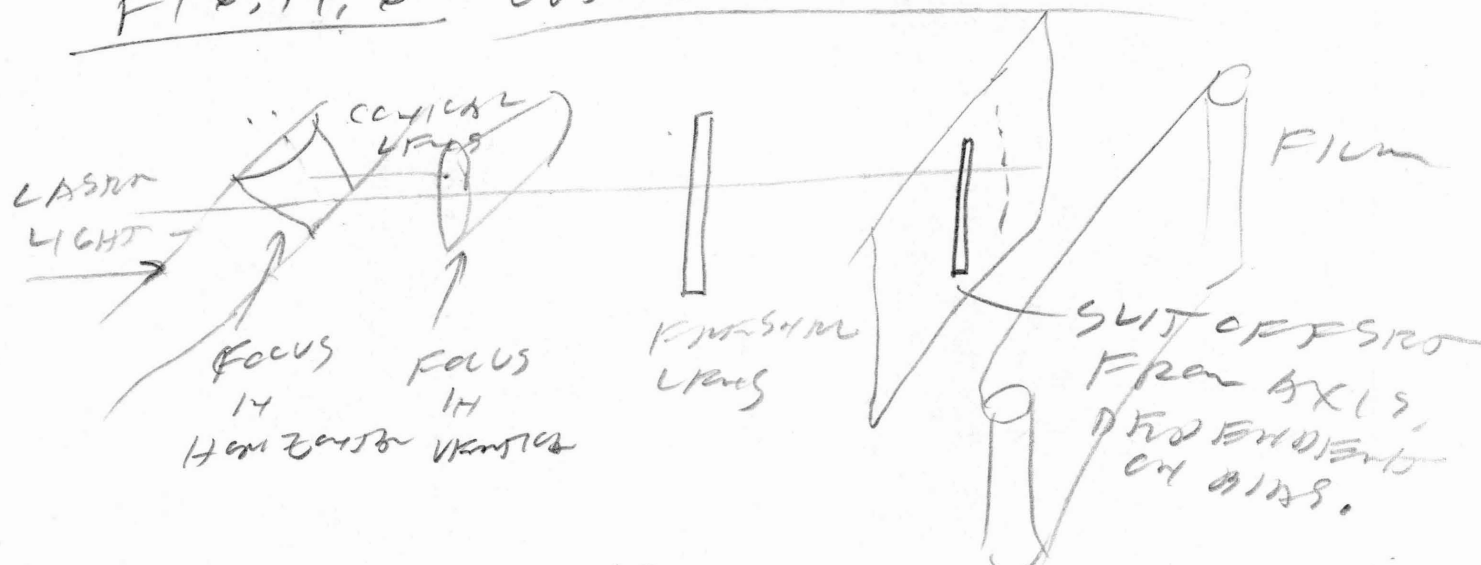
## FRESNEL LENS



BLOCK OUT DESTRUCTIVE  
INTERFERENCE  
SAME AS FILM RECORDING.

∴ HOLOGRAM PHOTO IS COMBINATION  
OF MANY FRESNEL LENSES.

## FIG. 14.6 OPTICAL PROCESS



HAVE TO REMOVE DC BIAS.

∴ PUT AC BIAS ON CRT WITH  
DC BIAS. (SAME AS NORMAL  
AMPLITUDE) ∴ CRT FACTOR  
OF TWO IN AMBIGUITY

## RADARS FOR REMOTE SENSING

- Conventional - Weather, clear air turbulence, birds, astronomy
- Imaging - Identifying culture activities, land use mapping, drainage and soil mapping, sea spectrum, ice mapping, oil spill location, crop census, forestry, geology
- Precision altimeter - Earth geoid, sea state, ice thickness
- Scatterometer - Sea state, ice observation
- HF radar - Sea state, sea spectrum, surface winds, ionospheric sounding

- VERTICAL POLARIZATION HAS MORE SCATTER FROM WAVES.
- OIL SPINS PRODUCE SMALL WAVES.  
∴ DARK ON SEASAT.
- HORIZONTAL POLARIZATION SHOWS SHIPS AND COASTS ON SEASAT MUCH BETTER.

- CROSS ANGLE

PHASE CORRECTION TERM

$$u(t) = B \cos\left(2\pi f_0 t - \frac{2\pi f_0 x^2}{cR}\right)$$

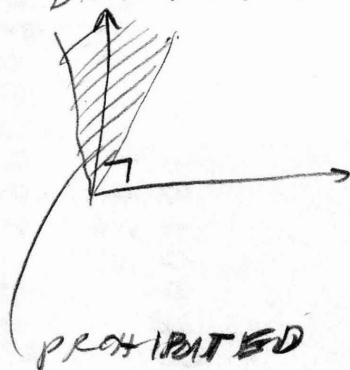
$$s(t) = A \cos\left(2\pi f_0 t + \frac{\pi B T}{T}\right)$$

PULSER COMPRESSION FOR CHIRP IS SAME AS SPATIAL COMPRESSION IN SAR.

DIGITAL PROCESSING NOW BEING WIDELY USED.

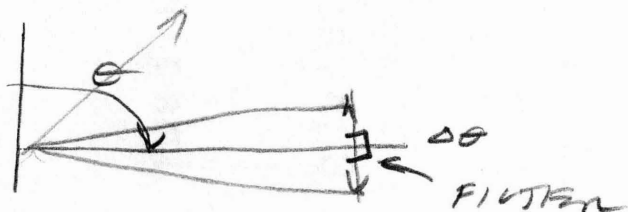
SQUINT MODE

WISAM PROPORTIONAL AS  $\cos \theta$ ,  
DIRECTION OF FLIGHT



$$f_d = \frac{2v}{\lambda} \cos \theta$$

$$\Delta f_d = \frac{2v}{\lambda} \sin \theta \Delta \theta$$



(DIFFERENT FOR DIFFERENT RANGE)  
FILTER  
DOPPLER  
DESIRER.

## STATUS OF REMOTE SENSING TECHNOLOGY

- EQUIPMENT AVAILABILITY IS GOOD, PRIMARILY BECAUSE OF NEEDS OF MILITARY. TECHNOLOGY TRANSFER HAS BEEN ADEQUATE AND IS NOT THE PACING ITEM.
- LIMITATION HAS BEEN IN UNDERSTANDING HOW TO EXTRACT USEABLE INFORMATION. BETTER METHODS ARE REQUIRED FOR INTERPRETATION OF SIGNALS.
- INTEREST IN REMOTE SENSING WILL PROBABLY WANE IF, WITHIN THE NEXT SEVERAL YEARS, ONE OR MORE MAJOR APPLICATIONS DO NOT SEE WIDESPREAD EMPLOYMENT ON A SUSTAINING BASIS.
- EACH SENSOR HAS ITS OWN SPECIAL LIMITATION:
  - RADIOMETRY - BETTER RESOLUTION
  - SAR - IMAGE INTERPRETATION, CROP IDENTIFICATION AND SOIL MOISTURE MEASUREMENT
  - HF OTH - WAVE SPECTRUM MEASUREMENT
- IT IS NOW NECESSARY TO DEVELOP MODELS AND THEORY IN CONJUNCTION WITH CONTROLLED EXPERIMENTS.
- AT PRESENT, INTEREST IN REMOTE SENSING HAS NEVER BEEN AS HIGH.

## DOPPLER BEAM SHARPENING

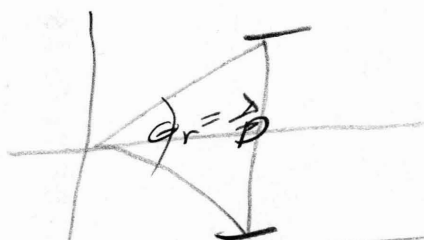
- VARY INTERGRATION TIME TO COMPENSATE FOR SIN  $\theta$  DEGRADATION.

BROADSIDE - L.P.F.

SEWINT - B.P.F. i.e. more difficult,

## SPOT LIGHT

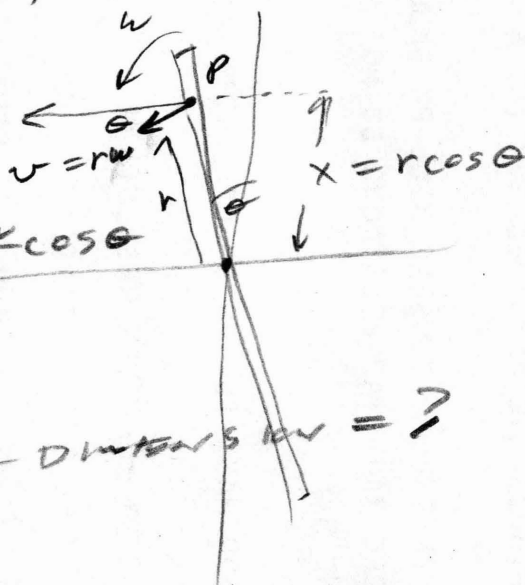
- DWELLS ON SCENE
- BETTER RESOLUTION THAN  $D/2$  BECAUSE OF LONGER TIME ON TARGET.



## INVERSE SAR

RANDOM STATIONARY + MOVING TARGET

RANDOM



$$f_d = \frac{2v}{\lambda} \cos \theta = \frac{2rw}{\lambda} \cos \theta$$

$$f_d = \frac{2u}{\lambda} x$$

RESOLUTION IN X-DIMENSION  $\Delta x = ?$

$$\Delta f_d = \frac{2u}{\lambda} \Delta x$$

$$\Delta x = \frac{\lambda \Delta f_d}{2u} \leftarrow \text{LIMITED BY TIME ON TARGET}$$

$$T = \frac{1}{\Delta f_d} \therefore \Delta x = \frac{\lambda}{2uT} \quad uT = \Delta \theta$$

$$\Delta x = \frac{\lambda}{2\Delta \theta} \quad \text{Assume } \lambda = 0.1 \text{ m}, \Delta \theta = 6^\circ = 0.1 \text{ rad.}$$

$$\therefore \Delta x = \frac{0.1}{2 \times 0.1} = \frac{1}{2} \text{ meter}$$

IMPROVES WITH TIME.

- USE RANGE RESOLUTION TO GET COMPARABLE RESOLUTION IN X-Y PLOTS OF S, A, R, ALONG Y-AXIS.
- MULTIPATH CAN ALIAS IMAGE.

GOOD ARTICLE ABOUT  
 → KOVALY J.J. "SYNTHETIC APERTURE RADAR"

SESSION X

ECCM

OVER-THE-HORIZON RADAR

MILLIMETER WAVES

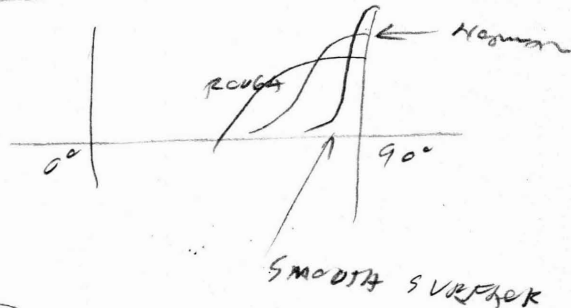
CURRENT PROBLEMS

"REMOTE SENSING" OF ENVIRONMENT  
 IMPLIED

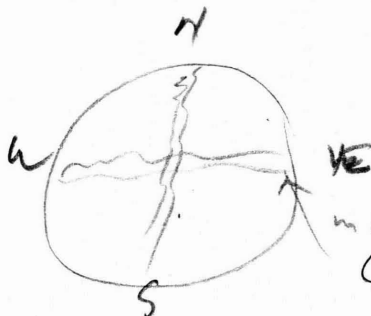
NASA (RADAR IS "ACTIVE REMOTE SENSING")

GEOD ⇒ MEAN SEA LEVEL.

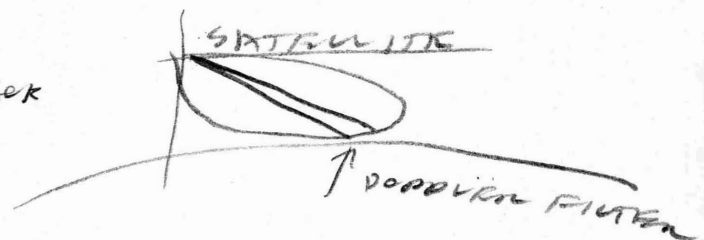
SCATTEROMETRY



∴  $\sigma_0$  VERSUS ANGLE  
 IS A MEASURE OF  
 SCATTER.



MIDWEST AIRBORNE P.O.I.  
 (TEMPERATURE, PARALLELNESS,  
 ROADS, FIELDS, ETC.)



M. A. Johnson & D. C. Stoner  
Heavy Military Equipment Department  
General Electric Company  
Court Street Plant, Syracuse, New York 13201

## INTRODUCTION

The previous paper by Steve Johnston might imply that for every possible mode of jamming, an appropriate counter has been invented and developed. Therefore, you all may be thinking there is little left to be concerned with. Apparently, all the radar designer need do is simply add sufficient counter techniques to satisfy the specified threat and ship the equipment.

Unfortunately, from the military customer's point-of-view (or should I say fortunately, from the continued engineering employment point-of-view), things are not quite that simple. There are four hurdles to cross before the Electronic Counter Counter Measures (ECCM) technique performance measured in the laboratory can be realized on an operating radar:

1. Many ECCM techniques require basic radar performance beyond that required in the absence of jamming. Improvement of the receiver stability, dynamic range, bandwidth rolloff or out-of-channel characteristics, and achievement of matched multiple receiver channels, for instance, may be necessary. Thus, it is usually necessary to review and possibly redesign the basic receiver in light of the ECCM techniques to be employed. In addition, some techniques make special demands on the transmitter and antenna.

2. When several ECCM techniques are to be employed, it may be found that they are incompatible with each other, so that they cannot be used simultaneously.

3. The presence of radar clutter of "friendly" interference may require counter techniques of their own which can work at cross purposes to the desired ECCM techniques.

4. One approach to the compatibility problem is to give the radar operator a jamming monitor and a set of switches so that he can choose those techniques which best counter the threat of the moment without using simultaneously incompatible techniques. There is a tendency with this approach, however, to give the operator so many choices that he is unable to find the right combination when he really needs it.

It is the intent of this paper to illustrate the kind of solution to these problems which has proven to be practical in the experience of the General Electric Company, and to show the general kind of

thinking which led to that solution. Due to the restrictions of time allotted and security, the answers to all threats and all design problems cannot be covered. However, the kind of approach necessary can be illustrated.

## DEFINITION OF AN ILLUSTRATIVE CASE

We shall consider a conventional 2-D air search radar which mechanically scans a fan beam in azimuth and radiates simple short pulses. The jamming and interference environment will include:

1. Multiple standoff jammers
2. Both narrow and wideband jamming
3. Continuous Wave (CW) and pulse interference.
4. Ground clutter
5. Weather clutter and/or chaff

Figure 1 illustrates an ECCM radar configuration we have evolved to meet this type of threat. It uses frequency domain, time domain, and spatial domain techniques combined to reduce the effect of the various kinds of jamming and interference, either singly or in combination. The techniques used are individually adaptive to the threat present to maximize radar performance with very little operator interaction required. Let us first briefly summarize its features, then detail them individually.

1. A frequency agile transmitter is adaptively programmed to the frequency of least interference.

2. Several auxiliary antennas and receivers are used to suppress sidelobe interference using both adaptive cancellation and short interval gating.

3. Ground clutter suppression is provided by appropriately tailored Moving Target Indicator (MTI) cancellation.

4. Chaff and weather clutter suppression is achieved by adaptively weighted cancellation.

5. A "clean" display presentation is provided by a Constant False Alarm Rate (CFAR) threshold utilizing split-window normalization.

6. Elimination of a synchronous pulse interference in the mainlobe is achieved by a pulse-to-pulse correlator.



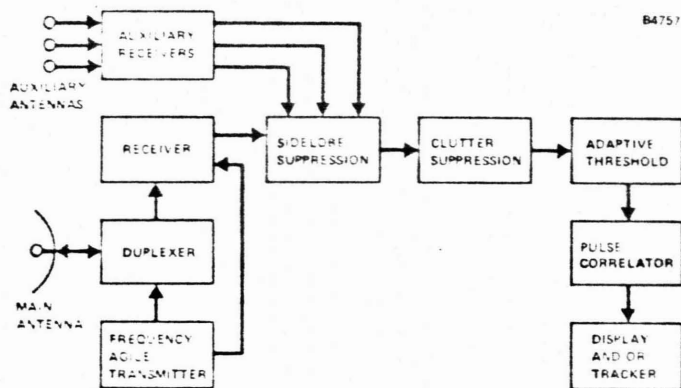


Fig. 1. ECCM Radar Configuration

## DESCRIPTION OF ECCM TECHNIQUES

### Transmitter

The basic technique applied here is frequency agility, appropriately programmed. An agility programmer is required to force a jammer to "spread" his energy over the entire agile bandwidth of the radar, thus reducing the effective jamming power. The agility programmer samples the interference prior to the next radar transmission (pre-look). This is done in such a way that the radar is not forced to change frequencies until the interference level is sufficient to degrade performance in a normal channel. The pre-look programmer is also very useful for the mainlobe jammer case in that spot jammers become less of a threat. It has been found that by examining the jammer spectrum and selecting a "hole" in this spectrum for the next radar transmission, a significant range improvement is obtainable. For typical parameters, the feature will also extend "burnthrough" ranges.

There are other benefits to be derived from the operation of this frequency agility over a wide bandwidth. If the frequency is varied over a reasonable percentage of the bandwidth in a systematic manner, it has the following advantages:

1. If the radar is used in an environment where a reflecting surface produces interference nulls in the elevation coverage pattern, the effects of a frequency agility will tend to fill in these nulls, hence eliminating the problem.

2. Pulse-to-pulse fluctuations of the target return caused by the frequency changes should increase the detection probability of the target.

In the "agile mode", the pre-look sampling of the environment occurs during the radar interpulse period (on a pulse-to-pulse basis) prior to each transmission. The next transmission then takes

place at the frequency of least interference. In the MTI mode, the pre-look sampling is accomplished after every fourth pulse to maintain the MTI processing.

### Receiver

The receiver uses dual conversion with a high dynamic range. Since the bandwidth at the receiver input will be broadband to accommodate the system frequency agility, the dual conversion assures that a jammer cannot transmit two frequencies separated by the first Intermediate Frequency (IF) and defeat the agility of the radar by producing a constant signal at the IF. The high dynamic range is essential to prevent a jammer of any realistic size from saturating the receiver and reducing system sensitivity.

A Sensitivity Time Control (STC) in the receiver reduces system sensitivity to avoid detections of birds, ground moving vehicles, etc. It also suppresses close-in ground clutter that may otherwise be acted upon by the sidelobe canceller system. By placing the STC actuators in front of the sidelobe cancellers, this problem was eliminated economically. Other solutions such as "sample-and-hold" techniques within the sidelobe canceller loop and directive auxiliary antennas are also viable solutions. One must take care that the former solution is not degraded in a "swept jamming" environment.

Since the Coherent Sidelobe Canceller (CSLC) used in this system represents considerable cost and capability, it is good strategy to use it only on jammers that are actually perturbing the used frequency of the radar. This is best accomplished by placing a filter matched to the radar transmission before each loop to reject out-of-band jamming. As an illustration: If a Radio Frequency ("RF") sidelobe canceller was used in the system which covered the entire agile bandwidth of the radar, it may devote all of its capabilities to the largest jammer in the agile band. If a smaller jammer is used to cover the transmission frequency, this CSLC arrangement may be effectively defeated. This, the loops preceded by the matched filter sees only the in-band jammer and simplification in the design of the auxiliary antenna system and the CSLC loops are achieved. To obtain maximum performance from the CSLC, each receiver (main and auxiliaries) must also be matched to each other.

### Sidelobe Suppression

The sidelobe suppression system consists of a coherent sidelobe canceller (CSLC) array (three loops) to remove barrage, CW and swept jamming and a compatible sidelobe blanking system to remove repeater and deception jamming.

The CSLC system is used to counter high-duty cycle jamming received in the sidelobes of the main antenna.<sup>1,2</sup> As shown in Figure 2, an auxiliary

antenna array is used to sample the jamming entering the sidelobes of the main antenna. This sampled signal is corrected in phase and amplitude to match that of the main antenna, and subtracted in a canceller system. The correlation between the jamming signal in the auxiliary antennas and the output signal to the summer are measured by the correlation mixer and the narrowband filter. This results in a weighted signal which is fed to the steering mixer and will amplitude weight and phase shift the auxiliary antenna signal also entering the steering mixer. These translated signals leaving the steering mixer are then subtracted from the main signal in the summing network. Cancellation thereby subtracts this array beam from the main antenna sidelobe pattern, forming a narrow null at the jammer location.

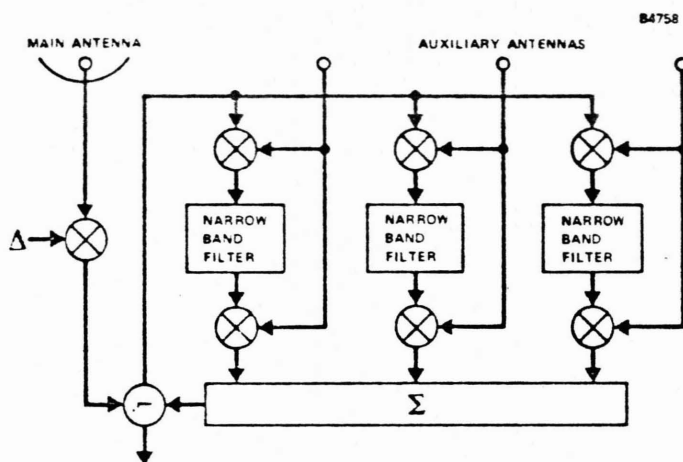


Fig. 2. 3-Loop Sidelobe Canceller

In addition to the interaction with a responsive sidelobe jamming threat, the CSLC must be configured, constrained and integrated into the radar system to insure it will perform its function without perturbing or degrading other system functions.

For example:

- It must not degrade noise figure or sub-clutter visibility in the normal environment where clutter may be present.

- It must perform in a multiple threat environment where Electronic Countermeasures (ECM), clutter and mutual interference may be present.
- It must be designed to not eliminate desired target signals.

Because this is a simple pulse system, the lockup time of the CSLC was made fast enough to achieve good cancellation without cancelling the signal.

The sidelobe blanker is used to remove low-duty cycle repeater of "spoofers" jammers entering the sidelobes of the main antenna in either a deception or saturation mode. The blanker utilizes two of the same auxiliary antenna and receiver systems as the CSLC to sample the signal, determine through logic processing the presence of these same signals in the sidelobes of the main antenna, and gate out the unwanted signals, as illustrated in Figure 3.

This logic is designed to allow compatible operation of the sidelobe blanking and the correlation sidelobe canceller in the presence of combined jamming.

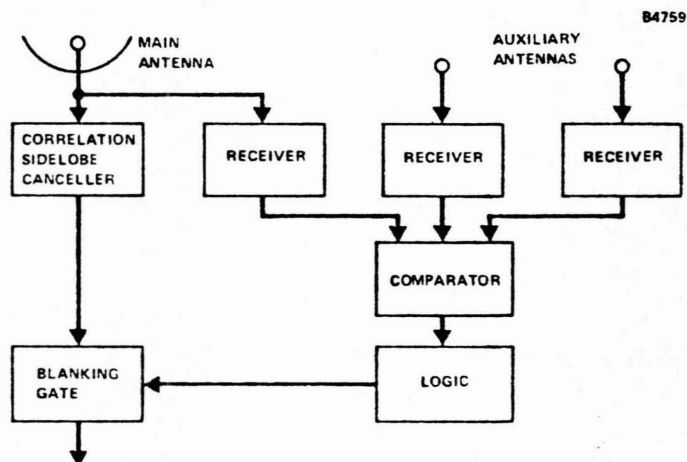


Fig. 3. Sidelobe Blanker

## Clutter, Chaff and Weather Suppression

The MTI system consists of two filters, a fixed-filter function for stationary clutter with the filter centered at zero Doppler and an adaptive-notch filter function for nonstationary clutter. The adaptive system is used to place the zero of the filter at the clutter Doppler response. This is shown in Figure 4.

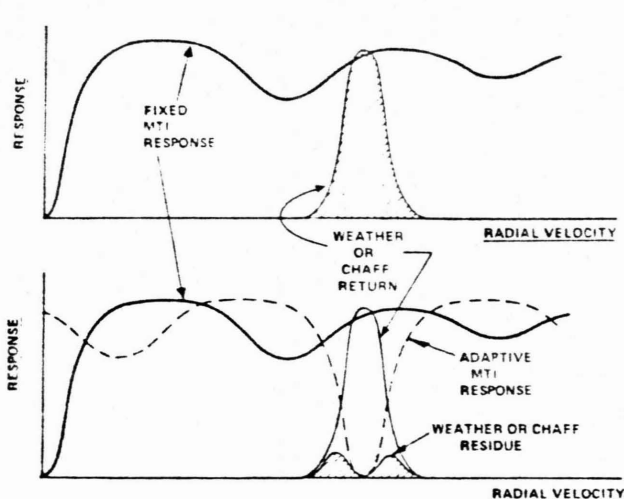


Fig. 4. MTI Response

The MTI function used for ground clutter is a conventional four-pulse MTI filter response with Pulse Repetition Period (PRP) stagger to remove the blind speeds. The system stability is adequate to support the improvement achievable with a four-pulse canceller. Any significant departure of the clutter spectrum from zero will result in poorer performance of the fixed-filter MTI.

To minimize the return from chaff and weather, the fixed-filter MTI is followed by the four-pulse adaptive MTI which is illustrated on Figure 5. The correlation loops placed at each tap output samples the output of the MTI filter and modifies the tap weights (phase and amplitude) to maximize the signal-to-interference ratio (SIR) at the sum output port. This configuration will maintain its performance in a continually varying clutter environment on a pulse-to-pulse basis.<sup>3</sup>

This clutter suppression scheme of a fixed and variable filter has worked well in a combination of mixed clutter spectra. The adaptive MTI varies its response to various clutter spectral shapes including both chaff and weather.

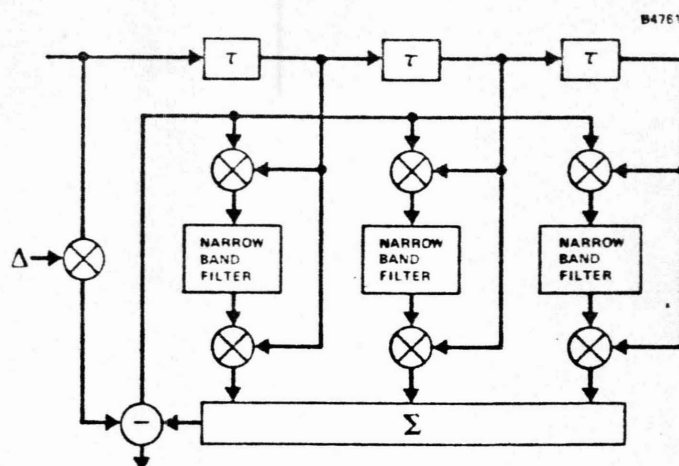


Fig. 5. Adaptive MTI

## Adaptive Threshold and Correlator

Automatic thresholding for target detection is provided by a normalizer (a CFAR device) and a two-pulse correlator [Pulse Repetition Frequency (PRF) discriminator] to reduce nonsynchronous interference. A functional diagram of the range normalizer and correlator is shown in Figure 6.

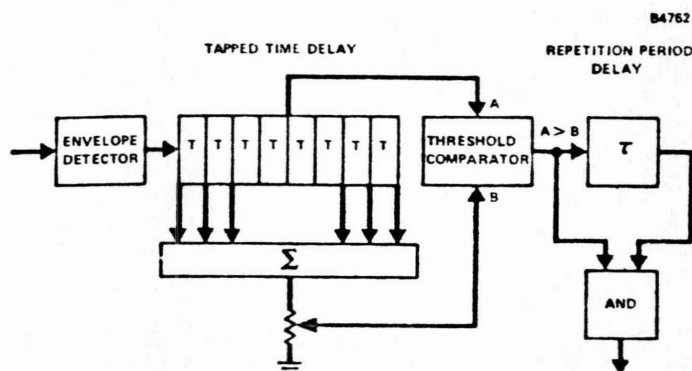


Fig. 6. Adaptive Threshold and Correlator

The range background estimator is probably the most cost-effective signal processing function one can implement. The adaptive threshold suppresses unwanted noise and other residual uniformly-distributed clutter while obtaining "super clutter visibility" on targets in the clutter region. This adaptive threshold is implemented as a range

normalizer to provide CFAR in a noise environment. While its primary purpose is CFAR in a receiver noise background, it also provides CFAR in any reasonably homogeneous interference. This device adjusts a threshold proportional to the mean background level in some number of range cells preceding and following the range cell under examination. When the range cell under examination is sufficiently large with respect to this background ( $A > B$ ), the normalizer gives a video output.<sup>4</sup> This output is then sent to the correlator, as shown in Figure 6. As stated before, the normalizer provides no sub-clutter visibility by itself, but it has proven an excellent adjustable threshold when as much interference as possible has been eliminated by the processor functions prior to its estimation processing. To prevent "capture" by a very large signal in a single range cell, the transfer characteristic preceding this device is a linear-logarithmic function.

This adaptive thresholding scheme is preferred over base clipping for an automatic detection system. With base clipping, if the detection level is set on the basis of receiver noise, then clutter returns over a large dynamic range will change the noise level and raise the false alarm probability drastically. This rise in the false alarms has an intolerable effect on automatic detection systems.

The two-pulse correlator following the normalizer serves several purpose. It essentially doubles the false-alarm rate of the adaptive threshold, thus decreasing the sensitivity required by the device alone. It also removes impulse jamming, even in the mainlobe, unless this interference has been synchronized to the radar PRF. The adaptive threshold and the correlator thus work together to reduce the false-alarm rate at the output of the radar system to a tolerable rate.

#### Other Design Considerations

The preceding portion of the paper has presented the selection and grouping of compatible techniques which enhance the sensor sensitivity to signal power while reducing sensitivity to clutter and jamming in a multiple threat environment. The incorporation of:

1. Frequency processing
2. Antenna pattern processing
3. Velocity processing
4. Time processing
5. Amplitude processing

have all been required to counter the environment.

It was important that these capabilities be "on-line" at all times and require minimum operator decisions to function properly. This not only insures

the proper response to the environment for maximum detection, but at the same time reduces operator training requirements. The operator is no longer required to recognize the total environment and adapt the radar lineup to that situation. Consequently, he needs to devote little time to this. The requirement that these features be self-compatible is a necessary condition.

In the system design, the compatibility of the frequency agility with the philosophy of MTI operation must be addressed. For this system, the ground rules were to maintain MTI operation at all times, giving it up only when the jamming becomes large enough to render it useless. This requires holding a single carrier frequency for at least four consecutive pulses. When extreme jamming is sensed, this requirement is automatically relaxed. Once the jamming has been effectively countered, MTI operation will resume.

It must also be remembered that this was a simple pulse, long range search radar with the PRP being compatible with the processing. With the advent of long duration waveforms, faster response times, higher PRP's, and more degrees-of-freedom care must be taken to avoid signal cancellation, distortion, low-level deception jamming and an increase in noise carryover or throughnoise in the range sidelobes of large Signal-to-Noise Ratio (SNR) returns. These will all degrade the performance of the ECCM processor if not handled properly. Since this particular design has worked well for this system does not mean it is appropriate for all situations. As always, each system must be examined in light of its own specification.

A radar ECCM processing lineup has not been designed to insure immunity from most ECM tactics. There are several additional tactics that come to mind which can with high probability defeat this radar processor. However, these tactics require that the jammer teams utilize considerable resource expenditures. This means that our processing performs its function well; that of maximizing the ratio of cost to defeat the system relative to the system cost.

#### QUALITATIVE PERFORMANCE RESULTS

Specific improvement performance cannot be given due to security restrictions. However, the following Plan Position Indicator (PPI) photographs were selected to give an indication of the performance of individual ECCM fixes and their working compatibility.

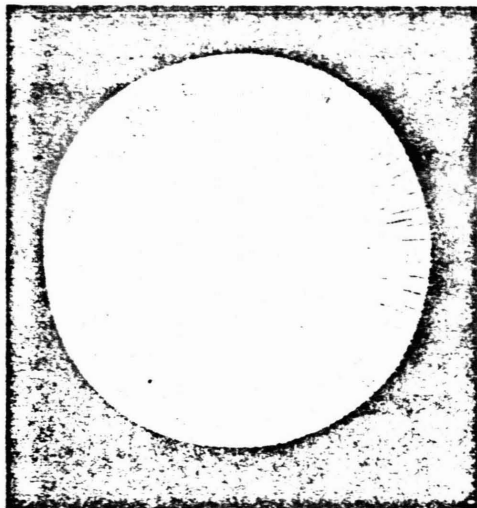
The photographs were taken at the General Electric facility with targets of opportunity and externally applied jamming signals. While the total ECCM processor is on-line in all the photos (i. e., the MTI is usually removing ground clutter that is always present) only the major ECCM contributor is described for its performance. The



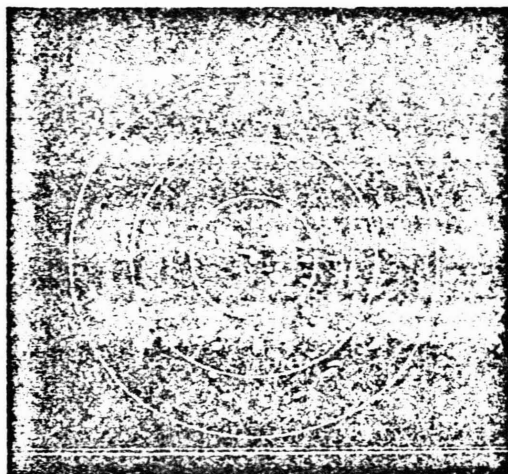
before photos are with basic receiver and the after photos are with the ECCM processor.

#### CSLC Against Swept CW

Figure 7(a) shows the effect of a narrowband swept CW jammer radiating 1000 W of Effective Radiated Power (ERP) without the CSLC connected. Figure 7(b) shows processed video due to the CSLC system. The range rings are 50 nmi each.



a. Cancellor Off



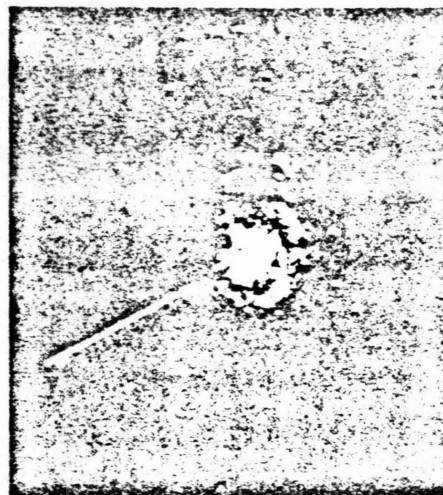
b. Cancellor On

Fig. 7. CSLC Performance with Swept CW

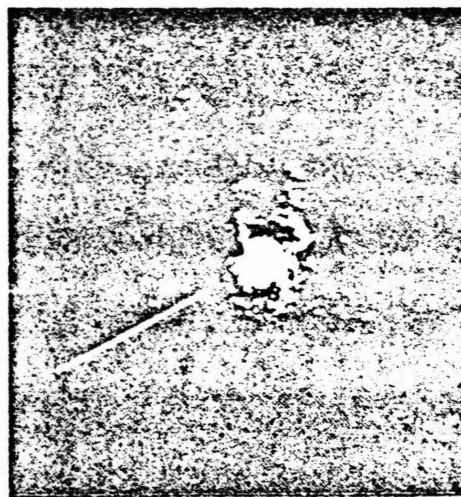
#### Sidelobe Blanker Operation

These photos were taken during flight tests at an operational site with controlled aircraft. The solid strobe line in the photograph is a result of instrumentation being used and would not normally be present.

Figure 8(a) shows the false target repeater in the false target mode of operation. The false targets are close to maximum range at 11 o'clock. The effectiveness of the sidelobe blanker is seen in Figure 8(b) where the true targets are visible and the false targets have been removed.



a. Sidelobe Blanker Off



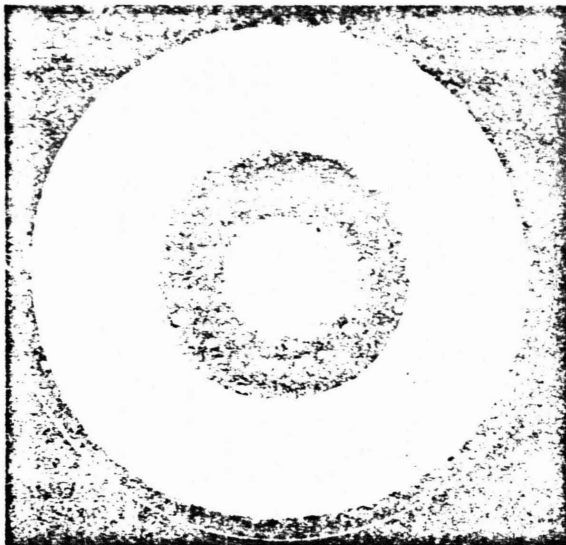
b. Sidelobe Blanker On

Fig. 8. Sidelobe Blanker Performance with False Targets

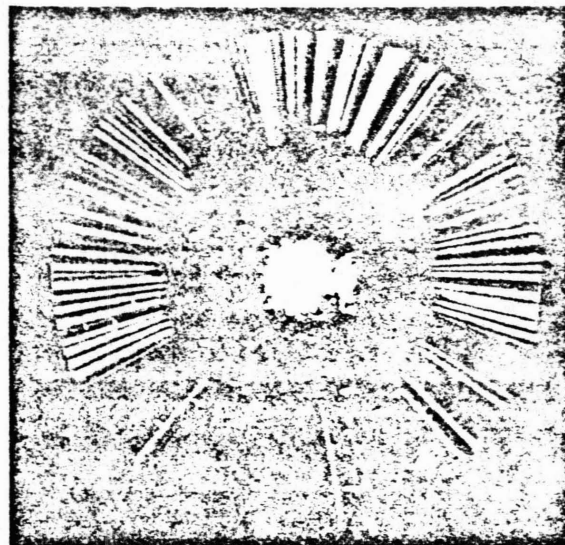
### Sidelobe Blanker and CSLC Compatibility

Figure 9 demonstrates the compatibility of the two sidelobe suppression techniques. Figure 9(a) shows a high-duty cycle jammer obscuring targets from maximum range into a fixed range with both sidelobe suppression fixes off. Figure 9(b) has only with the sidelobe blanker on and demonstrates how it "breaks down" under this high-duty cycle jamming to prevent it from shutting down the radar continuously. At these higher duty rates, the CSLC should turn on and cancel the jamming as shown in Figure 9(c). Note that with only the CSLC on in Figure 9(c),

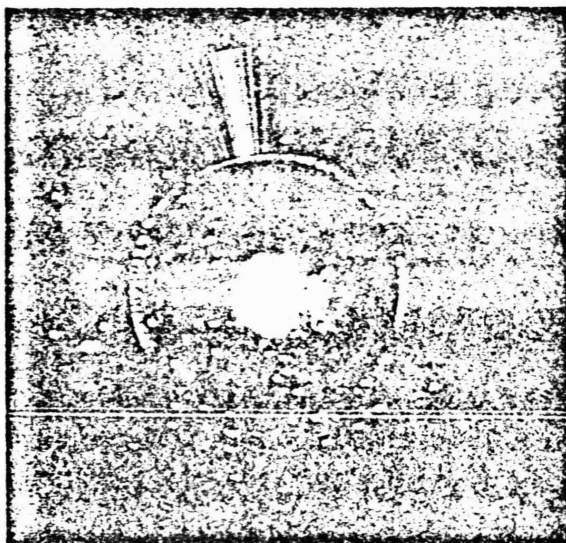
there is a continuous ring around the PPI photo at close range. This is caused by the CSLC lockup time. (The CSLC is continuously locking and unlocking on this high-duty cycle repeater jammer.) It is during this time that the radar is still vulnerable to any low-duty cycle jamming. Figure 9(d) is taken with the sidelobe blanker and the CSLC both on. Note that the ring in Figure 9(c) is now gone. The sidelobe blanker is now blanking any low-duty cycle jamming during the CSLC lockup time and the CSLC turns on to cancel the high-duty cycle jamming. The MTI was off-line during this photo sequence.



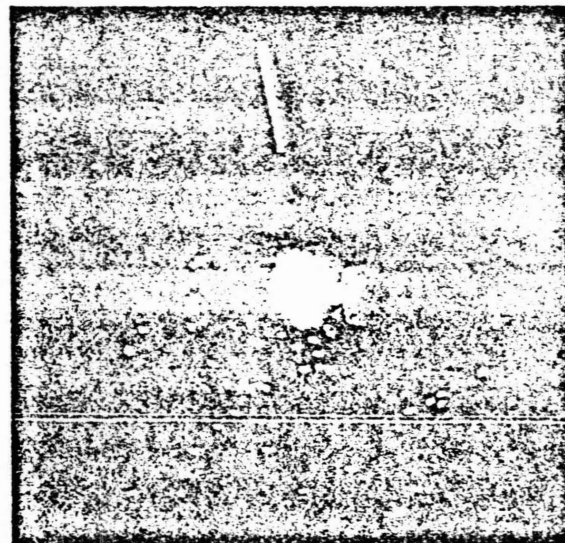
a. Both Blanker and CSLC Off



b. Only Sidelobe Blanker On



c. Only CSLC On

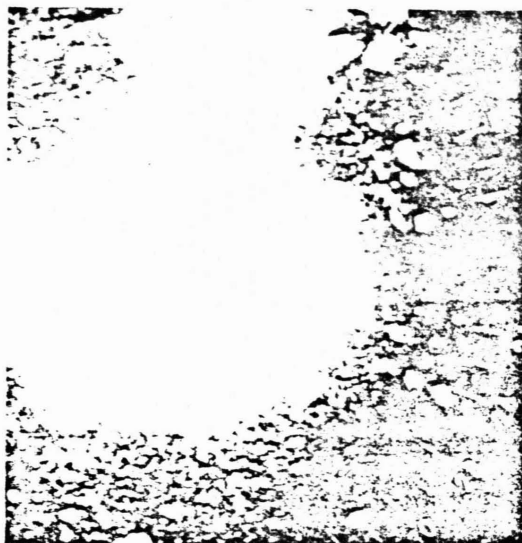


d. Both Blanker and CSLC On

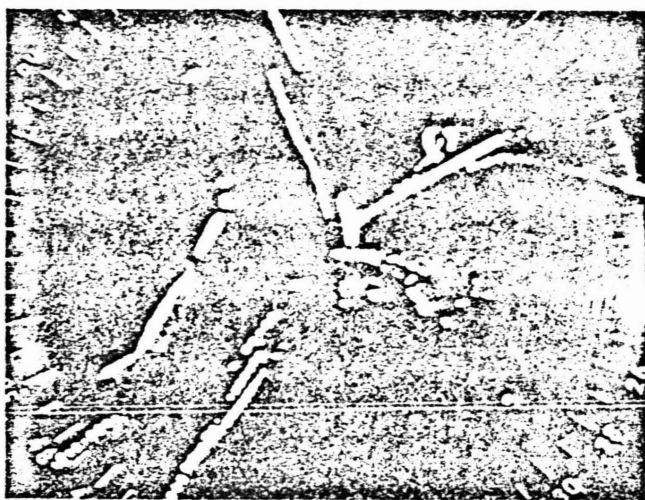
Fig. 9. Combined Sidelobe Blanker and CSLC Performance with High-Duty Cycle Pulse Jammer

### Clutter, Chaff and Weather Suppression

Figure 10 shows MTI and adaptive threshold performance. Figure 10(a) shows the close in ground clutter profile with no MTI or adaptive threshold. Figure 10(b) demonstrates the close in improvement achieved in this ground clutter. This photo has an elapsed exposure time to show the traceability of the targets.



a. MTI and Adaptive Threshold Off



b. MTI and Adaptive Threshold On

Fig. 10. Ground Clutter Suppression Performance

Figure 11 shows the adaptive MTI working against a chaff drop at 100 nmi. The top photos show a chaff drop with a test target ring inserted for test purposes. Both the PPI and A-scope photos are shown for clarity. The bottom set of photos are with the adaptive MTI, on-line.

### Compatibility of Sidelobe Suppression, Clutter Suppression and Adaptive Threshold Techniques

The three pictures on Figure 12 indicate the combined performance of the CSLC eliminating barrage jamming, the MTI eliminating ground clutter, the adaptive MTI eliminating a weather storm and the adaptive threshold action to maintain a false alarm rate to the PPI.

Figure 12(a) shows the profile of a weather storm out to approximately 60 nmi, where the ground clutter still exists at the site (shown previously in Figure 10(a)). Figure 12(b) is barrage noise jamming which is greater than 100,000 W of ERP from a standoff jammer at 100 nmi. Figure 12(c) gives an indication of the performance delivered by this compatible lineup operating to give a clear target presentation.

### Pulse-to-Pulse Correlation

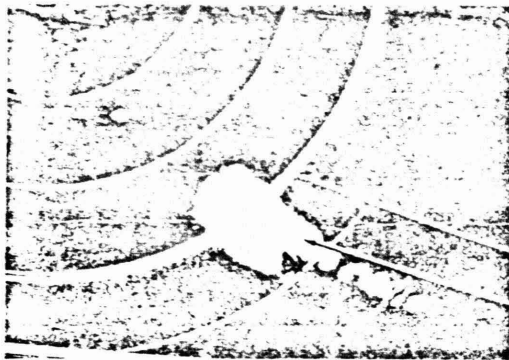
The effect of the correlator is shown in Figure 13. Figure 13(a) shows a PPI display with mutual interference present, and Figure 13(b) indicates the results of the correlator action to remove the interference.

### CONCLUSION

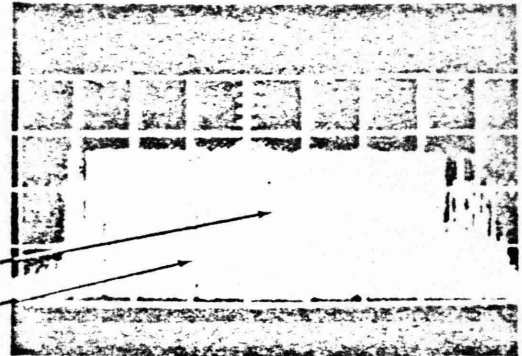
The ECCM radar configuration we have described has proven to be highly effective in operational use. It provides reliable performance and requires little operator intervention to counter a wide range of ECM and interference threats. It has extended the basic radar capability to cope with these threats at a cost which is only a fraction of the unprotected radar cost. This has been achieved by selecting a relatively small number of inherently adaptive and complementary ECCM techniques which had been individually proven, and carefully integrating them into the complete system. In view of the currently expected ECM threat and the success of this counter approach, we believe that it should be designed into or added to all currently considered operational military radar systems.

This obviously is not the end of the story. Both the total ECM threat and the types of radars employed are gradually but continuously growing. Consequently, it will be necessary not only to develop and evaluate effective new ECCM techniques, but also to integrate them into complete operational radars.

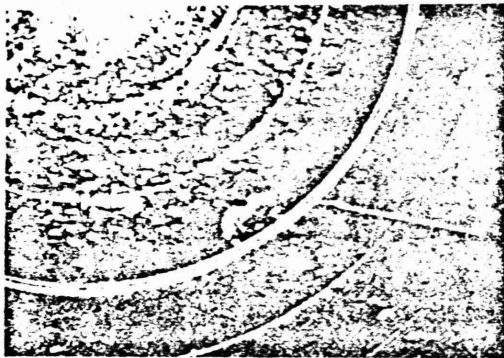




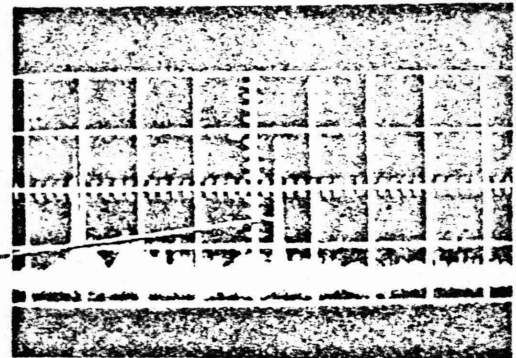
a. Scanning PPI Display -  
Adaptive MTI Off



c. Searchlight A-Scope Display -  
Adaptive MTI Off



b. Scanning PPI Display -  
Adaptive MTI On

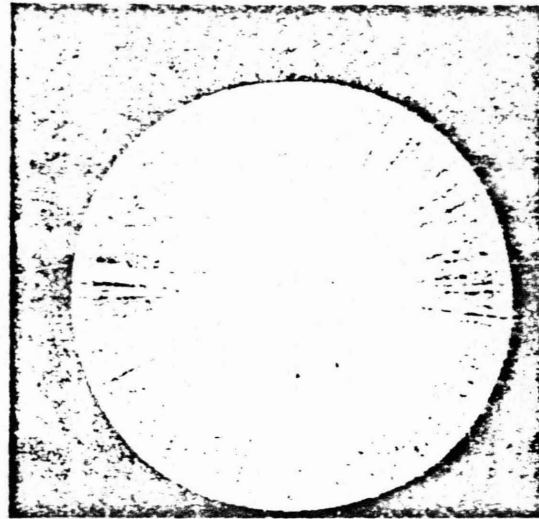


d. Searchlight A-Scope Display -  
Adaptive MTI On

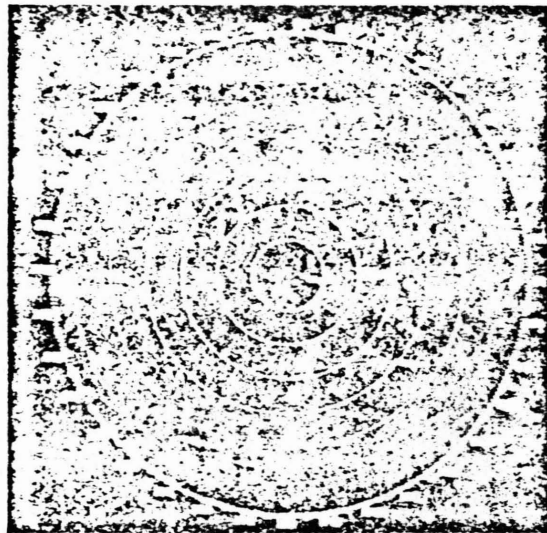
Fig. 11. Adaptive MTI Performance with Chaff



a. Weather and Ground Clutter

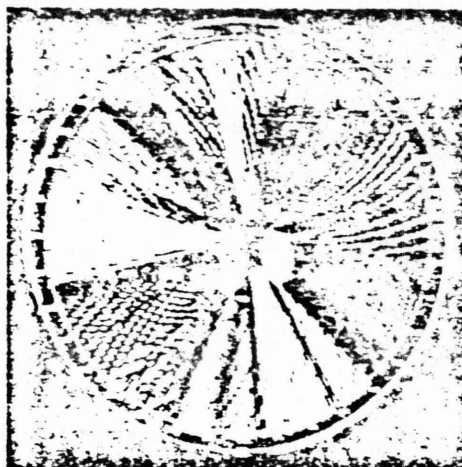


b. High-Power Barrage Noise Jamming

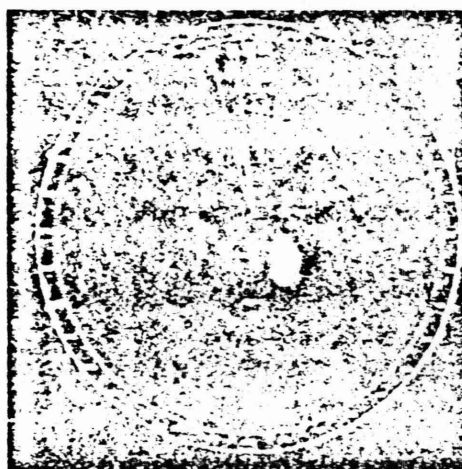


c. Sidelobe and Clutter Suppression Plus  
Adaptive Threshold

Fig. 12. Compatibility of Sidelobe Suppression, Clutter Suppression and  
Adaptive Threshold



a. Correlator Off



b. Correlator On

Fig. 13. Correlator Performance - With Mutual Interference

#### REFERENCES

1. Bernard L. Lewis and James P. Hansen, "Understanding and Optimizing Multiple Sidelobe Canceller Operation", NRL Report 7610, October 1973.
2. F. F. Kretschmer, "Effects of Cascading Sidelobe Canceller Loops", The Record of the IEEE 1975 International Radar Conference, April 1975.
3. Lloyd J. Spafford, "Optimum Radar Signal Processing in Clutter" (U), IEEE Transactions on Information Theory, Vol. IT 4, No. 5, September 1968, pp. 734-743.
4. L. W. Bauer, "Detection in the Sonar Environment" TIS No. R69EMH21, Class 1, GE Company, June 1969.

# H.F. OVER THE HORIZON RADAR

- IONOSPHERE PROVIDES OVER THE HORIZON CAPABILITY.

= IONIZATION OCCURS FROM SOLAR ENERGY.

- LAYERED. REFLECTS HIGH ALT (NOT ENOUGH PROBLEMS)  
LOW ALT. (NOT ENOUGH ENERGY)

- "D" LAYER 60-90 Km - ATTENUATION

- "E" LAYER 100-140 Km - PROPAGATE TO 1000 MILES  
AT LOWER FREQUENCIES,

WORKS { - "F"  
          - "F<sub>1</sub>" 230-400 Km (1800-2000 NAUTICAL MILES.)  
          - "F<sub>2</sub>" (HIGHER FREQUENCY)

REFRACTION VARIES WITH DENSITY AND  
HEIGHT

② VHF PASSES THROUGH,

MAXIMUM USEABLE FREQUENCY  
(HEIGHT AT WHICH REFRACTION  
BACK TO EARTH OCCURS AT 90  
DEGREES.)

H.F. (3-30 MHz) (5-30-TYPICAL USEABLE  
FOR RADAR)

- RADAR CAN AVOID BLACKOUTS BY LISTENING  
TO CHIRPSELF.

- ALSO MORE POWER.

- CHOICE OF FREQUENCY DEPENDS ON  
TIME OF DAY AND LOCATION OF  
TARGET.

- SKIP ZONE 500 MILES

∴ 500 - 2000 MILES TYPICAL RANGE.

Table 4.3. CHARACTERISTICS OF THE VARIOUS REGIONS  
IN THE IONOSPHERE

Particulars	D region	E region	F1 layer	F2 layer
Likely origin	(a) Ionization of NO with Lyman-alpha radiation (b) Ionization of all gases by soft X-rays	Ionization of all gases by soft X-rays	Ionization of O with fast decrease of recombination coefficient with height	Ionization of O by UV, X-rays and probably corpuscular radiation
Height, km	60-90 by day; disappears at night	100-140	180-240 by day; disappears at night	230-400
Molecular density, per cubic centimetre	$10^{14}$ - $10^{16}$	$5 \times 10^{11}$ - $10^{13}$	about $10^{11}$	about $10^{10}$
Electron or ion density, per cubic centimetre	$100$ - $10^3$ for electrons; $10^6$ - $10^8$ for ions	up to $10^5$ to $4.5 \times 10^5$ by day; fixed at about $5 \times 10^3$ to $10^4$ at night	$2 \times 10^3$ - $4.5 \times 10^5$	max. $2 \times 10^6$ by day in winter; max. $2 \times 10^5$ by day in summer, $3 \times 10^5$ at night in winter
Collisions, per second	$10^7$ at lower edge	$10^5$	$10^4$	$10^3$ - $10^4$
Recombination coefficient, cu. cm per sec	$10^{-8}$ - $10^{-7}$	$10^{-8}$	$4 \times 10^{-9}$	$8 \times 10^{-11}$ by day; $3 \times 10^{-11}$ at night

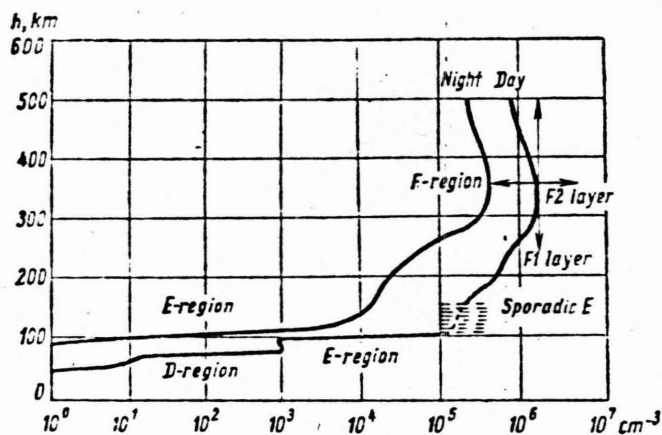


Fig. 4.8. Approximate distribution of electron density with height by day and at night. The arrows show the limits of variations for the height and electron density for the F2 layer

# "TYPICAL"

- 20 - 30 dB  $\hat{G}$  IN ANTENNAS
- 300 m RTING OR LONGER ANTENNAS
- SEVERAL HUNDREDS OF KW AVG, PWs
- PULSE DOPPLER - FM - CW  
TO REMOVE CLUTTER,
- DWRN TIME - SECONDS
- EXCELLENT RESOLUTION IN DOPPLER  
DOMAIN

microwave  $P_{max} = \frac{P_t G \lambda^2 \sigma_{th}}{(4\pi)^3 K T_0 F_n B (S/H)_0}$

USUAL SEPARATE ANTENNAS

H.F.

$P_{max} = \frac{P_{av} G_t G_r \lambda^2 \sigma F_p T_c}{(4\pi)^3 N_0 (S/H_0)}$

PROPAGATION

EXTERNAL NOISE + OTHER  
USING.

- LIKE 1 mhz PULSE WIDTH  
 $\therefore$  USE LONG PULSES.
- PICK LITTLE USED FREQ. BAND.



- MINIMIZE SKIP BY LOWER FREQUENCY.
- CHANGE ANGLE OF RADIATION TO CHOOSE  
DISTANCE  
 $\therefore$  BETTER HORIZONTAL HIGH UP  
TO STEER ANGLE,



# Over-the-Horizon Radar in the HF Band

JAMES M. HEADRICK, SENIOR MEMBER, IEEE, AND MERRILL I. SKOLNIK, FELLOW, IEEE

*Invited Paper*

**Abstract**—Over-the-horizon (OTH) HF radar using sky-wave propagation via refraction by the ionosphere is capable of detecting targets at distances an order of magnitude greater than conventional microwave radar limited by the line of sight. Some of the characteristics, capabilities, and limitations of OTH radar based on the experience of the MADRE radar as developed by the Naval Research Laboratory are described. Also discussed is the application of OTH radar to air-traffic control and to the remote sensing of sea conditions.

## I. INTRODUCTION

RADAR frequencies are generally synonymous with microwave frequencies. The standard radar bands (Fig. 1) established by the International Telecommunications Union (ITU) extend as low as VHF, but the lowest frequency band (137–144 MHz) is now used chiefly for experimental purposes. The next lowest band (216–225 MHz) has limited operational application, but the vast majority of radars in the United States operate at UHF or higher.

Radars at the lower frequencies suffer from a crowded spectrum, limited bandwidth, high ambient noise, and wide beamwidths. Nevertheless, there have been significant applications of radar in the HF band<sup>1</sup> in the past. The earliest "radars" were at HF and were used to measure the height of the ionosphere. In the middle 1920's Appellton employed FM-CW equipment, and Breit and Tuve used pulsed equipment to determine the ionospheric height by what would now be considered classical radar methods. The first operational military radar system was also at HF. This was the CH radar system installed by the British in 1938 for aircraft detection. These line-of-sight radars, which were crude by modern standards, were given credit for a major contribution in defending against German bombers during the Battle of Britain and conclusively demonstrated the worth of radar. They were built at HF because there was no other alternative available for a system that had to be installed in 1938. They did the job well, however. Just prior to World War II, radar frequencies reached up to about 200 MHz, and during the war the microwave region was exploited successfully.

UHF and microwave radars are used widely in both military and civilian applications, and it is unlikely that frequencies outside this relatively large portion of the electromagnetic (EM) spectrum will be competitive for the majority of current applications. However, there is a very important property of the HF region that has always been of interest to the radar designer, if it could be properly exploited. This property is the ability of HF radiation to propagate beyond the line of sight

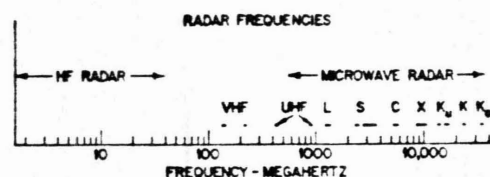


Fig. 1. Frequency spectrum showing the relationship between HF radar frequencies and conventional microwave radar bands (letter designations) as assigned by the ITU for Region II.

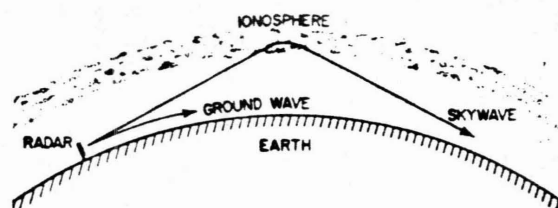


Fig. 2. Geometry of sky-wave and ground-wave propagation.

by either ground waves diffracted around the curvature of the earth or sky waves refracted by the ionosphere (Fig. 2). The range of a ground-wave HF radar typically might be of the order of 200–400 km, and the coverage of a sky-wave radar might extend from a minimum of 1000 to perhaps 4000 km or more. The HF over-the-horizon (OTH) radar can extend the 400-km range typical of a ground-based air-surveillance radar by an order of magnitude. The area covered increases by about two orders of magnitude.

The targets of interest to an HF OTH radar are the same as those of interest to microwave radar and include aircraft, missiles, and ships. The long wavelengths characteristic of HF radar also provide a means for gathering information about the sea and land, as well as aurora and meteors.

Experiments with OTH radar began at the Naval Research Laboratory early in the 1950's. It was realized that if targets of interest were to be seen, the extremely large undesired clutter echo returned from the ground must be suppressed relative to the target signal. For example, the echo from the ground might easily be 40–80 dB greater than an aircraft echo, depending upon antenna beamwidth and pulsewidth. To increase the target-to-clutter ratio requires high resolution in range and angle and excellent Doppler-frequency discrimination as in a moving target indicator (MTI) or pulse Doppler radar. At HF, sufficient resolution in angle and/or range to suppress completely the clutter echo is difficult to achieve. For example, a 1° beamwidth requires an antenna of the order of 2 km. Range resolution requires a wide-signal bandwidth, but it is seldom that the ionosphere can effectively support an instantaneous bandwidth greater than about 100 kHz, which corresponds to a range resolution of roughly 1½ km. Even with

Manuscript received September 18, 1973; revised January 7, 1974.

The authors are with the Naval Research Laboratory, Washington, D. C. 20375.

<sup>1</sup> Although the HF band is defined by the ITU to extend from 3 to 30 MHz, definitions are sometimes arbitrary. Here HF is meant to include those frequencies just above the broadcast band and extending up to 40 MHz or more.



SUMMER NOON IS WHEN<sup>MAX.</sup> POWER  
IS REQUIRED

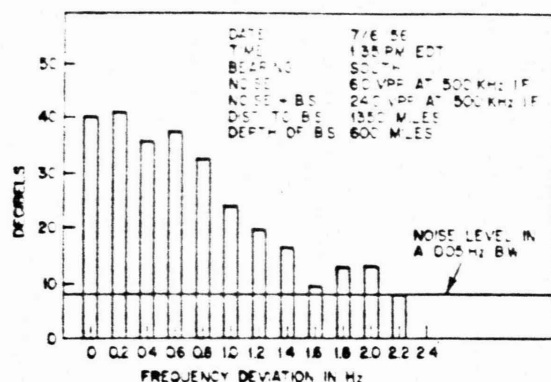


Fig. 3. A typical earth backscatter (BS) energy distribution showing the distribution of the backscattered energy and also the frequency at which this energy has diminished to the level of the noise in the 0.05-Hz bandwidth. The line structure of the graph is not due to a discrete modulation frequency since the backscatter signal is continuous with the frequency, but rather represents the average amplitude measured in a 0.05-Hz bandwidth filter over a 2-min period positioned in successive 0.2-Hz steps.

such range and angular resolution, sea clutter at a distance of 3000 km can be a target as large as perhaps  $10^6 \text{ m}^2$ . Doppler processing is thus clearly needed in an OTH radar for most targets.

In 1956 the Naval Research Laboratory concluded a definitive set of experiments that showed HF sky-wave radar could succeed for aircraft detection. First, aircraft targets were examined line-of-sight and found to give coherent echoes. The Doppler shift  $f_d$  from the radar carrier frequency  $f_0$  is given by the relation

$$f_d = \frac{2V_r f_0}{c} \quad (1)$$

where  $V_r$  is the target relative velocity and  $c$  is the velocity of light. For aircraft targets  $f_d$  was generally a very-well-defined frequency in the slightly above 0- to 50-Hz range. Second, one-way sky-wave paths had been measured to be frequency-stable at least for the order of seconds. The conclusive experiment that indicated OTH detection was feasible for aircraft targets employed a coherent pulse Doppler radar to examine the echo from the earth, and showed that the return from the earth by a sky-wave path was well-confined in spectral content to the very low Doppler frequencies. Fig. 3 taken from an early Naval Research Laboratory report describing that experiment, shows that the amplitude of the earth backscatter frequency spectrum is reduced at least 32 dB at a frequency 2.2 Hz removed from the carrier. In this measurement, the area of earth illuminated by the coherent pulse Doppler radar was 1100 by 1300 km, and included both land and ocean surface. (This is a cell size area about three orders of magnitude greater than would be used for an OTH radar.) Data such as these, and measured aircraft radar cross sections, were used to predict that OTH detection with a Doppler radar was possible. The limits of performance appeared to be controlled by the dynamic range achievable in receivers and in the signal processors. The Naval Research Laboratory then embarked on a program to apply Doppler processing to OTH radar. The heart of the initial development was a cross-correlation signal processor that utilized a magnetic drum as the storage medium. Under Air Force and Navy sponsorship, a

high-power transmitter and antenna suitable for testing aircraft detection feasibility were added, and in the fall of 1961 aircraft were detected and range tracked over the major portion of their flights across the Atlantic. Continual improvements in signal processing were made by the use of ferrite-core memory devices, capacitor-store devices, and digital processing. The signal processor has been the key element in the success achieved with OTH radar.

In this paper, the basic nature of OTH radar will be reviewed with emphasis placed on those properties and characteristics that differ from those found at microwaves. The sky-wave radar will be considered chiefly, but some brief mention will also be made of the shorter range OTH radar that utilizes the ground-wave mode of propagation.

## II. CHARACTER OF HF RADAR

Some of the characteristics and problems of HF OTH radar can be identified by an examination of the familiar radar range equation. A form commonly used in OTH Doppler radar analysis is

$$R_{\max}^4 = \frac{P_{\text{av}} G_t G_r \lambda^2 \sigma F_p T_c}{(4\pi)^3 N_0 (S/N) L_s} \quad (2)$$

where

$R_{\max}$	maximum range;
$P_{\text{av}}$	average power;
$G_t$	transmitting antenna gain;
$G_r$	receiving antenna gain;
$\lambda$	wavelength;
$\sigma$	target cross section;
$F_p$	factor to account for propagation effects;
$T_c$	coherent processing time;
$N_0$	noise power/unit bandwidth;
$(S/N)$	signal-to-noise ratio required for detection;
$L_s$	system losses.

The transmitting and receiving antenna gains are shown separately since in some OTH radars it is convenient to have separate antennas for these functions. It is in  $F_p$ ,  $N_0$ , and  $T_c$  that the major differences between sky-wave and microwave radar lie. The factor  $F_p$  contains ionospheric path energy loss, polarization mismatch loss, ionospheric focusing gain or loss, and losses due to the dynamic nature of the path [1], [2].  $N_0$  contains the noise power expected from natural sources [3] and in addition (and frequently more important) the effects of other HF band user interference. The processing time  $T_c$  [which is equal to the number of hits integrated divided by the pulse-repetition frequency (PRF)] is included in this form of the equation to emphasize that this is a Doppler radar that requires a dwell time of  $T_c$  seconds if a frequency resolution of  $1/T_c$  hertz is to be achieved.

In the design of an OTH radar an adequate signal-to-noise ratio (SNR) is not the only criterion for detectability. The signal-to-clutter ratio must also be sufficient. Thus such factors as the resolution cell size may be more important in an OTH radar than in conventional radar.

A "typical" OTH radar designed for the detection of aircraft at ranges out to 4000 km might have an average power of several hundreds of kilowatts, antenna gains from about 20-30 dB, and operating frequencies from several megahertz to several tens of megahertz. Antennas must be big to obtain

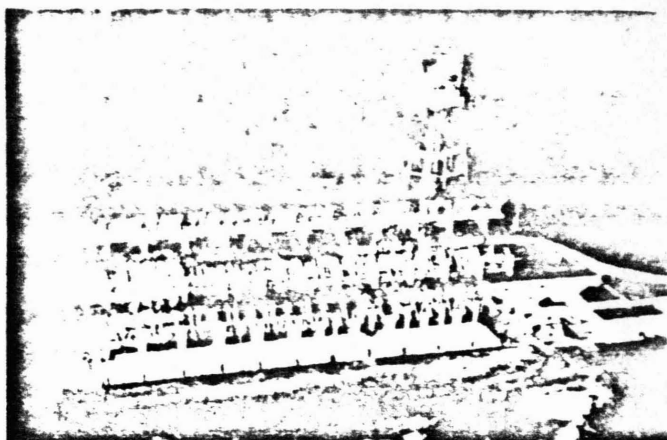


Fig. 4 MADRE OTH radar located at the Chesapeake Bay field site of the Naval Research Laboratory. The auxiliary rotatable antenna located above and behind the main planar antenna is used for experiments in directions not within the coverage of the main antenna.

reasonably small beamwidths. An antenna horizontal length of 300 m might be typical.

The transmitted waveform (signal format) can be CW, simple pulse, FM-CW, chirped pulse, or other coded waveforms [5]. Pulse compression is used for the same reasons as in microwave radar. Because of the skip zone, the HF OTH sky-wave radar does not detect targets within about 1000 km so that problems of minimum range, as might occur with sophisticated pulse waveforms, do not generally exist.

The Naval Research Laboratory's MADRE OTH radar is shown in Fig. 4. This is an experimental radar that first went into operation in 1961. The antenna is 98 m wide by 43 m high and consists of twenty corner reflector elements arranged in two rows of ten elements each. The beam is steered  $\pm 30^\circ$  in azimuth with mechanically actuated line stretchers. Shown above and behind this fixed main antenna is a rotatable antenna 27 m in width that is used to obtain coverage in directions other than that of the main antenna. This experimental radar has been generally operated with average powers from 5 to 50 kW.

In a microwave radar, the receiver sensitivity is usually determined by the internal noise generated within the receiver itself. External noise seldom affects the sensitivity. The opposite is true at HF. External noise due to atmospherics (lightning), cosmic noise, man-made noise, and other HF radiating sources can be significantly greater than internal receiver noise. The combined effects of interference from the many other users of the HF band is an especially major contribution to the receiver noise level. Fig. 5 plots a typical example of external noise in the HF band. The expected atmospheric and cosmic noise level would be at the bottom of the graph and is lower than the noise which is often experienced in practice. Note that the actual noise levels can be quite high and are not uniform across the band. If narrow-band operation can be tolerated (perhaps a spectral width of 5 or 10 kHz) many relatively clear regions can be found in which to operate. The nonuniformity of the ambient noise spectrum means that large-bandwidth systems might have to compete with a higher value of  $N_0$  (noise power per unit bandwidth) than might narrow-band systems.

External noise is not the only effect that can limit receiver sensitivity. As mentioned in the preceding, an OTH radar

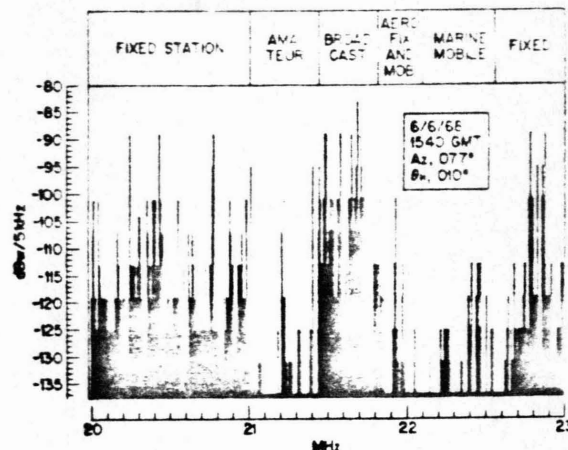


Fig. 5. Typical spectrum of the noise and interference experienced at HF as measured within a 5-kHz bandwidth. The noise due to atmospheric and cosmic sources is at a level of approximately -140 dBW (140 dB below 1 W). Note the correlation of the level with user allocations.

illuminates a large portion of the surface of the earth, and the land or sea echo is generally so large that it dominates the external noise level and the target echo. Generally, some form of Doppler signal processing is necessary to extract the desired moving target from the undesired background clutter. In principle, Doppler processing in an HF radar is similar to the MTI or pulse Doppler methods employed in microwave radar but with important modifications to allow for the specific characteristics of HF radar. Doppler filter bandwidths from 1 Hz down to 0.05 Hz may be used depending upon the target's characteristics and the stability of the propagation path. The addition of noncoherent processing is generally of benefit.

Just as other users of the HF band produce interference that can limit the sensitivity of HF radar, the HF radar can cause interference to other users if care is not taken. An approach to interference minimization is to use narrow-band waveforms (in the extreme, monochromatic continuous waves) whose spectral energy can be fitted within channels where no other user can be detected. The waveform in a radar like MADRE is a compromise between range resolution, which requires wide bandwidth, and interference elimination, which requires narrow bandwidth. To properly utilize narrow-band waveforms to minimize or eliminate interference by occupying quiet regions of the spectrum, frequency flexibility is necessary.

A narrow spectrum implies a long pulse. A long pulse is important in achieving the energy required for long-range detection. It is also desirable to shape the transmitted pulse (or pulse elements in a coded waveform) so as to reduce the spectral energy contained at frequencies far from the carrier. This precaution is also true for FM-CW, thus making it equivalent to a very long frequency-modulated pulse. A cosine-squared pulse shape has been successfully used with MADRE. When proper precautions are taken, experience has proven that there are but few complaints of HF radar interference to other users of the band.

Considering radar cross section, most targets are in the optical region for microwave radar. In contrast, for HF radar some targets can be in the resonance region and when operating at the lowest frequencies, even lie in the Rayleigh region. The cross section decreases rapidly with decreasing frequency in the Rayleigh region [4]. Fortunately, for many targets of

interest and for the usual frequency range of operation, the cross section seldom falls within this region.

A sky-wave OTH radar utilizes the ionosphere to refract the energy back to the earth's surface. The ionosphere determines the range of operation and introduces an additional path loss. The motions inherent in the ionosphere can limit the Doppler processing and the accuracy of the angular measurement. It is important in a radar of this type that the frequency of operation and the signal parameters be chosen to minimize the adverse effects of the ionosphere. It is generally easier to operate a radar to compensate for ionospheric propagation effects than it is with HF communications. In communications, two parties—the transmitter and receiver—must cooperate in order to have an effective path. In radar, there is only one party. Communicators usually operate with a limited set of frequency allocations. For the radar, it is assumed that the best frequencies are available, provided they do not interfere with others. The nature of the radar clutter echo can be used to determine the proper mode of operation. The effective use of frequency and signal waveform flexibility to operate successfully in spite of the vagaries of the ionospheric propagation path is an advantage of radar, as described in Section III.

The waveform repetition frequency of an OTH radar is generally low so as to avoid range ambiguities. A pulse-repetition frequency (PRF) of 50 Hz, for example, corresponds to an unambiguous range of about 3000 km. Because the PRF is low, Doppler ambiguities can result and a compromise is generally required between the range and Doppler ambiguities. Typical pulsewidths might vary from tens of microseconds to several milliseconds.

The magnetoionic part of the transmission path rotates the plane of polarization so that fading of the echo can occur if linear polarization is transmitted and received [1], [2]. Polarization fading can be reduced by receiving on two orthogonal linear polarizations when a single linear polarization is transmitted. Circular polarization can eliminate fading due to polarization rotation; however, it is expensive to achieve in a practical HF radar antenna. Because of the proximity of the antenna to the earth (relative to the wavelength), the ground must always be considered part of the antenna. The ground effects are generally different for horizontal and vertical polarization so that an initially circularly polarized wave might actually be launched as elliptical polarization and the ellipticity will be a function of the vertical radiation angle.

Multipath interference and dynamic irregularities in the ionospheric propagation path are two other sources of fading. Multipath effects with sky-wave radar are important and some will be identified. First, the previously mentioned polarization rotation can be considered a multipath effect. This rotation is due to the birefringence nature of the refracting medium (electrons in the presence of the earth's magnetic field). An incident linearly polarized wave can be thought of as decomposing into two circularly polarized components, one right handed and the other left handed, each traveling by its own distinct path and path length through the ionosphere, and upon emergence the combination of the two components can again give a linearly polarized wave, in general rotated from the incident wave. Second, waves refracted by an increasing electron density with height will generally have two paths from the radar to the target, a high ray and a low ray. The high ray experiences more loss and in analysis is frequently neglected. Third, the structuring of the ionosphere,

especially in the daytime, into separate height bands of high charge gradient provide, for some operating frequencies and distances, up to four paths between radar and targets. Fourth, for some operating frequencies and target distances both one- and two- (or more) refraction paths exist. All of the preceding sources of multipath can be multiplicative and the separate paths will either interfere causing fading or give distinct separate responses depending upon the radar's resolving capability in range, Doppler, and elevation radiation angle.

The antenna for an HF OTH radar is probably more demanding than for any other radar application. The antenna should be of high gain, cover an extremely wide-frequency range, be steerable in elevation, be rapidly steerable over a wide azimuth, and handle high power. Such an antenna will be of large size and require a large ground screen to keep the elevation launch angles low if vertical polarization is used. For example, if a vertical monopole element is used over a ground of poor conductivity and it is desired to put the maximum of the first lobe at  $4^\circ$ , a ground screen extending about 150 wavelengths (3000 m at 15 MHz) in front of the antenna is required.

The coverage of the radar on the earth's surface depends on the ionosphere. A "typical" patch of the ground illuminated by a single frequency might be 1000 km in the range dimension. The region from 1000–4000 km might, therefore, require three different frequencies for proper coverage. On the other hand, ionospheric conditions might be such that a single frequency could cover this range or perhaps five or six frequencies might be required. This illustrates the necessity for flexible radar management that senses the environment and adjusts the parameters of the radar for optimum operation. This subject will be treated in Section III.

If Doppler processing is used, the antenna beam must dwell on the target area for a time sufficient to achieve the Doppler resolution required and the degree of clutter attenuation needed. In MADRE, this dwell period might typically be 10 s.

The wide-area coverage of an OTH radar, the need to employ more than one frequency to cover the range interval under surveillance, and the need to dwell a sufficient time for Doppler processing means that a single-beam radar might require a relatively long time to scan a large surveillance area. The scan time can be reduced, if necessary, by the use of multiple simultaneous transmit and receive beams at the expense of increased equipment complexity. Another approach is to transmit with a broad beam and receive with multiple narrow beams covering the same area as the broad transmitting beam. This allows the more expensive transmitting antenna to be relatively small. (The transmitting antenna must be capable of high power so that it generally will be more costly than a receiving antenna of the same size.) The burden of providing narrow beams for resolution and accuracy then rests with the receiving antenna.

A problem confronting HF OTH radar is the clutter from meteors and aurora. Both phenomena can produce strong radar echoes that can hinder detection of desired echoes. Meteor and aurora clutter can be strong enough at times to enter the radar via the antenna sidelobes and from ranges greater than the maximum unambiguous range so that they are folded-over in range and can appear where targets might be expected. Again, by proper management of the flexible radar operation, limitations due to these effects can be minimized or eliminated.



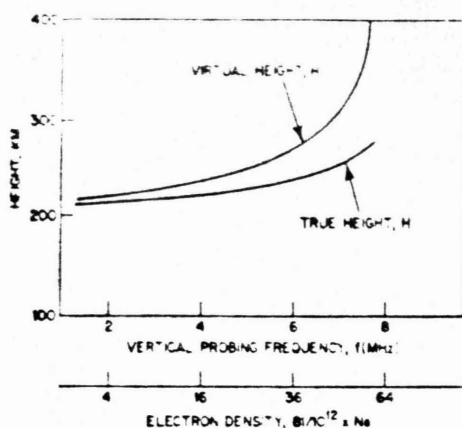


Fig. 6. Two vertical profiles of reflection height versus probing frequency are given. The upper trace is as would be derived from a vertical sounder and the  $H$  is a virtual height, generally identified by a prime:  $H' = (c\Delta t/2)$ , where  $c$  is the speed of light,  $\Delta t$  is the time delay for the signal to return from the ionosphere. The lower trace is the true height profile. The abscissa scale can be in terms of electron density because of the relationship  $N_e = f^2/81$ , where  $N_e$  is free electrons per cubic meter and  $f$  is the frequency in hertz.

### III. RADAR MANAGEMENT AND THE IONOSPHERE

Sky-wave propagation provides transmission paths from a station on the earth's surface to any other point on the earth's surface and to a large volume above the earth. A high-frequency EM wave launched at some oblique angle to the horizontal will bend away from the vertical as it travels into a region of increased electron density. The magnitude of this bending increases with decreasing radio frequency. Thus achieving a path back to the earth is just a matter of choosing the correct radio frequency to match the existing electron density distribution. The electron density distributions are caused by solar radiation exhibiting diurnal and seasonal variations. Since solar behavior is not precisely predictable, a future electron density distribution is not exactly predictable either. Effective radar operation requires that the electron density distributions be sensed in real time. Fig. 6 gives an example of an electron density profile and a vertical sounding profile, either of which is a common method of describing ionospheric parameters. This example shows a smooth increase of electron density with altitude typical of summer nights. Such a profile can be used to describe the ionosphere at each location on the earth. Fig. 7 shows a ray path for a frequency that gives refraction back to the earth. Earth reflections and successive ionospheric refractions can extend the path to any distance, including complete encirclement of the world. A complicating factor is that the vertical (altitude) profile of electron density may not be a smoothly varying function. Also electron density vertical profiles vary with time and geographic location. Fig. 8 is an example of daytime electron density profile and the virtual height as a function of the probing frequency. Fig. 9 shows the virtual ray paths associated with this ionospheric description for several radio frequencies. It can be seen that at some target distances a variety of paths are available.

Propagation losses are identified by three different processes. The first is in the lower part of the ionosphere ( $D$  region) where collisions of the free electrons (excited by the radio wave) with neutral particles absorb energy. This is called nondeviative absorption [1], [2]. The second is in the  $E$  region

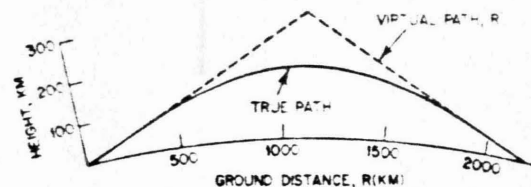


Fig. 7. A true path and virtual path are shown for the ionosphere as described in Fig. 6. It is frequently convenient to work with virtual paths. The virtual path length  $R' = (c\Delta t/2)$  is similar to the concept of virtual height. Below the ionosphere the true path and virtual path are identical.

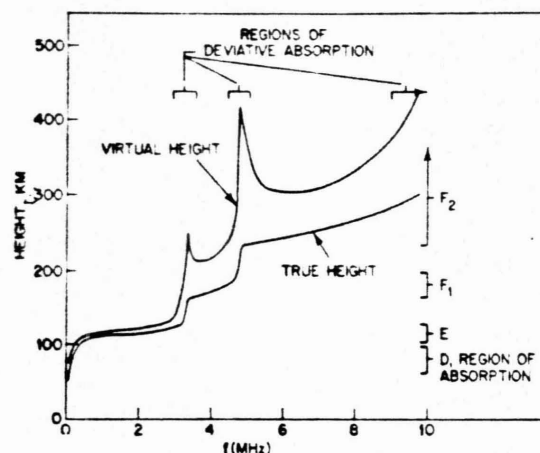


Fig. 8. A daytime vertical profile of the ionosphere is shown. This is a median profile based upon past soundings made at the particular location and time. The lower trace indicates the electron density structure with height as being other than smooth. The commonly used designators of height regions ( $F_1$ ,  $F_2$ ,  $E$ , and  $D$ ) are approximately bracketed and regions of absorption are indicated.

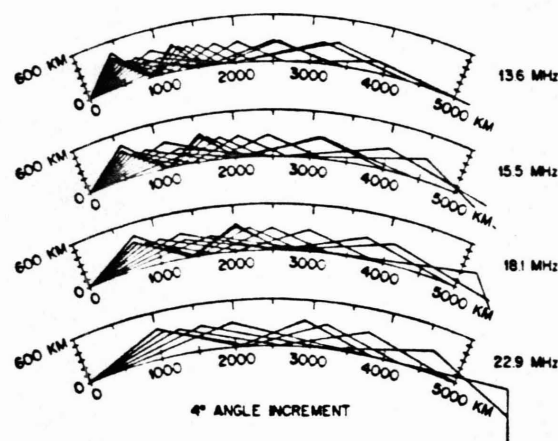


Fig. 9. This set of virtual path traces is based upon the ionospheric description given in Fig. 8. It would be more precise if each reflection from the ionosphere had used its own vertical profile. Although ionization changes with distance have been ignored, the general picture of radar range coverage achieved as a function of operating frequency is shown.

at an altitude a little over 100 km, where thin patches of high-density ionization may exist giving obscuration to the higher ionosphere. This has been called sporadic- $E$  obscuration. The third is the region where the true and virtual heights of the radio wave differ greatly, and this is called deviative absorption. In addition to these losses, there can be loss due to

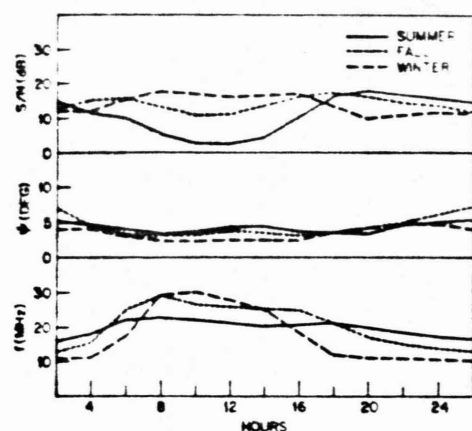


Fig. 10. The average performance calculated for a radar is used to show the variations in signal-to-noise ratio  $S/N$ , vertical radiation angle  $\psi$ , and operating frequency  $f$  versus time of day for three seasons but a single sun spot number. These computations are for a single target size and range, the range being about the maximum that can consistently be reached by one hop. A three-to-one frequency spread is required with the lowest frequency requirement being at winter night. The worst SNR occurs during the middle of summer day. Required radiation angles vary between  $3^\circ$  and  $6^\circ$ . Operation over an entire solar cycle requires more variation in launch angle and frequency.

polarization mismatch, ground reflection, and focusing or defocusing due to irregularities in ionization.

In practice, a system would be designed on the basis of the available information about the statistical behavior of the ionosphere. Since the electron density always increases with altitude (in the lower portion of the ionosphere), the existence of an ionospheric path can be considered certain but unpredictable in its detailed character. The reliability of performance that can be realized depends upon the antenna aperture size, radiated power, and the span of frequencies that can be used. One controlling limit is absorption in the lower atmosphere during summer days when the ionization extends to lower heights where the neutral particles are more dense. The result is increased path loss. A second controlling limit occurs on winter nights when the electron density is comparatively sparse and a low operating frequency is required to provide a path. Thus the first limit affects the long-range performance and the second, the short-range performance. Violent, but relatively infrequent, solar activity may result in short periods of similar behavior that can sometimes be more extreme. Fig. 10 shows the predicted performance of a hypothetical radar design.

In short, the sky-wave path can be made reliable if one is willing to pay the cost.

In addition to the question of path loss in HF sky-wave propagation, there are other aspects of the OTH radar environment that can be described as detrimental to radar operation. These may be classified as follows.

- 1) A multiplicity of paths from radar to target can exist causing either fading or multiple responses from a single target as has been previously discussed. There also may be patches of electron density in the lower ionosphere that are semi-transparent causing a ray to be refracted to the ground as well as permitting rays to be transmitted to a higher layer where they are likewise refracted back to the ground.

- 2) The ionosphere is dispersive in that the velocity of propagation depends on the frequency. Hence there are limits upon the information bandwidth that may be employed, and

extremely short pulses will be distorted, placing a limit on range resolution.

- 3) The nature of refraction by the ionosphere allows a specific area to be illuminated by only a limited band of frequencies.

- 4) The electron-density distribution in the ionosphere is in a state of continuous change so that the nature of the propagation path is subject to change with time.

- 5) The propagation space is studded with unwanted clutter echoes such as the earth, auroral ionization, meteor-caused ionization, and other large scattering areas that compete with the desired target echoes.

- 6) The part of the frequency spectrum appropriate for OTH radar is noisy due to cosmic, solar, and natural terrestrial sources, all of which, though not exactly white, extend smoothly across the band. The spectrum of man-made relations, both from radio transmissions and electrical machinery, tends to be colored. It is emphasized that the HF spectrum is crowded with users.

All of the preceding discussion shows that for successful HF OTH radar operation it is essential that the environment be sensed in real time and the radar be optimally matched to the environment. The operating frequency and the vertical radiation angle are the parameters available for securing desired illumination power density at a particular point on the earth. Monitoring of the occupancy of the HF spectrum can assist in the selection of the precise frequency and the emission bandwidth to minimize the interference level at the radar and to avoid interference to other users. The waveform repetition rate can be adjusted for the best compromise between range ambiguities, Doppler ambiguities, and obscuration by natural targets (clutter). It is evident that narrow antenna beamwidths in both the horizontal and vertical planes can provide discrimination against natural targets that obscure, and at the same time minimize interference with other users. Widening the emission bandwidth to achieve greater range resolution also can help reduce the echo from distributed natural targets.

All of the preceding serves to emphasize that for effective sky-wave radar operation it is important to have a real-time description of the transmission path and the band occupancy, and that the radar waveform and signal processing must be matched to the existing conditions. All of the common methods to determine the best operating conditions that have been developed for HF communications can be used with radar. These include vertical soundings of virtual height versus frequency, oblique soundings of virtual range versus frequency between the radar and fixed points, oblique soundings of backscatter amplitude versus frequency, estimates of the effect of solar activity, and HF band occupancy obtained from a search receiver. The sky-wave radar has a capability not available with HF communications that should always be used and which can provide additional description of the transmission path. The radar backscatter from the earth at a particular frequency can be used to infer the character of the ionosphere for all heights up to the height of maximum ionization. Thus normal radar operation has, as a byproduct, the data from which the transmission path can be described. The essential requirements for using these data are a knowledge of the scattering properties of the earth and some method of correlating virtual ranges with ground ranges, or virtual ranges with elevation radiation angle. If the earth has identifiable natural localized scatterers such as islands on the sea,

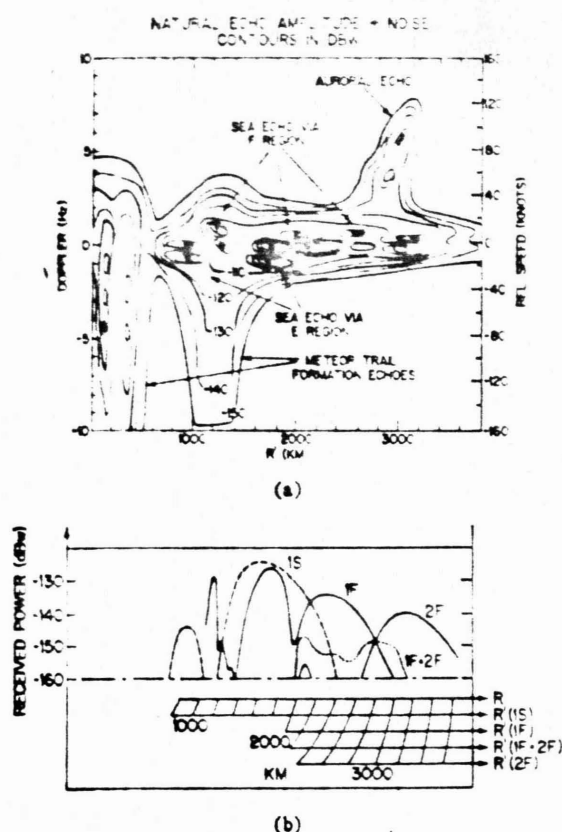


Fig. 11. In Fig. 11(a) Doppler range space is shown in contours of received power level in decibel-watts. Such descriptions of the earth (sea) echo can be used to determine the radar transmission path parameters. This analysis has been done and in Fig. 11(b) the received power for a 1000-m<sup>2</sup> target has been plotted for the several paths versus both great circle ground range  $R$  and virtual range  $R'$ . The paths drawn are: one refraction by sporadic ionization in the E region (1S); one refraction in the F region (1F); two refractions in the F region (2F); and the combination of the latter two (1F-2F). The ranges that permit multiple responses are evident. To indicate performance (either SNR or signal-to-clutter ratio) the noise or clutter power level from the appropriate range and Doppler on Fig. 11(a) must be divided into the signal power from Fig. 11(b). Performance is a decided function of target location in Doppler range space as well as power received from the target.

sea-land boundaries, or mountains or cities on land, these can be used to determine the correspondence between the virtual and ground range. If the radar has directive beams that can be readily steered in elevation, ground ranges can be associated with virtual ranges and ionospheric heights can be deduced. The earth echo provides a signal of sufficient quality to be used for automatic analysis of the transmission path. Even if the radar has no elevation angle control and there are no identifiable ground targets, the earth backscatter can still be useful in confirming estimates of the transmission path made by other means. The earth backscatter amplitude as a function of virtual range may not uniquely define the propagation path but it can be used to test the correctness of a particular assessment of the path. If the predicted backscatter distribution is similar to that observed, it gives confidence that the assessment is correct. Fig. 11 gives an example of performance assessment that has been deduced from an operating radar's earth (sea) echoes [6].

Radar performance depends on the geographical location. When the refracting part of the ionospheric path is in an auroral region, path losses and instabilities can be great. Even

when the propagation path does not traverse the aurora, unwanted echoes from aurora and other intense sources of field-aligned ionization can obscure targets by entering the radar via the antenna sidelobes.

Furthermore, OTH radar capability abruptly changes across the transition from one-hop to two-hop coverage. These transitions are somewhat variable with both time and location and nominally they are 2000–2200 km via the E region and 3000–4000 km via the F region. Thus when performance out to 4000 km is required, part of the time it must be achieved by a two-hop path.

#### IV. CAPABILITIES

A complete and detailed description of the capabilities of OTH radar cannot be fully discussed in a paper of this scope. Nevertheless, it is possible to indicate the following nominal performance characteristics that might be achieved:

range coverage	1000–4000 km; longer ranges are possible with multihop propagation, but with degraded performance;
angle coverage	can be 360° in azimuth, if desired; 60°–120° is more typical;
targets	aircraft and ships; also nuclear explosions, prominent surface features (such as mountains, cities, and islands), sea, aurora, meteors, and satellites below the ionosphere's altitude of maximum ionization;
range resolution	could be as low as 2 km, but is more typically 20–40 km;
relative range accuracy	typically 2–4 km for a target location relative to a known location observed by the same radar;
absolute range accuracy	10–20 km, assuming good real-time path assessments are made;
angle resolution	determined by the beamwidth; it can be less than 1° which corresponds to 50 km at a distance of 3000 km;
angle accuracy	beam splitting of 1–10 should be possible with sufficient SNR; ionospheric effects might limit the angle measurement accuracy to some fraction of a degree;
Doppler resolution	resolution of targets whose Doppler frequencies differ by 0.1 Hz or less is generally possible; at a radar frequency of 20 MHz, 0.1 Hz corresponds to a difference in relative velocity of about 1.5 knots.

#### V. APPLICATIONS

The order of magnitude increase in range possible with an HF OTH radar as compared with conventional radar makes it attractive for those geographical areas where it is not convenient to locate conventional microwave line-of-sight radars. Radar coverage of the sea is such an example. By way of illustration, two applications will be briefly mentioned:



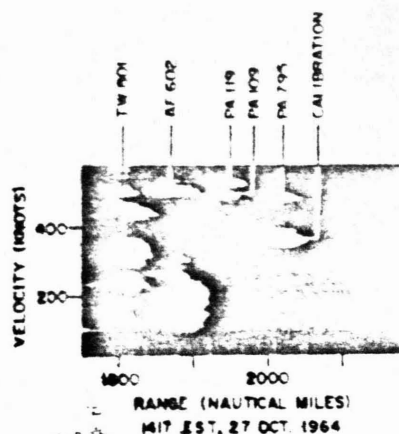


Fig. 12. Transatlantic aircraft targets on a Doppler-range display. In this example a clutter filter has been used to reject relative velocities up to about 100 knots and approach and recede targets have been folded upon each other so that direction is not obtained. The vertical streaks are meteor trail formation echoes. They persist but a short time. The aircraft echoes have been identified with flight information furnished by the FAA.

1) air-traffic control over the sea; and 2) the remote observation of sea conditions and the accompanying weather. Other applications are certainly possible.

1) *Air-Traffic Control:* An OTH radar with  $120^\circ$  angle coverage and a range coverage from 1000–4000 km can survey an area of almost sixteen million square kilometers. Aircraft within this area can be detected, located, and tracked by such a radar.

Fig. 12 shows a range-Doppler display of aircraft targets flying the North Atlantic air corridor between the United States and the United Kingdom. These data were taken with the MADRE radar. The azimuth measurement accuracy of this radar is not sufficient to track in angle, but excellent Doppler resolution permits targets to be separated in the frequency domain and measured in range. Fig. 13 is a plot of the ranges of these targets as measured by the radar (shown by the circle points) compared with the aircraft tracks (straight lines) obtained from the FAA. The agreement is quite good. Fig. 14 shows a Doppler-range display of aircraft targets made with the smaller MADRE rotatable antenna (see Fig. 4) looking West. Note how this radar is able to resolve in the Doppler domain targets that are unresolved in range alone.

Target height is not obtained with this OTH radar. It is possible to install HF transponders on each aircraft and relay back to the radar the height of the aircraft as determined by the on-board altimeter, as well as the identity of the aircraft. Limited communications can also be effected by this means.

An example of the possible OTH coverage of the North Atlantic air lanes is shown in Fig. 15 for two arbitrary radar sites.

Thus OTH radar offers a new capability for improving the safety and quality of over-ocean air traffic.

2) *Remote Sensing of Sea Conditions:* The extent of the Doppler frequency spectrum of the sea or land clutter is much less than the Doppler shifts expected from aircraft. Hence to separate aircraft echoes from sea or land echoes, the low-frequency portion of the spectrum is filtered out and only that region is passed in which aircraft or missile targets are expected. The lower portion of the spectrum that is filtered out, however, contains significant information about the nature of

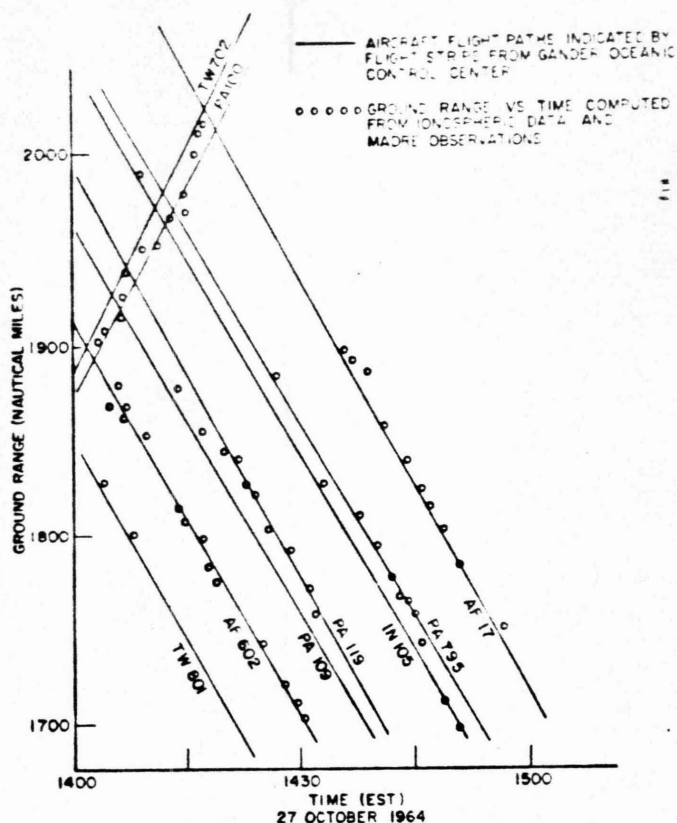


Fig. 13. FAA flight paths compared with radar data for a 1-h period.

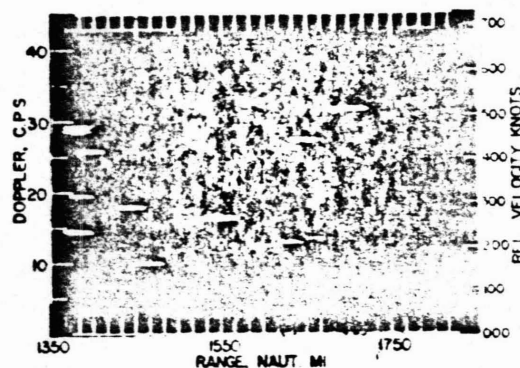


Fig. 14. A Doppler range of aircraft targets to the west of the MADRE site. Among the targets there is quite a spread in relative velocity. Notice that multiple targets at the same range are readily resolved by Doppler discrimination.

the clutter. Fig. 16 shows an example of the spectrum of the sea echo. Such spectra can be interpreted to give sea roughness and direction. Ionospheric effects, especially multipath, cause complications. Nevertheless, it has been possible to determine the direction of the waves, to estimate their magnitude, and to infer something about the winds that drive the waves. An example of radar derived wind direction is given in Fig. 17 [7]. Other papers in this issue of PROCEEDINGS treat this subject [8], [9].

## VI. GROUND-WAVE RADAR

Almost all of the preceding has been concerned with an OTH radar that utilizes the refractive properties of ionospheric sky-wave propagation to reach out and detect targets



Fig. 15. Possible OTH radar coverage of the North Atlantic from radar locations in northeastern USA and northern Spain.

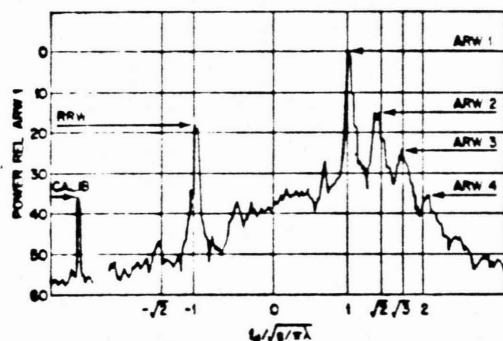


Fig. 16. A spectrum of the radar echo from the sea obtained from an area about 9.5 by 7.5 km via ground wave. The sea was developed by a 25-knot approaching wind and the operating frequency was 13.4 MHz. The Doppler  $f_d$  scale has been normalized so that the major returns occur at  $\pm 1$ . The major returns are the Approach Resonant Wave ARW 1 and Recede Resonant Wave RRW. The difference in amplitude between ARW 1 and RRW can be used to calculate the sea (and exciting wind) direction. The amplitude of the other peaks, ARW 2, ARW 3, ARW 4, and of the continuum between peaks can be used to indicate sea state (or driving wind speed).

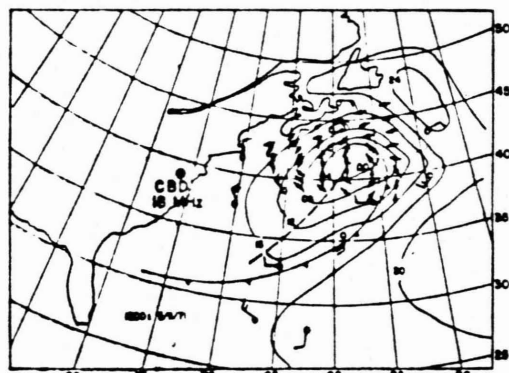


Fig. 17. Radar-derived wind direction has been plotted on a standard surface weather map in order to effect a comparison. The radar data are in good agreement with the weather map. The radar data can be obtained with a high density over the sea area surveyed.

beyond the horizon. It is also possible at HF to propagate energy around the curvature of the earth by diffraction. This is commonly called ground-wave propagation. The loss beyond the horizon in this ground-wave mode increases exponentially with range. Also the higher the frequency the greater the loss. A ground-wave radar can detect the same kind of targets as discussed for the sky-wave radar. Detection is somewhat easier than with sky-wave propagation since ionospheric effects are not present as they are with the sky-wave radar, and clutter returns from aurora can generally be eliminated by time gating. Furthermore, at night it may be possible to operate a ground-wave radar at a frequency too high for sky-wave transmission so that interference from distant sources that would normally propagate by sky wave is not present.

A ground-wave radar of a size and frequency comparable to the sky-wave radar discussed in this paper might have a range against aircraft targets of perhaps 200–400 km. Thus its capability is far less than that of the sky-wave radar. Detections are generally easier, for the reasons previously cited, but the ground-wave radar might not prove cost effective for general use. Unfortunately, the maximum range of ground-wave radar is considerably less than the minimum range of the sky-wave radar unless the sky-wave radar can operate at frequencies down to the broadcast band. However, the antenna dimensions would become large, and many targets of interest would certainly be in the Rayleigh scattering region where the cross section would be small. Thus it is impractical for ground-wave radar to fill in the skip zone of the sky-wave radar.

## VII. DISCUSSION

OTH radar offers a new and exciting means for sensing the environment and the detection of targets at distances an order of magnitude greater than conventional microwave radar. The technology has been developed and the capabilities demonstrated. The cost of the HF OTH radar might be expected to be high, but on the basis of cost per square mile of coverage it is probably comparable to other radar types. Its chief advantage is that it can cover areas not feasible with conventional radars.

## VIII. NOTE

In the United States, significant work on OTH radar using HF frequencies and both ground-wave and sky-wave propagation started in the late 1940's. The organizations engaged in this early work included the Watson Laboratories of the Army Air Force, the Lincoln Laboratory of the Massachusetts Institute of Technology, the National Bureau of Standards, the Raytheon Company, RCA, and Stanford University. In the early 1950's, the Naval Research Laboratory started a program to demonstrate the feasibility of sky-wave radar for aircraft targets. Later many other groups have significantly contributed to the advancement of HF OTH technology.

## REFERENCES

- [1] J. M. Kelso, *Radio Ray Propagation in the Ionosphere*. New York: McGraw-Hill, 1964.
- [2] K. Davis, "Ionospheric Radio Propagation NBS Monograph 80," 1965.
- [3] International Radio Consultative Committee, "World distribution and characteristics of atmospheric radio noise," International Telecommunications Union, Rep. 322, Geneva, Switzerland, 1964.
- [4] R. E. Kell and R. A. Ross, "Radar cross section of targets," in *Radar Handbook*, M. I. Skolnik, Ed. New York: McGraw-Hill, 1970, ch. 27.

- [5] C. E. Cook and M. Bernfeld, *Radar Signals: An Introduction to Theory and Application*. New York: Academic Press, 1967.
- [6] D. L. Lucas, J. L. Lloyd, J. M. Headrick, and J. F. Thomason, "Computer techniques for planning and management of OTH radars," NRL Memo. Rep. 250, Sept. 1972.
- [7] A. E. Long and D. B. Trizna, "Mapping of Northern Atlantic winds by HF radar sea backscatter interpretation," *IEEE Trans. Antennas Propagat.*, vol. AP-21, pp. 680-685, Sept. 1973.
- [8] D. E. Barrick, J. M. Headrick, R. W. Boger, and D. D. Crombie, "Sea backscatter at HF: Interpretation and utilization of the echo," this issue, pp. 673-680.
- [9] J. L. Ahearn, S. R. Curley, J. M. Headrick, and D. B. Trizna, "Tests of remote skywave measurement of ocean surface conditions," this issue, pp. 681-687.
- [10] D. E. Barrick, "Remote sensing of sea state by radar," in *Remote Sensing of the Troposphere*, V. E. Derr, Ed. Available from the U. S. Gov. Printing Office, Washington, D. C., ch. 12.
- [11] Y. A. Mishchenko, *Zagorizontnaya Radiolokatsiya*. Moscow, USSR: Military Publishing House, 1972. (Also available in English transl. from the National Technical Information Service, Springfield, Va. 22151, Rep. JPRS 56925.)
- [12] T. A. Croft, "Sky-wave backscatter: A means for observing our environment at great distances," *Rev. Geophys. Space Phys.*, vol. 10, pp. 73-155, Feb. 1972.

Merrill I. Skolnik

Naval Research Laboratory, Washington, D.C. 20375

The millimeter-wave portion of the electromagnetic spectrum has been challenging the engineer and the physicist for many years. The physicist has been reaching down (in frequency) using the techniques of the far infrared and of lasers, and the engineer has been reaching up using extensions of microwave techniques. Although these two technologies have been demonstrated to overlap in the spectrum (that is, coherent microwave techniques have been employed in systems at wavelengths as short as 0.5 mm, and lasers are available at wavelengths greater than 1 mm), there has been essentially no operational use of radar at wavelengths between 8.6 mm ( $K_a$  band) and 10.7  $\mu$ m (the  $CO_2$  laser band). The absence of high-power sources suitable for radar, sensitive receivers, and low-loss transmission lines has often been blamed for the lack of system applications. It is certainly true that there has not been an over-abundance of adequate components and subsystems in the millimeter wave region. However, there has been adequate technology at longer wavelengths (microwaves) and at shorter wavelengths (IR and optics) so there is reason to hope that Nature has not ruled out the attainment of similar capabilities in the region of the spectrum in-between. The paper by Dr. Godlove in this session describing the gyrotron high-power millimeter wave generator and the companion session on Millimeter Technology give evidence that there are opportunities for advancement in technology in this part of the spectrum.

A more important reason for the lack of current application is the large loss when propagating through the normal atmosphere, and the even greater loss in rain. The normal atmosphere is essentially "transparent" at wavelengths greater than 1 cm and less than 10  $\mu$ m. In-between, where the millimeter region lies, the losses are significant. The so-called "window" at 94 GHz has higher attenuation than the water vapor absorption line at 22 GHz. At 1 mm wavelength the loss is 10 dB/km at sea level, and at shorter wavelengths it is even greater. The high attenuation of the atmosphere in the millimeter-wave region will restrict radar applications to short ranges where extremely wide bandwidth is required or where high-resolution measurements in range, angle, or relative velocity are desired. Millimeter-wave radar will also be a candidate for radar applications in space, where there is no attenuation due to the earth's atmosphere.

The Papers in this session describe potential applications of millimeter radar within the above limitations. Short-range millimeter-radar missile-

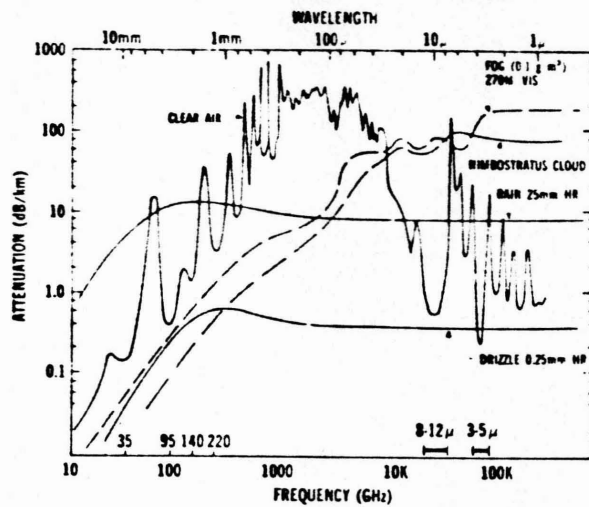
guidance systems at 35 and 94 GHz are the subject of Augustus Green's paper on applications to Army missile systems. George Jones mentions homing and fuzing applications in his paper on ballistic missile defense applications. Tresselt and Wu utilize the high resolution properties of millimeter waves in a short-range solid-state 36 GHz radar for the automatic braking of automobiles. An instrumentation radar at  $K_a$  band for obtaining target and clutter data is described by J. A. Scheer, J. L. Eaves, and N. C. Currie. R. B. Dybdal's paper also is concerned with target information, with emphasis on space object identification (SOI) applications.

Some of the millimeter radars described in this session operate at 35 GHz ( $K_a$  band). Although the wavelength is 8.6 mm, and can qualify as a millimeter radar, the technology is still basically that of the microwave region. Such technology cannot be extrapolated efficiently to the shorter wavelengths. The justification for working at  $K_a$  band is that it is the place one might start in order that one can crawl before walking. But to qualify as a real member of the millimeter-wave fraternity, one ought to be at shorter wavelengths.

The exploration of the microwave region had its beginnings in the experiments of Hertz in 1886. Experimentation with millimeters dates back almost to the same time. Experiments at 6 mm wavelength were first reported in 1895. In the early 1920s, millimeter wave work was reported in the U.S., Germany, and Russia, at wavelengths as short as 0.22 mm (reported by Nichols and Tear). The power sources in the early work were some form of spark generator. The first coherent source at 6 mm wavelength was from a split-anode magnetron employed by Cleeton and Williams at the University of Michigan in 1936.

Thus millimeter waves have an early history similar to that of microwaves, but as yet there has not been that desperately needed application resulting in a surge of developments that break down the technological barriers just as many other technological barriers in the electromagnetic spectrum were overcome in the past. Until the millimeter millennium arrives, it is incumbent upon the microwave engineer and the physicist to continue to combine their talents and experience for the basic exploration and understanding of this interesting and distinctive region of the electromagnetic spectrum.

# ATMOSPHERIC PROPAGATION LOSSES



A plot of atmospheric transmission from wavelengths of 10mm to 1μ shows the increased fog penetration of the millimeter waves.



From NRL Memorandum Report 2159, "Millimeter and Submillimeter Wave Applications," M. I. Skolnik, Aug 12, 1970.

## APPENDIX

### MILLIMETER WAVE SURVEILLANCE RADAR

The purpose of this appendix is to illustrate what the parameters might be of a surveillance radar operating at 94 GHz (3.2 mm) assuming realistic values for the radar characteristics. The equation governing this situation is

$$R_{\max}^4 = \frac{P_{\text{av}} G^2 \lambda^2 \sigma n E_i(n) \exp(-2 \alpha R_{\max})}{(4 \pi)^3 k T_o F_n (B_n \tau) f_r (S/N)_1 L_s}$$

where

- $R_{\max}$  = maximum radar range, m
- $P_{\text{av}}$  = transmitter average power, watts
- $G$  = antenna gain
- $\lambda$  = wavelength, m
- $\sigma$  = target cross section,  $\text{m}^2$  (assumed  $1 \text{ m}^2$ )
- $n$  = number of hits integrated
- $E_i(n)$  = integration efficiency
- $\exp(-2 \alpha R_{\max})$  = reduction in signal due to attenuation
- $\alpha$  = attenuation constant of the medium
- $k T_o = 4 \times 10^{-21}$  watts /Hz
- $B_n \tau$  = bandwidth-time product  $\approx 1$
- $f_r$  = pulse repetition frequency, Hz
- $(S/N)_1$  = signal-to-noise ratio required for detection
- $L_s$  = system losses.

At a frequency of 94 GHz, power sources with an average power of 200 watts might be available. Since we know a radar at this frequency will be limited, it is important to use as high an antenna gain as possible. Therefore, we select an antenna with a beamwidth of  $0.1^\circ$  in both azimuth and elevation. The gain is approximately 63 db. Since an elevation beamwidth of  $0.1^\circ$  would give poor coverage, it is assumed that the antenna beam will be spoiled in the vertical plane to give  $\text{csc}^2$  coverage and that a loss of gain of 3 db is had. Thus  $G = 60$  db. The antenna diameter would be close to 7 ft.

The number of hits integrated is  $n = \theta f_r / 6 \omega_m$  where  $\omega_m$  = the rpm of the antenna. Assuming a rotation rate of 5 rpm (12 sec data rate) and  $f_r = 1000$  Hz (about 80 nmi maximum unambiguous range)  $n = 0.1 \times 1000 / 6 \times 5 = 3.3$  hits/scan. The product  $n E_i(n) \approx 3$ .

The attenuation factor will be ignored for the present and will be taken account of later.

The noise figure of a good receiver might be 10 db and 10 db system losses are assumed. A signal-to-noise ratio of 15 db is also assumed.

Substituting into the range equation gives

$$R_{\max}^4 = \frac{2 \times 10^2 \times 10^{12} \times (3.2)^2 \times 10^{-6} \times 1 \times 3}{2 \times 10^3 \times 4 \times 10^{-21} \times 10 \times 1 \times 10^3 \times 3 \times 10}$$

$$= 2.5 \times 10^{20}$$

$$R_{\max} = 1.26 \times 10^5 \text{ m} = 68 \text{ nmi in free space}$$

Next, consider the neglected attenuation factor. At sea level, the attenuation rate at 94 GHz is about 0.4 db/km in clear weather. In 4 mm/hr rain the attenuation is 2.5 db/km. The range is reduced to about 16.5 nmi in clear weather and about 4.6 nmi in the rain. These figures are quite low and represent a significant reduction from the 68 nmi free space range.

If 4 such radars were used together as on a "merry-go-round" or some such other coordinated fashion, the theoretical improvement in detectability would be increased by a factor of about 5.5 db. Normally this would increase the range by a factor of 1.37, or to a range of 93 nmi if attenuation is ignored. The atmospheric attenuation will reduce so that the range in clear weather might be about 19 nmi. In rain, the improvement is even smaller so that the expense of employing four radars in unison is not worth the effort.

Thus the best that might be achieved in a millimeter wave surveillance radar is perhaps 15 to 20 nmi in clear weather, reduced to about 4 to 5 nmi in rain.



# RADAR TECHNOLOGY EVENTS 1960 - 1970

1960

1965

1970

Phase-frequency array (SPS-33)

Cassegrain antenna

OTH aircraft detection

BMEWS

Single-horn monopulse

Staggered prf MTI

OTH low-altitude aircraft detection

Kalman clutter filter

Stretch pulse compression

Track-before-detect

Clutter fence

Reflectarray

High-resolution SAR

Inverse scattering

Frequency-diversity glint reduction

Intrusion detection

Coherent sidelobe cancellation

Helicopter-blade radar

Coaxial magnetron

Lens-array

Interclutter visibility (MTI)

Digital MTI

Clutter CFAR (AVT)

OTH ship detection

95 GHz radar

Splash-detection radar

FFT MTI processor

Gemini rendezvous radar

1 m range resolution (APS-116)

Kalman tracking filter

Receiver design for non-Rayleigh clutter

OTH weather/sea-state observation

Scatterometer

# RADAR TECHNOLOGY EVENTS 1970 - 1980

1970

1975

1980

MTI transversal filter design

Ship collision avoidance (Digiplot)

Polyfrequency-SAR

Low sidelobe antennas

Practical low-noise front-ends

Minicomputers

Airborne TWS pulse doppler (AWG-9)

Apollo landing radar

SAW devices

Overland MTI (E2)

Associative processor

High-range-resolution monopulse

Spaceborne radar

Geoid measurement from space

Sea state from space

Long-range pulse doppler (AWACS)

Low-angle track

Scan-converter display

SAR - sea ice and oil spill

Microprocessors

Phase-phase array (SPY-1 and Patriot)

Adaptive processing

High-availability radar

Solid-state transmitter (TPS-59)

Balloon-borne radar

Active missile guidance (Harpoon)

Large phased array (Cobra Dane)

Integrated ADT

Airborne phased array (EAR)

Moving Target Detector (MTD)

Artillery locator (TPQ-37)

## REVIEW OF CURRENT RADAR INTERESTS

Merrill I. Skolnik

Naval Research Laboratory

Washington, DC

This introduction to the Technical Session on "Radar - Some Problems of Current Interest," will briefly indicate the major areas of radar application and a few of the problems that confront modern radar.

### Current Applications

Air Traffic Control - There are over 200 long range and medium range air surveillance radars in use by the FAA in the United States for the purpose of safely controlling air traffic. High resolution radar is used for surveillance of ground traffic at major airports. In addition, microwave landing systems and the widely used beacon system are based in large part on radar technology.

Aircraft Navigation - The weather avoidance radar used on aircraft to outline regions of high precipitation to the pilot is a classical form of radar. Although they may not always be thought of as radars, the altimeter (either FM/CW or pulse) and the doppler navigator are also radars. Sometimes ground mapping radars of moderately high resolution are used for aircraft navigation purposes.

Ship Navigation - In terms of numbers, this is one of the larger applications of radar, but in terms of physical size and cost it is one of the smallest. It is also one of the most reliable radar systems. Automatic detection and tracking equipments are commercially available for use with such radars for the purpose of collision avoidance. Shore-based radar of moderately high resolution is also used for the surveillance of harbors as an aid to navigation.

Space - Both the Gemini and the Apollo space vehicles used radar for rendezvous and docking, and Apollo also utilized it for landing on the moon. Some of the largest ground-based radars are for the detection and tracking of satellites.

Remote Sensing - All radars are remote sensors; however, as this term is now used it implies the sensing of geophysical objects, or the "environment." For some time, radar has been used as a remote sensor of the weather and the atmosphere. It was also used in the past to probe the moon and the planets, but this has been displaced by the successful use of manned and unmanned spacecraft. The ionospheric sounder, an important adjunct for HF (short wave) communications, is a radar and was first employed about fifty years ago. Current interests in remote sensing with radar deal with Earth resources, which include the measurement and mapping of sea conditions, water resources, ice cover, agriculture, forestry conditions, geological formations, and environmental pollution. The platforms for

such radars include satellites as well as aircraft.

Law Enforcement - In addition to the wide use of CW radar to measure the speed of automobile traffic, radar has been employed as a means for the detection of intruders.

Military - By far the biggest user of radar and the one who has paid for almost all of its development is the military. Its traditional role in the military has been for surveillance, navigation and for the control and guidance of weapons.

#### Current Problem Areas

Extending the Coverage of Radar - The coverage of microwave radar is basically limited by the line of sight, which depends on the height of the radar and the height of the target. No matter what coverage is obtained with radar, it is always natural to ask for more. Extending the range can be accomplished by elevating the radar, use of over-the-horizon radar in the HF band, or by taking advantage, when possible, of non-normal propagation conditions such as ducting.

Relief of the Operator - A man does very well as a radar operator so long as he is alert and is not confronted with too high an information rate. To assist the operator and to prevent saturation, digital computer techniques have been applied to the automatic detection and tracking of targets. The success of such techniques is due to the remarkable achievements in digital computer componentry

during the last twenty years. The computer is also useful for organizing and executing the control of the radar system and in the efficient use of its output.

Extraction of Target Information - The basic measurement of radar is the distance to the target. No other sensor can provide this as well as can radar. Radar also determines the angular location of targets and in some systems it uses the doppler frequency shift to measure relative velocity or to separate stationary from moving targets. Radar can obtain other information about targets, such as their size and shape, and can sort them by type. Means for extracting target information from the received signal is always of interest. A current example where significant progress has been made is in the remote sensing of the environment.

Operation in Clutter - Any method that allows a radar to perform its task in spite of the obstructions imposed by clutter is always welcome. Clutter includes unwanted reflections from land, sea, weather, clear air turbulence, birds, insects, meteors and aurora.

Electromagnetic Compatibility - Radar must be able to operate properly in spite of interference from other electromagnetic sources. Likewise, the radar must not interfere with other users of the electromagnetic spectrum.

Equipment Improvements - Better subsystems and components are always desirable. A few of the equipment advances that would be welcome include: better isolation

in CW radar, efficient linear transmitters, efficient low duty cycle solid-state RF power devices, wide dynamic range displays and receivers, wide-band wide-dynamic-range A/D converters, short-pulse high-power transmitters, and long-life highly reliable mechanically rotating antennas.

Affordable Phased Arrays - The value of the phased array antenna to the radar systems engineer is unquestioned. However, when economic matters are a consideration they are not usually competitive with other means for accomplishing the same objectives. The cost of computer software must be reduced, as well as array hardware costs.

Reasonable System Cost - Although it is a natural human trait to want to get the most for the least amount of money, this precept is not always practiced in the procurement of radar systems. It is easy in a highly sophisticated and changing technology like that of radar to be unknowingly extravagant. The cost of a radar is not just the dollars spent on acquiring the system. It also includes the costs to install, to finally make it work properly, and the cost of maintaining and operating it over its useful life. In addition to its cost in dollars there is the "cost" in weight and space if it is used in a mobile platform such as an aircraft or ship. There is also the cost of the platform itself if the radar installation makes special demands and the cost of the site if a land-based application. It is no secret as to how to minimize the total cost of a radar system. The user of a radar should ask only for what



he really needs rather than what he desires, and he should make certain that before he pays the bill the radar he has bought works as specified.

Dependability - A radar should be of long-life, reliable, maintenance free (or if not, at least it should be easy, cheap, and quick to fix), and be simple to operate. No one will deny the desirability of such things, but it is surprising how seldom they are taken seriously during development, when over-runs in money or time occur.

Of all the above the most important, in the writer's opinion, are the last two. The user of radar must be able to obtain what he needs at a reasonable price and it should operate as it is supposed to whenever it is required to do so. These are not usually thought of as research and development areas, but they are probably as important as anything else being conducted in the research laboratories and in industry, and they might very well become serious R & D projects.

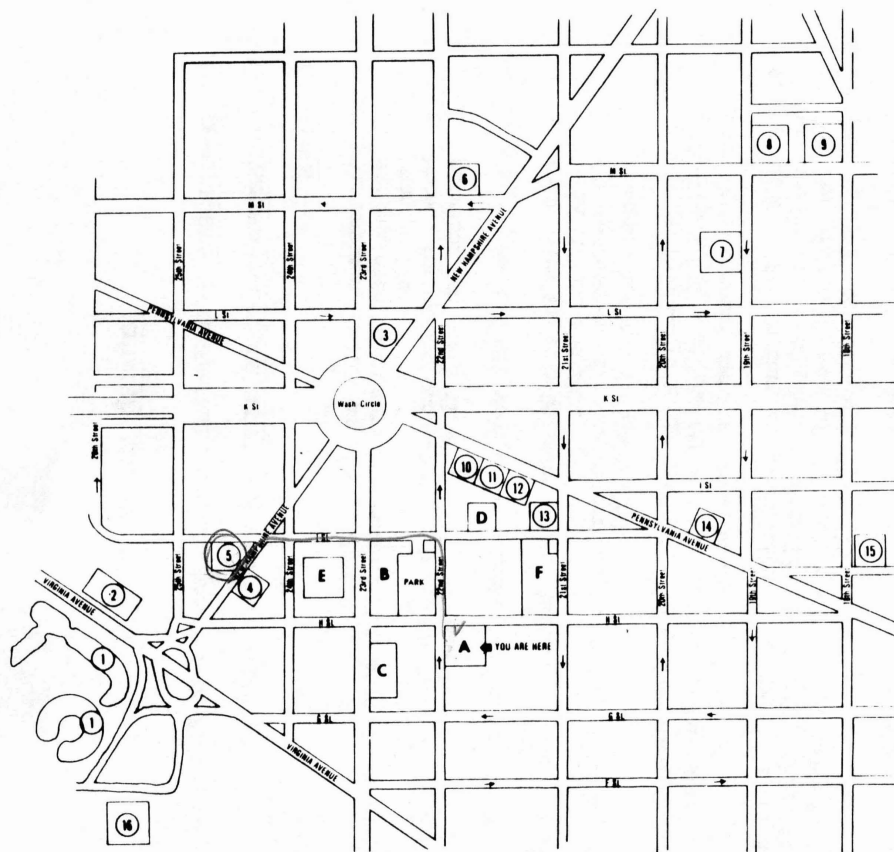
The above listing has been from the viewpoint of the systems engineer interested in applying radar for some useful purpose. They can be called problems in search of solutions. There are also solutions in search of problems. These are new techniques and components that their developers believe might offer improvements in radar. These will not be discussed here other than to state that they include such things as surface-wave acoustic devices,



charge-coupled devices, microwave transistors and other solid state RF devices, liquid crystal and solid state displays, microprocessors, adaptive antennas, conformal arrays, pattern recognition, and the whole myriad of techniques that are associated with millimeter waves. Progress in radar has been made by both the dogged pursuit of current problems one small step at a time, and by the occasional large advance introduced by some new, and usually unforeseen, technological development.

### ADMINISTRATIVE INFORMATION

1. COFFEE BREAKS — Coffee and doughnuts are outside Room 641. They are free.
2. RECOMMENDED PLACES FOR LUNCH — See attached chart.
3. PHONES —
  - a. For incoming calls, use (202) 676-6106.
  - b. See bulletin board outside classroom for messages and notes on incoming phone calls.
  - c. Phones for making outside calls are located in the foyer near the elevator, on sixth floor.
4. PARKING — We validate your parking tickets once per day for:
  - a. University Parking Building - use visitors' entrance on I Street between 22nd and 23rd.
  - b. Limited number of spaces under Marvin Center — use entrance on H Street between 21st and 22nd.
5. IN CASE OF FIRE — Exit via stairways located in elevator lobbies and in both back corners of the 6th and 7th floors. (These stairways have alarms which negate their use for normal entrance or exit.)
6. CRITIQUE — Please turn in the critique sheet on the final day at the time we present course completion certificate. Normally this will be just after the last coffee break. If you must depart early, leave your critique and pick up your certificate in Room 636.
7. SMOKING -- University policy is that there be no smoking in classrooms.
8. WASHROOMS — Men's and women's washrooms are directly across the corridor from classrooms on both 6th and 7th floors.
9. MARVIN CENTER
  - a. Bookstore — ground floor.  
Open Monday through Thursday 8:45 a.m. - 6:30 p.m.; Friday 8:45 a.m. - 5:00 p.m. During Summer Session, Monday through Friday 8:45 a.m. - 5:00 p.m.  
No special identification needed.
  - b. Gameroom -- 5th floor  
Open Monday through Thursday 1:00 p.m. - 11:30 p.m.;  
Friday & Saturday 11:00 a.m. - 1:30 a.m. Sunday 12:00 noon - 1:30 a.m.  
Bowling, billiards, and pingpong.  
Your name tag is sufficient identification.
10. Library:
  - a. Main library is open from 8:30 a.m. to midnight.
  - b. Circulation desk closes at 10:00 p.m.



#### UNIVERSITY

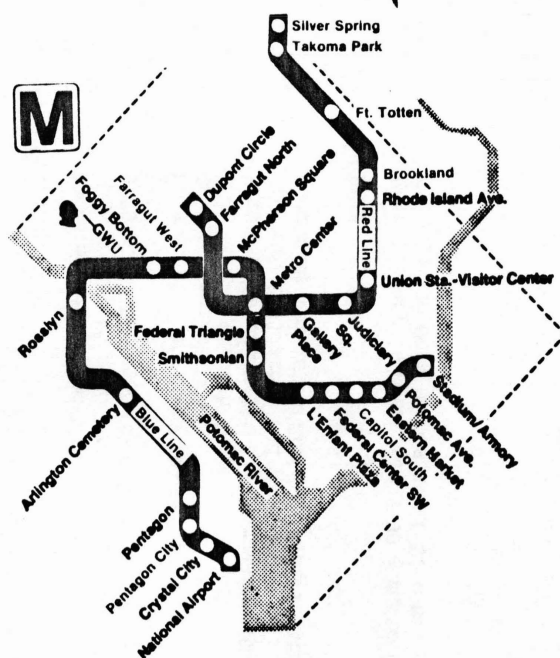
- A. GWU Library  
(Continuing Engineering Education—6th Floor)
- B. University Parking Bldg.  
(Visitors enter from I Street)
- C. Engineering School—Tompkins Hall
- D. University Administration—Rice Hall
- E. School of Medicine—Ross Hall
- F. Marvin Center  
-Bookstore (Basement)  
-Cafeteria (First Floor)  
-University Club (Third Floor)  
-Bathhouse (Fifth Floor)

#### HOTELS

- 1. Watergate
- 2. Howard Johnsons
- 3. One Washington Circle
- 4. Guest Quarters
- 5. Intrigue Hotel

#### RESTAURANTS

- 6. Blackie's House of Beef
- 7. Luigi's
- 8. Gusti's
- 9. The Astor
- 10. Trieste
- 11. Mr. Henry's
- 12. Swiss Chalet
- 13. Adams's Rib
- 14. Marrocco's  
(Italian)
- 15. Old Angus



The GW campus may be reached by METRO at the Blue Line's Foggy Bottom/GWU station located at 23rd and Eye St on the GW campus. From the Red Line, GW may be reached by transferring at METRO Center to the Blue Line going toward National Airport, and exiting at Foggy Bottom

## TRANSISTORS

1. OSCILLATORS - MAGNETRON (1 GHz AVG. MAXIMUM)
2. AMPLIFIERS - (GRID LEAK POWER) (TYPE O)  
 - TRIODE + TETRODES, KUTSTON + TWT  
 (BW ↓ TWT PWR ↑)  
 (BW ↑ KUTSTON PWR ↑)  
 - KUTSTONS RELIABLE  
 - CROSS FIELD AMPS (BROAD BW, GAIN LOW)  
 (PERFORM AS FINALS)  
 - SOLID STATE DEVICES  
 - TRANSISTORS, ETC. LOW PWR,

## DUPLEXERS

1. GAS TUBE - LIMITED LIFE, ERRATIC
2. CIRCULATORS
3. DIODE LIMITING

## ANTENNAS

1. PARABOLIC
2. PRISMED HORN - MECHANICALLY STRUCTURED  
 - ELECTRICALLY STRUCTURED

## RECEIVERS

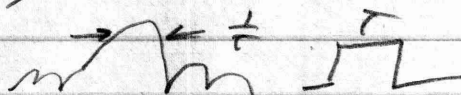
1. SUPERHET w/ LOW NOISE AMPLIFICATION OR MIXED  
 LNA - MASERS, PARAMPS, TRANSISTOR  
 - SUSCEPTIBLE TO JAMMING  
 - LOWERS DYNAMIC RANGE,

IF/ MATCHED FILTER FOR BEST S/N RATIO

$$H_n(f) = S^*(f)$$

$S(f)$  = FOURIER TRANSFORM OF SIGNAL

$$S(f) = \int s(t) e^{-j2\pi f t} dt$$



$BT \approx 1$   
 FOR MAX SENS.

## DETECTION

1. ENVELOPE (AMPLITUDE)  

 ⇒ TO VIDEO.

2. PHASE DETECTION (PHASE) ⇒ DOPPLER FILTER

DISPLAY P.P.I.

ANGLE  
 RANGE



- AS COPIE - RANGE VS. AMPLITUDE,
- COMPLEXION CONTRASTION

- DISTINCTION DECISION

- CFAR (CONSTANT FALSE ALARM RATE RECEIVER)

- CONTROLS GAIN TO KEEP FALSE ALARMS CONSTANT

- WITH AUTOMATIC DISTINCTION.

### RADAR EQUATION



$$\text{POWER DENSITY} = \frac{P_t}{4\pi R^2}$$

$$\text{DIRECTIVE POWER DENSITY} = \frac{P_t G}{4\pi R^2}$$

POWER CROSS SECTION  $\neq$  OBJECT CROSS SECTION

$$\sigma = \lim_{R \rightarrow \infty} (4\pi R^2) \frac{|E_H|}{|E_i|^2}$$

$$\text{POWER DENSITY @ RANGE} = \frac{P_t G}{(4\pi R^2)} \frac{\sigma}{(4\pi R^2)}$$

$$P_{\text{RECEIVED}} = \frac{P_t G}{4\pi R^2} \frac{\sigma}{4\pi R^2} A_e = P_r$$

← CAPTURE AREA

(1) ASSUMES RE-RADIATED IN ALL DIRECTIONS.

$$P_r = \frac{P_t G A_e \sigma}{(4\pi)^2 R^2}$$

WHEN  $P_r = 5 \text{ mW}$ ,  $R = R_{\text{max}}$

$$P_{\text{max}}^4 = \frac{P_t G A_e \sigma}{(4\pi)^2 5 \text{ mW}}$$

$$G = \frac{4\pi A_e}{\lambda^2}$$

$$P_{\text{max}}^4 = \frac{P_t G^2 \lambda^2 \sigma}{(4\pi)^3 5 \text{ mW}} = \frac{P_t A_e^2 \sigma}{4\pi \lambda^2 5 \text{ mW}}$$

0.6 TYPICAL  
 $A_e = \rho A$  ← PHYSICAL AREA

CONSTANT GAIN ANT. ∴ WANT LONG  $\lambda$   
 CONSTANT AREA ANT. ∴ WANT SHORT  $\lambda$ .

### SPECIFICATION OF ARSR

1. RELIABILITY - MTBF, MTTR

$$\text{AVAILABILITY} = \frac{\text{MTBF}}{\text{MTBF} + \text{MTTR}}$$

2. COVERAGE 243 mi @ 40,000 ft RANGE  
 3. TARGET,

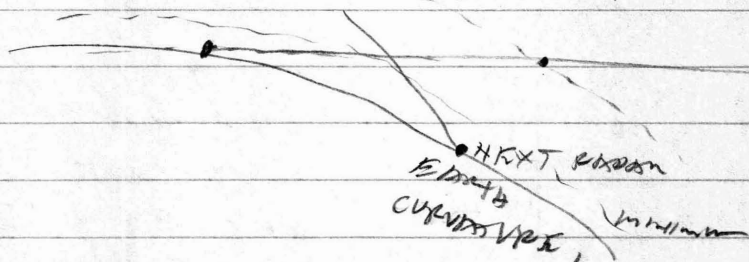


FIG. 20a RANGE RANGE - HEIGHT CHART.

4. COST (military cost) { \$, space, weight, power }  
 5. # TARGETS. (FDA 2500 TARGETS AT ONE TIME)  
 (TARGETS UNLIMITED)

6. ACCURACY. 3 miles. AZIMUTH,  
 RANGE IN ALTITUDE (USE  
 TARGETS SPECIFICATIONS)

7. WEATHER - FREQUENCIES FIXED FOR FRA (2044)

$$R_{\max} = \frac{P_{\text{av}} G^2 \lambda^2 \sigma_n E_{\text{in}}(n)}{(4\pi)^3 K T_0 F_n (BT) f_p (S/N), L_s}$$

NOT  
 UNIQUE  
 SOLUTION

$$n = \frac{\theta_a f_p}{6 \omega_n}$$

rpm

$$G = \frac{\pi^2}{\theta_a \theta_e}$$

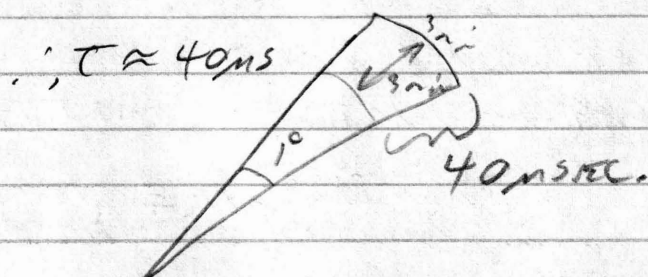
$$t_s = t_0 \times \frac{2\pi}{\theta_a}$$

$$t_0 = n / f_p$$

$$\theta \approx \frac{\lambda}{D}$$

For 243 km range  
 $f_p \approx 330 \text{ Hz}$  P.R.F.

$\theta_a \approx 1^\circ$  (3 miles @ 243 miles).



$\sigma = 2 \text{ m}^2$  For small AIRPLANE,  
 $t_s$  (PERIOD TIME) = 12 SEC.

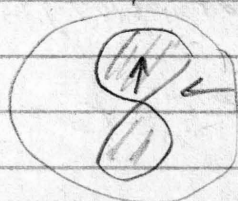
Range = 243 km.  
 (LOW ANGLE DEPENDENT ON  
 HEIGHT OF ANTENNA)

$n = \frac{\sigma_a t_p}{6 \text{ km}}$   $\therefore$  AVERAGE CHOSEN,

### LIST OF DESIGN PROBLEMS

- BACKGROUND NOISE
  - SURFACE CLUTTER (LAND & SEA)
  - WEATHER CLUTTER  $\propto f^4$
  - CIRCULAR BETTER THAN LINEAR
  - WITH PDH (10dB IMPROVEMENT)
  - BIRDS + INSECTS (BOTH HAVE PATTERNS)
- $\downarrow 10^{-4} \text{ m}^2$

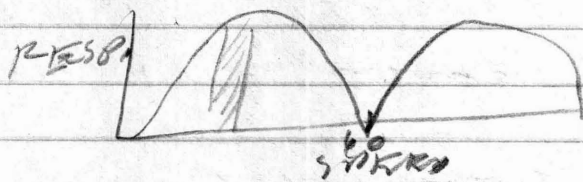
FOR  
 TRACKING  
 ONLY



WIND (ASPECT SENSITIVE)  
 ALSO WIND BEAT  
 MODULATIONS.



- AUTOMOBILES
- BLIND SORTEDS (AMBIGUITIES IN DOPTER)



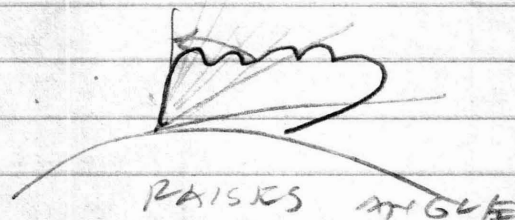
Assume 200 mi @ 15 g/m

1, @ 20 mi  $10^{-4} \text{ m}^2$  ( $\frac{1}{4}$  VARIATION RANGE)

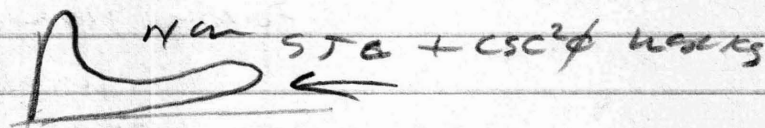
USE STC { AT SHORT RANGES TURN DOWN  
W/ 15H  
T-9 KLOS  
+ BROS } GAIN " SENSITIVITY TIME CONTRA

DUTOS - USE ANTENNA PATTERN (RAISE  
ANTENNA BEAM AT CLOSE IN  
RANGE.

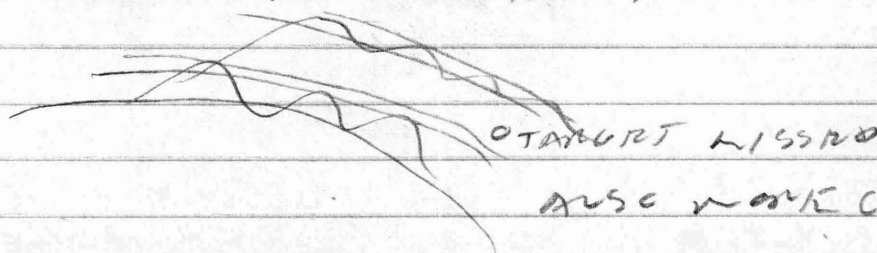
$$\csc^2 \phi \approx G(\phi)$$



STC +  $\csc^2 \phi$  = PROBLEM (HIGH FLYING  
TARGETS ABOVE AT SHORT  
RANGE WOULD NOT BE SEEN  
1, REDesign ANTENNA



- ANOMALOUS PROPAGATION.



ALSO WORK CLUTTER.

PRODUCING.

- GROUND REFLECTIONS

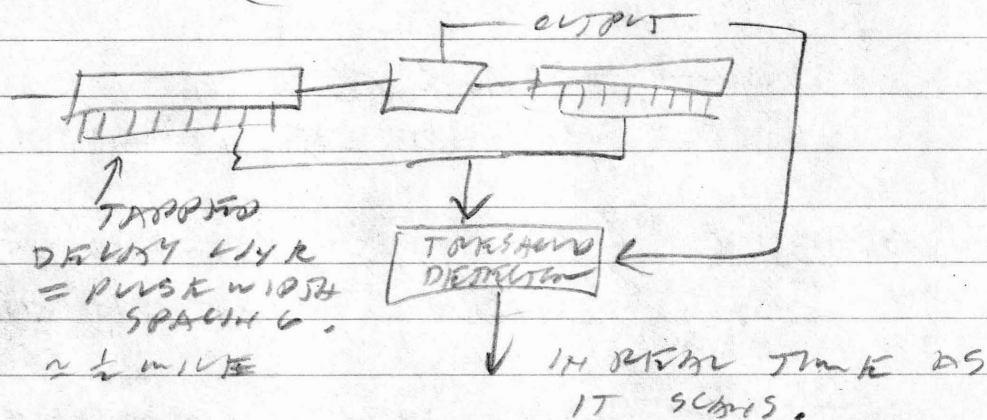
PULSE COMPRESSION - NECESSARY

WHEN LIMITED BY PEAK POWER.

- ~~NECESSARY~~ WITH TRANSISTORS, (DUTY CYCLE)

- AUTOMATIC DISTORTION + TRACKING

- CFAR (CONSTANT FALSE ALARM RATE)



- STC SENSITIVITY TIME CONTROL

### DETECTION CRITERIA

2 OUT OF 3 INTERCEPTS

3 OUT OF 4

3 OUT OF 5

### MULTIPLE REFLECTIONS

- LINEAR REFLECTION (LUTTER)

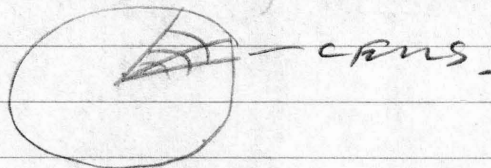
- MJI (DOOR)

- LOGARITHMIC (RAIN)

(VARY WITH BEARING + RANGE)

eg. COASTAL PHASE.

∴ COMPUTER CONTROLS RANGE,  
AZIMUTH GATING.



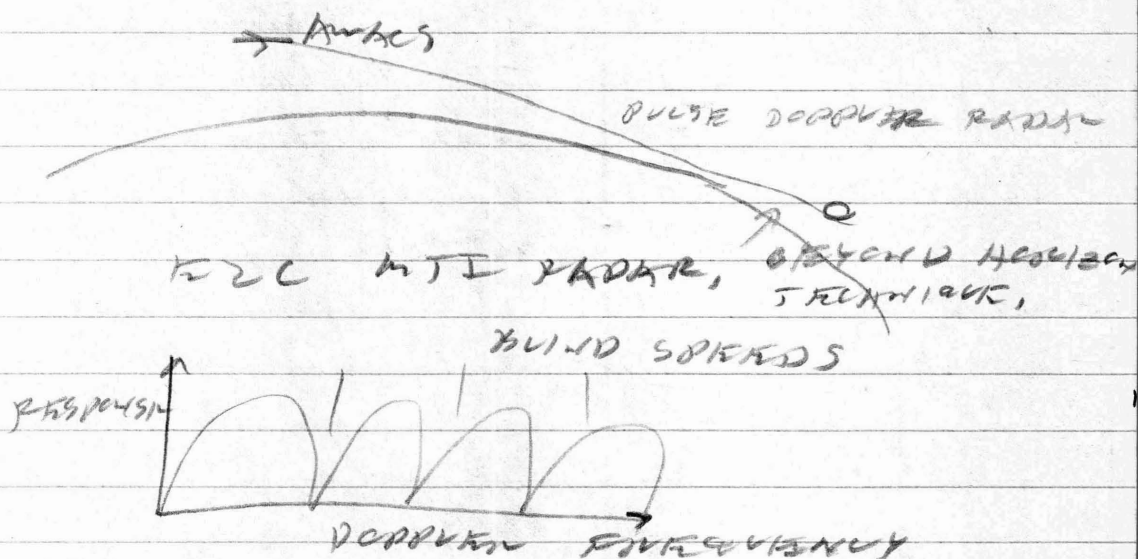
"FAMILY OF AIR TRAFFIC CONTROL RADARS" AT 5-15 MAY 1979  
 SALINA (ITALIAN) GOOD PAPER OF DESIGNER,

### 3D RADAR METHODS

- 1. NOODING BEAM HEIGHT FINDER (2 SYSTEMS)
- 2. SCANNING PENCIL BEAMS (MULTIPLEX TO SPEED UP)
- 3. MULTIPLEX FIXED BEAMS
- 4. TRANSPODER FFA.

### AWACS ECC (NAVY) PAGE ARRAY

- more clutter because looking DOWN AT CLUTTER.
- AWACS STAYS UP LONGER (SAME RADAR)



$$V_D (\text{KNOTS}) = \lambda (\text{m}) f (\text{Hz})$$

$$f_p = 20,000 \text{ Hz}$$

4 mVLC  
 16000000000  
 RANGE,



## DUTCH SYSTEM FOR TANKS

- NAMM BROWN RESOUTION OF MULTIPASS ROADING - X BAND STRUCT, FOR BAND NAMM BROWN.
- PRUETTICK 1st USA, TO BUILD DUTCH SYSTEMS.

$$v_p = 0.17 \times 300$$

$$v_p = 210 \text{ KNOTS}$$

(VHF)

$$v_d = 0.03 \times 300 = 9 \text{ KNOTS} \quad (\text{S-BAND})$$

IN AIRBORNE SYSTEM - KEEP NOTCH  
AT ZERO.

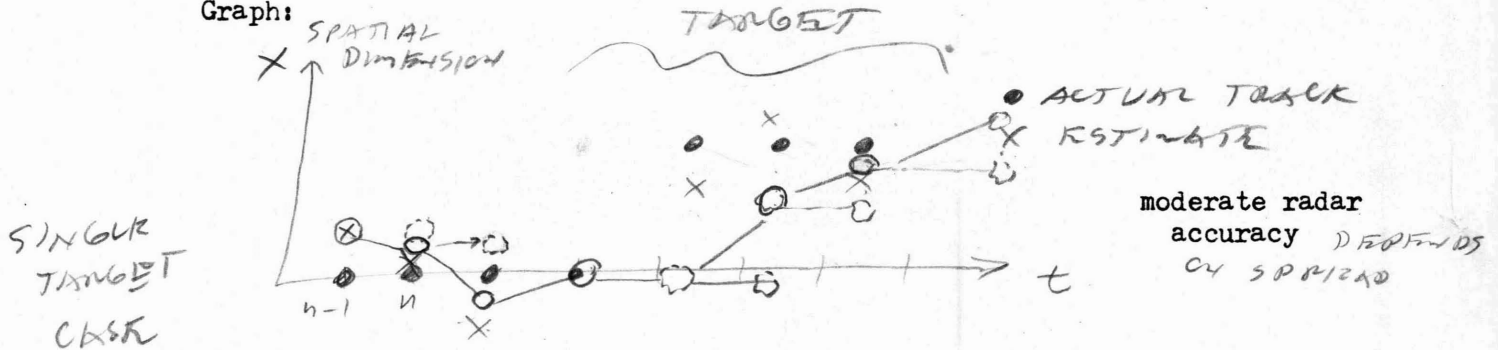
RTI { TACAN  
DPCA (DISABLED CENTER ANTENNA)  
ADAPTIVE

WORKSHEET

EXPONENTIAL TRACKING

1. A simple filter - take the predicted position and add to it just half of the difference between that and the newly measured position; consider this smoothed position to be the next predicted position.

Graph:



$\circ$  = PREDICTED POSITION  
 $\circ$  = INSTANT BEST ESTIMATE  
PREDICTION

$$X_{n-1} = X_{pn}$$

$$\bar{X}_n = X_{pn} + 0.5(X_n - X_{pn})$$

very accurate radar

"ALPHA" TRACKER (EXPONENTIAL TRACKER)

Formulas:

$$\bar{X}_n = X_{pn} + \alpha(X_n - X_{pn})$$

$$X_{pn} = X_{n-1} + \bar{X}_{n-1} T_s \quad , \quad \bar{X}_n = \bar{X}_{n-1} + \frac{\beta(X_{pn} - X_n)}{T_s}$$

MUCH BETTER ESTIMATOR

2. Consider how the next predicted position could be bettered by also estimating target velocity based off measured position.
3. How might the choice of alpha be influenced by your knowledge of the radar's accuracy? by your knowledge of the target's maneuverability? What's meant by the "gain" of a filter? by its "bandwidth"?

INACCURATE ADDITIONAL DATA DOES NOT DEGRADE ACCURATE DATA.

→ CAN CHANGE  $\alpha$  AND  $\beta$  FOR KNOW CONDITIONS  
eg. - LIGHTER WOULD BE CLOSER BUT LAGS TURNS,  
- USE  $\alpha$  TO TURN UP NEXT  $\alpha$  TO FOLLOW VELOCITY.

WORKSHEET

REPRESENTING PULSE COMPRESSION IN THE RADAR RANGE EQUATION

1. Write the Radar Range Equation, solving for  $R^4$  and leaving receiver noise in terms of receiver bandwidth  $B$ .

$$\frac{P_t G_t L_t}{4\pi R^2} \cdot \frac{1}{G \frac{1}{4\pi R^2}} \cdot A_{eff} = W \cdot K T B F$$
  

$$\therefore R^4 = \frac{P_t G_t G_r L_t L_r \lambda^2 \sigma}{(4\pi)^3 W K T B F}$$
  
 Annotations:
 

- $G_r = 4\pi \frac{A_{eff}}{\lambda^2}$  (RECEIVER GAIN)
- $A_{eff} = \frac{S}{4}$  (DETENTION CRITERION)
- ASSUMES  $B = \frac{1}{T}$  (PULSE DURATION BASIS)
- PRIME POWER (PULSE IN PULSE)

2. Consider two radars of equal peak power but a two-to-one pulse width difference. Write  $R^4$  in terms of pulse width considering receiver bandwidth to be well matched to modulation bandwidth of the pulse. No pulse compression here - this is to establish that range is indeed dependent upon signal energy, provided the receiver is matched to the signal bandwidth.

$$\text{① } R_1^4 = \frac{P_t \dots T_1}{\dots K T F}$$
  

$$\text{② } T_2 = 2(T_1) \quad R_2^4 = \frac{P_t \dots 2T_1}{\dots K T F}$$
  
 RANGE DEPENDENT ON DETECTION TEST

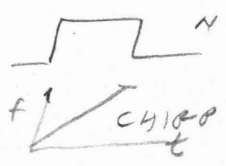
3. Consider two radars of the same waveform ( $P_t$  and pulse width) in one of which the receiver is well matched to the modulation bandwidth of the pulse and in the other of which the receiver is unnecessarily made  $N$  times broader in receiver bandwidth. Write the adjusted range equations and observe that range is reduced by the unfortunate reception mismatch. (Again, no pulse compression here.)

$$P_t \text{ [Pulse Width } T] \quad R^4 = \frac{P_t \dots T}{\dots K T F}$$
  
 NOW OPEN UP RECEIVER BW,  $R^4 = \frac{P_t \dots T}{N}$



(worksheet on pulse compression)

4. Consider a pulse compression radar of the same pulse width as in 3. above, but in which the time-bandwidth product of the transmitted pulse is  $N$ . Write the range equation using the factor  $N$  to restore the range over what the range had been in the mismatched receiver case. (Recall this restoration assumes the receiver is well matched, including phase and amplitude characteristics of its passband, to the transmitted signal.)



$$R^4 = R_t \frac{1 \dots 1}{1 \dots 1} \left( \frac{T}{N} \right) N$$

"PROCESSING GAIN"

$\frac{T}{N} = \text{compressed p.w. } T_c$

NOT ENERGY INDICATIVE

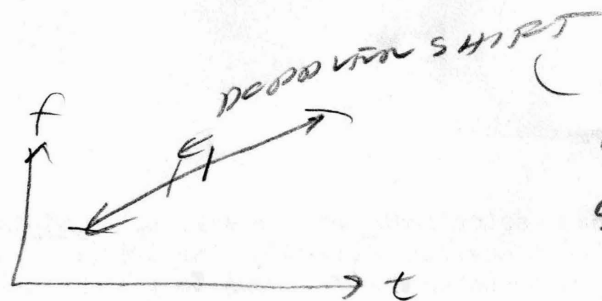
$$R^4 = R_t \frac{1 \dots 1}{1 \dots 1} \left( \frac{T}{N} \right) N$$

SIDE Lobe REDUCTION, EFFICIENCY RATIO

"PROCESSING GAIN" → (WEIGHTING EFFICIENCY)

5. Write the above in terms of the "compressed" pulse width, and note that the "restoring" factor  $N$  now appears in the numerator much as a gain term (like antenna gain) and, hence, is sometimes called the "processing gain" due to pulse compression. Recall, however, this "gain" merely restores the range to that due to the energy in the pulse; that energy, you see, is clearly more than the product of actual peak power and the compressed pulse width.

6. Can you imagine how the efficiency associated with "weighting" in the pulse compressor (to help form better range sidelobes, say) might be represented?



(CAN NOT TELL  
DIFFERENCE BETWEEN  
STATIONARY TARGET,

$\therefore$  AMBIGUITIES IN RANGE AND  
DOPPLER.

RULE OF THUMB

SINGLE PULSE, MATCHED FILTER

$1000 \text{ ft/sec} \rightarrow$  MATCH 1 TARGET, 1 kHz AT 1 GHz  
 $= 1 \text{ kHz}$

$\therefore$  ACTUAL RANGE WOULD BE  
2 kHz,

17,550 ft/sec @ 5 GHz GIVES 200 kHz  
2 kHz RANGE SHIFTS 400